2004

LANDSLIDE INVESTIGATION IN THE RIO AGUAS CATCHMENT, SOUTHEAST SPAIN

Hart, Andrew Barrie

LANDSLIDE INVESTIGATION IN THE RÍO AGUAS CATCHMENT, SOUTHEAST SPAIN

By

Andrew Barrie Hart

A thesis submitted to the University of Plymouth in partial fulfilment for the degree of

Doctor of Philosophy

School of Earth, Ocean and Environmental Sciences

Faculty of Science

University of Plymouth

April 2004

Abstract

Landslide Investigation in the Río Aguas Catchment, Southeast Spain

Andrew Barrie Hart

Many remote and/or rural communities live under the threat of major landslide activity. These remote areas are also increasingly the focus of development programmes which, without careful consideration of the ground conditions, will be at risk. The cost of mitigating against landslide activity can also be extremely high, possibly making prevention or avoidance the better long-term option. It is, therefore, of prime importance to assess the type and magnitude of the landslide activity affecting an area, particularly during the feasibility and planning stages of any project. The most straightforward approach to any landslide investigation is the compilation of a landslide inventory and the development of a geological and geomorphological ground model for the area under investigation.

Previous landslide inventory-based projects (for example, in UK, Hong Kong and Nepal) have utilised either desk study or remotely sensed sources (aerial photographs or satellite imagery) with only limited field mapping, have focused on wet monsoonal environments in either mountainous and/or heavily populated areas and have usually been completed without reference to a ground model for the area being investigated. Therefore, an investigation of the landslide activity affecting the 425 km^2 Río Aguas Catchment area has been completed. This is a remote and rural part of southeastern Spain, which has an arid to semi-arid climate and is periodically affected by both earthquake and flash-flood activity.

Through a combination of aerial photographic interpretation (API) and field verification and mapping, over 300 landslides have been mapped and documented. These data have been used to develop a landslide inventory and a conceptual geological and geomorphological ground model of the study area, with respect to the landslide activity. The landslide inventory data have been used to complete a statistical analysis investigating the factors that control the distribution, style and mechanisms of the landslide activity, as well as to examine the relationships between landslide volume, runout length and angle of reach. The basis of the ground model is a project-derived terrain classification for the study area.

The data analysis has shown that although a variety of landslide failure mechanisms are seen within the study area, the majority of the landsides are rock falls and topples and/or occur within incised sections of the drainage network. The analysis has also shown that the landslide activity is controlled by a combination of the discontinuities within the rock mass, as well as contrasts in the permeability and stiffness of the rock masses/types involved. The influence of human activity, as well as tectonic activity, rainfall and expansive clay soils has also been considered. However, a lack of detailed historical landslide and rainfall data limits the conclusions that can be drawn.

The mapped landslide distribution (supported by the geological and geomorphological ground model) has highlighted that the majority of the landslides in the Río Aguas Catchment are related to a major river capture and modification of the drainage network that occurred approximately 100Ka BP, and that they are a key component of the geomorphological processes active within the study area. This river capture, driven by differential tectonic uplift between sedimentary basins, has caused a wave of incision to pass through a substantial section of the south central part of the study area leading to the oversteepening of slopes, the incision of the drainage network and the majority of the landslide activity that is seen within the study area. The development of the drainage network has been recorded by a series of river terrace deposits that reflect the overall tectonically induced incision as well as the variable Quaternary climate. These river terrace deposits have been used to provide a relative temporal framework for the landslide activity, in the absence of any dated landslide chronology.

Contents

List of Appendices

Appendix A – Publications

Appendix B – Copy of the Landslide Inventory

Appendix C – Rating scheme for the Landslide Inventory

List of Figures

Chapter 1 – Introduction

Chapter 2 – Geology and Geomorphology

Chapter 3 – Landslide Investigation

Chapter 4 – Landslide Distribution Analysis

Chapter 5 – Case Studies

Chapter 6 – Río Aguas Ground Model and Summary

List of Tables

Chapter 1 – Introduction

Chapter 2 – Geology and Geomorphology

Chapter 3 – Landslide Investigation

Chapter 4 – Landslide Distribution Analysis

Chapter 5 – Case Studies

Chapter 6 – Río Aguas Ground Model and Summary

Acknowledgements

Author's Declaration

At no time during the registration for the degree of Doctor of Philosophy has the author been registered for any other University award.

This study was funded by the author, although assistance was received from two external bodies:

- The Geological Society of London Thomas Jefferson Fund for awarding me a grant of £1400 towards the cost of the fieldwork.

- The British Geomorphological Research Group (BGRG) Research and Publication Fund for awarding me a grant of £150 towards the cost of attending the Eighth International Symposium on Landslides in Cardiff during June 2000.

During the course of the study, relevant scientific seminars and conferences were attended at which work was presented. A number of papers have also been prepared for publication. The conferences attended and papers published are listed below:

Refereed Publications:

Griffiths, J.S., Mather, A.E. & Hart, A.B. (2002) Landslide susceptibility in the Rio Aguas Catchment, SE Spain. *Quarterly Journal of Engineering Geology and Hydrogeology*, **35**, 9-17.

Hart, M.B. & Hart, A.B. (2000) Global Climate Change: A geological perspective. *Geoscience in southwest England*, 10, 14-17.

Hart, A.B., Hearn, G.J. & Petley, D.N. (In press) Landslide susceptibility, hazard and risk mapping for infrastructure planning in mountainous areas. To be published in: *Quarterly Journal of Engineering Geology and Hydrogeology*, **37**, xxx-yyy.

Petley, D.N., Hearn, G.J. & Hart, A.B., (In press) Satellite remote sensing for planning and engineering purposes in Nepal and Bhutan. To be published in: *Quarterly Journal of Engineering Geology and Hydrogeology*, **37**, xxx-yyy.

Petley, D.N., Hearn, G.J. & Hart, A.B., (In press) Landslide risk assessment for rural regions in Nepal and Bhutan. In: Glade, T., Anderson, M. & Crozier, M. (eds) *Landslide Hazard and Risk*, xxx-yyy. To be published April 2004.

Conference Proceedings & Non-Refereed Publications:

Hart, A.B., Hearn, G.J. Petley, D.N., Tiwari, S.C. & Giri, N.K. 2003. Using remote sensing and GIS for rapid landslide hazard assessment: Potential public sector uptake in Nepal and Bhutan. *Proceedings for the Permanent International Association for Road Congresses (PIARC) Conference "Sustainable Slope Risk Management for Roads"*, Kathmandu, Nepal, March 2003.

Hart, A.B., Lamichhane, P., Jha, P., Subba, M. & GC, S. 2003. A Landslide Database for Nepal. *Proceedings for the Permanent International Association for Road Congresses (PIARC) Conference "Sustainable Slope Risk Management for Roads"*, Kathmandu, Nepal, March 2003.

Petley, D.N, Crick, W.D.O. and Hart, A.B. 2002. The use of satellite imagery in landslide studies in high mountain areas. *The Proceedings of the 23rd Asian Conference on Remote Sensing (ACRS 2002), Kathmandu*. Available online at: http://www.gisdevelopment.net/aars/acrs/2002/hdm/48.pdf

Hart, A.B., Griffiths, J.S. & Mather, A.E. (2000) The role of landsliding in landscape development in the Rio Aguas Catchment, South East Spain. In: Bromhead, E., Dixon, N. & Ibsen, M.-L. (eds.) *Landslides in research, theory and practice*, Thomas Telford, London, 701-706.

Hart, A.B. & Griffiths, J.S. (1999) Mass movement features in the vicinity of the town of Sorbas, South-east Spain. In: Griffiths, J.S., Stokes, M.R. & Thomas, R.G. (eds.) *Landslides: Proceedings of the Ninth International Conference and Field Trip on Landslides*, Bristol, UK, 5th-16th September 1999, A.A. Balkema, Rotterdam, 57-63.

Hart, A.B. (1999) An Introduction to the Landslides of the Sorbas Basin. In: Mather, A.E. & Stokes, M. (eds.) *BSRG/BGRG South East Spain Field Meeting Guide Book*, University of Plymouth, England, 124-133.

Conference Abstracts & Posters:

Hart, A.B., Griffiths, J.S. & Mather, A.E. (2001; abstract) Differentiating between susceptibility, hazard and risk: a case study of landsliding in South East Spain. Abstract for a paper that was presented by Griffiths, J.S. at the RGS/IBG Conference, held at the University of Plymouth, January 2001.

Mather, A.E., Hart, A.B. & Griffiths, J.S. (2000; abstract) Impact of Quaternary base-level change on hillslope erosion in the Rio de Aguas catchment, South-East Spain. Abstract submitted to the COST Conference, Almeria, September 2000.

Hart, A.B. (2000) Landslide activity, drainage development and risk assessment: The Sorbas Case Study, SE Spain. Poster presented at the European Union Concerted Action on Forecasting, Prevention and Reduction of Landslide and Avalanche Risks (CALAR) Conference "Living with Natural Hazards", Vienna, Austria 17th-19th January 2000.

Hart, A.B. (2000) Landslide activity, drainage development and risk assessment: The Sorbas Case Study, SE Spain. Poster presented at the 8th International Symposium on Landslides, Cardiff, Wales, 26th - 30th June 2000.

External Contacts:

- Dr Gareth Hearn, Scott Wilson Kirkpatrick & Co. Ltd – Engineering Geomorphologist at Scott Wilson and Project Manager on the Landslide Risk Assessment Project.

- Dr David Petley, University of Durham – Peer Review Consultant on the Landslide Risk Assessment Project.

Name: ANDREW HART

Signature: A-B. Hart

Date: 30/04/2004

Postscript

While printing the final version of this thesis, I was informed that a new rock fall had occurred at the site of the Maleguica landslide (described in Section 5.2.1). The April 2004 photograph is provided courtesy of Dr M. Stokes (University of Plymouth).

Chapter 1 – Introduction

1 Introduction

1.1 <u>Introduction</u>

The growth in global population and the expansion of settlements and communication routes in hazardous areas are increasing the impact of natural disasters in both the developed and developing world (Alexander, 1993). Casualties due to natural hazards tend to be larger in developing countries (Alexander, 1993; Shah, 1983), whereas economic losses are more severe in the industrialised world (Schuster & Fleming, 1986; Guzzetti *et al.*, 1999). Both may be increasing because of the higher value of endangered structures and the greater number of people potentially involved. Alexander (1993) stated that the cost of natural hazards to the global economy exceeded US$50,000 million per year, of which a third represents the cost of predicting, preventing and mitigating disasters and the other two thirds represent the direct costs of the damage.

Of the numerous natural hazards that affect many countries, the economic losses and casualties due to landslide activity is greater than commonly recognised. It has been well documented that in many countries, landslide activity generates a yearly loss of property larger than that from any other natural disaster, including earthquakes, floods and windstorms (Schuster & Fleming, 1986; Alexander, 1989; Swanston & Schuster, 1989; Olshansky, 1990; Schuster, 1996; Glade, 1998; Guzzetti *et al.*, 1999). Although it should not be forgotten that devastating landslides occur throughout the world (Table 1.1) *"highlighting the point that when a natural process strikes it does not stop to ask whether the recipients are developed or not"* (Brunsden, 1993).

Table 1.1 – Examples of high magnitude/low frequency landslide events in the latter part of the 20th Century (after Jones & Lee, 1994; Schuster 1996; Godt & Savage, 1999; Guadagno & Zampelli, 2000).

Year	Location	Name & Type	Volume (m³)	Trigger	Impact	Comment
1962	Peru (Ancash)	Huscaran Debris avalanche	13×10^6	?	4,000-5,000 killed; much of Ranrahirca village destroyed	Major debris avalanche from Nevado Huscaran; average velocity 170km/hr
1963	Italy	Vaiont rock slide	250×10^6	Filling Vaiont reservoir	c.2,000 killed; city of Longarone badly damaged; total cost in 1963 US$200 million	High velocity rock slide into reservoir caused 100m wave to overtop dam. Estimated maximum velocity 50m/s
1964	Alaska	The 1964 Alaskan landslide (spreading failures)	?	M6.4 earthquake	Damages in 1964 cost US$180 million	Spreading failures caused major landslide damage in Anchorage, Valdex, Whittle & Seward
1966	Rio de Janeiro (Brazil)	Rio de Janeiro avalanches debris & mud flows	?	Heavy rains	~1,000 killed	Many landslides around Rio de Janeiro
1966	Wales	Aberfan Tip flow slide (debris flow)	1.1×10^5	Loose tipping on a spring	144 killed including 112 school children	Flowslide of loose tipped colliery waste, estimated maximum velocity 8.8m/s; site of previous slides that did not reach the village
1970	Peru	Nevados Huscaran debris avalanche	?	M7.7 earthquake	18,000 killed; town of Yungay destroyed; Ranrahirca partially destroyed	Rock/debris avalanche from same peak as 1962; average velocity 280km/hr
1974	Peru	Mayunmarca rock slide – debris avalanche	1.6×10^9	Rainfall – river erosion	Mayunmarca village destroyed; ~450 killed; failure of 150m high landslide dam caused major downstream flooding	Debris avalanche with average velocity 140 km/hr; dammed Maataro River
1980	USA	Mount St Helens rotational rock slide followed by debris avalanche	2.8×10^9	Eruption of Mt St Helens	Worlds largest historic landslide; 5-10 killed – most people evacuated; major destruction to infrastructure	Began as rotational rock slide, degraded to 23km long debris avalanche with average velocity 125km/hr; surface remobilised into 95km debris flow

1982	USA	San Francisco Bay Region 18,000 debris flows	?	January 3-5 rainstorm	25 killed and landslide damage estimated at US$65 million	
1983	China (Gansu)	Salasham landslide	35×10^6	?	273 killed; 4 villages buried; 2 reservoirs filled with debris	Loess landslide
1985	Columbia	Nevado del Ruiz debris flow	?	Eruption of Nevado del Ruiz	4 towns & villages destroyed; killed 20,000+ in city of Amero; flow in valley of Langunillas River;	Death toll unnecessarily high due to no evacuation despite numerous hazard warnings
1986	Papua New Guinea	Bairaman rock slide – debris avalanche	200×10^6	M7.1 earthquake	Village of Bairaman destroyed by debris flow from breached landslide dam; evacuation prevented casualties; major environmental effects	Debris avalanche formed 210m high dam that impounded 50 million m^3 lake; dam failed causing 100m high debris flow – flood downstream
1987	Ecuador	Reventador landslides (mainly debris flows)	$75-110 \times 10^6$	M6.1 & M6.9 earthquakes	~1,000 killed; many kms of oil pipeline & highway destroyed; 1987 costs US$ 1 billion	Landslides mainly in saturated residual soils on steep slopes; thousands of thin debris flows in catchments
1994	Columbia	Paex landslides (mainly debris flows)	Area = 250km^2	M6.4 earthquake	271 killed; 1,700 missing; 32,000 displaced; several villages destroyed	Thousands of thin, residual soil slides on steep slopes becoming debris flows
1997/ 1998	USA	San Francisco Bay region – c.300 landslide events of all types	Largest individual failure: 13m^3 (Mission Peak Earthflow)	High rainfall	Landslide damage estimated at US$ 158 million; only one fatality	Rainfall recorded at more than twice the annual average as a result of a Type 1 El Nino Southern Oscillation
1998	Campani (southern Italy)	129 separate initial slides – predominantly debris flows	Area = 70km^2	Very high daily and antecedent rainfall	161 killed; towns of Quindici, Sarno, Bracigliano & Siano devastated	Rainfall return period calculated as 100 years; minimum flow rates of 10-20km/hr; failures mainly in colluvium and weathered pyroclastic material from Mt. Versuvius

Many remote and/or rural communities live under the threat of major landslide activity. There may be little understanding amongst these communities about the nature of such hazards, or how their everyday activities enhance the risk or can be modified to reduce such risks (Charman & Griffiths, 1993; Hearn *et al.*, 2003; Hart *et* al., 2003a,b; Hart *et al., in press*; Petley *et al., in press*). These remote areas are also increasingly the focus of development programmes which, without careful consideration of the ground conditions, will be at risk. There is also the problem of mitigating landslide activity. Costs can be extremely high, possibly making prevention or avoidance, if possible, the more sustainable long-term option. It is, therefore, of prime importance to assess the type and magnitude of the landslide activity affecting an area when considering any new development project or engineered structure, particularly during the feasibility and planning stages of a project.

However, to complete such assessments requires data that are frequently unavailable, such as detailed maps of topography or geology (Hearn *et al.*, 2003; Hart *et al.*, 2003a; Hart *et al., in press*). Therefore, these data need to be collected, which in turn requires suitable, reliable and often relatively rapid data collection techniques. In addition to this, there is a requirement to understand the countryside in which the landslide has occurred or the engineering project is to be carried out (Fookes, 1997).

1.2   The Ground Model & Terrain Evaluation

Prof. Peter Fookes (Fookes, 1997) argued that when working within the landscape a working conceptual ground model for the site should be developed as soon as possible through detailed desk study and field work. This would require consideration of the

regional and more local geological and geomorphological history together with an understanding of the current ground conditions. The information and data collected could then be used to plan and implement more detailed investigations.

Fookes (1997) states that *"the strength of the conceptual model is in providing an understanding of the geological processes that made the site. This enables predictions to be made or situations anticipated for which explanations need to be sought in the geological materials, geological structure and the ancient and active geological processes in the area"*. Although referring to engineering problems, this argument could also be made when dealing with landslide activity in general whether for regional or local planning, or for a specific engineering project.

The Second Working Party on Land Surface Evaluation for Engineering Practice have argued that one effective way to construct a conceptual model for an area or site is through land surface evaluation (Griffiths & Edwards, 2001). The Working Party has stated that the first objective of any land surface evaluation is to acquire the most comprehensive conceptual ground model that can be generated in order to maximise the value and justify the cost of any subsequent investigations and therefore minimise the geological unknowns (Griffiths & Edwards, 2001).

The First Working Party on Land Surface Evaluation defined land surface evaluation as: *"Land surface evaluation* (for engineering practice) *is the evaluation and interpretation of land surface features and recorded surface data using one or a combination of the ground mapping, interpretation, classification and visual remote sensing techniques... The object is to provide information about ground conditions likely to be of significance"* (Anon, 1982). The main recommended techniques of the First Working

6

Party were geomorphological ground mapping and aerial photographic interpretation (API) based on a framework of land classification. The Second Working Party extended this to include a detailed and extensive desk study, satellite image interpretation, and geological and terrain systems field mapping. They also recognised the increasing role of Geographical Information Systems (GIS) for the storing, analysis, interrogation, interpretation, and presentation of the collected data. This is especially true where large data sets are concerned.

The Second Working Party proposed an updated definition of land surface evaluation as: "*The evaluation and interpretation of land surface and near surface features using techniques that do not involve ground exploration by excavation or geophysics*" (Griffiths & Edwards, 2001). It was noted by the Working Party that this broader definition allowed land surface evaluation to be seen in its most common context as the process of data compilation, interpretation and conceptual ground modelling prior to undertaking engineering ground or site investigation work.

Although the Working Party was referring to the use of land surface evaluation techniques for engineering practice, these techniques are ideal for identifying "problem areas" such as areas of landslide activity (as in this study), soil erosion, karst development, land subsidence or flooding. An advantage of this approach over the "traditional" approach of investigating each slope of an area in turn (often referred to as the "slope by slope" approach) is that all features in the landscape are mapped, ensuring that all parts of the terrain are given due attention without being overlooked. The technique also allows for the production of inventory maps of the location, type, state, style of any engineering hazards encountered (e.g., landslide inventory maps – Wieczoek, 1984; Soeters & Van Westen, 1996). These data can then be used to

7

highlight areas needed for further investigation, as well as for completing assessments of the hazard affecting an area and the risk posed by that hazard to any potentially affected engineering project/structure.

As a well-established, simple, efficient and flexible technique land surface evaluation allows for the rapid assessment of large areas of terrain. It can be used to divide the landscape into areas of recurring patterns of topography, soils, geology and vegetation (Cooke & Doornkamp, 1990). It is, therefore, particularly suitable for mapping landslide activity in remote areas. The method can allow the elucidation of the presence or absence of landslide activity and can therefore be used to form the basis of a landslide distribution map.

The land surface evaluation approach can also be used to gain an understanding of the processes that have previously been active in an area (i.e., glacial, fluvial or previous landslide activity). This information can then be used to develop a model of how the landscape of an area has developed through time (and particularly through the recent past). Such information can then be used to identify those "events" or circumstances that have played the biggest role in creating the landscape of an area (Brunsden, 2001). The spatial and temporal scales used will depend on the scale, and therefore, the detail, of the data being used.

1.3   Examples of Possible "Best Practice"

There are a number of examples of where the land surface evaluation approach has been

adopted. These include:

- The "Review of Research on Landsliding in Great Britain" and the "National

  Landslide Database" for Great Britain;

- The Natural Terrain Landslide Investigation in Hong Kong; and

- The "Landslide Risk Assessment in the Rural Access Sector" project in Nepal

  and Bhutan.

1.3.1   National Landslide Database, UK

Jones & Lee (1994) stated that landslide activity was not a hazard that most people

associated with the UK. In 1984, the Department of the Environment commissioned the

project "Review of Landsliding in great Britain" and the development of the "National

Landslide Databank". A landslide database was established through a desk study

review of all reasonably accessible information held in the public domain regarding

landslides. The sources included books, journals, theses, geological maps and the files

of those engineering companies, local authorities and public utilities that granted access

to data. Each identified landslide was allocated a separate proforma upon which all

available information was entered. Analysis led to a series of regional reports, each

with accompanying folio of 1:25,000 scale county maps, along with a national summary

volume and map at 1:625,000 scale. By the time the review was completed in 1991, a

total of 8835 landslides had been identified (Lee *et al.*, 2000).

This study is considered to have provided the first coherent synthesis of the distribution, character and significance of mass movement and landslide activity in the UK. This study also included national reviews as to the extent, causes and significance to land use planning and development of: mining subsidence; natural underground cavities; foundation conditions; natural contamination; erosion; deposition and flooding; and a preliminary assessment of seismic risk (Brook, 1992). The hope was that this information would provide, for the first time, a comprehensive regional assessment of the then current knowledge regarding the ground conditions of the UK. Jones & Lee (1994) considered this essential base-line data for developing strategies to minimise the impact or losses of future hazards.

The study recognised that the distribution, concentration, extent, variety and significance of landslide activity in the UK had been seriously underestimated. To quote Lee *et al.* (2000) "Jones & Lee (1994) concluded that the pattern of recorded landslides was dominated by the results of a small number of detailed studies set against a backdrop of ignorance". Therefore, the database identifies only a sample of the actual number of landslides in existence (Lee *et al.*, 2000). This conclusion was considered to have serious implications for many sectors of the economy concerned with land development and construction. The recognition of landslide activity as a threat to property and a cause of recurring costs were largely confined to coastal areas, especially along the rapidly eroding clifflines of Eastern and Southern England stretching from Humberside to Devon. The recognition of landslide activity for inland areas was "generally poor" and extremely variable.

Jones & Lee (1994) argued that this initial study showed that further systematic studies were required before it would be possible to assess the true costs of landslide activity in the UK. Lee *et al.* (2000) noted that the study demonstrated the need for landslides to be properly considered in the land use planning process; especially during the preparation of local development plans and in determining individual applications for planning permission. The UK Government responded to this study by publishing guidance notes for local planning authorities on land instability issues (DoE, 1990, 1996). However, Lee *et al.* (2000) concluded that although there were some concerns over the quality and reliability of much of the available information on landslides held within the National Landslide Database, it has provided an excellent platform for desk studies for construction projects or the preparation of instability-related policies in land use plans.

1.3.2   Hong Kong Natural Terrain Landslide Investigation

Over 60% of the total land area of Hong Kong is characterised by steep natural slopes mantled with weak weathered rocks and superficial deposits. With frequent intense rainfall Hong Kong is frequently affected by landslide activity on natural slopes (Evans, 1998). The Geotechnical Manual for Slopes (Geotechnical Control Office, 1984) highlighted the costly and difficult nature of natural slope stabilisation works, and concluded that the avoidance of unstable natural terrain is usually the best approach. However, the demand for land in Hong Kong is such that building and infrastructure developments are increasingly spreading into areas adjacent to steep natural slopes and, over the last few years, the debris from a number of natural terrain landslides has reached areas of development (Evans, 1998).

12

Therefore it became clear that a better understanding was needed of the relative hazard from landsliding on natural terrain in order to define areas which may be particularly susceptible. In response to this the Geotechnical Engineering Office initiated the Natural Terrain Landslide Study (NTLS) in 1995.

Initially using high level (above 10,000 feet) aerial photographs, an inventory of landslide locations and approximate dates of landslides occurring on natural terrain slopes was compiled. This database is referred to as the Natural Terrain Landslide Inventory (NTLI) and contains records of 26,780 landslides (Evans, 1998). Each landslide within the NTLI is numbered, with its location and length of the resulting debris trail shown on a 1:5,000 scale map. The following parameters are recorded in associated data tables:

- The data on the aerial photograph on which the landslide was first observed and of the photograph immediately preceding it;

- The width of the landslide scar (less than or more than 20 m);

- The vegetation cover over the landslide source; and

- The ground slope angle across the landslide head.

The elevation at the toe and crest of each landslide was later manually recorded from the base map and added to the digitised tables. Most of the landslides recorded in the NTLI would probably be classified as debris slides, debris flows, complex debris slide-flows or composite debris slide-flow-falls (Varnes & Cruden, 1996). The landslides recorded in the inventory are divided into two groups:

1. Recent – if they occurred within the time scale of the available aerial photographs; and

2. Relict – if they occurred earlier.

Only natural terrain was surveyed for landslides, and the boundaries of the areas were recorded (Evans, 1998). Natural terrain was defined as terrain that has not been modified substantially by human activity, but includes areas where grazing, hill fires and deforestation may have occurred. Terrain modified substantially by human activity was taken to include both urban development and agricultural terraces. Coastal landslides apparently caused by direct undercutting from wave erosion were also excluded from the inventory.

Areas of intense gully erosion occur in Hong Kong and are clearly visible on high level aerial photographs. Landsliding may be a factor in the formation and on-going development of such gully systems, but due to the difficulty of recognising individual landslides in these areas, they were excluded from the survey, although their boundaries were also mapped (Evans, 1998).

The data in the NTLI have been digitised and incorporated with other datasets to form the NTLS Geographical Information System (GIS). These data sets include:

- The Hong Kong 1:20,000 scale geology maps;
- The Worldwide Fund for Nature digital vegetation map of Hong Kong; and
- GEO terrain classification data.

A Digital Terrain Model (DTM) has also been created, with the following surface modelling capabilities:

- Interpolation of surface elevation;
- Calculation of slope gradients;
- Calculation of aspect;
- Calculation of surface area;
- Calculation of surface length;
- Generation of profiles; and
- Analyses of flow paths, source areas and stream networks.

The NTLI data have been queried against the other datasets allowing other parameters to be extracted for each landslide. The data have also been used to create landslide distribution and isopleth maps.

A comparison of NTLI data and rainfall has been made for the period 1985 to 1994 inclusive. This involved using rolling 24 hour rainfall maxima, as well as overlaying isohyets of maximum 24 hour rainfall onto the landslide distribution maps for the study period (Evans, 1996, 1997, 1998).

The NTLI is currently being used to develop landslide susceptibility, hazard and risk zonation maps of natural terrain areas for the Hong Kong. The data are also being used to develop mitigation strategies and measures.

1.3.3 The Landslide Risk Assessment Project (Nepal and Bhutan)

It has often been argued by donor agencies and governments that the provision of rural roads will help reduce the high levels of poverty seen in the remote and rural areas of developing countries such as Nepal and Bhutan (Hearn *et al.*, 2003; Hart *et al.*, 2003a, b; Hart *et al.*, *in press*; Petley *et al.*, *in press*). In both of these countries the existing road network is undergoing rapid expansion with plans to carry this on into the future. However, it has also been noted that the planning of rural access corridors or other infrastructure in the remote and rural areas of these developing countries was often carried out in a haphazard fashion (Hearn, 2002; Hearn *et al.*, 2003). In particular, there are many examples where the planning, design, construction and maintenance of rural roads in mountainous areas such as Nepal often led to the occurrence of landslides and subsequent loss of life, infrastructure, the road and/or other valuable land. Therefore the "Landslide Risk Assessment in the Rural Access Sector" (LRA) Project, funded by the Department for International Development (DFID) commenced in November 2000. The LRA Project has focused on the Himalayan Kingdoms of Nepal and Bhutan, working in three remote areas in each country. The philosophy behind the LRA Project was:

- To review techniques commonly used for landslide susceptibility, hazard and risk assessment, both globally and locally in Nepal and Bhutan;

- To identify, develop and assess both field-based and desk study based techniques that would be applicable to the assessment of landslide susceptibility, hazard and risk in the context of rural access development. This included field mapping, engineering walkover surveys, and remote sensing techniques;

- To develop a set of best practice guidelines that can be used by planners, engineers and developers for rural access development;

- To complete a landslide susceptibility, hazard and risk assessment for each of the six study areas;

- To disseminate the results and findings of the project through project reports, training workshops and seminars; and

- To train government engineers and planners in the above techniques.

To date, the LRA Project has involved the following activities:

- The completion of aerial photographic and satellite image interpretation for each of the study areas. The project has used Landsat ETM, SPOT, IKONOS (both colour and black and white), and IRS (Indian Remote Sensing) satellite imagery (Petley *et al., in press*).

- Field verification of the findings of the remote sensing.

- Factor mapping in each of the six study areas. This included the landslide distribution, geology, geomorphology, existing infrastructure and land use. The project has mapped over 2,200 km^2 of Himalayan terrain and over 1,300 landslides.

- The development of a GIS database containing the field collected data and any available digital data (i.e., contours, population and infrastructure).

- Interrogation and statistical analysis of the data held within the GIS. This involved comparing the landslide distribution with each of the factor layers (or combinations of the factor layers) within the GIS. The aim was to identify those factor layers that appeared to explain the landslide distribution with a degree of statistical confidence.

- Development of techniques for the assessment of landslide susceptibility, hazard and risk.

- Production of landslide susceptibility, hazard and risk maps for each of the six study areas.

- Field assessments of the interaction between the local population, land use, engineering work along the road corridor or other infrastructure and landslide activity, for each of the six study areas and a two other smaller study areas.

- The testing of the techniques in two further study areas through the use of remote sensing and published desk study data (i.e., topographic and geological maps).

All of the aspects of the project that have been discussed here have been documented in a series of Project Reports (LRA, 2001a, b, 2002a, b, 2003a, b, c) or published papers (Petley *et al.*, 2002; Hart *et al.*, 2003a,b; Hearn *et al.*, 2003). The intention is that at some point in the future all of these reports will be available on-line. It is hoped that the governments of Nepal and Bhutan (and others) will adopt these techniques as they seek to both expand, as well as maintain, their existing road networks. At present, both governments are looking at the institutionalisation of these techniques and recommendations, within the relevant government departments.

1.3.4 Synopsis

Each of the three projects listed above has required the establishment of a landslide inventory, as part of an investigation into the landslide activity affecting a given area. The three projects have each dealt with this problem differently.

The National Landslide Database in the UK used desk study sources only and no primary data collection. Therefore, many landslides that were not recorded in the

Chapter 1 - Introduction

literature or on maps were missed. It is also a "snap-shot" database – it was set up to establish the situation at that time, but with no programme of updating. However, there are now projects updating different parts of the database (Griffiths & Foster, *pers. comm.*). The publication by Jones & Lee (1994), which stems from the landslide database (despite the concerns over its accuracy and how up-to-date it is), does provide a good overall ground model for the UK with respect to landslide activity Lee *et al.* (2000).

The NTLI in Hong Kong has used an extensive (and continually growing) aerial photograph collection supported by ground investigations to establish a detailed database and GIS. This has been used to carry out detailed statistical analysis of the database. In many ways the Hong Kong NTLI is seen as "best practice", with the database and the statistical analysis being updated yearly. However, this is over a relatively small area (approximately 1090 km^2). It is also a politically driven project, with a relatively large budget working in a heavily populated and urbanised area (Chan, Y.C., *pers. Comm.* – head of the GEO in Hong Kong, 2001).

The LRA Project in Nepal and Bhutan has sought to use primary data obtained from aerial photograph and satellite image interpretation, as well as field mapping, while working in relatively remote rural areas. Frequently there was limited topographical and geological map coverage, as well as other data such as rainfall records. This was especially the case in Bhutan. A GIS was used to compile and statistically analyse the data, leading to the development of a scheme that can be used for the assessment of landslide susceptibility, hazard and risk in such areas. Although landslide inventories were established for each of the study areas where the project worked, the main thrust of the project was the development of "best practice" guidelines and training of engineers

18

and others from relevant government agencies. The results have not yet been used to develop a geological and geomorphological ground model for the areas studied, although such models do exist for the Himalayas (TRL, 1997).

1.4   The Rio Aguas Landslide Investigation

1.4.1   Introduction

The previous section has shown that although the development of landslide inventories has been undertaken in a number of places around the globe, it is generally:

1. In areas where the data are available through either desk study sources or remote sensing;

2. Has involved the use "high-tech" methods for analysis of the data (i.e., the use of Geographical Information Systems);

3. Has usually been done without reference to a ground model for the area being considered (i.e., the landslides are almost studied in isolation from their geological and geomorphological setting); and

4. Has usually been carried out in wet (monsoonal environments) with significant vegetation cover. These areas are also often mountainous and/or populated areas.

Very few landslide inventory based projects have sought to use primary field mapping (in conjunction with remote sensing) and then to evaluate the data in its geological and geomorphological context. Therefore, this project has sought to use land surface evaluation techniques to carry out a landslide investigation and develop a landslide inventory following the guidelines of the Working Party on the World Landslide

Inventory (WP/WLI, 1991, 1993, 1994, 1995) and the Working Party on Land Surface Evaluation for Engineering Practice (Griffiths, 2001 and references therein). The work of these working parties is discussed in more detail in Chapter 3. Land Surface Evaluation techniques are regarded as the ideal way of developing a conceptual geological and geomorphological ground model for the study area and allow for a better understanding of the landslide activity affecting the study area to be gained.

The area that has been chosen for this study is a relatively remote, rural and arid to semi-arid region of southeastern Spain, which has, in recent years, seen considerable investment and subsequent development of the infrastructure (i.e., improvements to the road network). However, this investment may be put at risk if little or no account is taken of the natural hazards that affect the region. Due to the remoteness of the region, there is very little information available about the observed (or relict) landslide activity affecting the area, or some of the triggering factors that will influence its occurrence.

Previous geomorphological and geological research in the Andalucían Province of Almería, south eastern Spain (Figures 1.1 and 1.2), has shown how the underlying geology, differential tectonic uplift and changing Quaternary climate have affected the evolution and development of the drainage network (Harvey, 1987; Harvey & Wells, 1987; Mather, 1991; Mather & Harvey, 1995; Harvey *et al.*, 1995; Stokes, 1997; Kelly *et al.*, 2000; Schulte & Julià, 2001; Schulte, 2002; Stokes *et al.*, 2002; Mather *et al.*, 2002; Candy *et al.*, 2003). In particular, the catchment area for the Río Aguas and its major tributaries have been well studied and its evolution and long-term landscape development are well understood (as will be shown in Chapter 2). It has also been shown that those same factors listed above, have also influenced the formation and development of the landslide activity that affects the Río Aguas catchment area (Hart,

1999; Hart & Griffiths, 1999; Hart *et al.*, 2000; Griffiths *et al.*, 2002, 2003). This ongoing research is seeking to study and quantify the interactions between the landscape, the drainage network and the observed landslide activity.

1.4.2 The Study Area

The study area (Figure 1.3) has been defined as the catchment area for the Río de Aguas (or Río Aguas) in Almería Province, Andalucía, in Southeast Spain. This is an ephemeral river system that drains an area of approximately 425 km^2. A catchment area was chosen as it is the *"fundamental unit of geomorphology"* (Gregory & Walling, 1973). The Sierra Bédar, Sierra de Los Filabres and Sierra Cabrera help define the catchment area, to the north, north-west and south-east respectively. The southern margin of the study area is the Cuesta d'Encantada that runs parallel but slightly to the north of the Sierra Alhamilla. The north-eastern and western margins of the study area are poorly defined topographic highs. Selected spot heights for each of these areas are shown in Figure 1.3.

The region in which the study area is located is one of the driest parts of Western Europe. It has a mean annual precipitation of less than 210mm (Estaban-Para *et al.*, 1998). Most of this precipitation falls in autumn or winter as relatively short duration but high-intensity storms. Field observations have shown that the rainfall pattern varies across the study area, depending on physiographic factors such as closeness to the coast or the surrounding mountains. The daytime temperature can vary from c. 15°C in January to c. 40°C in July and August (Mather *et al.*, 2001a).

Figure 1.1 – Map of Spain, showing the location of Almería Province (Map courtesy of www.theodora.com/maps - used with permission).

Figure 1.2 – Map of Almería Province showing the location of the study area (Map courtesy of www.costacasa.com – used with permission).

Figure 1.3 - The Río Aguas Catchment Study Area
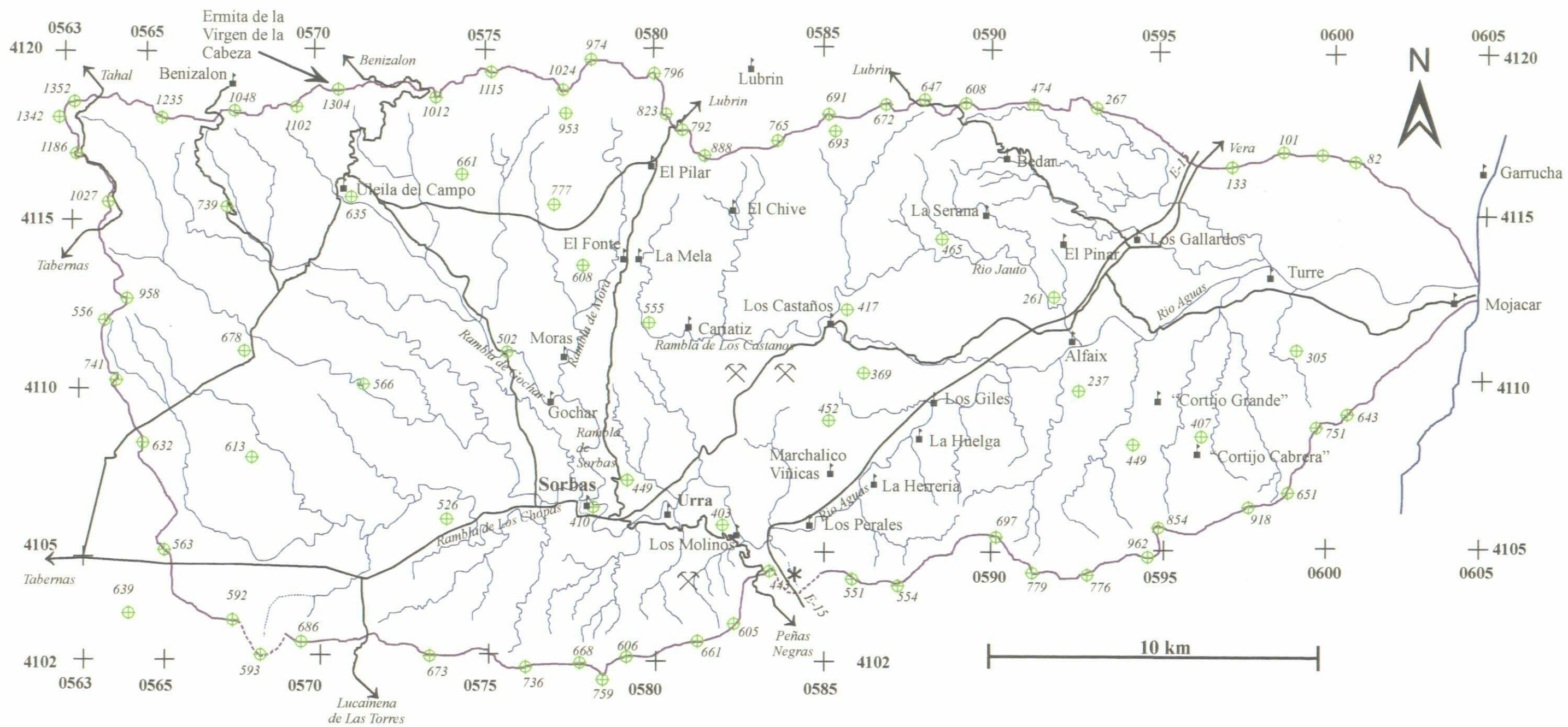
Legend

686 ⊕	Spot Heights (m.a.s.l.)
∿	Drainage System
—	Major Roads/Motorway
—	Study Area Boundary
⚒	Settlements
⚒	Gypsum Quarries
✳	Rio Agua/Rambla Feos "Wind Gap"

The region is seismically active. The city of Almería was virtually destroyed by an earthquake in 1522, and the small town of Vera suffered a similar fate during the last century. The Andalucían earthquake of 25th December 1884 affected the area near Alhama de Granada and reached intensity IX on the Mercalli scale, killing 800 people (López-Arroyo *et al.*, 1980). The most frequent earthquakes that affect the Almería Province (about 5 each year) are magnitude 3 to 4. Information regarding the latest earthquakes is available from the website of the Institute of Andalucían Geophysics at the University of Granada (www.ugr.es/~iag/).

The economy of the study area is a mixture of beach tourism along the coast, rural/"Eco" tourism in parts of the inland areas, agriculture and quarrying. Traditionally, the agriculture within the study area was predominantly small groves of olive, almond and fruit trees. However, recently, there has been a move towards more intensive methods, involving the ploughing up of land and use of intensive irrigation techniques. Historically, there were small mining operations (for example, iron) in some of the mountainous areas surrounding the study area, but the large scale quarrying of gypsum has now replaced these.

Over the last decade, with the help of European Union funding, there has been substantial investment in the transport infrastructure and agricultural industries within the region (Walsh, *pers. comm.*, 2000). The E-15 motorway has been constructed linking the major cities along the Mediterranean coast. Within the study area, there has been significant upgrading of the rural road network, including the upgrading with metalled road surfaces of previous dirt tracks. Recently work has started on a rail link being constructed through the region, again linking the main population centres with each other and the rest of the country (Walsh, *pers. comm.*, 2003; Hearn, *pers. comm.*,

2003). This expansion of the transport network has followed the growth of the local population. However, the growth of the local population and expansion of the region's infrastructure has frequently meant coming into contact with either active or relict landslide features.

The study area is covered by a series of 1:25,000 and 1:50,000 topographic maps (Table 1.2). A number of 1:50,000 geological maps produced by the Instituto Geológico y Minero de España (IGME) are also available for the region. The geological map of the region produced by Weijermars (1991) was also used in this study.

Table 1.2 – The topographic map sheets that cover the Río Aguas Study Area and have been used by this project.

1:25,000 Topographic Map Sheets (Mapa Topografico Nacional de España, Instituto Geographico Nacional)	1:50,000 Topographic Map Sheets (Mapa Militar de España)
1013-IV (Uleila del Campo)	1013 (Macael)
1014-III (Lubrín)	1014 (Vera)
1014-IV (Vera)	1015 (Garrucha)
1030-II (Los Yesos)	1030 (Tabernas)
1030-IV (Lucaiñena de las Torres)	1031 (Sorbas)
1031-I (Sorbas)	1032 (Mojacár)
1031-II (Turre)	1046 (Carboneras)
1031-III (Polopos)	
1031-IV (El Agua Del Medio)	

1.4.3 Previous Landslide Research in SE Spain

An extensive review of the published literature was undertaken as part of this project. It revealed that within southeastern Spain, landslide research has focused on:

- The use of remotely sensed imagery to identify and map landslide features;

- The use of GIS-based analysis techniques to assess the landslide hazard affecting an area; and

- The computer modelling of selected slopes to try and gain an understanding of the controls influencing the stability of those slopes.

The remote sensing work has frequently focused on how the acquired imagery can be manipulated, processed and enhanced to identify different types of landslide activity. This has sometimes investigated the potential of using automatic classification techniques (for example, Eyers et al., 1998). Much of this work has stemmed from the postgraduate remote sensing courses at a number of UK universities including Imperial College and the University of Greenwich. The proximity to the UK, as well as the geological, geographical and environmental conditions, makes the region an ideal training area for remote sensing studies (Mather & Stokes, 2000). The different imagery sources that have been tested are Airborne Thematic Mapper (ATM), Landsat Thematic Mapper, SPOT panchromatic and ERS-1 synthetic aperture radar (SAR) imagery (Eyres et al., 1998; Mason et al., 1998; García-Meléndez et al., 1998).

Davis et al. (2000) demonstrated how ortho-photographs could be combined with a digital elevation model (DEM) to create three-dimensional views of an area. It was argued that this would allow for an improved interpretation of a number of the previously mapped landslides in the area. However, the actual details of how the

26

interpretations were improved and the extra knowledge gained have not been described. To date, the work has only focused on a small number of very large, previously mapped landslides that have been used as "test sites". However, as the techniques are improved, and more high-resolution data become available this may change, particularly with the increasing use of Geographic Information Systems (GIS).

A large amount of work in the region that has utilised GIS-based analysis techniques has been published (Chacón *et al.*, 1993, 1994, 1996; Hamdouni *et al.*, 1996; Fernández *et al.*, 1994, 1996; Irigaray *et al.*, 1994, 1996a,b, 1999, 2000). This work, which is almost solely based in Granada Province, has investigated the use of GIS-based analytical techniques for the mapping, investigation and determination of landslide causative factors. For example, many of the papers listed above describe areas where the landslide distribution and a number of factor layers are mapped and then their spatial relationships analysed using a GIS. The factor layers are a mixture of field derived data (i.e., lithology or soil type), GIS derived data (i.e., slope angle, slope aspect, or elevation) and published/field mapped data (i.e., land use). However, the factor layers that are being analysed do not take account of the geomorphological evolution of the slopes that are being considered.

The data stored in the GIS are used to complete bivariate or multivariate statistical analyses of the numerous factor layers with respect to the known landslide distribution. This is based on either the landslide densities or the landslide areal densities for an area (i.e., either the number of landslides or the areal extent of the landslides occurring in the "limestone" part of the geology factor layer). The results from such analyses have then been used to identify those factor layers that are the most statistically significant in explaining the mapped landslide distribution. Those factor layers that have been

deemed to be the most statistically significant have then been "combined" (often using unspecified calculations) to produce landslide susceptibility or hazard maps for the areas concerned. The resulting maps have then been statistically compared with the mapped landslide distribution, and the "effectiveness" at "predicting" the known landslide distribution evaluated. Attempts have also been made to verify these "landslide susceptibility maps" in the field, particularly after significant rainfall events (Irigaray *et al.*, 1999, 2000). Similar techniques have been developed and tested in other parts of the world such as Hong Kong (Evans, 1998; Dai & Lee, 2002) and the Landslide Risk Assessment Project in Nepal (LRA, 2001, 2002, 2003a, b, c).

Another area of landslide research in the region has involved the computer modelling of hillslope processes. This has particularly focused on seeking to model the processes that are acting on the slopes in the Guadelfeo valley area of Granada Province and how they interact with each other (Alcántara-Ayala & Thornes, 1996a,b). Factors that have been analysed are the climate, hydrology, geology, structural geology, topography and the erosional conditions that are present on the slopes. Thornes & Alcántara-Ayala (1998) concluded from their results that on the mountainous slopes of the Guadelfeo valley (i.e., the slopes of the Alpujarras) that slope morphology is controlled by the long-term geomorphological and erosional history, as well as rare, but extreme, climatic events (i.e., flood events). The climate is considered to be important for controlling shallow slope failures.

The above summary of the landslide-related research that has previously been undertaken in the region has shown that it has particularly focused on either the more "high-tech" approach to investigating landslides or on the modelling of individual slopes within an area. The literature review for this project has also shown that much of

28

this research has not sought to develop or utilise a working geological and geomorphological model for the region. If such a model was developed it could be used to investigate and explain the observed landslide distribution, as well as to identify areas of potential instability (Hart *et al.*, 2000; Griffiths *et al.*, 2002).

1.5 Aims & Objectives

The above sections have described the background to, and rationale behind, this landslide investigation. Therefore, the aims of this project are to:

1.   Identify the types of landslide and landslide activity affecting the study area.

2.   Identify the main factors and controlling conditions that lead to the observed landslide activity within the study area.

3.   Investigate the link between the development of the drainage network, the Quaternary river terrace deposits, the landscape and the observed landslide activity.

4.   Develop a conceptual ground model for the chosen study area in SE Spain.

The specific objectives for this project are:

1.   To use a detailed and extensive desk study to develop an initial conceptual ground model for the study area.

2.   To use aerial photographs as part of the desk study to produce an initial landslide and terrain map of the study area.

3.   To undertake an extensive period of detailed field mapping to ground truth the aerial photographic interpretation (API), to map those landslides that were not identified in the API, and to collect more detailed geological, discontinuity and geomorphological data.

4.   To use the results from the fieldwork to add detail to the conceptual ground model for the study area.

5.   To use the landslide data collected both from the API and the fieldwork to compile a landslide inventory for the study area, following the guidelines suggested by the Working Party on the World Landslide Inventory.

6.   To undertake a statistical analysis of the data held in the landslide inventory.

7.   To use the results from the data analyses and investigations, the data held within the landslide inventory, as well as other geological and geomorphological observations/information, to develop a conceptual ground model for the study area

8.   To use the results from the data analyses and investigations, as well as the above conceptual ground model for the study area, to seek to identify areas of landslide susceptibility within the study area.

9.   To look at the implications of the results from this project locally, regionally and globally.

1.6 **Project Assumptions**

The work undertaken by this landslide investigation has sought to follow the guidelines, recommendations, suggestions, and definitions of BS5930 (1990), WP/WLI (1990, 1991, 1993, and 1994), Soeters & Van Westen (1996), Turner & McGuffey (1996), TRL (1997) and Griffiths (2001). A number of standard and fundamental assumptions have also been made based on the work of Varnes (1984), Hutchinson (1995), Turner & Schuster (1996) and Aleotti & Chowdhury (1999). These assumptions are:

1. *All types of slope failure leave discernible morphological features that can be recognised, classified and mapped.*

2. *The present is the key to the past* and that the past and present are possibly keys to the future (based on Hutton's "Principle of Uniformitarianism"). If applied to landslides, this would suggest that landslides will have occurred in the past under similar geological, geomorphological, hydrogeological and climatic conditions to those that cause landslides at present, and that slope failures in the future are more likely to occur under conditions that have previously led to instability.

3. *The main conditions that cause landslides are controlled by identifiable physical factors that can be investigated and determined.* This information can be used to build predictive models of landslide occurrence.

4. *Landslide processes are controlled by mechanical laws* that can be determined using empirical, statistical and/or deterministic techniques.

5.   Landslide occurrence, either spatially or temporally, can be inferred from heuristic investigations, computed through the analysis of environmental information, or inferred from physical models.

6.   The distribution of existing and future landslides can be approximated by reference to conditioning factors alone, such as rock type or slope angle.

The first assumption in the above list is possibly the most important. If the landslides affecting an area cannot be identified, classified and mapped then an inventory and distribution map of their occurrence cannot be produced. As indicated above, it is also important to be able to identify the controlling and triggering factors of previous landslide activity. It may be feasible to use this information to predict where, and possibly even when, future landslides might occur. However, the occurrence of a landslide is seldom linked to a single causative/controlling factor. This, therefore, makes it difficult to determine all of the factors involved and their complex relationships with each other.

The assumptions listed above are also affected by:

• The experience of the investigator(s) in working in a particular type of environment or mapping landslides, geology or geomorphology (Hearn & Griffiths, 2001);

• The age, size and activity of the landslide – the morphological differences between a very recent landslide and a relict feature that has become degraded and overgrown;

• The classification scheme being used and viewpoint of the investigator(s) – there is a "grey-area" at the smaller end of the scale where landslide activity, slope

deterioration and soil erosion overlap with one another, depending on the landslide classification scheme that is being used; and

• The availability of historical data (discussed in Chapters 4 and 5).

1.7   Chapter Summary & Thesis Structure

This chapter has introduced the landslide investigation that has been completed within the Río Aguas catchment area. It has introduced the concept of developing a ground model based on the geology and geomorphology of a given area as a method for gaining a fuller understanding of that area. This model can then be used to develop a better understanding of how the landslide activity of an area has developed and those factors that are controlling it. An essential part of this ground model is the development of a landslide inventory database. Examples of other landslide inventory based projects that are considered as "best practise" have been described. This has been used to establish the rationale behind this landslide investigation, including the choice of the Río Aguas catchment area as the project's study area.

A brief description of the study area has been presented here. A detailed account of the geology and geomorphology, as well as the geological and geomorphological setting of the study area is presented in Chapter 2. This forms the fundamental basis for the ground model, and is based on the findings from the desk study, aerial photographic interpretation (API) and field mapping that have been completed as part of this project.

The API and field mapping have used Land surface Evaluation techniques to define a classification scheme for the study area, which is described in Chapter 3. This scheme

has helped to sub-divide the study area into a number of mappable units with similar characteristics and terrain. Chapter 3 also describes the definitions and techniques that have been used in developing the landslide inventory database that forms the core database for this project. A statistical analysis of the landslide inventory has been completed, which highlights the numerous factors that have influenced or controlled the landslide activity within the Río Aguas catchment area (Chapter 4). A number of examples from the landslide inventory are described and discussed in Chapter 5 as a series of "Landslide Type Localities".

The results of the desk study, API, field mapping and statistical analysis of the landslide inventory are brought together to form a working ground model for the study area in Chapter 6. This final chapter also summarizes the main project findings, highlighting potential areas for future research either in the study area or in the field of landslide investigation. The local, regional and international implications for this project are also discussed.

2 Geology and Geomorphology of the Río Aguas Catchment

2.1 <u>Introduction</u>

The previous chapter has outlined the aims, objectives and rationale behind this Project. The aims included developing a geological and geomorphological ground model and landslide inventory for the study area and investigating the main factors and controlling conditions of the observed landslide activity (Section 1.5). The aim of this chapter is, therefore, to introduce the geology and geomorphology of the study area. This is based on an extensive literature review and will also include data that were collected in the field. There will be a description of:

- The geological setting of the region;

- The geological history of the study area;

- The geology of the study area;

- The stratigraphic terminology used by this study;

- The geomorphology of the study area; and

- The formation of the Río Aguas Catchment area.

This information is needed so as to provide an understanding of how the landscape and drainage system of the study area (and therefore the geomorphology of the study area) has developed and is influenced by the material strengths and geological structures of the underlying geology. This is also true for the landslides that have been studied by this project. As will be demonstrated in Chapters 4 and 5, the landslide activity of the study area is controlled by the rock mass properties and structural discontinuities of the underlying bedrock geology.

2.2 Geological Setting of Southeast Spain

The study area covers the Sorbas Basin and the southern part of the Vera Basin (Figure 2.1). These Neogene sedimentary basins are situated within the Internal Zone of the Betic Cordillera of southern Spain (Weijermars, 1991). There has been a considerable body of work published concerning the geological setting and history of southern Spain. This work has focused on the tectonic setting of the region, the development of the major fault zones that cut through the region, the formation, development and stratigraphy of the numerous sedimentary basins and the basement highs that surround them. These include Fallot (1948), Egeler (1963), Egeler & Simon (1969), Weijermars *et al.* (1985), Larouziére *et al.* (1988), Montenat (1990), Sanz de Galdeano (1990), Weijermars (1991), Biermann (1995), Stapel *et al.* (1996), Montenat & Ott d'Estevou (1999), Poisson *et al.* (1999), Mather *et al.* (2001), Gibbons & Moreno (2002), Braga *et al.*, (2003) and Mather & Stokes (2003) and references therein.

2.2.1 The Betic Cordillera

The Betic Cordillera forms part of the Alpine orogenic belt, which originated from the relative movements and interaction of the African and Iberian Plates, and relates to the rifting of the Atlantic Ocean and the closure of Tethys (Dewey *et al.*, 1973; Biju-Duval *et al.*, 1977; Biermann, 1995; Stapel *et al.*, 1996). This began in the early Mesozoic and has continued through to the present day.

The Betic Cordillera is usually subdivided into the *Internal* and *External Zones*, each relating to a separate continental block distinguished on the basis of lithological,

tectonic and palaeogeographical criteria (Fallot, 1948; Sanz de Galdeano, 1990; Montenat & Ott d'Estevou, 1999).

The External Zone forms the northern part of the Betic Cordillera and comprises an autochthonous folded terrain linked to the Spanish Meseta (the Pre-Betics) and an allochthonous domain thrust northwards over the Pre-Betics (the Sub-Betic) (Fallot, 1948; Garcia-Hernandez *et al.*, 1980; Sanz de Galdeano, 1990). It represents the Late Jurassic-Cretaceous passive continental margin of Iberia (Stapel *et al.*, 1996).

The Internal (or "Betic") Zone is located within the southern part of the Betic Cordillera and is formed by a stack of metamorphic nappe units – the Nevado-Filabride, Alpujarride and Malaguide Complexes (Egeler & Simon, 1969; Sanz de Galdeano, 1990; Sanz de Galdeano & Vera, 1992). The nappe units represent the deep structure of an Upper Cretaceous subduction complex (Bakker *et al.*, 1989, Stapel *et al.*, 1996) and was formed by the closure of the Tethys Ocean. These nappes were thrust to the north onto the External Zone during the Oligocene to earliest Miocene (Sanz de Galdeano, 1990).

The closure of the Tethys led to crustal thickening under Morocco and Spain (Weijermars, 1985) and the formation of the Betic-Rif Arc (or Arc of Gibraltar) and the Alborán Basin in the western Mediterranean. The continuity of this orogenic arc, which stretches from Minorca to Calabria via Gibraltar, Morocco and Tunisia, indicates a lack of significant movement between the African and Iberian Plates since the Oligocene (Smith & Woodcock, 1982).
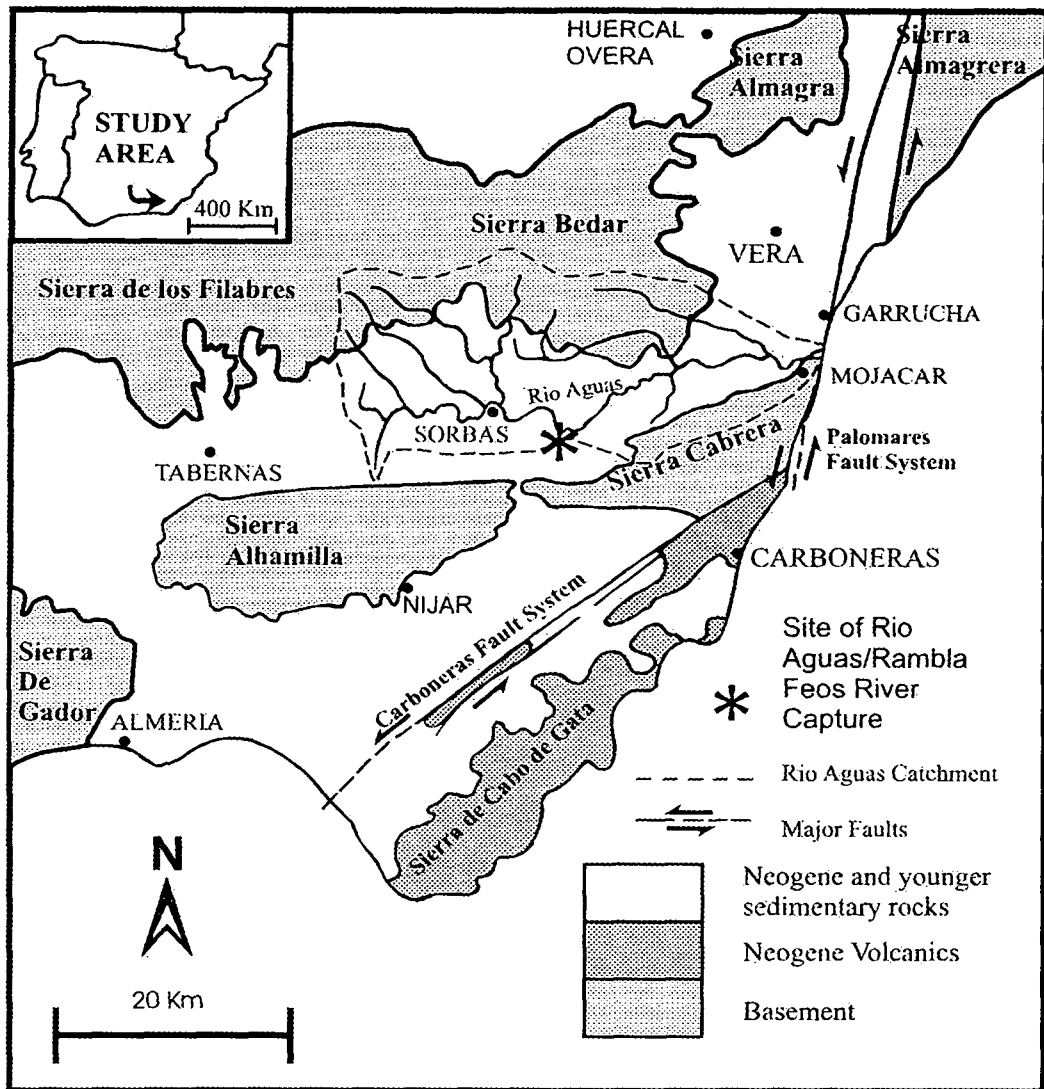
Figure 2.1. Map showing the study area, the regional geology, the catchment area for the Rio Aguas and the key geographical locations mentioned in the text. Based on Hart *et al.* (2000) and Mather & Harvey (1995).

Final emplacement of the nappe structures occurred during the early to mid-Miocene (Platt & Vissers, 1989; Biermann, 1995). The compression was in a NNW-SSE and N-S direction (Coppier *et al.*, 1989; Sanz de Galdeano, 1990) and was the result of the continuing convergence between the African and Iberian plates.

The subsequent compressive interaction between these plates lead to the formation of a series of major strike-slip fault systems collectively termed the Trans-Alborán Shear Zone (Larouziere *et al.*, 1988). Orientated NE-SW, this shear zone is characterised by an overall sinistral movement which can be traced for several hundred kilometres and runs onshore between Almería and Alicante (Hernandez *et al.*, 1987), cutting through several of the nappe structures of the Betic Cordillera. In the Almería region, the Trans-Alborán Shear Zone consists of a series of large fault systems that include the Palomares and Carboneras Faults. These faults play an important role in defining the sedimentary basins of the region. Variations in the displacement along these faults have resulted in localised compression and extension forming networks of basement highs and sedimentary basins (Keller *et al.*, 1995).

2.2.2 Neogene Sedimentary Basins

Various different models for the formation of the Neogene basins in the Betic Internal Zone have been proposed (Longergan & White, 1987; Montenat *et al.*, 1987; Montenat & Ott d'Estevou, 1990; Weijermars, 1991; Sanz de Galdeano and Vera, 1992; Frizon de Lamotte *et al.*, 1991, 1995; Biermann, 1995; Vissers *et al.*, 1995; Stapel *et al.*, 1996; Martinez-Martinez & Azanon, 1997 and Poisson *et al.*, 1999). The sedimentary basins in the eastern Internal Zone are a result of:

1. Late Tertiary regional strike-slip tectonics along a major NE-SW trending, sinistral strike-slip fault zone (Montenat *et al.*, 1987; Montenat & Ott d'Estevou, 1990);

2. East-west trending, dextral strike-slip faults (Sanz de Galdeano, 1989; Sanz de Galdeano and Vera, 1992; Stapel *et al.*, 1996); and

3. North-south extension associated with late orogenic collapse (Vissers *et al.*, 1995).

Rapid subsidence of Neogene basement accompanied the deformation (Cloetingh *et al.*, 1992) and resulted in a mountain belt which presently forms a discontinuous chain of more or less isolated Sierras separated by Miocene to Quaternary basins. The basins are filled with mainly flat lying or slightly tilted or folded sediments, while the strongly deformed Middle Miocene sediments are restricted to the basin margin fault zones (Stapel *et al.*, 1996).

The down-faulted sedimentary basins are filled with predominantly Neogene sediments, including marine calcareous mudstones, limestones, sandstones and gypsum. Within the study area the sequence is thought to represent at least three transgressive/regressive episodes. Importantly, for stratigraphic and lithostratigraphic studies, there is a lack of continuity of the stratigraphic units between the Sorbas Basin and the adjoining Vera and Tabernas Basins (Mather, 1991).

2.2.3 Outline Geological History of the Study Area

The study area is defined by the Sierra de Los Filabres and Sierra Bédar to the north and north west respectively, the Cuesta del Encantada to the south and the Sierra Cabrera to the south-east (Figure 2.1). These mountain ranges are composed of Palaeozoic and Permo-Triassic basement (Egeler & Simon, 1969; García-Hernández *et al.*, 1980; Sanz de Galdeano, 1990). The western and north eastern margins to the Rio Aguas catchment area are relative topographic highs within the Neogene sedimentary basins.

Weijermars (1991) and Mather *et al.* (2001) provide a detailed overview of the geology of the region and, therefore, the area that is covered by the study area for this project. The lithostratigraphy and nomenclature for the Neogene basin fill used here (Figures 2.2, 2.3 and 2.4) will follow that used by Mather (1991) and Stokes (1997), which is based on the work of Ruegg (1964) and Völk & Rondeel (1964).

The Neogene sedimentary rocks of the study area range in age from Burdigalian to Quaternary (i.e., 22 Ma BP and younger) and represent three major transgressive/regressive cycles, which occurred during the Serravallian-Tortonian, the Messinian and the Pliocene. Völk and Rondeel (1964) divided the Neogene rocks into the Older Neogene (Burdigalian - Serravallian) and the Younger Neogene (Tortonian - Pliocene), based on a change in the source area of the sediments. The Older Neogene sequences represent the first phases of deposition during the early to mid-Miocene (Burdigalian/Serravallian through to Tortonian). The Younger Neogene sequences represent the main depositional phase during the mid- and late Miocene and include sediments of Tortonian, Messinian and Pliocene age. The Older Neogene sequences are

dominated by Alpujarride-derived sediment and devoid of Nevado-Filabride material (Volk, 1967a,b), which could imply that the Nevado-Filabride Nappe was not unroofed at this time.

The Older Neogene sediments (coarse terrigenous clastics to deeper water turbidites) overstep the basement massifs. Uplift led to the deformation of these Tortonian sediments, which, in turn, are overstepped by the Younger Neogene sequence of bioclastic and reef carbonates, basinal marls, evaporites and shallow marine to terrestrial clastic deposits (Martin & Braga, 1994, 1996; Braga & Martin, 1996). The Younger Neogene sediments are also characterised by the presence of large amounts of crystalline rock fragments derived from the Nevado-Filabride Complex.

The Tortonian to Messinian transgressive sequence is represented by the shallow marine sandstones and conglomerates of the Azagador Member, Turre Formation (Figures 2.2 and 2.3) (Weijermars, 1985; Mather et al., 2001). During deposition of the Azagador Member, the Sorbas, Vera, Tabernas and Carboneras Basins were interconnected (Ott d'Estevou, 1980). The Azagador Member unconformably overlies (at up to 60° angular unconformity) the Tortonian sediments (Tortonian II of Ott d'Estevou, 1980; Mather, 1991). The period of maximum flooding is marked by the deposition of approximately 120m of marine marls in the Sorbas Basin (the Abad Marls of the Turre Formation; Figures 2.2 and 2.3) (Weijermars, 1985). These contain foraminifera that indicate a maximum water depth in the region of approximately 100-300m (Troelstra et al., 1980; Baggley, 2000). The reefs of the Cantera Member (Turre Formation, Figures 2.2, 2.3 and 2.4) developed along the margins of this seaway and over the Alhamilla/Cabrera topographic high (Mather, 1991; Mather et al., 2001).
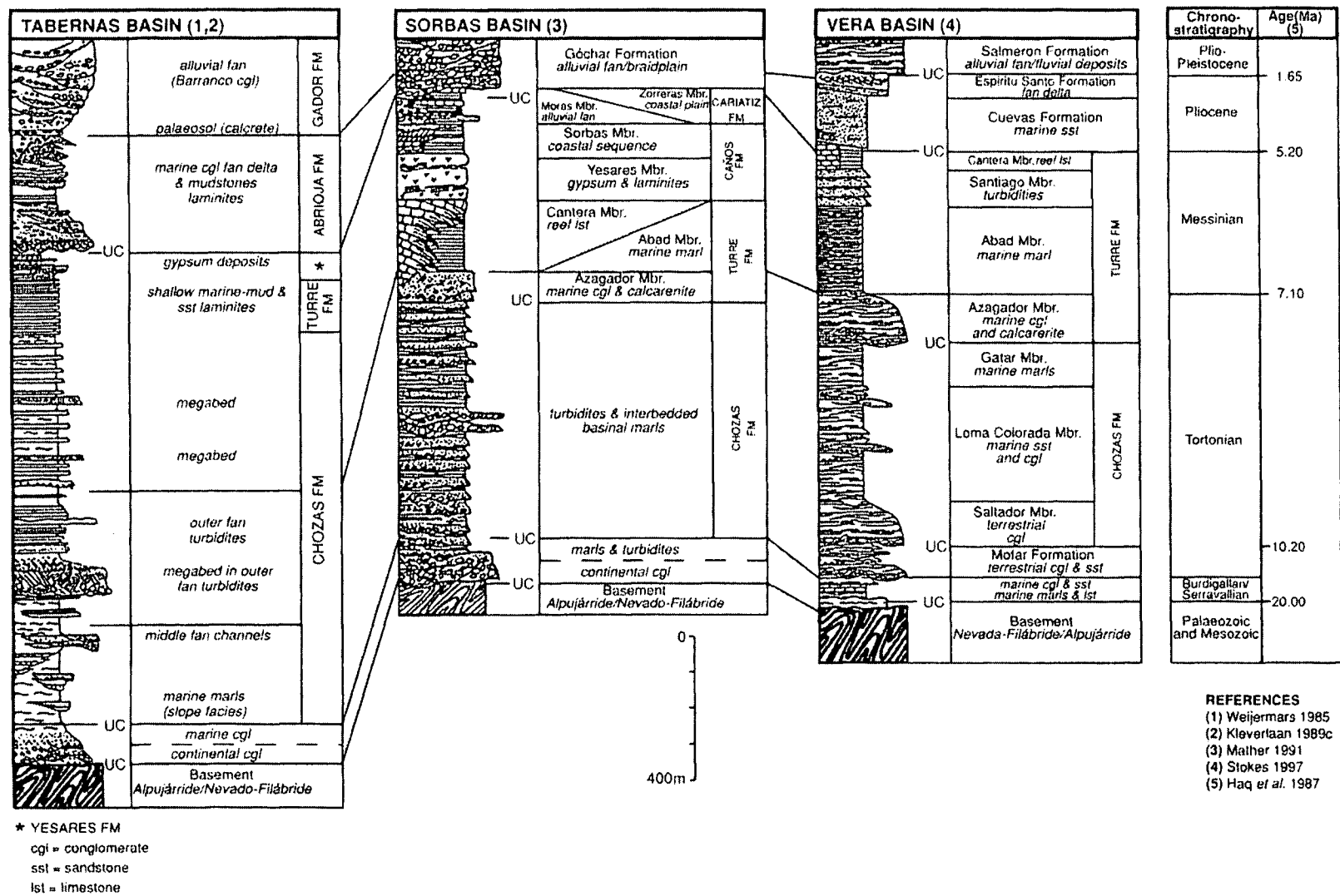
Figure 2.2 – Simplified geological sections of the Tabernas, Sorbas and Vera Basins. (Modified after Weijermars, 1985; Kleverlaan, 1989; Mather, 1991; Stokes, 1997; Mather *et al.*, 2001).
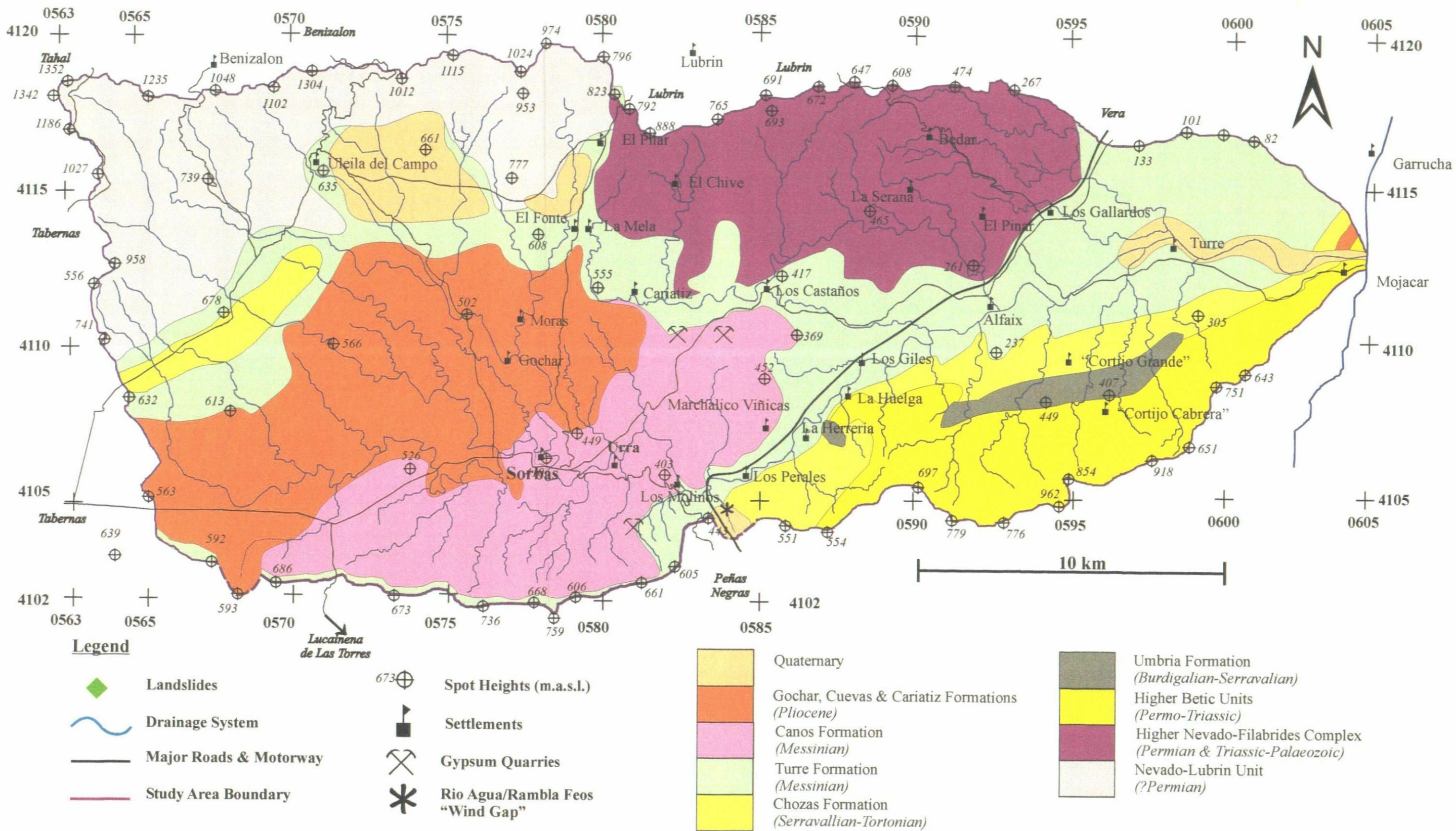
Figure 2.3 - The Geological Formations of the Río Aguas Catchment Study Area (after Weijermars, 1991; Mather, 1991; Stokes, 1997).
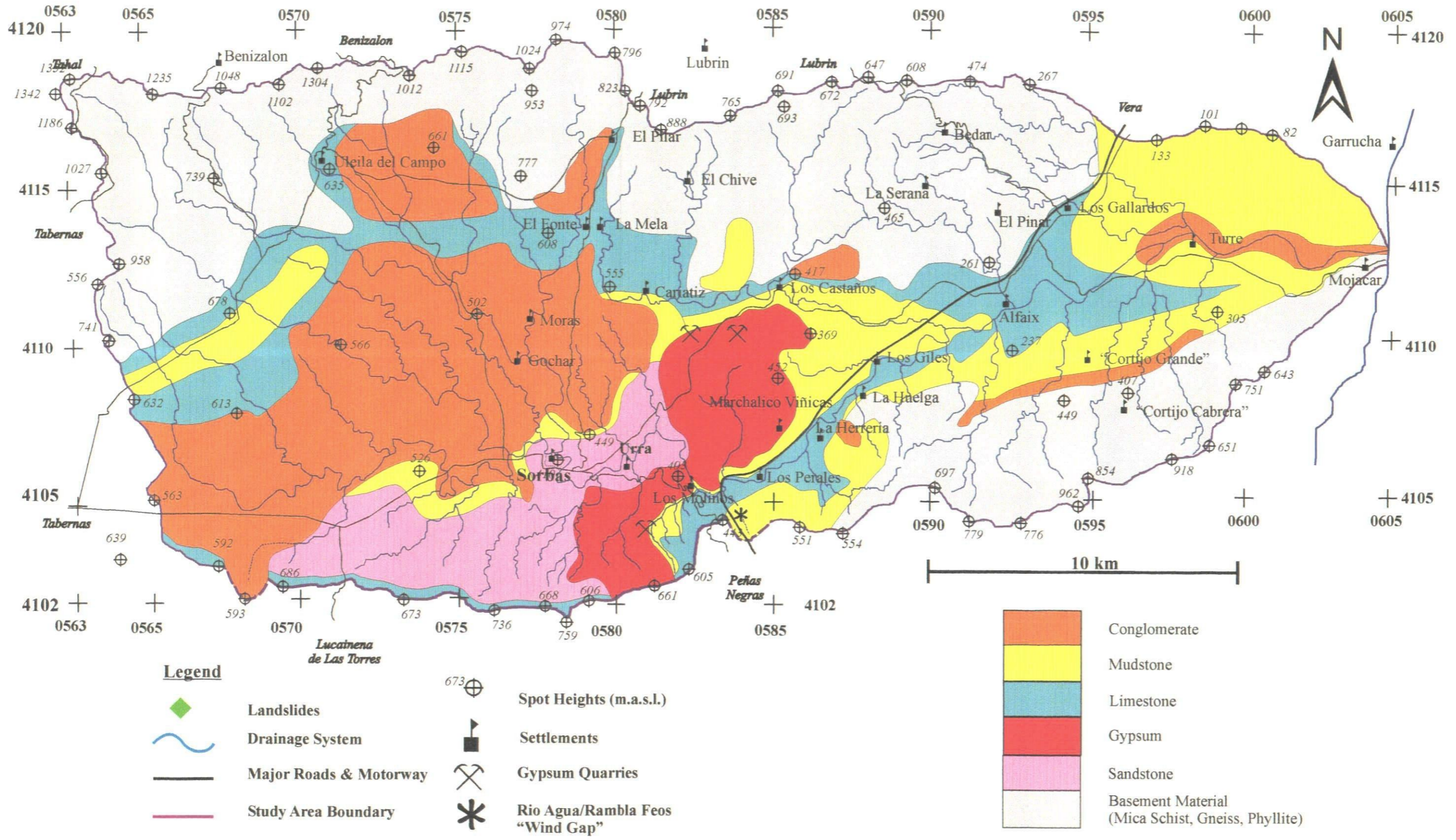
Figure 2.4 - The Lithology Map for the Río Aguas Catchment Study Area.

Legend

- ◆ Landslides
- ∿ Drainage System
- — Major Roads & Motorway
- — Study Area Boundary
- ⊕ 673 Spot Heights (m.a.s.l.)
- ⚑ Settlements
- ⚒ Gypsum Quarries
- ✳ Rio Agua/Rambla Feos "Wind Gap"

- Conglomerate
- Mudstone
- Limestone
- Gypsum
- Sandstone
- Basement Material (Mica Schist, Gneiss, Phyllite)

10 km

The reef development in progressively less elevated, more central basin positions marks a gradually falling sea level after the peak of the transgression (Mather, 1991 and references therein). Hypersaline conditions developed in the Sorbas Basin centre, depositing up to 130m of gypsum (Yesares Member, Caños Formation; Figures 2.2, 2.3 and 2.4). The faunal and micro-faunal assemblages indicate water depths may have varied between 10 to 100m during the deposition of the Yesares Member (Dronkert, 1976; Pagnier, 1976). Laminates of mud, marl and limestone are frequently intercalated with the gypsum. They show no evidence of wave ripples or desiccation cracks, implying deposition below wave base. The fall in sea level is generally considered to be related to the "Messinian Salinity Crisis" of Hsü *et al.* (1972, 1977, 1978).

The Yesares Member is overlain by the Sorbas Member (Caños Formation; Figures 2.2, 2.3 and 2.4) which is represented by a sequence of finely laminated clay and lime muds in its lower part, and calcareous sandstone and conglomerate of a beach-barrier system in its upper part (Roep *et al.*, 1979). Hypersaline conditions have again been inferred from the nature of deposition of this member (Pagnier, 1976). Towards the end of deposition of the Sorbas Member, access to the Vera and Tabernas Basins was restricted, the main connecting basin becoming the Carboneras Basin to the south. A switch to continental conditions occurred after the deposition of the Sorbas Member.

In the stratigraphic classification of Ruegg (1964), the Zorreras Member was classified as part of the Caños Formation. However, the Caños Formation within the Sorbas Basin represents an evaporitic sequence (Dronkert, 1976) whereas the Zorreras Member represents a switch to continental sedimentation after the evaporitic period (Mather, 1991). Mather (1991) proposed that the Zorreras Member and a newly identified member (the Moras Member) should be grouped together to form the Cariatiz

Formation (Figures 2.2, 2.3 and 2.4). The Moras Member consists dominantly of conglomerate and the Zorreras Member consists dominantly of sandstone and siltstone. Mather (1991) also suggested that during the time of deposition of the Cariatiz Formation the Pliocene sea was to the south in the Carboneras/Almería Basin. A small part of the southern Sorbas Basin was also under marine conditions connected to the Carboneras/Almería Basin through a restricted opening in the Sierra Alhamilla/Cabrera. The majority of the Sorbas Basin was a coastal plain (the Zorreras Member), although a series of alluvial fans developed along the northern margin of the Basin (the Moras Member). Sedimentation was punctuated by the development of lacustrine conditions across the Basin, partly reflecting the low gradient of the coastal plain, and the restricted topography. The lakes would have been fairly shallow, unstratified and probably retaining a connection to the open sea to the south (Mather, 1991; Mather *et al.*, 2001).

The conglomerates of the Góchar Formation represent the Pliocene sedimentation within the study area, which mark the last phase of deposition before basin inversion in the Sorbas Basin (Ott d'Estevou, 1980; Mather, 1991). Continued uplift stimulated incision of the drainage networks, and the development of the contemporary landscape. This incision history is recorded as a series of Quaternary river terrace deposits that have been documented by Harvey (1984), Harvey & Wells (1987), Mather (1991, 1993a,b), Mather *et al.* (1991), Mather & Harvey (1995), Harvey *et al.* (1995), Stokes (1997), Kelly *et al.* (2000) and Mather *et al.* (2001). These will be discussed further in Section 2.4.

2.3   Geology of the Río Aguas Catchment

The information presented in the following section is based on the literature review combined with supplementary data that were collected in the field.

2.3.1   Alpine Basement Geology

The study area is bordered to the northwest, north and southeast by mountains composed of Mesozoic, Palaeozoic and older basement (Figures 2.1 to 2.4).   The basement can be divided into three major units based on their relative age, degree of metamorphism, the number of phases of deformation and their correlation with regional basement lithological patterns.   The terminology used here is based on the established classification of Egeler & Simon (1969).   The differences between the three major units are summarised in Table 2.1.   The stratigraphic relationship of the basement complexes is a result of their structural superimposition as a series of thrust nappe units which relate to the development of the Betic Cordillera and their subsequent geodynamic evolution (Egeler & Simon, 1969).

Table 2.1 – Stratigraphic Relationship of the Basement Units (after Gomez-Pugnaire, 2001).

Complex Name	Dominant Rock Types	Deformation	Relative Age
Malaguide Complex (pre-Permian)	Mica Schist overlain by sandstones and limestones	Little or no deformation	Youngest
Alpujarride Complex (pre-Permian)	Harzburgite, eclogite, metagranite, granulite, gneiss, migmatite and mica schist, overlain by phyliite, quartzite and limestone, mudstone and dolostones	Some deformation	
Nevado-Filabride Complex	Mica schist, quartzite, mafic and ultramafic rocks, marbles and carbonates	Highly deformed	Oldest

2.3.1.1 *Nevado-Filabride Complex*

The Nevado-Filabride Complex was first described by Egeler (1963) to include all of the metamorphic rocks beneath the nappes of Higher Betic Units. Brouwer (1926a,b) sub-divided the eastern Betic region on the correlation of two lithologically distinct tectonic units found in the Sierra Nevada area. These were described by Weijermars (1991) as:

- The "Upper Tectonic" or "Higher Nevado-Filabrides Unit"; and

- The "Lower Tectonic" or "Nevado-Lubrín Unit".

These units are characterised lithologically by a general medium to high-grade greenschist facies metamorphism relating to the early emplacement of the Nevado-Filabride Complex during the early geodynamic history of the Betic Cordilleras (Weijermars, 1991).

Nevado-Lubrín Unit (The Lower Tectonic Unit)

The underlying Nevado-Lubrín Unit (Weijermars, 1991), referred to as the Tahal Schists by Bicker (1966), occupies the bulk of the Sierra de los Filabres to the north of the study area. This unit consists of graphitic, black, garnet-bearing mica-schists, overlying garnet-bearing, albite-chlorite, and yellowish, chloritoid-garnet, mica-schist (Weijermars, 1991). The Unit is "capped" (Weijermars, 1991) by a brecciated marble that is approximately 75 m thick, containing both angular and rounded clasts of both the underlying and overlying geology. Weijermars (1991) suggested that this might represent some sort of fault gouge.

Higher Nevado-Filabrides Unit (The Upper Tectonic Unit)

Within the eastern Sierra de los Filabres, bordering the Vera Basin, the crystalline schists of the Higher Nevado-Filabride Unit that are found in the Sierra Nevada are absent and several localised, stratigraphically and lithologically distinct tectonic units can be identified (Bicker, 1966; Table 2.2).

Table 2.2 – Units of the Higher Nevado-Filabride Unit (after Weijermars, 1991)

Relative Age	Name	Description
Youngest ↓	**Lisbona Unit**	Triassic mica-schists and meta-carbonates with local intercalations of amphibolite.
	Chivé Unit	Permo-Triassic chlorite mica-schists, amphibolites and tourmaline gneisses.
	Nevado-Lubrín Unit	Palaeozoic to Permo-Triassic mica-schists, garnet mica-schists and quartzites with localised intercalations of carbonate and gypsum.
Oldest	**Bédar Unit**	Palaeozoic and older graphite schists and tourmaline gneiss complex.

At least three of these individual thrust sheets have been mapped along the southwestern flank of the Sierra de los Filabres (Linthout & Vissers, 1979; Weijermars, 1991).

The Bédar Unit (found in the Sierra de Bédar) comprises a tourmaline granitic intrusion that was then emplaced (Weijermars, 1991). The Rb-Sr isochron of the Bédar Unit granite suggests that the intrusion took place in the Early Permian 269 ± 6 Ma BP (Priem *et al.*, 1966). The emplacement of the Bédar Unit has largely deformed the Bédar granite into tourmaline-gneiss with large feldspar augen (Weijermars, 1991). The Bédar Unit outcrops towards the north of the study area in the Sierra de Bédar.

2.3.1.2 *Alpujarride Complex*

The Alpujarride Complex is not as spatially extensive as the Nevado-Filabride Complex within the sierras surrounding the study area. There are minor exposures of the Complex within the Sierra de los Filabres (Bicker, 1966) and Sierra Cabrera (Rondeel,

1965). Weijermars (1991) described the Sierra Alhamilla as a basement inlier with the Alpujarrides enveloping a core of the Nevado-Filabrides.

The Alpujarrides Complex was thrust over the Nevado-Filabride Complex in a north to northwest direction (Platt *et al.*, 1983). The Alpujarride nappes comprise low-grade metamorphosed Triassic carbonate rocks, phyllite and quartzite, with localised black greenschist facies mica-schist (Weijermars, 1991).

2.3.1.3 *Malaguide Complex*

Also known as the Betic of Malaga, the Malaguide Complex occurs as minor outcrops within the Sierra Cabrera. It has been extensively eroded away prior to the onset of Neogene sedimentation, leaving only small outcrops preserved as klippen (Weijermars, 1991).

The Complex consists of low grade metamorphic schists, phyllite and pelites and non-metamorphosed greywackes, sandstones, conglomerates and carbonates of Palaeozoic to Oligocene age (Rondeel, 1965; Bicker, 1966).

2.3.2 The Umbria/Mofar Formation

The Umbria/Mofar Formation forms part of the "Older Neogene" rocks of Burdigalian to Serravallian age (Figures 2.2, 2.3 and 2.4). This Formation outcrops in narrow faulted zones in the steeply dipping cuestas along the northern margin of the Sierra Cabrera. It is represented by calcareous mudstones, claystones, sandstones, and

conglomerates and reaches a maximum thickness of approximately 600m with unconformable upper and lower boundaries (Rondeel, 1965). However, the lack of exposure and intense deformation of the Older Neogene sediments makes a study of these units quite difficult.

2.3.3   Chozas Formation

The Chozas Formation (Serravallian - Tortonian) within the study area is represented by four Members (Table 2.3) (Rondeel, 1965; Volk, 1967, Alvado, 1986, Martin-Penela & Barragán, 1995; Stokes, 1997). It is significant as it marks the first Neogene marine transgression within the study area and occupies much of the southern part of the Sorbas Basin along the north flank of the Sierra Cabrera (Figures 2.2, 2.3 and 2.4). It can be sub-divided into a lower sequence (?Seravallian/lower Tortonian or Tortonian I of Ott d'Estevou, 1980) and an upper sequence (upper Tortonian or Tortonian II of Ott d'Estevou, 1980). The lower sequence is the least developed in the Sorbas Basin, outcropping along the southern margin of the basin around Gafarillos (Ott d'Estevou, 1980; Mather, 1991). This lower sequence is separated from the upper sequence by a marked angular discordance. The upper part of the sequence dominates and is locally some 2000m thick (Ott d'Estevou, 1980; Mather, 1991). It comprises basinal marls and intercalated turbidites that have been derived from the north (Weijermars et al., 1985). The Tortonian sediments are strongly deformed into open to tight folds as a result of the emergence of the Sierra Alhamilla (Weijermars et al., 1985).

Table 2.3 – Descriptions of the four Members of the Chozas Formation sequence (based on Rondeel, 1965; Stokes, 1997)

Member Name	Description	Depositional Environment
Gafarillos Member	Mainly confined to the SE of the Sorbas Basin Thickly bedded brownish-red sandstones and conglomerates (tabular-shaped coarse clastics (micaceous marble, garnet-mica schist, and garnet-staurolite schist) predominantly from the Nevado-Filabride Complex).	Alluvial fan activity within a continental environment.
Gatar Member	Mainly very well bedded, alternating white to yellowish calcareous mudstones, siltstones, sandstones and marine conglomerates. These rocks contain a very characteristic spherical weathering pattern. The lower part of the member contains many poorly consolidated sandstone layers.	Deep marine basin.
Loma Colorada Member	Mainly grey to yellow/brownish, very poorly sorted boulder conglomerates with irregular beds, composed of rocks of different coarseness, alternating with more evenly bounded sandstone layers, approximately 60cm in thickness. The boulders (in the boulder conglomerate) are rounded mesometamorphic rocks (garnet-mica schists, garnet-staurolite schists, biotite quartzites, epidote-rich mica schists, epidote-amphibolite schists, amphibolites, marbles, and gneisses). This material is predominantly from the Nevado-Filabride Complex.	Near shore, shallow marine, possible shoreline environment.
Salador Member	Red conglomerates.	Alluvial fan activity within a continental environment.

2.3.4 Turre Formation

The Turre Formation (Figure 2.2; Ruegg, 1964) in the study area has been divided into three Members and represents a transgressive sequence that is approximately 500 m thick (Dronkert, 1976, 1985). Oldest to youngest, these units are the Azagador, the Abad and the Cantera Members (Figure 2.2 and 2.3). The Azagador and Abad Members are considered to be partly contemporaneous with each other (Rondeel, 1965; Braga *et al.*, 2001).

2.3.4.1 *Azagador Member*

The Azagador Member outcrops in both the Sorbas Basin (Riding *et al.*, 1991; Braga & Martín, 1996) and the Vera Basin (Barragán, 1997; Braga *et al.*, 2001) sections of the study area (Figures 2.3 and 2.4). In the Sorbas Basin the outcrops form part of the Cuesta d'Encantada, and some of the small hills below the Sierra de los Filabres to the north east of the study area. It also outcrops along parts of the Rio Aguas from Los Molinos (Sorbas Basin) to Turre in the Vera Basin. Along the northern flanks of the Sierra Cabrera (southern edge of the Vera Basin) the steeply dipping Azagador Member forms a series of ridges that are composed of strong (after BS5930, 1991) and compact limestone units with well developed jointing. Rondeel (1965) noted that disintegration occurs along these joint planes, resulting in numerous wedge failures that locally cover many of the slopes.

The basal units of the Azagador Member rest unconformably on the underlying basement of the Alpujarride Complex. The basal unit is a terrestrial conglomerate,

derived locally from the underlying basement material, containing well-rounded clasts of Alpujarride mica-schist. These conglomerates rest unconformably on the underlying basement.

The rest of the Azagador Member consists of thickly bedded, algal-rich, mica-rich, light coloured (ochre-yellow through to brownish-yellow) sandstones, limestones and conglomerates. The overall thickness of the units varies considerably across the study area, as does the degree of folding and jointing.

2.3.4.2 *Abad Member*

The Abad Member (as with the Azagador Member) outcrops in the parts of the study area covered by both the Sorbas and Vera Basins (Figures 2.2, 2.3 and 2.4). The Río Aguas follows the outcrop of the Abad Member and/or its boundary with the Azagador Member.

The Abad Member is represented by dark coloured (dark yellow-brown-grey-black) calcareous mudstones and siltstones interbedded with, more resistant, thin beds of lighter coloured limestones and brownish sandstones. The mudstones are moderately weak, reasonably friable, and weather to form a dark coloured weathering surface/crust

The Abad Member macrofauna includes sponges, bryozoans, encrusted nodules and molluscs, while the microfauna is dominated by foraminifera (Baggley, 2000). The vast majority of the samples studied by Baggley (2000) contained benthonic foraminifera, which, in general, show excellent preservation. Re-crystallisation, pressure distortion of the tests and mechanical damage to, or dissolution of, the tests impeded the

identification of only 3.5% of the samples. From the 120,000 specimens of foraminifera that were picked (60,000 planktonics and 60,000 benthonics), 394 different benthonic species and 111 different planktonic species were identified. Such high diversities and abundances would only be expected in completely open marine environments of normal salinity. The quality of preservation of the fauna would indicate little post-depositional diagenesis or other alteration (Hart, M.B., *pers. comm.*, 2002).

XRD analysis of some samples that were collected in the field in the Los Molinos area, showed that the calcareous mudstone layers contained quartz, calcite, the expansive clay mineral smectite (chlorite/montmorillonite) and, possibly, a small amount of pyrite.

2.3.4.3 *Cantera Member*

The Cantera Member is only found in the Sorbas Basin part of the study area (Figures 2.2, 2.3 and 2.4). It caps the Cuesta del Encantada that forms the drainage divide between the Río Aguas and the Rambla de Lucaiñena (and therefore the southern margin of the study area). This prominent ridge is the result of the tectonic uplift that has affected the area since the Messinian (Mather, 1991). The Cantera Member also outcrops in the foothills of the Sierra de los Filabres (south of Uleila) and in the area north of the village of Cariatiz. In the Cariatiz area the limestone is part of a reef talus slope that is being reworked to form a distinctive escarpment and modern talus slope.

The Cantera Member is a lightly coloured, strong to moderately strong (after BS5930, 1991) barrier reef limestone (10-30 m thick) containing *Porites* coral (Van de Poel *et*

al., 1984). This limestone is thought to represent the maximum flooding of the Messinian transgression in the region (Dronkert, 1976).

2.3.5 Caños Formation

The Caños Formation in the Sorbas Basin represents a regressive sequence that has been described as one of the best preserved continental remnants of the Messinian Salinity Crisis. Numerous workers have suggested that this was a catastrophic event that led to the (complete) desiccation of the Mediterranean area 7-5 Ma (Hsü *et al.*, 1972, 1977, 1978). In the study area it is only found in the Sorbas Basin, where it can very clearly be divided into the Yesares and Sorbas Members (Figures 2.2 and 2.3).

2.3.5.1 Yesares Member

The Yesares[Ψ] Member outcrops over approximately 25 km^2 of the central part of the study area to the east of Sorbas and Cariatiz (Figures 2.3 and 2.4). The unit has been described in detail by Dronkert (1976, 1977, and 1985), Riding *et al.* (1999), Calaforra (1996) and Calaforra & Pulido-Bosch (1997, 2003). The sequence comprises eight, approximately 30m thick, beds of moderately strong gypsum intercalated with thinly laminated, moderately weak calcareous mudstones. The mudstone layers strongly control the groundwater flow through the rock mass and, ultimately, the karstification processes that occur within it. The groundwater passing through the Yesares Member

---

[Ψ] The term Yesares is derived from the Spanish word for gypsum - "*Yeso*"

cave system forms part of a subterranean tributary to the Río Aguas (Calaforra & Pulido-Bosch, 2003).

On occasion, the mudstone layers also exercise a net geomorphological control, which is evidenced on the surface by the morpho-structural escarpments and extensive karst systems that are found in the region (Calaforra & Pulido-Bosch, 1997). These geomorphological features are discussed in Section 2.5.1.

The Yesares Member represents a period of relatively dramatic environmental conditions within the Mediterranean region that are well documented in the literature. The period is often referred to as the *"Messinian Salinity Crisis"* and is thought to represent a time when the sea in the Mediterranean area became desiccated, leaving extensive and thick deposits of gypsum and other evaporitic minerals (Martín & Braga, 1994, 1996; Krijgsman *et al.*, 1999; Braga, 2003). In the study area the Yesares Member is economically significant with at least three large working quarries.

2.3.5.2 Sorbas Member

The Sorbas Member outcrops over an area of approximately 25 km^2 the central part of the study area around the town of Sorbas, after which it is named (Figures 2.2, 2.3 and 2.4). The Sorbas Member generally represents a regressive post-evaporite sequence deposited under "normal marine conditions" (Ott d'Estevou, 1980; Doyle *et al.*, 2000). However, the continuity with the underlying evaporite sequence of the Yesares Member and the sporadic presence of gypsum arenites (Pagnier, 1976) suggest the continuing presence of hypersaline conditions during at least the earliest stages of deposition.

The Sorbas Member is represented by lightly coloured (mainly off-white), thickly bedded, moderately strong calcareous sandstones and thinner beds of laminated moderately weak, calcareous mudstones. There are also some minor conglomeratic units. The dip direction of the beds around Sorbas is generally to the north and northwest, although there are fluctuations in the amount of dip. The member is approximately 75 m thick and contains bird and wolf foot imprints, as well as other fossil remains (Roep & Van Harten, 1979; Roep *et al.*, 1979; Ott d'Estevou, 1980; Doyle *et al.*, 2000).

2.3.6   Cariatiz Formation

The Cariatiz Formation, as defined by Mather (1991), is divided into the Zorreras Member and the Moras Member. The members were mapped and logged as part of a detailed study by Mather (1991).

The Cariatiz Formation outcrops in the northern and central parts of the Sorbas Basin (Figures 2.2 and 2.4). It conformably overlies the Sorbas Member and is capped conformably at the basin centre, but unconformably at the basin margins, by a laterally extensive "marine unit" (Mather, 1991; Mather & Stokes, 2001) There are two other, laterally extensive white carbonate beds that, along with the marine unit, are extremely useful as marker beds, as they are easily identifiable and can be traced quite easily over substantial parts of the central zone of the Sorbas Basin part of the study area.

2.3.6.1 *Moras Member*

The Moras Member is composed of coarse sediments that are laterally equivalent to the Zorreras Member. The Moras Member varies across the Sorbas Basin; coarser sediments at the basin margins which become finer towards the basin centre.

In the area around the village of Moras and the Rambla de Góchar, the member comprises of moderately well sorted conglomerates, laminated silts and fine sands with some scattered small pebbles. Part of the conglomerate succession is clast supported with weak imbrication, while other parts are matrix supported. The conglomerate clasts are derived from the Sierra de los Filabres or are reworked laminated carbonate clasts in a matrix of poorly sorted sand containing scattered, smaller carbonate fragments. The top part of the conglomerate succession fines upwards into poorly sorted sandstones.

In the Cinta Blanca area (Grid Reference 0573041090) the Moras Member is represented by a moderately to well sorted conglomerate with imbricated clasts, and weakly laminated sandstones (Mather, 1991). The conglomerate clasts are all from the Sierra de Los Filabres.

Where the Moras Member outcrops in the valley side slopes to the south of Cariatiz, it comprises a clast-supported conglomerate with metabasic clasts (derived from the Sierra de Bédar), finely laminated red mudstone, graded sandstone units and granular/very coarse sand to very fine sandstone and siltstone.

Mather (1991) suggested that the Moras Member represents an alluvial fan environment, with material being derived from both the Sierra de los Filabres and Sierra Bédar. The fans would have developed over the existing topography (i.e., the

62

Messinian limestone reef "cliffs" that developed at the basin margins). Distally these fan deposits interfinger with the coastal plain sediments of the Zorreras Member.

2.3.6.2 *Zorreras Member*

Mather (1991), who described the Zorreras Member as being continental in nature, identified six different lithofacies within the Zorreras Member succession. The member is represented by laminated, red-coloured siltstones and medium to fine grained sandstones (1-2m thick) horizontal bands of carbonate nodules and poorly sorted, channelised to well sorted and imbricated conglomerates (Sierra de Los Filabride derived clasts). There is sedimentological evidence in numerous places for localised desiccation, pedological/soil development and/or calcium carbonate accumulation. The top of a section in the Sorbas area, for example, shows increasing redness associated with soil development (Mather, 1991).

Mather (1991) suggested that the sediments of the Zorreras Member represent a low gradient coastal plain depositional environment. East of Sorbas the plain formed a shallow depression which possibly acted as a focal point for the fluvial drainage within the Sorbas Basin.

2.3.6.3 *The Marker Beds*

Mather (1991) described three distinctive beds within the Cariatiz Formation that can be traced over large parts of the Sorbas Basin. These "Marker Beds" are two light coloured/white *"Carbonate Beds"* and a yellow bioturbated sandstone bed *("Marine Unit")*.

The two carbonate beds range in thickness from 20cm to 2m, with the upper carbonate bed being typically thinner and less well developed than the lower carbonate bed. They are both laterally extensive and occur within the Zorreras and Moras Members. Mather (1991) identified six lithofacies within the carbonate beds - grey mudstone, red clay, fine-grained laminated carbonate, calcarenites and clastics in approximate order of stratigraphic appearance.

The fine-grained carbonate is generally restricted to the more central areas of the Sorbas Basin and is more extensive in the lower carbonate band. It reveals no internal structure and is composed of pure white micrite (Mather, 1991). The fine-grained millimetre-centimetre scale laminated carbonate occurs in the marginal areas of the Sorbas Basin and is frequently intercalated with sub-millimetre thick, grey clay laminae. The carbonate beds in the northern and western margins of the Sorbas Basin become calcarenitic, and contain low angle stratification, cross stratification and scour sedimentary structures. The clastic lithofacies is also restricted to the margins of the Sorbas Basin and comprises centimetre-thick silt and sand layers, decimetre-thick, graded sandstone units and thick, poorly sorted calcarenite (Mather, 1991).

The carbonate units of the lower marker bed contain ostracods and external moulds of bivalves, while the fauna of the upper bed is more diverse (Ott d'Estevou, 1980). The fauna includes the ostracod *Cyprideis pannomania pseudo-argentina* (of Messinian age; Mather, 1991) and gastropod moulds (dominantly *Melanopsis*; Mather, 1991). The carbonate beds in the northern margins of the basin also contain ichnofossils such as feeding traces and burrows.

The carbonate beds within the Cariatiz Formation reflect deposition in a warm, shallow, unstratified, well-oxygenated brackish lagoon which extended across a low-gradient geomorphological surface (Mather, 1991). The lagoon would have been connected to the sea to the south (i.e., where the Carboneras Basin is located) (Mather, 1991).

The so-called *"Marine Band"* is Pliocene in age (Montenat & Ott d'Estevou, 1977) and marks the top of the Cariatiz Formation. The band lies conformably on the Zorreras Member in the central and southern parts of the Sorbas Basin. However, along the eastern margin of the Sorbas Basin there is a weakly developed unconformity between the Zorreras Member and the Marine Band. This unconformity is most strongly developed along the northern margin of the basin over the Moras Member.

The Marine Band is dominated by a persistent bioturbated, yellow sandstone that typically contains shell fragments (including oysters and small bivalves). The strong yellow colour is probably due to the presence of limonite, which readily oxidises from chamosite. Oxidation could be related to uplift, but Mather (1991) has suggested that it could be due to the extreme bioturbation of this facies thoroughly aerating the sediments, enabling early oxidation, particularly as less bioturbated units remain greenish in colour.

Although the Marine Band is dominated by the yellow sandstone described above, Mather (1991) identified a further eight lithofacies within the unit. These are a grey/green bioturbated sandstone, a laminated yellow clay, micro-conglomerate, marginal conglomerate, cross-laminated sands and gravels, channel bodies, carbonate developments and a basal conglomerate and sandstone. Mather (1991) suggested that the marine band facies of the Carbonate Bands indicate more open marine conditions in

the southern area of the Sorbas Basin and, therefore, a marine connection in this area. The opening for the marine incursion was possibly through a narrow gap in the Sierras that formed the southern basin margin.

Field mapping in a number of different areas around the study area highlighted that parts of the Marine Band are highly erosive and susceptible to piping and other related dissolution features. Samples taken from the Marine Band in the Los Beneficios area were analysed using X-ray diffraction techniques. The results showed the presence of dispersive clay minerals such as smectite and chlorite which could explain the observed dissolution features and weathering.

2.3.7   Cuevas Formation

The Cuevas Formation represents a Lower to mid-Pliocene transgressive marine sequence within the Vera Basin (Figures 2.2 and 2.3; Stokes, 1997). It marks the third, and final, marine transgression that is identified within many of the Neogene sedimentary basins in the region and corresponds to a relative rise in regional sea level following the Messinian salinity crisis within the Mediterranean area.

The contact between the members of the Cuevas Formation and the underlying Messinian sediments of the Turre Formation shows an erosional unconformity. The Cuevas Formation shows two distinct facies (Stokes, 1997):

- massive, grey coloured siltstones and fine-grained sandstones rich in planktonic microfossils (*Globorotalia margaritae*, *Globorotalia puncticulata*, *Globorotalia*

crassaformis and *Globorotalia inflata* - (Volk, 1967a; Ott d'Estevou, 1990)) but

with limited macrofossils; and

- thickly bedded, yellow, fossiliferous medium to coarse-grained sandstones.

2.3.8 Góchar Formation

The Góchar Formation, of Pliocene age, immediately overlies the Marine Band at the

top of the Cariatiz Formation and represents a regressive and continental facies (Figure

2.2). It is dominated by fluvial conglomerates, with the type locality of Mather (1991)

being in the Rambla de Góchar (Grid Reference: 752 108). Ott d'Estevou (1980)

describes various forms of Helicidae (terrestrial gastropods) in the lower parts of the

succession which imply a Plio-Pleistocene age for the sediments (Mather, 1991). These

alluvial fan and braid plain conglomerates may locally reach a thickness of up to 100m

and are sometimes difficult to distinguish from the Quaternary deposits.

The Góchar Formation outcrops over much of the western part of the study area (the

western and central parts of the Sorbas Basin – Figures 2.3 and 2.4). It is best studied in

the canyon walls of the Rambla de Góchar, near to the village of Góchar after which it

and the Rambla are named. In this area the lithology is a polymict, matrix supported,

terrestrial conglomerate containing sub-rounded pebbles and cobbles of mica schist,

quartz and limestone. The matrix is fine-grained orange-red, silty sandstone. The rock

mass is strong to moderately strong, forming (in this area) near vertical canyon walls

approximately 50m high. On the basis of clast assemblages and palaeocurrent analysis

it is possible to identify four drainage systems within the Góchar Formation (Mather,

1991).

2.3.8.1 *The Góchar Fluvial System*

Draining from the northern basin margin, this is the largest system and forms a sequence of conglomerates up to 45 m thick. The clast assemblage is dominated by high grade metamorphics derived from the Tahal Unit of the Filabride Nappe in the northwest of the Sorbas Basin. The unit is represented by poorly sorted sandstone that coarsens upwards. The unit also contains some palaeosol horizons that are typically lacking in carbonate and are coloured red (Maunsell colour chart designation 5YR 5/8; Mather, 1991). The Góchar Fluvial System has a relatively consistent southeast palaeocurrent direction, and was dominated by a fluvial braided stream environment with highly fluctuating discharges. The channels were typically shallow, cut by floods and filled by smaller scale, more frequent run-off events (Mather, 1991).

2.3.8.2 *The Marchalico Fluvial System*

The smallest of the systems, the Marchalico Fluvial System, contains a clast assemblage of metamorphic and igneous material derived from the Sierra Bédar. Mather (1991) further sub-divided the system into schist-rich and reef-rich sub-systems. The system comprises a basal red sandstone unit which coarsens upwards into a series of intercalated hematite-rich sandstones and generally well sorted, intercalated gravels and conglomerates. Locally they contain a persistent non-pedogenic calcrete unit and towards the top of the system the conglomerate bodies become thicker and more channelised (Mather, 1991). The two suites of clast assemblages suggest the development of two alluvial fans sourced from different catchments. The palaeocurrent directions are dominantly towards the south and southwest.

2.3.8.3 *The Mocatán Fluvial System*

Located along the southern margin of the Sorbas Basin, the clasts of the Mocatán Fluvial System are derived from the Alpujarride Complex of the Sierra Alhamilla (i.e., low grade metamorphosed Triassic carbonates). In the vicinity of the Barranco del Mocatán, the system reaches a thickness of approximately 200m and is dominated by fine-grained sandstone and siltstone with coarser, laminated, grey sandstone beds. The sequence coarsens upwards into conglomerate. Mather (1991) suggested that this could represent flood events in a dominantly braided channel environment.

2.3.8.4 *The Los Lobos Fluvial System*

The Los Lobos Fluvial System is probably the largest of the four systems and drains the basin from west to east. The clast assemblage is characterised by a mixture of the clast types found in the other three Góchar sub-systems (Mather, 1991). The system, which reaches a maximum thickness of approximately 120m, comprises poorly sorted sandstone, overlain by conglomerate and intercalated with red sands and silts. The sequence reflects deposition in a braidplain environment (Mather, 1991).

2.3.8.5 *Synthesis*

The four systems described above represent the initiation of the drainage network within the Sorbas Basin and the study area. Mather (1991) demonstrated how the sea that deposited the Cariatiz Formation retreated and fluvial systems began to prograde across the Sorbas Basin. Uplift of the Sierras at the basin margins led to the formation of a basinal drainage network that was roughly centripetal. The Góchar, Marchalico and Mocatán Fluvial Systems were low-gradient fluvial systems that developed in the more central parts of the Sorbas Basin. These then fed into the larger Los Lobos Fluvial

System. This flowed from the Sorbas Basin to the south via a topographic low between the Sierra Alhamilla and Sierra Cabrera, into the palaeo-Mediterranean, which at this time occupied the Carboneras Basin to the south.

Geomorphological controls at this time were generally masked by the active structural controls. The presence of mature, well-drained pedogenic profiles lacking in any carbonate development despite a readily available source in the surrounding environment, indicates that leaching was prominent at this time. This may suggest a fairly humid environment.

2.4   Geomorphological Setting of the Río Aguas Catchment

2.4.1   Introduction

The previous section has described the geological formations and units of the study area. The material properties and structural controls of the underlying geology, along with the tectonic, climatic and geomorphological activity acting upon it have led to the formation of the present landscape. Those processes and controlling factors have been studied in some detail by numerous authors. For example, Mather (1991, 1993a,b), Mather & Harvey (1995), Harvey *et al.*, (1995), Stokes (1997), Mather & Stokes (2001), Stokes *et al.* (2002) and Mather *et al.* (2001, 2002 and 2003) have particularly focused on the initiation and development of the drainage networks across the Sorbas and Vera Basins. This has included the initiation and development of the Río Aguas, which forms the basis for the study area used by this project. The aim of this next section is to:

- Describe the transition from marine to continental conditions and the initiation of the drainage network across the study area;

- Describe the evolution of the Río Aguas and the contemporary landscape; and

- Describe the role of the different controlling factors in this development.

2.4.2   Marine to Continental Transition

With continued tectonic uplift of the region, many of the sedimentary basins became elevated above sea level, despite a global rise in sea-level during the Pliocene (Haq *et al.*, 1988; Mather & Stokes, 2001). The continued deformation associated with this uplift also led to the increasing isolation of the basins from each other. The history of the marine to continental transition is recorded within the Upper Messinian, Pliocene and Pleistocene sediments of the basins. However, the timing of the transition varied between the basins as a function of different relative uplift rates (Mather & Stokes, 2001).

Within the Sorbas Basin the marine to continental transition was initiated in the Late Messinian, with the development of marginal alluvial fans and coastal plain deposits in the basin centre. The later fluvial systems developed as a function of the early emergence of the basin-fed, low-relief, Plio-Pleistocene fan-deltas in the Almería Basin to the south (Mather, 1993b; Mather & Stokes, 2001). The earlier Pliocene in the Vera Basin (as well as the Tabernas and Almería Basins) is marked by the development of Gilbert-type fan-deltas (Postma, 1984; Postma & Roep, 1985; Boorsma, 1992; Stokes & Sendra, 1996; Stokes, 1997). This suggests low-energy, restricted basins with sediment being supplied from the adjacent sierras. It is thought that true continental deposition

within these basins did not appear until the ?Early Pleistocene, when alluvial-fan deposition dominated the basin margins (Mather & Stokes, 2001).

2.4.2.1 *Messinian*

From the Messinian onwards, regression was experienced by the main sedimentary basins due to a fall in relative sea-level. This was first experienced in the Sorbas Basin after the regression of the Sorbas Member seas and was associated with the development of alluvial-fan sediments accumulating at the basin margins (Moras Member, Cariatiz Formation; Mather, 1991) and coastal plain sediments (Zorreras Member, Cariatiz Formation; Mather, 1991) in the basin centre (described in Section 2.3.6).

During the latest Messinian-Pliocene the Sorbas Basin continental sediments were affected by two basin-wide brackish water lacustrine incursions, with similar deposits found in the Vera Basin (Van de Poel, 1991; Mather & Stokes, 2001). These are represented by the "Carbonate Marker Beds" of Mather (1991). Sediments within the Sorbas Basin show signs of more marine influence only towards the southern margin of the basin, implying a link with the Almería Basin across the Feos Gap between the Sierra Alhamilla/Cabrera (Figure 2.5). Links between the Sorbas Basin and the Tabernas and Vera Basins are absent. The presence of an angular unconformity in the sediments at the northern basin margin indicate continued uplift of the Sierra de Los Filabres at this time (?Late Messinian-Pliocene; Mather & Stokes, 2001).

When the sea that deposited the Cariatiz Formation retreated, the fluvial systems (of the Moras Member) began to prograde across the Sorbas Basin. Uplift of the Sierras at the

basin margins led to the formation of a roughly centripetal basinal drainage network. The basin still an intermittent marine connection with the Carboneras Basin (and the palaeo-Mediterranean) to the south (Mather, 1991).

Geomorphological controls at this time were generally masked by the active structural controls (Mather, 1991). The presence of mature, well-drained pedogenic profiles lacking in any carbonate development despite a readily available source in the surrounding environment, indicates that leaching was prominent at this time. Mather (1991) argued that this may suggest a relatively more humid environment.
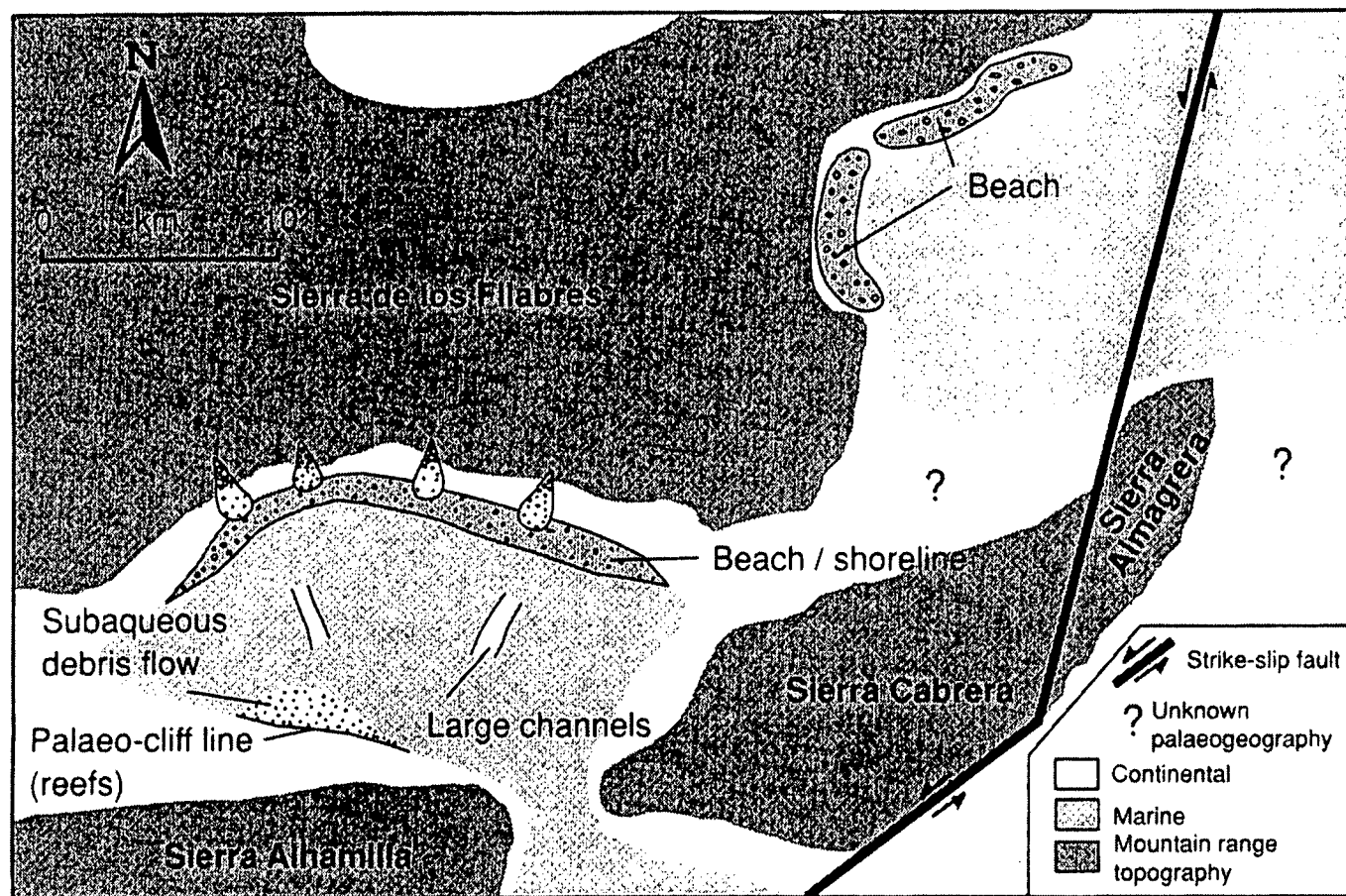
Figure 2.5 – Early Pliocene reconstruction of the continental to marine transition for the Sorbas and

Vera Basins. (Modified after Mather, 1991; Stokes, 1997; Mather & Stokes, 2001).

2.4.2.2 Plio-Pleistocene

The top of the Cariatiz Formation in the Sorbas Basin is marked by a yellow, basin-wide marine unit. The fauna in this unit is thought to imply a link to more open marine conditions in the south. This incursion, of Late Pliocene age (Roep & Beets, 1977; Ott d'Estevou, 1980) most probably reflects flooding in response to global sea-level rise recorded at this time (Haq *et al.*, 1988). In the Sorbas Basin, continental sedimentation subsequently became dominated by alluvial-fan and braided-river sedimentation (Figure 2.5; Ruegg, 1964; Mather, 1991). The sediment from the Sorbas Basin exited to the south across the axis of the Sierra Alhamilla and Cabrera, forming low-relief fan-deltas in the north of the Almería Basin (Mather, 1993b). It is thought that this was the only connection that the Sorbas Basin had with any of the adjacent basins.

During the Pliocene deposition of the upper units of the Cariatiz Formation in the Sorbas Basin, the adjacent Vera and Almería Basins were dominated by shallow marine deposition marked by the Cuevas Formation. The base of these deposits in the Vera Basin marks the Mediterranean-type locality for the Mio-Pliocene boundary (Fortuin *et al.*, 1995). As sea level reached its maximum, Gilbert-type fan-deltas developed where suitable conditions and accommodation space were available (i.e., adjacent to pronounced topography, in the sheltered northern parts of the Vera Basin; Figure 2.6). In the Vera Basin this is represented by the Espíritu Santo Formation (Völk & Rondeel, 1964; Postma & Roep, 1985; Stokes, 1997). With continued uplift and regression the fan-deltas gave way to continental sedimentation, such as the Salmerón Formation (Völk, 1979; Stokes, 1997; Stokes & Mather, 2000). Both of these units lie outside of the study area.
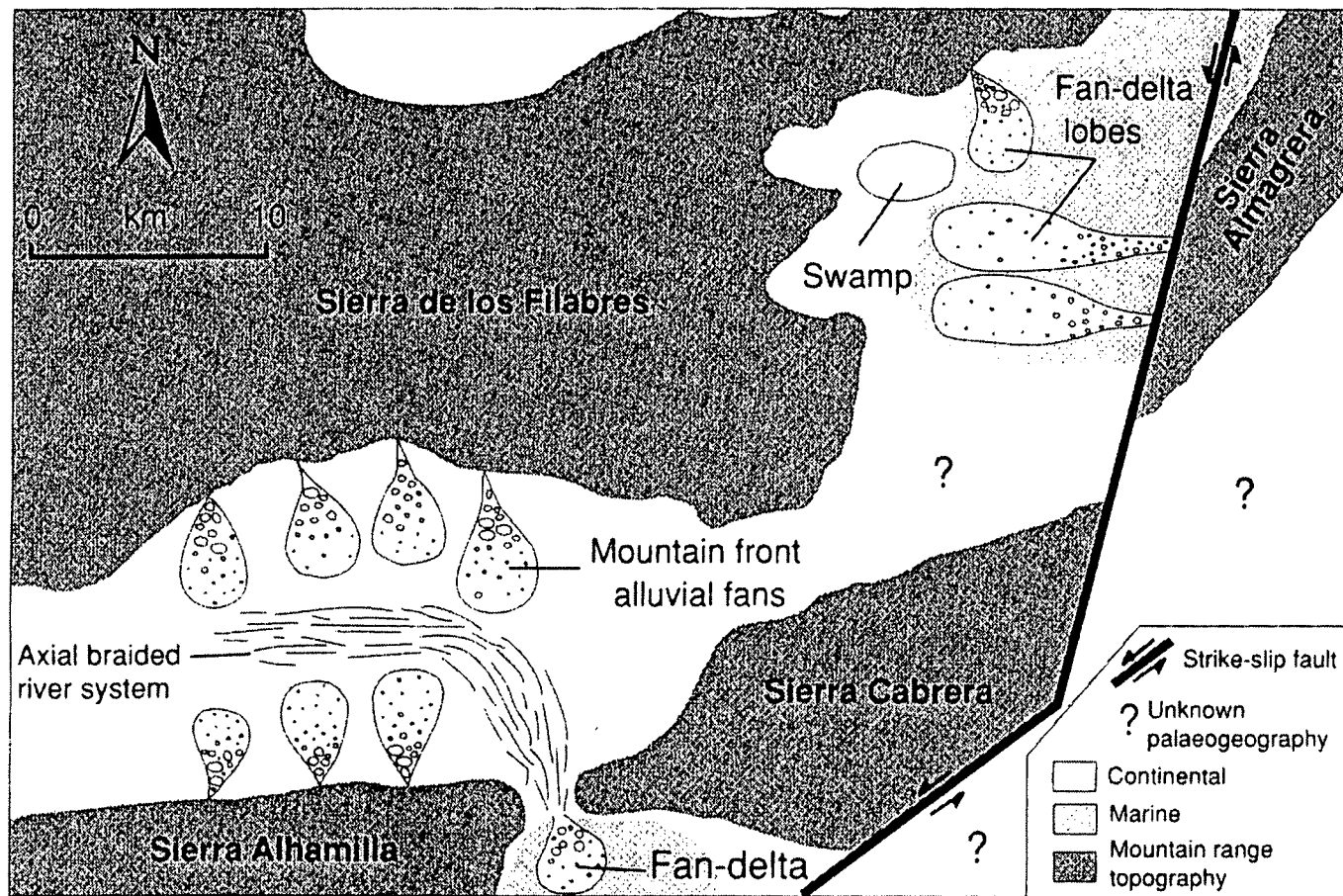
Figure 2.6 – Late Pliocene reconstruction of the Sorbas and Vera Basins. (Modified after Mather, 1991; Stokes, 1997; Mather & Stokes, 2001).

Within the study area, the transition from marine to continental conditions occurred first in the Sorbas Basin (Early-Middle Pliocene) and then in the Vera Basin (Plio-Pleistocene). As marine conditions withdrew across the study area, alluvial sediments were deposited. Analysis of the sedimentology, the clast assemblages and the available palaeocurrent information has allowed the palaeogeography and palaeoenvironmental conditions to be reconstructed.

This analysis has shown that a basinally convergent drainage network existed within the Sorbas Basin, represented by the alluvial deposits of the Góchar Formation (Mather, 1991, 1993a; Mather & Harvey, 1995; Section 2.3.8). Braided river systems developed in the more central parts of the Sorbas Basin fed by the broader, low-gradient marginal fluvial systems. These braided systems drained from the Sorbas Basin into the Carboneras Basin through an opening between the Sierra Alhamilla and Sierra Cabrera.

Intense deformation related to uplift along the southern margin of the Sorbas Basin indicates active tectonism. Subsidence, relating to the deformation, generated topographic lows where small lakes developed. Mather (1991) also concluded that the influence of climatic and geomorphological controls were difficult to ascertain.

During the "late" Góchar (after Mather, 1991) the existing fluvial systems reached their maximum extent. However, these systems were not mature braid systems (Mather, 1991). They were dominated by infrequent flood events, which typically produce simple unit bars as opposed to more complex, braid bars that are associated with more mature deposits.

At this time, a difference developed in the principal controlling factors governing the behaviour of the drainage systems. Tectonic controls were now only of minor importance, affecting local uplift and subsidence rates, whereas geomorphological controls became more influential. The exception to this was along the southern margin of the basin along the Sierra Alhamilla/Cabrera axis, where the main drainage was slowly displaced towards the basin centre. This was due to uplift-generated, gentle basinward tilt.

Within the Vera Basin, the Upper Pliocene alluvial sediments of the Salmerón Formation, indicate the onset of continental conditions and the establishment of a convergent drainage network which flowed eastwards towards a Pliocene Mediterranean coastline (Stokes, 1997). This initial drainage network comprised a series of distinct coalescent mountain front alluvial fans which prograded over the former Pliocene shelf and shoreline areas, as recorded by the underlying Cuevas and Espíritu Santo Formations. Modification of the original drainage network occurred towards the end of Salmerón Formation times during the Early Pleistocene, when extensional tectonic activity resulted in significant changes in the sediment load and rerouting of the drainage network (Stokes & Mather, 2000; Mather & Stokes, 2001).

2.4.3   Quaternary Landscape & Drainage Evolution

The main continental drainage systems developed during the Pliocene. Drainage lines that were transverse to the structure were superimposed and became antecedent following uplift (Harvey, 1987, 2001; Harvey & Wells, 1987; Mather & Harvey, 1995; Stokes, 1997; Stokes & Mather, 2000; Mather & Stokes, 2001). The Río Aguas/Rambla

Feos became established as the master drainage channel of the Sorbas Basin. It is thought that this drained into the Alias and eastwards through the Carboneras Fault Zone. The Vera Basin, with less uplift, had become a receiving basin for drainage systems originating outside of the basin.

The area between the Sorbas and Vera Basins is drained by the lower Río Aguas system. It becomes a transverse drainage across the Sierra Cabrera and the Palomares Fault Zone near to the present coastline. A major tributary to the Lower Río Aguas, the Río Jauto, is also a transverse drainage across the structures of the Sierra de Bédar. This is presumably through a combination of superimposition and antecedence (Harvey, 2001).

Controls on the drainage were dominated by geomorphological adjustment to tectonic uplift (Mather, 1991). The main drainage at this time was inherited from the end-Góchar land surface and comprised a series of moderately graded surfaces that grade into the basin centre. These surfaces have subsequently been incised by the Quaternary drainage network. Modification of this network took place through river capture and re-routing, especially at the basin margins. For example, Tabernas drainage captured the western headwaters of the Sorbas drainage, as well as two substantial river captures in the southern part of the Sorbas Basin. There was also interaction between the Sorbas drainage and the Lower Río Aguas tributary system, the Río Jauto/Rambla de Los Castaños system in the north-east of the Sorbas Basin (Mather, 1991, 1993a; Harvey, 2001).

2.4.3.1 *River Capture*

The incision history of the Río Aguas and some of its main tributaries (i.e., the Rambla de Sorbas, Rambla de Góchar and Rambla de Mora) is recorded as a series of well-developed river terrace deposits (Harvey, 1987a, 2001; Harvey & Wells, 1987; Miller, 1991; Harvey *et al.*, 1995, Kelley *et al.*, 2000; Schulte & Julià, 2001; Candy *et al.*, 2003). These different terrace levels have been identified on the basis of field observations and relationships and, therefore, represent a relative time-scale. They are correlated on the basis of soil development (Harvey *et al.*, 1995; Table 2.4). The deposits lie unconformably on the older basin fill and post-date the youngest Góchar sediments and the main deformation within the Sorbas Basin.

Mapping of the river terrace levels has shown that during the early part of the Pleistocene the Sorbas Basin was still draining to the south through a topographic low between the Sierra Alhamilla and Sierra Cabrera into the Carboneras Basin (via the Rambla de Los Feos; Harvey & Wells, 1987; Mather, 1991, 1993a,b). This is marked by the terrace levels A to C of Harvey & Wells (1987) and Harvey *et al.* (1995).

Terrace levels A, B and C all have a distinctive red colouring and show aggradational thickness of up to c.20m between Sorbas and Los Molinos, but up to c.10m elsewhere. Dating from the ?Early to Middle Pleistocene, the terrace gravels rest unconformably on basement or Neogene rocks. They are usually well cemented both at the surface, by strongly developed calcretes derived from pedogenic carbonate, and at the base at the gravel/bedrock contact. For example, river terrace level A has developed on top of an erosional geomorphic surface that truncates the Plio/Pleistocene fill (Mather, 2000a) and grades into a mature calcrete (Stage V-VI, after Machette, 1985). All three of the terrace levels have carbonate-accumulating red soils, with well-developed Bt horizons

and well developed Bk or K horizons with at least Stage III carbonate accumulation (Harvey *et al.*, 1995; terminology after Gile *et al.*, 1966; Machette, 1985). The colours of the Bt horizons generally reach 5YR Munsell colour hues or stronger. Harvey & Wells (1987) suggested a pre-Würm age for the youngest stage C gravels.

Where the deposits overlie the horizontally bedded conglomerates of the Moras Member or the Góchar Formation they are often difficult to distinguish from the older deposits, especially where they have similar palaeocurrent directions and clast assemblages. More commonly, however, they lie unconformably over the older deposits. Present day morphology of the sites (inset below the top of the Góchar sequence), and the development of well-developed soil profiles are often good indicators of the presence of terrace gravels.

The soils on the younger (Late Pleistocene and Holocene, D and E) terraces show much less maturity. Only on terrace D1 does the Bt horizon reach 7.5YR colouration, and carbonate accumulation reach Stage II. Terrace D is usually subdivided into three aggradational terraces. The older D1 terrace usually comprises up to c.10m of gravels, sometimes weakly cemented or capped by a thin, immature calcrete. The younger D3 terrace is more extensive but thinner (generally <3m), and comprises non-cemented gravels. In the vicinity of Cortijo Urra, between Sorbas and Los Molinos, the middle D2 terraces comprise of very thick sequence (>35m) of fine sediments that developed in response to local deformation (Mather *et al.*, 1991). Kelly *et al.*, (2000) dated a calcrete from the D1 terrace level at 8.97 +/- 0.28Ka (Table 2.5) which seemed to be at variance with the expectations of Harvey *et al.* (1995).

Table 2.4 – Summary of soil properties on terrace surfaces of the Río Aguas (modified after Harvey *et al.*, 1995; CaCO$_3$ Stages after Giles *et al.*, 1966; Machette, 1985).

Relative Age		Holocene	Late Pleistocene		Late-Mid Pleistocene		
Terrace Level		E	D3	D1	C	B	A
Characteristic	Approx. depth 9cm)	<50	<80	>150		150-200	
soil property	CaCO$_3$ Stage*	0	I	I-II	II-III	III-IV	IV
B Horizon							
Hue¥		10YR	10YR	7.5YR	5YR	2.5YR	2.5YR
Redness Index Φ	Mean	<1.0	<1.0	4.2	9.1	12.7	14.0
	Approx. range			1-7	7-14	9-16	12-16
Percentage clay, max		na	13	13	35	46	Na
Fe$_d$ percentage range		0.1-0.5	0.3-0.6	0.6-1.0	1.0-2.2	1.4-3.0	1.3-2.6
Activity ratio€		0.34-0.66	0.31-0.57	0.29-0.35	0.17-0.34	0.13-0.27	0.13-0.27
Mineral magnetic characteristics, B Horizon Ψ							
Magnetic susceptibility X (range) $10^{-8} m^3 kg^{-1}$		23	76	135	135-220	83-173	105-110
Frequency dependent susceptibility percentage X_{fd} (range), $X_{LF} - X_{HF} \times 100$		4.5	9.8	1.2	2.2-7.8	4.9-7.7	5.2-9.2
Anhysteretic Remnant Magnetization (ARM) (range), $10^{-6} Am^2 kg^{-1}$ at 1 Tesla		34	121	145	128-368	84-145	74-150
SIRM (range)		2,620	7,601	15,052	13,259-16,378	7,270-8,132	9,179-10,192

* = After Gile *et al.*, (1966) and Machette (1985) / ¥ = Munsell colour hues / Φ= After Hurst (1977); Table modified from Harvey *et al.* (1995) and Harvey (2001) /

€ = See text / Ψ = See Thompson & Oldfield (1986) for definitions.

After the initial dissection of the D1 terrace to near present river level, up to 35m of mainly silts and sands were deposited under limnic/paludal conditions (D2 terrace) (Mather *et al.*, 1991), followed by further dissection (D3 terrace). The soils of these terraces are (from oldest to youngest) typically coloured 5YR, 7.5YR and 10YR (standard Munsell colour chart for hue/chroma), and the carbonate accumulation of the younger D soils reach Stage I. They are believed to be of a Würm to Holocene age (Mather, 1991; Mather *et al.*, 1991). A ^{14}C radiocarbon date for a sample taken from the E terrace is 2310 +80/-90 years BP (Harvey & Wells, 1987; Kelly *et al.*, 2000).

Table 2.5 – Comparison of age estimates for terrace features

Terrace	Soil & landform development / ka (Harvey *et al.*, 1995)	U/Th date / ka (Kelly *et al.*, 2000)	Period
E		2310 +80/-90	Holocene
D3	10 - 20		Holocene
D2		8	Holocene
D1	Early Würm (80?)	9	Holocene/late Würm?
Early D1 ?		31	Würm (c10-70 ka)
C	> 100	88 (68 - 104)	Tyrrhenian III (c.95 ka)
B		145	Tyrrhenian II? (c.125 ka)
A	700 < 1600	224 > 380	mid-Pleistocene

The river terrace levels have been used to demonstrate that the drainage network has been substantially modified by at least two major river capture events (Mather, 2000a,b). The earliest occurred in the Early Pleistocene and isolated approximately 15% of the original Sorbas Basin drainage network from its source area in the Sierra Alhamilla (Mather, 1993a, 2000a,b). This part of the drainage network (i.e., the Rambla de Lucaiñena) had progressively extended headwards as a strike-orientated

stream, capturing some of the basinal drainage lines in the south of the Sorbas Basin (Mather, 1991, 1993a; Mather & Harvey, 1995; Harvey, 2001). These were then diverted southwards into the Carboneras Basin.

The second river capture (referred to here as the "Río Aguas/Rambla Feos River Capture") occurred in the late Pleistocene, approximately 100,000 years BP, leading to approximately 73% of the original Sorbas Basin drainage being re-routed eastwards into the Vera Basin (Harvey & Wells, 1987; Harvey et al., 1995; Mather, 1991, 1993a, 2000a,b; Mather et al., 1991). The river capture was the result of the Lower Río Aguas headward erosion and retreat westwards along the regional strike of the sedimentary basin fill and the similarly orientated basin margin fault systems (Harvey & Wells, 1987). This was driven by the relatively higher uplift of the Sorbas Basin with respect to the Vera Basin. The site of the river capture is considered to be the "Wind Gap" or Col area between the villages of Los Molinos and Los Perales. The river terrace remains of the Rambla Feos can be found in this area. The E-15 motorway now passes through this Col area.

The evidence for this river capture are the differences in the clast assemblages, as well as the spatial distribution of the river terraces in the Río Aguas (both upstream and downstream of the river capture Col) and the Rambla Feos.

The main sediment sources feeding the Río Aguas headstreams are the metamorphic rocks of the Sierra de los Filabres. The differing importance of this sediment source upstream and downstream of the capture site is expressed in the pre- and post-capture sediments in the terrace gravels (Table 2.6). In the upstream reach there is little difference between the pre- and post-capture sediments, either in terms of size or in

terms of lithology (Table 2.6). The distinctive amphibolite mica schist and garnet mica schist, outcropping in the Filabres north and west of Uleila (Figure 2.2), has been traced in decreasing proportions of the total clast assemblage, in the A-C terraces downstream from the Upper Aguas into the Feos system (Harvey & Wells, 1987; Harvey *et al.*, 1995), and through to the south of the Sierra de Alhamilla (Mather, 1991). Along the route of the Rambla Feos, post-capture sediments are much finer than the earlier sediments and contain only rare reworked Filabride clasts (Harvey & Wells, 1987; Harvey *et al.*, 1995). In contrast, in the Lower Aguas no distinct Filabride clasts can be found in the pre-capture terrace sediments, but they are present in the post-capture sediments (Harvey & Wells, 1987; Harvey *et al.*, 1995).

Table 2.6 – Clast lithologies from river terrace deposits pre- and post- river capture, upsteam and downstream of the capture site (percentage occurrence). Modified from Harvey *et al.* (1995).

	Upper Río Aguas		Rambla Feos		Lower Río Aguas	
	Urra		Arojos		La Huelga	
River Terrace*	C	D3	B	D1	C	F
Clast Lithology						
Green spotted gneiss (F)	34	38	20	2	0	7
Mica Schists (B)	28	20	10	11	35	33
Black Phyllite (A)	0	0	15	26	0	0
Quartz (B)	27	23	7	6	7	9
Sandstone (T, Mt)	0	5	4	9	15	6
Dark Limestone (T)	0	0	11	20	15	11
Pale Limestone (Mm)	9	13	32	23	15	18
Mudstone (Mt, m)	0	0	0	0	4	11
Misc. (X)	2	0	2	4	9	5

(A) = Sierras de Alhamilla/Cabrera; (B) = Basement; (F) = Sierra de los Filabres; (M) = Miocene rock; (m) = Messinian rocks; (t) = Tortonian rocks; (T) = Triassic rocks; (Mm) = Quaternary calcrete or unidentified rocks; (X) = other sources (i.e. gypsum)
* Terraces B and C = pre-river capture; Terraces D and F = post-river capture

The episodic nature of the incision is apparent in the terrace sequence A-C. All three terraces are present throughout the headstream areas mapped, and are separated altitudinally by up to c. 20m. They become divergent downstream, perhaps indicating

increasing rates of incision downstream. There is then an incision of several tens of meters through the early stages of terrace D, especially downstream of Sorbas. Harvey *et al.* (1995), Harvey (2001), Mather *et al.* (2002) and Stokes *et al.* (2002) have all argued that this represents the accelerated capture-induced incision working headwards from the capture site.

Downstream of the capture site, along the Feos Valley, the A-C sequence is similar to that upstream of the capture. All three terraces can be traced across the southern margin of the Sorbas Basin and through the mountains. There, terrace B at least, has been deformed by faulting (Harvey & Wells, 1987; Harvey *et al.*, 1995). South of the mountains, terrace A is impossible to follow and may be deformed and buried by younger deposits. Faulted fluviatile gravels overlying Góchar-age (?) fan delta deposits in the Polopos/Lower Feos area, may be the equivalent of this terrace (Mather, 1991; Harvey *et al.*, 1995).

There has been almost no dissection since terrace C times in the Feos Valley. Terrace D deposits bury terrace C. The abundance of terrace D-age colluvial and tributary junction alluvial fan deposits attests to the "underfit" nature of the Feos in post-C times (Harvey *et al.*, 1995).

In the Lower Aguas the picture is almost the reverse of that in the Feos Valley. From the capture site downstream to La Huelga, no A-C terraces are present. The whole area is deeply incised, as a result of the headwards erosion through the calcareous mudstones of the Abad Member (Section 2.3.4.2), that brought about the capture in terrace C times. Red soils only occur on the uppermost hillslopes on the southern side of the valley, above a zone of landslides induced by the rapid incision. The northern side of the

valley is occupied by rapidly eroding badlands below the gypsum caprock escarpment (Harvey, 1987; Section 2.5). downstream of La Huelga an extensive terrace with a red soil appears to be the local equivalent of terrace C. The clast content indicates a local and Cabrera source area, indicating a pre-capture origin. Terrace fragments, apparently equivalent to D1, D3 and E terraces can be traced intermittently from Los Molinos, through the post-capture course of the Lower Aguas, downstream to beyond La Huelga.

2.4.3.2 *The Effects of River Capture*

The result of the Río Aguas/Rambla Feos River Capture was to dramatically decrease the base level and increase the stream power of the Río Aguas at the capture site, and the propagation upstream of a wave of incision (Harvey *et al.*, 1995; Mather, 2000a; Harvey, 2001; Griffiths *et al.*, 2002; Stokes *et al.*, 2002; Mather *et al.*, 2002, 2003). The presence of this wave of incision is reflected in the development of a number of nick points within the river profiles of many of the drainage lines in the study area (Figure 2.7). Some of these nick points reflect:

- Lithological boundaries – the first nick point above the capture site;

- Increased stream power as a function of discharge changes at the confluences of rivers – the nick point at the Ramblas Gochar and Cinta Blanca 10-17 km upstream); and

- Nick points that are within specific lithologies, suggesting that the nick point must have actively migrated from the lithological boundary – examples seen around Sorbas.
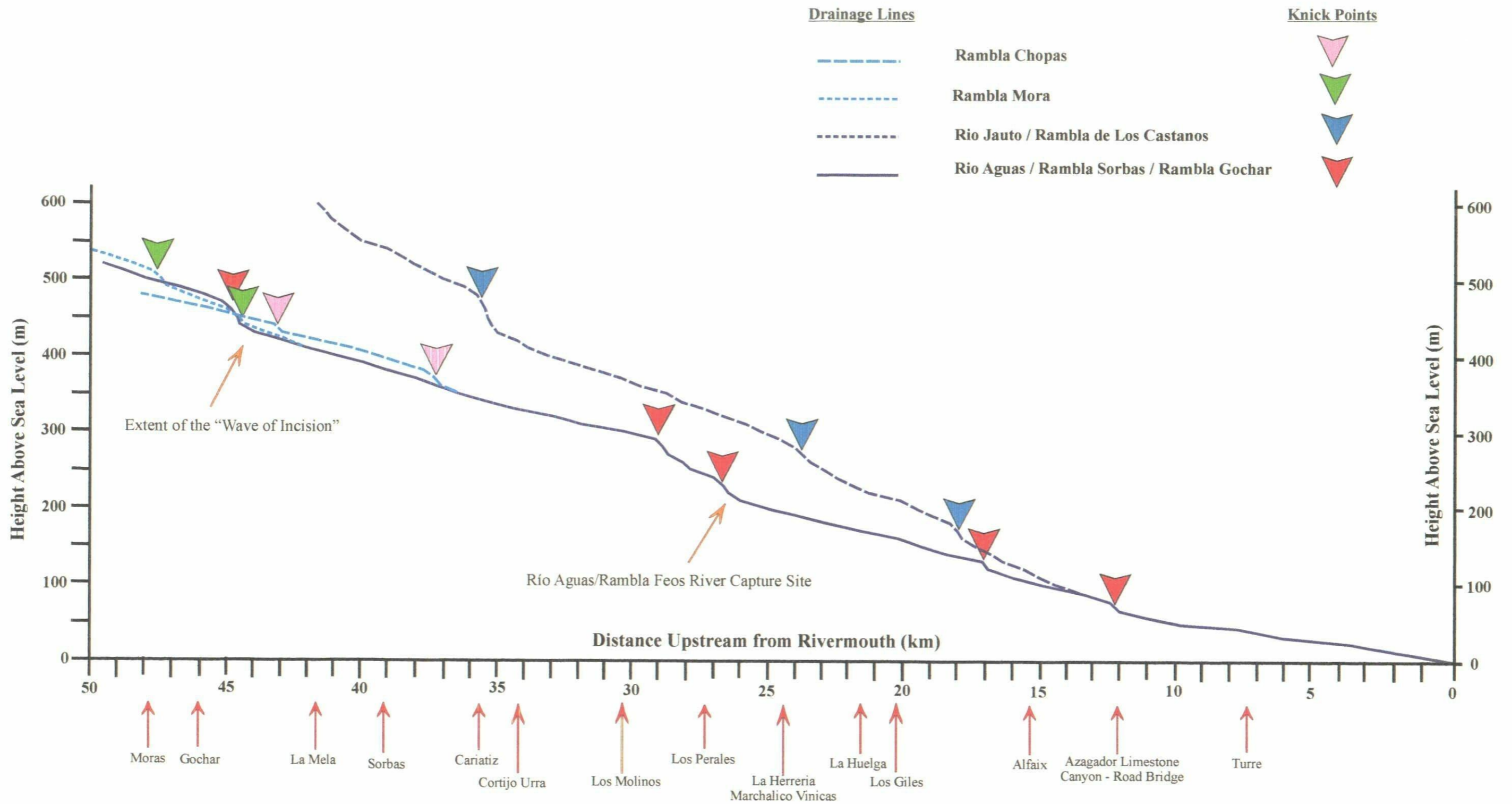
Figure 2.7 - Profiles of the Río Aguas, the Río Jauto and some of their major tributaries.

Above these knick points the river profiles appear to be relatively unaffected. This suggests that the headward propagation of the wave of incision is still active via a series of nick points and that it has reached approximately 18 km upstream from the Río Aguas/Rambla Feos capture site (Table 2.7). It also suggests that there is much scope for continued elevated levels of erosion within the fluvial system as a function of its response to the base level change which occurred as a result of the Río Aguas/Rambla Feos River Capture approximately 100 K years BP (Stokes, *et al.*, 2002; Mather *et al.*, 2002, 2003). This will probably decay with time, as suggested from empirical and field observations (Begin *et al.*, 1981; Begin, 1988; Gardiner, 1983).

Table 2.7 – Distances upstream of the nick points relating to the Río Aguas/Rambla Feos River Capture.

River	Total Distance Upstream (km)	Distance Upstream from Capture Site (km)
Rambla Sorbas / Rambla Gochar	45	18
Rambla Mora	45 & 47.5	18 & 20.5
Río Jauto	17 & 35	NA

Examination of how the Río Aguas/Rambla Feos River Capture has affected the drainage network (particularly focusing on the Rambla Feos, Lower Aguas and the Upper Aguas as far as the knick points) has demonstrated that the resulting wave of incision has led to the development of over steepened valley side slopes and canyons, the lowering of the land surface, especially in the areas closest to the capture site and changes in the amount and rate of incision (Table 2.8; Mather *et al.*, 2002; Stokes *et al.*, 2002).

Table 2.8 – Summary of the Pre- and Post-River Capture valley incision.

	Pre-Capture	Post-Capture
Amount of Valley Incision	Terrace sequence is characterised by low to moderate amounts of incision	Terrace sequence typically shows higher amounts of incision and a greater degree of variance between valley zones – incision amounts are moderate to high within the Upper and Lower Aguas Valleys but only negligible within the Feos Valley
Rate of Valley Incision	Terrace sequence is characterised by low-moderate rates of incision, although there is some spatial variance, with the highest values recorded from the Feos Valley	Terrace sequence shows higher rates of incision but with more spatial variance – the highest rates of incision are recorded from the Lower Aguas Valley and contrast with the negligible rates recorded from the Feos Valley.
Valley Shape	Mean width to depth ratio of 25	Mean width to depth ratio of 3

2.4.3.3 *Coastal Section of Río Aguas*

The coastal section of the Río Aguas has also been modified during the Pleistocene. In the area to the north of Mojacár, the modern Río Aguas, when in flood, flows across an extensive flat plain that overlies the deep-water calcareous mudstones of the Turre Formation. In the coastal areas this flat plain is punctuated abruptly by a series of basement inliers which relate to fault "slithers" or "pop-up" structures, exposed by strike-slip movement along the Palomares Fault Zone (Stokes, 1997). The spacing of

these basement inliers would suggest that the ancestral Río Aguas once flowed around them, eventually joining the Mediterranean Sea within the Garrucha area (Stokes, 1997). This is confirmed by the presence of conglomeratic deltaic sediments with an overall northeasterly transport direction within the Garrucha area, suggesting that a major river system once joined the Mediterranean Sea at this locality (Stokes, 1997). Presently, the Río Aguas joins the Mediterranean Sea to the south of Garrucha town, whilst the Río Antas and Almanzora join to the north.

Stokes (1997) was able to demonstrate that these deltaic sediments are not part of the ancestral Río Antas or Almanzora drainage systems. During the Pleistocene the ancestral Río Almanzora is thought to have joined the Mediterranean Sea in more or less the same location as it does today. Terrace remnants corresponding to the ancestral Río Antas are characterised by conglomerate only within the oldest, most proximal mountain front regions, becoming dominated by sand grade material within younger, more distal regions. Therefore they do not match those that are found in the Garrucha area (Stokes, 1997).

2.4.3.4 *The Role of Climate*

The Iberian Peninsula lies between the climate patterns of the Atlantic Ocean, the Mediterranean Basin, northern Africa and northern Europe. The majority of the Quaternary climate research has focused on what was happening in each of these areas and how they may have interacted with each other (i.e., northern Europe and the Atlantic Ocean). However, assessing the climate pattern interactions over boundary areas, such as the Iberian Peninsula, can be complex.

Carrion *et al.* (2000, 2001) considered that a basic outline of the vegetational history (and therefore possibly the climate history) of the Iberian Peninsula (and SE Spain in particular) still remains elusive. This is in-spite of the fact that over the last few decades there have been numerous workers studying pollen spore, micro- and macro-fossil (including isotopic analysis) and archaeological evidence taken from peat bog cores, cave deposits and cores taken form either the Mediterranean Sea or the Atlantic Ocean (Table 2.9 provides a summary of some of this work). However, this evidence is sparse with sites in southern and eastern Spain, as well as a combination of coastal and mountainous areas (i.e. Alicante, Valencia, Cordoba and Granada). This, therefore, limits the amount of interpretation and extrapolation between the sites.

A number of trends or key points have been identified in the findings from these studies:

- Large parts of southern Spain were covered by pine forests during the coldest phases of the last glacial (Carrion, 1992b).

- A period of significant landscape change with extensive fluvial erosion, transport and deposition during the "Oxygen Isotope Stage 2" period (Macklin *et al.*, 1995).

- The presence of steppe grassland and mixed deciduous forest in southeast Spain during the Quaternary (Huntley & Birks, 1993).

- The mid-Holocene landscape of southeast Spain seems to have been open with a wide range of mesothermophilous taxa, and that the coastal belt could maintain significant reserves of biodiversity throughout the pleniglacial stages (Carrion *et al.*, 1999).

- The Younger Dryas Event (between 11K and 10K years BP) appears to have been characterised by a severe cold period with dramatic drops in both temperature and precipitation over approximately a 400-year period (Pons & Reille, 1988; Carrion & Dupre, 1996; Carrion & Van Geel, 1999).

- Pollen and dinoflagellate data from western Mediterranean Sea cores reveal arid conditions on the neighbouring continent during the first deglaciation phase and the Younger Dryas interval, which contrasts with the improvement during the Bølling/Allerød Period (Perez-Obiol & Julia, 1994).

Very little work has been published concerning the Quaternary climate of the study area. This is unfortunately due to a lack of evidence, apart from the river terrace deposits (which are discussed in more detail in Section 2.5.2). Investigation of the river terrace deposits found in the study area indicate that terrace formation occurred along with major dissection of the drainage network during milder interglacial periods. The major aggradation phases, resulting in sustained fluvial deposition, appear to relate broadly to cold, dry but stormy climates which equate temporally with the northern European glacials (Amor & Florschutz, 1964; Butzer, 1964; Sabelberg, 1977; Rhodenburg & Sabelberg, 1980; Harvey, 1987a, 2001; Harvey *et al.*, 1995; Stokes & Griffiths, 1999; Mather, 2000a,b).

The fluctuating climate would have influenced the vegetation cover, surface runoff, rates of erosion and rates of sediment supply to the drainage network (Stokes & Griffiths, 1999; Mather, 2000a, b). These factors in turn would have also influenced, and been influenced by, slope stability. For example, Harvey (1990), Stokes & Griffiths (1999) and Mather (2000a,b) have all argued that during glacial periods a decrease in

vegetation cover due to more arid, cooler conditions would have allowed an increase in erosion and, therefore, sediment supply. Hart (1999), Hart *et al.* (2000), Griffiths *et al.* (2002) and this study (Section 4.2.14) have shown that a significant proportion of the sediment would have come from mass movement activity.

At present, the study area is considered one of the driest parts of Europe, with a semi-arid to arid thermomediterranean climate (Canton *et al.*, 2001). Rainfall events are produced by rain bearing fronts, associated with the Atlantic Ocean, coming from the west, principally in the cold season (Canton *et al.*, 2001). The pronounced semi-arid climate of the region is determined by its geographical location, in the rainfall shadow of the main Betic ranges and the proximity of northern Africa (Rodriguez-Puebla *et al.* 1998). Rodriguez-Puebla *et al.* (1998) argued that precipitation over the Almerían region was influenced by both the December North Atlantic Oscillation and by the October Southern Oscillation. Autumnal rainfall is associated with incoming fronts from the Mediterranean Sea, which sometimes result in storms and torrential rains. The average annual rainfall for the Sorbas area is less than 210 mm, most of which falls in autumn or winter, in relatively short duration but high intensity storms (Walsh *pers. Comm.*; Thornes, 1974; Esteban-Parra *et al.*, 1998; Mather *et al.*, 2001; Table 2.10). Daytime temperatures range from approximately 15°C in January to approximately 40°C in July and August. Frosts are rare except in the Sierras.

Table 2.9 – Palaeoclimate research in Southern Spain or the Mediterranean Region

Pons & Reille (1988)	Analysis of pollen from a Holocene peat record in Padul (Granada Province)
Carrion (1992a, b)	Pollen analysis from cave deposits near Granada & Alicante
Harrison & Digerfeldt (1993)	European lake levels
Huntley & Birks (1993)	pollen analysis for northern Europe
Perez-Obiol & Julia (1994)	Pollen record from a lake near Barcelona
Macklin *et al.* (1995)	Overview of the Mediterranean regional climate
Carrion & Dupre (1996)	Vegetational history from pollen analysis taken from a peat sequence in Navarres (Valencia Province)
Goy et al. (1996)	Coastlines and changing sea levels along the coast of southern Spain
Torres-Giron & Recio-Espejo (1997)	Periglacial features from Cordoba Province
Carrion *et al.* (1998)	Palynology of cave deposits (Granada Province)
Carrion *et al.* (1999)	Late Quaternary pollen sequence from a cave in Granada Province
Carrion & Van Geel (1999)	Palynology from Valencia
Terral & Mengil (1999)	Holocene climate reconstruction using olive wood and charcoal (caves in Valencia)
Rose *et al.* (1999)	Climate change in the western Mediterranean for the last 140Ka based on deep sea cores
Navarro *et al.* (2000)	Palynology of cave deposits in Alicante Province
Jalut *et al.* (2000)	Holocene climate changes along the Mediterranean coast from SE France to SE Spain (based on pollen analysis)
Carrion *et al.* (2000)	Forest successions in southern Spain
Carrion *et al.* (2001)	Vegetational history from lake and peat deposit in Albacete Province

Table 2.10 – Rain station data for Almería, Alicante and Murcia (after Esteban-Parra *et al.*, 1998).

Station	Almería	Alicante	Murcia
Altitude (m.a.s.l.)	7	82	66
Period	1911 – 1991	1856 – 1992	1862 – 1984
Average (mm)	210	357	316
Minimum (mm)	63	122	99
Maximum (mm)	552	673	765

2.5 Geomorphology of the Río Aguas Catchment Study Area

The study area has a predominantly erosional landscape, with depositional zones restricted to the coastline, the main river valleys and alluvial fans in mountain-front zones. The erosion of the landscape was controlled by changes in base level relating to the incision of the drainage system. Therefore, the resultant erosional landform patterns partly reflect the regional tectonic patterns and history, partly the resistance of the bedrock lithologies and partly the Quaternary climate. The main erosional landforms that are present in the study area are canyons, badlands and scarplands, while the main depositional landforms are coastal sediments and river terrace sediments (Figure 2.8; Harvey *et al.*, 2001). The information and observations presented here were then used to develop a terrain classification model for the study area. This is presented in Chapter 3.

2.5.1 Quaternary Erosional Landforms

2.5.1.1 *Canyons*

Deep canyons and incised valleys developed where rapid vertical incision coincided with the outcrop of more resistant rocks. They occur within uplifted mountains both on rivers originating from the mountains and on superimposed/antecedent transverse rivers. For example, where the Rambla de Lucaiñena crosses the Sierras Alhamilla and Cabrera, the Río Almanzora (Stokes & Mather, 2003) or the Río Jauto crossing the Sierra de Bédar (Figure 2.9A). They also occur where vertical incision coincides with the outcrop of more resistant rocks within the basin-fill sequences. For example, the Río Aguas and Rambla de Sorbas canyons that cut through the limestones of the Azagador Member or the sandstones of the Sorbas Member (Figure 2.9B).

Harvey *et al.* (2001) noted another interesting feature associated with some of the canyons in the study area – abandoned incised meander loops. Examples of these are:

- Cut-offs in the headwaters at Moras;

- A meander in the hillside above the Rambla de Sorbas, just upstream from the town of Sorbas;

- The meander that isolates the "knoll" on which the town of Sorbas is built; and

- A number along the Barranco de Hueli near Urra.

Legend

K   **Knick Points**

Drainage System

Canyons and Incised Channels

Study Area Boundary

Major Roads & Motorway

673 ⊕   **Spot Heights (m.a.s.l.)**

Settlements

Gypsum Quarries

Rio Agua/Rambla Feos "Wind Gap"

Limestone Escarpment

Gypsum Escarpment

Level terrain

Badlands

Gypsum

Hill areas with valley side slopes

Hill areas incised by canyons and gullies

Mountainous terrain

Figure 2.8 - A map of the landforms found in the Río Aguas Catchment Study Area Developed by this Study.

Yesares Member (Gypsum)

A.

Higher Nevado-Filabrides Complex (Gneiss)
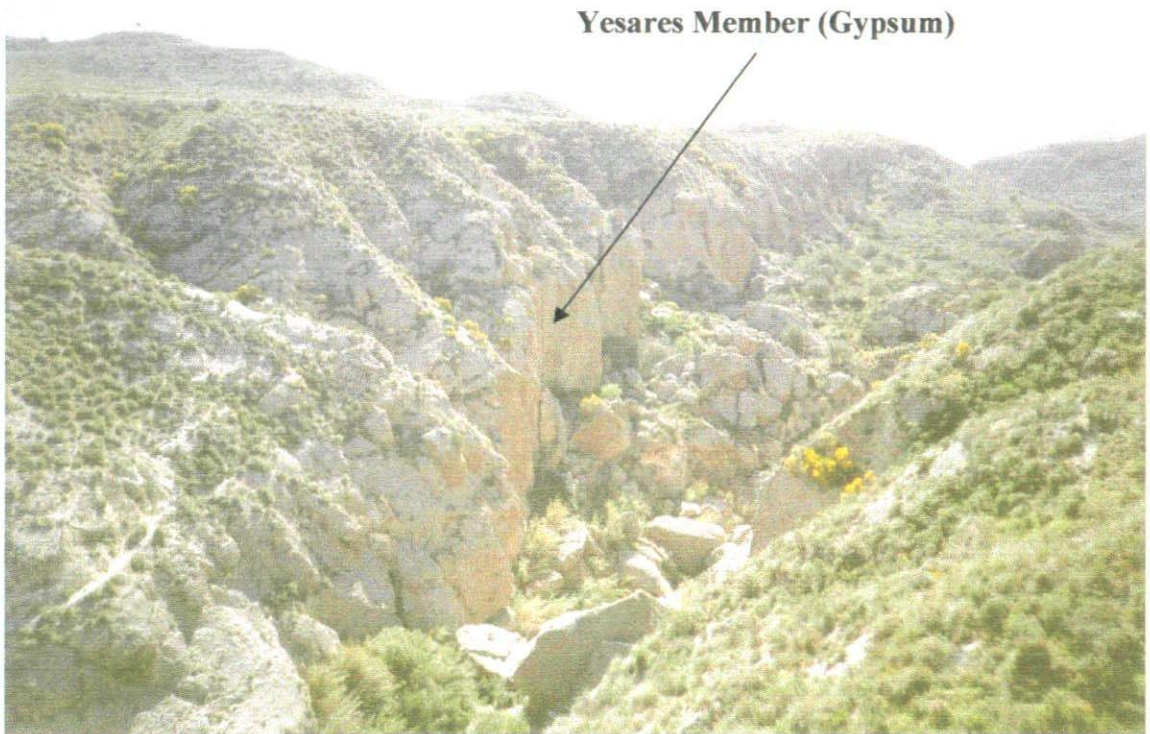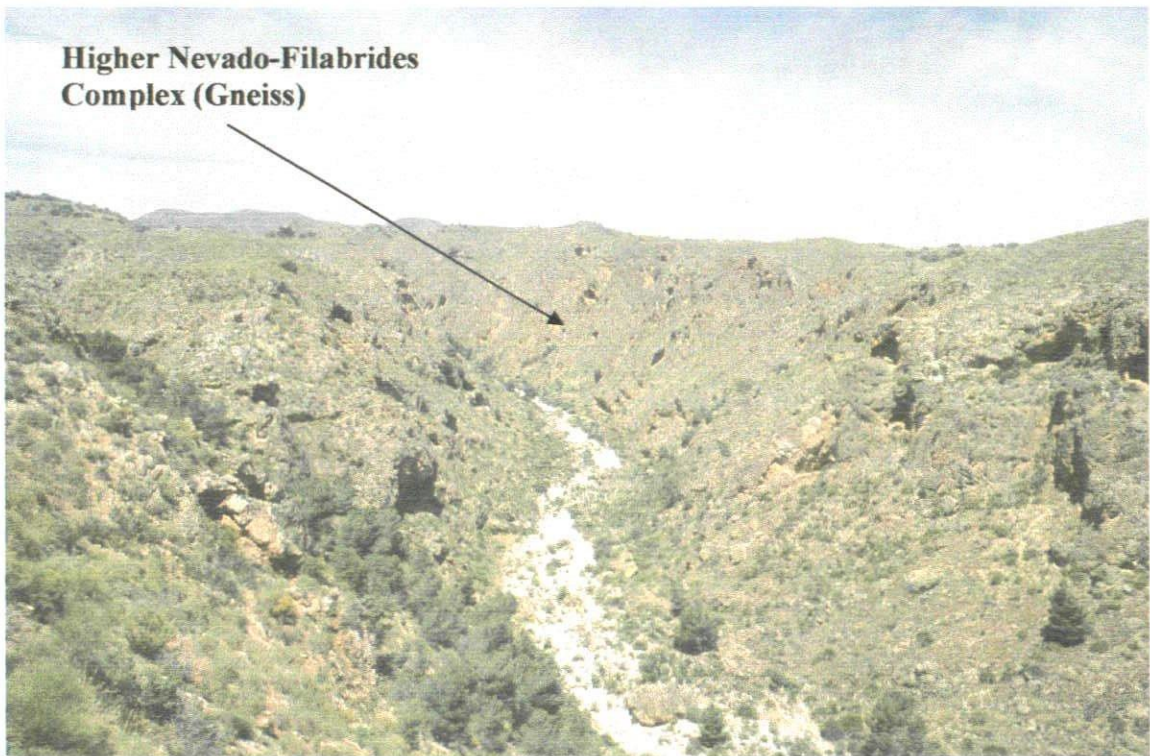
B.

Figure 2.9 – Canyons in the study area. **A**. Río Aguas passing through Yesares Member gypsum at Los Molinos (Grid Reference: 0582141059 / Facing southeast). The canyon is approximately 70m deep. **B**. Río Jauto passing through gneiss outcropping in the Sierra Bédar (Grid Reference: 0591641125 / Facing northwest). The canyon is approximately 90m deep.

2.5.1.2 *Dissected Erosional Landscapes & Badlands*

Where rapid incision coincides with the outcrop of weaker rocks, selective weathering and erosion of soft rock areas has produced deeply dissected erosional landscapes, characterised by gullying and, in extreme cases, by badlands (Calvo-Cases *et al.*, 1991a). The Tabernas badlands are considered by some the most spectacular in Europe (Harvey, 2001). The Tabernas badlands dissect a considerable thickness of Tortonian mudstones. This dissectional relief is the result of tectonic activity. It is thought that they date back to the Pleistocene (Alexander *et al.*, 1994).

There are two distinct areas of badlands within the study area (Figure 2.8). These are:

- "The Gypsum Escarpment Badlands", which are found along the Río Aguas between Los Molinos and La Huelga (Figure 2.10A); and

- The Barranco de Mocatán area = erosion of mudstones, sands and silts of the Zorreras and Góchar Formations (Figure 2.10B).
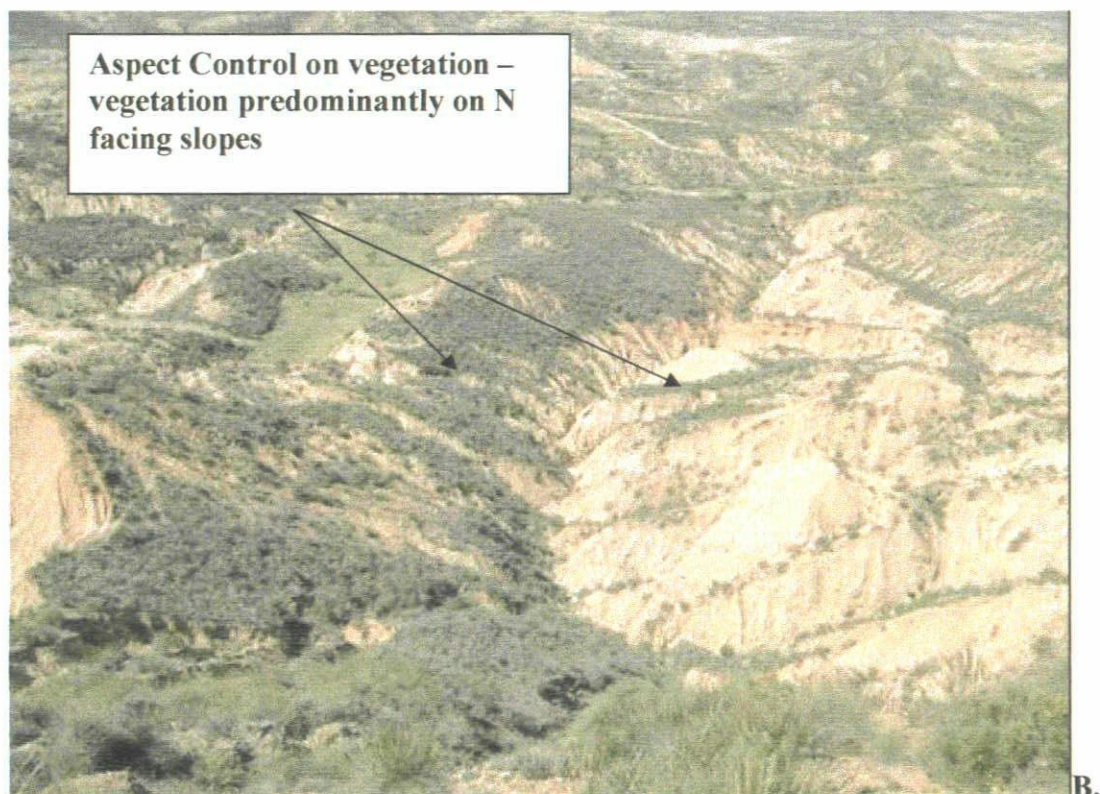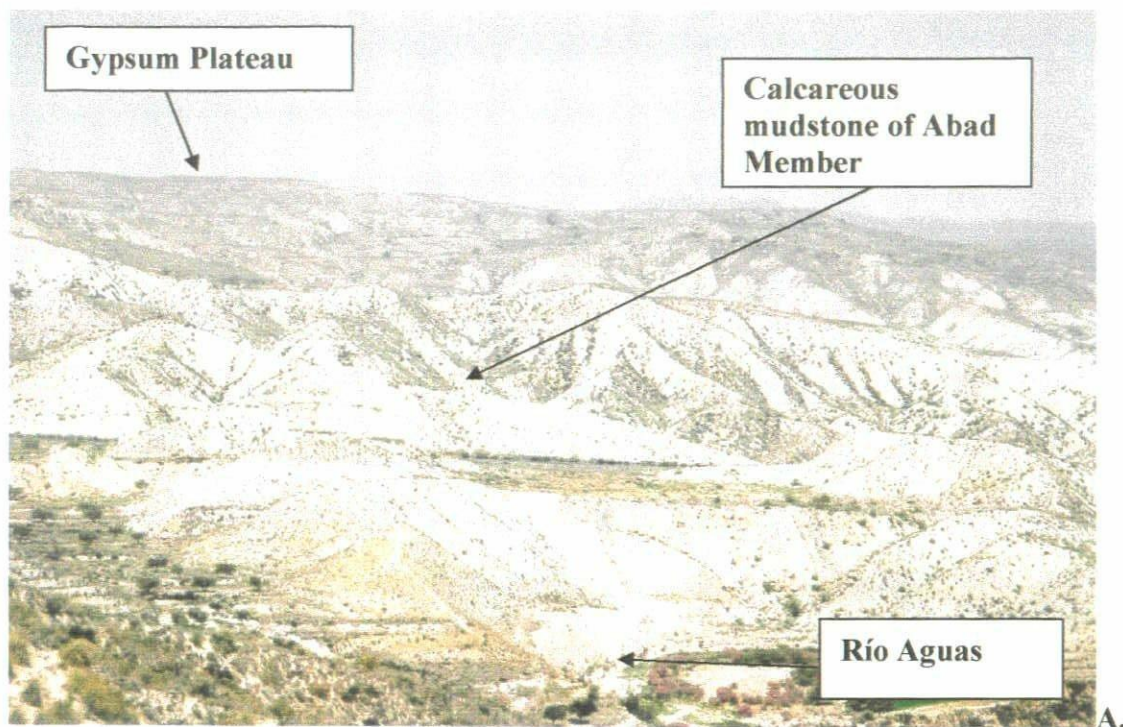
Figure 2.10 – Dissected erosional landscape and badlands. **A.** Los Molinos Badlands showing gullying and rilling formed on slopes with very little vegetation cover (Grid Reference: 0587641078 / Facing northwest. **B.** Mocatán Badlands near Sorbas showing aspect control on vegetation cover (Grid Reference: 0576541045 / Facing north).

Both of these areas have been affected by deep dissection of the landscape following the Río Aguas/Rambla Feos River Capture. The styles of modern processes operating within the badland areas reflect the interactions between geological, topographic and climatic factors (Harvey, 1982; Calvo-Cases *et al.*, 1991a,b; Alexander *et al.*, 1994). The badlands themselves range from apparently simple zones of relatively recent dissection, some of it undoubtedly human-induced, to zones of complex multiple sequences of badland development and stabilization.

The so called "Gypsum Escarpment Badlands" refer to an area of badlands that occur along the Río Aguas from the Los Molinos area northwards (undercutting the Gypsum Plateau escarpment) to near to the village of Los Castaños. They also stretch eastwards to the villages of La Huelga and Alfaix in the Vera Basin. The badlands have formed within the calcareous mudstones of the Abad Member, and undercut the gypsum of the Yesares Member.

Some parts of the Zorreras Member are highly erosive and susceptible to piping and other related dissolution features. In a number of places around the study area they weather to form badland-type topography. One example is the Mocatán area where Spivey (1997), Alexander *et al.* (1999) and Faulkner *et al.* (2000) have studied the geochemical and ecological aspects of badland weathering and morphology. This much smaller area of badlands occurs approximately 2km south of Sorbas. The Mocatán Badlands occur within part of the Zorreras Member and part of the overlying Góchar Formation (Spivey, 1997; Alexander *et al.*, 1999; Faulkner *et al.*, 2000). The highly erosive nature of the material is related to the clay mineral content (Alexander *et al.*, 1999; Faulkner *et al.*, 2000). Samples that have been analysed using X-ray diffraction

techniques have highlighted the presence of dispersive clay minerals such as smectite and chlorite.

2.5.1.3 *Scarplands*

Where erosion has coincided with alternating strong and weak rocks, the resistant bands form ridges or escarpments (Figure 2.8). The main resistant rocks and escarpment formers within the study area are:

- Limestones of the Azagador Member – southern margin of the study area.

- Reef limestones of the Cantera Member – southern margin of the study area and in the Cariatiz area (Figure 2.11A).

- Gypsum of the Yesares Member – in the Los Molinos area and along the Río Aguas valley downstream to La Huelga and northwards to Los Castaños (Figure 2.11B).
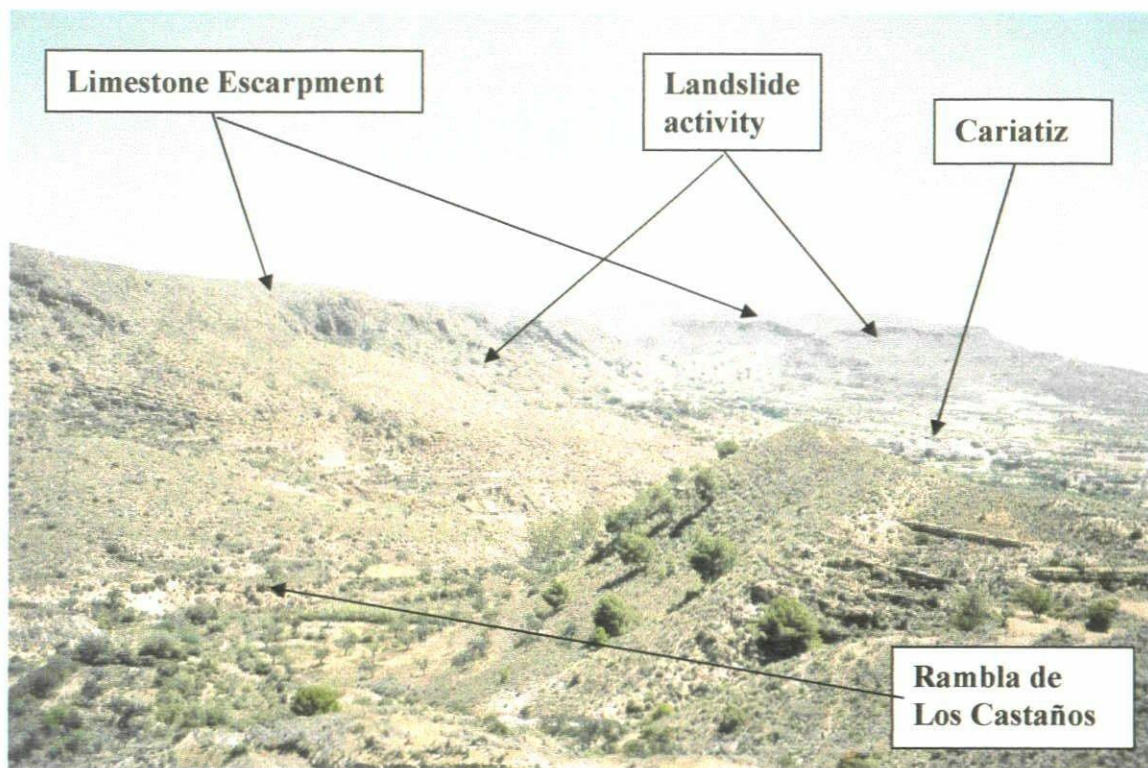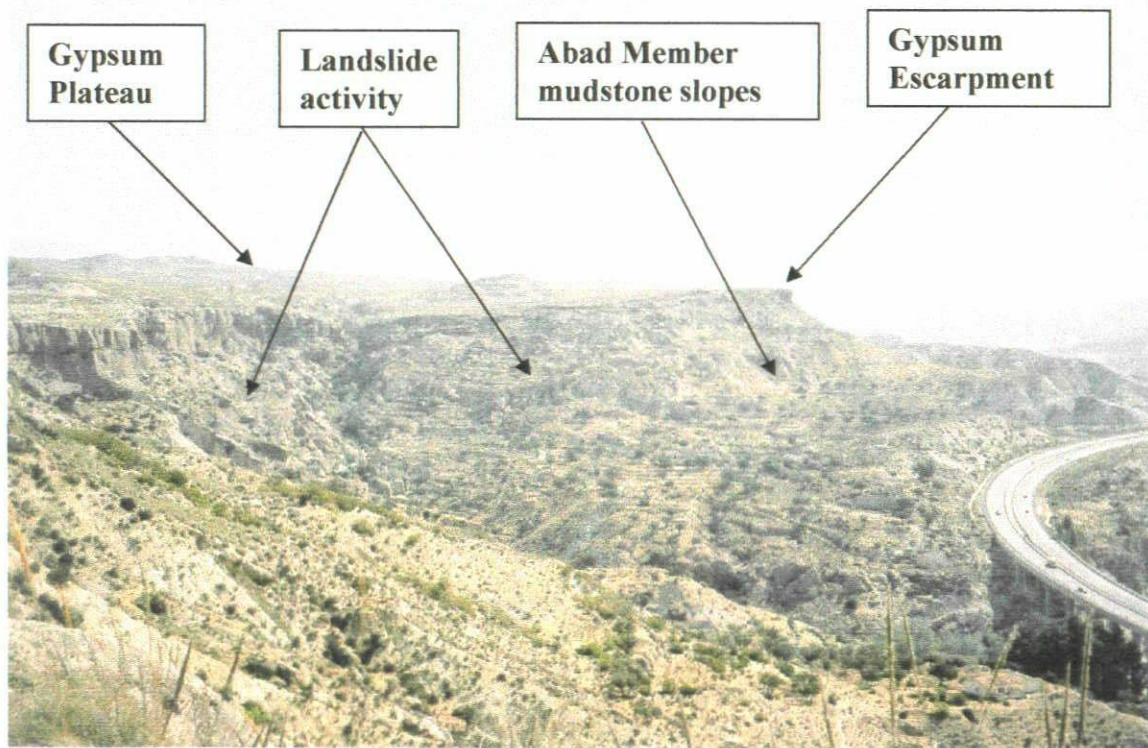
Figure 2.11 – Escarpments of the study area. **A.** Limestone escarpment above Cariatiz (Grid Reference: 0579641113 / Facing east). The limestone (Turre Formation) is dipping slightly out of the slope. **B.** Gypsum plateau and escarpment of the Yesares Member above El Tesoro (Grid Reference: 0583141060 / Facing east).

2.5.1.4 *Relict Depositional Surfaces and Pediments*

Zones of less intense erosion include relict depositional surfaces and uplifted pediments. In basin centres, away from tectonically induced dissection, are relict landscapes dominated by the remnants of the last stages of basin filling. Little-dissected Plio-Pleistocene depositional surfaces occur on conglomerates in the west of the Sorbas Basin (Harvey, 1987).

In some areas of soft rock, where the vertical incision has been limited, erosional pediment landscapes have developed. These occur on the margins of uplifted mountain areas in the Almería Basin, and in the eastern part of the Vera Basin. In many places the pediments are mantled by a thin depositional veneer of Early Pleistocene gravels.

2.5.1.5 *The Gypsum Plateau & Karst*

The Gypsum Plateau covers approximately 25km^2 of the study area, located to the east of the Sorbas Basin part of the study area (Figures 2.3, 2.4 and 2.8). The Yesares Member contains some exceptional examples of gypsum karst morphology, which have been described in detail by Calaforra & Pulido-Bosch (1997).

There are eight gypsiferous levels, each with a thickness of up to 30 m. The interbeds of calcareous mudstone strongly control the hydraulic flow through the gypsiferous series and, ultimately, the karstification processes that occur. On occasion, the calcareous mudstone also exercises a net geomorphological control, which is evidenced on the surface by the morpho-structural escarpments to be found in the region.

The solution and collapse dolines are small and only a few of them are over 30 m in diameter. The collapses are caused by the breakdown of the gypsiferous material when the layers of calcareous mudstone have eroded away. This is a special phenomenon that occurs in the gypsum karst of Sorbas (Calaforra & Pulido-Bosch, 1997).

The karren landforms in the outcrop are well represented, but are frequently affected by the texture of the gypsiferous material (Calaforra, 1996). The types of morphology seen within the outcrop suggest that the solution of the gypsiferous material is controlled by the gypsum crystallography. The greatest crystal solution takes place through the exfoliation planes and the selenitic gypsum twins, while solution is least on the crystal faces (Calaforra & Pulido-Bosch, 1997).

One of the most important features of the Yesares Member in the Sorbas Basin is the interstratification karst. These have developed as a result of the presence of the calcareous mudstone intercalations within the gypsiferous sequence. The cave passages frequently develop along the interstratification planes, between the calcareous mudstone and the gypsum. This usually means that the roof and floor are within the gypsum and the walls formed of the calcareous mudstone.

The origin of these interstratal cavities is related to the hydrogeological development of the gypsiferous aquifer (Calaforra, 1996). During the initial stages, the gypsiferous aquifer may be considered a multilayer aquifer under confined conditions. In this situation, the gypsum only dissolves by the formation of small proto-conduits, the position of which is determined by fracturing and by the presence of the calcareous mudstone, (which make up the impervious levels of the different gypsum layers). In the secondary stage, characterised by the present-day vadose conditions, the gypsum hardly

dissolves at all; instead, there is an intensely erosive action within the interstratal calcareous mudstone, producing the typical triangular section of the passages. In this situation, it is normal to find the presence of proto-conduits that form as a result of the presence of the interstratified calcareous mudstones, and its meandriform advance along the roof of the passage. These proto-conduits might be considered "false ceiling channels", as their origin is unrelated to the posterior filling of the passage with detrital materials.

Many of the longest caves in the area are configured to different levels marked by the presence of interbedded marls. The genesis of these features is related to the hydrogeological history of the multi-layer aquifer from phreatic conditions (when predominance of gypsum solution took place) to vadose conditions (predominance of marl erosion).

In the southern part of the study area, close to the site of the Rambla Feos/Río Aguas river capture, the gypsum plateau is underlain by the calcareous mudstones of the Abad Member. The relative weakness and high erosion potential of this member has meant that it has formed a fairly distinctive badland topography, as well as undercutting the overlying gypsum. This has resulted in the formation of a very prominent scarp-slope escarpment that follows the course of the Río Aguas in this area.

2.5.2 Quaternary Depositional Landforms

2.5.2.1 Coastal Sediments

Quaternary coastal deposits are restricted to the modern Mediterranean coast. Only in the Almería area is there a sequence of Quaternary coastal deposits, spanning from the Early to the Late Quaternary (Zazo *et al.*, 1981; Goy & Zazo, 1986; Goy *et al.*, 1986). Offlap and interdigitation between terrestrial and coastal sediments in this zone reflects interaction of the Alhamilla uplift and the Almería/Rioja downfaulting with Pleistocene sea-level change (Ovejero & Zazo, 1971; Zazo *et al.*, 1981).

A number of shoreline sequences have been identified along parts of the western Mediterranean coastline of the Vera basin. These shoreline sequences have been investigated by a number of authors:

1. Volk (1979) – mapped and described Pleistocene "strandlines" as part of an examination of the Quaternary relief of the Vera Basin.

2. Goy & Zazo (1982) – mapped and surveyed the Pleistocene shoreline sequences within the Mojacár-Garrucha region as part of a regional study.

3. Goy & Zazo (1986) – described the Pleistocene shoreline sequences in the Mojacár-Garrucha region and the affect of neotectonics on them as part of a regional study.

4. Bull (1988) – surveyed Pleistocene shoreline sequences in the Mojacár-Garrucha region as part of a local study into the geomorphology and soils of the Vera Basin.

5. Harvey (1997) – described the shoreline sequence in the Macenas area, south of Mojacár, as part of a regional study of the geomorphological development of the Almería region.

6. Stokes (1997) – reviewed the previous work by the above authors and examined the Pleistocene shoreline sequences along the Vera Basin coastline from around Garrucha southwards to Mojacár and Macenas.

Stokes (1997) includes detailed descriptions of the shoreline sequences that can be observed at each of these loctions. Using the distribution of the shoreline sequences and the geomorphology of the area, Stokes (1997) was able to infer that the Río Aguas once drained into the present Mediterranean Sea in the area around Garrucha.

The Pleistocene shoreline sequences within the Vera Basin are consistently characterised by gravel-pebble conglomerates deposited within a relatively high-energy, wave-dominated "beachface" environment, which received and reworked large inputs from nearby river systems (Stokes, 1997). However, as none of these shoreline sequences are directly involved with the observed landslide activity that is seen within the study area, they will not be described any further. Information on these sequences is available in the publications of the authors mentioned above.

It is likely that these deposits relate only to the late Pleistocene Tyrrhenian I (Völk, 1979; Mather *et al.*, 2001). Some of the deposits also show deformation relating to either the Caboneras or Palomares Faults (Angelier *et al.*, 1976; Goy & Zazo, 1986).

The modern shoreline within the study area ranges from shingle to sand beaches.

2.5.2.2 *River Terrace Sediments*

A well developed series of river terrace deposits can be found along the major river valleys, representing an alternating sequence of incision punctuated by major phases or aggradation. The incision is considered to represent an erosional response to regional uplift (Harvey, 1987; Harvey *et al.*, 1995). The major aggradation phases, resulting in sustained fluvial deposition, appear to relate broadly to cold, dry but stormy climates which equate temporally with the northern European glacials. The major dissection phases, producing the terraces, appear here, as elsewhere in the western Mediterranean region, to relate broadly to the milder interglacials (Amor & Florschutz, 1964; Butzer, 1964; Sabelberg, 1977; Rhodenburg & Sabelberg, 1980; Harvey, 1987; Harvey & Wells, 1987; Harvey *et al.*, 1995).

However, there are local variations, some of which may be related to tectonic activity (i.e., the lake at Tabernas). Other variations can be related to topographical and base-level changes following river capture, and include the complex and deformed terrace sequence at Urra (Mather *et al.*, 1991).

In the northern part of the Almería Basin, along the Río Alias, there is a sequence of several terraces. The gravels of the oldest terrace level have been deformed by the Carboneras Fault Zone near El Argamasón (Mather *et al.*, 2001). However, the relationship between this terrace sequence and the previously described terrace sequence of the Río Aguas is unknown.

In the Vera Basin, there are major terrace sequences along the Río Antas and Río Almanzora. These record the sequence of fluvial dissection following Early Pleistocene

alluvial fan sedimentation (Stokes, 1997; Stokes & Griffiths, 1999; Stokes & Mather, 2000).

Along most of the river valleys the modern floodplain sediments range between silts on the smaller streams, to sands and gravels, especially on rivers fed from mountain catchments. In a number of places, the sediments record relationships between lateral and vertical accretion: for example, the Río Aguas at Urra. The modern river channels tend to be wide, shallow, ephemeral, braided rivers although locally meandering does occur (Mather *et al.*, 2001).

2.6   Chapter Summary

The aims of this Project include developing a geological and geomorphological ground model and landslide inventory for the study area and investigating the main factors and controlling conditions of the observed landslide activity (Section 1.5). To meet these aims requires an understanding of the geology and geomorphology of the study area, including how the landslides, landscape and drainage system of the study area have developed and is influenced by the material strengths and geological structures of the underlying geology. This chapter has, therefore, provided a detailed review and description of:

- The geological setting of the study area and surrounding region;

- The geology of the study area;

- The transition from a marine to the present continental environment;

- The development of the drainage network; and

- The geomorphology of the study area.

This chapter has shown that the study area covers parts of two Neogene sedimentary basins; the Sorbas and Vera Basins. The northwestern and southeastern sections of the study area are bordered by Sierras composed of predominantly metamorphic rocks. The present drainage network was initiated during the Plio-Pleistocene and has incised through the sedimentary succession. This drainage network, which originally flowed southwards, has been modified by a number of river capture events.

One of these events (referred to here as the Río Aguas/Rambla Feos River Capture) has had a significant impact on the landscape in the south central part of the study area closest to the capture site. The river capture has led to:

- A relatively rapid drop in base level;

- A wave of incision to pass through a section of the drainage network, leading to the over-steepening of many of the valley sides slopes and formation of river canyons;

- The incision of the drainage network in the area closest to the capture site into the underlying bedrock geology; and

- An increase in the rate of incision, erosion and land surface lowering, especially in the areas closest to the river capture site.

It is this combination of events that has contributed to the landslide activity that is seen in the study area. It is argued here, therefore, that to understand the landslide activity one needs to appreciate the details of the underlying geology, the tectonic and structural setting of the region, the transition from marine to continental conditions and the formation and subsequent development of the drainage network. How this has affected

the distribution, style and nature of the landslide activity in the study area will be described and discussed as part of the data analysis in Chapter 4 and the case study examples in Chapter 5. The final ground model, based on the geology and geomorphology of the study area (as described here) will be presented in Chapter 6. The following chapter (Chapter 3) will describe the landslide investigation, including the use of aerial photographic interpretation, field mapping, a project-derived terrain classification, and the project-derived landslide inventory.

Chapter 3 – The Landslide Investigation

*"We only observe that which we can see, but we can
only see that which is already in the mind."*
– Detective Bertillion

3 The Landslide Investigation

3.1 <u>Introduction</u>

This landslide investigation that has been undertaken in the Río Aguas Catchment area of southeast Spain has involved the multi-disciplinary approach of land surface evaluation, as outlined in Chapter 1. The rationale behind this approach, and the definitions of the terms used will be further described in this chapter. This approach makes use of standard mapping techniques such as geological and geomorphological investigations.

Therefore, this chapter will include a description of:

- Land Surface Evaluation techniques;

- The considerations and assumptions that were made when designing the investigation;

- The data sources and collection techniques that were used;

- The landslide definitions and classification schemes that were used; and

- The landslide inventory database that was developed by this project.

3.2 Land Surface Evaluation

3.2.1 Rationale

As discussed in Chapter 1, the First Working Party on Land Surface Evaluation for Engineering Practice defined the technique as *"the evaluation and interpretation of land surface features and recorded surface data using one or a combination of the ground mapping, interpretation, classification and visual remote sensing techniques... The object is to provide information about ground conditions likely to be of significance"* (Anon, 1982). The Second Working Party has recently proposed an updated definition of land surface evaluation as *"the evaluation and interpretation of land surface and near surface features using techniques that do not involve ground exploration by excavation or geophysics"* (Griffiths & Edwards, 2001). As such, land surface evaluation is the process of data compilation, interpretation and conceptual ground modelling. The Working Party suggested that the technique should be used prior to undertaking any engineering ground or site investigation work. It is argued here that the technique can also be adopted for either geological, geomorphological or landslide investigations (or a combination of the three as in this study). It is also argued here that this technique is ideal for covering large areas of relatively remote terrain.

The Second Working Party stated that the first objective of any land surface evaluation is to acquire the most comprehensive conceptual ground model that can be generated. The aim being to maximise the value and justify the cost of any subsurface investigation and laboratory testing and to minimise the engineering geological unknowns (Griffiths & Edwards, 2001). Both of the Working Parties proposed the combined use of remote sensing and field mapping backed up by a detailed and extensive desk study. The field-

based techniques recommended were geological, geomorphological, engineering geological and land classification (terrain systems) field mapping (Anon, 1972, 1982; Griffiths & Edwards, 2001). These mapping techniques have been extensively reviewed in the literature (i.e., Brunsden *et al.*, 1975; Doornkamp *et al.*, 1979; Goudie, 1981; Anon, 1982; de Graf *et al.*, 1987; Cooke & Doornkamp, 1990; Lawrance *et al.*, 1993; Fookes, 1997; Petley, 1998; Griffiths, 2001; Hutchinson, 2001; Lee, 2001, Phipps, 2001) and it is not the intention to repeat that here.

Through the use of aerial photographic interpretation or satellite image interpretation land surface evaluation can be used to cover large areas of terrain, particularly that which is remote or where access is limited, difficult or dangerous. Another advantage of this approach is that all features in the landscape are mapped, ensuring that all parts of the terrain are given due attention without being overlooked. It can be used to divide the landscape into areas of recurring patterns of topography, soils, geology and vegetation, thereby summarising the physical aspects of a terrain. These are then analysed to decide the degree of influence that each may have, in order to derive a ground model that takes account of all factors in appropriate measure (Cooke & Doornkamp, 1990; Lawrance *et al.*, 1993; Lee, 2001). This means that land surface evaluation techniques are ideal for identifying "problem areas" such as areas of landslide activity, soil erosion or karst development and, therefore, the production of inventory maps. These maps would include information on the location, type, state, style of any engineering hazards encountered (i.e., landslide inventory maps; Finlayson, 1984; Wieczoek, 1984; Soeters & Van Westen, 1996). These data can then be used to highlight areas requiring further investigation, as well as for completing assessments of the hazard(s) affecting an area and the risk posed by that hazard to any proposed or existing engineering project/structure.

The land surface evaluation approach can also be used to gain an understanding of the processes that have previously been active in an area (i.e., glacial, fluvial or previous landslide activity). This information can then be used to develop a model of how the landscape of an area has developed through (for example) the Quaternary. Such information can then be used to identify those "events" or circumstances that have played the biggest role in creating the landscape of an area over that period of time (Brunsden, 1993). However, this will depend on how long evidence of processes such as landslide activity or geomorphological features such as river terraces or meanders are discernable in the landscape. This in turn will depend on the size and nature of the "signature" left in the landscape by the feature being studied (Brunsden & Thornes, 1979; Schumm, 1979). For example, the LRA Project in Nepal identified that within that particular terrain and environment, relatively small landslides (generally formed from relatively weak material) remained discernable in aerial photographs for approximately 15 years (LRA, 2001b). Much larger landslides (such as the Maleguica landslide described in Chapter 5) will have a much longer lasting "signature" in the landscape, possibly several thousand years.

The increasing use of remote sensing techniques and compilation of large inventory databases has required the use of computer systems such as Geographical Information Systems (GIS) that can be used to store, analyse, interrogate and interpret large quantities of data. There is a rapidly growing number of examples and reviews of how GIS-based techniques have been used in landslide investigations (Wadge, 1988; Carrara *et al.*, 1991, 1999; Leroi *et al.*, 1992; Rengers *et al.*, 1992; Dikau *et al.*, 1996; Mantovani *et al.*, 1996; Soeters & Van Westen, 1996; Turner & Schuster, 1996; Cruden & Fell, 1997; Van Westen *et al.*, 1997; Aleotti & Chowdhury, 1999; Guzzetti *et al.*,

1999; Lazzari & Salvaneschi, 1999; Thurston & Degg, 2000; Hearn *et al.*, 2001; Nathanial & Symonds, 2001, Petley *et* al., 2002; LRA, 2003c; Hart *et al.*, 2003a; Hart *et al.*, *in press*; Petley *et al.*, *in press*.) and it is not the intention to repeat that here.

The GIS approach requires a large amount of accurate and detailed data to be effective and a substantial investment of time for data input. At the start of this project no digital data were available, which would have meant a considerable amount of time would have been spent just digitising all of the required data. There were also "holes" in the published map data at scales below 1:50,000. However, digital contour data have now become available and as a continuation of this project it could be used in conjunction with the results from this study to develop a substantial database for the study area combining contour (and therefore slope data) with the geological, geomorphological and landslide information presented here. It is however beyond the scope of this present project.

3.2.2 Definitions

The term "terrain systems mapping" originated in the 1930's and early 1940's when the requirement to be able to classify large areas of terrain for the purposes of locating potential agricultural and economic resources, as well as identify suitable sites for development in mainly undeveloped rural areas was identified (Mitchel, 1991; Phipps, 2001). Phipps (2001), following Christian & Stewart (1968), suggested that the terms "terrain" and "land" were synonymous.

The mapping units for a land (or terrain) classification are defined by several terrain attributes in combination: landform, parent material and hydrological regime (Table

3.1). The most important aspect of a land classification is a choice of mapping units that are (a) essentially homogeneous for the purpose of the intended land use and (b) easy to recognise and, therefore, easy to map quickly and accurately (Lawrance *et al.*, 1993). The landscape of any area, however, is highly complex making this task difficult. A seven-fold hierarchical system of describing a given landscape has been developed and has been reviewed extensively (i.e., Cooke & Doornkamp, 1990; Mitchell, 1991; Lawrance *et al.*, 1993; Phipps, 2001). This study will use the three "lowest" (or "smallest") terrain units from this system – the "Land System", "Land Facet" and "Land Element" (Figure 3.1). These have been used as they are easily mapped at scales of between 1:25,000 and 1:50,000 and provide the most detailed picture of the landscape.

Land System   Gentle hills with broad terraced river valleys

Land Facets

3. Terrace   1. Hill

2. Minor valley

Land   4. Major valley

Elements

3b. Bluff 3a. Surface   2a. Floor 2b. Stream   4a. Abandoned   1a. Slope
                                                          channel   1b. Gully side
                                                       4b. Stream   1d. Stream
                                                    4c. Floodplain   1c. Gully floor
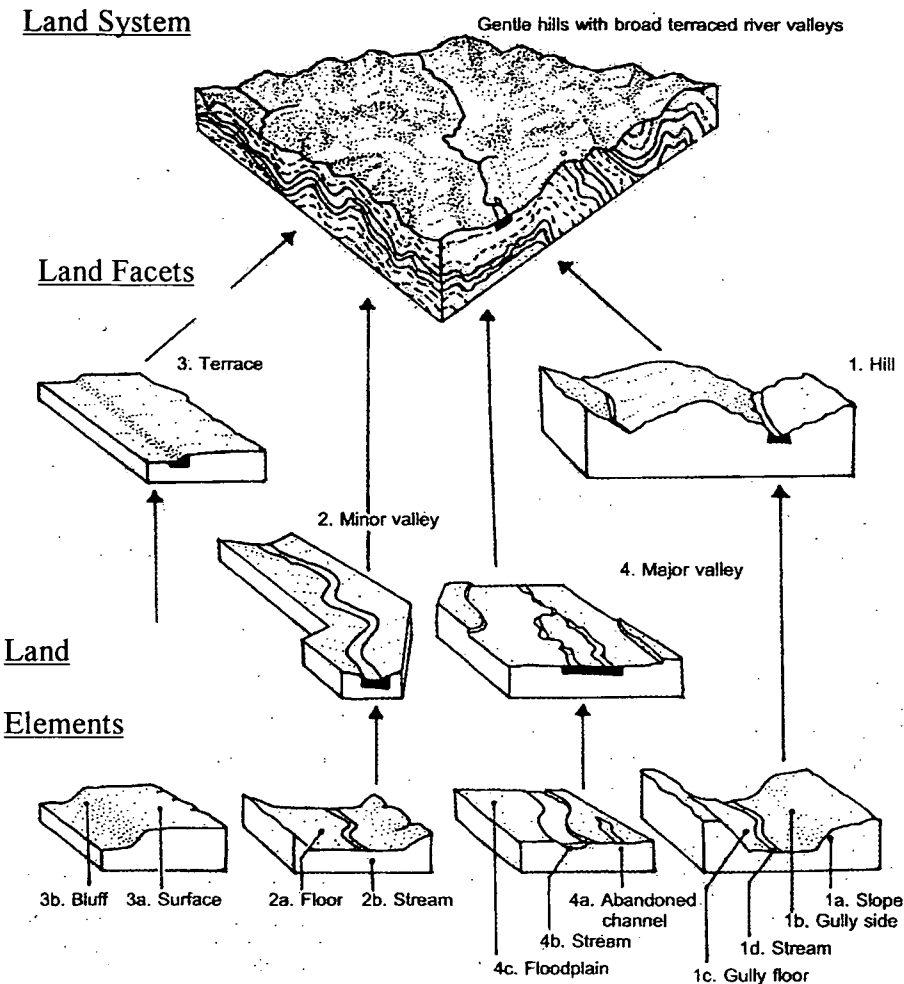
Figure 3.1 – Relationship between Land Systems, Land Facets and Land Elements

(Modified from Lawrance *et al.*, 1993; Phipps, 2001).

Table 3.1 – Definitions and key characteristics of Land Systems, Land Facets and Land Elements

Land System	Land Facet	Land Element
• A large area with a recurring pattern of landforms, soils and hydrological regimes. Its physical attributes give it a distinctive, unified character, recognisable on the ground but more especially from the air or space, when the regular arrangement of surface features are apparent. • Is recognised and mapped by its pattern of streams, landforms and vegetation. A substantial change in any one of these indicates a new land system. • Vegetation, although an important factor in the recognition of land systems (being a major contributor to air photograph patterns), is not used in the definition of land systems. This is because vegetation can be temporary, especially in areas of marginal habitability, and can be destroyed or modified by such events as fire, successive years of drought, changes in agricultural activity, overgrazing and deforestation.	• The land facet is the fundamental unit of the classification, the "building block" that makes up a land system. • A land facet is a terrain unit of uniform slope, parent material, soils and hydrological conditions. It is sufficiently homogeneous to be considered uniform for most practical purposes.	• A land element is a sub-division of a land facet, although it has no specified minimum size. • It is the smallest unit of the classification. Land facets can contain minor features that are too small to be called facets themselves. These are often too small to be mapped at any practicable scale, yet they are of significance to a project. • Examples would be the inside or outside of a meander in a river, a scarp-slope escarpment or a river terrace
Key Characteristics		
1. Area of at least 100km²; 2. Mappable at about 1:250,000 - 1:1,000,000 scale; 3. The climate is uniform at a similar altitude; 4. It is developed on a parent material that is either uniform, or consists of several closely related rock types, or contains a range of rock types (e.g. a sequence of bedded sandstones and mudstones); 5. A recurrent land pattern that is clearly identifiable in the aerial photographs is a good indication of consistent land forming processes, and hence of uniform ground conditions; and 6. Land systems are contiguous: there are no gaps of unclassified land between systems.	1. The land facets of a land system are geomorphologically related to each other; 2. Mappable at scales between 1:10,000 and 1:100,000; 3. The hydrological characteristics are consistent for all occurrences of the same facet within a land system; 4. Parent material can vary in the same manner as for a land system, although the total range of variation within a facet would normally be much smaller than variation of parent material within a land system. Ideally it is uniform; 5. Land facets are named after the landform that they comprise (e.g. "river terrace", "plateau top"). These simple names are not unique. 6. Land facets are contiguous: there are no gaps of unclassified land between facets.	1. The land elements of a land facet are geomorphologically related to each other; 2. Mappable at scales below 1:50,000; 3. Parent material can vary in the same manner as for a land facet, although ideally it is uniform; 4. Land elements are named after the landform that they comprise although these names are not unique. 5. Land facets are contiguous: there are no gaps of unclassified land between facets.

3.2.3 Project Defined Terrain Classification Model

The geomorphological setting and geomorphology of the study area was described in Chapter Two. This included a description of the main landforms and processes that are found in the study area. This information and the results from the initial aerial photographic interpretation have been used to develop a terrain classification scheme based on the concept of Land Systems, Facets and Elements for the study area. This was then refined through the fieldwork and field validation of the API results (described in the following section of this chapter). The final version of that scheme is presented here (Figure 3.2 and Table 3.2) with a series of photographs and examples of these Land Systems taken from the study area (Figures 3.3 to 3.9).

The Land Systems defined for this study are:

1. Mountain slopes incised by gullies, canyons and river channels;

2. Mountain slopes with gullies;

3. Hill areas incised by canyons and gullies;

4. Hill areas with river valley side slopes;

5. Gypsum plateau and karst;

6. Badlands; and

7. Level terrain.
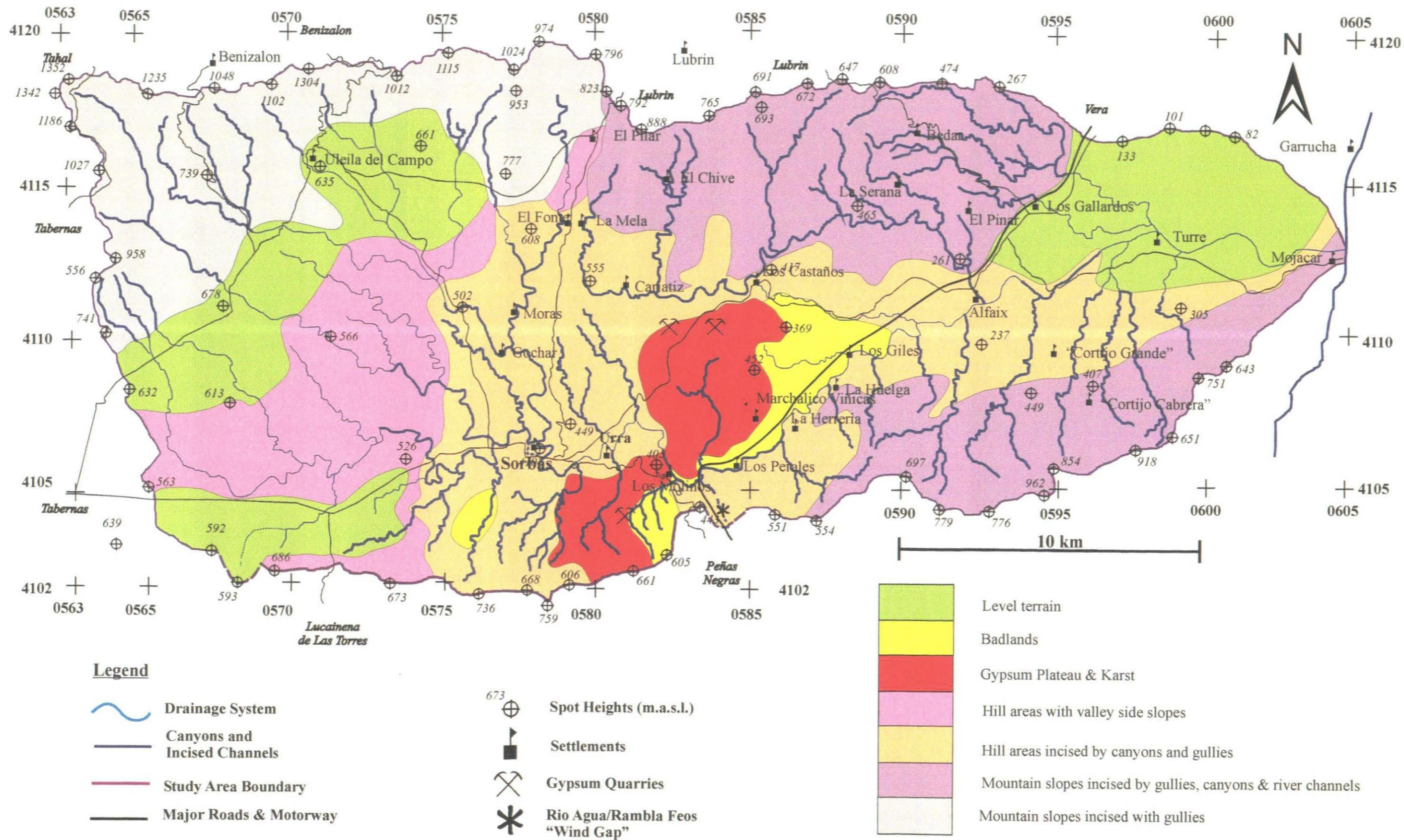
Figure 3.2 - The Land Systems Map for the Río Aguas Catchment Study Area Developed by this Study.

Table 3.2 – Terrain Classification developed by this project for the Río Aguas Study Area.

Land System	Location	Description	Geology	Fig. No.
Mountain slopes incised by gullies, canyons and river channels	Sierra Cabrera and Sierra Bédar	Steep mountain slopes, drainage channels are incised, narrow and steep, basin margin fault systems.	Basement Material (gneiss, mica schist, phyllite)	3.3
Mountain slopes with gullies	Sierra Filabres	Steep mountain slopes covered by scree material. Very little dissection of the drainage channels. Very steep slopes.	Basement Material (gneiss and mica schist)	3.4
Hill areas incised by canyons and gullies	The central western parts of the study area	Areas that have been incised by the drainage network. Characterised by steep sided gullies and canyons.	Neogene sediments	3.5
Hill areas with river valley side slopes	The central western parts of the study area away from the main drainage channels	Areas with valley side slopes formed by the dissection of the drainage channel. Some gullies, but generally open side slopes	Neogene Sediments	3.6
Gypsum Plateau and Karst	Central part of the study area	Large area of level terrain. Very thin or no soil cover. Sparse vegetation cover. Characterised by dissolution features such as sinkholes, and cave systems, as well as other karstic features. The eastern edge of the plateau is marked by a distinctive escarpment.	Yesares Member – gypsum interbedded with calcareous mudstone	3.7
Badlands	1. Between the Gypsum Plateau Land System and the Río Aguas 2. Mocatán area	Typical "Badland" landscapes. Areas of high rates of erosion and dissection.	Zorreras and Góchar Formations	3.8
Level Terrain	NE and SW parts of the study area, as well as areas below the Sierra Filabres	Relatively level terrain. Some parts of this area (i.e. central parts of Sorbas Basin) will relate to the Góchar erosion surface	Neogene and Quaternary sediments	3.9

A.

B.

Figure 3.3 – "Mountain slopes with incised drainage" Land System.

A. Mica schist slopes (part of the Higher Betic Units) within the Sierra Cabrera (Grid Reference: 0594841079 / Facing almost due east). The southern basin margin faults of the Vera Basin also pass through this area. **B.** Gneiss slopes (part of the Higher Nevado-Filabrides Complex) within the Sierra Bédar (Grid Reference: 05854113 / Facing south).
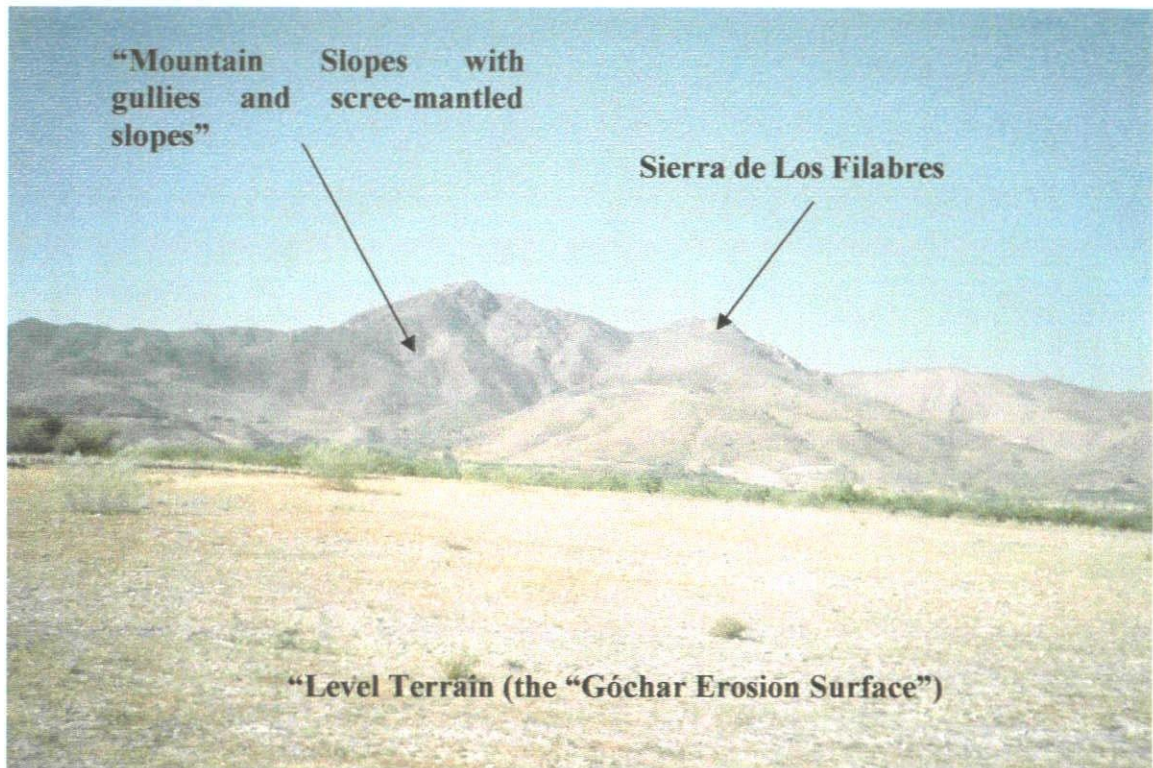
Figure 3.4 – "Mountain slopes with gullies and scree-mantled slopes" Land System.

The photograph is taken looking to the north from the roadside of the AL-813, approaching the village of Uleila del Campo. The highest peak in the picture is the "Ermita de la Virgen de la Cabeza" (1304 m above sea level). The slopes of this part of the Sierra de Los Filabres are formed from garnet mica schist of the Nevado-Lubrín Unit.

Landslide occurring within the Zorreras Member conglomerate & mudstone

A.

Scarp-slope formed from Azagador Member limestone overlying Chozas Formation mudstone

Large rock fall

Very large landslide on a dip-slope formed from Azagador Member limestone overlying Chozas Formation mudstone

Río Aguas
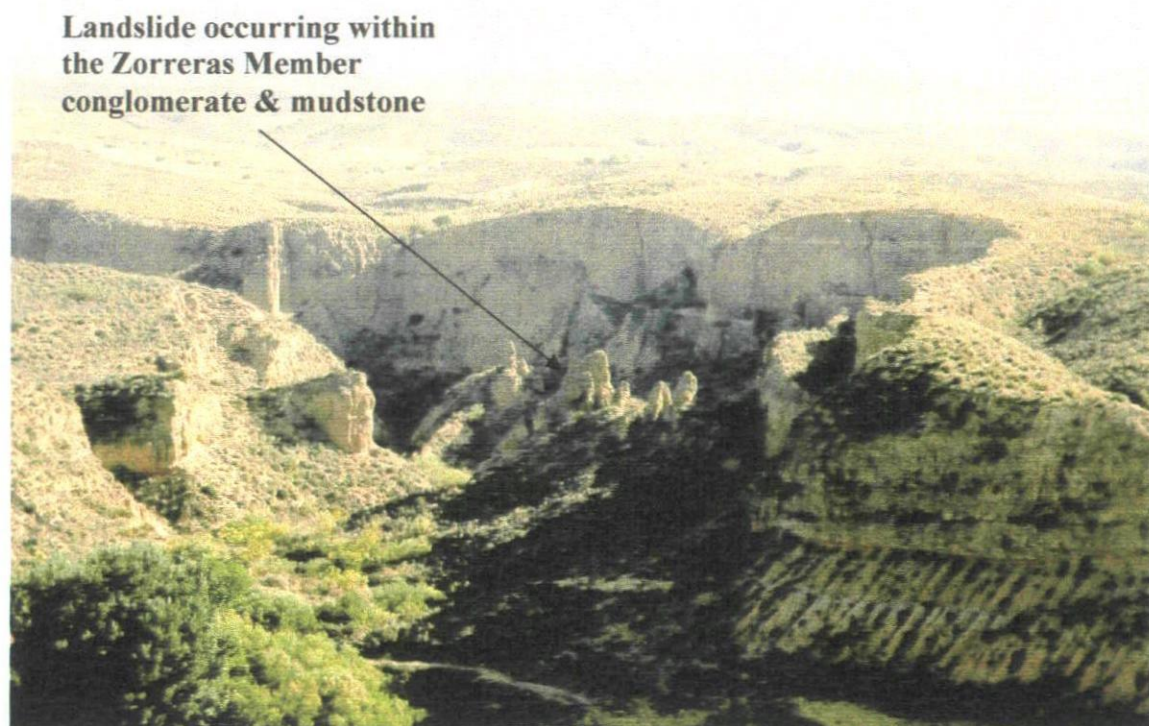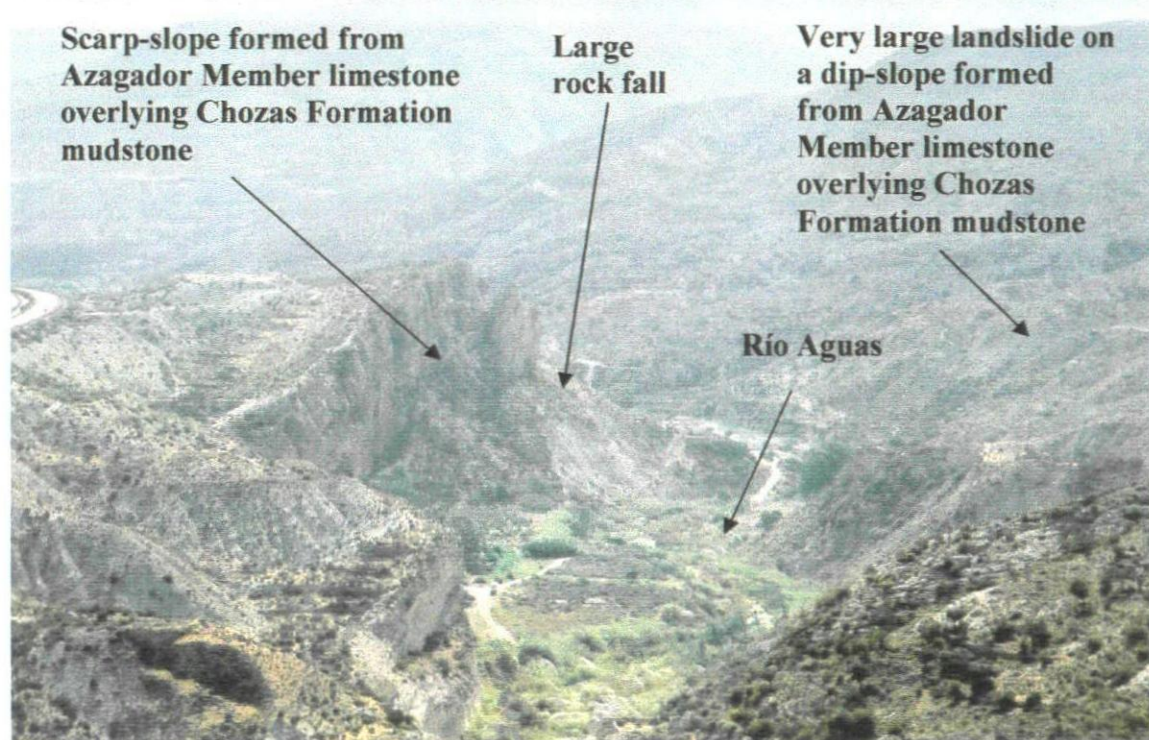
B.

Figure 3.5 – "Hill areas with incised drainage" Land System.
A. The incised Rambla del Aguarón (Grid Reference: 0579041074 / Facing northeast from Alto de Zorreras / the incision is approximately 30-40m at this point).
B. A view along the incised section of the Río Aguas at Los Perales (Grid Reference: 0583041056 / Facing east). The scarp slope indicated above is approximately 70m high.

A.
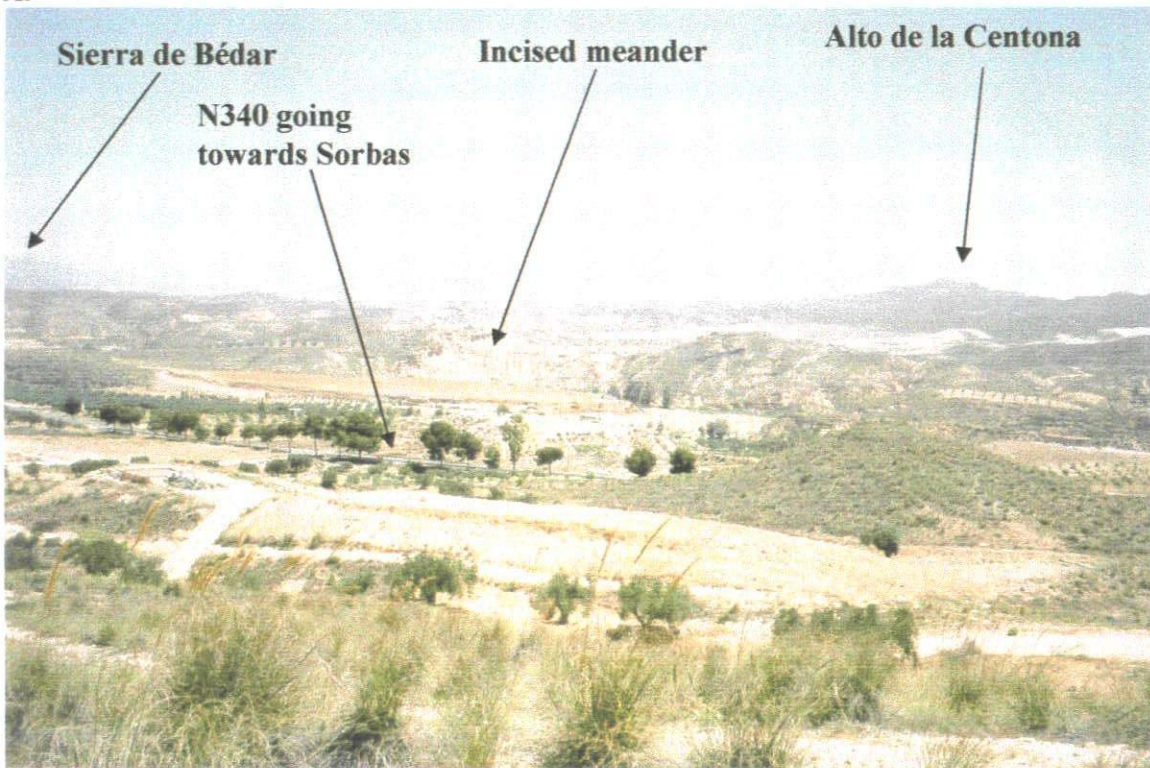
B.

Figure 3.6 – "Hill areas with valley side slopes" Land System.

A. Río Aguas valley near Urra (Grid Reference: 0579541050 / Facing northeast from near to the farm "La Clauda")

B. Rambla de Los Chopas near to Cortijo de Mojonera (Grid Reference: 0573641058 / Facing southeast from Alto de la Mojonera)
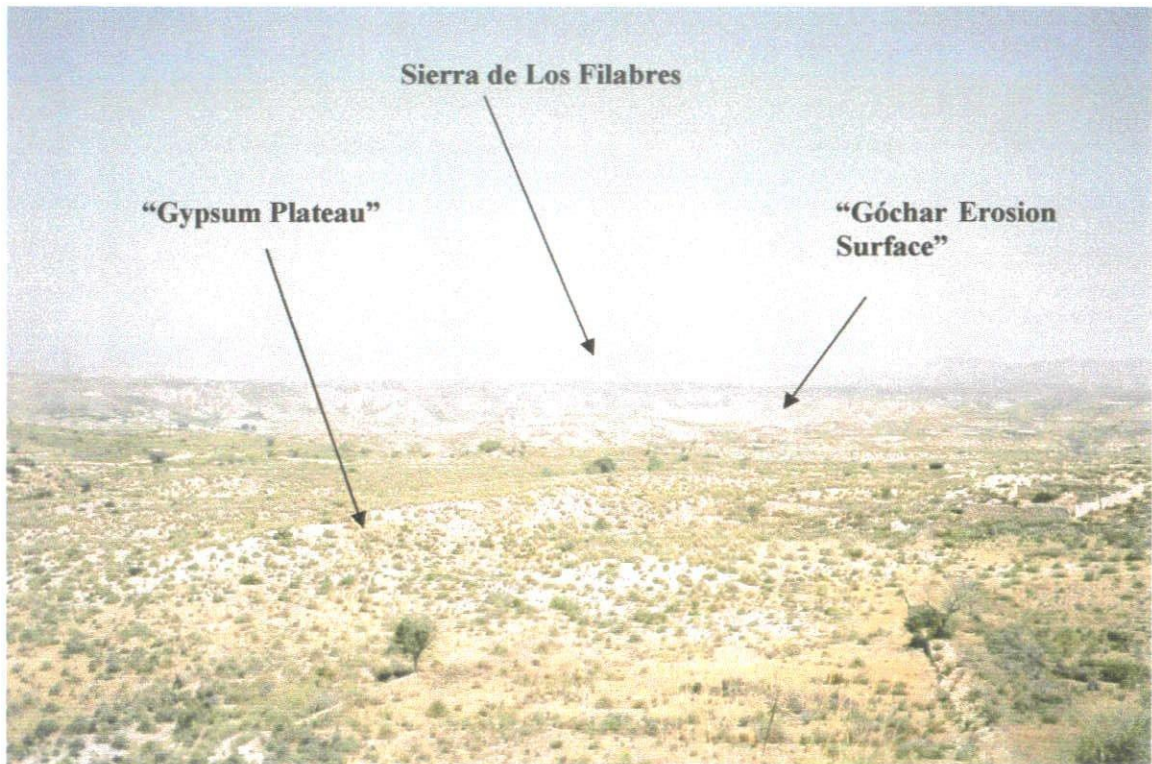
A.

B.

Figure 3.7 – "Gypsum plateau and karst" Land System.

A. View across the Gypsum Plateau towards the Sierra de Los Filabres (Grid Reference: 0583441066 / Facing northwest). The "Gypsum Plateau" is at approximately the same level as the "Góchar Erosion Surface". **B.** Gypsum karst feature (tumulus dome structure that has collapsed). Photograph taken near to Marchalico Viñicas (Grid Reference: 0585541074).
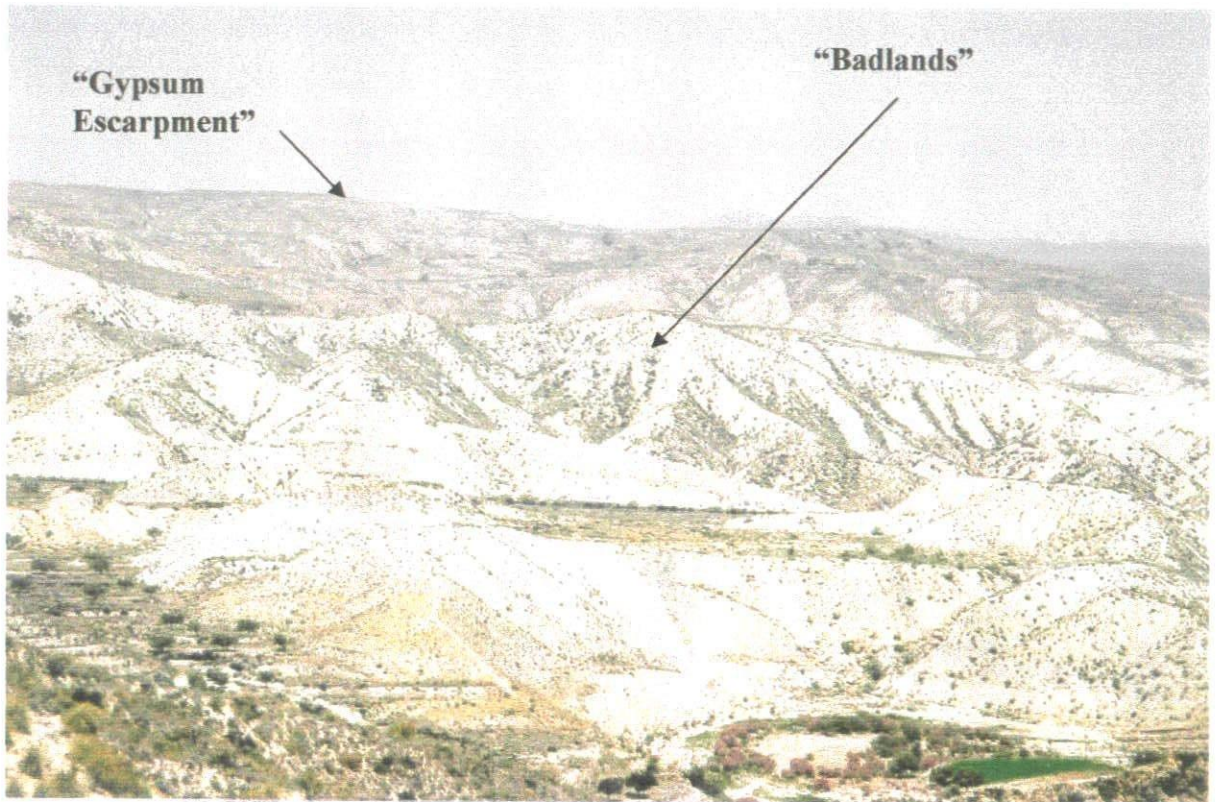
Figure 3.8 – "Badlands" Land System. The Badlands are forming in the calcareous mudstones of the Abad Member. The photograph was taken from the southern side of the Río Aguas above the village of La Herrería, looking towards the northwest.
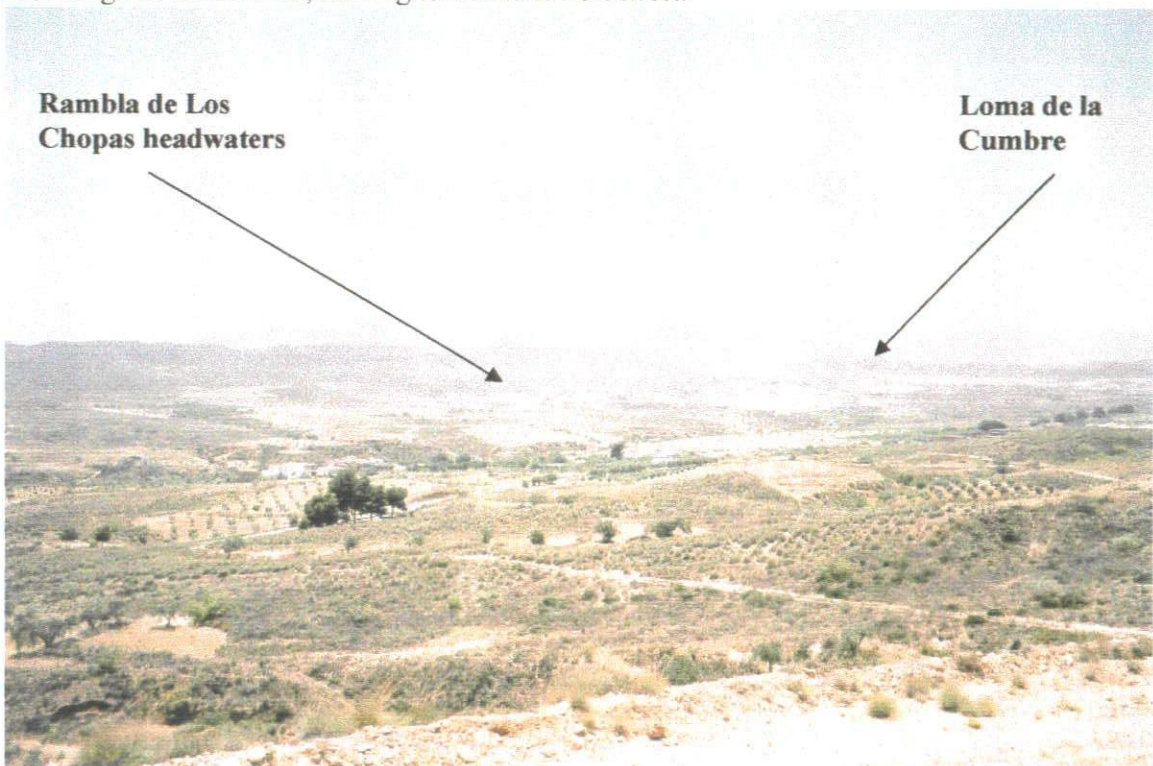
Figure 3.9 – "Level terrain" Land System. View across the southwestern corner of the study area, taken from "Alto de la Mojonera" (Grid Reference 0573641058) looking towards "Loma de la Cumbre".

3.3   Data Sources & Collection

Landslide activity is the result of the interaction of a large number of different factors. Any landslide investigation, therefore, needs to adopt a multi-disciplinary approach, such as that championed by Fookes (1997), Hutchinson (2001) and Brunsden (2002). The Land Surface Evaluation approach to landslide investigation utilises data from a number of different sources (Section 3.2; Griffiths, 2001 and references therein). This landslide investigation has used an extensive and detailed desk study, along with a detailed aerial photographic interpretation (API), backed up by an extended period of field mapping.

The amount, type and quality of the data collected by any landslide investigation will subsequently determine the type of susceptibility, hazard and risk analysis that can be completed using that information (Soeters & Van Westen, 1996). This could range from purely qualitative assessment through to a complex statistical, and/or analytical assessment. However, the prime concern of any project should be data quality, as this will influence the results obtained regardless of the method of assessment or techniques used. Data quality should, therefore, be continually assessed throughout the lifetime of the investigation. This can be undertaken by independent experts in the subject area or by the investigator(s) themselves. This study has sought to question the accuracy of the data being used and results at every stage of the investigation.

3.3.1 Aerial Photographic Interpretation

One of the predominant advantages of remote sensing interpretation techniques is that they allow for an individual site (i.e., a landslide) to be placed within the overall landscape. This information can be added to any desk study-based ground model that is being developed. Aerial photographic interpretation (API) techniques, particularly those utilising stereo-images, are well suited to landslide investigations. The stereo-images can provide diagnostic information concerning the type of movement (Crozier, 1973), as well as information concerning the overall terrain conditions, which are critical in determining the susceptibility of a site to slope instability (Soeters & Van Westen, 1996; TRL, 1997). Landslide information, extracted from aerial photographs (as well as other remotely sensed images), is mainly related to the morphology, vegetation and drainage conditions of the slope (see the tables of the characteristic features used in landslide identification by Soeters & Van Westen, 1996). Identification is based on studying the variations in tone, texture, shape and any lineaments in relation to the expected ground conditions and landforms associated with slope instability processes. (Allum, 1982; Soeters & Van Westen, 1996; TRL, 1997)

The interpretation of landslides from aerial photographs is based on recognition or identification of elements associated with slope instability and the interpretation of their significance to landslide activity. The implication is that a particular type of slope failure is seldom recognised directly but is interpreted to exist by analysis of a certain number of elements pertaining to slope instability features that are observed on the images. Therefore, the interpretation of landslides from aerial photographs requires knowledge of the distinctive features associated with slope movements and of the image

characteristics associated with these features (see the tables of the characteristic features used in landslide identification by Soeters & Van Westen, 1996). The contrast between a landslide feature and the surrounding landscape (resulting from either spectral or spatial differences) will affect the image characteristics and, therefore, the ease of interpretation. Spectral differences may relate to shadowing affects from a backscar, differences in vegetation or the differences between the disturbed and undisturbed parts of a slope. Factors that will affect image interpretation are (not in specific order):

- The size of the landslide;

- The age of the landslide (and therefore the time period between the landslide occurring and the image being taken);

- Local topography;

- Erosional processes within or around the landslide;

- Vegetation growth within or around the landslide;

- Shadowing affects caused by either vegetation or slope aspect;

- Landslide activity and rate of movement; and

- The severity of the landslide movements and their effect on slope morphology, drainage and vegetation.

Soeters & Van Westen (1996) discuss in detail the role of image resolution and interpretability in landslide inventory mapping and the advantage of using stereo pairs. They suggested the use of two scales of photographs. Small-scale aerial photographs (i.e., 1:25,000 to 1:50,000) can be used for determining the regional spatial landslide distribution of variables affecting landslide activity. Large-scale aerial photographs (i.e., 1:5,000 to 1:15,000) could be used for landslide inventory mapping and analysis of

possible casual factors. Due to the availability, this project has used 1:30,000 and 1:13,333 scale aerial photographs (Table 3.3).

Table 3.3 – Details of the aerial photographs used by this study.

Source	Flight Details	Scale / Description	Areas Covered	Quality
Spanish Catalunya Cartographic Institute	September 1984, April 1985 & October 1985	1:30,000 / Black and White	Complete coverage	Reasonable quality, some problems with shadowing, some patches of cloud cover
Natural Environment Research Council	Spring 1996	1:13,333 / Colour	Two runs – southern margin of the study area between Sorbas and Los Molinos	Good quality, no cloud cover problems
Natural Environment Research Council	April 2001	1:13,333 / Colour	Four runs – northern margin of the study area between the Sierra Bédar, Rambla de Mora (in the west) and Los Gollardos (in the east)	Good quality, no cloud cover problems

The API has been an ongoing part of the project. The aerial photographs (Table 3.3) were used as part of the initial desk study in order to gain an initial overview of the area and to provide a more focused approach to the fieldwork. The desk study API enabled an initial landslide inventory to be established. Subsequent use of the aerial photographs (in light of the knowledge gained through the fieldwork) meant that more meaningful results could be obtained for areas that could not be reached during the fieldwork, or that areas visited in the field could be "revisited". This technique proved very useful while trying to link the observed landslide activity with the development of the Río Aguas.

Each stereo-pair of photographs was viewed stereoscopically. The information was recorded onto a series of acetate overlays and then transferred onto topographic base

maps (Allum, 1982). The same information was collected following the same procedure for each aerial photographic print analysed:

1.   The drainage in as much detail as possible;

2.   The ridge crests or escarpments;

3.   Any identifiable landslide backscars and/or deposits;

4.   Any other identifiable areas of unstable ground and/or accumulations of colluvium (unattributed debris);

5.   Any areas of creep or erosion;

6.   Locations of deep shadow – these often coincide with steep slopes or canyon walls and might obscure any landslides;

7.   Outcrops of geological exposure;

8.   Terrain units;

9.   Areas of standing water or spring lines; and

10.   Land use.

All this information was recorded in ink using a symbol, line and colour system. Any other potentially useful information was also recorded including observations such as structural control, and dip and dip direction lineations and any unusual features. A number of acetate sheets were used for each photographic print so as not to over clutter them with data. Where appropriate these data were transferred to the topographic base maps for the study area.

While undertaking an API the distortion effects that occur at the edge of the prints must be taken into account. The distortion effects are dependent on the relative relief of the area being studied. As the topography of the study area has a relatively subdued relative relief then the distortion effects are not considered to be that significant, in this case.

3.3.2 Fieldwork

Field investigations have long been recognised as the central and decisive part of any investigation into landslide activity and landslide-prone regions (Turner & Schuster, 1996). During the period from spring 1998 through to spring 2000, over 17 weeks of field mapping were undertaken in the study area. An additional 2-week visit was made to the study area in June 2003. The field mapping involved carrying out a number of activities. These were:

1. Field validation of the results from the API (including those areas that are not covered by the aerial photographs);

2. Mapping of the landslides and development of the landslide inventory;

3. Mapping of the geology, structural geology and geomorphology (this information has been used to develop the ground model for the study area);

4. Collection of more detailed data that could not be obtained from the aerial photographs (i.e., rock mass properties and structural information);

5. Repeat visits and monitoring of certain key sites;

6. Consultation with members of the local population or local landowners; and

7. Selecting areas within the study area for further investigation, including more detailed fieldwork, data collection and analysis (described in Chapter 4).

3.3.2.1 *Field Validation of API*

This process is often referred to as "Ground-Truthing". The aim is to check whether the features that have been mapped during the API have been identified properly/correctly. The field validation for this study involved:

- Checking the locations and details of as many of landslides identified by the API as possible;

- Mapping the locations and details of any landslide features that were not identified by the API;

- Checking the accuracy of the geological and geomorphological mapping that was completed using the API (i.e., lithological contacts, significant breaks of slope, drainage patterns);

- Monitoring of certain key sites;

- Check for any new infrastructure that may have been built since the aerial photographs were acquired; and

- Mapping any other details that cannot or were not identified by the API which are significant to the project.

3.3.2.2 *Field Mapping*

Standard geological and geomorphological field mapping techniques were used (i.e., Brunsden *et al.*, 1975; Barnes, 1981; Tucker, 1982; Fry, 1984; Thorpe & Brown, 1985; McClay, 1991; BS5930, 1990; Cooke & Doornkamp, 1990; TRL, 1997; Griffiths, 2001; Lee, 2001; Phipps, 2001). The data collected during the field mapping (and the API validation) were recorded using field notebooks in conjunction with a series of proforma tables, as well as onto a number of topographic base maps. A number of field samples were also collected for further laboratory-based analysis.

3.3.2.3 *Local Knowledge*

While undertaking the field mapping, various members of the local population were consulted as to the nature and frequency of some of the landslides encountered in the study area. This approach yielded limited (and sometimes contradictory) results. It is heavily dependant on the individual's understanding of landslide activity, their memory for such events and, above all, their actual observation of the landslide in the first place (as distinct from second or third hand "information"). Often the only reason for a member of the local population noticing a landslide was when it affected their property, or their daily life, in some way. However, the information provided by the local population was useful in gaining a longer-term understanding of how the landscape behaves.

3.4 The Landslide Inventory

3.4.1 The Database

The most straightforward approach to any landslide investigation is the compilation of a landslide inventory (Soeters & van Westen, 1996). Therefore, the landslide inventory is the principal database for this project. It contains information on all of the landslides that have been mapped for this study, including the geometry, geology, and slope morphology of the landslides (Table 3.4). A printout of the database is included as Appendix B. The data have been stored electronically as a *Microsoft Access* database. The reasons for using this software are:

- The ability to set up a "front page" onscreen form that can be used for quicker data entry;

- The ability to search and interrogate (or "query") the database; and

- The ability to export the data into a number of different spreadsheet and GIS computer packages, so that more detailed data manipulation and analysis can be completed in more detail.

To minimise on file space, the majority of the data are stored as a series of numerical codes. The codes used by this project are shown in Appendix C. The use of codes also has the advantage of making the data language-independent (i.e., only the code lookup tables as show in Appendix C need to be translated and not the entire database).

A reliable landslide inventory defining the type and activity of all landslides, as well as their spatial distribution, is essential before any analysis of the occurrences of landslides and their relationship to environmental conditions can be undertaken (Soeters & Van Westen, 1996; Evens, 1998). All assessments of landslide susceptibility, hazard or risk require the compilation of a detailed landslide inventory. As previously discussed, this can be developed using data obtained during an aerial photographic interpretation, satellite image interpretation, ground survey or a literature review (concerning the historical occurrences of landslides in an area).

A landslide distribution map based on the landslide inventory will give the spatial distribution of mass movements, which may be indicated as either affected areas (drawn to scale) or as point symbols (Wieczorek, 1984). Landslide inventory maps can also be used as an elementary form of hazard map because they display the location of a

particular type of slope movement. They provide information only for the period shortly preceding the date that aerial photographs were taken or the fieldwork was conducted. They may not, however, provide an insight into any temporal changes in the distribution of mass movement activity. This can be achieved, to a certain extent, by using aerial photographs of various ages and/or numerous field visits, as well as any available historical information. These data can be presented as a landslide activity map and used to assess the temporal variability of a factor, such as land use.

3.4.2 Definitions

During the United Nation's International Decade for Natural Disaster Reduction (IDNDR), the International Association of Engineering Geology (IAEG) Commission on Landslides and Other Mass Movements set up the Working Party on the World Landslide Inventory (WP/WLI). It was set up to examine the terminology that is used to describe landslide activity and the way in which landslide data is collected and recorded. The WP/WLI has since published a series of papers defining the various facets of landslide classification (WP/WLI, 1990, 1993, 1994, 1995; Cruden, 1991). This has included a definition of a landslide and the different parts of a landslide, as well as the state, style, distribution, and rate of movement of the observed landslide activity. These guidelines and definitions have been used during this investigation, along with the works of Dikau *et al.* (1996), Cruden & Varnes (1996), Turner & Schuster (1996) and Cruden & Fell (1997).

Table 3.4 – Details of the data contained in the landslide inventory database.

Category	Data that were collected
Location	The geographical location of the landslide including the grid reference and the longitude and latitude co-ordinates of the centre of the landslide.
Certainty of Identification	The data source used (i.e. field mapping and/or API) and the certainty of identification of the landslide.
Land use	The land use of the area in which the landslide has occurred and the relative position of the landslide to the land use. Any remedial measures that have been undertaken were also recorded.
Elevation	The elevation of the crown and toe area of the landslide.
Geometry	The height, width and length of the backscar and debris accumulation, as well as the area covered by the landslide and the volume of the debris accumulation.
Angle of Reach	The angle of reach of the landslide, measured from the crown to the toe.
Landslide Mechanisms	Up to six landslide mechanisms were recorded for each landslide, using the definitions described by Cruden (1991), Dikau *et al.* (1996) and Turner & Schuster (1996) and outlined in Section 3.4.2
Landslide Activity	The state, style, distribution and rate of the landslide, based on the definitions of the WP/WLI (1990, 1993, 1994, 1995).
Landslide Age	Relative age of the landslide based on a project-derived scheme.
Causative Factors	Up to ten factors attributed to either controlling or actually triggering the landslide, per landslide using the WP/WLI definitions (WP/WLI, 1990, 1993, 1994, 1995).
Slope Morphology	The aspect, profile and angle of the slope on which the landslide has occurred.
Geomorphology	The Land System, Land Facet and Land Element in which the landslide has occurred, as described in Section 3.2.3.
Geology	The geology of the slopes in which the landslide has occurred. Additional information concerning the geotechnical properties of both the rock material and rock masses involved in the landslide are contained within a second database.
Vegetation	The type and density of the vegetation covering the slopes on which the landslide has occurred.
Drainage	The type of drainage within and around the landslide.
References	Any published or unpublished material referring to the landslide.
Other Information	Any other relevant information.

3.4.2.1 *Landslides*

For this investigation a landslide is defined as "*The movement of a mass of rock, earth, or debris down a slope*" (Cruden, 1991). However, because it is not practical to report every single "landslide" (using the above definition) that has occurred within the study area, it was necessary to establish a working definition of a "significant landslide". Based on the suggestion made in WP/WLI (1990), it is proposed that for the purposes of this research, a significant landslide must satisfy at least one of the following criteria: -

1. Has a measurable backscar and/or debris accumulation; and

2. Covers a minimum plan area of $10m^2$.

3.4.2.2 *Landslide Mechanisms*

One of the conclusions of Dikau *et al.* (1996) was that the most important information required about a landslide is the correct recognition of the failure type, mechanisms and causes. The topic of landslide classification is, however, a complex one, with many workers approaching the subject from a variety of different perspectives. These include soil or rock mechanics, engineering/applied geology, engineering/applied geomorphology, or "pure" geomorphology. Each different perspective has brought a different set of terms, definitions and classification schemes to the subject. The most widely accepted and used schemes are those of Varnes (1958, 1978, 1984), Hansen (1984), Crozier (1986), Hutchinson (1988), Dikau *et al.* (1996) and Cruden & Varnes (1996). This landslide investigation has adopted the classification scheme proposed by Dikau *et al.* (1996), which was based on the schemes proposed by Hutchinson (1988) and EPOCH (1993). These classification schemes are based on the morphology, the

processes and types of material involved, as well as the rate of movement (Table 3.5 and Appendix C).

The terminology used by this study for landslide mechanisms are (Figure 3.10):

- A fall is taken to denote the free-fall movement of material from a steep slope or cliff;

- A topple normally involves a pivoting action rather than a complete separation at the base of the failure;

- Movements occurring on a distinct slope or shear surface are termed slides. These may be subdivided into rotational and translational according to the geometry of the failure surface.

- Rotational landslides involve a semi-circular shear surface;

- Translational failures usually occur on planar slip surfaces;

- Non-rotational landslides involve movement on a curved, but non-circular slip surface. The slip surface may have a high angle in the upper part of the failure;

- Lateral spreading is characterised by the low-angled slopes involved and the unusual form and rates of movement;

- Flows normally behave as a fluidised mass in which water or air is significantly involved; and

- The complex failures are principally a combination of two or more of the previously described movements.

In reality nearly all landslides involve more than one type of movement either acting concurrently in different parts of the failure (compound landslides) or evolving downslope over time into a different process (i.e., initial failure to subsequent deformation (complex landslides)). Many rotational slides, therefore, develop into a flow form at the toe, described by some authors as a slump-earthflow (Dikau *et al.*, 1996). A rockslide or rockfall may also advance into a flow form, known as a rock avalanche or sturzstrom. This type of failure is very destructive, with a high velocity run-out of rock debris. The high velocities associated with these failures have been attributed to one of the following processes: fluidisation, cohesionless grain flow, heat or steam generation, frictionite production or strength changes caused by the rate of shear (Dikau *et al.*, 1996). Another complicated form of landslide is the debris flow. It begins and is fed by debris slides, rotational slides, bank collapse, bed erosion and falls. The result is a mixture similar to "wet concrete". It may also be on a free rectilinear slope confined in a valley or so catastrophic that it overwhelms the topography (Dikau *et al.*, 1996).

Table 3.5 – The Landslide Mechanism Classification Scheme used by this Landslide Investigation (after Brunsden, 1985; Hutchinson, 1988; EPOCH, 1993; Dikau *et al.*, 1996). Each category should be read continuously from left to right.

TYPE OF MOVEMENT	FORM OF INITIAL FAILURE SURFACE		SUBSEQUENT DEFORMATION
FALL Detachment from a	(a) planar (b) wedge (c) stepped (d) vertical	failure surface	Free fall, may break up, roll bounce, slide flow down slopes below. May involve fluidisation, liquefaction, cohesionless grain flow, heat generation, chemical, rate effects or other secondary mechanisms
TOPPLE Detachment from	(a) single (b) multiple	(a) pre-existing discontinuities (b) tension failure surfaces	As above.
SLIDE Rotational movement (sliding) on a	(a) single (b) successive (c) multiple	circular failure surface	Toe area may deform in a complex way. May bulge, override, flow, creep. May be retrogressive.
Non-rotational compound movement (sliding) on a	(a) single (b) progressive (c) multistoried	non-circular (i) listric / (ii) bi-planar failure surface	Often develops a graben at the head. May have a toe failure of different type.
Translational movement (sliding) on a	(a) planar (b) stepped (c) wedge (d) non-rotational	failure surface	May develop complex run-out after disintegrating. As for falls and flows.

SPREAD

Lateral spreading of
ductile or soft material
which deforms in

(a) a layer beneath hard rock
(b) a weak interstratified layer
(c) a collapsible structure

topographic
surface

Can develop sudden spreading failure in
quick clays. Slope opens up in blocks and gulls
or fissures. Liquefaction can occur and the whole slope
spreads either as a totally collapsed flow or with
"floating" blocks and grabens.

FLOW

Debris movement
by flow on a

(a) natural slope
(b) complex slope

(i) unconfined slope
(ii) channelised slope

Flow will involve complex run-out from source.
May move in sheets or lobes and involve viscous
or rheological mechanisms.

Movement by creep on

any hillslope

Creep may be gravity, seasonal, pre-failure or progressive.

Rock flow (sagging,
Sackung) movement on

(a) single sided
(b) double sided

mountain slope
(a) of rotational
(b) compound form
    (i) listric / (ii) bi-planar

May be slow gravity creep or early stages of landsliding,
but not displaying toe deformation other than bulging.

(c) stepped

discontinuity

May involve toppling.

COMPLEX - movements involving two or more of the categories above.
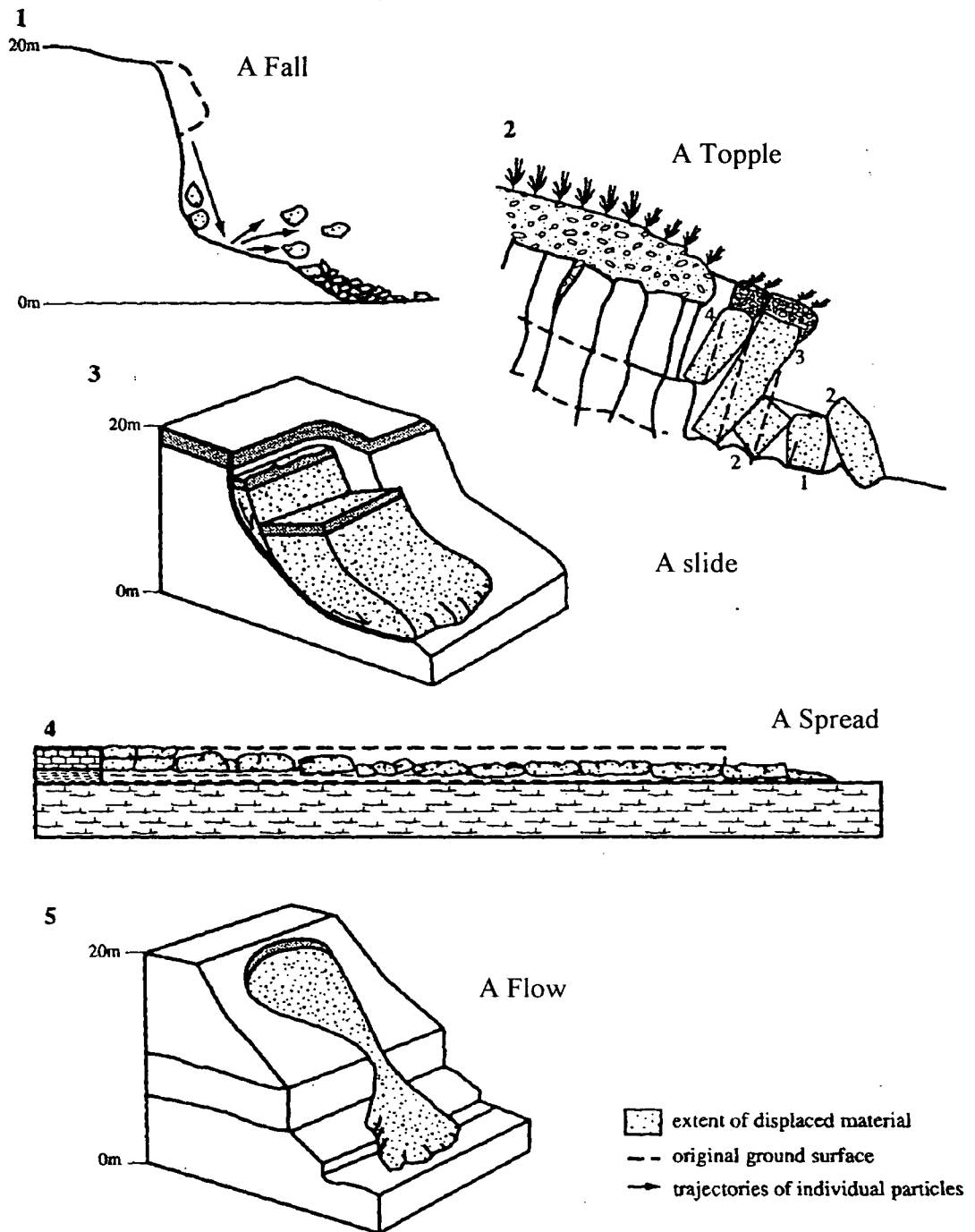
Figure 3.10 – Landslide Mechanisms (after Dikau *et al.*, 1996). The descriptions are given overleaf.

The descriptions for the different types of landslide mechanism shown in Figure 3.10 as stated by Dikau *et al.* (1996):

1. A fall starts with detachment of soil or rock from a steep slope along a surface on which little or no shear displacement takes place. The material then descends largely through the air by falling, saltation or rolling.

2. A topple is the forward rotation, out of the slope, of a mass occurring dominantly on surfaces of rupture or relatively thin zones of intense shear strain.

3. A slide is the downslope movement of a soil or rock mass occurring dominantly on surfaces of rupture or relatively thin zones of intense shear strain.

4. A spread is an extension of cohesive soil or rock mass combined with a general subsidence of the fractured mass of cohesive material into softer underlying material. The rupture surface is not a surface of intense shear. Spreads may result from liquefaction of flow (and extrusion) of the softer material.

5. A flow is a spatially continuous movement in which surfaces of shear are short-lived, closely spaced and usually preserved. The distribution of velocities in the displacing mass resembles that in a viscous fluid.

The type of material involved in the landslide should also be defined. Debris is material that is coarser than 2mm but usually describes an assortment of material including clasts incorporated into a matrix. Soil is finer than 2mm and rock is considered as a coherent, consolidated mass of a significant size and volume (BS5930, 1990).

While undertaking field mapping, it was observed that many of the slopes (including many of the landslides) exhibited smaller scale failure mechanisms than those described above. Nicholson *et al.* (2000) described these as slope deterioration processes. They defined it as the progressive alteration, detachment and removal of material from the surface of a parent rock mass by mechanical and chemical processes.

The slope deterioration scheme of Nicholson *et al.* (2000) was based on observations of man-made slopes and limited to relatively small scale surface processes (Figure 3.11). It was therefore designed with these slopes and processes in mind and not natural terrain landslides. However, it was decided to record which landslides in the landslide inventory for this project were affected by these processes and therefore use the Nicholson *et al.* (2000) scheme to classify them. This enables a more detailed understanding to be gained of the processes acting on the slopes of the study area, especially due to the large number of canyon slopes in the Rio Aguas study area.

However, this landslide investigation has already defined a minimum size limit for the landslides that are included in the landslide inventory. The criterion is a plan area of 10m^2, as well as identifiable/measurable backscar and/or debris accumulation. Therefore this means that slopes affected by the smaller-scale failures described in Figure 3.11 were considered too small to be mapped as individual landslides for this

project. However, where these mechanisms were present as secondary or tertiary mechanisms, they were recorded in the landslide inventory.

3.4.2.3 *Landslide Activity*

The terminology used in this landslide investigation to describe the state, style, distribution and rate of landslide movement, as well as the anatomy of the mapped landslides has followed that of the Working Party on the World Landslide Inventory (WP/WLI, 1990, 1993, 1994, 1995). The suggestions and recommendations of Hutchinson (1988), Dikau *et al.* (1996) and Turner & Schuster (1996) have also been followed. The definitions and codes used in the database are listed in Appendix C.
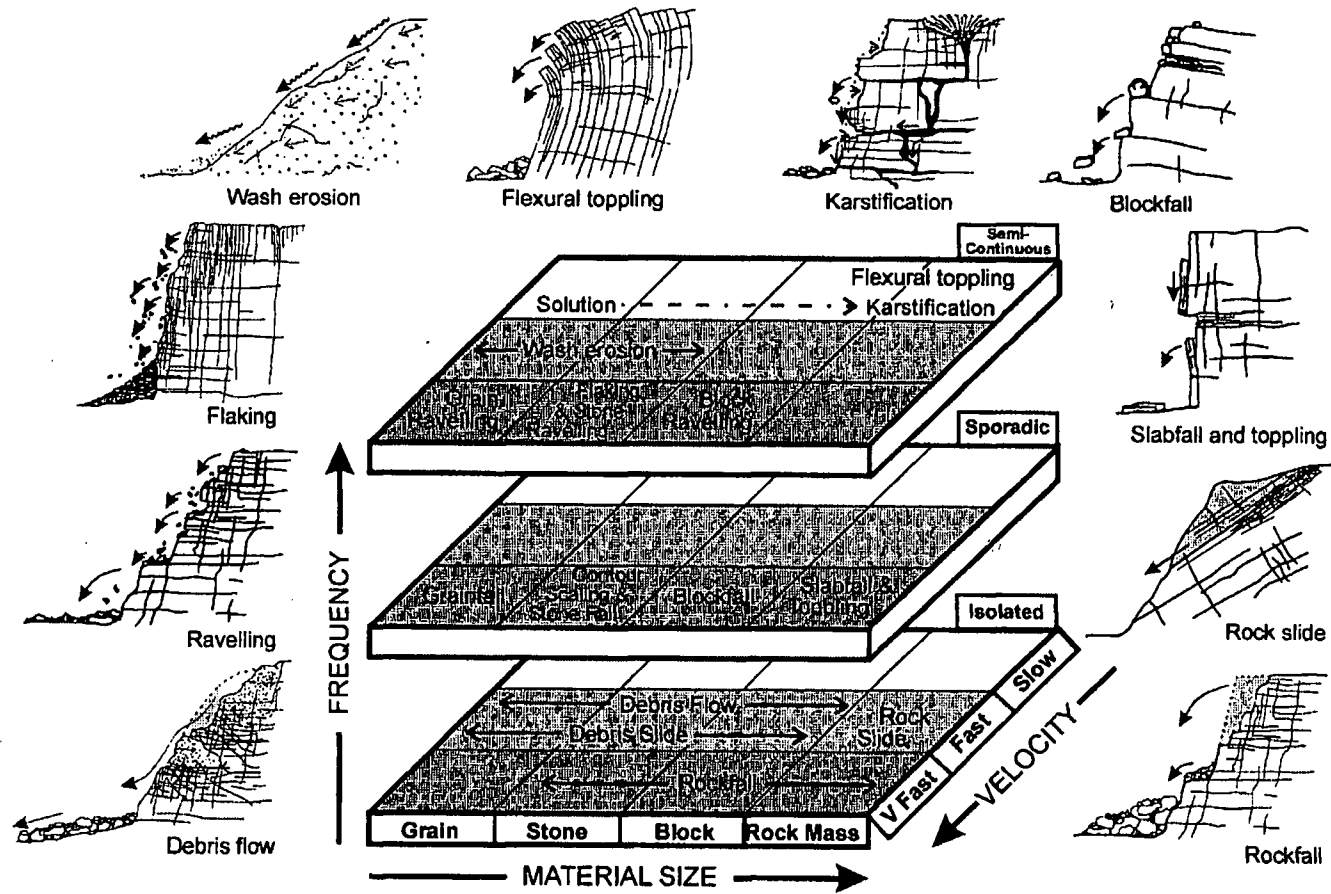
Figure 3.11 – Classification of slope deterioration processes (after Nicholson *et al.*, 2000).

3.4.2.4 *Landslide Causes*

The factors that cause landslides to occur can be differentiated into three categories

(Terzaghi, 1950; Crozier, 1986; Brunsden, 1988; WP/WLI, 1994; Dikau *et al.*, 1996;

Turner & Schuster, 1996):

1. Preparatory factors – the cumulative events which prepare the slope for failure but

    do not necessarily produce movement;

2. Triggering factors – those factors that initiate landsliding to occur; and

3. Sustaining factors – those factors that keep the material involved in motion, either

    intermittently or continuously.

For this investigation, those factors that could be identified (or inferred) as influencing

the stability of a slope or landslide were recorded in the landslide inventory (Appendix

C).

3.5 Chapter Summary

This chapter has described the "building blocks" of the Project – land surface evaluation and terrain classification, aerial photographic interpretation, field mapping and the landslide inventory. This description has included discussion of the various techniques, definitions and classifications that have been used

As part of the Land Surface Evaluation of the study area, a terrain classification has been developed for the Río Aguas Catchment study area. This terrain classification is based on the results of the aerial photographic interpretation and field mapping, and divides the study area into seven areas of similar geology, geomorphology and topography. It is this terrain classification that will form the basis of the ground model that will be presented in Chapter 6.

The design of the landslide inventory has been introduced, as well as the definitions of the different categories of the data which it contains. This database forms the fundamental database for this Project and was produced as a result of the landslide mapping which was a major part of the aerial photographic interpretation and field mapping. The results from a statistical analysis of this database will be presented in the following chapter (Chapter 4). A number of the landslides will also be presented as a series of "Landslide Type Localities" in Chapter 5.

Chapter 4 – Landslide Distribution Analysis

4 Landslide Distribution Analysis

4.1 Introduction

The landslide inventory map (Figure 4.1) shows the distribution of landslides in the study area. By studying the distribution of the landslides with respect to the geology and geomorphology of the study area, it is possible to gain a better understanding of how the landscape and drainage network have evolved over time. By studying the data recorded in the landslide inventory it is also possible to estimate the volume of material within the study area that is involved in landslide activity. This provides an insight into the rates of slope processes acting within the Río Aguas catchment study area.

Analysis of the landslide distribution will also highlight some of the factors that have been controlling the stability of the slopes in the study area, and allow the possible identification of those combinations of geology and geomorphology that are the most susceptible to failure. Field observations have shown that certain combinations of rock type and geomorphological setting tend to give rise to particular landslide failure mechanisms or other geological hazards (i.e., dissolution features). This information is vital when attempting to assess the nature and extent of the landslide susceptibility and hazard affecting the study area.

The aim of this chapter is, therefore, to present the results that have been obtained during this landslide investigation and specifically to discuss:

- The observed landslide distribution (Section 4.2);

- The role of geology and geomorphology in explaining the landslide distribution (Section 4.2);

- The observed mechanisms involved in slope failure (Section 4.2);

- The state, style and activity of the observed landslides (Section 4.2); and

- The controlling and triggering factors behind the landslide distribution (Section 4.3).
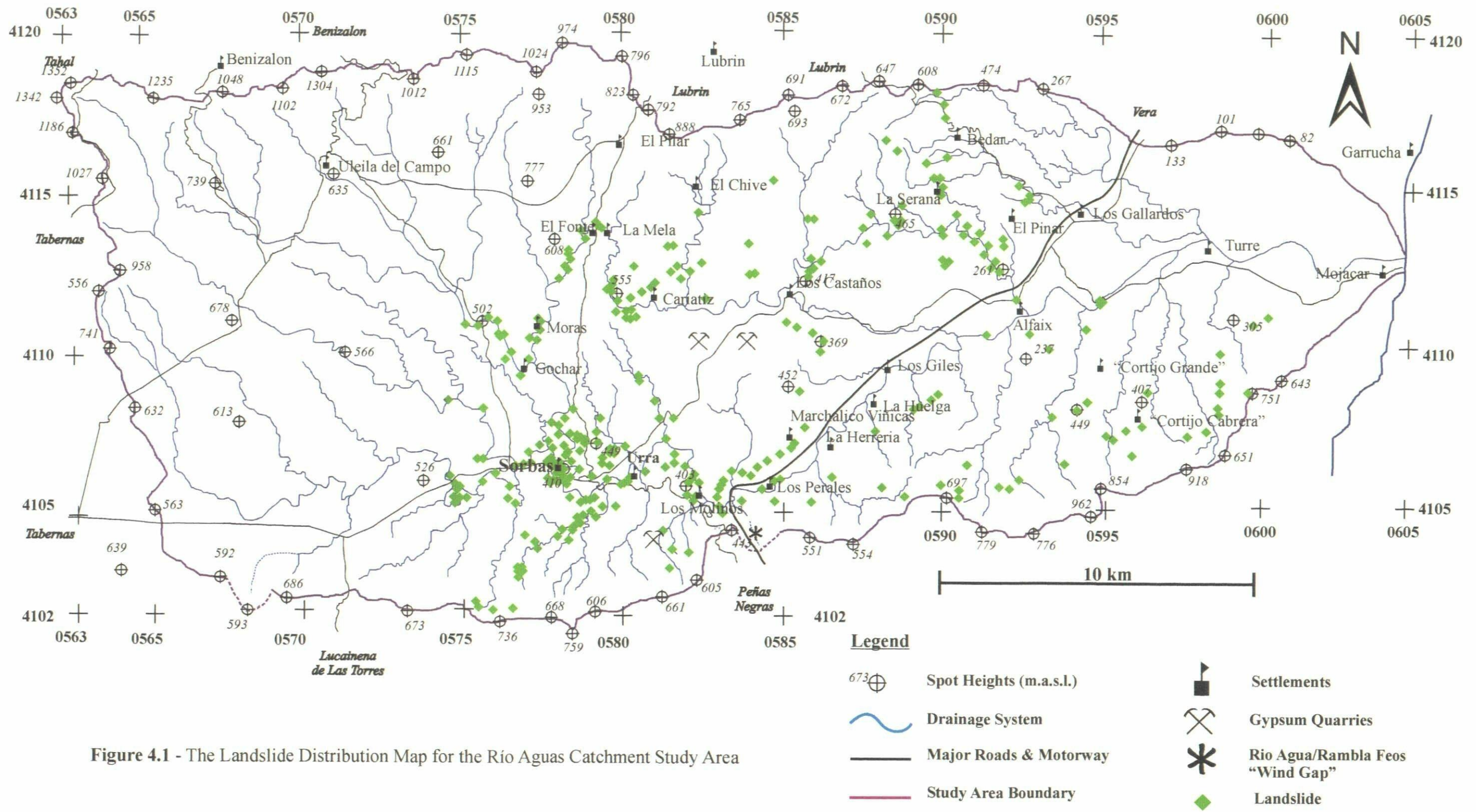
Figure 4.1 - The Landslide Distribution Map for the Río Aguas Catchment Study Area

Legend

$673 \oplus$ Spot Heights (m.a.s.l.)

〰 Drainage System

— Major Roads & Motorway

— Study Area Boundary

▪ Settlements

⚒ Gypsum Quarries

✳ Rio Agua/Rambla Feos "Wind Gap"

◆ Landslide

4.2 Analysis of the Landslide Inventory

Over 300 hundred landslides or areas of slope instability were identified within the study area. Of these, 316 have been described in detail in the landslide inventory. The remaining landslides or unstable areas were not mapped in detail because of either uncertainty in identification, difficulty in access, and/or a lack of suitable aerial photographic coverage for those areas. Over 75% of the mapped landslides have been described as "Clearly Identifiable" – a landslide where both the backscar and accumulation zone were clearly mappable without uncertainty (Figure 4.2). Landslides where there was a slight degree of uncertainty when mapping either the backscar or accumulation zone accounted for 6.6% and 8.2% of the 316 landslides respectively (Figure 4.2). The remaining 9.2% of the landslides (classified as "Other") are where the exact location of the backscar or accumulation zone was slightly debatable due to either the remote location not allowing full access to the landslide, or vegetation cover or shadowing affects on the aerial photographs.

As described in Chapter 3 the landslide mapping comprised an API (using 3 sets of aerial photographs) followed by field verification. Interestingly, the API accounted for only 54.4% of the landslides that were mapped (Figure 4.3). Of these approximately 21.5% were verified with limited fieldwork (observed at a distance due to difficult access) and approximately 25% with detailed field mapping. This means that over 45% of the landslides contained within the landslide inventory were only identifiable in the field (Figure 4.3). These figures may reflect the nature and size of the majority of the landslides that were mapped, as well as the scale of the black and white aerial photographs that were used for the majority of the study area.
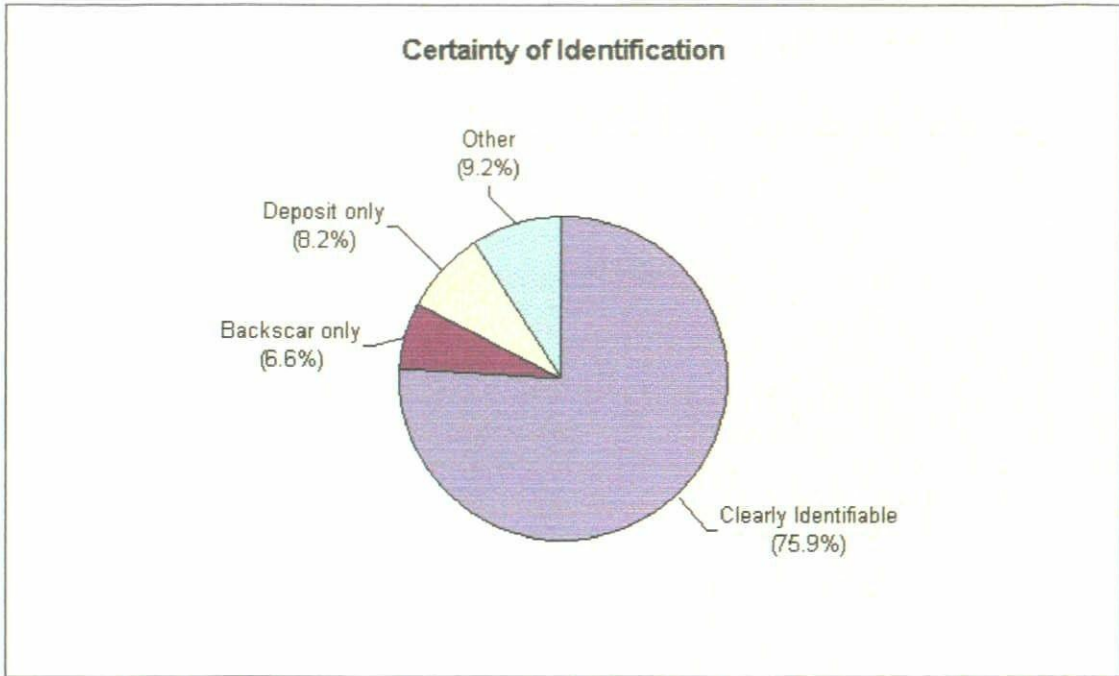
Figure 4.2 – Graph showing the certainty of identification of the mapped landslides
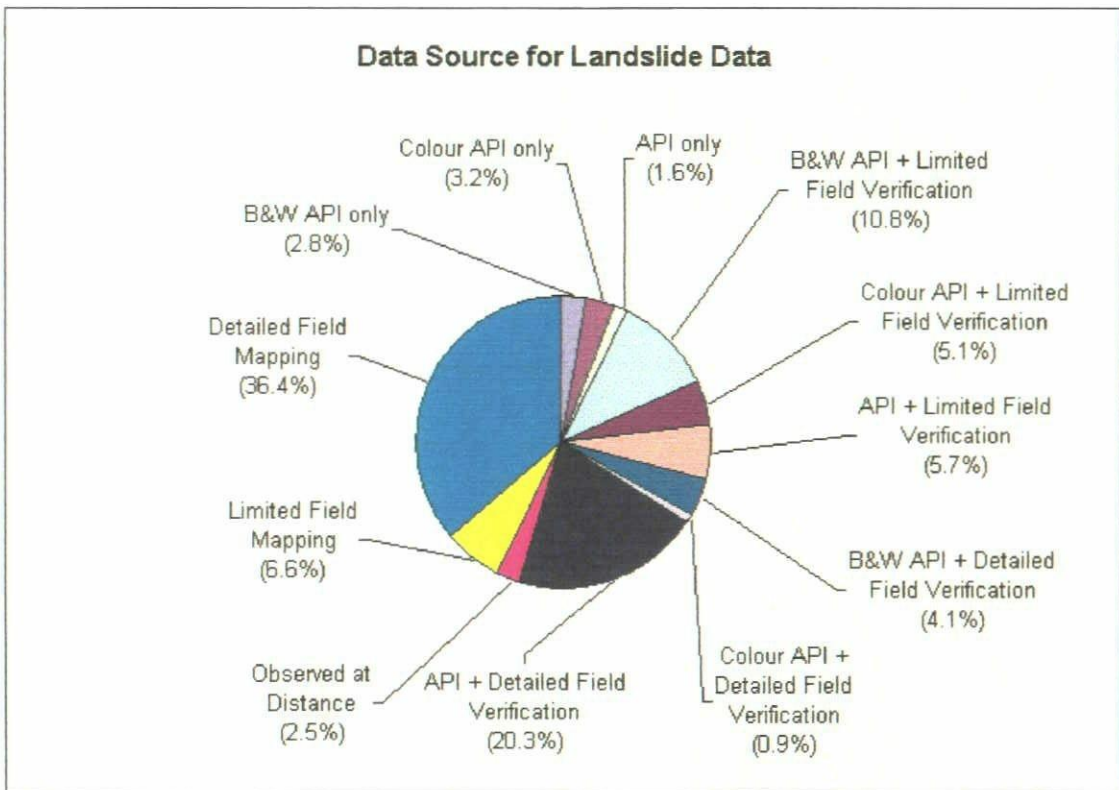
Figure 4.3 – Graph showing the data sources used to identify the mapped landslides

Of the 240 landslides that were classified as being "Clearly Identifiable" only 9 landslides (2.8%) were mapped using only the aerial photographs, and 78 of the landslides (24.7%) mapped using a combination of API and detailed field verification (Figure 4.4). The remaining 132 landslides (approximately 42%) were only identifiable in the field. The majority of the landslides that were classified as "Backscar Only" (where the backscar was clearly identifiable but there was some uncertainty of the exact location of the accumulation zone) were mapped using the aerial photographs and with only limited field verification (Figure 4.4).

The age and state of activity of a landslide will affect how clearly it is visible within the landscape. It is important, therefore, to consider how this may influence the landslide mapping and the data being used in this study. Of the 76% of the mapped landslides that are considered "Clearly Identifiable", almost 58% of them are considered "dormant" (Figure 4.5). A dormant landslide is defined as "a landslide that has not moved for more than one annual cycle of seasons, but where the causes of movement apparently remain" - WP/WLI, 1993). "Relict" landslides (WP/WLI, 1993) which would normally be considered to be the most difficult to identify within a landscape, would perhaps be expected to make up a large proportion (if not the majority) of the landslides not established as "Clearly Identifiable". However, this is not the case. The majority of "relict" landslides were in fact classified as being "Clearly Identifiable" (Figure 4.5). This could be a reflection of the relatively "young" nature of this landscape and/or the size and type of failures involved.

A more detailed analysis of the state of landslide activity within the study area will be described later.
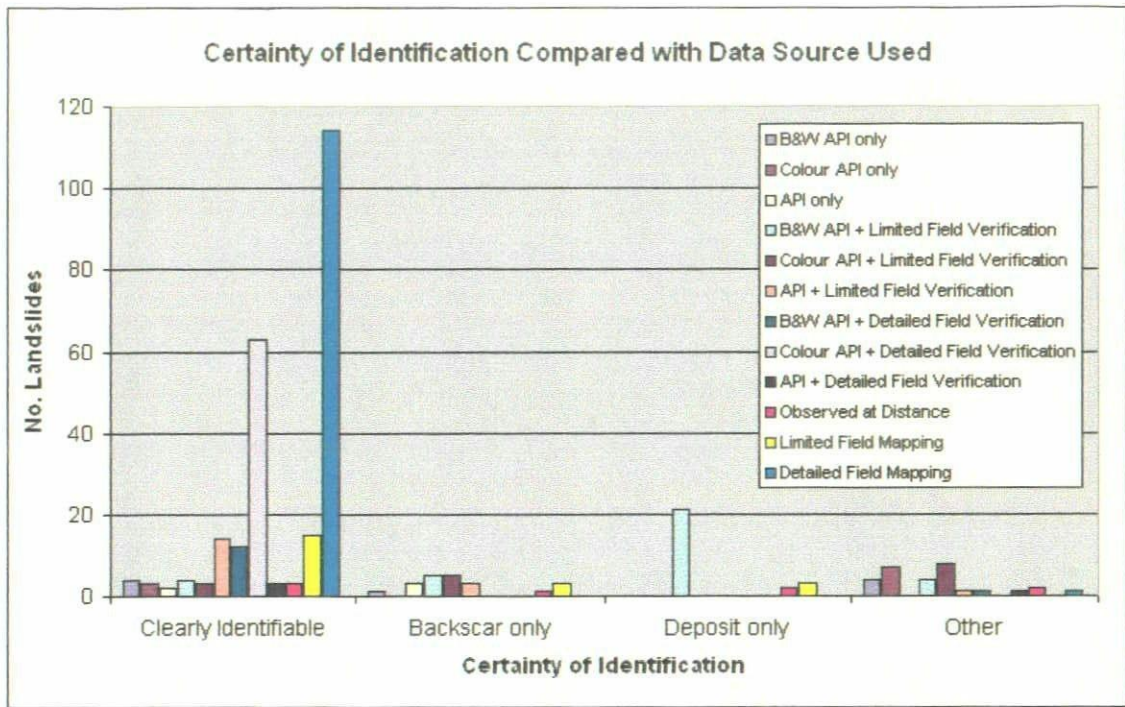
Figure 4.4 – Graph showing the certainty of identification of the mapped landslides compared with the source of the data used.
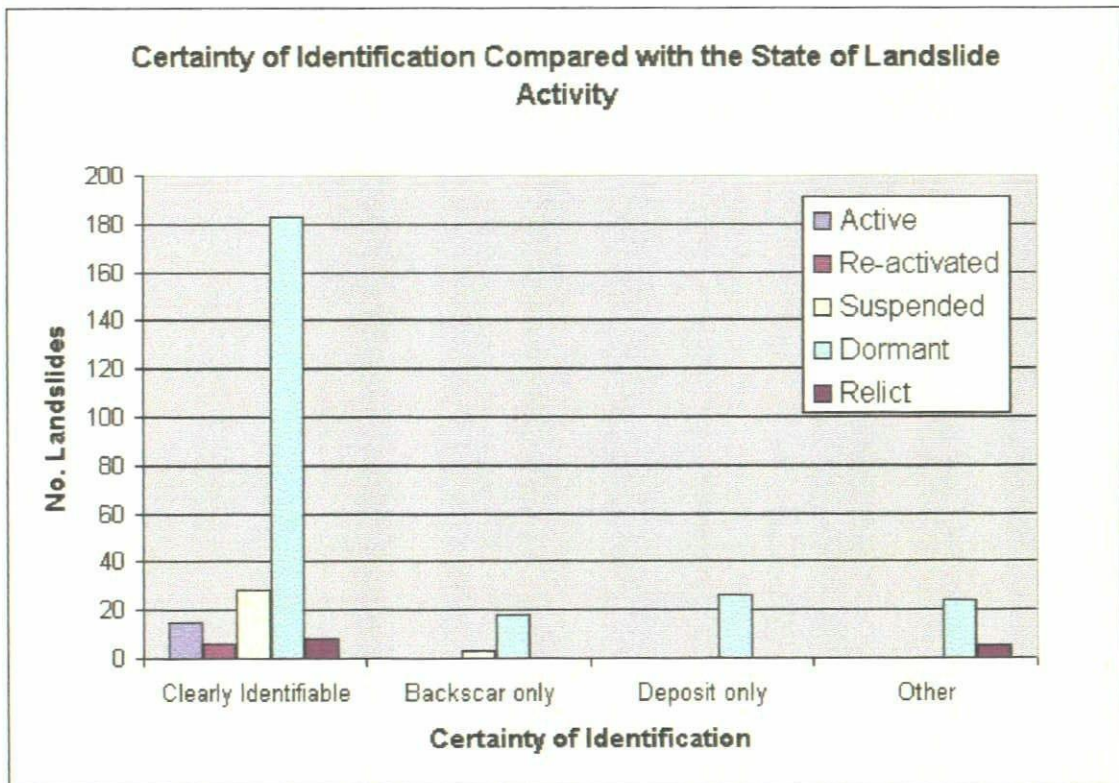
Figure 4.5 – Graph showing the certainty of landslide identification compared with the state of landslide activity.

The following sections describe the analysis of the landslide inventory that has been completed. This analysis has helped to identify those factors that are relevant in either controlling or leading to, the observed landslide activity within the study area. Subsequently these results have been used to develop a ground model for the study area.

4.2.1   Landslide Distribution & Density

The landslide inventory for this study contains detailed data for 316 landslides for a study area of approximately 425km^2. This means that the Río Aguas Catchment (and therefore this study area) has a landslide density of approximately 0.75 landslides/km^2. Compared with other areas in southern Spain (Table 4.1) this figure is relatively low. However, this may reflect the nature of the study area. The other areas listed in Table 4.1 are more specific areas that were studied because of their high concentration of landslide activity, whereas the study area used by this project is based on the fundamental unit of geomorphology – a catchment area.

Table 4.1 – Landslide density figures for other areas in southern Spain

Area	Area (km^2)	No of Landslides	Landslide Density (landslides/km^2)	Reference
Río Aguas Catchment	425	316	0.75	This study
Albunelas river basin, Granada	89	215	2.42	Hamdouni *et al.*, 1996
Contraviesa area, Granada, south of the Sierra Nevada and the Guadalfeo river	94	898	9.55	Fernández *et al.*, 1996
Colmenar area, Malaga	234	133	0.57	Irigaray *et al.*, 1996a
Genil River area	503	800	1.6	Irigaray *et al.*, 1996b

However, this figure for the Río Aguas Catchment Area does not reflect the actual distribution of the observed landslide activity. Even with a cursory glance at the landslide distribution map for the Río Aguas (Figure 4.1) it is apparent that the majority

of the landslides are very closely associated with the drainage network and are primarily found in four parts of the study area:

1. Close to the town of Sorbas – this is the largest "cluster" of landslides in the study area

2. Close to the village of Cariatiz

3. Close to the village of Góchar

4. Along a section of the Río Jauto

There also are a number of smaller clusters of landslides within the Sierra Cabrera.

The landslide distribution has been investigated further with the use of a landslide isopleth or density map (Figure 4.6). This map has been constructed using the technique described by Hansen (1984) and Wright & Nilsen (1974). However, due to the scale of the maps being used and the size of the majority of the landslides that have been mapped it was decided to count the number of landslides per counting circle instead of calculating the areas of the landslides within the counting circle. Figure 4.6 confirms the presence of the clusters described above.

The largest concentration of landslides is found in the south central part of the study area (around the town of Sorbas). This is 10 km upstream from the area where the Río Aguas/Rambla Feos river capture occurred (as described in Section 2.4) approximately 100,000 years BP (Harvey & Wells, 1987). Interestingly, the landslide distribution and landslide isopleth maps (Figures 4.1 and 4.6) show that this cluster of landslides only extends upstream as far as a series of nick points that have been mapped in the field (Figure 4.7). It is argued here that these nick points relate to the "Wave of Incision" (Griffiths et al., 2002, 2003) that has worked upstream from the site of the river capture.

These nick points are picked out in the river profile diagrams in Section 2.4 (Figures 2.6 and 4.8) where the gradient becomes relatively steeper.

When the landslide distribution is added to these profiles it is noticeable that the landslides are clustered along those sections of the drainage network with the steepest gradients, which for the Río Aguas is upstream of the Río Aguas/Rambla Feos river capture site near to Los Molinos (Figures 4.8). The following sections will look more closely at the relationship between the mapped landslide activity and the geomorphological, morphological and slope settings of those landslides. It should also be noted that there are a number of sizeable landslides downstream of the river capture site.

Interestingly, the western end of the study area is almost conspicuous by the absence of any mapped landslides. The southwest corner of the study area is relatively flat terrain with few slopes. The reasons for the apparent absence of landslides in the Sierra de Los Filabres (the northwestern corner of the study area) will be discussed later in this chapter.
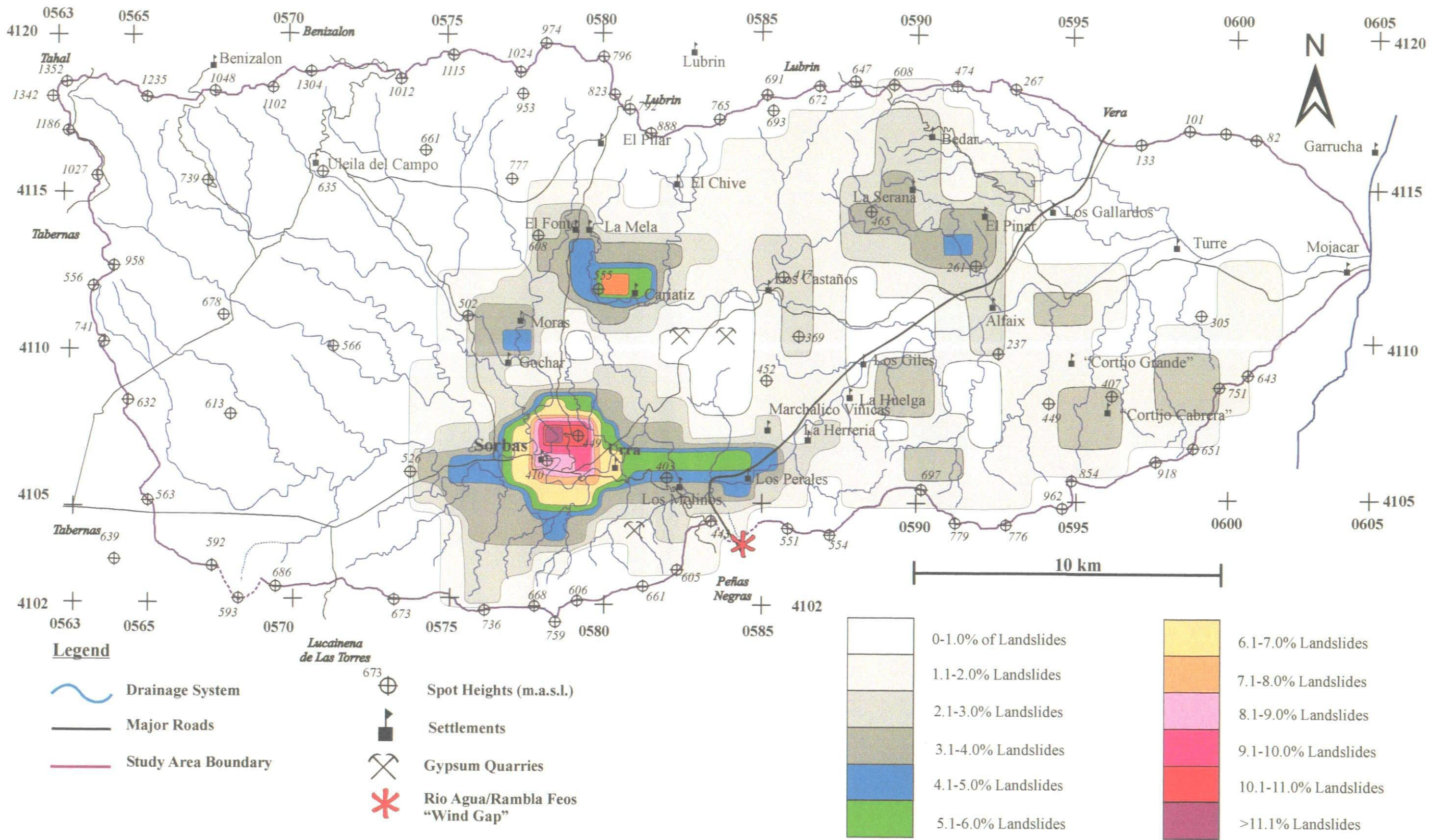
Figure 4.6 - Landslide Isopleth Map for the Rio Aguas Catchment Study Area.
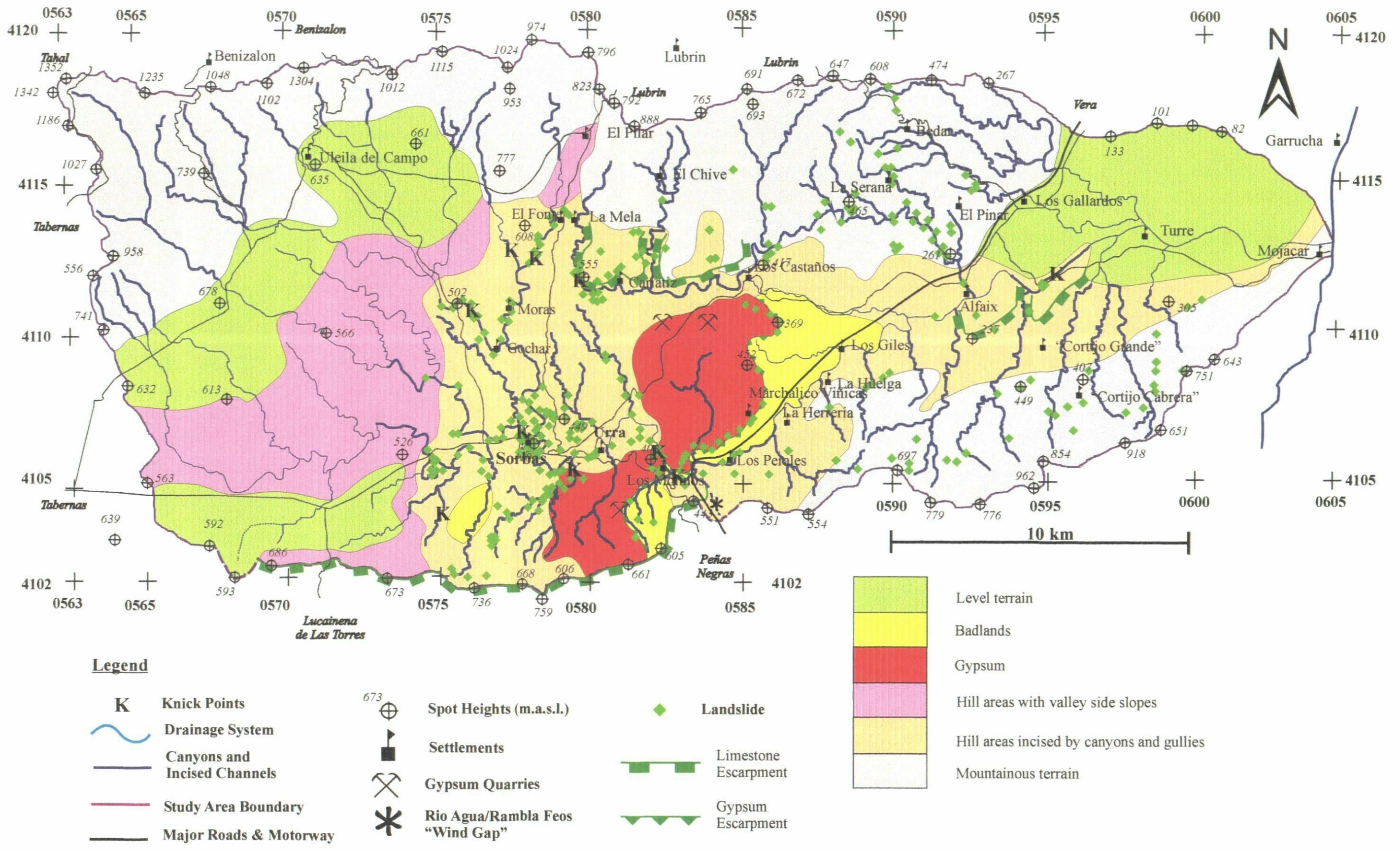
Figure 4.7 - A map of the landforms found in the Río Aguas Catchment Study Area and the landslide distribution. .

Legend

K   Knick Points

Drainage System

Canyons and Incised Channels

Study Area Boundary

Major Roads & Motorway

$\oplus$ 673   Spot Heights (m.a.s.l.)

Settlements

Gypsum Quarries

Rio Agua/Rambla Feos "Wind Gap"

Landslide

Limestone Escarpment

Gypsum Escarpment

Level terrain

Badlands

Gypsum

Hill areas with valley side slopes

Hill areas incised by canyons and gullies

Mountainous terrain

10 km
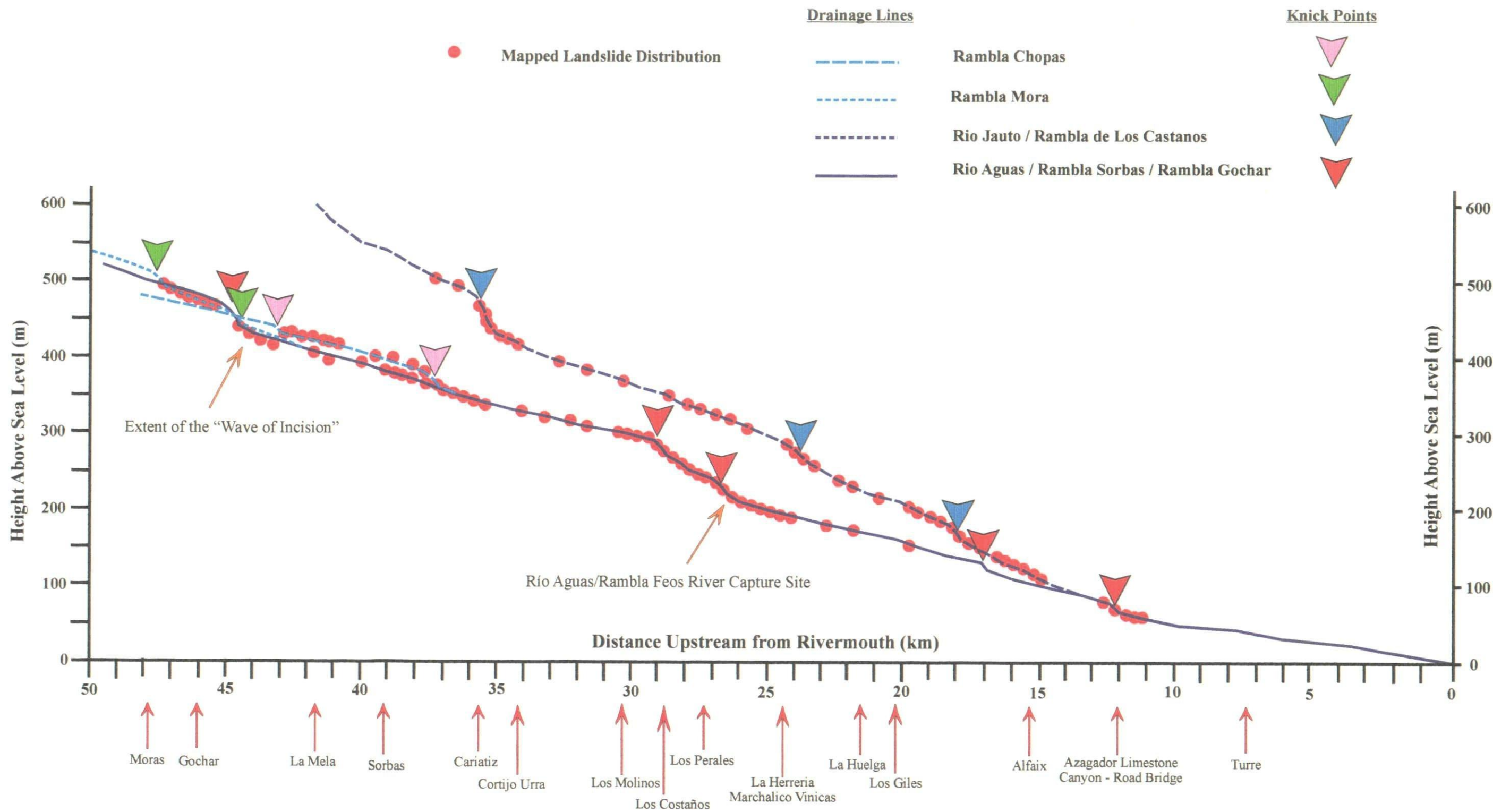
Figure 4.8 - Profiles of the Río Aguas, the Río Jauto and some of their major tributaries with the landslide distribution.

4.2.2 Slope Setting & Morphology

The majority of the mapped landslides (44.6%) in the study area were classified as occurring along "escarpments" (Figure 4.9). This also included those landslides that occurred on cliffs or canyon walls. This observation is in agreement with the analysis of the slope angle data.

The slope angle class data show that as the angle of the slope on which the landslide occurred increases so does the landslide incidence (Figure 4.10). A comparison of the slope angle classes with the simplified slope profile data shows a similar relationship (Figure 4.11). The majority of the backscars of the mapped landslides occur on slopes above 75° have been classified as being either canyon walls or escarpments.

Slope aspect does not appear to be influential in controlling the mapped landslide distribution (Figure 4.12). However, there do appear to be slightly more landslides on west facing slopes. This could be a reflection of the drainage pattern, which in some parts of the study area trends roughly north – south. This pattern is also a reflection of the tectonic setting of the study area and surrounding region.
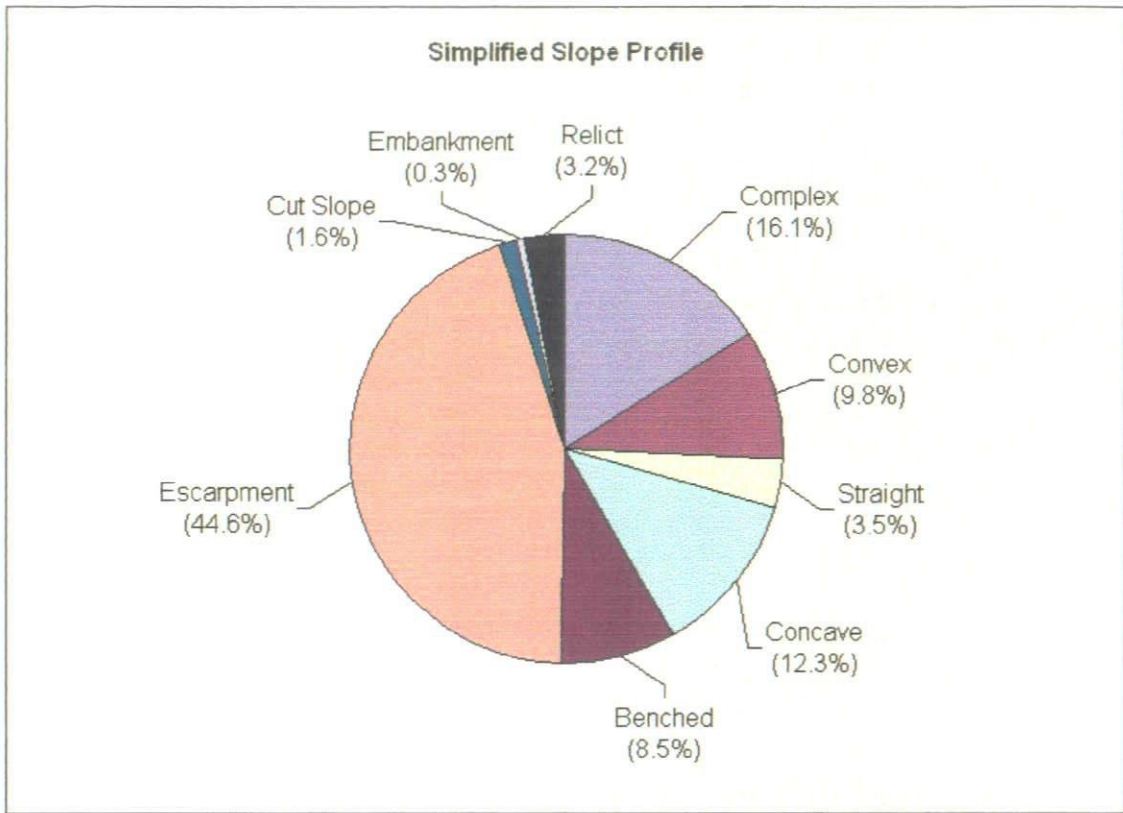
Figure 4.9 – Graph showing the breakdown of mapped landslides in the simplified slope profile units used by this study.
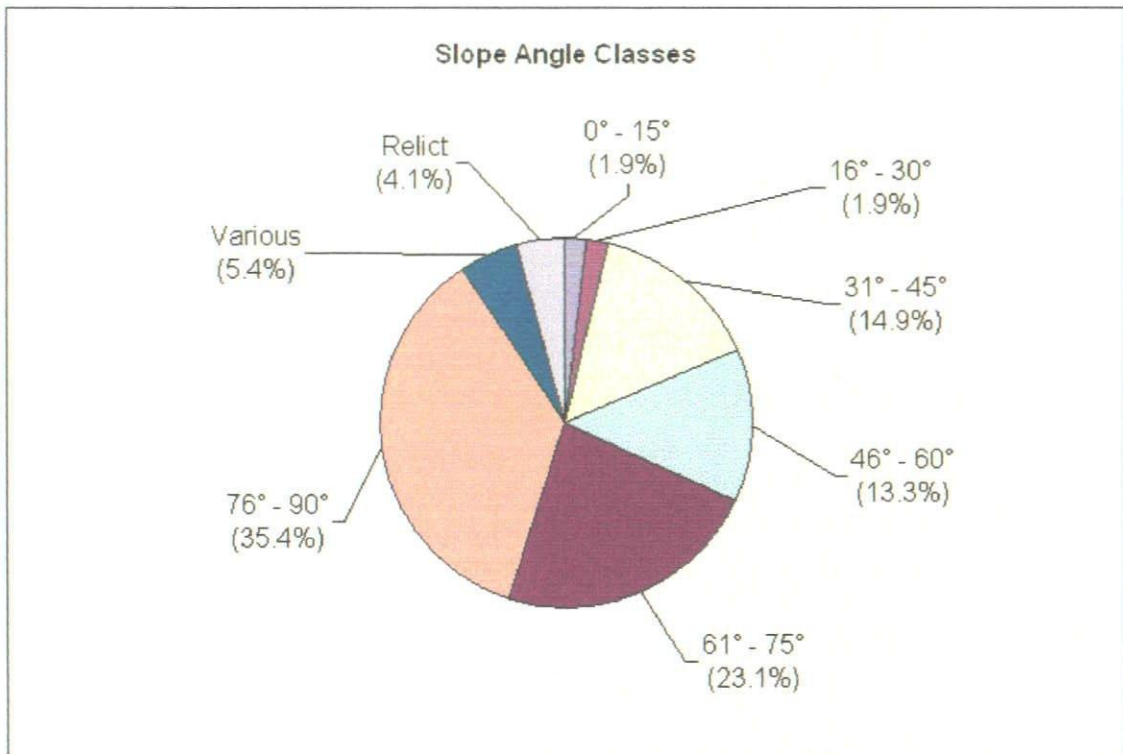
Figure 4.10 – Graph showing the breakdown of mapped landslides in the slope angle classes used by this study.
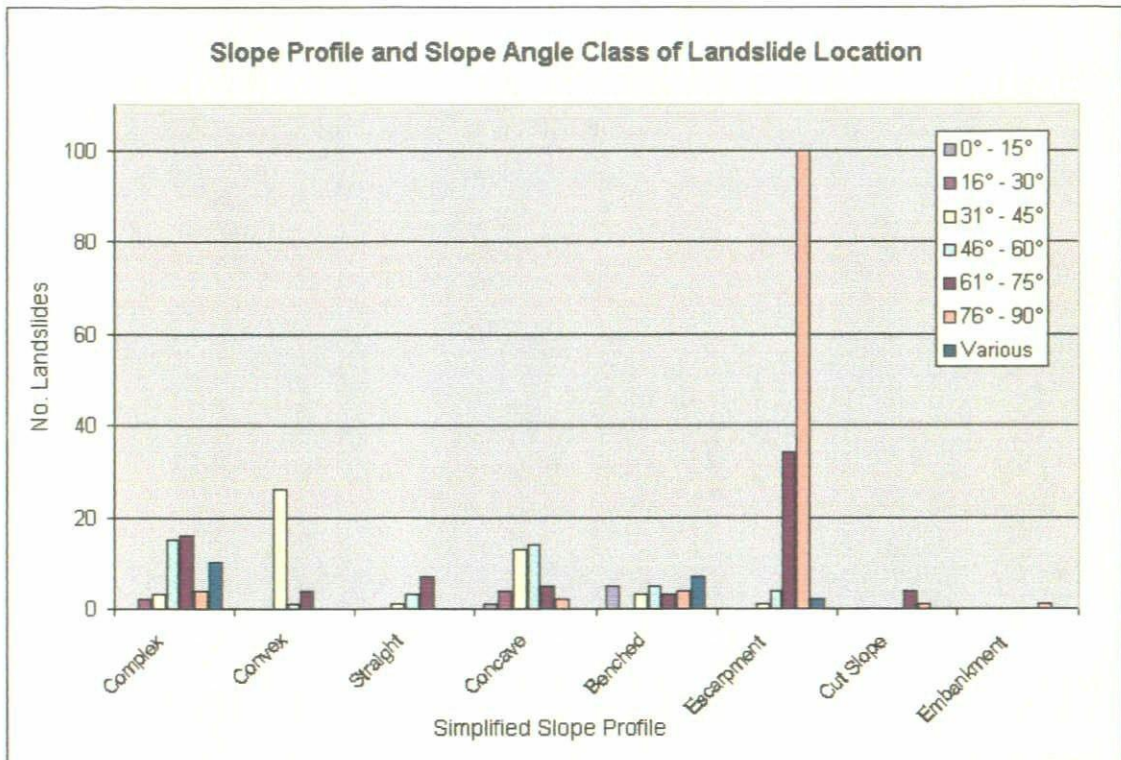
Figure 4.11 – Graph showing the slope angle classes compared with the simplified slope profile data for the landslides mapped by this study
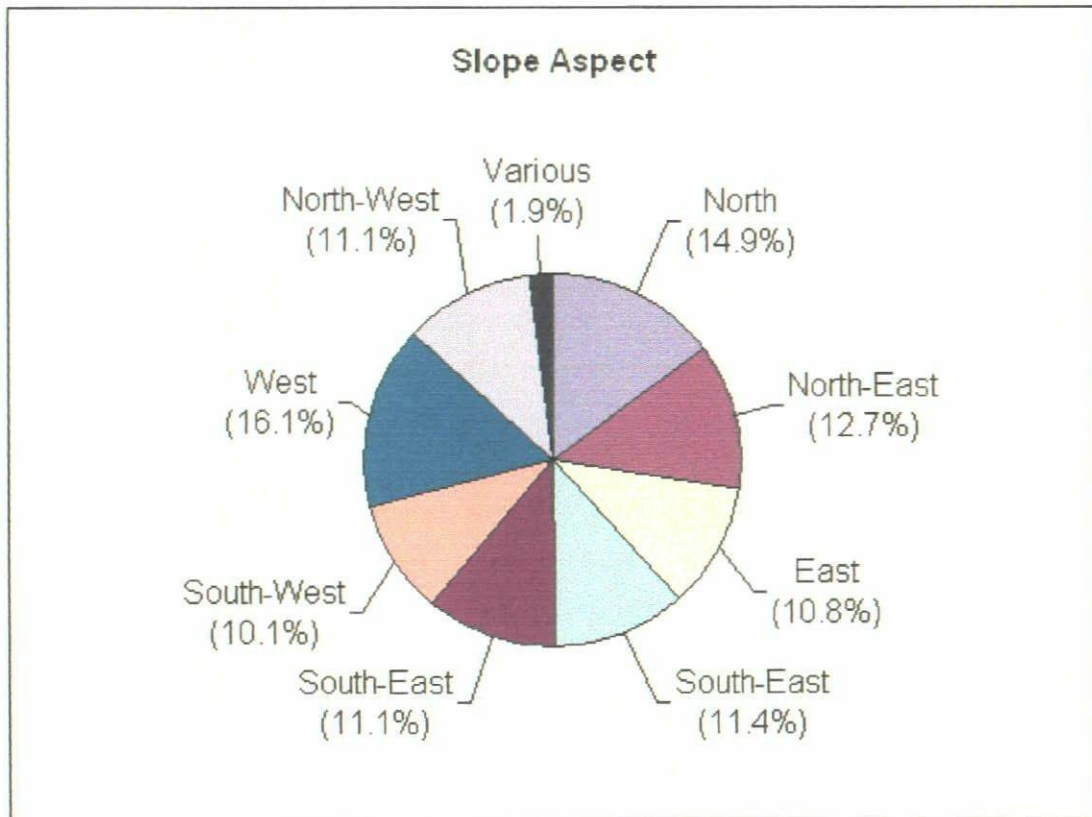
Figure 4.12 – Graph showing the breakdown of mapped landslides in the slope aspect classes used by this study

4.2.3 Terrain Classification

During the aerial photographic interpretation and field mapping it was apparent that the landslides occurred in certain geomorphological settings. This is because the Land Systems, Facets and Elements of the study area will reflect the underlying geology and the geomorphological history of the study area. Therefore, this section will consider which are the most susceptible combinations of Land Facet and Land Element within each of the Land Systems used by this study, for landslide activity.

Using the descriptions of the study area described in Section 3.2.3, 52.8% of the mapped landslides occur in "hill areas incised by canyons and gullies" (Figure 4.13 and Table 4.2). It should be noted that this class covers a large part of the central part of the study area. Landslides occurring in areas classified as being either "mountainous slopes incised by gullies, canyons and river channels" or "hill areas with river valley slopes" account for 24.4% and 13.3% of the landslides respectively.

Table 4.2 shows the results from a detailed analysis of the landslide inventory database. It shows the number of landslides occurring in each of the combinations of Land System, Facet and Element that were encountered in the study area. In the majority of these combinations only a small number of landslides were mapped. In these cases it is unlikely that this is a "susceptible" combination and there could be other reasons for the mapped landslide activity. However, the analysis has highlighted some combinations that could be regarded as "susceptible combinations". These combinations have been highlighted in Table 4.2 by a five-fold colour scheme, as well as summary Table 4.3.

Land Systems of the Rio Aguas Study Area affected by landslide activity

Gypsum Plateau & Karst 2.5%

Neogene Hill areas with river valleys 13.3%

Mountains in Basement Material 24.4%

Neogene Hill areas with incised drainage 59.8%
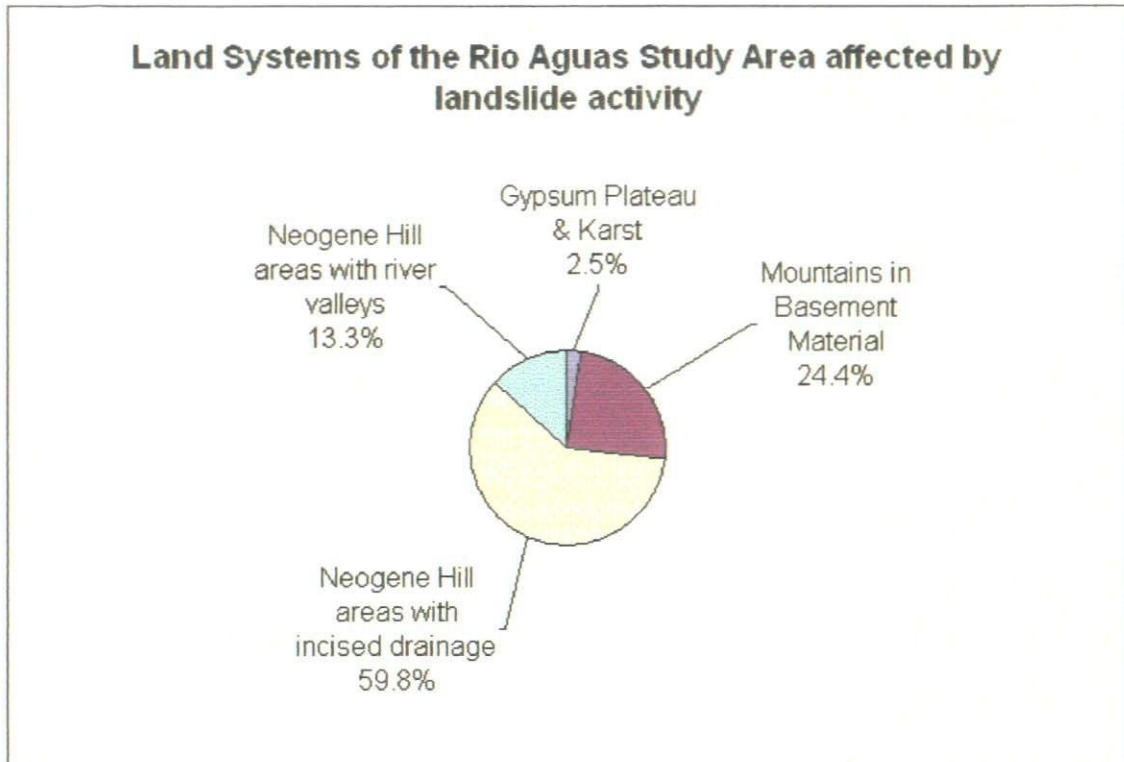
Figure 4.13 – Graph showing the breakdown of mapped landslides in the Land System classes used by this study

Legend for Table 4.2

No. Landslides	% Range
> 6	> 1.9%
7 – 12	2.2 – 3.8
13 – 18	4.1 – 5.7
19 – 25	6.0 – 7.9
< 26	< 8.2%

Table 4.2 – Distribution of mapped landslides within the terrain classification used by this study

Land System	Land Facet	Land Element
1. Gypsum Plateau & Karst (2.5%)	Open river valley formed by the dissection of the drainage channel without river terraces (2.5%)	Scarp-slope escarpment (2.5%)
2. Mountain slopes incised by gullies, canyons and river channels (24.4%)	Hill and Mountain slopes (10.4%)	Ridge crest (7.0%)
		Scarp-slope escarpment (0.6%)
		Valley side slopes (0.3%)
		Outside meander of active drainage channel (0.3%)
		Mountain side slope (1.3%)
	Incised drainage channels without river terraces (13.9%)	Ridge crest (1.3%)
		Valley side slope (0.9%)
		Canyon side slope (5.4%)
		Inside meander of active drainage channel (0.9%)
		Outside meander of active drainage channel (3.2%)
		Outside meander of abandoned drainage channel (0.6%)
		Mountain side slope (1.6%)
4. Hill areas with river valley side slopes (13.3%)	Open river valley formed by the dissection of the drainage channel with river terraces (4.7%)	Ridge crest (0.3%)
		Dip-slope mid-slope (0.3%)
		Mountain & valley side slopes (0.9%)
		Gully side slope (0.3%)
		Outside meander of active drainage channel (2.5%)
		Outside meander of abandoned drainage channel (0.6%)
		Inside meander of abandoned drainage channel (0.3%)
	Open river valley formed by the dissection of the drainage channel without river terraces (4.7%)	Dip-slope escarpment (0.9%)
		Valley side slope (0.9%)
		Outside meander of active drainage channel (1.6%)
		Gully side slope (1.3%)
		Gully side slope (0.6%)
		Valley side slope (1.9%)
	Hill and Mountain slopes (1.3%)	Dip-slope mid-slope (1.3%)

3. Hill areas with incised by canyons and gullies (59.8%)	Hill and Mountain slopes (0.9%)	Dip-slope mid-slopes (0.3%)
		Valley side slopes (0.6%)
	Incised drainage channel with river terraces (38.3%)	Scarp-slope escarpment (5.4%)
		Dip-slope escarpment (6.6%)
		Scarp-slope mid-slope (0.3%)
		Dip-slope mid-slope (0.6%)
		Valley side slope (2.8%)
		Canyon side slope (3.5%)
		Gully side slope (0.9%)
		Inside meander of active drainage channel (2.2%)
		Outside meander of active drainage channel (12.0%)
		Inside meander of abandoned drainage channel (0.3%)
		Outside meander of abandoned drainage channel (2.2%)
		Cut slope (1.3%)
	Incised drainage channel without river terraces (14.6%)	Scarp-slope escarpment (0.6%)
		Dip-slope escarpment (2.8%)
		Dip-slope mid-slope (0.9%)
		Valley side slope (1.3%)
		Canyon side slope (1.3%)
		Gully side slope (0.3%)
		Inside meander of active drainage channel (0.3%)
		Outside meander of active drainage channel (7.0%)
	Gully system (6.0%)	Dip-slope mid-slope (0.3%)
		Gully side slope (3.2%)
		Inside meander of active drainage channel (1.3%)
		Outside meander of active drainage channel (0.9%)
		Mountain side slope (0.3%)

Table 4.3 – Summary table of the distribution of mapped landslides within the terrain classification used by this study

Land System (Approximate % of mapped landslides)	Key Findings from Table 4.2 (Land Facet / Land Element / % of the mapped landslides*)
1. Gypsum Plateau and Karst (2.5%)	• River valley formed by the dissection of the drainage system • Scarp-slope escarpment • 2.5% of the mapped landslides (8 landslides)
2. Mountain slopes incised by gullies, canyons and river channels (24.4%)	• Hill and mountain area • Ridge crests • 7.0% of the mapped landslides (22 landslides)
	• Incised drainage channels with river terraces • Canyons side slopes • 5.4% of the mapped landslides (17 landslides)
	• Incised drainage channels without river terraces • Outside meanders of active drainage channels • 3.2% of the mapped landslides (10 landslides)
3. Hill areas with incised drainage channels (59.8%)	• Incised drainage channels with river terraces • Outside meanders of active drainage channels • 12.0% of the mapped landslides (38 landslides)
	• Incised drainage channels with river terraces • Dip-slope escarpments • 6.6% of the mapped landslides (21 landslides)
	• Incised drainage channels with river terraces • Scarp-slope escarpments • 5.4% of the mapped landslides (17 landslides)
	• Incised drainage channels with river terraces • Canyon side slopes • 3.5% of the mapped landslides (11 landslides)
	• Incised drainage channels without river terraces • Outside meanders of active drainage channels • 7.0% of the mapped landslides (22 landslides)
	• Gully system • Gully side slope • 3.2% of the mapped landslides (10 landslides)
4. Hill areas with gentle valley side slopes (13.3%)	• No combination with significant numbers of mapped landslides

* = These percentages will not add up to 100% as this is a summary table showing extracts from Table 4.2.

The above table (Table 4.3) highlights the apparent importance of both incised drainage channels (with river terraces) and the outside meanders of active drainage channels. This fits with observations made during the field mapping and aerial photographic interpretation.

Within the "mountain slopes" Land System, the most "susceptible" combinations for landslide activity involve ridge crests or areas where the drainage has been incised to form canyons. The most "susceptible" combinations within the "hill areas with incised drainage" Land System involve the outside meanders of active drainage channels that have been incised. Dip-slope and scarp-slope escarpments are also seen to be "significant" for landslide activity. The majority of these landslides fall within the area influenced by the Río Aguas/Rambla Feos river capture and the subsequent "wave of incision" that has influenced the formation of the present Río Aguas.

Although 13.3% of the mapped landslides occur within the Land System "hill areas with gentle valley side slopes", they do not occur in any "significant" concentrations in any of the possible Land System, Facet and Element combinations. Interestingly, considering the number of landslides used in this study (316 mapped landslides) there are not many combinations of Land System, Facet and Elements with "significant" clusters of landslides. This is probably due to the fact that due to the complexity of the classification scheme used by this study, there are a large number of combination possibilities.

4.2.4   Geology and Lithology

The field mapping involved the mapping of the geology and geomorphology of the study area, as well as the landslide distribution. This means that for each entry within the landslide inventory, the geological formations and/or members were recorded as well as the lithological units that were involved in the observed landslide. Both sets of data have been analysed.

By overlaying the landslide distribution on the geology map for the study area it is possible to quickly identify those lithological units or combinations of units that are involved with the landslide activity of the study area (Figure 4.14).

The majority of the mapped landslides have occurred within the Nevado-Filabride Complex, the Sorbas Member, the Góchar Formation or the Azagador Member (16.8%, 15.5%, 12.3% and 9.5% of the mapped landslides respectively; Figure 4.15). However, there is not much of a difference between these units and the other units that have been mapped. This result does not help gain an understanding of the landslide activity in the study area. This is due to the fact that geological formation or member names do not necessarily indicate the rock type (or lithology) of the material involved in the landslide. Therefore it is crucial to analysis the lithological data that have been collected.

The majority of the mapped landslides were seen to occur in conglomerate, limestone, sandstone or mica schist (14.6%, 13.9%, 10.1% and 10.4% of the mapped landslides respectively; Figure 4.16). Approximately 26% of the landslides involve basement geology such as mica schist, gneiss, phyllite or combinations of these. It should also be noted that over 42% of the mapped landslides involve more than one rock type, and that these combinations are predominantly "hard rock" over "soft rock".

Figure 4.14 - The Lithology Map for the Río Aguas Catchment Study Area & the Landslide Distribution.
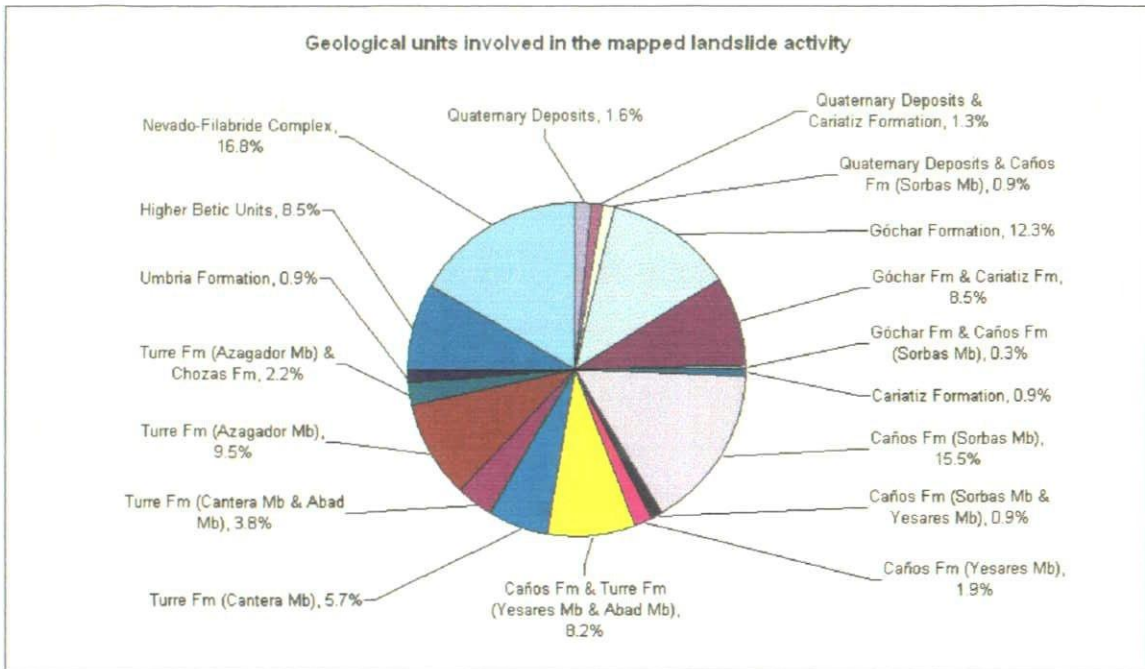
Figure 4.15 – Graph showing the geological units involved in the mapped landslide activity of the study area.
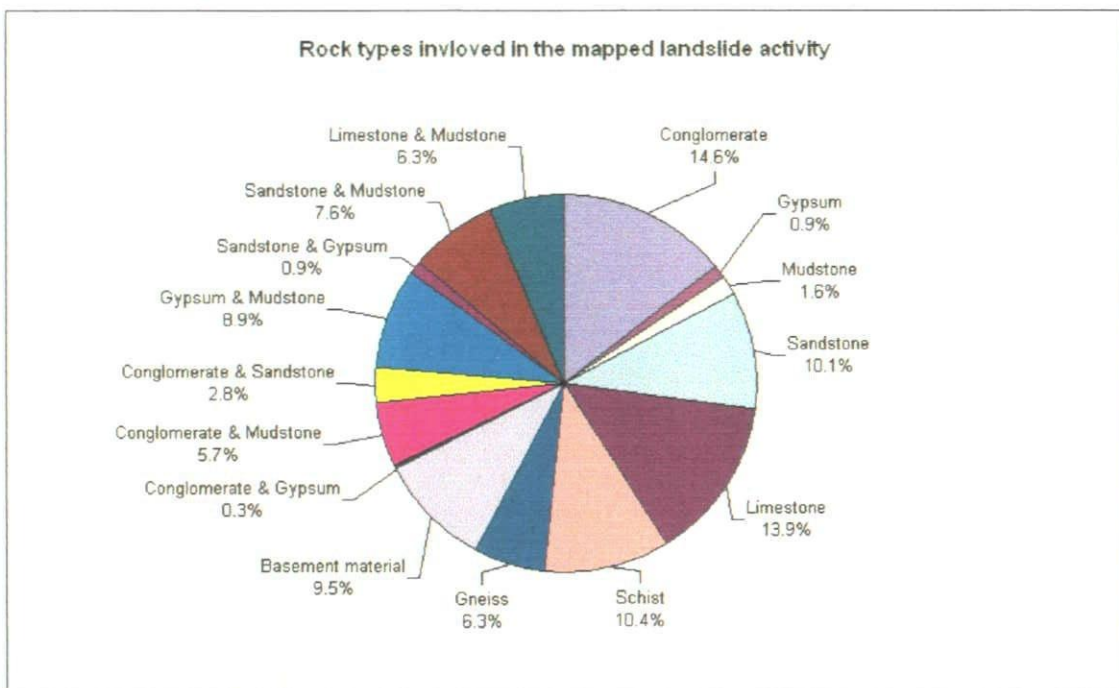
Figure 4.16 – Graph showing the lithological units involved in the mapped landslide activity of the study area.

Again, the spread of the data is not very large, restricting the number of conclusions that can be drawn. To gain a better idea of how the geology is controlling the landslide activity of the study area further analysis has been completed comparing the geology with the geomorphological location and failure mechanisms of each mapped landslide. The results from these analyses will be described in subsequent sections of this chapter.

4.2.5 Geology and Terrain Classification

The occurrence of a landslide is related to the material involved and the geomorphological location. It has been shown in previous sections that the majority of the landslides occur in areas where the drainage channel has been incised, and particularly in the outside of active meanders. But which are the rock types that are least favourable to slope stability in these locations?

An analysis has been completed looking at the number of landslides occurring in the different combinations of Land System, Facet and Element and rock type which were recorded in the landslide inventory. The results from the analysis are presented in Table 4.4 and a summary of those combinations with the highest percentages are presented in Table 4.5.

Table 4.4 – Distribution of mapped landslides within the terrain classification and rock type combinations used by this study.

Land System	Land Facet	Land Element	Rock Type
1. Gypsum Plateau & Karst (2.5%)	Open river valley formed by the dissection of the drainage channel without river terraces (2.5%)	Scarp-slope escarpment (2.5%)	Gypsum over lying mudstone (2.5%)
2. Mountain slopes incised by gullies, canyons and river channels (24.4%)	Hill and Mountain slopes (10.4%)	Ridge crest (7.0%)	Schist (2.2%)
			Basement (4.7%)
		Scarp-slope escarpment (0.6%)	Limestone (0.6%)
		Valley side slopes (0.3%)	Limestone (0.3%)
		Outside meander of active drainage channel (0.3%)	Gneiss (0.3%)
		Mountain side slope (1.3%)	Schist (0.6%)
			Gneiss (0.3%)
			Basement material (1.3%)
	Incised drainage channel without river terraces (13.9%)	Ridge crest (1.3%)	Schist (0.3%)
			Basement material (0.9%)
		Valley side slope (0.9%)	Gneiss (0.9%)
		Canyon side slope (5.4%)	Schist (4.7%)
			Gneiss (0.6%)
		Inside meander of active drainage channel (0.9%)	Schist (0.3%)
			Basement material (0.6%)
		Outside meander of active drainage channel (3.2%)	Schist (1.3%)
			Gneiss (1.3%)
			Basement material (0.6%)
		Outside meander of abandoned drainage channel (0.6%)	Schist (0.6%)
		Mountain side slope (1.6%)	Gneiss (0.6%)
			Basement material (0.9%)
4. Hill areas with river valley side slopes (13.3%)	Open river valley formed by the dissection of the drainage channel without river terraces (4.7%)	Ridge crest (0.3%)	Gypsum & Sandstone (0.3%)
		Dip-slope mid-slope (0.3%)	Gypsum & Sandstone (0.3%)
		Mountain & valley side slopes (0.9%)	Conglomerate & Sandstone (0.6%)
			Sandstone & Mudstone (0.3%)
		Gully side slope (0.3%)	Conglomerate & Mudstone (0.3%)
		Outside meander of active drainage channel (2.5%)	Conglomerate & Mudstone (0.3%)
			Conglomerate & Sandstone (0.3%)
			Conglomerate (0.3%)
			Sandstone (0.9%)
		Outside meander of abandoned drainage channel (0.6%)	Sandstone (0.6%)
		Inside meander of abandoned drainage channel (0.3%)	Mudstone (0.3%)
	Open river valley formed by the dissection of the drainage channel without river terraces (4.7%)	Dip-slope escarpment (0.9%)	Limestone (0.9%)
		Valley side slope (0.9%)	Conglomerate (0.6%)
			Limestone & Mudstone (0.3%)
		Outside meander of active drainage channel (1.6%)	Conglomerate (1.6%)
		Gully side slope (1.3%)	Sandstone & Mudstone (0.9%)
			Conglomerate (0.3%)
	Incised drainage channel with river terraces (0.6%)	Gully side slope (0.6%)	Sandstone (0.3%)
			Conglomerate & Mudstone (0.3%)
	Incised drainage channel without river terraces (1.9%)	Valley side slope (1.9%)	Gneiss (1.6%)
			Conglomerate (0.3%)
	Hill and Mountain slopes (1.3%)	Dip-slope mid-slope (1.3%)	Limestone (1.3%)

Table 4.4 (Continued) – Distribution of mapped landslides within the terrain classification and rock type combinations used by this study

Land System	Land Facet	Land Element	Rock Type
3. Hill areas with incised by canyons and gullies (59.8%)	Hill and Mountain slopes (0.9%)	Dip-slope mid-slopes (0.3%)	Limestone (0.3%)
		Valley side slopes (0.6%)	Gneiss (0.6%)
	Incised drainage channel with river terraces (38.3%)	Scarp-slope escarpment (5.4%)	Sandstone (0.3%)
			Limestone (0.3%)
			Conglomerate & Mudstone (0.3%)
			Limestone & Mudstone (0.3%)
			Conglomerate & Gypsum (0.3%)
			Gypsum & Mudstone (3.8%)
		Dip-slope escarpment (6.6%)	Sandstone (2.2%)
			Limestone (1.6%)
			Gypsum & Mudstone (1.9%)
			Sandstone & Mudstone (0.6%)
			Limestone & Mudstone (0.3%)
		Scarp-slope mid-slope (0.3%)	Gypsum & Mudstone (0.3%)
		Dip-slope mid-slope (0.6%)	Limestone & Mudstone (0.6%)
		Valley side slope (2.8%)	Limestone (0.9%)
			Conglomerate (1.6%)
			Limestone & Mudstone (0.3%)
		Canyon side slope (3.5%)	Conglomerate (1.6%)
			Conglomerate & Mudstone (1.3%)
			Sandstone (0.3%)
			Gypsum & Mudstone (0.3%)
		Gully side slope (0.9%)	Gypsum (0.3%)
			Limestone & Mudstone (0.3%)
			Mudstone (0.3%)
		Inside meander of active drainage channel (2.2%)	Conglomerate (0.6%)
			Sandstone (1.3%)
			Limestone & Mudstone (0.3%)
		Outside meander of active drainage channel (12.0%)	Conglomerate (3.2%)
			Conglomerate (0.9%)
			Sandstone (0.3%)
			Limestone (0.6%)
			Conglomerate & Mudstone (1.6%)
			Conglomerate & Sandstone (1.6%)
			Sandstone & Mudstone (0.6%)
			Limestone & Mudstone (2.5%)
			Mudstone (0.6%)
		Inside meander of abandoned drainage channel (0.3%)	Conglomerate (0.3%)
		Outside meander of abandoned drainage channel (2.2%)	Sandstone (0.3%)
			Conglomerate & Mudstone (0.3%)
			Conglomerate (0.3%)
			Sandstone (0.6%)
			Limestone & Mudstone (0.6%)
		Cut slope (1.3%)	Sandstone (1.3%)

	Incised drainage channel without river terraces (14.6%)	Scarp-slope escarpment (0.6%)	Limestone (0.6%)
		Dip-slope escarpment (2.8%)	Gypsum (0.3%)
			Limestone (1.9%)
			Sandstone & Mudstone (0.6%)
		Dip-slope mid-slope (0.9%)	Limestone (0.6%)
			Conglomerate & Sandstone (0.3%)
		Valley side slope (1.3%)	Limestone (0.9%)
			Schist (0.3%)
		Canyon side slope (1.3%)	Limestone (0.9%)
			Basement material (0.3%)
		Gully side slope (0.3%)	Limestone & Mudstone (0.3%)
		Inside meander of active drainage channel (0.3%)	Limestone (0.3%)
		Outside meander of active drainage channel (7.0%)	Conglomerate (2.2%)
			Gypsum (0.3%)
			Mudstone (0.3%)
			Limestone (1.3%)
			Sandstone & Mudstone (2.2%)
			Conglomerate & Mudstone (0.6%)
	Gully system (6.0%)	Dip-slope mid-slope (0.3%)	Conglomerate & Sandstone (0.3%)
		Gully side slope (3.2%)	Sandstone (0.6%)
			Limestone (0.6%)
			Conglomerate (0.3%)
			Conglomerate & Sandstone (1.6%)
		Inside meander of active drainage channel (1.3%)	Conglomerate (0.3%)
			Sandstone (0.9%)
		Outside meander of active drainage channel (0.9%)	Sandstone (0.6%)
			Sandstone & Mudstone (0.3%)
		Mountain side slope (0.3%)	Sandstone & Mudstone (0.3%)

Legend for Table 4.4

No. Landslides	% Range
> 6	> 1.9%
7 – 12	2.2 – 3.8
13 – 18	4.1 – 5.7
19 – 25	6.0 – 7.9
< 26	< 8.2%

Table 4.5 – Summary table of the distribution of the mapped landslides within the terrain classification/rock types combinations used by this study

Land System (Approximate % of mapped landslides)	Key Findings (Land Facet / Land Element / Lithology / % of the mapped landslides*)
1. Gypsum Plateau and Karst (2.5%)	• River valley formed by the dissection of the drainage system • Scarp-slope escarpment • Gypsum overlying calcareous mudstone • 2.5% of the mapped landslides (8 landslides)
2. Mountain slopes incised by gullies, canyons and river channels (24.4%)	• Hill and mountain area • Ridge crests • Basement material (Mica schist, gneiss, phyllite) • 4.7% of the mapped landslides (15 landslides)
	• Hill and mountain area • Ridge crests • Mica schist • 2.2% of the mapped landslides (7 landslides)
	• Incised drainage channels with river terraces • Canyons side slopes • Mica schist • 4.7% of the mapped landslides (15 landslides)
3. Hill areas with incised drainage channels (59.8%)	• Incised drainage channels with river terraces • Outside meanders of active drainage channels • Conglomerate • 3.2% of the mapped landslides (10 landslides)
	• Incised drainage channels with river terraces • Outside meanders of active drainage channels • Limestone and calcareous mudstone • 2.5% of the mapped landslides (8 landslides)
	• Incised drainage channels with river terraces • Scarp-slope escarpments • Gypsum overlying calcareous mudstone • 3.8% of the mapped landslides (12 landslides)
	• Incised drainage channels with river terraces • Dip-slope escarpments • Sandstone • 2.2% of the mapped landslides (7 landslides)
	• Incised drainage channels without river terraces • Outside meanders of active drainage channels • Conglomerate • 2.2% of the mapped landslides (7 landslides)
	• Incised drainage channels without river terraces • Outside meanders of active drainage channels • Sandstone and Mudstone • 2.2% of the mapped landslides (7 landslides)
4. Hill areas with gentle valley side slopes (13.3%)	• No combination with significant numbers of mapped landslides

* = These percentages will not add up to 100% as this is a summary table showing extracts from Table 4.4.

In many ways, the above summary table (Table 4.5) highlights many of the results seen in Table 4.3. The Land Elements that appear to be most "susceptible" to landslide activity are again the outside meanders within active and incised drainage channels, or the presence of dip-slope or scarp-slope escarpments. However, by increasing the number of possible combinations, the result is to decrease the number of "significant" clusters of landslides occurring in any given combination.

The prominence of either mica schist or "basement material" (a combination of mica schist, gneiss, phyllite and other basement rock types) within the "mountain slopes" Land System is not surprising, and reflects the nature of this Land System. Within the "hill areas with incised drainage channels" Land System, it appears that combinations of rock types (usually involving mudstone), in conjunction with the previously noted outside meanders of incised and active drainage channels is the most "susceptible" to landslide activity. This fits with previous observations that the "classic" combination of "hard" rock over "soft" rock (which in this case is calcareous mudstone) is a combination that is "susceptible" to landslide activity within this study area. This observation is also true for the gypsum escarpment, scarp-slope that occurs along the edge of the "Gypsum Plateau" Land System.

4.2.6 Landslide Mechanisms

The Río Aguas catchment area is affected by a wide variety of different failure mechanisms. In most cases, each mapped landslide itself is a combination of different failure mechanisms acting together, either at the same time or at different stages during the development of the landslide. The landslide mechanism classification and

definitions that were used in the database were described and discussed in Chapter 3. Where it was applicable, up to six different failure mechanisms were recorded for each of the mapped landslides. These were recorded on the basis of which mechanisms were judged to be the primary, secondary, tertiary failure mechanisms, etc., for that particular landslide. However, the majority of the landslides mapped by this study only involved two failure mechanisms. This analysis has, therefore, only considered the first two failure mechanisms (Table 4.6 and Figure 4.17).

Analysis of the landslide inventory shows that approximately 67% of the mapped landslides involve rock falls and topples, and 21% of the mapped landslides are non-rotational landslides (Table 4.6 and Figures 4.17 and 4.18) as the primary mechanism. A further 9% of the mapped landslides involve rock falls and topples as secondary mechanisms (Table 4.6). This means that approximately 80% of the mapped landslides involve rock falls or topples and approximately 40% of these failures involve slope deterioration processes as a secondary mechanism. These relatively high figures reflect the rocky nature of the topography, with oversteepened canyon walls and other cliff faces or escarpments. Interestingly, only 15% of the mapped landslides just involve rock falls and topples with no other failure mechanism. This reflects the complex nature of landslide activity within the study area and highlights the need for considering more than one failure mechanism for any given landslide. It also highlights the need for a relatively "flexible" landslide classification scheme that allows for multiple mechanisms to be considered.

Only 8.2% of the landslides within the study area have been classified as "Other" Landslides (Table 4.6 and Figures 4.17 and 4.18). The term "Other" is used here to

describe landslides involving debris movements, rock avalanches, rock flows, Sackung (as defined in Table 3.5 and Dikau *et al.*, 1996) and slope cambering. Translational landslides account for approximately 3.8% of the landslides mapped within the study area (Figures 4.17 and 4.18).

The classification scheme that has been used in this project also sub-divides failures such as rock falls into specific types of rock fall based on the shape or orientation of the failure surface. For example, the majority of the rock falls (as a primary failure mechanism) occur on joint-controlled wedge-shaped failure surfaces (45.3% of the mapped landslides; Figure 4.19).

Table 4.6 – Table showing the breakdown of the primary and secondary failure mechanisms of the mapped landslides

<table>
<tr><td rowspan="2"></td><td rowspan="2"></td><td colspan="4">**Primary Failure Mechanism**</td><td rowspan="2"></td></tr>
</table>

		Falls & Topples	Non-rotational Landslides	Translational Landslides	"Other" Landslides#	Totals
Secondary Failure Mechanism	**Falls & Topples**	62 (19.6%)	16 (5.1%)	2 (0.6%)	10 (3.2%)	90 (28.5%)
	Non-rotational Landslides	14 (4.4%)	6 (1.9%)	1 (0.3%)	13 (4.1%)	34 (10.8%)
	Translational Landslides		5 (1.6%)			5 (1.6%)
	"Other" Landslides		3 (0.9%)			4 (1.3%)
	Slope Deterioration	87 (27.5%)	14 (4.4%)			101 (32.0%)
	Primary Mechanism Only	48 (15.2%)	23 (7.3%)	9 (2.8%)	2 (0.6%)	82 (25.9%)
	Totals	211 (66.8%)	67 (21.2%)	12 (3.8%)	23 (8.2%)	316

"Other" Landslides includes here rock flow and debris movements, although these have been plotted separately in Figure 4.17.
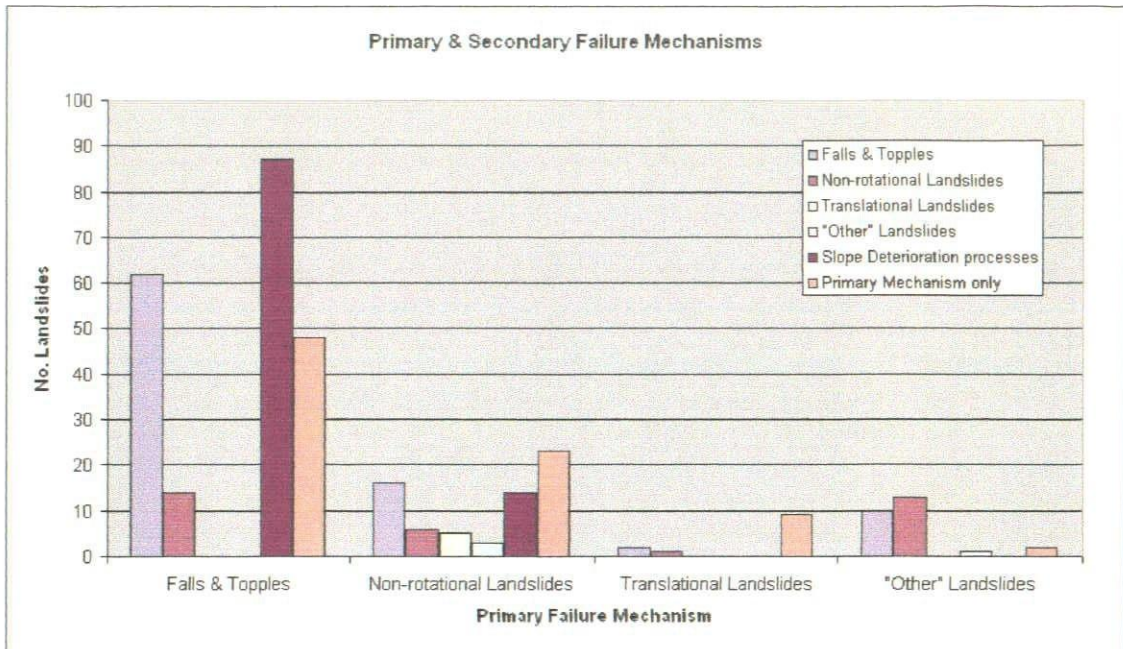
Figure 4.17 – Graph showing the breakdown of the primary and secondary landslide failure mechanisms mapped within the study area.
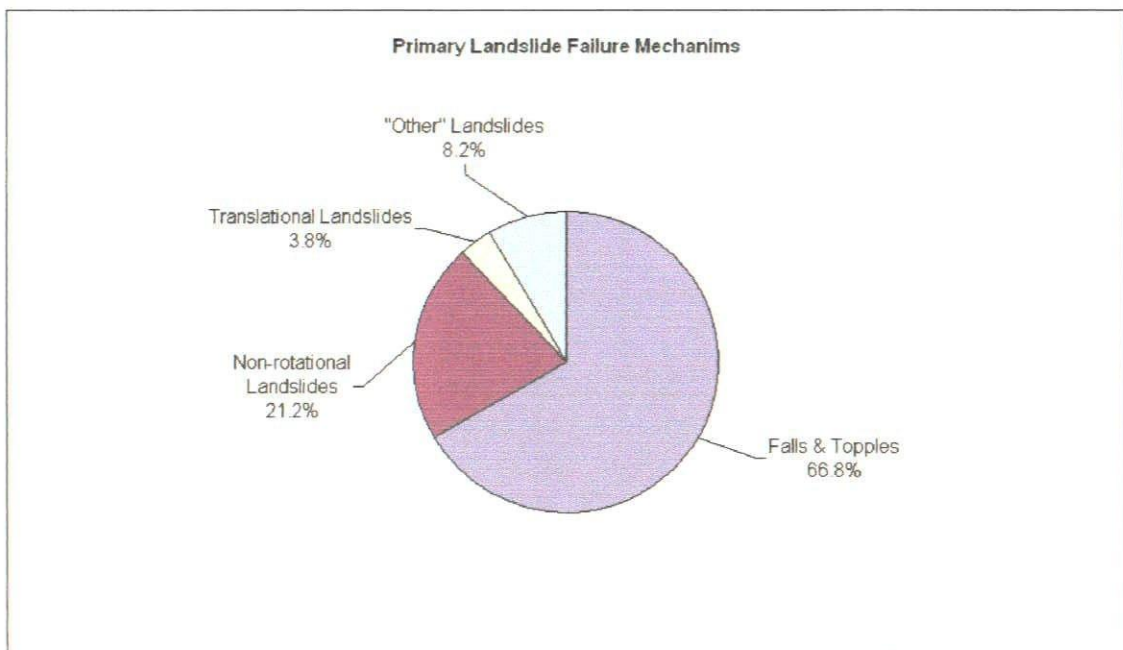
Figure 4.18 – Graph showing the breakdown of the primary landslide failure mechanisms mapped within the study area.

Detailed Landslide Failure Mechanisms

Rock Falls (wedged failure surface), 143.0

Rock Falls (planar failure surface), 16.0

Rock Falls, 7.0

Complex combination of Cambering & Sackung, 24.0

Debris Movement (natural channelised slope), 1.0

Rock Flow, 1.0

Translational Landslides (non-planar failure surface), 5.0

Translational Landslides (planar failure surface), 3.0

Translational Landslides, 4.0

Rock Falls (vertical failure surface), 44.0

Rock Topples (multiple pre-existing discontinuities), 1.0

Non-rotational Landslides, 9.0

Non-rotational Landslides (single, non-circular, listric, failure surface), 31.0

Non-rotational Landslides (progressive, non-circular, listric, failure surface), 21.0

Non-rotational Landslides (multi-storied, non-circular, listric, failure surface), 6.0

Figure 4.19 – Graph showing the detailed landslide failure mechanisms mapped within the study area.

4.2.7 Landslide Mechanisms and Geology

The relationship between the different landslide failure mechanisms that have been mapped and the rock types involved has been investigated. Approximately 66.5% of the mapped landslides have been described as "Rock Falls". Within this group, the majority of the mapped landslides occur within limestone (12.7%; Figure 4.20) and a further 3.2% involve limestone overlying mudstone. Landslides occurring within mica schist, gneiss or "basement material" account for approximately 10.1%, 3.5% and 9.5% of the mapped landslides respectively. Sandstone and conglomerate account for a further 7.6% and 8.5% of the total number of mapped landslides respectively, which are involved with rock falls and topples.

The majority of the landslides classified as involving either rock flow, rock avalanche or "other" failure mechanisms were found to occur within gypsum overlying mudstone (7.3%; Figure 4.20). This matches with field observations from along the gypsum escarpment.

The relationships seen in Figure 4.20 also match with the field observations and expectations. For example, the majority of the rock falls and topples and slope deterioration processes occur within hard or brittle rocks (i.e., sandstone or limestone). Failure mechanisms involving sliding either along a rotational, non-rotational or linear shear surface are seen to occur within lithological combinations involving a brittle rock unit (i.e., limestone) overlying a more ductile lithological unit (i.e., mudstone).
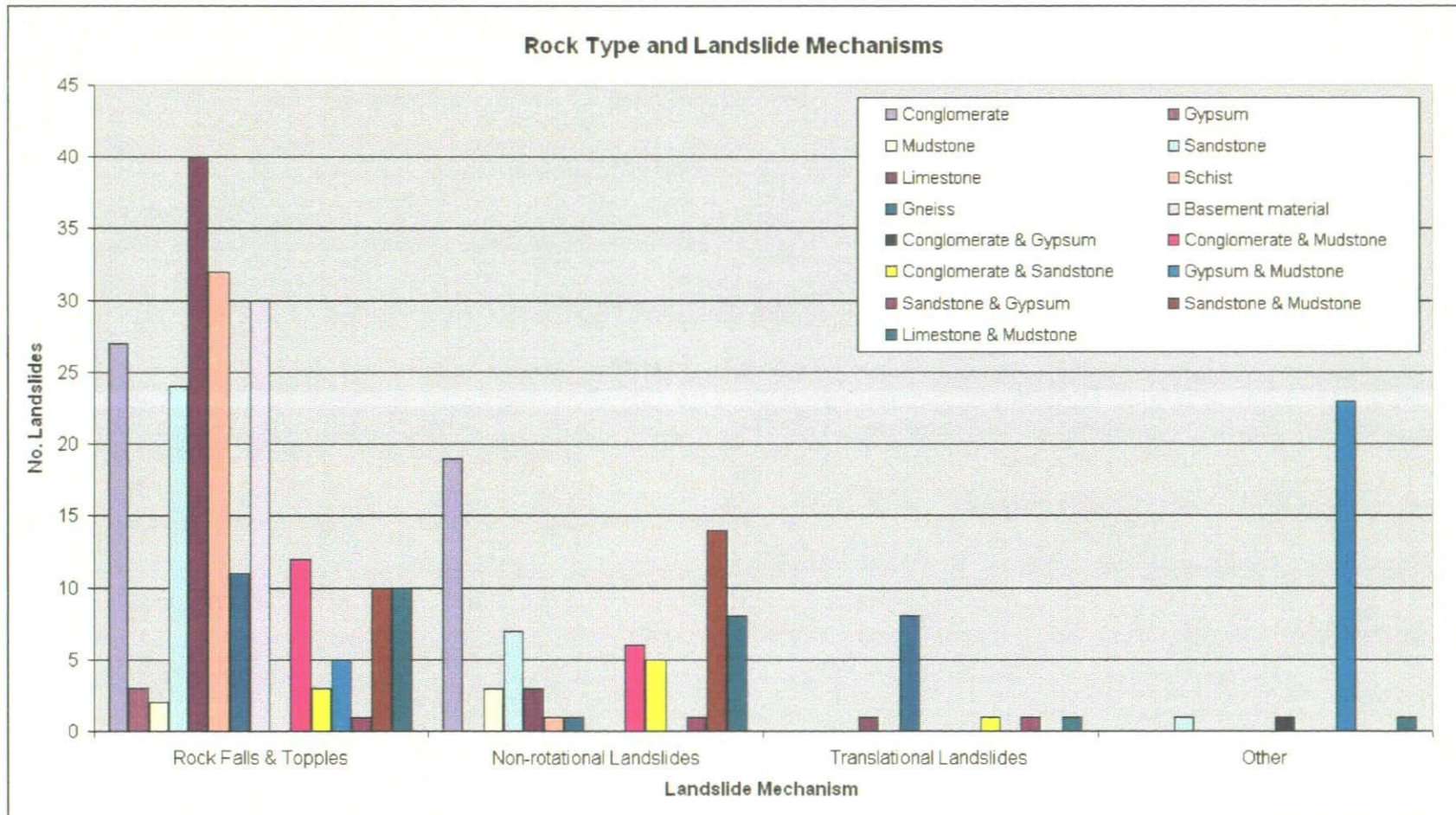
Figure 4.20 – Graph showing the breakdown of landslide mechanisms compared with the lithological units involved with the mapped landslide activity of the study area.

4.2.8 Landslide Mechanisms and Terrain Classification

In the previous section the relationship between landslide failure mechanism and rock type was investigated. The landslide mechanism by which a slope fails is also controlled by the geomorphology of the slope.

An analysis has been completed looking at the number of landslides with specified failure mechanisms occurring in the different combinations of Land System, Facet and Element which were recorded in the landslide inventory. The results from the analysis are presented in Table 4.7 and a summary of those combinations with the highest percentages are presented in Table 4.8.

Legend for Table 4.7

No. Landslides	% Range
> 6	> 1.9%
7 – 12	2.2 – 3.8
13 – 18	4.1 – 5.7
19 – 25	6.0 – 7.9
< 26	< 8.2%

Table 4.7 – Distribution of mapped landslides within the terrain classification/landslide failure mechanism combinations used by this study.

Land System	Land Facet	Land Element	Mechanism
1. Gypsum Plateau & Karst (2.5%)	Open river valley formed by the dissection of the drainage channel without river terraces (2.5%)	Scarp-slope escarpment (2.5%)	Other / Complex Combinations (2.5%)
2. Mountain slopes incised by gullies, canyons and river channels (24.4%)	Hill and Mountain slopes (10.4%)	Ridge crest (7.0%)	Falls & Topples (7.0%)
		Scarp-slope escarpment (0.6%)	Falls & Topples (0.6%)
		Valley side slopes (0.3%)	Falls & Topples (0.3%)
		Outside meander of active drainage channel (0.3%)	Translational Landslide (0.3%)
		Mountain side slope (1.3%)	Falls & Topples (1.3%)
	Incised drainage channel without river terraces (13.9%)	Ridge crest (1.3%)	Falls & Topples (0.3%)
		Valley side slope (0.9%)	Falls & Topples (0.6%)
			Non-rotational Landslide (0.3%)
		Canyon side slope (5.4%)	Falls & Topples (5.4%)
		Inside meander of active drainage channel (0.9%)	Falls & Topples (0.9%)
		Outside meander of active drainage channel (3.2%)	Falls & Topples (3.2%)
		Outside meander of abandoned drainage channel (0.6%)	Falls & Topples (0.6%)
		Mountain side slope (1.6%)	Falls & Topples (1.6%)
4. Hill areas with river valley side slopes (13.3%)	Open river valley formed by the dissection of the drainage channel without river terraces (4.7%)	Ridge crest (0.3%)	Non-rotational Landslide (0.3%)
		Dip-slope mid-slope (0.3%)	Translational Landslide (0.3%)
		Mountain & valley side slopes (0.9%)	Non-rotational Landslide (0.9%)
		Gully side slope (0.3%)	Falls & Topples (0.3%)
		Outside meander of active drainage channel (2.5%)	Falls & Topples (0.6%)
			Non-rotational Landslide (1.3%)
		Outside meander of abandoned drainage channel (0.6%)	Non-rotational Landslide (0.6%)
		Inside meander of abandoned drainage channel (0.3%)	Falls & Topples (0.3%)
	Open river valley formed by the dissection of the drainage channel without river terraces (4.7%)	Dip-slope escarpment (0.9%)	Falls & Topples (0.9%)
		Valley side slope (0.9%)	Falls & Topples (0.3%)
			Non-rotational Landslide (0.3%)
			Translational Landslide (0.3%)
		Outside meander of active drainage channel (1.6%)	Falls & Topples (0.9%)
			Non-rotational Landslide (0.6%)
		Gully side slope (1.3%)	Falls & Topples (0.9%)
			Non-rotational Landslide (0.3%)
	Incised drainage channel with river terraces (0.6%)	Gully side slope (0.6%)	Falls & Topples (0.6%)
	Incised drainage channel without river terraces (1.9%)	Valley side slope (1.9%)	Falls & Topples (0.3%)
			Translational Landslide (1.6%)
	Hill and Mountain slopes (1.3%)	Dip-slope mid-slope (1.3%)	Falls & Topples (1.3%)

Table 4.7 (Continued) – Distribution of mapped landslides within the terrain classification and landslide failure mechanism combinations used by this study

Land System	Land Facet	Land Element	Mechanism
3. Hill areas with incised by canyons and gullies (59.8%)	Hill and Mountain slopes (0.9%)	Dip-slope mid-slopes (0.3%)	Non-rotational Landslide (0.3%)
		Valley side slopes (0.6%)	Translational Landslide (0.6%)
	Incised drainage channel with river terraces (38.3%)	Scarp-slope escarpment (5.4%)	Falls & Topples (1.3%)
			Other (4.1%)
		Dip-slope escarpment (6.6%)	Falls & Topples (6.0%)
			Other (0.3%)
			Non-rotational Landslide (0.3%)
		Scarp-slope mid-slope (0.3%)	Other (0.3%)
		Dip-slope mid-slope (0.6%)	Non-rotational Landslide (0.6%)
		Valley side slope (2.8%)	Falls & Topples (0.9%)
			Non-rotational Landslide (1.9%)
		Canyon side slope (3.5%)	Falls & Topples (2.8%)
			Other (0.6%)
		Gully side slope (0.9%)	Falls & Topples (0.6%)
			Non-rotational Landslide (0.3%)
		Inside meander of active drainage channel (2.2%)	Falls & Topples (1.9%)
			Other (0.3%)
		Outside meander of active drainage channel (12.0%)	Falls & Topples (7.6%)
			Non-rotational Landslide (4.4%)
		Inside meander of abandoned drainage channel (0.3%)	Falls & Topples (0.3%)
		Outside meander of abandoned drainage channel (2.2%)	Falls & Topples (0.6%)
			Non-rotational Landslide (1.6%)
		Cut slope (1.3%)	Falls & Topples (1.3%)
	Incised drainage channel without river terraces (14.6%)	Scarp-slope escarpment (0.6%)	Falls & Topples (0.6%)
		Dip-slope escarpment (2.8%)	Falls & Topples (2.2%)
			Non-rotational Landslide (0.6%)
		Dip-slope mid-slope (0.9%)	Falls & Topples (0.3%)
			Translational Landslide (0.6%)
		Valley side slope (1.3%)	Falls & Topples (0.9%)
			Non-rotational Landslide (0.3%)
		Canyon side slope (1.3%)	Falls & Topples (1.3%)
		Gully side slope (0.3%)	Falls & Topples (0.3%)
		Inside meander of active drainage channel (0.3%)	Falls & Topples (0.3%)
		Outside meander of active drainage channel (7.0%)	Falls & Topples (2.8%)
			Non-rotational Landslide (4.1%)
	Gully system (6.0%)	Dip-slope mid-slope (0.3%)	Non-rotational Landslide (0.3%)
		Gully side slope (3.2%)	Falls & Topples (1.3%)
			Non-rotational Landslide (1.9%)
		Inside meander of active drainage channel (1.3%)	Falls & Topples (1.3%)
		Outside meander of active drainage channel (0.9%)	Falls & Topples (0.9%)
		Mountain side slope (0.3%)	Falls & Topples (0.3%)

Table 4.8 – Summary table of the distribution of the mapped landslides within the terrain classification/landslide failure mechanism combinations used by this study

Land System (Approximate % of mapped landslides)	Key Findings (Land Facet / Land Element / Mechanisms / % of the mapped landslides*)
1. Gypsum Plateau and Karst (2.5%)	• River valley formed by the dissection of the drainage system • Scarp-slope escarpment • "Other" – complex combination of mechanisms • 2.5% of the mapped landslides (8 landslides)
2. Mountain slopes incised by gullies, canyons and river channels (24.4%)	• Hill and mountain area • Ridge crests • Rock Falls and Topples • 7.0% of the mapped landslides (22 landslides)
	• Incised drainage channels with river terraces • Canyons side slopes • Rock Falls and Topples • 5.4% of the mapped landslides (17 landslides)
	• Incised drainage channels with river terraces • Outside meanders of active drainage channels • Rock Falls and Topples • 3.2% of the mapped landslides (10 landslides)
3. Hill areas with incised drainage channels (59.8%)	• Incised drainage channels with river terraces • Outside meanders of active drainage channels • Rock Falls and Topples • 7.6% of the mapped landslides (24 landslides)
	• Incised drainage channels with river terraces • Dip-slope escarpments • Rock Falls and Topples • 6.0% of the mapped landslides (19 landslides)
	• Incised drainage channels with river terraces • Scarp-slope escarpments • "Other" – complex combination of mechanisms • 4.1% of the mapped landslides (13 landslides)
	• Incised drainage channels without river terraces • Outside meanders of active drainage channels • Non-rotational Landslides • 4.1% of the mapped landslides (13 landslides)
	• Incised drainage channels without river terraces • Outside meanders of active drainage channels • Rock Falls and Topples • 2.8% of the mapped landslides (9 landslides)
	• Incised drainage channels without river terraces • Dip-slope escarpments • Rock Falls and Topples • 2.2% of the mapped landslides (7 landslides)
4. Hill areas with gentle valley side slopes (13.3%)	• No combination with significant numbers of mapped landslides

* = These percentages will not add up to 100% as this is a summary table showing extracts from Table 4.7.

In many ways, the above summary table (Table 4.8) highlights many of the results already seen in Table 4.3 (i.e., the Land Elements that appear to be most "susceptible" to landslide activity are again the outside meanders within active and incised drainage channels, or the presence of dip-slope or scarp-slope escarpments). Again, by increasing the number of possible combinations, the result is to increase the number of "significant" clusters of landslides occurring in any given combination, but to decrease the number of landslides occurring within those clusters.

The dominance of rock falls and topples is not surprising considering the results presented in Section 4.2.6 (section on landslide failure mechanisms). However, there are some noticeable exceptions. For example, within the "hill areas with incised drainage channels" Land System 4.1% of the mapped landslides were classified as "other" and occur on scarp-slope escarpments (Table 4.8). An additional 4.1% of the mapped landslides within this Land System also occur as non-rotational landslides in the outside meanders of incised and active drainage channels.

4.2.9 Landslide Mechanisms, Geology and Geomorphology

In developing a ground model for the study area it is essential to have some understanding of which combination of lithology and geomorphological setting will potentially give rise to which types of landslide failure mechanisms. Therefore a relatively complex analysis has been completed combining these three sets of variables. These will be presented by Land System unit.

An analysis has been completed looking at the number of landslides with specified failure mechanisms occurring in the different combinations of terrain classification and rock type which were recorded in the landslide inventory. The results from the analysis are presented in Table 4.9 and a summary of those combinations with the highest percentages are presented in Table 4.10.

Legend for Table 4.9

No. Landslides	% Range
> 6	> 1.9%
7 – 12	2.2 – 3.8
13 – 18	4.1 – 5.7
19 – 25	6.0 – 7.9
< 26	< 8.2%

Table 4.9 – Distribution of mapped landslides within the terrain classification/rock type/landslide failure mechanism combinations used by this study

Land System	Land Facet	Land Element	Rock Type	Mechanism
1. Gypsum Plateau & Karst (2.5%)	Open river valley formed by the dissection of the drainage channel without river terraces (2.5%)	Scarp-slope escarpment (2.5%)	Gypsum over lying mudstone (2.5%)	Other / Complex Combinations (2.5%)
2. Mountain slopes incised by gullies, canyons and river channels (24.4%)	Hill and Mountain slopes (10.4%)	Ridge crest (7.0%)	Schist (2.2%)	Falls & Topples (2.2%)
			Basement (4.7%)	Falls & Topples (4.7%)
		Scarp-slope escarpment (0.6%)	Limestone (0.6%)	Falls & Topples (0.6%)
		Valley side slopes (0.3%)	Limestone (0.3%)	Falls & Topples (0.3%)
		Outside meander of active drainage channel (0.3%)	Gneiss (0.3%)	Translational Landslide (0.3%)
		Mountain side slope (1.3%)	Schist (0.6%)	Falls & Topples (0.6%)
			Gneiss (0.3%)	Falls & Topples (0.3%)
			Basement material (1.3%)	Falls & Topples (1.3%)
	Incised drainage channel without river terraces (13.9%)	Ridge crest (1.3%)	Schist (0.3%)	Falls & Topples (0.3%)
			Basement material (0.9%)	Falls & Topples (0.9%)
		Valley side slope (0.9%)	Gneiss (0.9%)	Falls & Topples (0.6%)
				Non-rotational Landslide (0.3%)
		Canyon side slope (5.4%)	Schist (4.7%)	Falls & Topples (4.7%)
			Gneiss (0.6%)	Falls & Topples (0.6%)
		Inside meander of active drainage channel (0.9%)	Schist (0.3%)	Falls & Topples (0.3%)
			Basement material (0.6%)	Falls & Topples (0.6%)
		Outside meander of active drainage channel (3.2%)	Schist (1.3%)	Falls & Topples (1.3%)
			Gneiss (1.3%)	Falls & Topples (1.3%)
			Basement material (0.6%)	Falls & Topples (0.6%)
		Outside meander of abandoned drainage channel (0.6%)	Schist (0.6%)	Falls & Topples (0.6%)
		Mountain side slope (1.6%)	Gneiss (0.6%)	Falls & Topples (0.6%)
			Basement material (0.9%)	Falls & Topples (0.9%)
4. Hill areas with river valley side slopes (13.3%)	Open river valley formed by the dissection of the drainage channel without river terraces (4.7%)	Ridge crest (0.3%)	Gypsum & Sandstone (0.3%)	Non-rotational Landslide (0.3%)
		Dip-slope mid-slope (0.3%)	Gypsum & Sandstone (0.3%)	Translational Landslide (0.3%)
		Mountain & valley side slopes (0.9%)	Conglomerate & Sandstone (0.6%)	Non-rotational Landslide (0.6%)
			Sandstone & Mudstone (0.3%)	Non-rotational Landslide (0.3%)
		Gully side slope (0.3%)	Conglomerate & Mudstone (0.3%)	Falls & Topples (0.3%)
		Outside meander of active drainage channel (2.5%)	Conglomerate & Mudstone (0.3%)	Falls & Topples (0.3%)
			Conglomerate & Sandstone (0.3%)	Falls & Topples (0.3%)
			Conglomerate (0.3%)	Non-rotational Landslide (0.3%)
			Sandstone (0.9%)	Non-rotational Landslide (0.9%)
		Outside meander of abandoned drainage channel (0.6%)	Sandstone (0.6%)	Non-rotational Landslide (0.6%)
		Inside meander of abandoned drainage channel (0.3%)	Mudstone (0.3%)	Falls & Topples (0.3%)
	Open river valley formed by the dissection of the drainage channel without river terraces (4.7%)	Dip-slope escarpment (0.9%)	Limestone (0.9%)	Falls & Topples (0.9%)
		Valley side slope (0.9%)	Conglomerate (0.6%)	Falls & Topples (0.3%)
				Non-rotational Landslide (0.3%)
			Limestone & Mudstone (0.3%)	Translational Landslide (0.3%)
		Outside meander of active drainage channel (1.6%)	Conglomerate (1.6%)	Falls & Topples (0.9%)
				Non-rotational Landslide (0.6%)
		Gully side slope (1.3%)	Sandstone & Mudstone (0.9%)	Falls & Topples (0.9%)
			Conglomerate (0.3%)	Non-rotational Landslide (0.3%)
	Incised drainage channel with river terraces (0.6%)	Gully side slope (0.6%)	Sandstone (0.3%)	Falls & Topples (0.3%)
			Conglomerate & Mudstone (0.3%)	Falls & Topples (0.3%)
	Incised drainage channel without river terraces (1.9%)	Valley side slope (1.9%)	Gneiss (1.6%)	Translational Landslide (1.6%)
			Conglomerate (0.3%)	Falls & Topples (0.3%)
	Hill and Mountain slopes (1.3%)	Dip-slope mid-slope (1.3%)	Limestone (1.3%)	Falls & Topples (1.3%)

Table 4.9 (Continued) – Distribution of mapped landslides within the terrain classification, rock type and landslide failure mechanism combinations used by this study

Land System	Land Facet	Land Element	Rock Type	Mechanism
3. Hill areas with incised by canyons and gullies (59.8%)	Hill and Mountain slopes (0.9%)	Dip-slope mid-slopes (0.3%)	Limestone (0.3%)	Non-rotational Landslide (0.3%)
		Valley side slopes (0.6%)	Gneiss (0.6%)	Translational Landslide (0.6%)
	Incised drainage channel with river terraces (38.3%)	Scarp-slope escarpment (5.4%)	Sandstone (0.3%)	Falls & Topples (0.3%)
			Limestone (0.3%)	Falls & Topples (0.3%)
			Conglomerate & Mudstone (0.3%)	Falls & Topples (0.3%)
			Limestone & Mudstone (0.3%)	Falls & Topples (0.3%)
			Conglomerate & Gypsum (0.3%)	Other (0.3%)
			Gypsum & Mudstone (3.8%)	Other (3.8%)
		Dip-slope escarpment (6.6%)	Sandstone (2.2%)	Falls & Topples (2.2%)
			Limestone (1.6%)	Falls & Topples (1.6%)
			Gypsum & Mudstone (1.9%)	Falls & Topples (1.6%)
				Other (0.3%)
			Sandstone & Mudstone (0.6%)	Falls & Topples (0.3%)
				Non-rotational Landslide (0.3%)
			Limestone & Mudstone (0.3%)	Falls & Topples (0.3%)
		Scarp-slope mid-slope (0.3%)	Gypsum & Mudstone (0.3%)	Other (0.3%)
		Dip-slope mid-slope (0.6%)	Limestone & Mudstone (0.6%)	Non-rotational Landslide (0.6%)
		Valley side slope (2.8%)	Limestone (0.9%)	Falls & Topples (0.9%)
			Conglomerate (1.6%)	Non-rotational Landslide (1.6%)
			Limestone & Mudstone (0.3%)	Non-rotational Landslide (0.3%)
		Canyon side slope (3.5%)	Conglomerate (1.6%)	Falls & Topples (1.6%)
			Conglomerate & Mudstone (1.3%)	Falls & Topples (1.3%)
			Sandstone (0.3%)	Other (0.3%)
			Gypsum & Mudstone (0.3%)	Other (0.3%)
		Gully side slope (0.9%)	Gypsum (0.3%)	Falls & Topples (0.3%)
			Limestone & Mudstone (0.3%)	Falls & Topples (0.3%)
			Mudstone (0.3%)	Non-rotational Landslide (0.3%)
		Inside meander of active drainage channel (2.2%)	Conglomerate (0.6%)	Falls & Topples (0.6%)
			Sandstone (1.3%)	Falls & Topples (1.3%)
			Limestone & Mudstone (0.3%)	Other (0.3%)
		Outside meander of active drainage channel (12.0%)	Conglomerate (3.2%)	Falls & Topples (3.2%)
			Conglomerate (0.9%)	Non-rotational Landslide (0.9%)
			Sandstone (0.3%)	Falls & Topples (0.3%)
			Limestone (0.6%)	Falls & Topples (0.6%)
			Conglomerate & Mudstone (1.6%)	Falls & Topples (0.9%)
				Non-rotational Landslide (0.6%)
			Conglomerate & Sandstone (1.6%)	Falls & Topples (0.3%)
				Non-rotational Landslide (1.3%)
			Sandstone & Mudstone (0.6%)	Falls & Topples (0.6%)
			Limestone & Mudstone (2.5%)	Falls & Topples (1.6%)
				Non-rotational Landslide (0.9%)
			Mudstone (0.6%)	Non-rotational Landslide (0.6%)
		Inside meander of abandoned drainage channel (0.3%)	Conglomerate (0.3%)	Falls & Topples (0.3%)
		Outside meander of abandoned drainage channel (2.2%)	Sandstone (0.3%)	Falls & Topples (0.3%)
			Conglomerate & Mudstone (0.3%)	Falls & Topples (0.3%)
			Conglomerate (0.3%)	Non-rotational Landslide (0.3%)
			Sandstone (0.6%)	Non-rotational Landslide (0.6%)
			Limestone & Mudstone (0.6%)	Non-rotational Landslide (0.6%)

Landform	Slope type	Geology	Failure type
Incised drainage channel without river terraces (14.6%)	Cut slope (1.3%)	Sandstone (1.3%)	Falls & Topples (1.3%)
	Scarp-slope escarpment (0.6%)	Limestone (0.6%)	Falls & Topples (0.6%)
	Dip-slope escarpment (2.8%)	Gypsum (0.3%)	Falls & Topples (0.3%)
		Limestone (1.9%)	Falls & Topples (1.9%)
		Sandstone & Mudstone (0.6%)	Non-rotational Landslide (0.6%)
	Dip-slope mid-slope (0.9%)	Limestone (0.6%)	Falls & Topples (0.3%)
			Translational Landslide (0.3%)
		Conglomerate & Sandstone (0.3%)	Translational Landslide (0.3%)
	Valley side slope (1.3%)	Limestone (0.9%)	Falls & Topples (0.9%)
		Schist (0.3%)	Non-rotational Landslide (0.3%)
	Canyon side slope (1.3%)	Limestone (0.9%)	Falls & Topples (0.9%)
		Basement material (0.3%)	Falls & Topples (0.3%)
	Gully side slope (0.3%)	Limestone & Mudstone (0.3%)	Falls & Topples (0.3%)
	Inside meander of active drainage channel (0.3%)	Limestone (0.3%)	Falls & Topples (0.3%)
	Outside meander of active drainage channel (7.0%)	Conglomerate (2.2%)	Falls & Topples (0.9%)
			Non-rotational Landslide (1.3%)
		Gypsum (0.3%)	Falls & Topples (0.3%)
		Mudstone (0.3%)	Falls & Topples (0.3%)
		Limestone (1.3%)	Falls & Topples (0.6%)
			Non-rotational Landslide (0.6%)
		Sandstone & Mudstone (2.2%)	Falls & Topples (0.6%)
			Non-rotational Landslide (1.6%)
		Conglomerate & Mudstone (0.6%)	Non-rotational Landslide (0.6%)
Gully system (6.0%)	Dip-slope mid-slope (0.3%)	Conglomerate & Sandstone (0.3%)	Non-rotational Landslide (0.3%)
	Gully side slope (3.2%)	Sandstone (0.6%)	Falls & Topples (0.6%)
		Limestone (0.6%)	Falls & Topples (0.6%)
		Conglomerate (0.3%)	Non-rotational Landslide (0.3%)
		Conglomerate & Sandstone (1.6%)	Non-rotational Landslide (1.6%)
	Inside meander of active drainage channel (1.3%)	Conglomerate (0.3%)	Falls & Topples (0.3%)
		Sandstone (0.9%)	Falls & Topples (0.9%)
	Outside meander of active drainage channel (0.9%)	Sandstone (0.6%)	Falls & Topples (0.6%)
		Sandstone & Mudstone (0.3%)	Falls & Topples (0.3%)
	Mountain side slope (0.3%)	Sandstone & Mudstone (0.3%)	Falls & Topples (0.3%)

Table 4.10 – Summary table of the distribution of the mapped landslides within the terrain classification/landslide failure mechanism/rock type combinations used by this study.

Land System (Approximate % of mapped landslides)	Key Findings (Land Facet / Land Element / Lithology / Mechanisms / % of the mapped landslides*)
1. Gypsum Plateau and Karst (2.5%)	• River valley formed by the dissection of the drainage system • Scarp-slope escarpment • Gypsum overlying calcareous mudstone • "Other" – complex combination of mechanisms • 2.5% of the mapped landslides (8 landslides)
2. Mountain slopes incised by gullies, canyons and river channels (24.4%)	• Hill and mountain area • Ridge crests • Basement Material (Mica schist, gneiss, phyllite) • Rock Falls and Topples • 4.7% of the mapped landslides (15 landslides)
	• Hill and mountain area • Ridge crests • Mica Schist • Rock Falls and Topples • 2.2% of the mapped landslides (7 landslides)
	• Incised drainage channels with river terraces • Canyons side slopes • Rock Falls and Topples • Mica Schist • 4.7% of the mapped landslides (15 landslides)
3. Hill areas with incised drainage channels (59.8%)	• Incised drainage channels with river terraces • Outside meanders of active drainage channels • Conglomerate • Rock Falls and Topples • 3.2% of the mapped landslides (10 landslides)
	• Incised drainage channels with river terraces • Dip-slope escarpments • Sandstone • Rock Falls and Topples • 2.2% of the mapped landslides (7 landslides)
	• Incised drainage channels with river terraces • Scarp-slope escarpments • Gypsum overlying calcareous mudstone • "Other" – complex combination of mechanisms • 3.8% of the mapped landslides (12 landslides)
4. Hill areas with gentle valley side slopes (13.3%)	• No combination with significant numbers of mapped landslides

* = These percentages will not add up to 100% as this is a summary table showing extracts from Table 4.7.

Once again, the above summary table (Table 4.10) highlights many of the results previously seen in Tables 4.3 and 4.8. However, once again, by increasing the number of possible combinations, the result is to increase the number of "significant" clusters of

landslides occurring in any given combination, while at the same time decrease the number of landslides occurring within those clusters.

The two most "susceptible" combinations of Land System, Facet and Element with rock type and failure mechanism for landslide activity occur within the "mountain slopes" Land System. These are:

1. Basement material (mica schist, gneiss and/or phyllite) failing as rock falls and/or topples along ridge crests in "hill and mountain areas" (4.7%).

2. Mica schist failing as rock falls and/or topples on canyon side slopes in "incised drainage channels" (4.7%).

This is despite the fact that the majority of the landslides occur within the "hill areas with incised drainage channels" Land System. However, the third and fourth most "susceptible" combination for landslide activity occurs within that Land System:

3. Gypsum overlying calcareous mudstone failing as a complex combination of cambering and high-angle non-rotational landsliding (classified here as "other" landslides) on scarp-slope escarpment above incised drainage channels (3.8%).

4. Conglomerate failing as rock falls and/or topples in the outside meanders of incised and active drainage channels (3.2%).

However, it should be noted that out of the 316 landslides that have been considered in this investigation, these four "susceptible" combinations account for only 51 (16.4%) of the mapped landslides. This means that the majority of the mapped landslides are not occurring in these "susceptible" combinations. This is a result of the complexity of the

analysis that has been completed here and the total number of possible combinations of terrain classification, rock type and landslide failure mechanism that could occur.

4.2.10 Landslide Mechanisms, Slope Angle and Geology

The relationship between rock type and slope angle is very important for slope stability (LRA, 2003a, b). It will also influence the type of failure mechanism by which a slope may fail. Therefore, a comparison was made between the incidence of landslides of different failure mechanisms with slope angle (Figures 4.21). This was then repeated using rock type combined with failure mechanism (Figures 4.22 to 4.25).
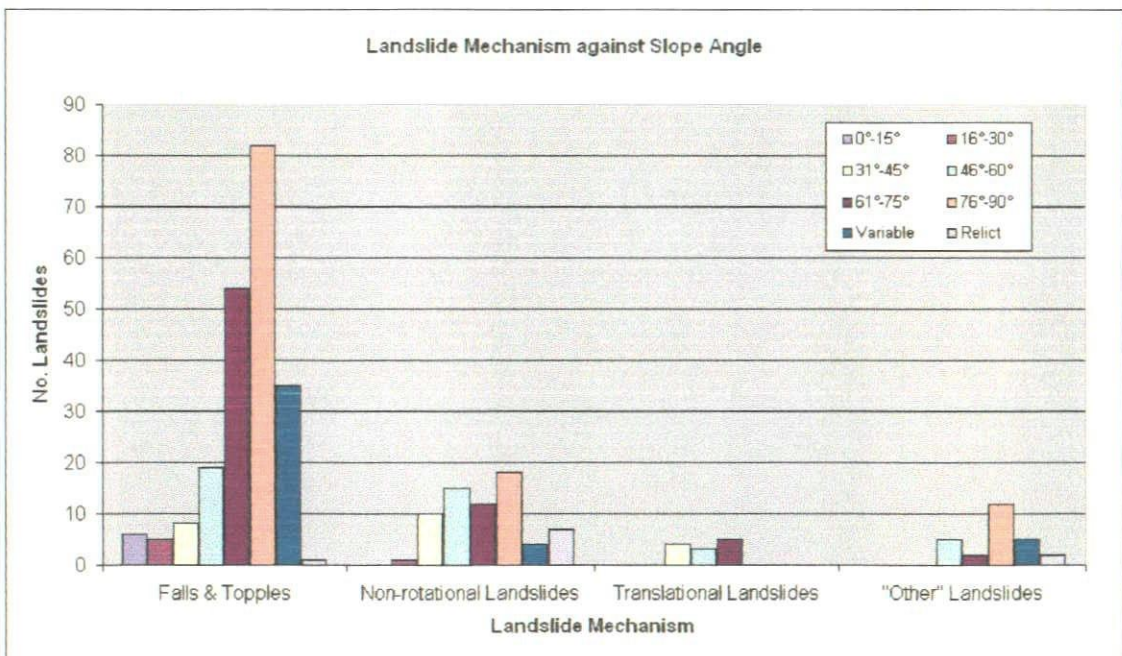
Figure 4.21 – Graph comparing the incidence of mapped landslides within the slope angle classes used by this study

The majority of rock falls and topples (43.0% of the mapped landslides) occur on slopes between 61° and 90°, with almost 26% of the mapped landslides occurring on slopes above 76° (Figures 4.21 and 4.22). A further 11.4% of the mapped landslides occur on slopes classified as having a variable slope angle. There is also an increase in the number of landslides occurring as the slope angle increases. These are not surprising observations, as rock falls and topples, by definition, require a steep slope on which to occur. It also fits with the observations that the largest concentration of landslides was found in the canyons and incised drainage channels in the Sorbas area (Figure 4.6).

The largest proportion of non-rotational landslides are found on slopes between 76° and 90° (5.7% of the mapped landslides; Figure 4.23). Again, the number of landslides occurring increases with slope angle, except for slopes between 46° and 60°, where the second largest proportion of landslides are seen to occur (Figure 4.23). This is partly due to the relatively higher number of landslides involving limestone and limestone and mudstone. This could, therefore, be a lithological control.

The twelve translational landslides that have been mapped in the study area occur on slopes between 61° and 75° (1.6% of the mapped landslides) and between 31° and 45° (1.3% of the mapped landslides) (Figure 4.24). Again, this is not a surprising result as translational landslides will tend to only occur on moderately steep slopes (Hutchinson, 1988; Dikau *et al.*, 1996). A lithological control is also apparent with the translational landslides involving gneiss only occurring on the steeper slopes, while all of the other translational landslides occur on the slopes between 31° and 45°. This is probably due

to the more competent and relatively stronger nature of the gneiss compared with the relatively weaker sedimentary rocks (i.e., limestone & mudstone).

All of the landslides classified as "other" (landslides involving combinations of rock flow, cambering, non-rotational or high angle rotational landslides) occur on slopes greater than 46° or were classified as occurring on slopes with a "variable" slope angle. The majority of these landslides occur on slopes between 76° and 90° (Figure 4.25). This probably reflects the nature of the landslide failure mechanisms involved, as well as the lithologies involved. All but three of the landslides being considered here (7.3% of the mapped landslides) involve failure of gypsum overlying calcareous mudstone along the Gypsum Escarpment.
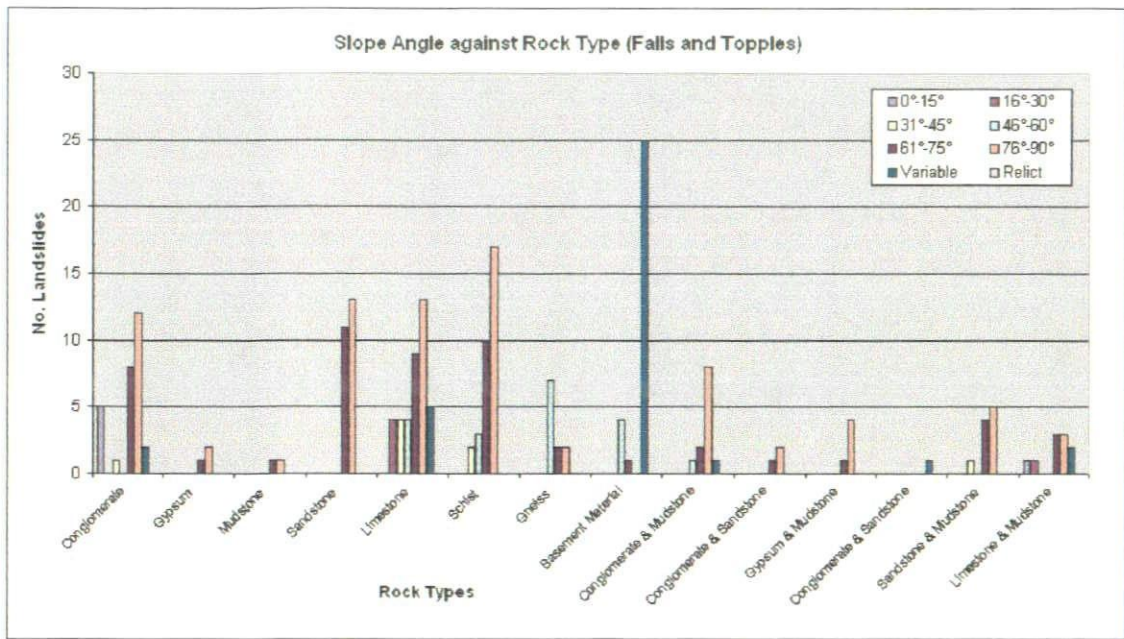
Figure 4.22 – Graph comparing the incidence of rock falls and topples within the slope angle classes used by this study for different rock types
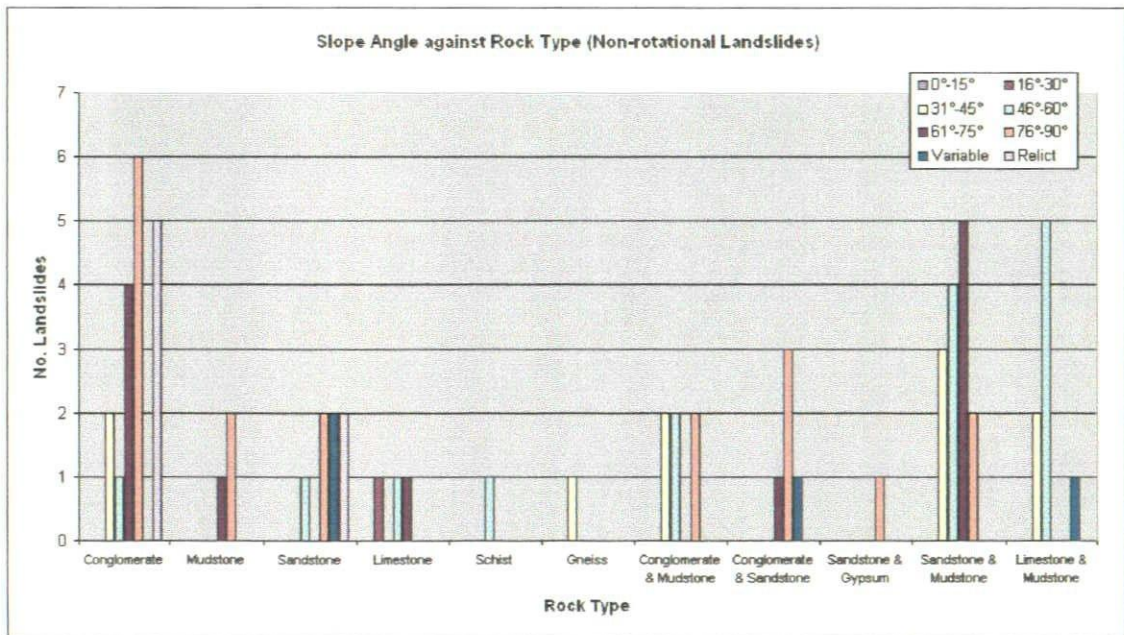
Figure 4.23 – Graph comparing the incidence of non-rotational landslides within the slope angle classes used by this study for different rock types.
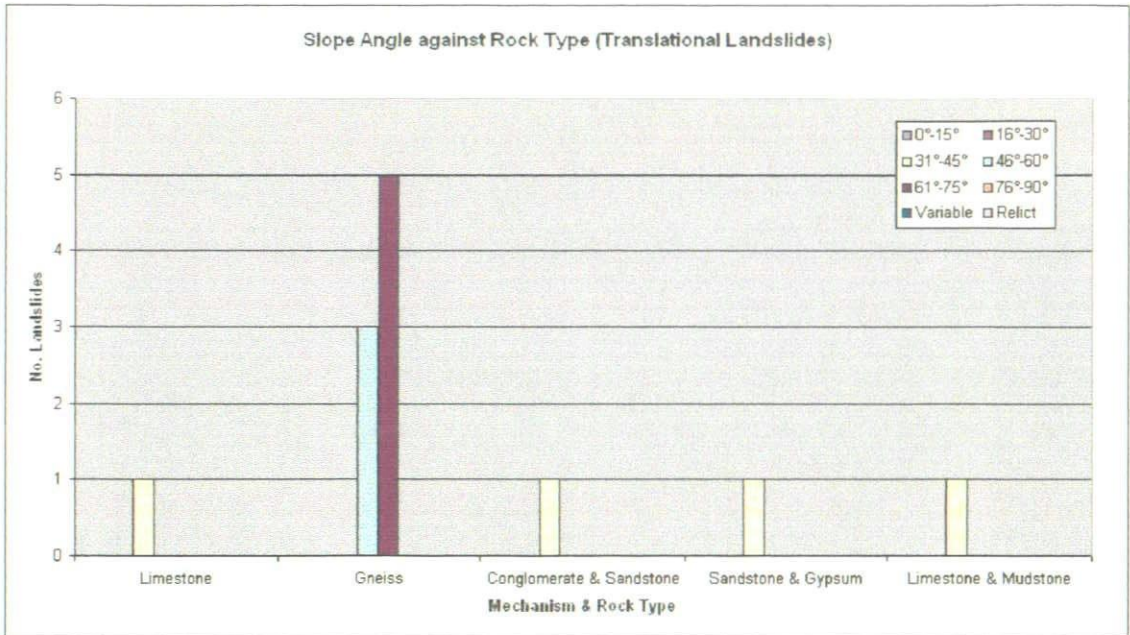
Figure 4.24 – Graph comparing the incidence of translational landslides within the slope angle classes used by this study for different rock types.
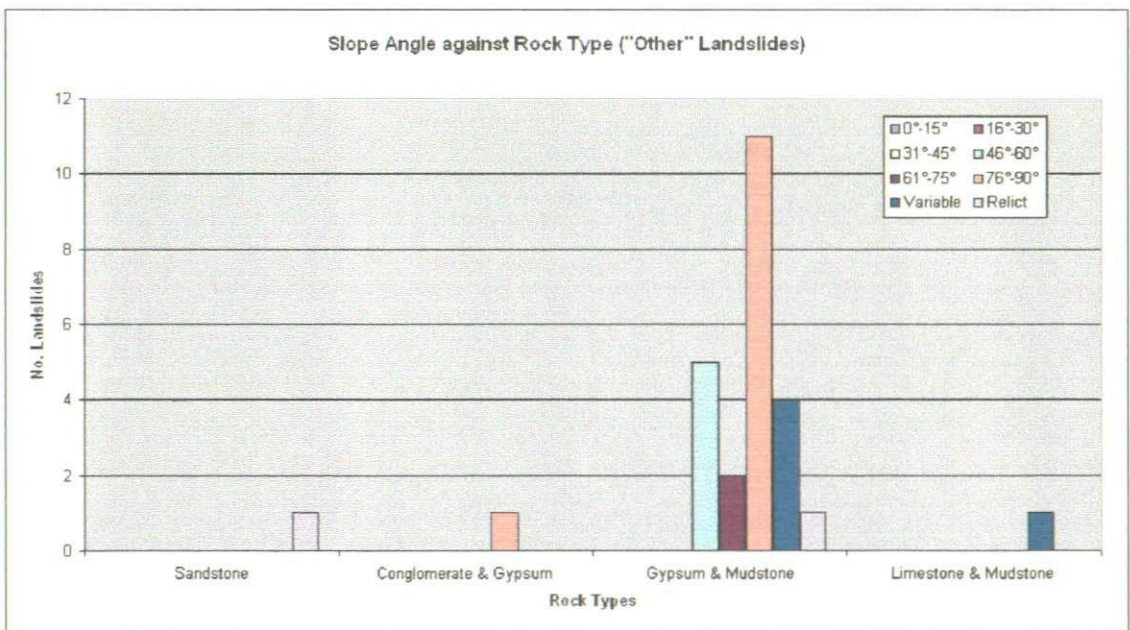
Figure 4.25 – Graph comparing the incidence of "Other" landslides within the slope angle classes used by this study for different rock types

4.2.11 Landslide Activity

The state of landslide activity in the study area is difficult to assess without constant monitoring. However, this can be partially overcome by using a combination of geomorphological mapping and repeat visits to some of the landslide sites. This led to approximately 80% of the mapped landslides being classified as "dormant" ("a landslide that has not moved for more than one annual cycle of seasons, but where the causes of movement apparently remain" – WP/WLI, 1993) (Figure 4.26). This is quite significant because it means that the vast majority of the landslides, although considered not to be currently active, still have the potential to become active. Suspended landslides (those that have "moved within the last annual cycle of seasons, but is not moving at present") account for 8.5% of the mapped landslides.

However, the classification of the above landslides depends on the accuracy of being able to identify when the landslides were last active. Within the study area, this depends on field observations, as well as sometimes on eyewitness accounts. Therefore, it depends on how easy it is to be able to determine how frequently a landslide is active.

Through the combination of aerial photographic interpretation and geological and geomorphological field mapping it was possible to map a number of "Relict" landslides within the study area. These accounted for just over 4% of the total number of the mapped landslides (Figure 4.26).

The majority of the mapped landslides in the study area (approximately 80%; Figure 4.27) have been classified as "Multiple". WP/WLI (1993) states that a multiple

landslide exhibits "repeated development of the same type of movement along the same rupture surface and involving the same displaced material".

Three-quarters of the mapped landslides (Figure 4.28) are classified as "retrogressing". WP/WLI (1993) defined a "retrogressing" landslide as one where "the rupture surface is extending in the direction opposite to the movement of the displaced material". Approximately 17% of the mapped landslides are considered as "enlarging" (i.e., having a rupture surface that is extending in two or more directions - WP/WLI (1993); Figure 4.28).
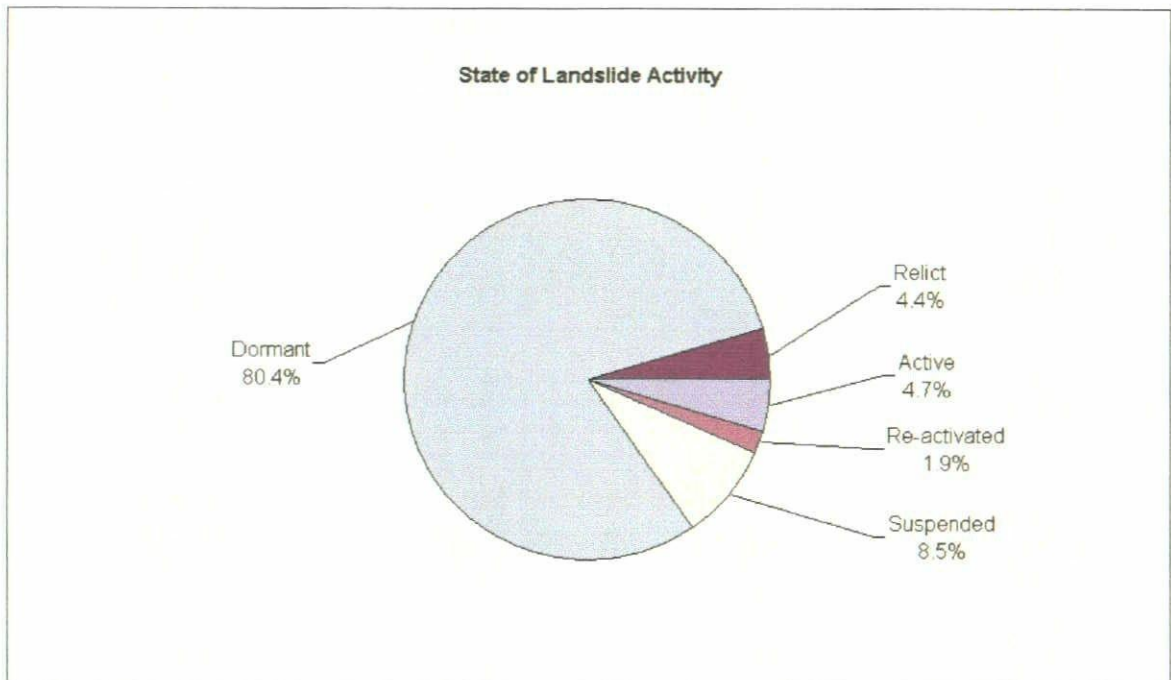
Figure 4.26 – Graph showing the breakdown of mapped landslides within the "State of Landslide Activity" classes used by this study.
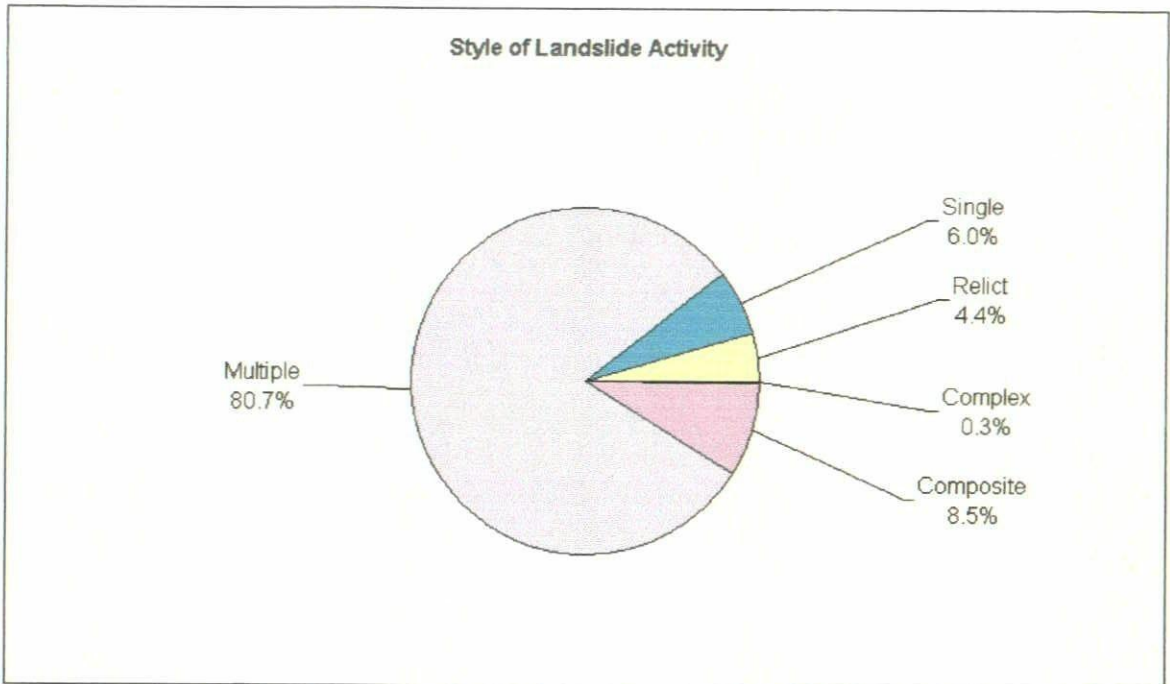
Figure 4.27 – Graph showing the breakdown of mapped landslides within the "Style of Landslide Activity" classes used by this study.
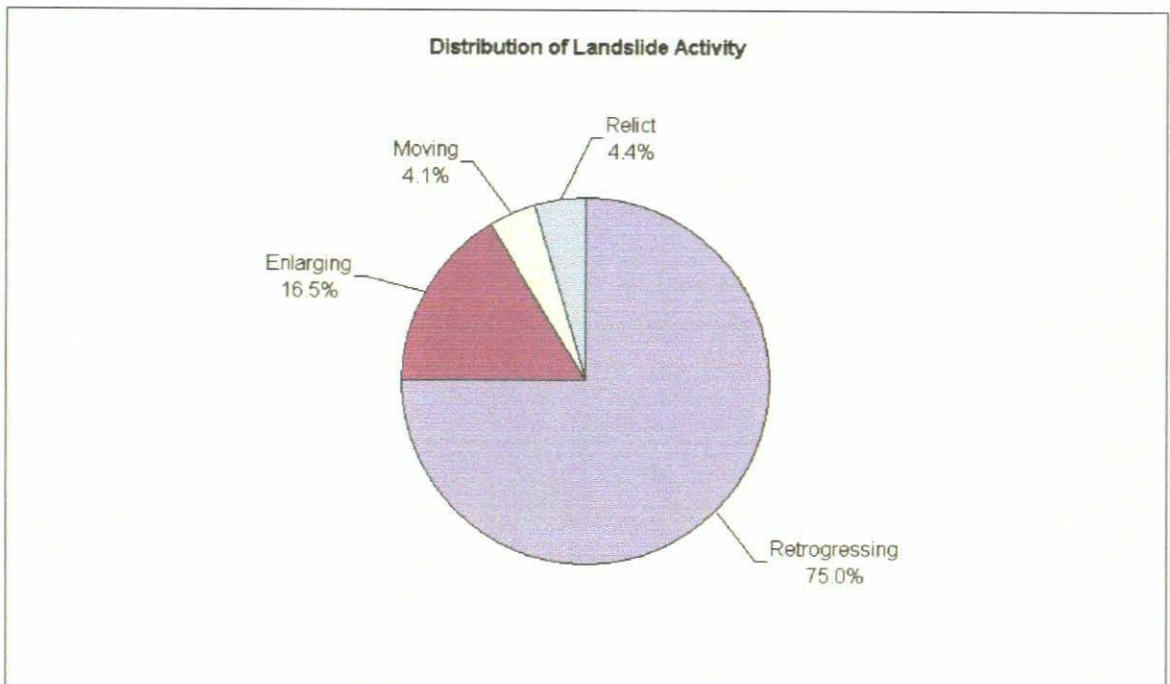
Figure 4.28 – Graph showing the breakdown of mapped landslides within the "Distribution of Landslide Activity" classes used by this study.

4.2.12 Landslide Activity & Failure Mechanism

Examination of the relationship between the state, style and distribution of the mapped landslide activity has highlighted the following points (Figures 4.29, 4.30 and 4.31):

- That the vast majority of either suspended or dormant landslides are rock falls and topples.

- That most of the mapped relict landslides are non-rotational landslides

- That the majority of "composite" landslides have been classified as "other" (landslides involving cambering, rock flow or debris movements).

- That the majority of retrogressing landslides are rock falls and topples, while the majority of enlarging landslides are non-rotational landslides.
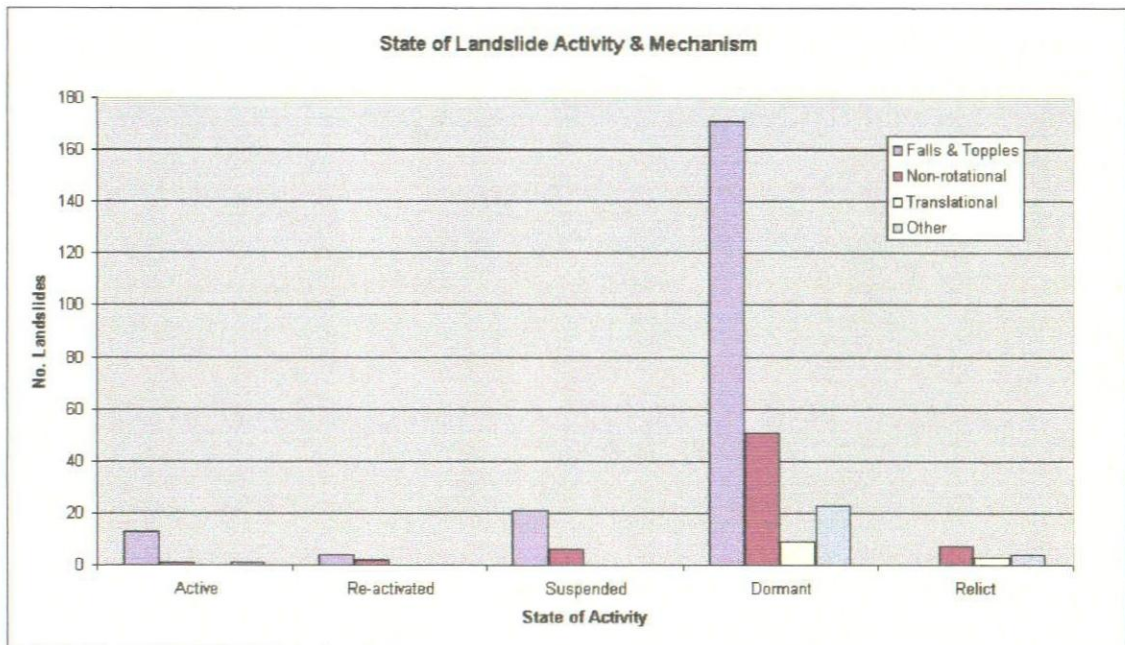
Figure 4.29 – Graph comparing the state of the mapped landslide activity against landslide failure mechanism.
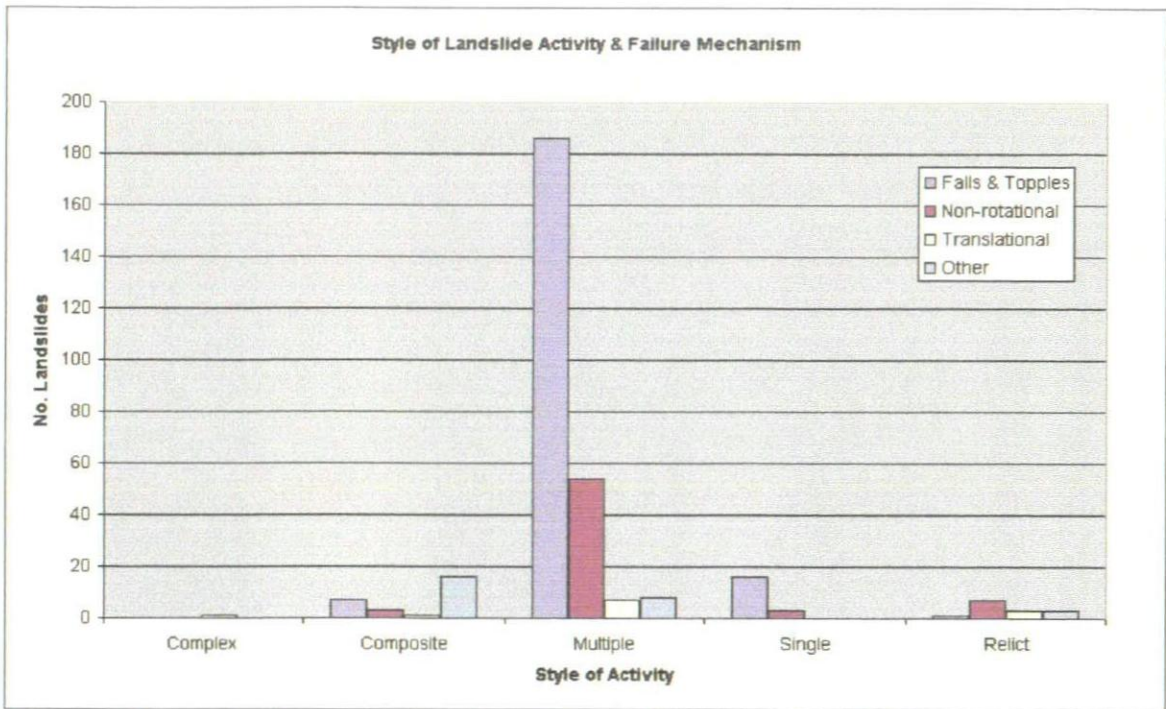
Figure 4.30 – Graph comparing the style of the mapped landslide activity against landslide failure mechanism
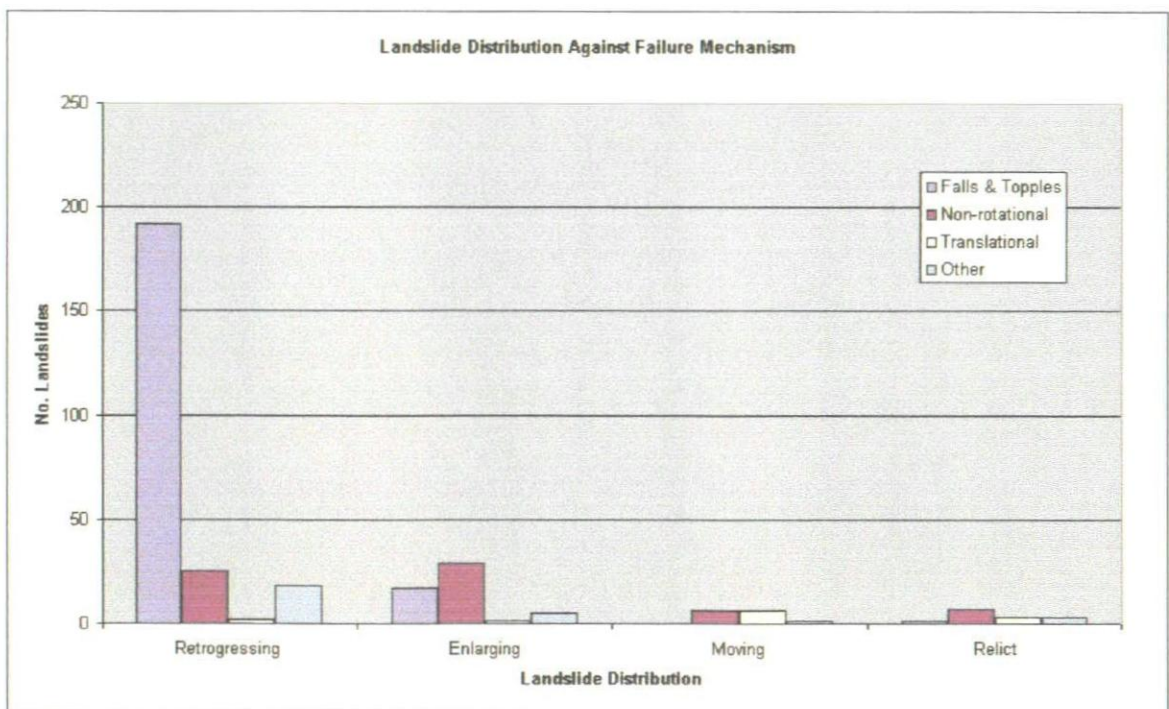
Figure 4.31 – Graph comparing the distribution of the mapped landslide activity against landslide failure mechanism

4.2.13 Landslide Activity & Geomorphology

The relationship between the geomorphological location (using the previously described terrain classification for the study area) and the state of landslide activity has been investigated. As already stated in the previous section, the overwhelming majority of the landslides mapped in this study have been described as being "Dormant" using the classification scheme of the WP/WLI (1993). This result would suggest that the state of landslide activity is not dependant on the geomorphological location of the landslide.

Unfortunately, due to the fact that the majority of the landslides in every Land System have been classified as "dormant" it is not possible to draw any conclusions as to how the geomorphological location of a landslide may affect its state of activity. This may reflect the nature of the landslide activity in the study area. However, it may also reflect the problem of having very limited historical records of landslide activity within the study area – a problem with most landslide studies (Griffiths, *pers. comm.*).

4.2.14 Landslide Statistics

The landslides recorded in the landslide inventory vary greatly in size and volume (Table 4.11). For example, the smallest landslides (involving a few cubic metres of material) measured a few metres in width, whereas the largest (measuring approximately 300×10^6 cubic metres) was approximately 2 km wide. However, the majority of the landslides recorded in the inventory are at the smaller end of the scale.

Table 4.11: Selected statistics relating to the geometry of the mapped landslide activity, as recorded in the landslide inventory.

Parameter	Max	Mean	Median	Skewness[1]
Height (m)	250	54.44	40	1.52
RS Width (m)	2000	162.01	75	3.10
AZ Length (m)	900	92.42	32.5	2.61
AZ Area (m^2)	1.50×10^6	19,782.53	50	11.54
AZ Volume (m^3)	1.47×10^8	2.32×10^6	3.67×10^4	10.79
Angle of Reach	84	39.99	39.5	-0.06

RS = Rupture Surface / AZ = Accumulation Zone

The landslide geometry data that has been collected shows that at least 700 million cubic metres (0.7 km^3) of material is currently involved in landslide activity, covering an area of over 6 million square metres (6 km^2). This implies that 1.4% of the study area is covered by landslide activity. The mapped landslides vary in volume from 10m^3 to 147 million m^3 of material (Figure 4.32). The largest 15 landslides are listed in Table 4.12 and shown in Figure 4.33. This landslide distribution map shows that the largest 13 landslides are found in two relatively distinct clusters; in the area close to the Rio

---

[1] Positive skewness indicates a distribution with an asymmetric tail extending toward more positive values. Negative skewness indicates a distribution with an asymmetric tail extending toward more negative values.

Aguas/Rambla Feos river capture and in the highest part of the Sierra Cabrera. The 14th and 15th largest landslides are found along the Rambla de Los Castaños and Río Jauto respectively.

Table 4.12 – Table showing the maximum estimated volumes of the 15 largest landslides in the Río Aguas study area.

No.	Grid Reference	Landslide Location or Name	Volume (10^6 m^3)
1	0585041055	Cuesta del Honor	147.3
2	0581541034	Barranco Los Barrancones	58.9
3	0599541085	Cerro de Cucar	32.7
4	0595841075	Cerro de Los Peralicos	29.3
5	0594541085	Loma del Colorado 2	28.4
6	0598241075	Barranco de Mofar 1	27.5
7	0586541064	La Parrica	26.2
8	0598541080	Barranco de Mofar 2	23.6
9	0585341074	Marchalico Viñicas 2 ("Relict")	17.0
10	0598541083	Barranco de Mofar 3	16.8
11	0585141071	Marchalico Viñicas ("Recent")	15.1
12	0583841053	Tension Crack Ridge	14.7
13	0593841065	La Carrasca	12.6
14	0581041122	Limestone Escarpment Failures (near to Cariatiz)	11.5
15	0590541135	Río Jauto Canyon 4	10.5

When compared with a selection of well known landslides described in the literature (Table 4.13) it is seen that these landslides are on a comparable scale. It should be noted that in the majority of cases these volumes are estimates as it is almost impossible to measure the dimensions of a landslide accurately and, therefore, calculate the volume of displaced material.

216

Table 4.13 – Table showing the volumes of a number of landslides selected from the literature (Turner & Schuster, 1996; Varnes, 1978; Voight, 1978).

Landslide Location or Name	Volume (10^6 m^3)
Blackhawk Slide	300
Nevados Huscaran (1970)	50-100
Medicine Lake	86.0
Vancouver Slide (Ok Tedi, PNG)	61.0
Hope Slide	47.3
Frank Slide	30.0
Nevados Huscaran (1962)	13.0
Sherman Glacier Rock Avalanche	10.1
Elm	10.0
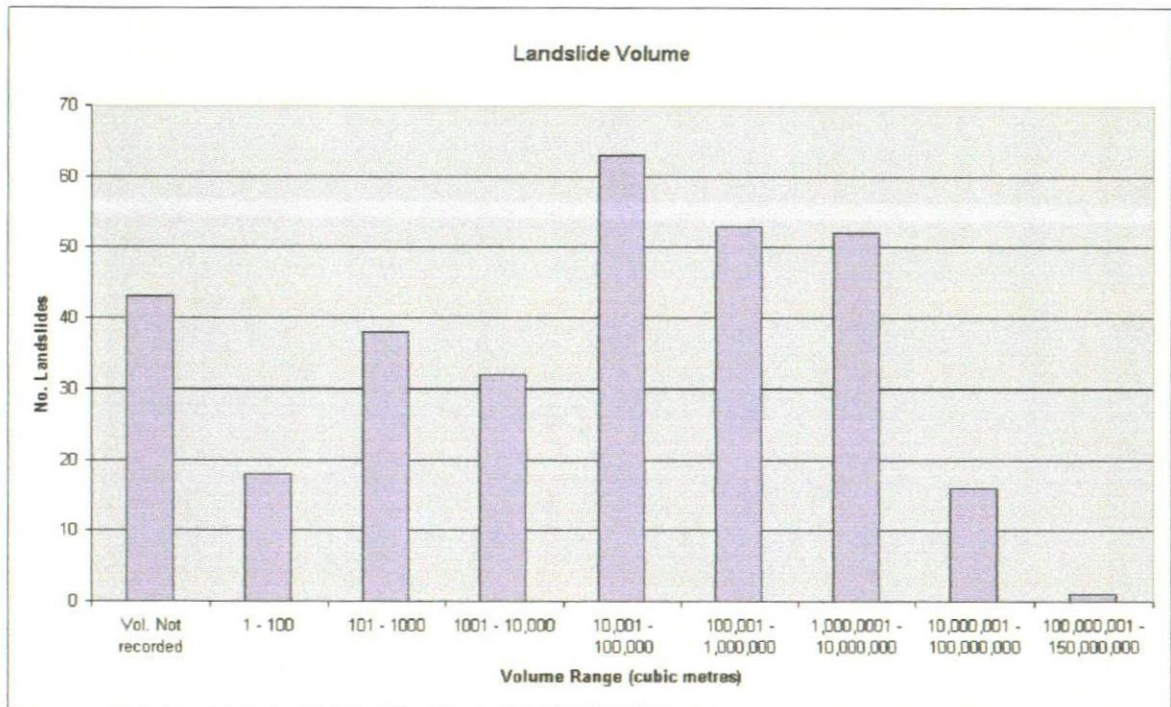
Figure 4.32 – Graph showing the distribution of the volumes of the mapped landslide activity.

Figure 4.33 - The Landslide Distribution Map for the Río Aguas Catchment Study Area Showing the Locations of the 15 Largest Landslides.

Legend

■ Settlements

⊕ *673* Spot Heights (m.a.s.l.)

⋈ Gypsum Quarries

〜 Drainage System

✳ Rio Agua/Rambla Feos "Wind Gap"

━━ Major Roads & Motorway

◆ Landslide

━━ Study Area Boundary

10◆ Numbered Landslide relating to Table 4.12 (The 15 Largest Landslides in the study area)
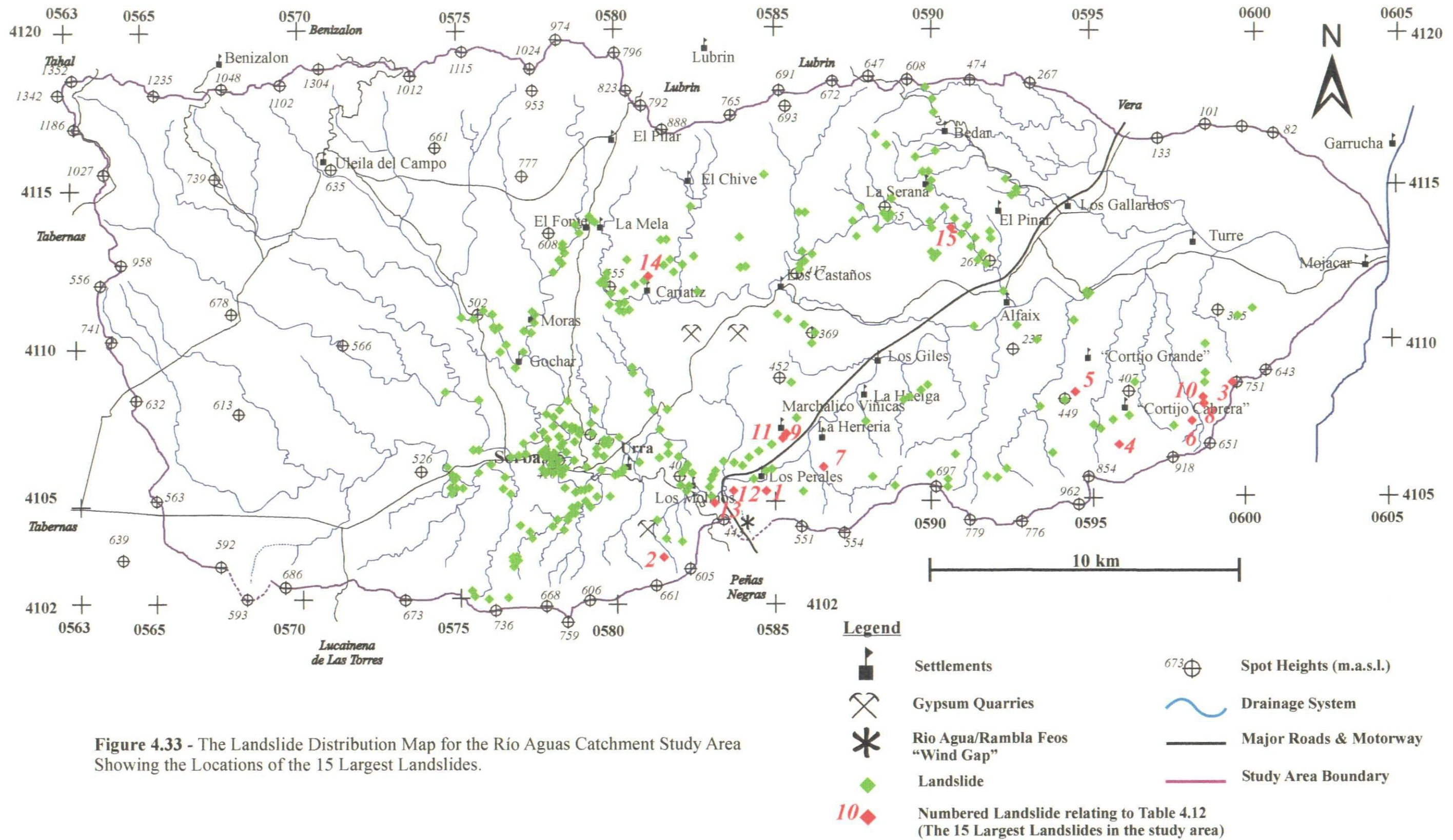
Mather *et al.* (2002) and Stokes *et al.* (2002) both estimated that between 1.29 and 1.39 km^3 of material has been removed from the upper section of the Río Aguas catchment area due to surface lowering and incision of the drainage system. Their study area was approximately 0.76 km^2. This research project has mapped 180 landslides within this area, with a combined volume of approximately 0.23 km^3. This would suggest that landslide activity accounts for approximately 17.8% of this material.

4.2.15 Runout Length and Volume

The runout length for all of the landslides has been plotted against the volume of the landslide (Figure 4.34). The runout length of a landslide is the distance from the crown of the landslide scar to the toe of the landslide debris (Corominas, 1996) and has been measured for each of the landslides recorded in the landslide inventory.

Analysis of the relationship between the runout length of the mapped landslides and their volumes has shown a strong positive relationship (R^2 value of 0.9162 with 263 degrees of freedom and a t-test percentile of greater than 0.995 suggesting that this relationship is statistically significant; Table 4.14). There is very little scatter in the data when all plotted together (Figure 4.34). A general trend of increasing runout length with increasing volume can be seen in the data when combined together. The scatter in the data increases at the higher runout lengths. This may indicate that some of the landslides may have travelled slightly further than might be expected.

By studying the relationship between the runout distance and the landslide volume for landslides involving different rock types and/or failure mechanisms, it may be possible to gain an understanding of how any future landslide might behave. The best correlation was between landslide volume and runout length based on the basis of the rock type or types involved in the landslide (Figures 4.35 and 4.36). A series of best-fit lines were calculated for each rock type or failure mechanism examined (Table 4.14).
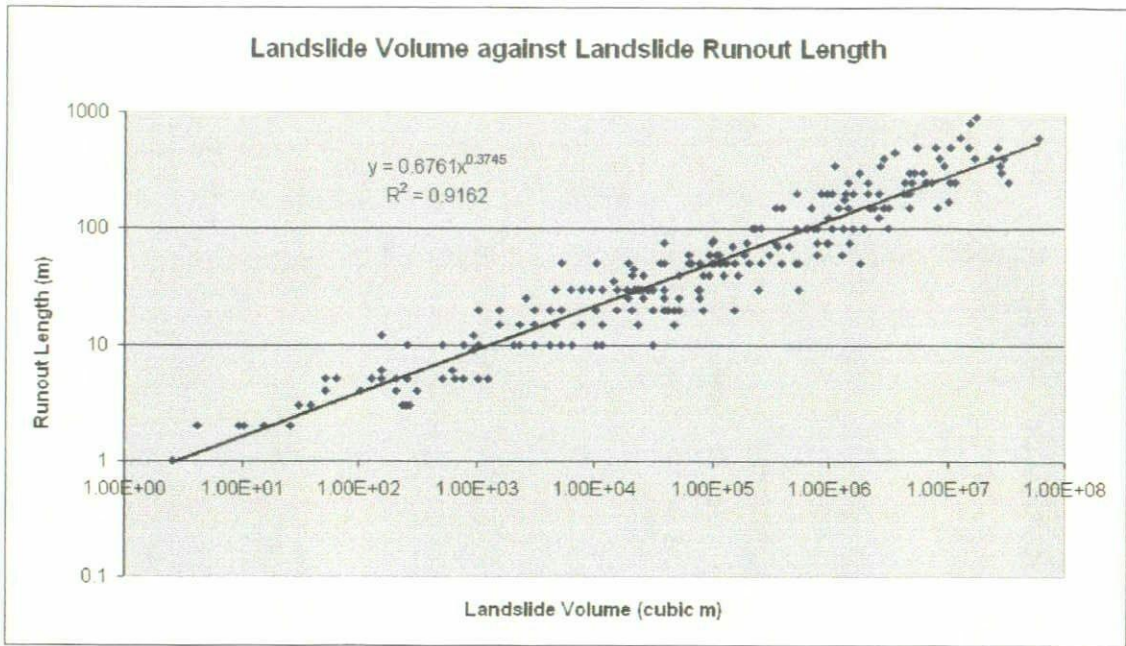
Figure 4.34 – Graph comparing the relationship between landslide volume and runout length.
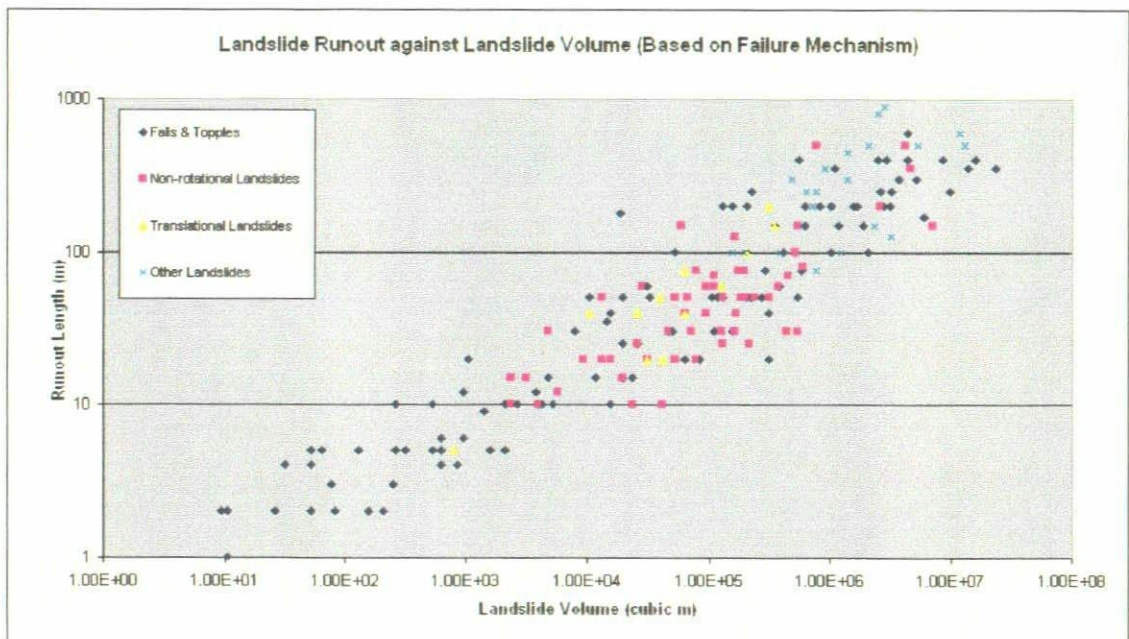
Figure 4.35 – Graph comparing the relationship between landslide volume and runout length based on primary landslide failure mechanisms.

Table 4.14 – Table showing the R-squared values and best fit equations for the relationships between landslide runout and volume of the mapped landslide activity.

Geology	Equation	Degrees of Freedom	R^2	t-test Percentile
All Data	$y = 0.6761 \, x^{0.3745}$	263	0.9162	0.995
Conglomerate	$y = 1.1708 \, x^{0.2943}$	35	0.8792	0.995
Mudstone	$y = 0.8949 \, x^{0.3619}$	3	0.9871	0.995*
Sandstone	$y = 0.886 \, x^{0.3684}$	24	0.886	0.995
Limestone	$y = 0.4891 \, x^{0.3893}$	31	0.9512	0.995
Schist	$y = 0.3219 \, x^{0.8523}$	27	0.8523	0.995
Gneiss	$y = 0.7297 \, x^{0.3651}$	16	0.7985	0.995
Basement Material	$y = 0.6614 \, x^{0.3793}$	17	0.6337	0.995
Conglomerate & mudstone	$y = 4\text{Ex-05}x + 28.556$	16	0.8747	0.995
Conglomerate & sandstone	$y = 5\text{Ex-05}x + 18.513$	7	0.9082	0.995*
Gypsum & mudstone	$y = 0.8378 \, x^{0.3839}$	22	0.7309	0.995
Sandstone & mudstone	$y = 1.3054 \, x^{0.3128}$	25	0.8531	0.995
Limestone & mudstone	$y = 0.7833 \, x^{0.3747}$	17	0.894	0.995
Rock falls & topples	$y = 0.5297 \, x^{0.4018}$	170	0.8906	0.995
Non-rotational landslides	$y = 0.5080 \, x^{0.3898}$	58	0.6029	0.995
Translational landslides	$y = 0.1385 \, x^{0.5389}$	10	0.8192	0.995
"Other" landslides	$y = 0.8016 \, x^{0.4057}$	22	0.4017	0.995

* = Ignored due to less than 10 degrees of freedom. A t-test percentile of 0.995 implies that the probability of the relationship occurring by chance is less than 1 in 500 ($p \leq 0.005$).

When examining the relationships between landslide runout and volume for landslides of differing rock types or failure mechanisms, the following observations were made:

- Landslides with larger volumes and long runout lengths involve mica schist, gneiss, "basement material" or gypsum overlying mudstone.

- Non-rotational and translational landslides tend to have moderate volumes and runout lengths.

- Landslides classified as "Other" tend to have the largest volumes and runout lengths. These are also the landslides that involve gypsum overlying mudstone.
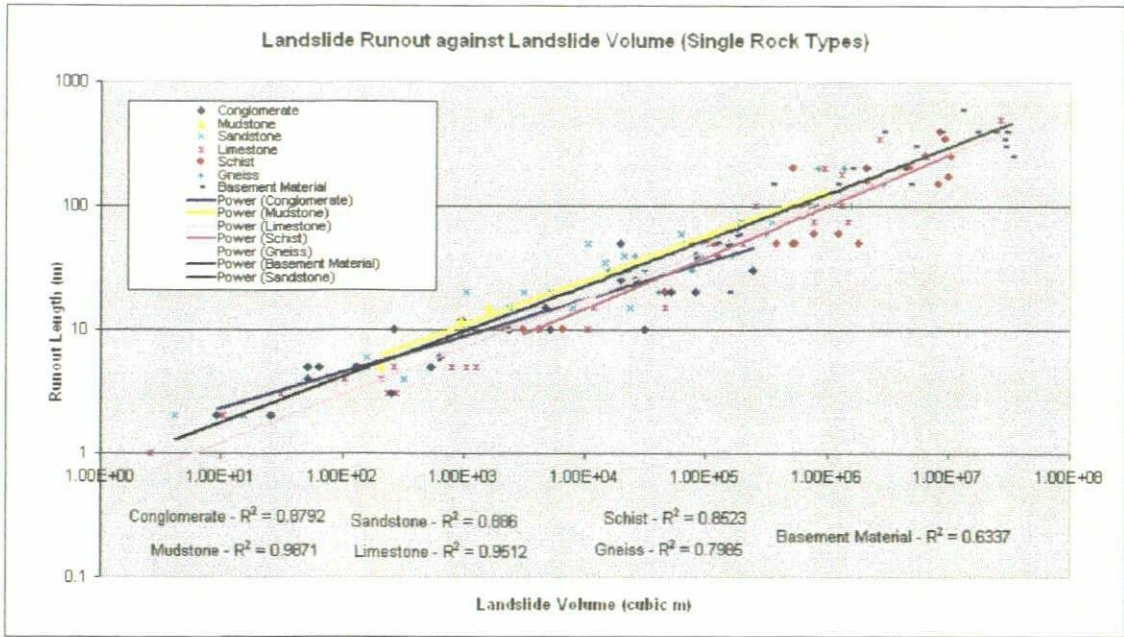
A.
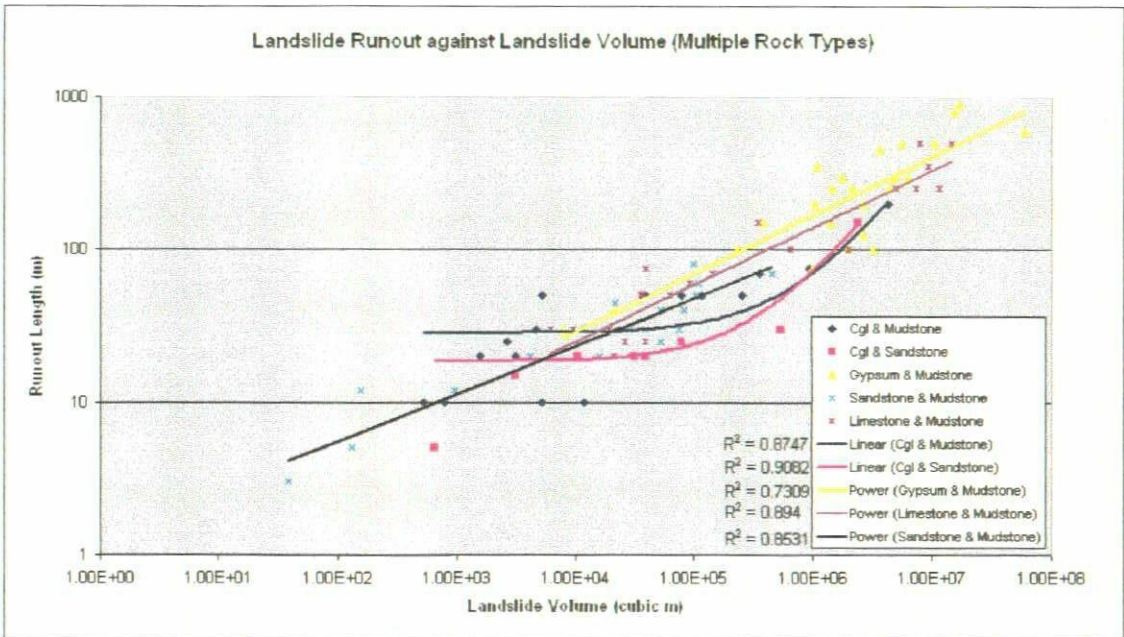
B.

Figure 4.36 – Graphs comparing the relationship between landslide volume and runout length for different rock types. **A.** Single rock types. **B.** Multiple rock types.

4.2.16 The Angle of Reach

The angle of reach of a landslide is the angle of a line connecting the head of the landslide source to the distal margin of the displaced mass (Corominas, 1996). Heim (1932) called this the "fahrböschung angle" and proposed that it was a measure of the relative mobility of rock avalanches or sturzstroms. Shreve (1968) called this angle the equivalent coefficient of friction, and Scheidegger (1973) claimed that for a sliding body the tangent of the reach angle is the coefficient of friction of the surface of contact between the sliding mass and the ground. However, Hsü (1975) and Voight (1978) both showed that Scheidegger's assumption is valid only in the case of the slope of the line linking the centres of gravity of the landslide source and deposit (Corominas, 1996).

Plots of the tangent of the angle of reach (expressed as the ratio between the vertical drop H and the horizontal projection of the distance L) versus the landslide volume show that large landslides tend to develop lower angles of reach than smaller ones, and because of this, they are considered more mobile (Scheidegger, 1973; Hsü, 1975; Lucchitta, 1978; Tianchi, 1983; Voight et al., 1983). Corominas (1996) noted that Skermer (1985) insisted that there is no relationship between the angle of reach and the volume of a landslide. He argued that the increase in mobility in large landslides is mostly due to the height of the fall. A greater height of fall should correspond to longer horizontal displacements.

Corominas (1996) has also stated that a volume threshold was observed in landslide mobility. Scheidegger (1973) had stated that a decrease in the angle of reach occurs when the volume of the landslide approaches or exceeds 1×10^5 m^3. For lesser volumes, a constant coefficient of friction can be assumed in most cases. Hsü (1975)

225

revised this limit up to 0.5×10^6 m^3, the volume below which the *H/L* relation is approximately equal to 0.6, the value of the coefficient of friction of most natural rock types. Other authors do seem to agree with this value (McEwen, 1989). However, additional data suggest that small landslides display a variable angle of reach that can be similar to those for large landslides. For example, Hutchinson (1988) demonstrated how flow slides and chalk failures of relatively small dimensions exhibited *H/L* ratios similar to those of large landslides. It has also been noted by Corominas *et al.* (1988) that some rock falls, planar slides and debris flows between a few hundred and several thousand cubic meters in volume exhibit relatively low angles of reach and that the reach is also controlled by the landslide failure mechanism.

This highlights a lack of agreement between researchers, with opposing conclusions being derived from these simple relations. Corominas (1996) then argued that this seems to suggest that a direct inference from the plots of volume versus the tangent of the angle of reach cannot be made and that additional considerations are needed to properly understand the relationship between the volume of a landslide and the angle of reach of that landslide. Other factors that were looked at by Corominas (1996) that were argued to control the angle of reach of a landslide were the type of failure mechanism and the runout path of the landslide, including any obstacles in that path.

Corominas (1996) concluded that:

- All movements, regardless of mechanism, experience a continuous reduction in the angle of reach with increasing volume.

- The scattering in the plots relating to landslide volume to angle of reach is mostly due to the effect of obstacles and topographic constraints on the runout path.

- The horizontal distance covered is not only dependent on the volume of the landslide but on the height of fall which, in turn, is a result of the steepness of the path. Potential highly mobile landslides will not develop long runout unless the path is steep enough. Because of this, in order to express the degree of mobility in terms of distance reached, the use of a relative index such as the relative excess of travel distance (*Lr*) was recommended.

- Many small landslides appear to have relative excess of travel distance similar to some large landslides. However, the relative mobility increases with the volume of the landslide.

- Slow-moving landslides display angles of reach as low as very rapid rock avalanches. For these movements, no special mechanism like air trapping, vapour fluidisation, or acoustic fluidisation can be used to explain their high degree of mobility.

- The continuous and rapid decrease of the angle of reach from the smallest volumes suggest that beside pore-water pressure, scale effects must be considered to play an important role in the mobility of landslides.

- The angle of reach is an index of the efficiency of landslide motion because all of the movements displaying lowest angles of reach attain the farthest horizontal distance in relation to the height of fall or the potential energy of the moving mass. The angle of reach can also be used as an index of relative mobility.

- The angle of reach and the distance travelled are the result of the process of emplacement of the landslide; this includes its mass, debris properties, mechanism of motion, geometry of the runout path, presence of obstacles, presence of pore-water pressures, and scale-effects.

Corominas (1996) concluded that he agreed with the statement made by Heim (1932) that the travel distance of a sturzstrom depends on height of fall, regularity of the pathway, and size of the fallen mass.

The angle of reach for each of the landslides recorded in the Landslide Inventory was calculated using the geometric parameters that were collected either in the field or from the API. The angle of reach was also measured in the field wherever possible. In all cases where the angle of reach was both measured in the field and calculated using the measured geometric parameters there was very good correlation.

The relationships between the angle of reach and landslide runout length and the angle of reach and the landslide volume have both been investigated. In both cases, there is a negative correlation with some scatter in the data (Figures 4.37 and 4.38). However, in both cases the R^2 values are significant with over 99.999% confidence (Tables 4.15 and 4.16). The data show that the angle of reach decreases with increasing landslide volume and landslide runout length. This fits with the trend of increasing runout length with increasing landslide volume described in the last section.

These relationships were then investigated on the basis of either the rock type (or types) or landslide failure mechanism involved in the landslide (Figures 4.39 to 4.42). The best fit relationships were calculated for all of these relationships (Tables 4.15 and 4.16).
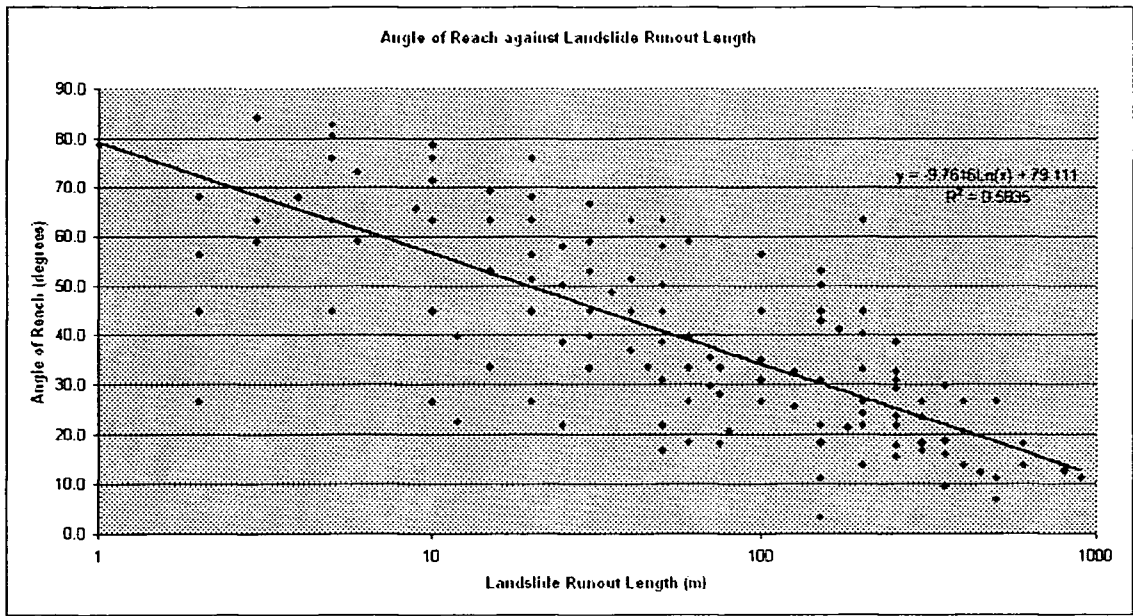
Figure 4.37 – Graph comparing the relationship between landslide runout length and the angle of reach for all mapped landslides with the specified data.
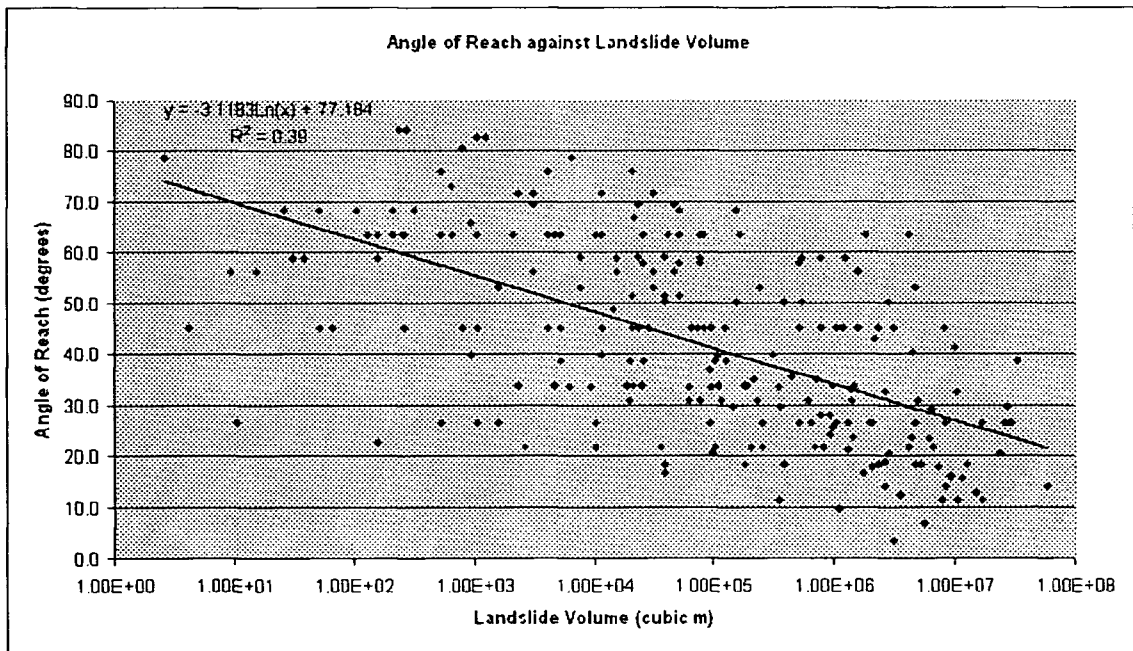
Figure 4.38 – Graph comparing the relationship between landslide volume and the angle of reach for all mapped landslides with the specified data.
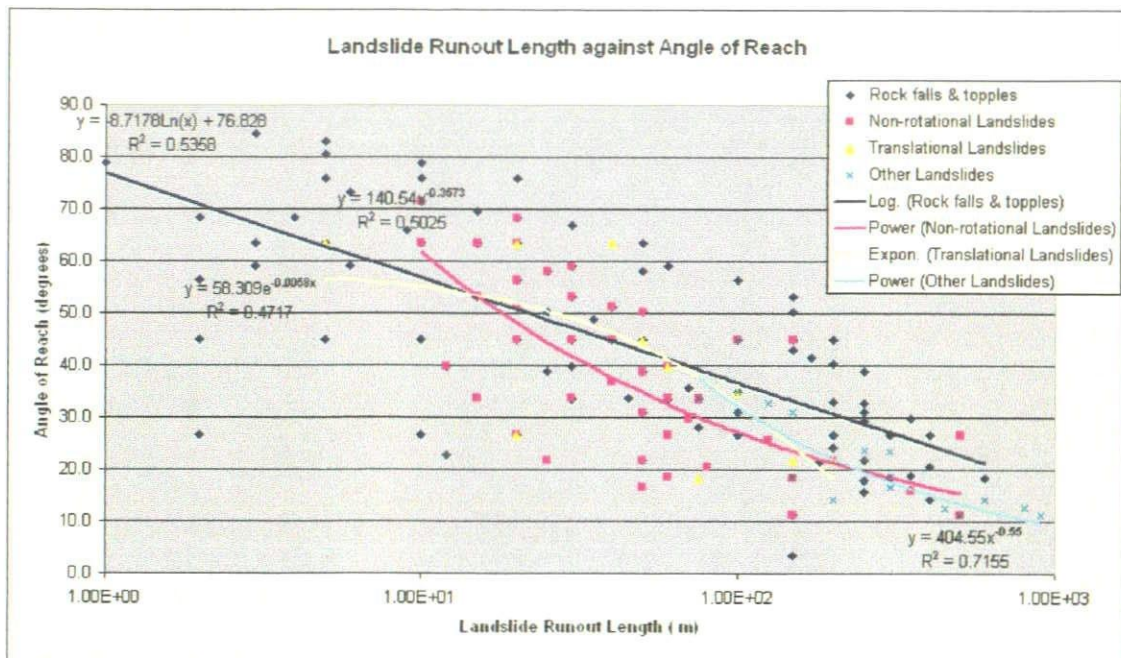
Figure 4.39 – Graph comparing the relationship between landslide runout length and the angle of reach based on the primary landslide failure mechanism.
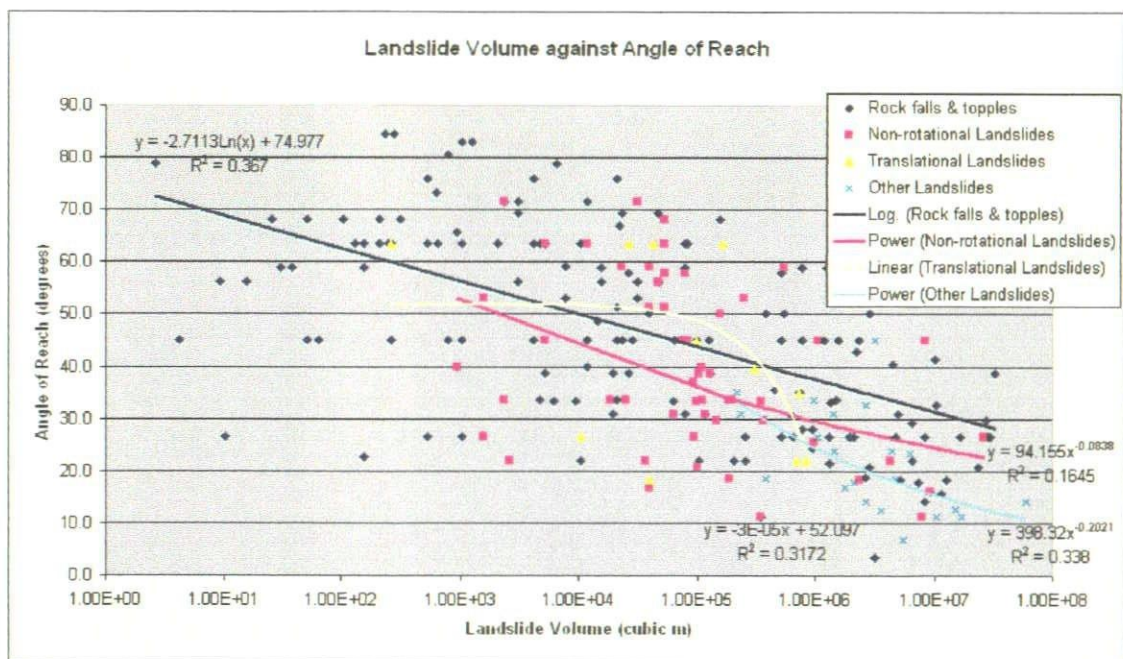
Figure 4.40 – Graph comparing the relationship between landslide volume and the angle of reach based on the primary landslide failure mechanism.
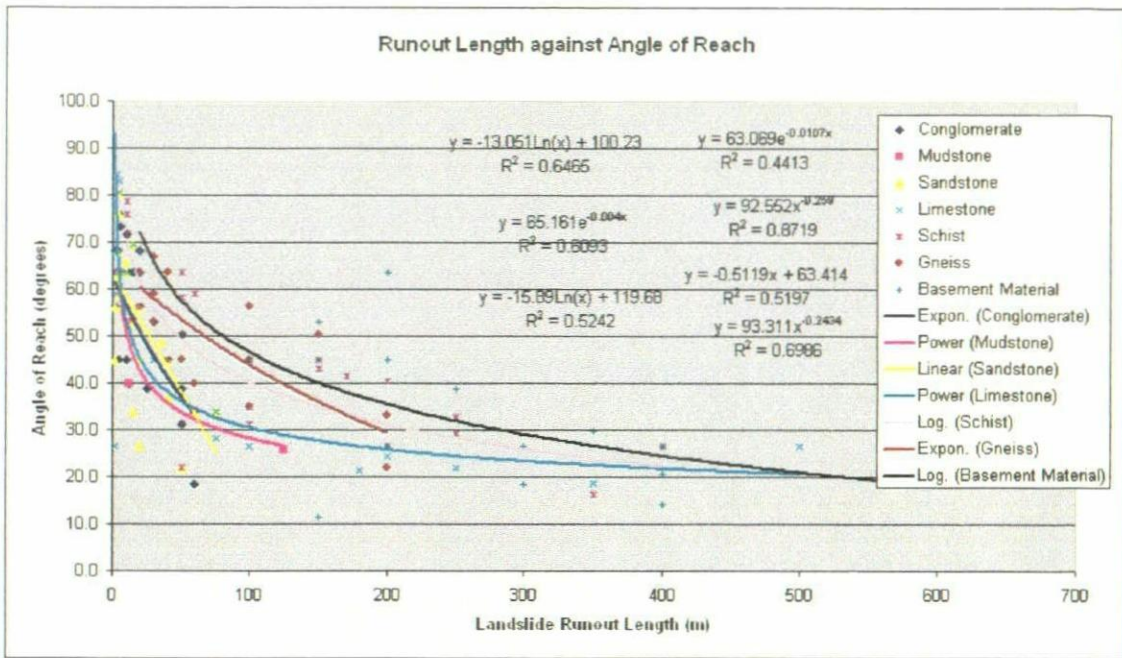
A.
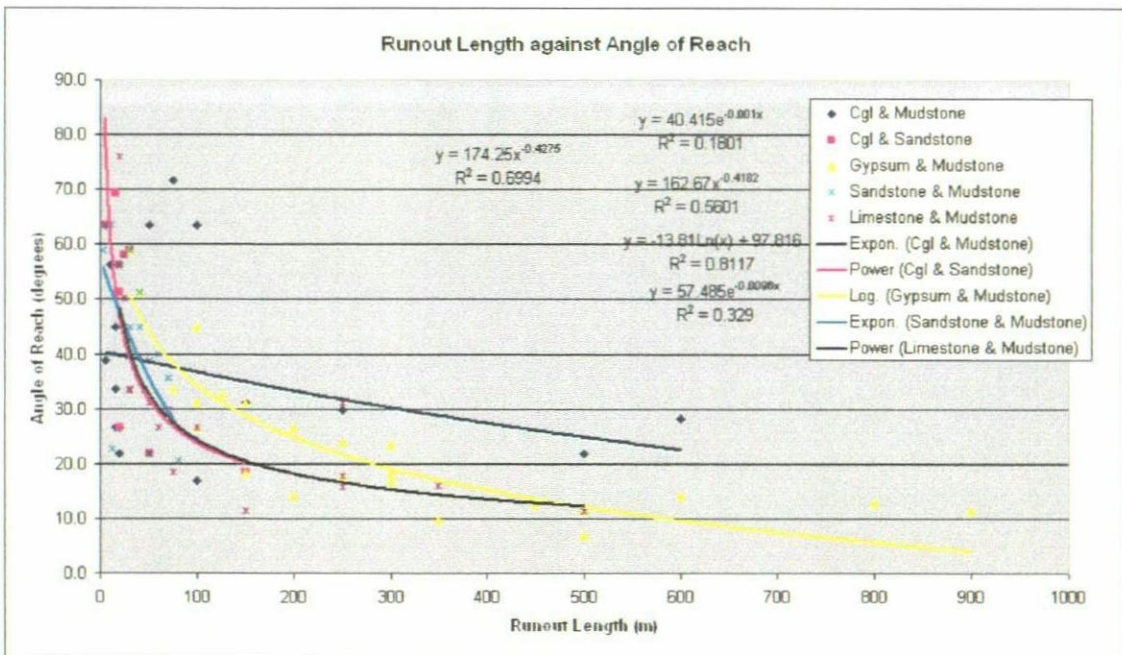
B.

Figure 4.41 – Graph comparing the relationship between landslide runout length and the angle of reach based on the rock type involved in the landslide. **A.** Single rock types. **B.** Multiple rock types.
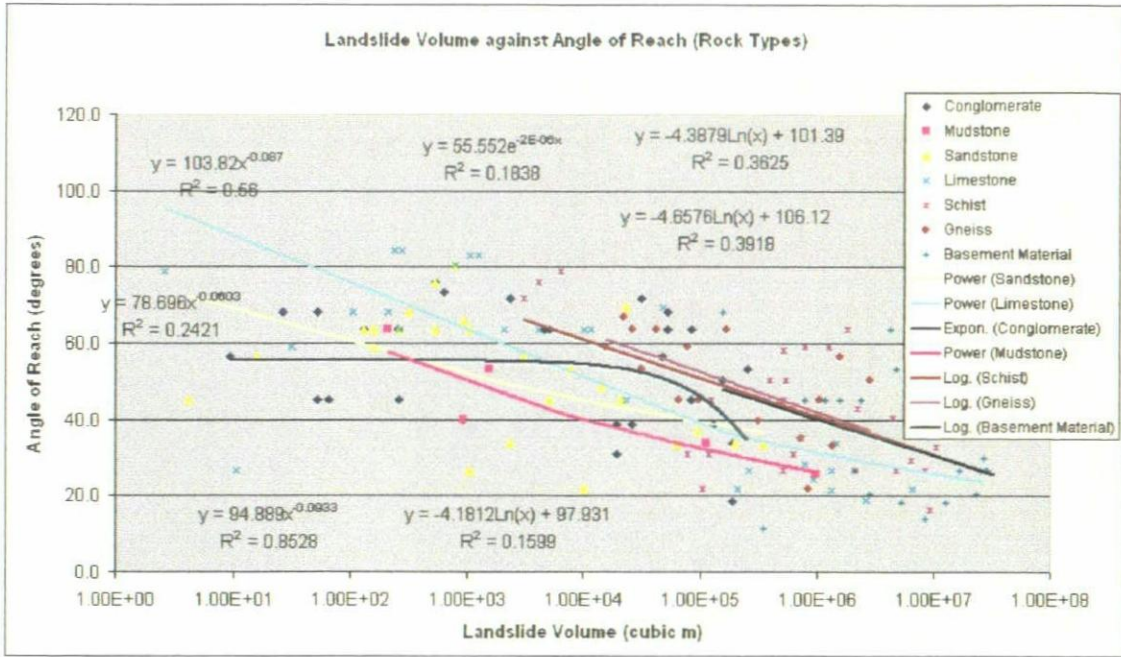
A.
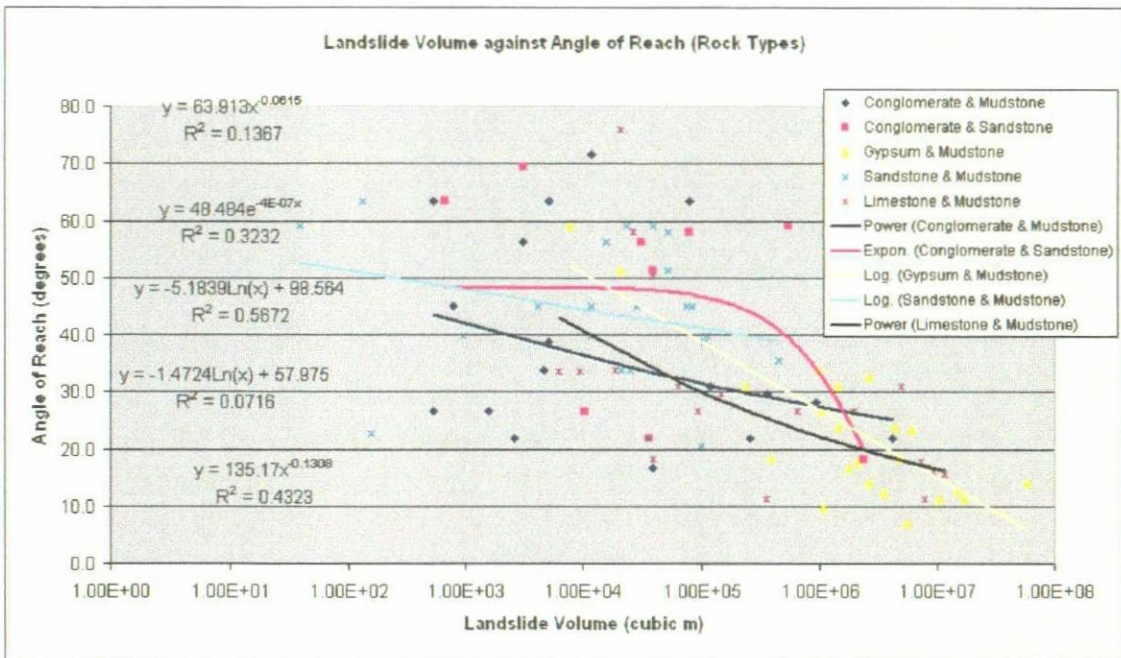
B.

Figure 4.42 – Graph comparing the relationship between landslide volume and the angle of reach based on the rock type involved in the landslide. **A.** Single rock types. **B.** Multiple rock types.

Table 4.15 – Table showing the R-squared values and best fit equations for the relationships between the landslide angle of reach and runout length of the mapped landslide activity.

Geology	Equation	Degrees of Freedom	R^2	t-test Percentile
All Data	$y = -9.7616 \text{Ln}(x) + 79.111$	263	0.5835	0.995
Conglomerate	$y = 63.069 x^{-0.0107}$	35	0.4413	0.995
Mudstone	$y = 92.552 x^{-0.2590}$	3	0.8719	0.975*
Sandstone	$y = -0.5119x + 63.414$	24	0.5197	0.995
Limestone	$y = 93.311 x^{-0.2434}$	31	0.6986	0.995
Schist	$y = -13.051 \text{Ln}(x) + 100.23$	27	0.6465	0.995
Gneiss	$y = 65.161 e^{-0.004}$	16	0.6093	0.995
Basement Material	$y = -15.89 \text{Ln}(x) + 119.68$	17	0.5242	0.995
Conglomerate & mudstone	$y = 40.415 e^{-0.001}$	16	0.1801	0.950
Conglomerate & sandstone	$y = 162.67 x^{-0.4182}$	7	0.5601	0.990*
Gypsum & mudstone	$y = -13.81 \text{Ln}(x) + 97.816$	22	0.8117	0.995
Sandstone & mudstone	$y = 57.485 e^{-0.0096x}$	25	0.3290	0.995
Limestone & mudstone	$y = 174.25 x^{-0.4275}$	17	0.6994	0.995
Rock falls & topples	$y = -8.7178 \text{Ln}(x) + 76.828$	170	0.5358	0.995
Non-rotational landslides	$y = 140.54 x^{-0.3573}$	58	0.5025	0.995
Translational landslides	$y = 58.309 e^{-0.0058}$	10	0.4717	0.990
"Other" landslides	$y = 404.55 x^{-0.55}$	22	0.7155	0.995

* = Ignored due to less than 10 degrees of freedom. A t-test percentile of 0.995 implies that the probability of the relationship occurring by chance is less than 1 in 500 ($p \leq 0.005$).

Table 4.16 – Table showing the R-squared values and best fit equations for the relationships between the landslide angle of reach and volume of the mapped landslide activity.

Geology	Equation	Degrees of Freedom	R^2	t-test Percentile
All Data	$y = -3.1183 Ln(x) + 77.184$	263	0.3900	0.995
Conglomerate	$y = 55.552 e^{-2E-6x}$	35	0.1838	0.995
Mudstone	$y = 94.889 x^{-0.0933}$	3	0.8528	0.975*
Sandstone	$y = 78.696 x^{-0.0603}$	24	0.2421	0.995
Limestone	$y = 103.82 x^{-0.0870}$	31	0.5600	0.995
Schist	$y = -4.3879 Ln(x) + 101.39$	27	0.3625	0.995
Gneiss	$y = -4.6576 Ln(x) + 106.12$	16	0.3918	0.995
Basement Material	$y = -4.1812 Ln(x) + 97.931$	17	0.1599	0.950
Conglomerate & mudstone	$y = 63.913 x^{-0.0615}$	16	0.1367	0.900
Conglomerate & sandstone	$y = 48.484 e^{-4E-7}$	7	0.3232	0.950*
Gypsum & mudstone	$y = -5.1839 Ln(x) + 98.564$	22	0.5672	0.995
Sandstone & mudstone	$y = -1.4724 Ln(x) + 57.975$	25	0.0716	0.900
Limestone & mudstone	$y = 135.17 x^{-0.1308}$	17	0.4323	0.995
Rock falls & topples	$y = -2.7113 Ln(x) + 74.977$	170	0.3670	0.995
Non-rotational landslides	$y = 94.155 x^{-0.0838}$	58	0.1645	0.995
Translational landslides	$y = -3.E-5x + 52.097$	10	0.3172	0.950
"Other" landslides	$y = 398.32 x^{-0.2021}$	22	0.3380	0.995

* = Ignored due to less than 10 degrees of freedom. A t-test percentile of 0.995 implies that the probability of the relationship occurring by chance is less than 1 in 500 ($p \leq 0.005$). A t-test percentile of 0.950 implies that the probability of the relationship occurring by chance is less than 1 in 20 ($p \leq 0.05$).

In particular, the analysis seems to agree with the observations of Scheidegger (1973) that a decrease in the angle of reach occurs when the volume of the landslide approaches or exceeds $1 \times 10^5 \text{ m}^3$ (Figure 4.43). For example, the analysis highlighted the following points:

- Very few of the low volume landslides have low angles of reach;

- That the converse is also true – that very few large volume landslides develop high angles of reach;

- Landslides with volumes less than approximately $1 \times 10^5 \text{ m}^3$ tend to have relatively high angles of reach; and

- Landslides with volumes greater than approximately $1 \times 10^5 \text{ m}^3$ tend to have relatively low angles of reach.
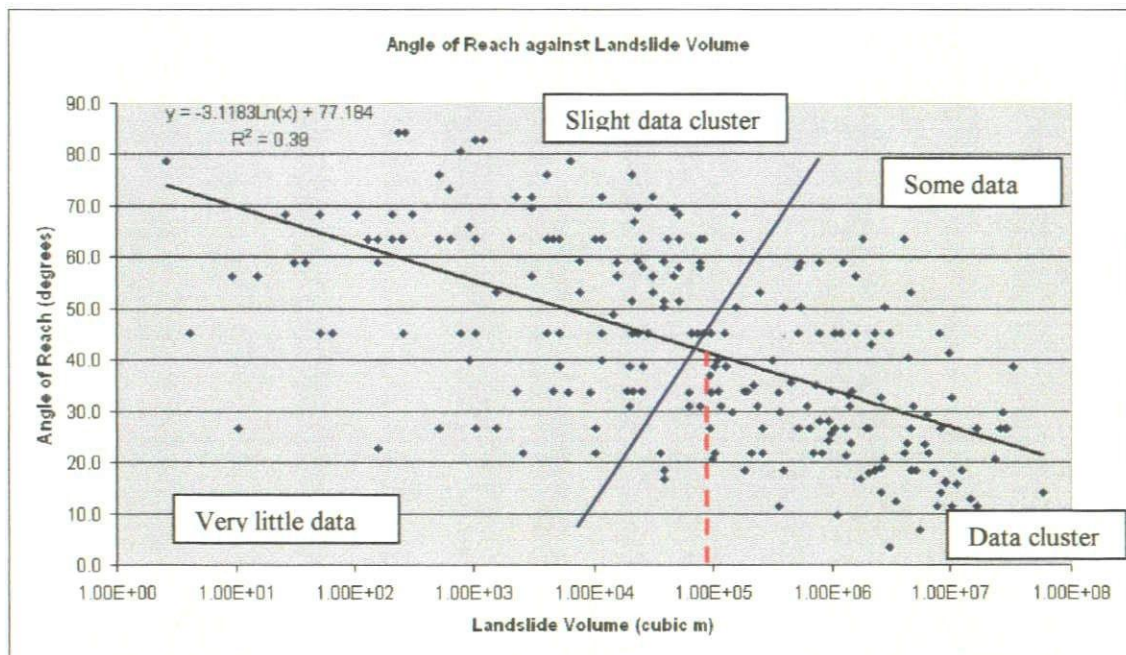
Figure 4.43 – Annotated graph comparing the relationship between landslide volume and angle of reach for all mapped landslides with the specified data.

This analysis agrees with the observations of Scheidegger (1973), Hsü (1975), Lucchitta (1978), Tianchi (1983), Voight *et al.* (1983) and Corominas (1996) who all stated that larger volume landslides tend to develop lower angles of reach. They all suggested that this showed a higher mobility in the larger volume landslides with respect to the smaller volume landslides. This analysis has shown that:

- The majority of the landslides involving gypsum overlying mudstone (as well as those landslides classified as being "Other") had large volumes and low angles of reach (and therefore fell into the fourth category listed above). The majority of the "Other" landslides involve gypsum overlying calcareous mudstone and occur along the edge of the Gypsum Escarpment.

- The majority of the landslides involving either mica schist, gneiss or "basement material" tend to have higher volumes and higher angles of reach. This could be a reflection of the fact that the majority of these landslides occur on mountain slopes with relatively steep slope angles. Therefore, the slope morphology is affecting the angle of reach and the apparent mobility of the landslide.

- A large number of the non-rotational landslides have volumes of approximately 1×10^5 m^3, but a range of angles of reach. This may also be a reflection of the slope and morphological setting of the landslide.

- The statistical analysis of the best fit lines for the different relationships studied (using the t-test) has shown that almost all of these relationships are statistically significant, with percentile values above $t_{0.995}$. This indicates that the relationships studied have a less than 1 in 500 probability of occurring by chance.

Many of these observations seem to agree broadly with the observations and conclusions of Corominas (1996) that were described earlier in this section. It should also be noted that the data set used by this study is larger than the data set used by Corominas (1996).

4.2.17 Land Use

The land use of a landslide site and its location with respect to the landslide has been recorded in the landslide inventory. These data would be required for both landslide susceptibility and landslide risk analysis.

Unsurprisingly for a relatively remote and rural area, the majority of the mapped landslides (approximately 73%) do not affect any particular land use or infrastructure (Figure 4.44). Those landslides that affect agricultural land or abandoned agricultural land account for 8.9% and 1.9% of the mapped landslides respectively (Figure 4.44).

An observation that may be of some concern for a remote rural area, are the 3.3% of the mapped landslides that occur above or below private, residential buildings (Figure 4.44). Another concern would be the number of mapped landslides occurring either above, below or crossing the roads and tracks of the study area (9.3% of the mapped landslides; Figure 4.44).

It is difficult to ascertain whether land use influences slope stability within the study area. In many cases it is a question of either cause or effect or both. For example, agricultural land may be abandoned due to landslide activity, as in the case of the

landslides at Casa del Aguarico (Figure 4.45; Grid reference: 0579341077), or a landslide may occur because of agricultural land (and associated irrigation ditches) not being maintained. For example, poorly maintained drainage lines may result in water seeping into the ground and causing dissolution and/or soil erosion. Field observations suggest that this can lead to slope instability.

The situation is further complicated by the suggestion that a particular land use may lead to slope instability. In the example of Casa Del Aguarico, the blocks (sliding on a high-angle, non-rotational compound shear surface) incorporate ploughed ground, which was obviously in use at the time of the landslide occurring (Figure 4.45). An important consideration to be made would be whether it was the irrigation of the area that actually led to the landslide occurring, or whether that was just coincidental. After talking with local residents about this particular example, it is highly unlikely that the plants being grown in the area where the landslide occurred were being irrigated. This would suggest that the landslide was a natural occurrence and not the result of human activity.

In general, the results from this analysis and observations made in the field would suggest that the majority of the landslides mapped in the study area are natural terrain landslides, and not the result of human interference in the landscape. However, as expansion of the transport network, intense agricultural practises and settlements continues this picture may change.
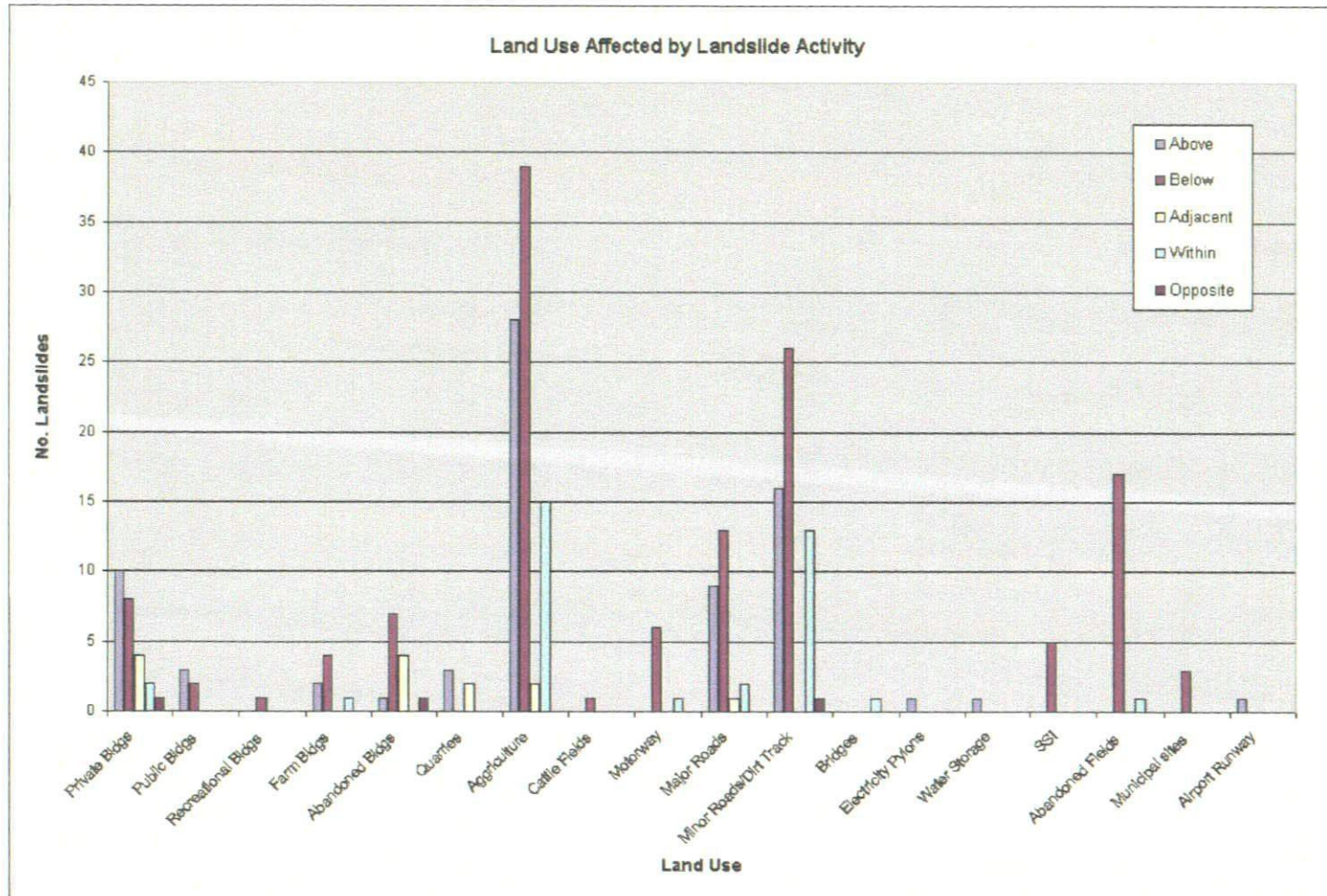
Figure 4.44 – Graph showing the different types of land use (as defined by this study) affected by the mapped landslide activity in the study area.

Another high-angle, non-rotational landslide on the other side of the valley

Rows of planted crops

Landslide Backscar (throw is approximately 10m)
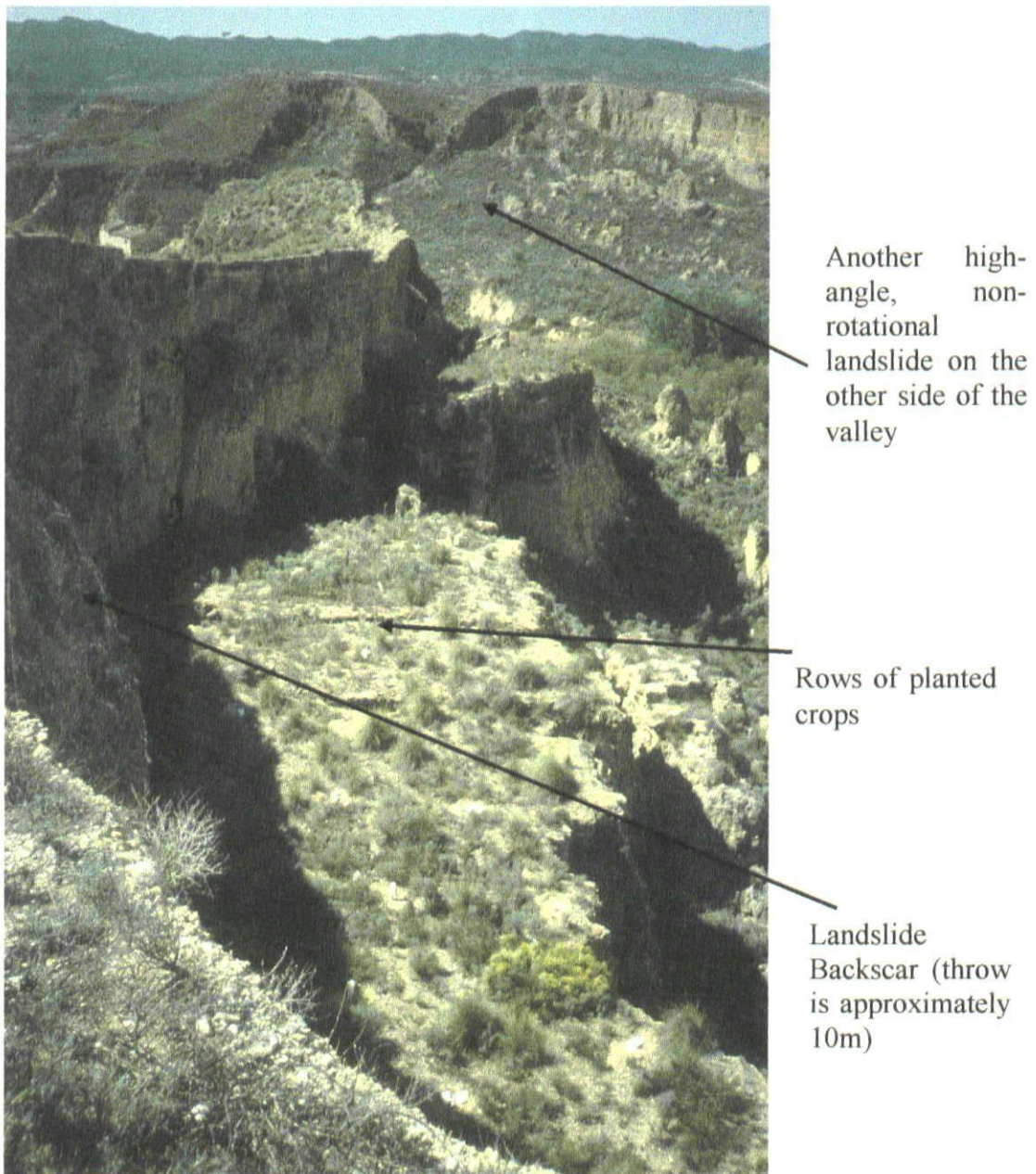
Figure 4.45 – Photograph of a back tilted block with remains of crops growing on its surface at Casa Del Aguarico (Grid Reference: 0579341079 / Facing to the South). The landslide occurs in the conglomerate and mudstone of the Zorreras Member. The back tiled block is approximately 10m across.

4.3   Landslide Causes

Part of the landslide investigation has included an investigation of the possible causes of the observed and mapped landslide activity.   The Working Party on the World Landslide Inventory proposed two classes of factors that lead to landslide activity (WP/WLI, 1994):

1. Preparatory Casual Factors – those factors, which make the slope susceptible to movement without actually initiating it and thereby tending to place the slope in a marginally stable state

2. Triggering Casual Factors – those factors, which initiate movement. These casual factors shift the slope from a marginally stable to an actively unstable state.

The identification of Preparatory Factors can be achieved through a combination of geological and geomorphological mapping as well as more detailed geotechnical investigations.   However, the identification of those factors that actually trigger a particular landslide are more difficult to identify, particularly in the absence of detailed historical evidence or actual eye witnesses to the event.   Therefore, this study has sought to identify only the Preparatory Casual Factors that are thought to be significant in leading to the observed landslide activity in the study area.   This has been through field mapping only.   There is also the argument that many landslides may have numerous causes but only one triggering factor.   Therefore, this study has sought to identify as many of the causes as possible.   However, the landslide inventory database was designed to record up to a maximum of twelve causes for each landslide.

The Working Party identified a list of factors that they considered to be significant in causing instability or landslide activity. This list can be sub-divided into four categories – geology, morphology, physical and human factors. These will be discussed in the following sections.

4.3.1 Geological Factors

All of the landslides mapped within the study area had some degree of geological control that was responsible for decreasing the stability of the slope (i.e., acting as preparatory factors). Within the study area the geological factors identified were:

-   Jointed or fissured material;

-   Adversely orientated mass discontinuities (bedding, cleavage, faults or unconformities);

-   Contrasts in permeability and its effects on groundwater;

-   Alternating sequences of "hard rocks" over "soft rocks"; and

-   Contrasts in stiffness (stiff, dense material over plastic material).

4.3.2 Morphological Factors

The role of the morphological factors acting on a slope or landslide is often speculative. As with the geological factors, the morphological factors acting on a slope or landslide will predominantly act to reduce slope stability rather than actually trigger a landslide. The majority of the landslides (203 or 64.2% of the mapped landslides) are closely related to the drainage network and therefore are influenced, if not directly affected by fluvial activity. For example, in the case of one landslide, an eyewitness account did

suggest that fluvial erosion of a slope during a river flood event led to the initiation of that particular landslide. However, as this was during a rainstorm event it is unclear as to how much the rainfall also influenced the triggering of this landslide.

Therefore, those factors that were assessed in the field as being significant in explaining the majority of the observed landslide activity in the study area were:

- Tectonic uplift of the study area;

- Fluvial erosion of many of the slopes;

- Subterranean erosion through piping and dissolution features (Figure 4.46); and

- Vegetation removal (by erosion, forest fire or drought).

Interestingly, the Working Party includes "tectonic uplift" as a morphological factor and not a geological factor. This is not helped by a lack of explanation for the scheme.

Large subterranean soil pipes and dissolution features were found in a number of locations around the study area. They were found in both very fine grained sandstone and mudstone (Figure 4.46) or within the gypsum of the Yesares Member. A number of these features were found in close proximity to approximately 99 (31.3%) of the mapped landslides. In some of the cases field mapping identified that some of the pipes and dissolution features were possibly channelling water into the landslides.

The dissolution features within the gypsum are related to the karst features that are widely seen within the Gypsum Plateau Land System (Section 2.4).

The presence of the pipes and dissolution features also highlights the highly erosive nature of some of the rocks units within the study area. This is related to the presence of expansive soils and highly erosive clay minerals being present in these rock units. It is, therefore, possible that this characteristic acts to decrease the stability of the rock material or rock mass and subsequently for a landslide to form.
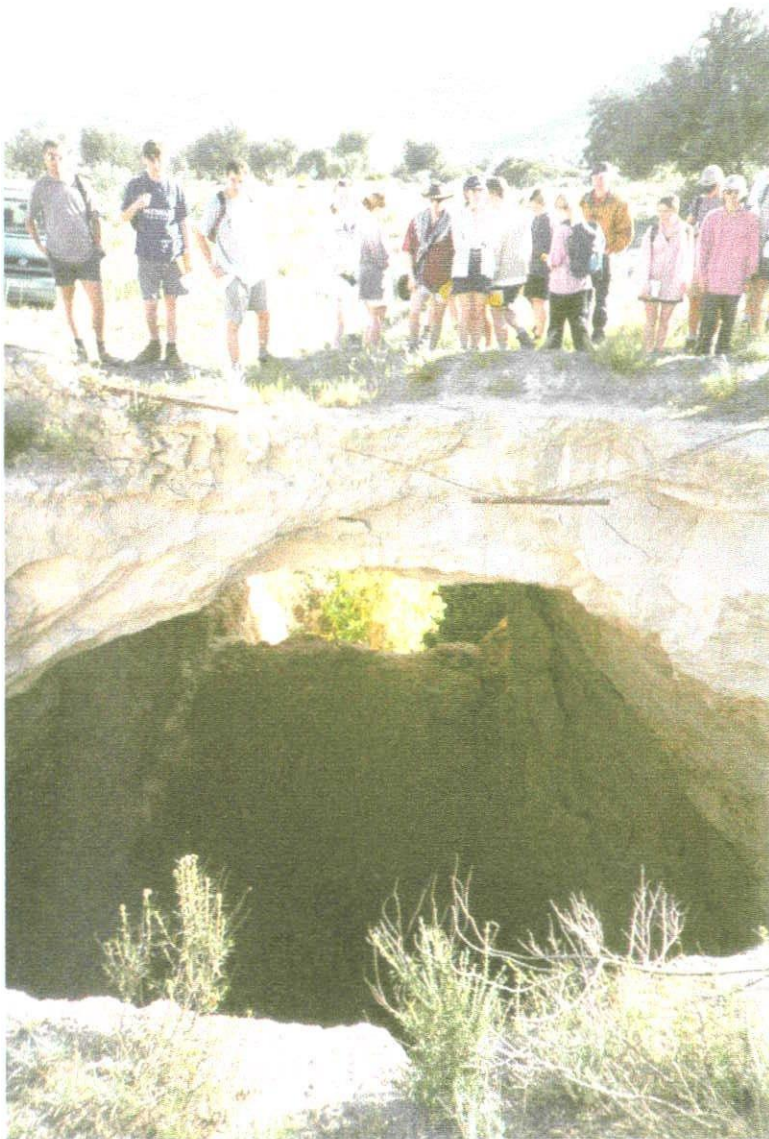
Figure 4.46 – Photograph of soil pipe within fine grained sediment (Grid Reference: 0600741114; approximately 1.5km west of Mojacár). The pipe has collapsed, leaving the large open cavern that is seen above. Third year students and staff for scale.

4.3.3 Physical Factors

The physical factors acting on a slope can act to reduce the stability of the slope, reactivate an existing landslide or actually trigger a new landslide. These factors are all heavily dependent on either historical documentation and/or eye witness accounts. As these two sources of information are very limited in the study area, this study has had to rely heavily on circumstantial evidence. Therefore, the following list of factors that are considered as being significant in causing the observed landslide activity in the study area is speculative. The factors are:

- Intense, short period rainfall;

- Earthquake activity; and

- Shrink and swell weathering of expansive soils and clays.

Unfortunately, detailed rainfall records (i.e., 24 hour records) over an extended period of time (i.e., several decades or longer) are not available for the study area. However, eyewitness accounts do suggest that a small number of the landslides have occurred during periods of intense rainfall (Thornes, 1974; Walsh, *pers. comm.*). However, in at least one example the rainstorm had led to the Río Aguas being in flood. This means that the landslide could have been triggered by either the rain or the flood event (or both). Unfortunately this means that it was impossible to complete an analysis of how many of the mapped landslides have been caused or influenced by rainfall.

Globally, earthquakes have long been recognised as a major cause of landslides (Keefer, 1984, 1999). Earthquake-induced landslides have been documented from at least as early 373 or 372BC (Seed, 1968). Despite their geomorphological and economic

significance, earthquake-induced landslides are still not well understood. In his key paper, Keefer (1984) argued that among the unanswered questions are: How does the number and distribution of landslides depend on earthquake magnitude, ground-shaking intensities and other seismic parameters? What types of landslides are caused by earthquakes? Which types of landslides are most hazardous to human life and property? What geological materials are most susceptible to landslides in earthquakes? Do earthquakes reactivate landslides originally triggered by non-seismic causes?

In answer to these questions, Keefer (1984, 1999) sought to investigate the relationship between the distribution and nature of landslide activity compared with earthquake activity of different magnitudes and intensities. He also considered the role of geology and other environmental parameters.

Keefer (1984, 1999) concluded that the area affected by landslides in an earthquake correlates with the magnitude of the earthquake (Figure 4.47). This area increases from almost 0 at $M \approx 4.0$. to approximately $500,000km^2$ for a $M = 9.2$ earthquake. Factors other than magnitude that control the area affected by landslides include the local geological conditions, earthquake focal depth, and the specific ground motion characteristics of a particular event. Certain threshold levels of ground shaking are necessary for triggering the various types of landslides. Indirect measures of these thresholds are the smallest earthquakes that cause landslides, the maximum distance of landslides from the epicentre or fault rupture (Figures 4.48) and the minimum intensity for landslides (Figure 4.49).
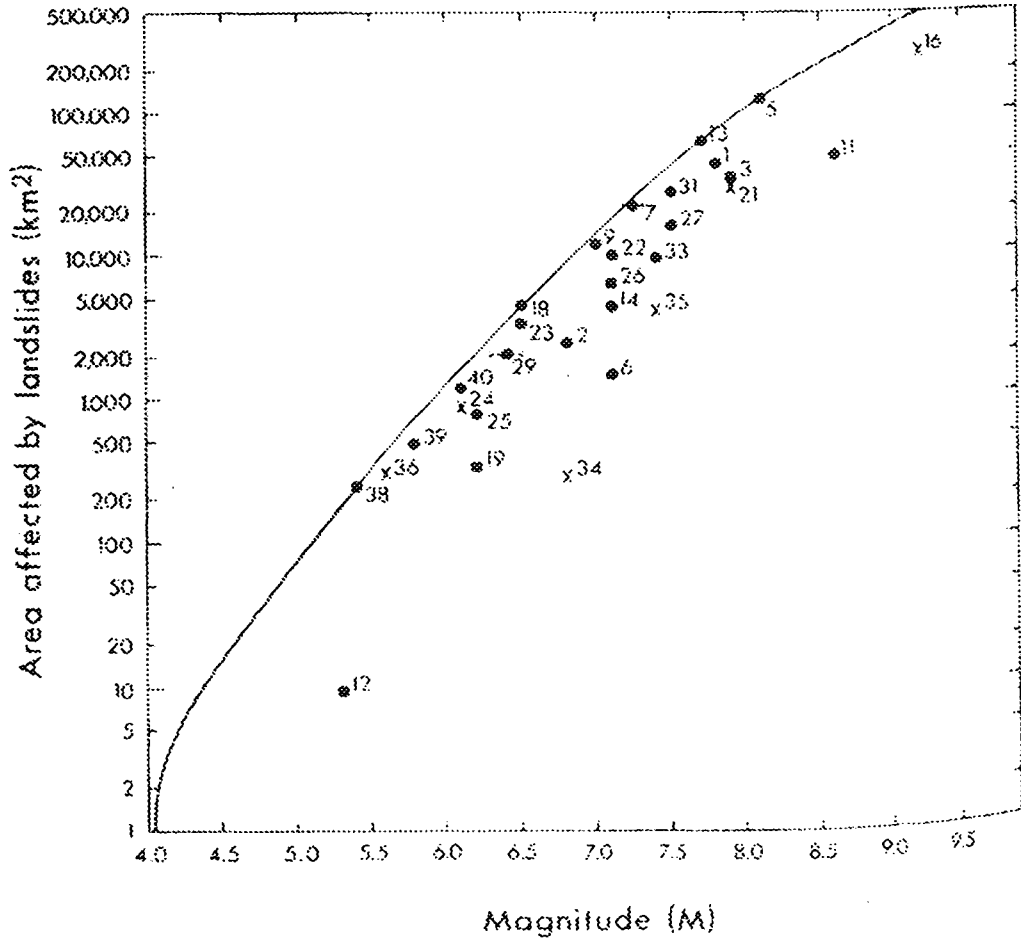
Figure 4.47 – Area affected by landslides in earthquakes of different magnitudes. Number beside data points are earthquakes listed in Table 1 of Keefer (1984). Dots = onshore earthquakes; x = offshore earthquakes. Horizontal bars indicate range in reported magnitudes. Solid line is approximate upper bound enclosing all data (Taken from Keefer, 1984).
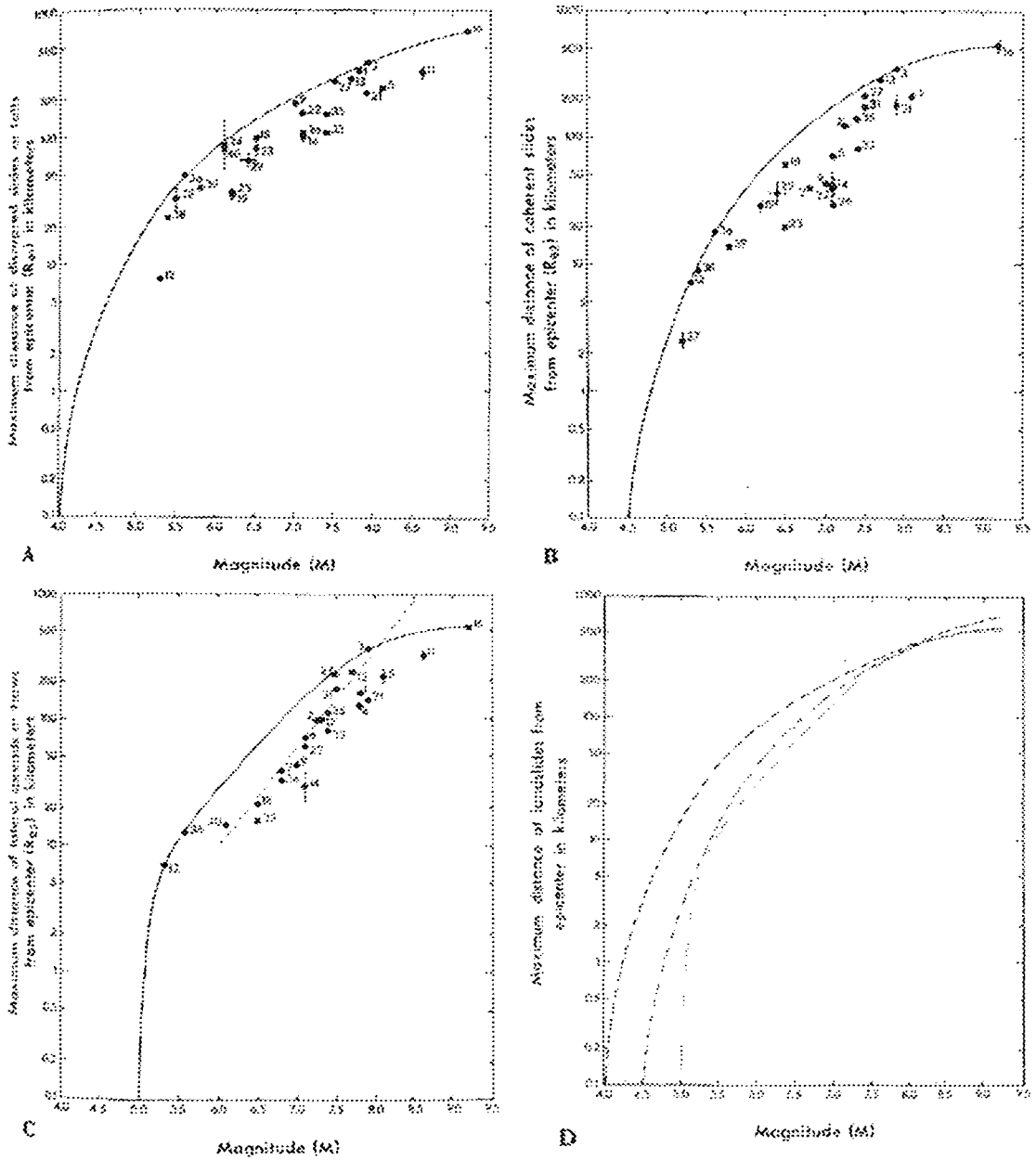
Figures 4.48 – Maximum distance from epicentre to landslides for earthquakes of different magnitudes. Numbers beside data points are earthquakes listed in Keefer (1984, table 1). Vertical bars indicate uncertainties, where known, in locations of epicentres, in locations of most distant landslides, or both. Horizontal bars indicate range in reported magnitudes. **A.** Maximum distance from epicentre to disrupted slide or fall. Solid line is approximate upper bound enclosing all data. **B.** Maximum distance from epicentre to coherent slide. Solid line is approximate upper bound enclosing all data. Dot-dash line is upper bound determined by Kurbayashi & Tatsuoka (1975, 1977) for soil-liquefaction phenomena in earthquakes in Japan. **D.** Comparison of upper bounds from **A, B** and **C.** Dashed line is bound for disrupted falls and slide, dash-double-dot line is bound for coherent slides, and dotted line is bound for lateral spreads and flows. Taken from Keefer (1984).
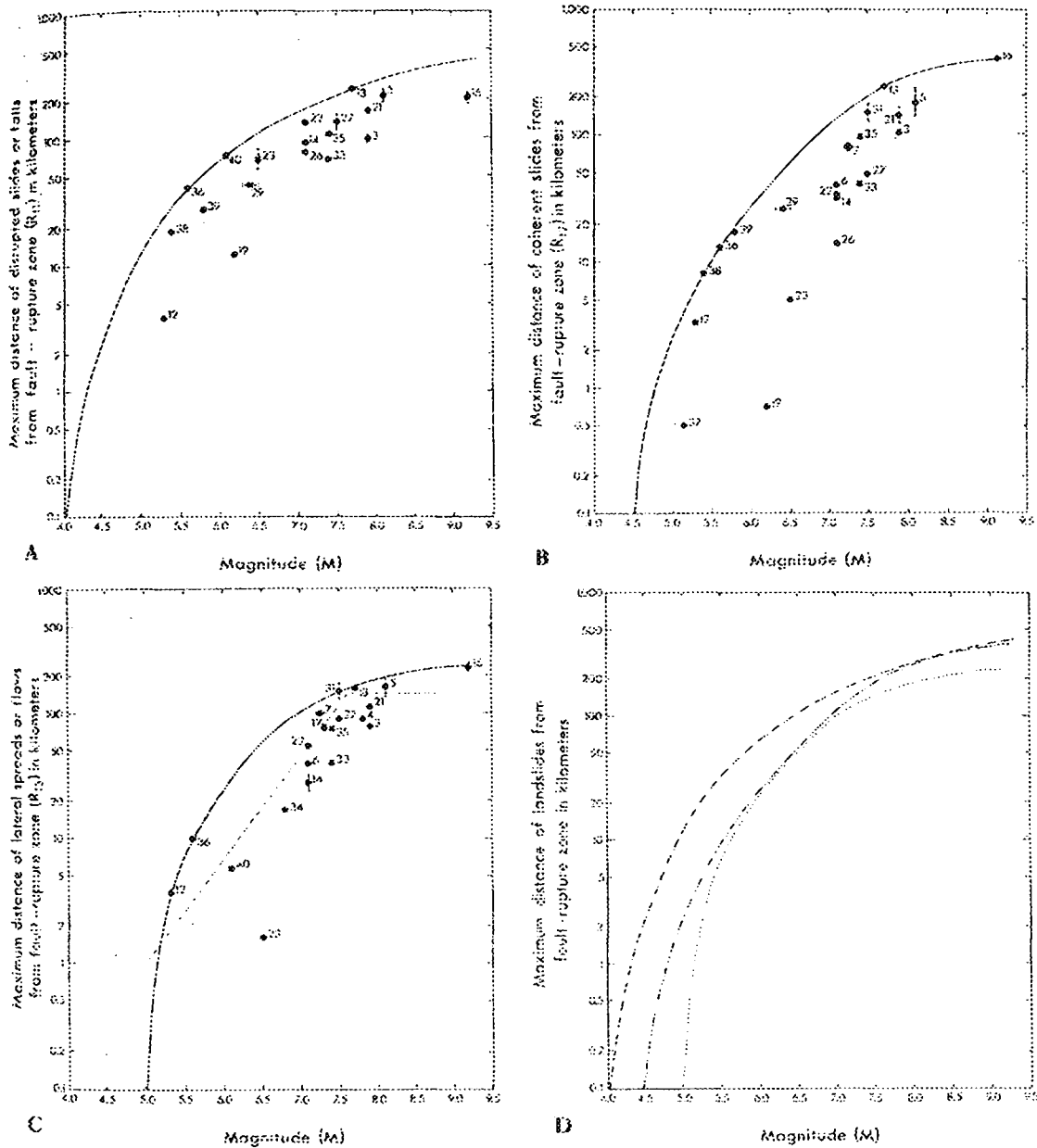
Figure 4.49 – Maximum distance from fault-rupture zone to landslides in earthquakes of different magnitudes. Numbers beside data points are earthquakes listed in Keefer (1984, table 1). Vertical bars indicate uncertainties, where known, in boundaries of fault-rupture zones, in locations of most distant landslides, or both. Horizontal bars indicate range in reported magnitudes. **A.** Maximum distance from fault-rupture zone to disrupted slide or fall. Solid line is approximate upper bound enclosing all data. **B.** Maximum distance from fault-rupture zone to coherent slide. Solid line is approximate upper bound enclosing all data. **C.** Maximum distance from fault-rupture zone to lateral spread or flow. Solid line is approximate upper bound enclosing all data. Dot-dash line is upper bound determined by Youd & Perkins (1978) for significant soil-liquefaction phenomena. **D.** Comparison of upper bounds from **A, B** and **C.** Dashed line is bound for disrupted slides and falls, dash-double-dot line is bound for coherent slides, and dotted line is bound for lateral spreads and flows. Taken from Keefer (1984).

These measurements indicate that rock falls, rock slides, soil falls, and disrupted soil slides are initiated by the weakest shaking. In particular, these shallow, highly disrupted landslides from steep slopes are probably susceptible to the short-duration, high-frequency shaking characteristic of small earthquakes. Coherent, generally deep-seated landslides are initiated by stronger and probably longer-duration shaking, and lateral spreads and flows by shaking that is still longer and stronger. With possible rare exceptions, rock avalanches and soil avalanches have the highest thresholds of all (Keefer, 1984).

Keefer (1984) also concluded that the Modified Mercalli shaking intensities for landslides determined by comparing isoseismal maps with maps of landslides distribution are one to five levels lower than those indicated by explicit criteria on the Modified Mercalli scale. He argued that this discrepancy suggests that the landslide-related criteria on the scale need to be revised to conform to intensities based on other criteria. These could be:

1. that shallow, highly disrupted landslides from steep slopes are common at MMI VI;

2. that rapid soil flows, soil lateral spreads, and coherent deep-seated slides from gentler slopes are common at MMI VII; and

3. That landslides of all types occasionally occur at intensities one to two levels lower than the levels at which they are common.

The study (Keefer, 1984) also identified several materials that appear especially susceptible to earthquake-induced landslides. The materials and the predominant types of landslides in each are:

- weakly cemented, weathered, sheared, intensely fractured, or closely jointed rocks – rock falls, slides, avalanches, slumps and block slides;

- "more-indurated rocks" with prominent discontinuities – rock falls, slides, block slides, and, possibly slumps;

- unsaturated residual or colluvial sand – disrupted soil slides and soil avalanches;

- saturated residual or colluvial sand – rapid soil flows;

- saturated volcanic soils containing sensitive clay – disrupted soil slides, soil avalanches and rapid soil flows;

- loess – rapid soil flows;

- cemented soils – soil falls;

- deltaic sediments containing little or no clay – soil lateral spreads and sub-aqueous landslides;

- flood-plain alluvium containing little or no clay – soil slumps, block slides and lateral spreads; and

- uncompacted or poorly compacted man-made fill containing little or no clay – soil slumps, block slides, lateral spreads and rapid soil flows

Seismic data for the majority of places around the globe can be downloaded from the website of the National Earthquake Information Centre (NEIC) of the United States Geological Survey (USGS). The available seismic data for the study area and surrounding region have been downloaded. The data set dates back to 1973 and

contains over 660 entries (or seismic events) and includes the time, magnitude, location of the epicentre and the focal depth of the earthquakes.

A plot of the distribution of these earthquakes shows that they are predominantly associated with the basin margin fault systems as well as the major strike-slip Carboneras and Palomares Fault Zones (Figure 4.50). These fault zones (which were also identified in Chapter 2) are probably responsible for the majority of the earthquakes affecting the study area. All of these earthquakes occur within 33km of the Earth's surface, and are therefore considered as being shallow.

The majority of the earthquakes (66%) occurring in the region during 1973-2002 had a magnitude of between 2.0 and 2.9 on the Richter Scale (Figure 4.51). Approximately 16% of the earthquakes had a magnitude of between 3.0 and 3.9 on the Richter Scale and 14% between 1.0 and 1.9 on the Richter Scale.

By comparing the earthquake data set that has been downloaded from the USGS with the mapped landslide distribution it is unlikely that any of the earthquakes triggered any of the landslides mapped within the study area. This is based on assessing the distance, depth and magnitude of the earthquake in comparison to the location of the landslides (Figure 4.47).
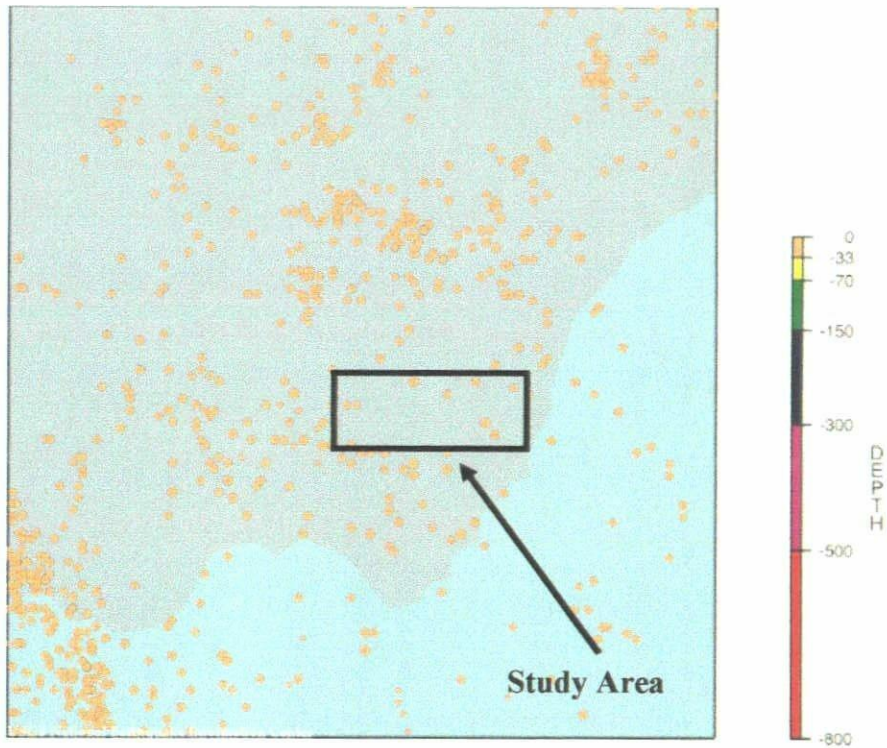
Figure 4.50 – Map of SE Spain showing the distribution of earthquake epicentres recorded in the USGS Data.
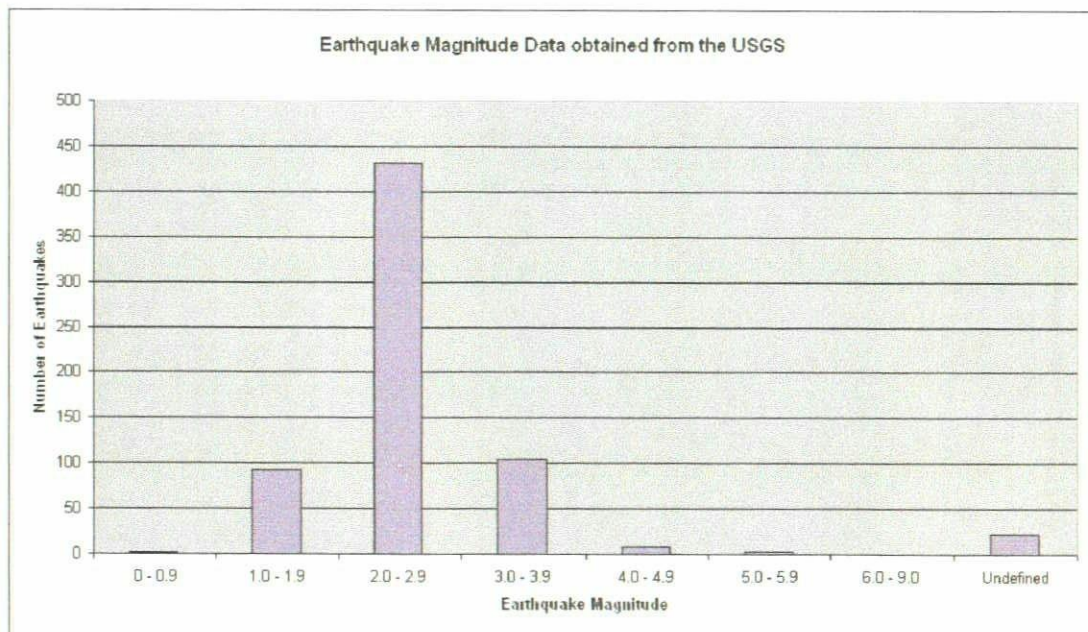
Figure 4.51 – Graph showing the distribution of earthquakes of given magnitudes as recorded in the USGS database.

Approximately 34% of the mapped landslides (107 out of 316) were associated with units that exhibited features relating to shrink and swell weathering of the rock and/or soil, and therefore the presence of expansive clays and soils. These also tended to be related to the dissolution features described in Section 4.3.2. Soil samples from some of these locations were collected and analysed for the presence of expansive clay minerals. Preliminary XRD analysis of these samples highlighted the presence of smectite, montmorillonite, chlorite and illite. All of these clay minerals are commonly associated with shrink and swell weathering, high rates of erosion and subterranean dissolution features in the Sorbas and Tabernas region (Spivey, 1997; Alexander *et al.*, 1999; Faulkner *et al.*, 2000; Bell, 1993).

An interesting question that is still under consideration is how the presence of these minerals within the soil or rock mass of a slope affects slope stability. It is likely that the presence of these minerals leads to the formation of the observed dissolution features and discontinuities within the rock or soil mass and it is these that decrease the stability of the slope, leading to the observed landslide activity in these areas.

4.3.4 Human Factors

The identification of those factors that were significant in causing the observed landslide activity in the study area came down to circumstantial evidence. For example, the excavation and/or loading of slopes around the town of Sorbas may have influenced and/or caused many of the landslides seen in this area. The landslide inventory records that 41 of the mapped landslides (13.0%) were affected by human activity. In some cases more than one factor were identified for an individual landslide (Figure 4.52). Those factors that were assessed in the field as being significant in explaining the observed landslide activity were:

- excavation of slopes;

- loading of the slope or at its crest;

- defective maintenance or leaking of service pipes;

- vegetation cover removal (deforestation); and

- quarrying.

Loading and excavation of slopes accounted for approximately 4.4% and 3.8% of the mapped landslides respectively. This fits with the observations made around the town of Sorbas where many of the landslides are the result of human activity. These examples will be discussed further in Chapter 5. The removal of vegetation was also seen as a significant factor. This was seen in areas where the removal of vegetation exposed highly erosive soils to slope erosion processes such as rilling and gullying which then progressed further to affect a larger area and greater volume of material and therefore become a landslide.
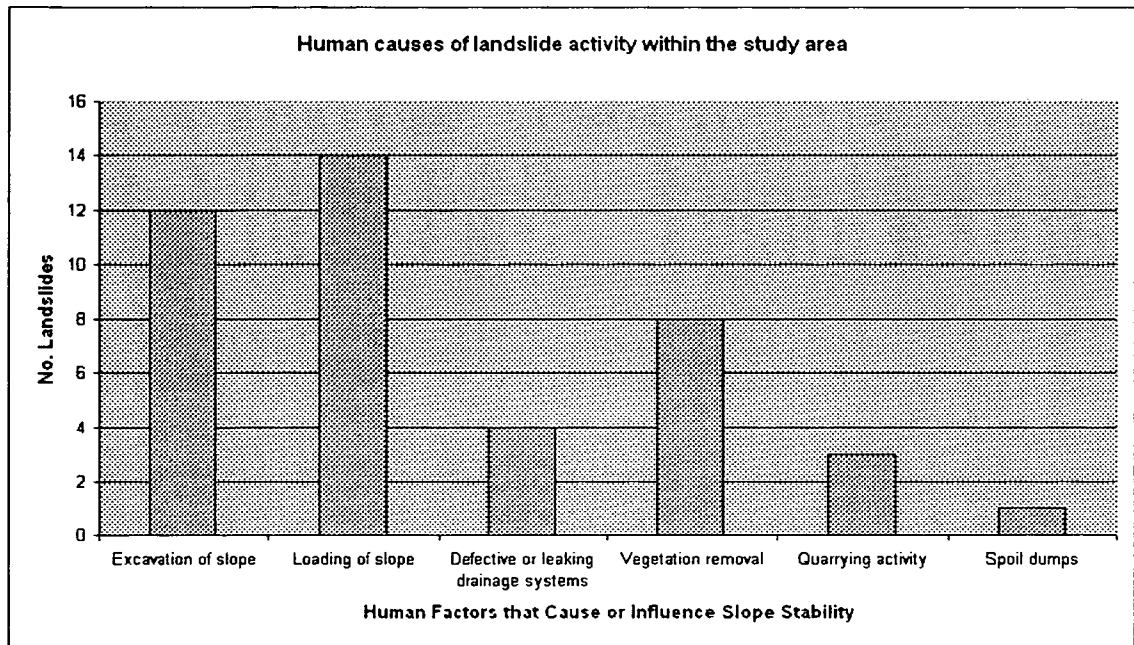
Figure 4.52 – Graph showing the number of mapped landslides related to human activity within the study area.

4.4 Age of Landslide Activity

An understanding of the spatial and temporal occurrence of landslides and other slope movements is useful for obtaining a better understanding of what might have caused or triggered those landslide movements in the past (González-Díez *et al.*, 1999). As the climate is both an important conditioning and triggering factor for slope movements, landslide chronologies may help to establish or test climate models for the past. However, the correlation between slope movements and climatic change is dependant on the ability to date periods of landslide activity and periods of climatic change, and therefore link the two.

The incision history of the Río Aguas has been recorded by a series of river terrace levels (Section 2.4; Harvey & Wells, 1987; Mather, 1991; Harvey *et al.*, 1995; Kelly *et al.*, 2000). If the relationship between the landslides and these river terraces is known, then they can be used to provide a relative chronological framework for the landslide activity in that same area. Also, work is currently underway to determine absolute ages for some of these river terrace levels (Kelley *et al.*, 2001).

Geomorphological mapping of the area between the site of the Río Aguas/Rambla Feos River Capture site and the area around the town of Sorbas, has indicated that the distribution of the landslides may represent at least three distinguishable stages of landslide activity (Hart & Griffiths, 1999):

1. Present day landslide activity.

2. Those that have occurred post the Río Aguas/Rambla Feos River Capture approximately 100,000 years BP (Harvey & Wells, 1987).

3. Those that occurred prior to the Río Aguas/Rambla Feos River Capture.

Therefore, it has been possible to "date" a large number of the landslides with respect to the river terraces and the stages listed above. Examples, of how this "relative dating scheme" has been used and some examples of the landslides from each of the different stages listed above are described and discussed in the following Case Studies chapter.

When examining the landslide data for the whole study area, the majority of the landslides occurred post the Río Aguas/Rambla Feos River Capture (60.4% of the mapped landslides) with a further 38.0% of the mapped landslides being classified as having an "Unknown" age (Figure 4.53). However, all of these "Unknown" landslides are within the areas that were not directly affected by the Río Aguas/Rambla Feos River

Capture. Being outside of this area means that they cannot be correlated easily to the river terraces that have been mapped in the Río Aguas/Rambla Feos area.

Ongoing research in the study area (i.e., along the Rambla de Los Castaños and Río Jauto), suggests that the presence of clusters of landslides (i.e., not single landslides), may highlight further anomalies within the landscape and drainage network. This may be related to other drainage network reorganisations within the Río Aguas catchment area, or other geological or geomorphological factors that have affected the region (i.e., landslides occurring along fault zones).

Of the 316 landslides found in the study area, 183 (57.9% of the mapped landslides) are located upstream of where the Río Aguas/Rambla Feos River Capture took place (referred to here as the "Upper" Río Aguas). Half of these (29.4% of the mapped landslides) are classified as "Recent" landslides with the majority of the remaining landslides (26.9% of the mapped landslides) being classified as occurring since the river capture event (Figure 4.54). Only 1.6% of the mapped landslides upstream from the capture site are thought to have occurred prior to the Río Aguas/Rambla Feos River Capture.
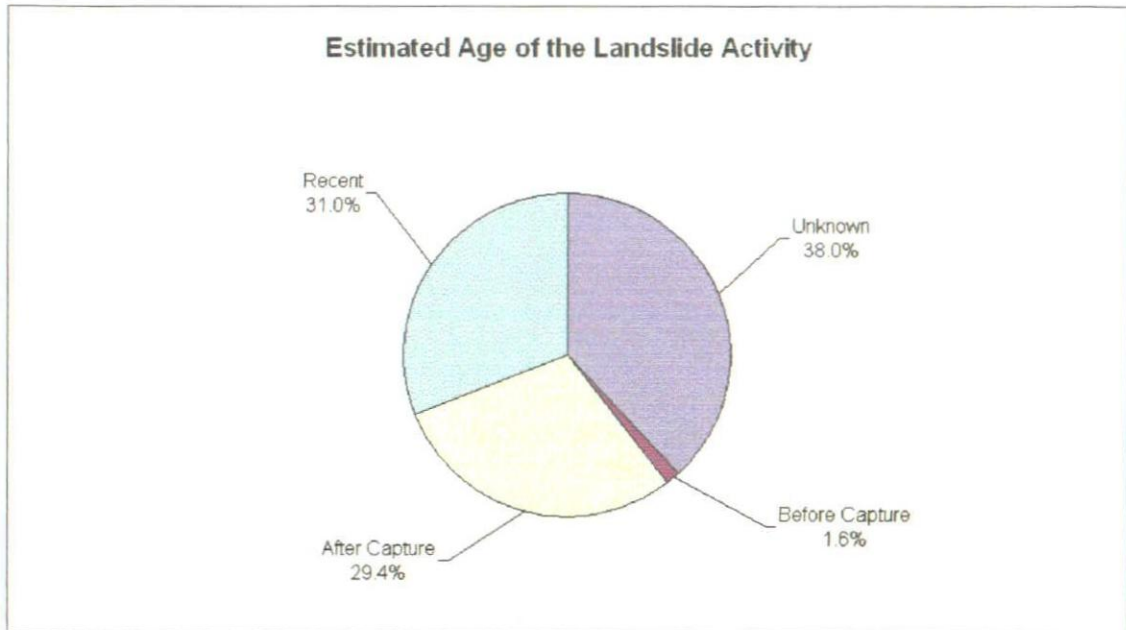
Figure 4.53 – Graph showing the estimated ages of the mapped landslide activity within the study area.
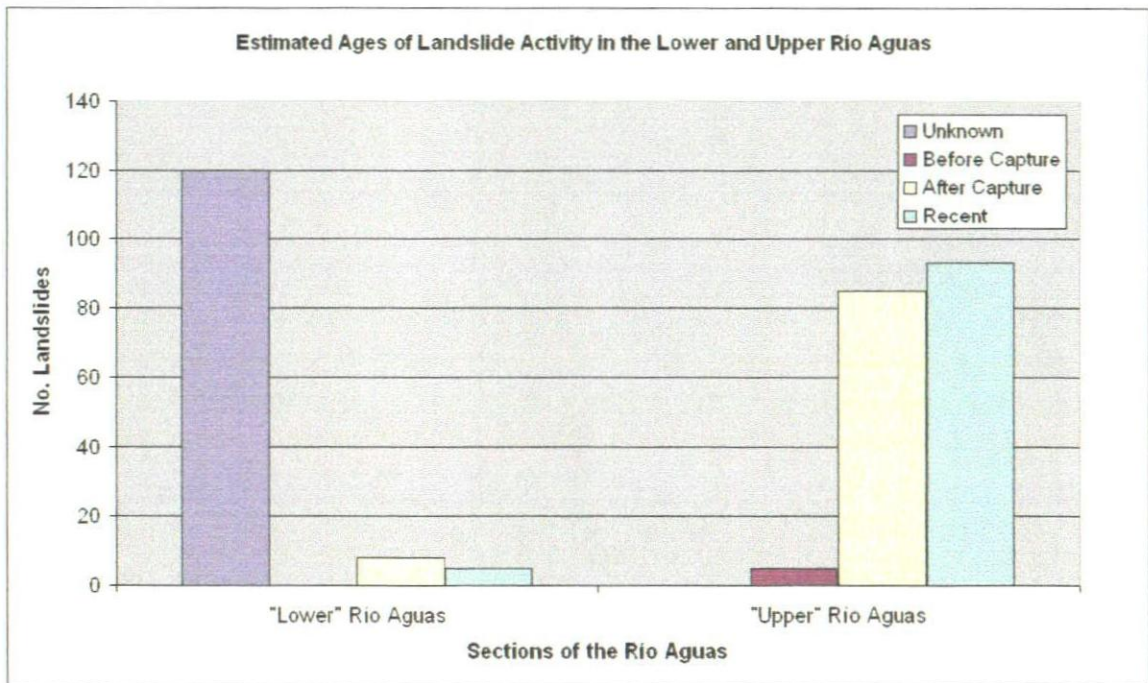
Figure 4.54 – Graph comparing the estimated ages of the mapped landslide activity upstream and downstream of the Río Aguas/Rambla Feos capture site.

These observations are also confirmed when the Land System locations of the mapped landslides are considered. The majority of landslides with the "Unknown" age grouping are found in the "mountain slopes with incised drainage channels" Land System (24.1% of the mapped landslides; Figure 4.55). The majority of the landslides are found in the "Neogene hills with incised drainage channels" Land System (Figure 4.54). A similar picture is also observed at the Land Facet level of description. The majority of the landslides are found in "incised areas with river terraces" or "incised areas without river terraces" (38.9% and 28.5% of the mapped landslides respectively; Figure 4.56).

The 18.7% of the mapped landslides (59 landslides) that are classified as being of an "Unknown" age and in the "incised areas without river terraces" Land Facet are the landslides that were mapped along some sections of the Rambla de Los Castaños (Figure 4.56). In the Cariatiz area (Figure 4.1) this river has been incised by approximately 90-100 m below the surrounding countryside/Góchar erosion surface. This area has also not been affected by the Río Aguas/Rambla Feos River Capture and therefore cannot be related to the river terrace sequence in that part of the study area. However, the aerial photographic interpretation completed for this study and other ongoing research projects in that area (Mather & Griffiths, *pers. comm.*) would suggest that the Rambla de Los Castaños/Rio Jauto have been affected by a number of drainage re-organisations. These may have influenced the stability of some of the slopes in this area, and therefore given rise to the observed landslide activity. This is currently being investigated as part of another ongoing research project. Unfortunately, at present there are no identifiable terrace sequences that can be used to "date" any of the landslide activity that affects this area.
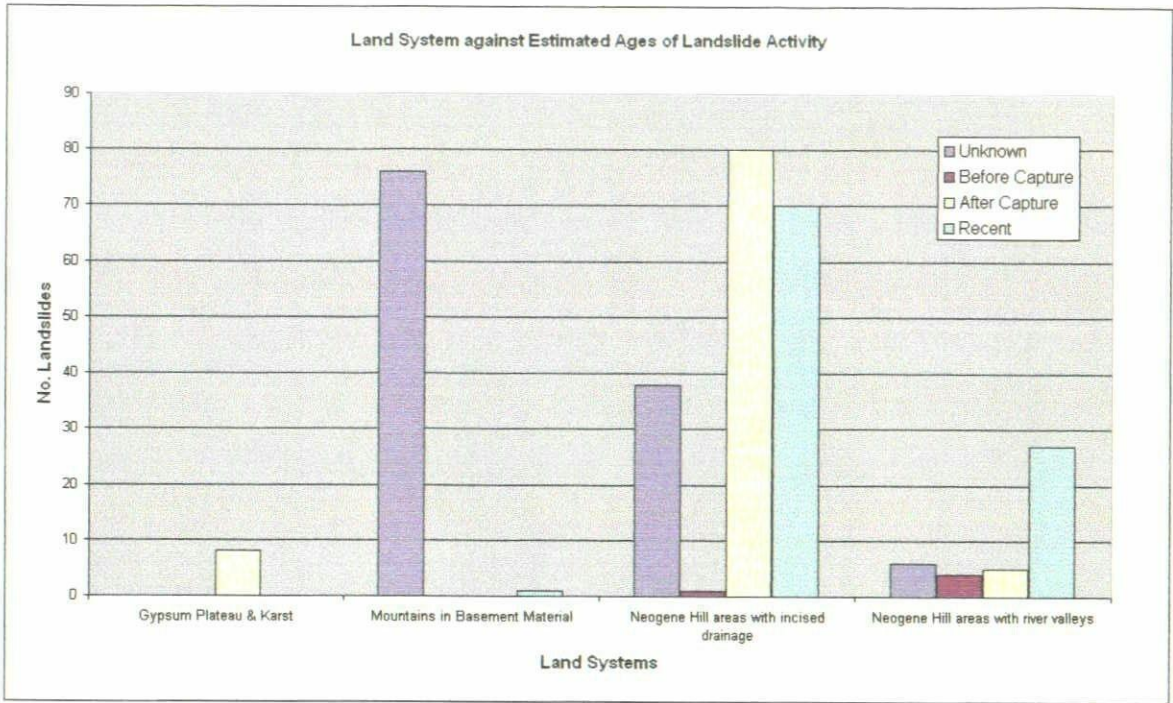
Figure 4.55 – Graph comparing the Land System classification against the estimated age of the mapped landslide activity within the study area.
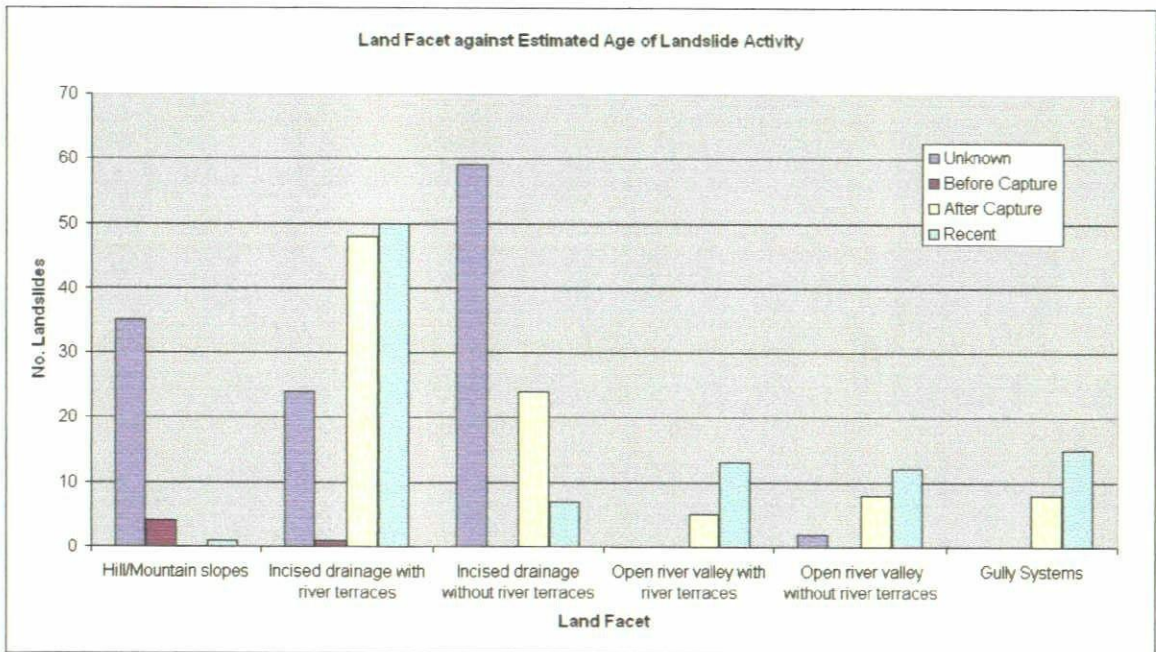
Figure 4.56 – Graph comparing the Land Facet classification against the estimated age of the mapped landslide activity within the study area.

The Río Aguas river terrace sequence is thought to possibly reflect an overall tectonically induced incision onto which climate change is superimposed, producing minor aggradations of sediment within an overall framework of incision (Harvey, 1987; Harvey & Wells, 1987; Mather, 1991; Harvey *et al.*, 1995). Periods of aggradation and river terrace formation are thought to have occurred during Quaternary glacials and periods of degradation and incision during Quaternary interglacials. The geomorphological mapping would suggest that the larger landslides are likely to have occurred during periods of incision and, therefore, possibly during interglacial periods.

Therefore, as well as reflecting the incision of the drainage network, the "stages" listed above may also reflect changes in the Quaternary climate. As the climate changed there would have been fluctuations in the amount of available water in the system, including:

- The level of the water table;

- The presence or absence of standing water;

- The frequency of intense rain storm events and associated flood events; and/or

- The frequency of light or heavy frosts.

These factors would all have influenced the style and frequency of landslide activity in the area.

Berrisford & Matthews (1997) and González-Díez *et al.* (1999) identified a number of periods of landslide activity within northern and western Europe (Figure 4.57). This was based on examining the landslide activity in Cantabria, the Pyrenees, the Swiss Alps, the French Alps, Italy, Germany, the Carpathians, Scandinavia and the UK, as part of two research projects – the "European Palaeoclimate and Man since the Last

Glaciation" Project and the TESLEC Project (temporal stability and activity of landslides in Europe with respect to climatic change). This work has highlighted some possible clusters at about 5,000 and 10,000 years BP. However, the figure (Figure 4.57) displays a lot of scatter in the data, which could be interpreted as showing landslide activity as occurring continuously throughout the last 10,000 years. Also the lack of dated landslides prior to 10,000 years BP makes attempting any correlations difficult. This does raise the question of how long a landslide can remain recognisable in the landscape. This will of course depend on their size, location, style of landslide activity and failure mechanism.

Unfortunately, due to the lack of dated landslides in the Rio Aguas study area, it is not possible to fit the landslides described here with the chart shown in Figure 4.57 beyond what is shown.
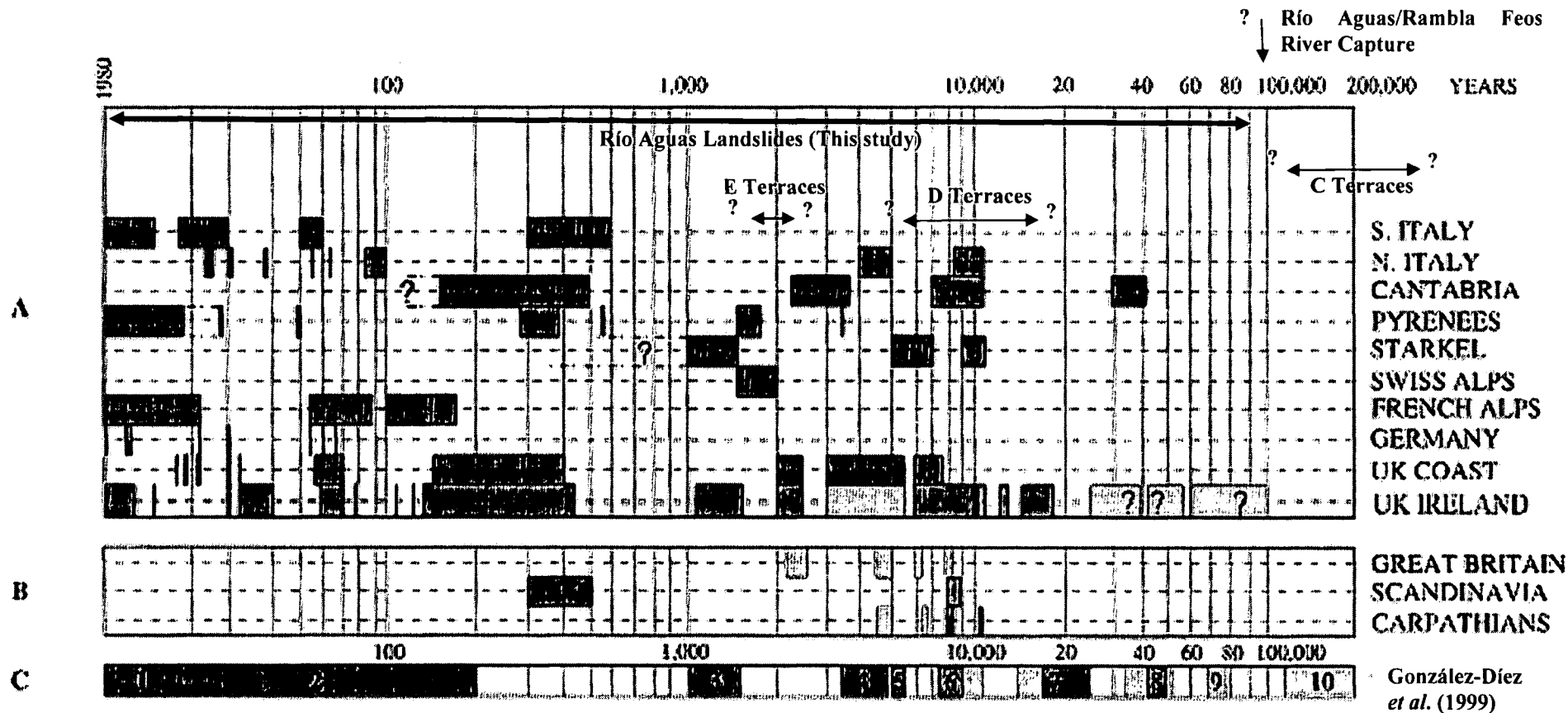
Figure 4.57 – Comparison between the information on temporal occurrence of landslides in the study area and periods of major landslide activity in Europe derived from data of an EPOCH (European Programme on Climate and Natural Hazards) project. (A) From Brunsden *et al.* (1996a); Brunsden & Ibsen (1997) (Starkel refers to Starkel (1996); Cantabria refers to a former analysis by Cendrero *et al.* (1994)). (B) From Starkel (1985). (C) From González-Díez *et al.* (1999). Diagram modified after González-Díez *et al.* (1999). Terrace dates for the Río Aguas study area are from Harvey *et al.* (1995).

4.5 Chapter Summary

This chapter describes the results of the statistical analysis that has been completed by this project. It has examined the spatial and temporal distribution of the mapped landslide activity. The analysis (based on regression analysis) has sought to identify those geological or geomorphological factors and/or settings that are significant in explaining the observed distribution. These factors include the underlying geology, the steepness of the slope, as well as the proximity of the landslides to the Río Aguas/Rambla Feos River Capture.

Regression analysis has been used because it is a method that helps to identify dependant and independent relationships within the data. Geomorphological data are often skewed and inter-correlated (Griffiths, *pers .comm.*) which means that it does not normally meet the requirements and assumptions for other higher level parametric statistical tests such as Principle Component Analysis (PCA), discriminate function analysis or cluster analysis. These techniques require that the data have a normal distribution and variables that are not correlated with each other. However, future statistical analysis of this database (and refinements of it) could potentially utilise such techniques, in conjunction with the use of a Geographical Information System (GIS).

The landslide inventory database contains data on 316 landslides. As the Río Aguas study area covers approximately 425 km^2, this is a landslide density of approximately 0.75 landslides/square km. The results of the regression factor analysis of the landslide inventory database are summarised below (Tables 4.17 and 4.18). The analysis has also sought to identify those factors that have either caused or controlled the landslide activity (Table 4.19).

Table 4.17 – Summary of the results from this landslide investigation. The table shows those factors with the highest incidence of landslides, for each of the main factors considered by this study. All percentages are percentages of the total number of mapped landslides.

Landslide Factor Analysis	
Landslide Mechanism:	Rock falls and topples = 66.8% Non-rotational Landslides = 21.2%
Geological Unit:	Nevado-Filabride Complex = 16.8% / Sorbas Member = 15.5% Góchar Formation = 12.3% / Azagador Member = 9.5%
Rock Types:	Conglomerate = 14.6% / Limestone = 13.9% / Mica Schist = 10.4% / Sandstone = 10.1%
Slope Angle & Mechanism:	• Falls & Topples & Non-rotational Landslides = increasing landslide incidence with slope angle • Translational Landslides = highest landslide incidence on moderately steep slopes • "Other" Landslides = Highest landslide incidence on very steep slopes
Slope Angle & Rock Type:	• The highest incidence of landslides involving conglomerate, sandstone, limestone and schist occur on slopes > 60°. • For landslides involving gneiss the slope angle is >45° • For landslides involving gypsum overlying mudstone the highest incidence is on slopes >75°
Landslide Activity	
State of Landslide Activity:	Dormant = c.80% ("a landslide that has not moved for more than one annual cycle of seasons, but where the causes of movement apparently remain" – WP/WLI, 1993)
Style of Landslide Activity:	Multiple = 80% (a landslide that exhibits "repeated development of the same type of movement along the same rupture surface and involving the same displaced material" – WP/WLI, 1993).
Distribution of Landslide Activity:	Retrogressing = 75% ("a landslide where the rupture surface is extending in the direction opposite to the movement of the displaced material" – WP/WLI, 1993).

Table 4.18 – Summary of the results from the statistical analysis of the number of landslides occurring in the different combinations of geology, terrain classification and landslide failure mechanism considered by the project.

Geomorphology	Geomorphology & Mechanism	Geomorphology & Lithology	Geomorphology, Lithology & Mechanism
• Hill areas with incised drainage channels • Incised drainage channels with river terraces • Outside meanders of active drainage channels • 12.0% of the mapped landslides (38 landslides)	• Hill areas with incised drainage channels • Incised drainage channels with river terraces • Outside meanders of active drainage channels • Rock Falls and Topples • 7.6% of the mapped landslides (24 landslides)	• Mountain slopes incised by gullies, canyons and river channels • Hill and mountain area • Ridge crests • Basement material (Mica schist, gneiss, phyllite) • 4.7% of the mapped landslides (15 landslides)	• Mountain slopes incised by gullies, canyons and river channels • Hill and mountain area • Ridge crests • Basement Material (Mica schist, gneiss, phyllite) • Rock Falls and Topples • 4.7% of the mapped landslides (15 landslides)
• Hill areas with incised drainage channels • Incised drainage channels without river terraces • Outside meanders of active drainage channels • 7.0% of the mapped landslides (22 landslides)	• Mountain slopes incised by gullies, canyons and river channels • Hill and mountain area • Ridge crests • Rock Falls and Topples • 7.0% of the mapped landslides (22 landslides)	• Mountain slopes incised by gullies, canyons and river channels • Incised drainage channels with river terraces • Canyons side slopes • Mica schist • 4.7% of the mapped landslides (15 landslides)	• Mountain slopes incised by gullies, canyons and river channels • Incised drainage channels with river terraces • Canyons side slopes • Rock Falls and Topples • Mica Schist • 4.7% of the mapped landslides (15 landslides)
• Mountain slopes incised by gullies, canyons and river channels • Hill and mountain area • Ridge crests • 7.0% of the mapped landslides (22 landslides)	• Hill areas with incised drainage channels • Incised drainage channels with river terraces • Dip-slope escarpments • Rock Falls and Topples • 6.0% of the mapped landslides (19 landslides)	• Hill areas with incised drainage channels • Incised drainage channels with river terraces • Scarp-slope escarpments • Gypsum overlying calcareous mudstone • 3.8% of the mapped landslides (12 landslides)	• Hill areas with incised drainage channels • Incised drainage channels with river terraces • Scarp-slope escarpments • Gypsum overlying calcareous mudstone • "Other" – complex combination of mechanisms • 3.8% of the mapped landslides (12 landslides)

Geomorphology	Geomorphology & Mechanism	Geomorphology & Lithology	Geomorphology, Lithology & Mechanism
• Hill areas with incised drainage channels • Incised drainage channels with river terraces • Dip-slope escarpments • 6.6% of the mapped landslides (21 landslides)	• Mountain slopes incised by gullies, canyons and river channels • Incised drainage channels with river terraces • Canyons side slopes • Rock Falls and Topples • 5.4% of the mapped landslides (17 landslides)	• Hill areas with incised drainage channels • Incised drainage channels with river terraces • Outside meanders of active drainage channels • Conglomerate • 3.2% of the mapped landslides (10 landslides)	• Hill areas with incised drainage channels • Incised drainage channels with river terraces • Outside meanders of active drainage channels • Conglomerate • Rock Falls and Topples • 3.2% of the mapped landslides (10 landslides)
• Mountain slopes incised by gullies, canyons and river channels • Incised drainage channels with river terraces • Canyons side slopes • 5.4% of the mapped landslides (17 landslides)	• Hill areas with incised drainage channels • Incised drainage channels with river terraces • Scarp-slope escarpments • "Other" – complex combination of mechanisms • 4.1% of the mapped landslides (13 landslides)	• Gypsum plateau and karst • River valley formed by the dissection of the drainage system • Scarp-slope escarpment • Gypsum overlying calcareous mudstone • 2.5% of the mapped landslides (8 landslides)	• Gypsum plateau and karst • River valley formed by the dissection of the drainage system • Scarp-slope escarpment • Gypsum overlying calcareous mudstone • "Other" – complex combination of mechanisms • 2.5% of the mapped landslides (8 landslides)
• Hill areas with incised drainage channels • Incised drainage channels with river terraces • Scarp-slope escarpments • 5.4% of the mapped landslides (17 landslides)	• Hill areas with incised drainage channels • Incised drainage channels without river terraces • Outside meanders of active drainage channels • Non-rotational Landslides • 4.1% of the mapped landslides (13 landslides)	• Hill areas with incised drainage channels • Incised drainage channels with river terraces • Outside meanders of active drainage channels • Limestone and calcareous mudstone • 2.5% of the mapped landslides (8 landslides)	

Table 4.19 – Summary of the results from the analysis of landslides causative factors. All percentages are percentages of the total number of mapped landslides.

Landslide Causes	
Geological Factors:	These factors were identifiable in the field: • jointed or fissured material; • adversely orientated mass discontinuities (bedding, cleavage, faults or unconformities); • contrasts in permeability and its effects on groundwater; • alternating sequences of "hard rocks" over "soft rocks"; and • contrasts in stiffness (stiff, dense material over plastic material).
Morphological Factors:	These factors were inferred from field observations or eye-witness accounts: • tectonic uplift of the study area; • fluvial erosion of many of the slopes; • subterranean erosion through piping and dissolution features (Figure 4.45); and • vegetation removal (by erosion, forest fire or drought).
Physical Factors:	Insufficient detailed information and no dated landslides to allow for a full investigation of these factors. However, these factors were inferred from field observations or eye-witness accounts: • Intense, short period rainfall; and • Shrink and swell weathering of expansive soils and clays are important.
Human Factors:	These factors were inferred from field observations or eye-witness accounts: • excavation of slopes; • loading of the slope or at its crest; • defective maintenance or leaking of service pipes; • vegetation cover removal (deforestation); and • quarrying.

The data analysis has also included investigating the relationship between the runout length and angle of reach of a landslide with its volume and/or the elevation difference between the crown and toe of the landslide. The results from this investigation have been compared with the findings of other projects detailed in the literature. This has shown how this study has come to very similar conclusions as these other projects, in many cases using a larger database. This information could be used to estimate the runout lengths of potential landslides within the study area, if an estimate can be made of the size or volume of any potential landslide.

The above summary has shown that the landslides of the study area involve a number of different failure mechanisms, rock types and slope angle combinations. The comparison of the landslide distribution with the terrain classification has shown that the majority of the landslides are in areas of incised drainage, relatively steep terrain or areas of active erosion. The landslides also vary greatly in volume ($10m^3$ to 1.47×10^8 m^3), the area covered by landslide debris and runout length (up to 900m).

The following chapter will use a number of examples from the landslide inventory database to bring together some of the results from statistical analysis described here, and the results of the API and field mapping. These examples are presented here as a series of "Landslide Type Localities" (similar to geological type localities).

Chapter 5 – Case Studies

5 Case Studies

5.1   Introduction

A number of case studies have been chosen from within the study area to highlight

some of the findings from the aerial photographic interpretation, the field investigations

and some of the results and observations that were described and discussed in the

previous chapter. These case studies are grouped into two "case study areas" – the town

of Sorbas (and surrounding area) and the area immediately upstream and downstream of

the Río Aguas/Rambla Feos Wind Gap (Figure 5.1). Both of these areas are within the

part of the study area most greatly affected by the Río Aguas / Rambla Feos River

Capture and provide some of the best examples of the landslide problems being

addressed by this research project (Hart & Griffiths, 1999; Hart, 2000; Griffiths *et al.*,

2002, 2003). These two areas will also allow for the individual landslides and the

statistics from the analysis of the landslide inventory to be seen in the context of the

ground conditions in each of these case study areas. Therefore, the landslides are

presented here (Table 5.1) as a series of "Landslide Type Localities" that can be used to

highlight:

- The effects of the Río Aguas / Rambla Feos River Capture;

- The link between the geology, geomorphology and observed landslide activity;

- The factors controlling the landslide activity and how these vary across the study

  area depending on the geological and geomorphological setting;

- The range of landslide activity that is seen within the study area (styles, failure

  mechanisms and geomorphological setting); and

- The interaction between landslide activity and the infrastructure and population of

  the study area.

Table 5.1 – Landslides mapped in the case study areas. "River Capture" refers to the Río Aguas/Rambla Feos river capture (Mb = Member / Fm = Formation).

Locality	Mechanism	Volume	Geology	Rock Type	Geomorphology	Relative Age	Comment
Maleguica	Complex	3.14×10^6 m³	Sorbas Member	Sandstone	Dip slope / outside of a meander	Post River Capture	Large scale failure associated with the River Capture
Alfarería	Sackung	5.50×10^5 m³	Góchar Fm & Cariatiz Fm	Sandstone & Mudstone	Outside of a meander	Post River Capture	Large scale failure associated with the River Capture
Sorbas Theatre	Rock fall & topple	1.05×10^4 m³	Sorbas Member	Sandstone	Canyon wall	Recent	Urban risk & construction activity
Los Beneficios	Complex	2.36×10^6 m³	Góchar Fm & Cariatiz Fm	Sandstone, Mudstone & Conglomerate	Outside of a meander	Post River Capture	Large scale failure associated with the River Capture
Bird's Footprint	Rock fall & topple	9.43×10^2 m³	Sorbas Member	Sandstone	Canyon wall	Recent	Urban risk &
New Museum	Rock fall & topple	45 m³	Sorbas Member	Mudstone & Sandstone	Canyon wall	Recent	Urban risk & Human activity
Abandoned Meander & Cave Collapse landslides	Various	Various	Sorbas Member	Sandstone	Abandoned incised meander	C to D terrace level & Recent	Urban risk & Human activity
Los Molinos Relict Feature	Debris flow / complex	1.10×10^6 m³	Yesares Mb & Abad Mb	Gypsum & Mudstone	Within incised canyon	Post River Capture	Large scale failure associated with the River Capture
Cerro Molatas/Carrasco	Complex – translational & non-rotational movements	4.91×10^6 m³	Azagador Mb & Chozas Fm	Limestone & Mudstone	Dip slope adjacent to River Capture site	Post River Capture	Large scale failure associated with the River Capture
El Tesoro	Rock falls and topples	1.05×10^6 m³ & 12.5×10^6 m³	Yesares Mb & Abad Mb	Gypsum & Mudstone	Scarp slope	Post River Capture	Large scale failures associated with the River Capture
Tension Crack Ridge	Complex	14.7×10^6 m³	Azagador Mb & Chozas Fm	Limestone & Mudstone	Dip slope / active erosion on 2 sides	Prior & Post to River Capture	Large scale failure associated with the River Capture
Cuesta del Honor	Complex	147.3×10^6 m³	Azagador Mb & Chozas Fm	Limestone & Mudstone	Dip slope	Prior & Post to River Capture	Large scale failure
Marchalico Viñicas ("Recent")	Complex	15.1×10^6 m³	Yesares Mb & Abad Mb	Gypsum & Mudstone	Scarp slope	Prior & Post to River Capture	Large scale failure
Marchalico Viñicas ("Relict")	Complex	17.0×10^6 m³	Yesares Mb & Abad Mb	Gypsum & Mudstone	Scarp slope	Prior & Post to River Capture	Large scale failure

Figure 5.1 - The Case Study Areas within the Rio Aguas Catchment Study Area
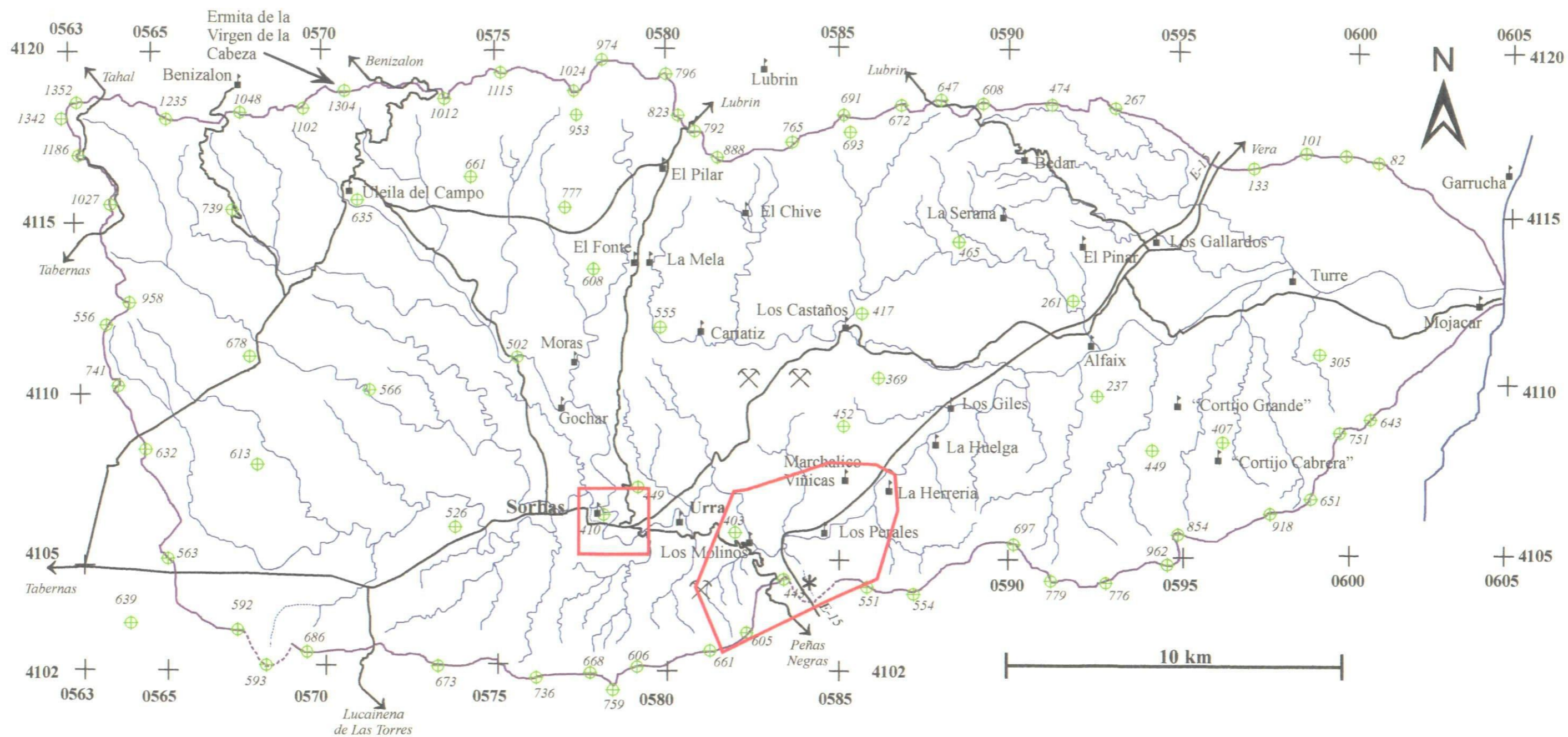
Legend

673 ⊕	Spot Heights (m.a.s.l.)
∿	Drainage System
—	Major Roads & Motorway
—	Study Area Boundary
▮	Settlements
⚒	Gypsum Quarries
✳	Rio Agua/Rambla Feos "Wind Gap"
☐	Case Study Areas

5.2   The Sorbas Area

The town of Sorbas (Figures 5.1 and 5.2) provides some of the best examples of the landslide problems being addressed by this research project (Hart & Griffiths, 1999; Hart, 2000; Griffiths *et al.*, 2002, 2003). The API and subsequent field validation of the area around Sorbas and its environs identified over 30 landslides. The landslide isopleth map for the study area (Figure 4.6) highlights this area as having the highest density of landslides within the study area (approximately 7.5 landslides per km^2).

Geomorphological mapping of the area has shown that the majority of the landslides are associated with the Quaternary development of the drainage network (Hart & Griffiths, 1999). The mapping also highlighted the presence of several relict landslide features, and confirmed the importance of understanding the geomorphological history of an area before undertaking engineering works. Therefore, the geomorphological mapping undertaken by this study has allowed for the identification of at least three stages of landslide activity in the Sorbas area, reflecting the incision history of the drainage network as described in Sections 2.4 and 4.4; see also Hart & Griffiths (1999). The Sorbas area is also a good example of how human interaction with the landscape has led to a number of the landslides around the town. It is this combination of Quaternary history, relict features and human activity that has led to the high number of landslides in this part of the study area.
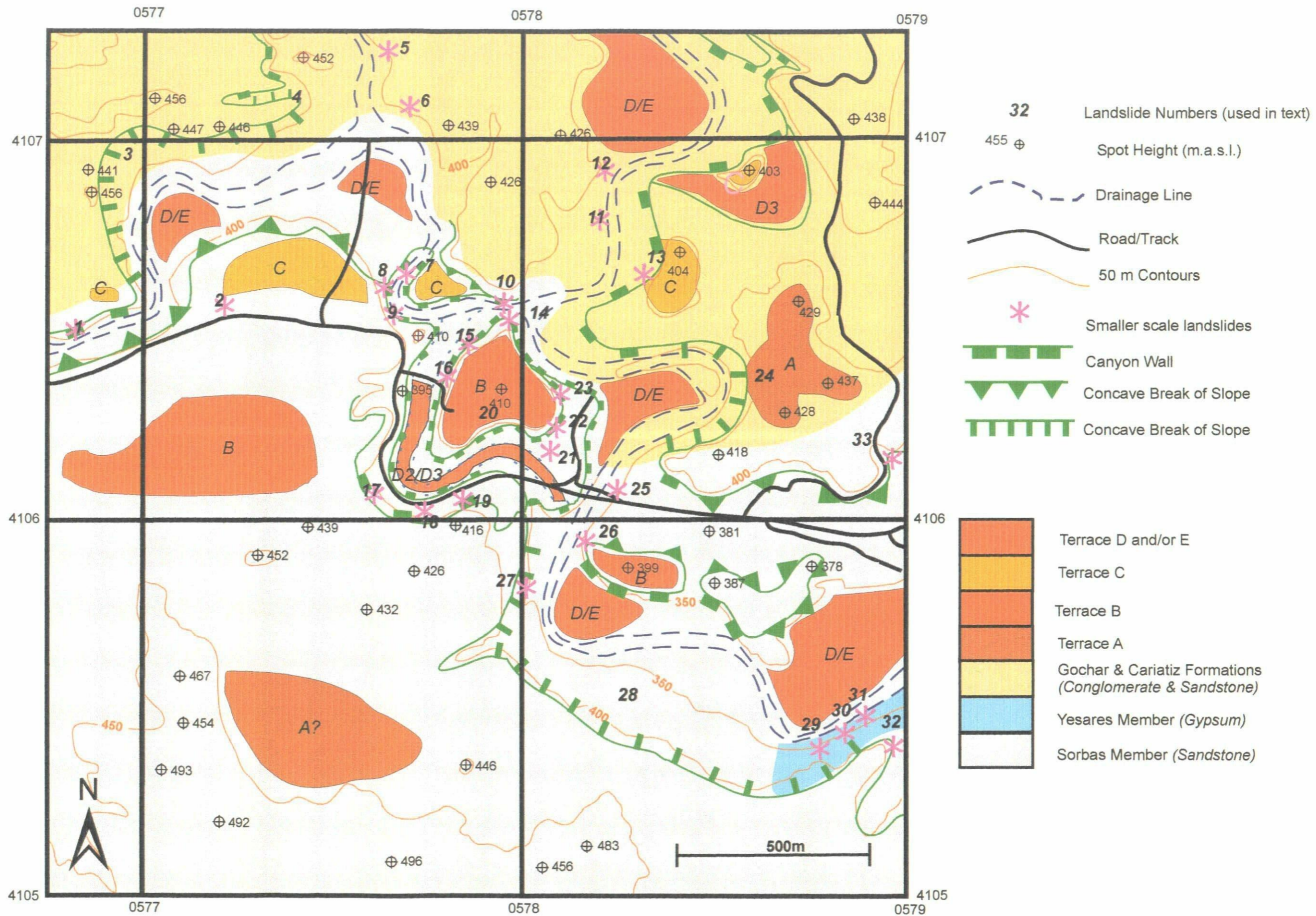
Figure 5.2 - Map of the Sorbas Case Study Area. River terrace levels are after Harvey *et al*. (1995).

Sorbas (37°06'00''N and 2°07'30'' W) is split into two parts, with the old town built on a "knoll" within an incised drainage system (Figure 5.2). The active channel of the Río Aguas drains around the eastern part of the town. A tributary of the Río Aguas (the Rambla de Los Chopas) is located to the north of the town where it joins the Río Aguas. An abandoned channel runs around the western and southern part of the "knoll" on which Sorbas is built. The newer parts of Sorbas are found to the west of the old town, on either side of the main Almería to Murcia road (the N-340).

The majority of the town is built upon moderately strong, thickly bedded sandstone that is occasionally interbedded with thin laminations of calcareous mudstone (the "Sorbas Member"). The rock is heavily jointed and fractured, with the joint sets almost perpendicular to the bedding. To the north of the town, the Sorbas Member is overlain by a sequence of fine to medium grained sandstones and conglomerates (the "Zorreras Member"). This moderately strong unit is also jointed and fractured in a similar fashion to the Sorbas Member. These rock units have been described more fully in Section 2.3 respectively. River terrace deposits also cap many of the slopes in the area (Harvey & Wells, 1987; Harvey et al., 1995; Hart & Griffiths, 1999).

The river terrace deposits record the incision of the drainage system, particularly after the Río Aguas/Rambla Feos river capture (Harvey & Wells, 1987; Mather, 1991; Harvey et al., 1995). These river terrace deposits therefore provide an insight into the formation of the present day Río Aguas valley, and are therefore helpful in "dating" some of the observed landslide activity that is seen in the case study area.

Sorbas is situated approximately 10 km upstream from the site of the Río Aguas/Rambla Feos river capture (Section 2.4) and is within the area most heavily affected by it. The river capture led to the formation of the canyon system around which the town is located. The canyon that passes around the northern and eastern sides of the older part of Sorbas contains the active drainage channels (the Rambla de Los Chopas and the Río Aguas respectively) and reaches a depth of about 90 m. The confluence of the Rambla de Los Chopas and Rambla de Sorbas (to form the Río Aguas) is located at the northeastern corner of the Sorbas knoll. The canyon that passes around the western and southern sides of the old town has been abandoned since the formation of the D2 river terrace (Harvey & Wells, 1987; Harvey *et al.*, 1995; Harvey, 2001). This canyon was abandoned when two meanders, one on the Rambla de Los Chopas and another on the Rambla de Sorbas, cut back into each other (Figure 5.3). The Rambla de Sorbas was probably at a slightly lower level than the Rambla de Los Chopas and therefore "captured" this drainage line (Harvey, 2001).

The 32 landslides that have been identified in and around the town of Sorbas vary greatly in their size, activity and failure mechanisms. Only seven of them are included here. The landslide mechanisms observed include rock fall, rock topple, high-angle rotational sliding, non-rotational sliding, and Sackung (after Dikau *et al.*, 1996), with the majority of failures involving rock falls. However, many of the larger landslides tend to exhibit a combination of different failure mechanisms. This reflects the geology, as well as the geomorphological setting of this area. For example, the formation of the steep canyon slopes allows for the formation of rock falls and topples. Rotational or translational landslides are often the result of combinations of harder, more brittle rock, overlying weaker, more ductile rock. Therefore, the factors affecting slope instability around Sorbas include:

- Unloading of the canyon walls (due to the incision of the drainage network);

- Discontinuities within the rock mass and their orientation;

- Collapse of man-made cavities within the canyon walls; and

- Construction activity in the area.

The examples presented below are three of the largest landslide complexes in the study area, as well as a number of smaller landslides that were chosen to illustrate the points and issues referred to above. These include the link between the landslide activity and the relatively rapid incision of the drainage network, the relative ages of the mapped landslide activity and the relationship between the mapped landslide activity and human activity in the area. The case studies are presented in the order one would encounter them moving upstream through the case study area.
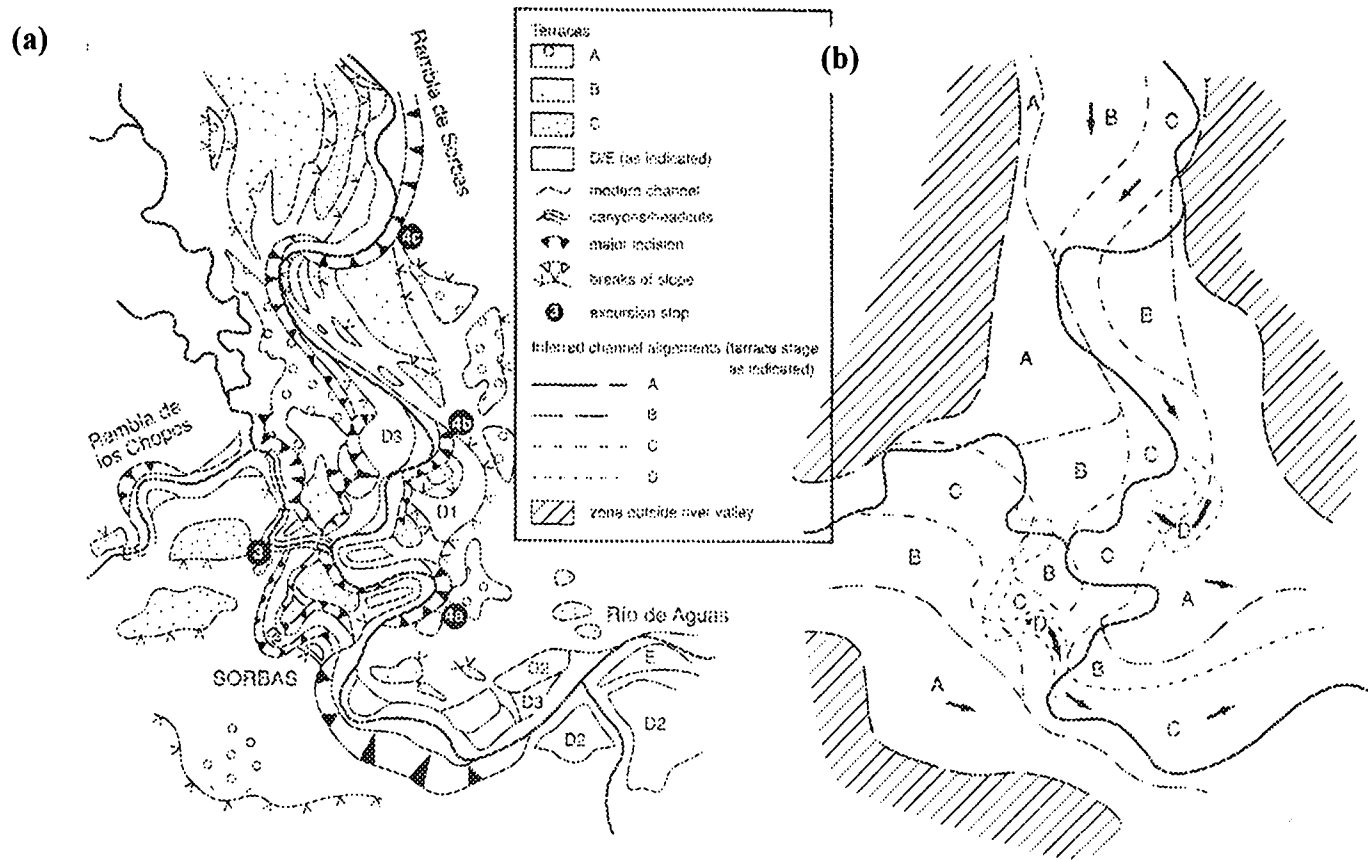
Figure 5.3 – Map of the drainage evolution in the Sorbas area **(a)** Map of the terrace sequence on the Río Aguas feeder streams at Sorbas. **(b)** Interpretation of the sequence of valley development during incision of the Río Aguas at Sorbas. Note cut-off valley meander loops. (Modified after Harvey *et al.*, 1995; Harvey, 2001).

5.2.1 The "Maleguica Landslide"

The Maleguica landslide is an extensive mass movement situated to the south-east of the older part of Sorbas (Landslide No. 28; Figure 5.2) that has been described by Hart (1999), Hart & Griffiths (1999), Hart *et al.* (2000) and Griffiths *et al.* (2002). The landslide was also identified and very briefly described by Eyers *et al.* (1998) as part of a satellite image interpretation study in the region, and is clearly identifiable on aerial photographs (Figure 5.4; Hart, 1999).

The landslide occurs on the outside of a meander in the Río Aguas contemporary active channel. This part of the Río Aguas has been incised below the level of the surrounding countryside to a depth of about 80m below the Góchar erosion surface. The "canyon" is approximately 500m wide at its widest point and is related to the incision that occurred after the Río Aguas/Rambla Feos river capture, and can be mapped through a number of different river terrace levels in the area (Mather, 1991; Harvey *et al.*, 1995; Mather *et al.*, 1995).
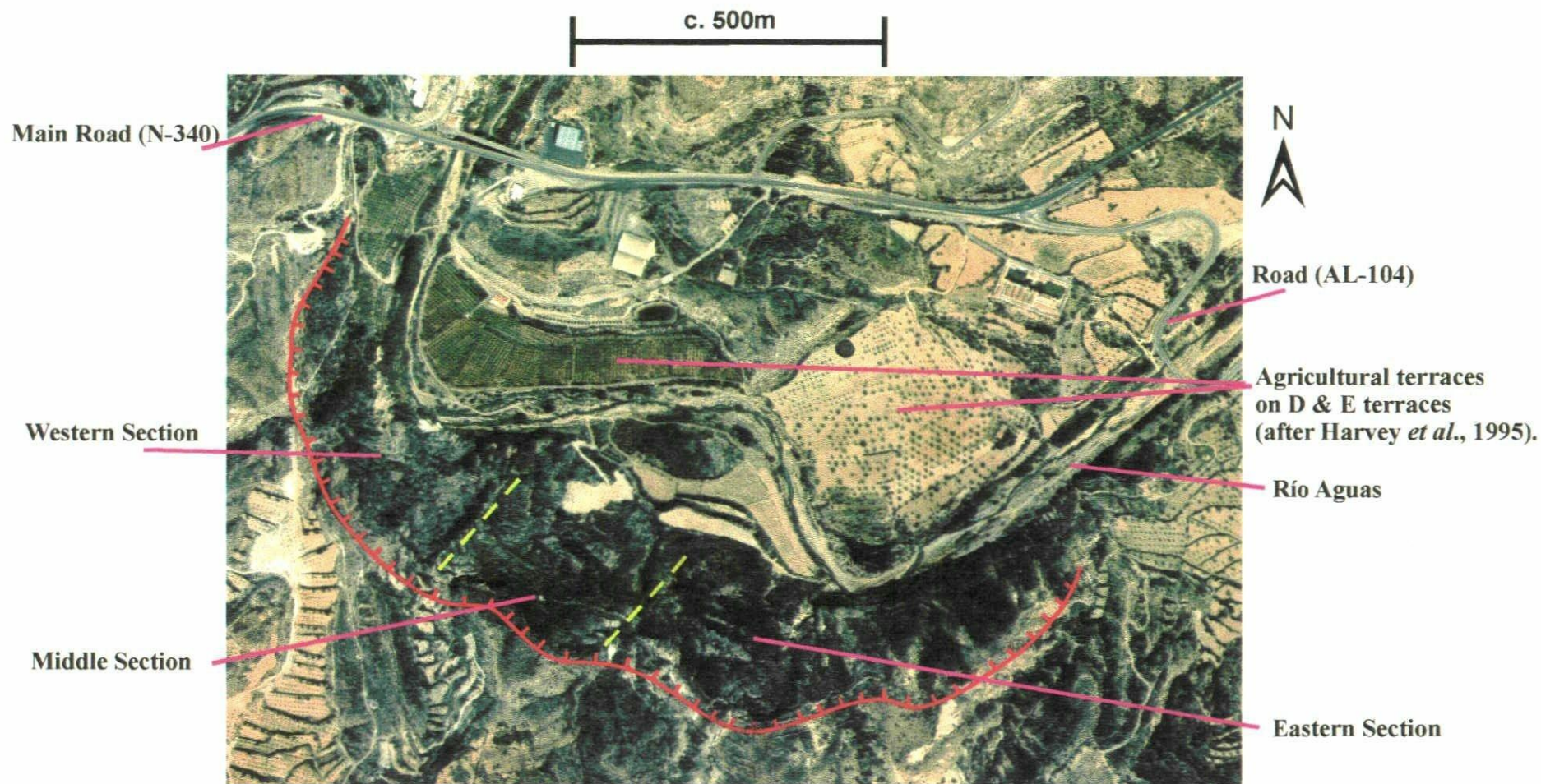
Figure 5.4 - Enlargement of a Colour Aerial Photograph showing the Maleguica Landslide. Reproduced courtesy of NERC Earth Observation Data Centre. The Photograph was taken in 1996.

The geology of the case study area consists of the sandstones and calcareous mudstones of the Sorbas Member and the underlying gypsum and calcareous mudstones of the Yesares Member. The dip of these units in this area is to the north and north-east and, therefore, out of the backscar cliff face and into the Río Aguas, although there is a slight variation in the amount of geological dip across the landslide area. The thickly bedded sandstone of the Sorbas Member is well jointed, with the jointing being perpendicular to the dip of the bedding.

A number of faults were identified cutting through the landslide, including the Infierno-Marchalico Lineament (Mather, 1991). This feature is visible at the far eastern end of the main landslide complex and follows the trend of the Río Aguas, which changes direction at this point from NW-SE to SW-NE. The other, minor faults, were either parallel to this orientation of perpendicular to it.

The Maleguica Landslide is a complex landslide exhibiting different types of failure mechanism (Dikau *et al.*, 1996). These are rock falls, rock topples and non-rotational landslides. Some of the details included in the landslide inventory are shown below (Table 5.2). This landslide is one of the largest in the study area, with a width of approximately one kilometre and a volume of over 3 million cubic metres of material. However, the exact runout length of the landslide is difficult to ascertain. It may have been removed by fluvial activity in the Río Aguas or been buried by the river terraces within the valley floor area .

Table 5.2 – Maleguica landslide data

Landslide No.:	28
Grid Reference:	05780 41055
Height:	50 – 60 m
Length:	150 m
Width:	1,000 m
Angle of Reach:	18.0°
Volume:	3.14×10^6 m^3

The landslide can be divided roughly into three sections, on the basis of its geomorphology, mode of failure and state, style and distribution of activity (Figures 5.5 and 5.6).

The western section of the landslide appears to be the most active with very little vegetation and a substantial accumulation of debris. This section is bounded by three large cliff faces that are approximately 50-60 m in height. The backscar cliff face trends NW-SE, while the two cliff faces that form the flanks of the landslide trend at approximately NE-SW. Geological mapping shows that this NE-SW and NW-SE trend fits within the regional discontinuity pattern. Geomorphological mapping of this section of the landslide was used to identify a number of back-tilted blocks, the size and shape of which are controlled by the discontinuity pattern. The back-tilted nature of the blocks indicates that they have undergone some degree of discontinuity controlled rotational sliding along a very high angle shear surface.
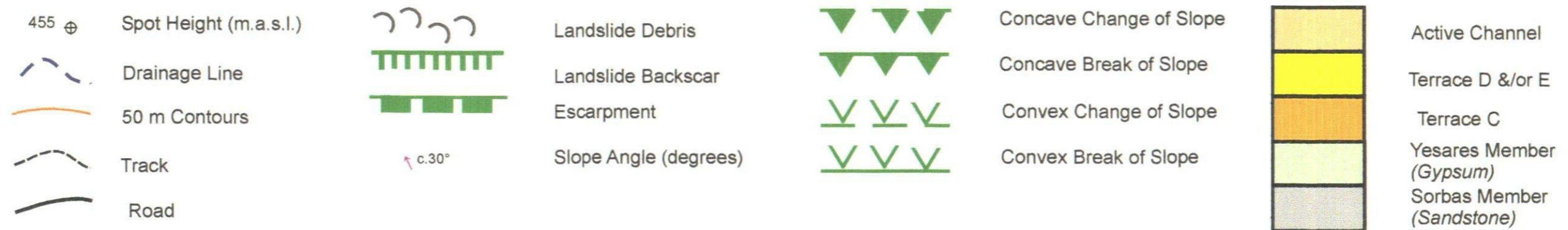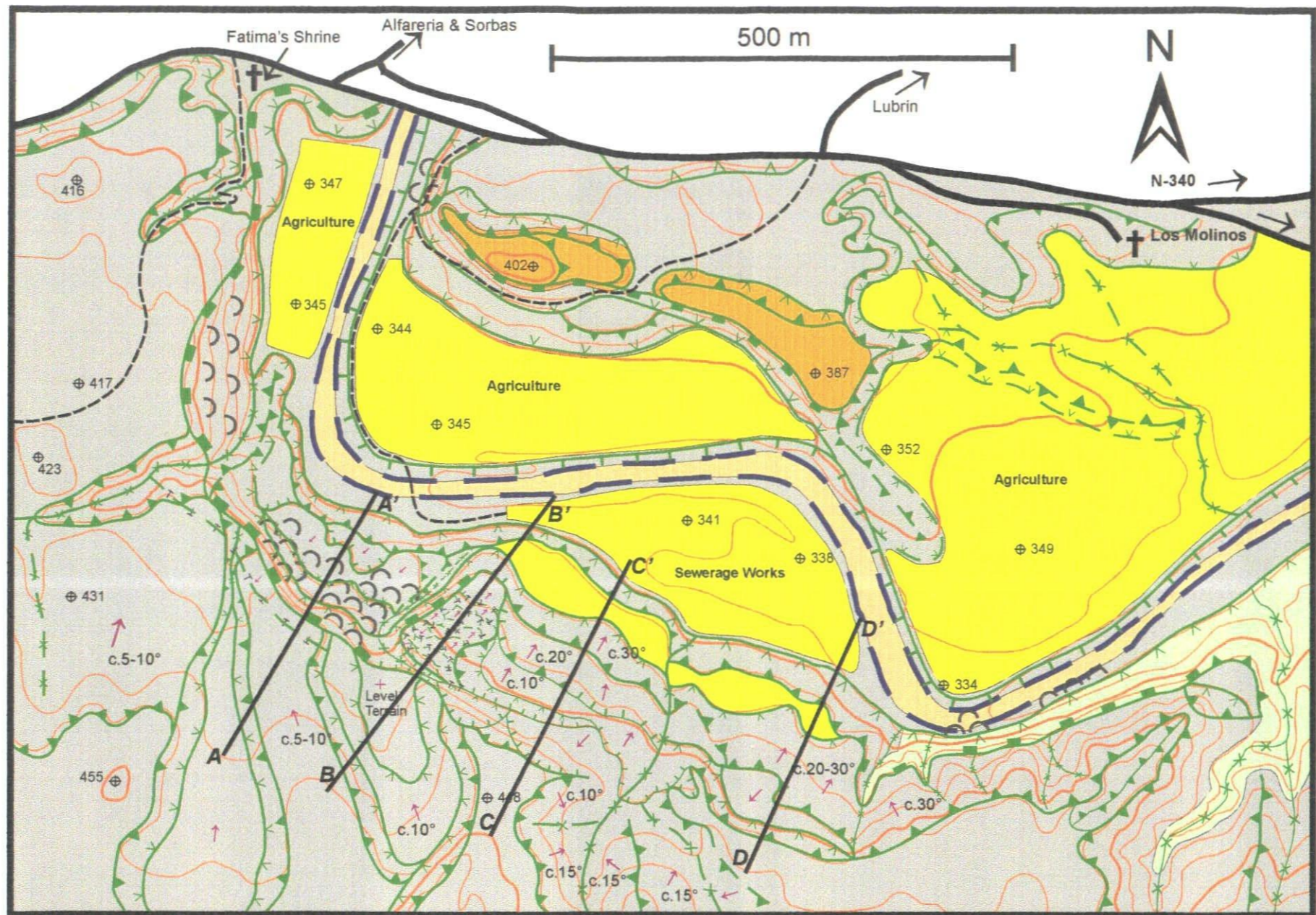
Figure 5.5 - Map of the Maleguica Landslide

Profile A

Terrace Level A - B (Pre-capture)

Major bedding plane discontinuity

Rock fall debris

Sorbas Member Sandstone

Displaced blocks

Yesares Member Gypsum

Terrace Levels D & E ?

Inferred shear surfaces   Rio Aguas

Profile B

The "Chasm"

Sorbas Member Sandstone

Inferred shear surfaces

Agricultural Terrace

Sewage Works

Yesares Member Gypsum

Rio Aguas

Terrace Levels D &/or E ?

Profile C

Terrace Level A - B (Pre-capture)

Vegetated & Degraded Slopes

Sorbas Member Sandstone

Yesares Member Gypsum

Terrace Level E

Inferred shear surfaces   Rio Aguas

Profile D

Vegetated & Degraded Slopes

Sorbas Member Sandstone

Agricultural Terrace
Terrace Levels D & E

Yesares Member Gypsum

? Inferred shear surfaces   Rio Aguas

Figure 5.6 - Profiles through the Maleguica Landslide

There have also been a number of large rock falls, with the debris covering some of the older back-tilted blocks (Figure 5.7). The rotational movements involve most of the cliff face, while the rock falls seem to only occur in the upper parts of the cliff face. The difference in failure mechanism could indicate a change in the ground conditions or discontinuity pattern within the rock mass. They could also simply reflect two stages of slope failure within this section of the landslide. For example, the discontinuity pattern of the rock mass will allow for the development of the back tilted blocks. As these blocks progress towards failure, smaller rock falls could occur along the edge of the cliff face (the backscar of the previous failures). The rock falls could also relate to smaller blocks that initiated as high angle non-rotational/rotational slides but then subsequently failed as rock falls.

The crown area of this western section of the landslide is extensively affected by tension cracks. The largest tension crack (which runs approximately parallel to the NW-SE cliff face) defines a block that is approximately 200m in length and up to 40-50 m wide (Figure 5.8). Parts of this block have moved over 2m both horizontally and vertically (Figure 5.9). The block itself is broken up into several smaller blocks by a set of smaller tension cracks that follow the overall discontinuity pattern of the hillside. The front of this block has failed as a series of smaller rock falls.

Top of Tilted Block
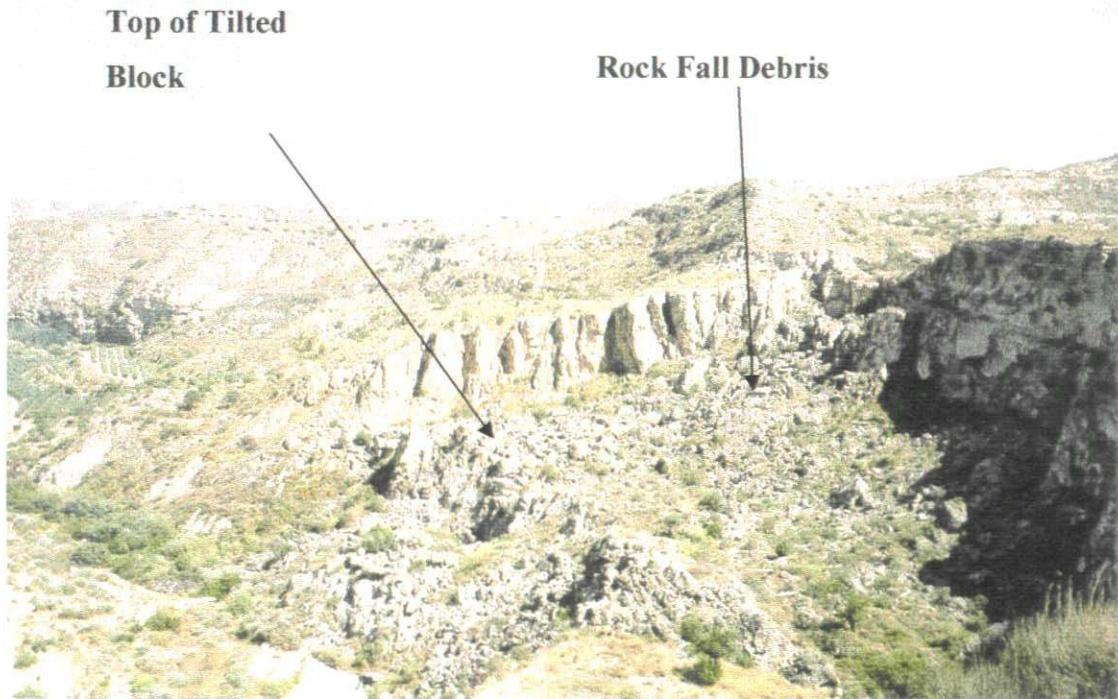
Rock Fall Debris

Figure 5.7 – Photograph of the back tilted blocks with rock fall debris at Maleguica The height of the cliff above river level is approximately 50 m (Grid Reference: 0577941057 / Facing approximately south southeast).
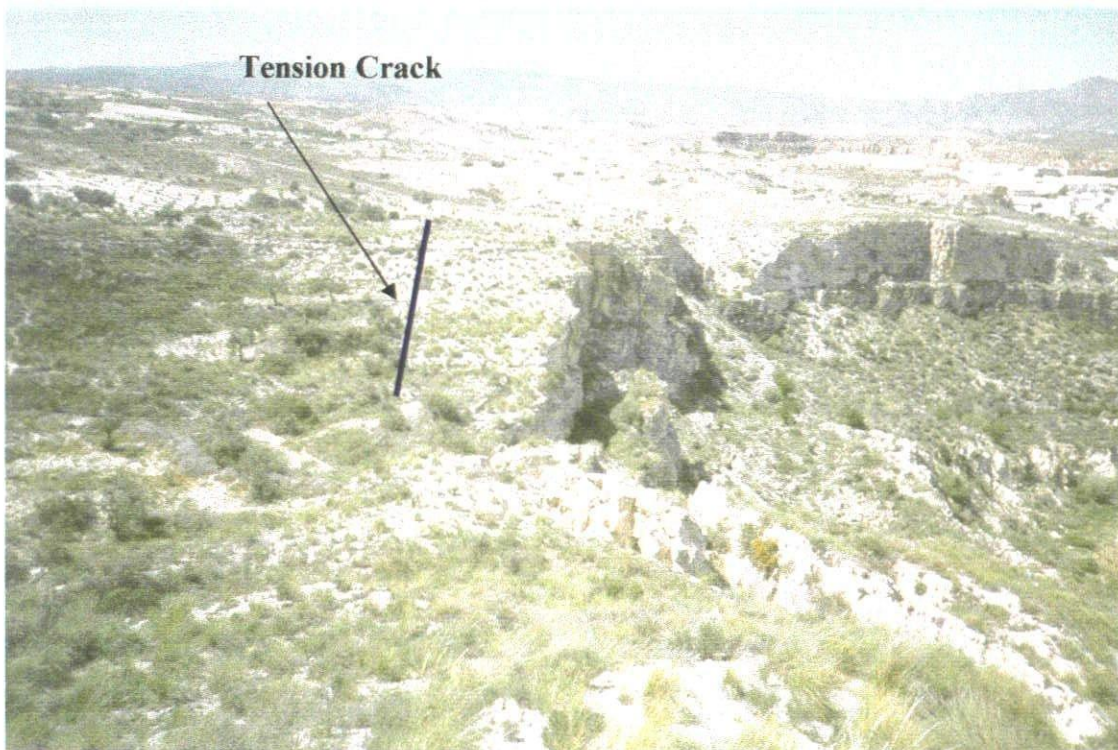
Tension Crack

Figure 5.8 – Photograph of the back scar to the western section of the landslide and the tension crack and large block that has been displaced (Grid Reference: 0578441054 / Facing approximately west northwest). The line indicates the location of the tension crack shown in Figure 5.9.

The middle section of the landslide has undergone a series of reasonably complex discontinuity controlled movements. These movements are partially picked out by the heavily jointed NE-SW orientated cliff that marks out the eastern side of the western section of the landslide (Figure 5.10). Using a combination of discontinuity and geomorphological mapping it is possible to show that this cliff face was actually a series of separate blocks. The lower blocks have undergone a small amount of non-rotational sliding, while some of the higher blocks have ridden up against them. These movements can be picked out by the discontinuities that are clearly visible in the cliff face that separates this section of the landslide from the western section. The movement of these blocks has resulted in a very large tension crack opening between the backscar and the uppermost moving block (Figure 5.11).

The eastern section is relatively well vegetated which tends to mask the underlying disturbed ground (Figure 5.12). Field mapping highlighted the presence of a number of back-tilted blocks that have undergone high-angle rotational sliding. The shape and size of these blocks, as before, are controlled by the discontinuities affecting the area. The relatively thick vegetation cover suggests that this section of the landslide is currently slightly less active than the other two sections. This may relate to the ground conditions or that this section is away from the active river channel, and therefore is less affected by toe erosion than it would have been in the past.

Tension crack with 2 m displacement in white, moderately strong sandstone (Sorbas Member)

2 m Ruler

Figure 5.9 – Photograph of the tension crack and backscar associated with the displaced block shown in Figure 5.8 (Grid Reference: 0578041056).

Río Aguas

c. 20 m high

Rock fall debris & tops of rotated blocks
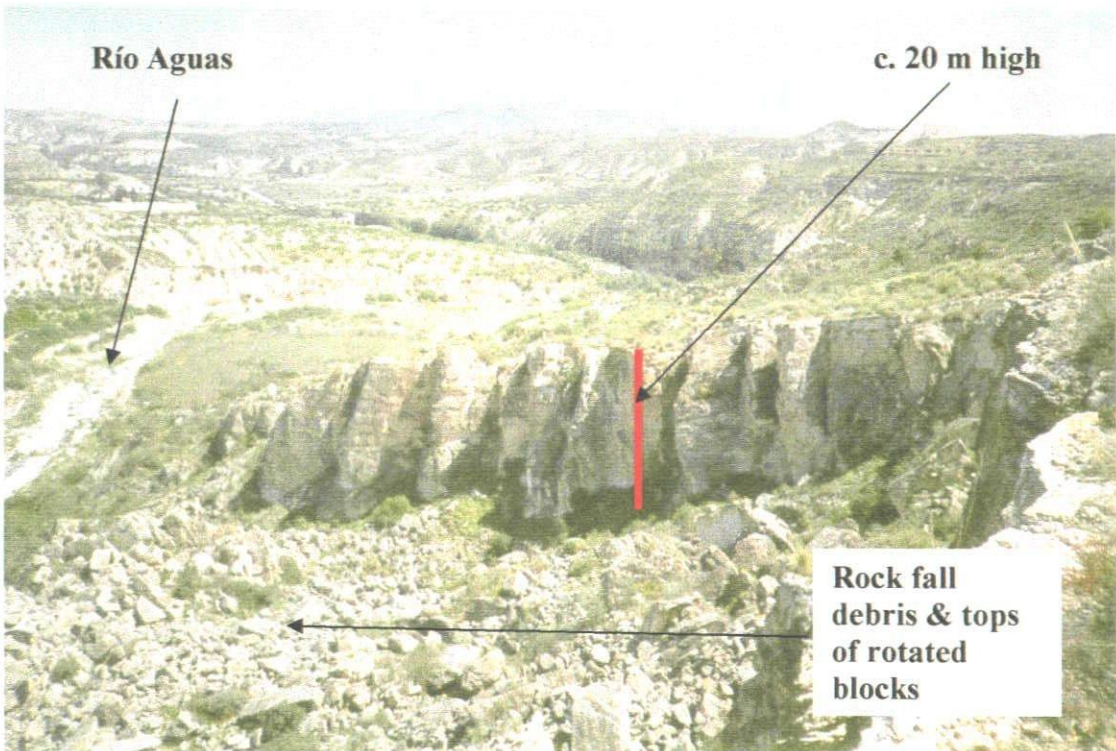
Figure 5.10 – Photograph of the jointed cliff face in the western section of the landslide (Grid Reference: 0578041056 / Facing east).
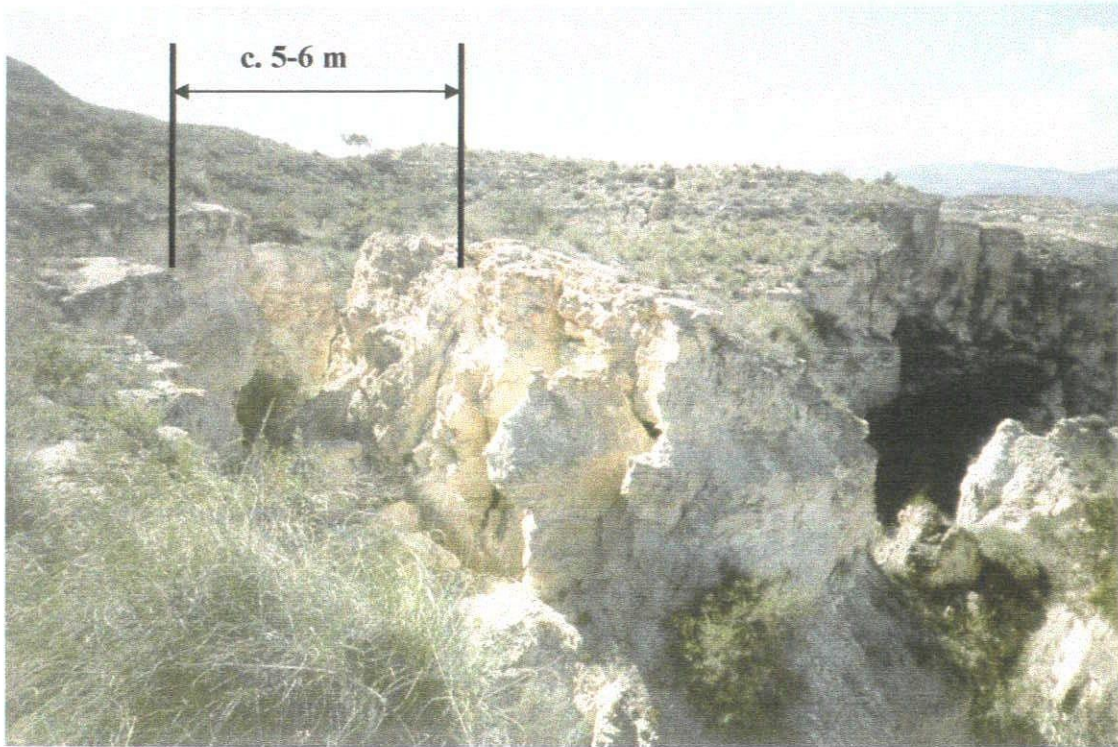
Figure 5.11 – Photograph of the chasm behind the central part of the Maleguica landslide (Grid Reference: 0578341055 / Facing northwest).
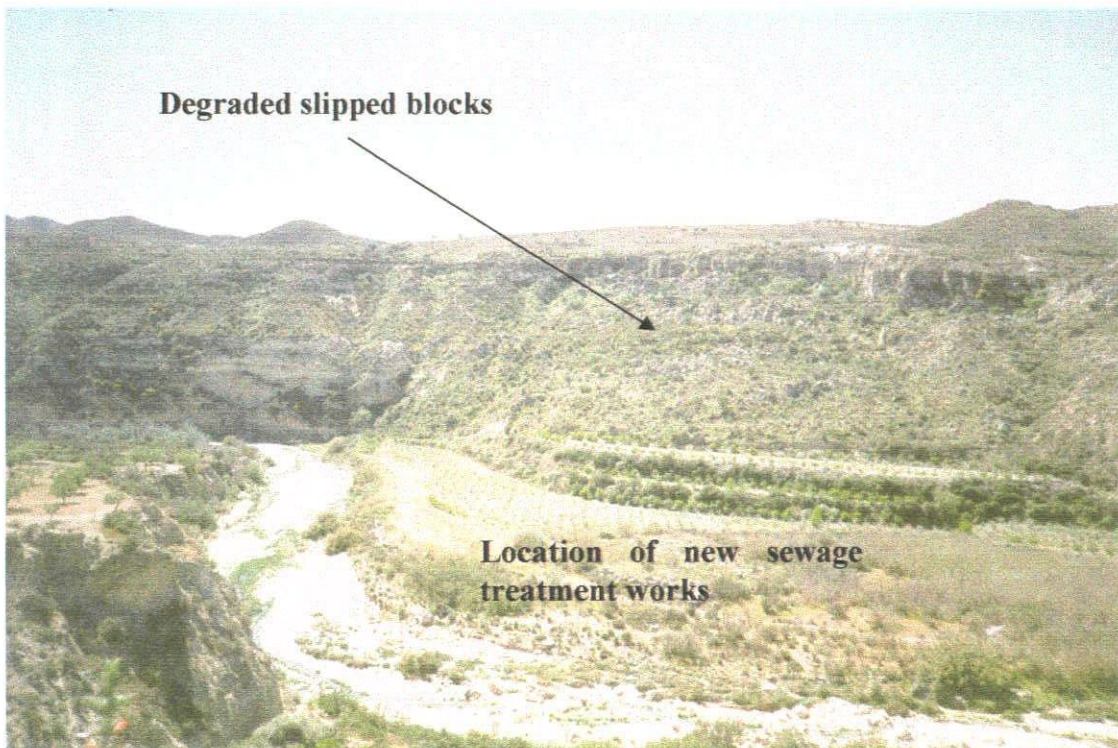
Figure 5.12 – Photograph of the Eastern-section of the Maleguica landslide (Grid Reference: 0578541058 / Facing south). The sewage treatment works are now located on the terrace at the foot of the landslide.

An interesting question is whether this landslide has ever blocked the Río Aguas. Field mapping failed to find any evidence that would support this hypothesis. However, that does not mean that the course of the Río Aguas has not been affected by the landslide. The canyon floor is probably sufficiently wide enough, that if a landslide had occurred the river would have had room to alter its course and, therefore, not be blocked.

Geomorphological mapping of the landslide and surrounding area identified a number of river terrace levels within the valley, as well as the presence of numerous "hanging" valleys and gullies along the edge of the backscar cliff face. The river terraces, although modified by human activity, still help to highlight the previous river course.

The hanging valleys and gullies can be picked out (particularly in the aerial photographs for the area) by the presence of agricultural terraces that have been built along the drainage lines. These terraces have been constructed to make use of the natural drainage of the hillside. The fact that they have been truncated by the current drainage, and are approximately 50 m above the present river level confirms the relatively rapid incision of the current drainage system (i.e., the landscape is still adjusting to the incision). Mather (2000) estimated that tributary catchments in the Sorbas area experienced up to a ten-fold increase in the rate of incision post the Río Aguas/Rambla Feos River Capture.

The crown area of the landslide (and the top of the canyon wall) is at approximately the same height as the C river terrace level. A number of D terrace levels have been

identified along the canyon floor (Harvey *et al.*, 1995; Mather *et al.*, 1995; Harvey, 2001). These level areas within the canyon floor are currently being used for agriculture. This spatial distribution of the river terraces would suggest that the incision of the river has occurred post river terrace C and prior to the formation of the D river terraces, which fits in with the incision history of the Río Aguas described previously. It would also imply that the landslide was initiated during this time interval, and is a relatively old feature within the landscape, but remains "active" (the fresh tension cracks and rock falls within the western section of the landslide).

This relative age of the landslide may help to explain the differences in landslide activity described earlier in the three different sections of the landslide. After the Río Aguas/Rambla Feos River Capture, the rate of incision of the drainage channel was relatively high (Mather, 2000) leading to the formation of over steepened slopes and the present canyon system. This is when the landslide could have been initiated. As the canyon then developed further, and the rate of base level change slowed down after the initial wave of incision through the drainage system, the activity of the landslide would have also changed. This would have occurred in different parts of the landslide as the drainage pattern in the canyon evolved and shifted course.

As far as the risk being posed by this landslide to infrastructure or the local population, the landslide complex is not located near to any of the houses or roads associated with the main town of Sorbas. However, in the spring of 2000 a new sewage treatment works was built on the D3/E river terrace at the foot of the central to eastern section of the landslide (on the terrace level shown in Figure 5.12). If a significant failure was to occur in this central section, the runout could affect the

sewage works. Also during the spring of 2000, a local farmer started to dig out agricultural terraces within parts of the western section of the landslide. Some of these were based on the slipped blocks from previous failures. However, by 2003 these agricultural terraces seem to have been abandoned for no apparent reason.

5.2.2 The "Alfarería Landslide"

The Alfarería landslide is located immediately to the east of the old part of Sorbas in an area known as "Alfarería" (Figure 5.2). Sorbas is well known for its pottery and it is within Alfarería that most of the pottery is made. The landslide has been previously described in Hart & Griffiths (1999).

The landslide is located in the outside of a meander in the active channel of the Río Aguas. The river channel is within the canyon that surrounds Sorbas and is approximately 50 m below the level of the surrounding countryside and the Góchar erosion surface. However, due to its location, on the inside of the meander, Alfarería is located only just above the level of the river on a post D3 river terrace level. The canyon is approximately 400-500 m wide in this area. The incision is related to the incision that occurred after the Río Aguas/Rambla Feos river capture, which occurred approximately 10 km downstream from the landslide.

The geology of the Alfarería landslide consists of the Góchar Formation overlying the Cariatiz Formation. The lithology of the landslide area is a succession of near-shore and inter-tidal sandstones, interbedded with calcareous mudstones and overlain by terrestrial conglomerates. There are also three distinctive beds within the succession

that can be used to correlate across the landslide, as well as to correlate the landslide

deposit with the backscar. These are the medium grained yellow sandstone "Marine

Band" and the two fine grained white "Carbonate Bands" described by Mather (1991)

and Section 2.3.

The geological dip of the bedding (which is approximately 10-15°) is to the north and

northeast, although there is some variation in the dip across the landslide area. A

number of small normal faults were also identified within the area.

The Alfarería Landslide is a complex landslide dominated by high-angle rotational

movements, as well as rock falls and topples and some sagging-type movements

(Dikau *et al.*, 1996). The landslide also exhibits a number of different other type of

failure mechanism such as sporadic stone fall and rock fall. Some of the details

included in the landslide inventory are shown below (Table 5.3).

Table 5.3 – Alfarería landslide data

Landslide No.:	24
Grid Reference:	05785 41063
Height:	50 m
Length:	30 m
Width:	700 m
Angle of Reach:	59.0°
Volume:	$5.5 \times 10^5 \text{ m}^3$

The measured runout length for the landslide is much shorter than would be expected

for this type of landslide. This is because the debris from the landslide is highly

erodible and, therefore, easily removed by flood activity in the Río Aguas. The runout

from this landslide is likely to have blocked or affected the course of the Río Aguas,

and may explain the reasonably large river terrace (topographically) below the Alfarería area (Figures 5.2 and 5.13).

The crown area of the landslide (and the top of the canyon wall) is capped by an outcrop of river terrace level A. The inside of the meander is possibly a D3/E river terrace (Harvey *et al.*, 1995; Mather *et al.*, 1995). This would suggest that the incision of this section of the river has occurred post formation of the river terrace A and prior to the formation of the D/E river terraces. This fits with the previously described incision history of the Río Aguas. It would also imply that the landslide was initiated during this time interval although this covers most of the recent history of the study area. Geomorphological mapping and analysis of the spatial distribution of the river terraces in the area would suggest that the landslide is probably related to the wave of aggression and incision after the Río Aguas/Rambla Feos River Capture (i.e., post Terrace C formation and prior terrace D formation).

The landslide is not located near to any of the roads or other infrastructure associated with the main town of Sorbas. Alfarería is located opposite the landslide, although it is unlikely that any activity within the landslide area would affect Alfarería directly. An interesting scenario would be if the landslide blocked the Río Aguas. Any backflow from a landslide dam could affect the farmhouses and/or farmland that are located within the canyon floor or some of the lower parts of Alfarería.
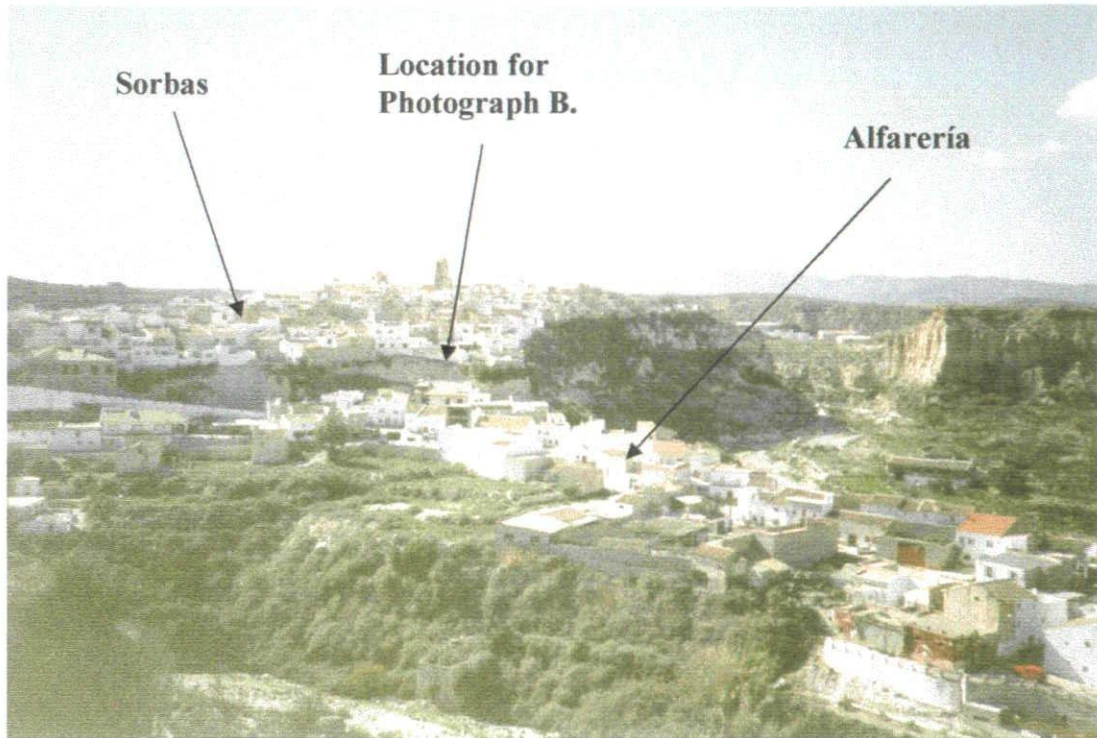
A.
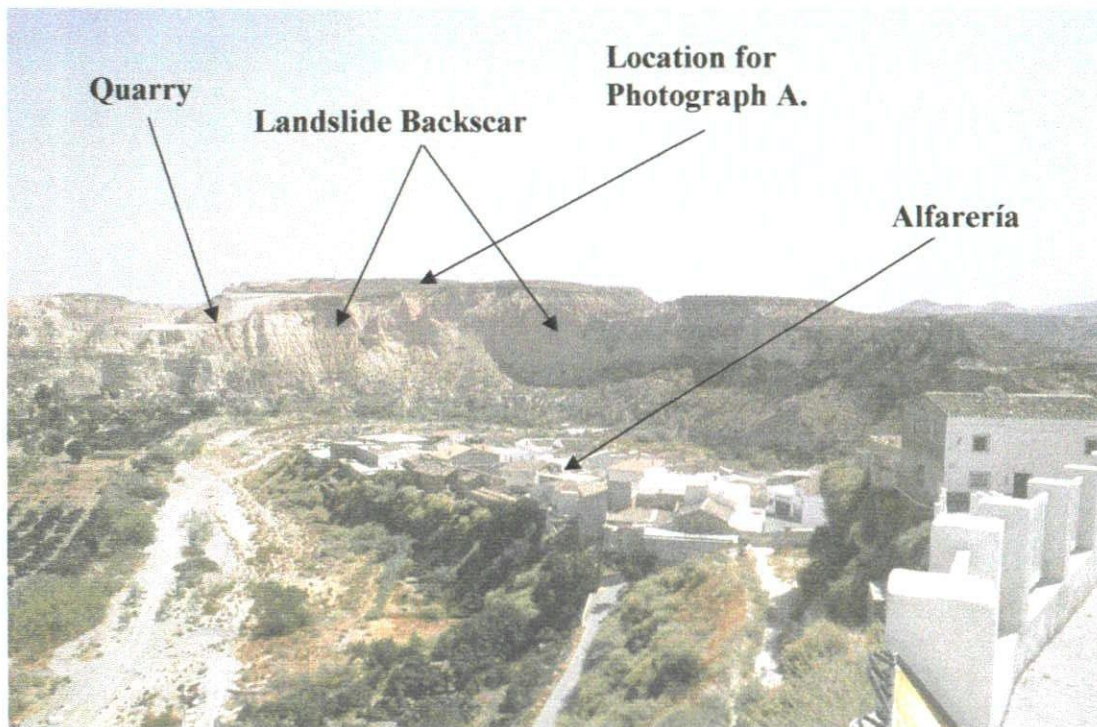
B.

Figure 5.13 – Photographs of Alfarería and the Alfarería Landslide. **A.** Photograph of Alfarería taken from the crown of the landslide looking towards the west (Grid Reference: 0578641064). **B.** The Alfarería Landslide taken from Sorbas looking towards the east. Alfarería is in the foreground (Grid Reference: 0578341064).

297

Interestingly, the landslide is slowly being removed by quarrying activity in the crown area. This part of the landslide is within fine-grained sandstone that is used locally for brick making. Within the last 4-5 years, the size of the operation has increased rapidly, with a large portion of the northern part of the backscar being removed. Some material has been spoiled over the edge of the canyon wall into the river below, causing some minor rock falls and topples. This quarrying activity could result in the removal of the majority of the head area of this landslide. This could reduce the activity and impact of the landslide.

5.2.3 The Sorbas Theatre Rock Fall

This rock fall is named after the Sorbas Theatre that is built directly above the backscar of the landslide. The theatre, which is located on the northern side of the Sorbas "knoll", was opened in the autumn of 1997 (Landslide 15; Figure 5.2). The landslide had already occurred when the author first visited the site in the spring of 1998, but is not seen in the colour aerial photographs that were flown in 1996. The site is of particular interest as it is an example of how construction activity in the area influences slope stability and how the local population sometimes tries to deal with the instability. It has been described in Hart & Griffiths (1999) and Hart et al. (2000).

The site is located above a river terrace level that lies at what would have been the area of the confluence of the Rambla de Los Chopas and the abandoned meander. However, the river terrace is below the level of the abandoned meander and is therefore younger than the D3 age of the floor of the abandoned meander. Due to the

current drainage pattern, the river terrace (and therefore the landslide site) is now in the outside of a meander, in the active drainage channel of the Rambla de Los Chopas.

This part of the drainage system is incised below the surrounding countryside and the Góchar erosion surface. The depth of the drainage channel below this level is approximately 30-40 m. The canyon is approximately 20-25 m wide at this point.

The canyon wall consists of the thickly bedded, white sandstone interbedded with thin intercalations of calcareous mudstone of the Sorbas Member. At least two, well defined joint sets have been identified in the rock mass. The very top of the canyon wall consists of made-ground, involving building waste and other debris. A number of river terrace levels have also been mapped in this area, particularly on top of the canyon wall on the other side of the drainage channel (Harvey *et al.*, 1995).

The canyon wall under the Sorbas Theatre is affected by rock fall activity (Dikau *et al.*, 1996) initiating from a wedge failure surface (Table 5.4). It is thought that this rock fall occurred at some point during the construction of the theatre, possibly as a result of the new building loading the edge of the canyon wall. The spoiling of building material over the edge of the canyon wall may have also affected the stability of the slope. At present, this rock fall does not appear to affect the foundations of the theatre. However, in June 2003 there were some cracks beginning to form along the back wall of the theatre, which could be related to subsidence of the building. It is unclear at present whether this is related to the rock fall or further instability of the canyon wall.

Table 5.4 – Sorbas Theatre landslide data

Landslide No.:	15
Grid Reference:	05777 41064
Height:	20m
Length:	50m
Width:	15-20m
Angle of Reach:	22.0°
Volume:	3,000 m³

The author has been able to observe the degradation of the landslide over a period of six years (1998-2003). This has enabled the author to investigate how quickly the backscar and debris have degraded during this period (Figure 5.14). In this time, vegetation has started to grow up over the backscar and deposit of the landslide. Some of the debris was also removed shortly after the landslide occurred so that an agricultural terrace below the landslide could be re-instated. An understanding of how quickly the vegetation has grown over the landslide and how quickly the back scar has degraded could be used to assess the relative ages of other failures in the canyon walls around the Sorbas area and therefore (possibly) gain some idea of their frequency of occurrence.
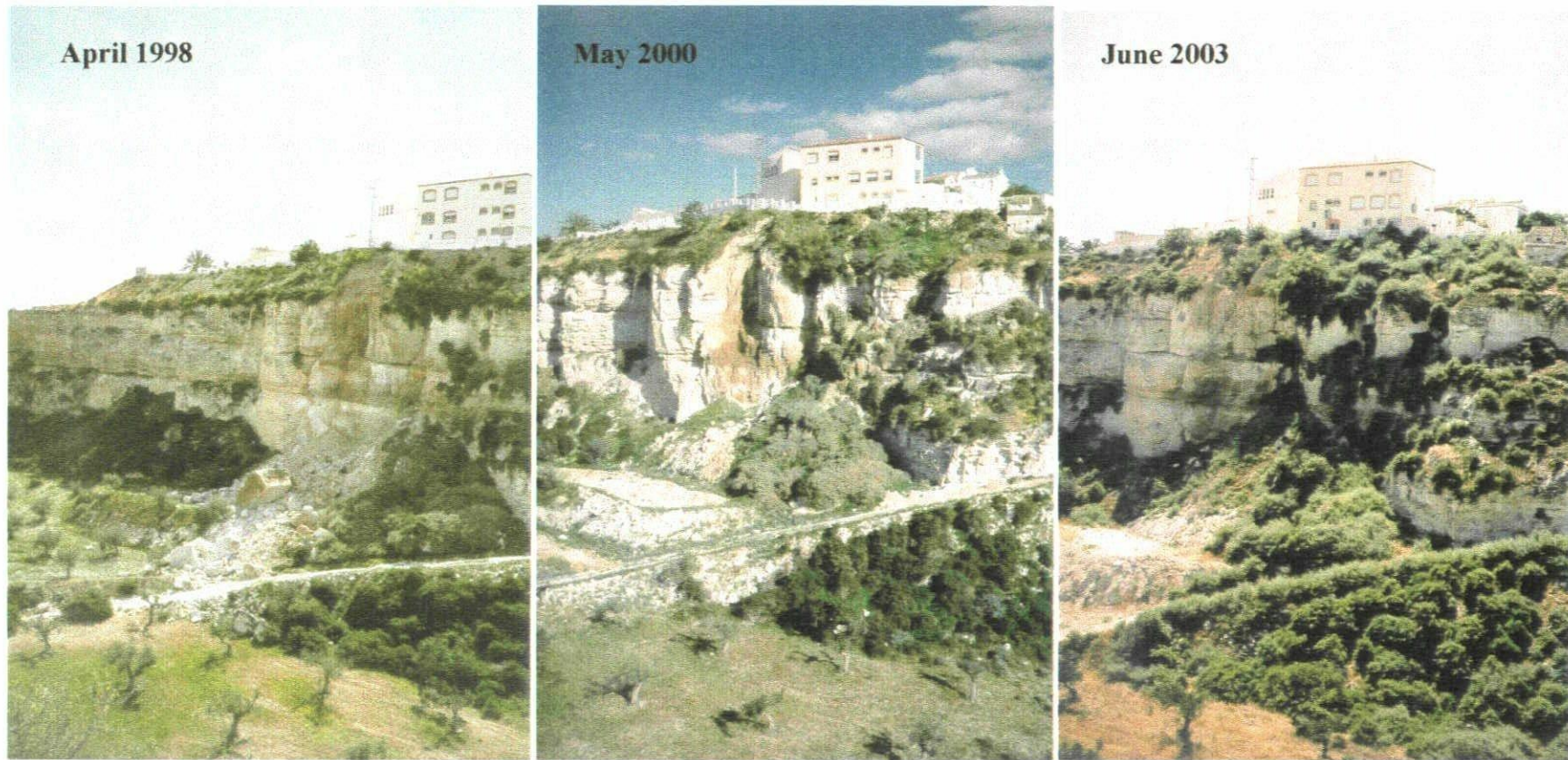
Figure 5.14 – Photographs of Sorbas Theatre during the period 1998 to 2003 showing the changes in slope morphology and vegetation cover (Grid Reference: 0577641065 / Facing east southeast).

5.2.4   The "Los Beneficios Landslide"

The Los Beneficios Landslide has been described in Hart & Griffiths (1999) and Hart *et al.* (2000). It is a reasonably extensive mass movement, which is identifiable on aerial photographs. It is located to the north-west of the new part of Sorbas (Landslide No. 3; Figure 5.2).

The landslide is located within the outside of a meander in the active channel of the Rambla de Los Chopas. This part of the river system is a relatively open valley, but has been incised below the level of the surrounding countryside to a depth of about 34-40 m below the Góchar erosion surface and is related to the incision that occurred after the Río Aguas/Rambla Feos river capture 11-12 km downstream from the landslide, as described in Section 2.4.

The geology of the Los Beneficios area is very similar to the Alfarería area, consisting of the Cariatiz Formation overlain by the Góchar Formation. The lithology of the landslide area is a succession of sandstones, interbedded with calcareous mudstones and overlain by terrestrial conglomerates.

As in the case of the Alfarería landslide area, the same three distinctive marker horizons described by Mather (1991) are seen within the succession, and facilitate correlation across the landslide and the identification of some of the moved materials. Dissolution features were found within some of the units of this succession. These highlight the highly erosive nature of some of the rock material involved in this landslide.

The dip direction of the bedding is approximately to the north and northeast, although there is some variation in the amount of dip across the landslide area. The amount of dip is also variable, between almost horizontal and 10-15°. A number of smaller faults were also identified within the rock mass. These are predominantly small-scale normal faults with throws of < 1-2 m.

The Los Beneficios Landslide is a complex landslide dominated by both high-angle and low-angle rotational and non-rotational movements (Dikau *et al.*, 1996). It is also one of the largest landslides in the study area with a volume of several tens of millions of cubic metres. These are picked out by a number of large back-tilted blocks (Figures 5.15 and 5.16). The landslide also exhibits a number of different types of failure mechanism such as backward topples, rock fall, sporadic stone fall, and non-rotational sliding. Some of the details included in the landslide inventory are shown below (Table 5.5).

Table 5.5 – Los Beneficios landslide data

Landslide No.:	3
Grid Reference:	05769 41069
Height:	50 m
Length:	150 m
Width:	600 m
Angle of Reach:	18.0°
Volume:	$2.36 \times 10^6 \text{ m}^3$
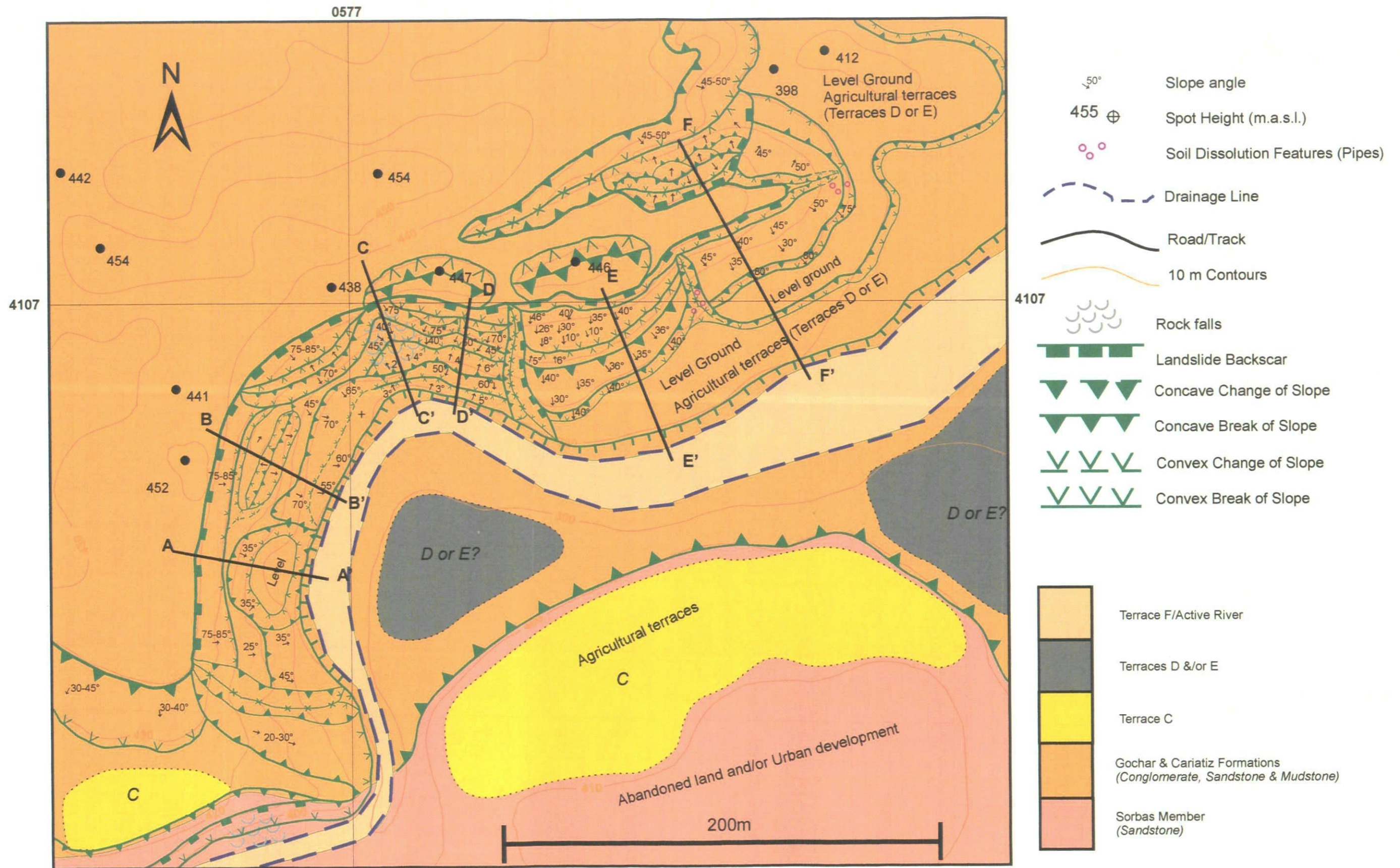
Figure 5.15 - Map of the Los Beneficios Landslide
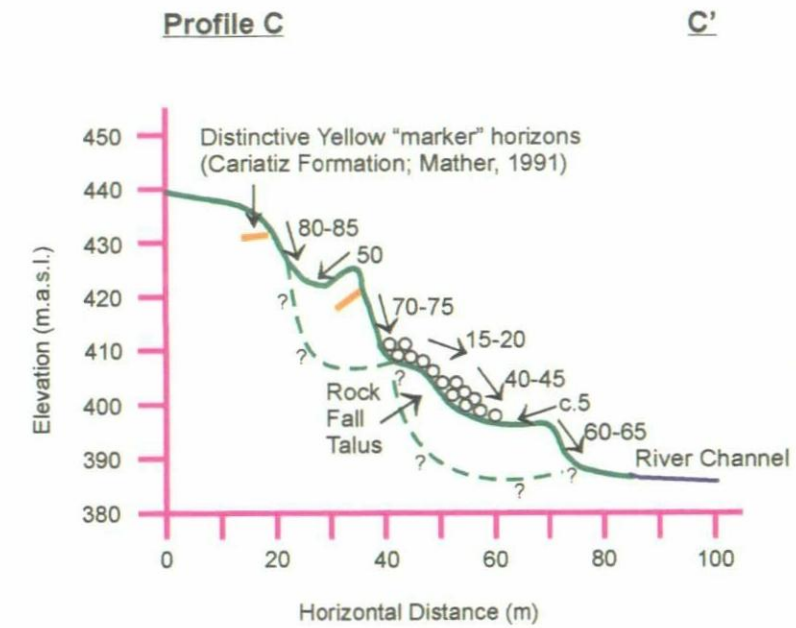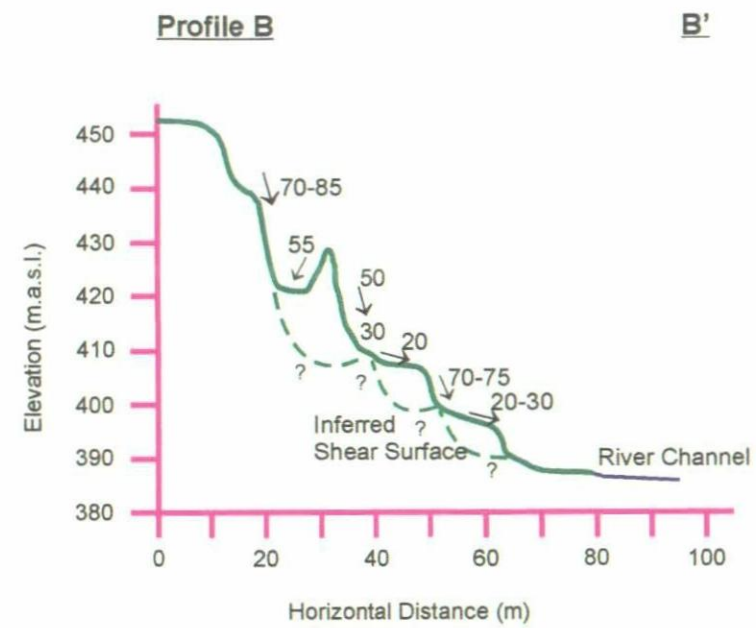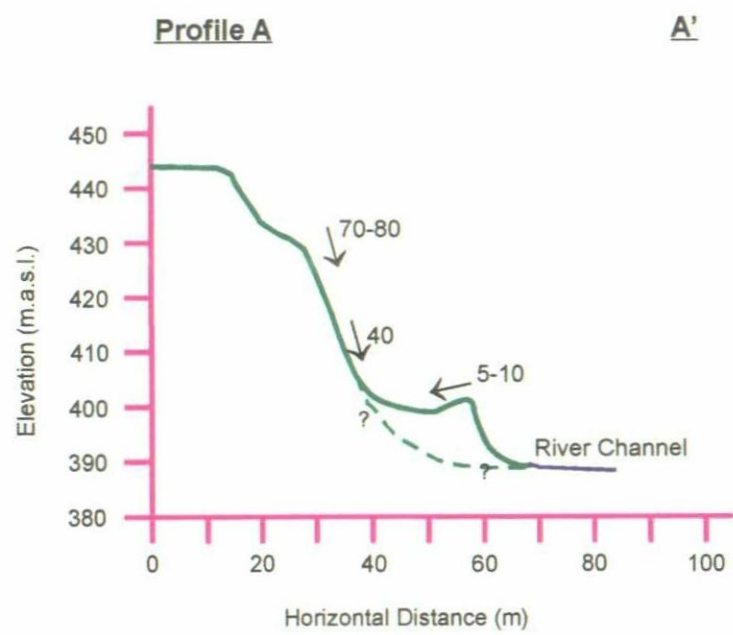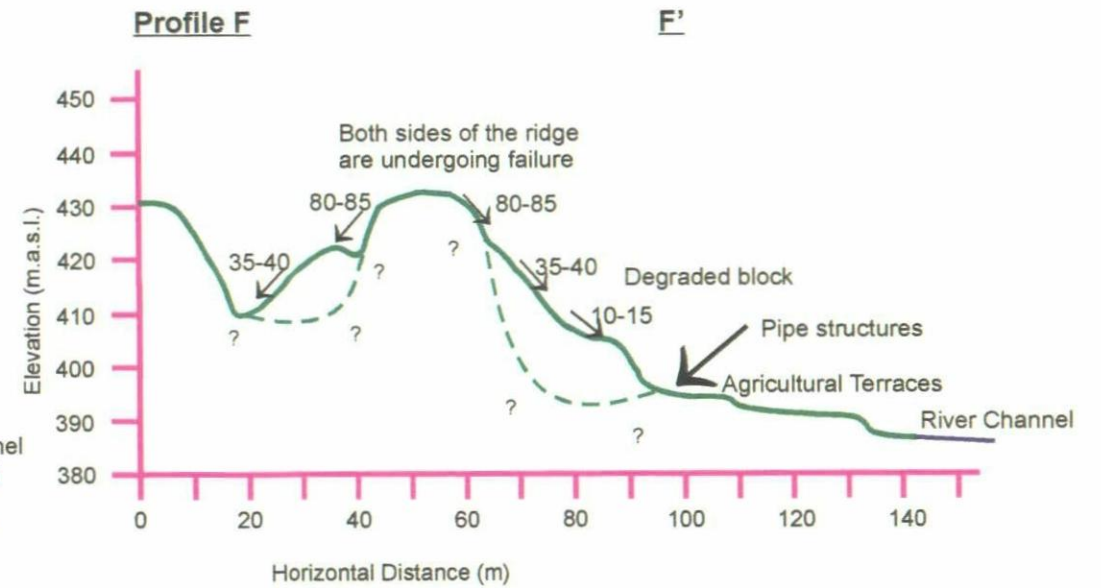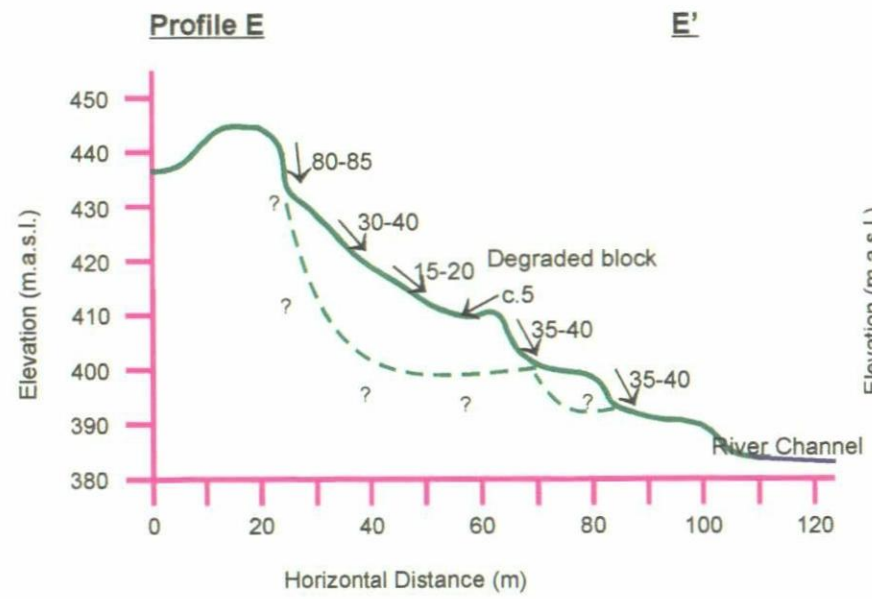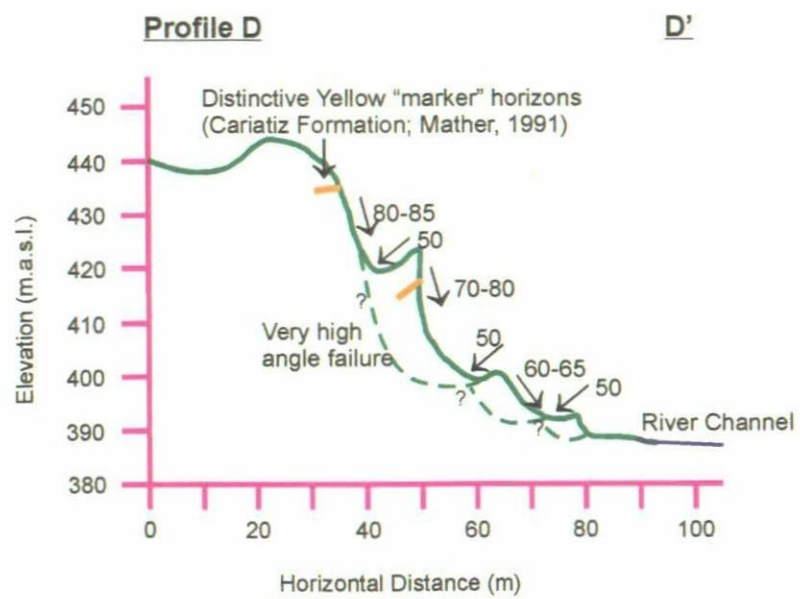
Figure 5.16 - Profiles through the Los Beneficios Landslide

The landslide can be roughly divided into four different sections, based on the state, style, and distribution of the landslide, as well as the geomorphology of the landslide (Figure 5.15). This is also dependent on the relative position of the geological units within the meander, and the geological dip of the beds.

The western section of the landslide lies within the outside of the meander of the Rambla de Los Chopas. This section is marked by a 30 m high, almost vertical cliff face which forms the backscar to the landslide and a number of back-tilted blocks (Figure 5.17). Only one of these is clearly defined, while the others are all fairly degraded, but they can be picked out on the profiles (Figure 5.16). Slope angles within this section of the landslide vary between 30° and 70°. Most of the cliff face is composed of conglomerate (Góchar and Cariatiz Formations). However, there are one or two lithological units within the cliff face that can be traced through different parts of the landslide complex. One of these is a moderately weak, coarse grained sandstone bed.

To the north and centre of the landslide complex there is a large rock debris cone. This seems to be a combination of a rock fall and back-tilting block that subsequently broke up to form a rock fall (Figure 5.18). The remains of the block can be found under parts of the rock fall debris. Another, smaller block can be seen at the top of the cliff above the rock fall debris. This block has dropped by a few metres and is now slowly breaking up to form a rock fall.
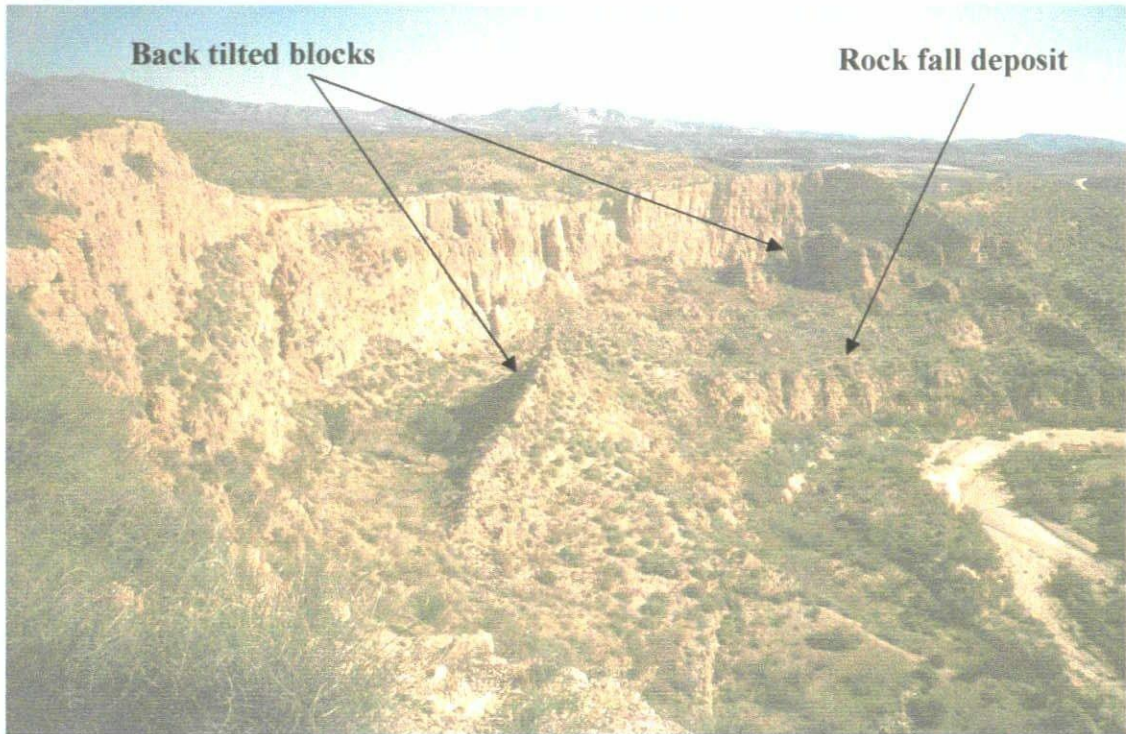
Figure 5.17 – Photograph of the western section of the Los Beneficios landslide (Grid Reference: 0576941066 / Facing north), showing back tilted blocks and rock fall deposits are clearly visible.
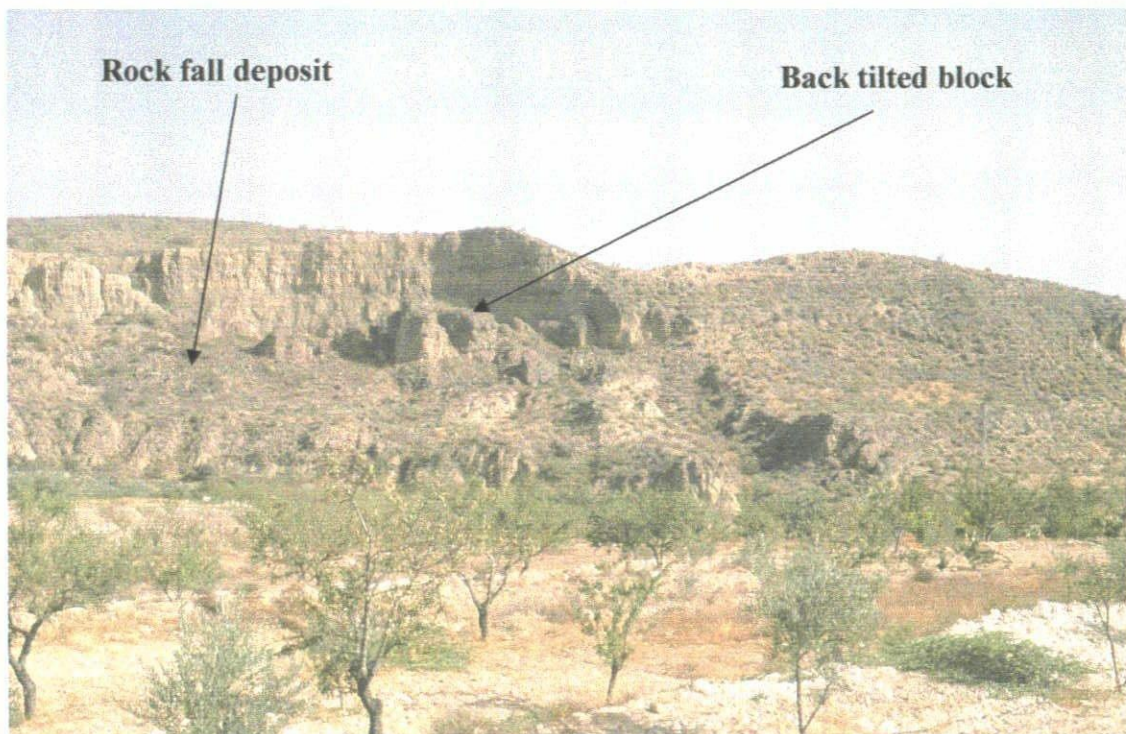
Figure 5.18 – Photograph of the central section of the Los Beneficios landslide (Grid Reference: 0577241067 / Facing north). The rock fall deposits and back tilted block are clearly visible.

The eastern section of the landslide is very different from the western and central northern section described above. The slope angles are gentler and the slopes are not mantled with rock fall debris. Both sections are characterised by an undulating slope profile (Figure 5.16 – profiles E and F). These undulations may indicate the presence of very degraded blocks or lithological boundaries within the hillside, but this is uncertain. The underlying rock mass appears to be weaker giving rise to the more subdued profile. However, this is capped by a more resistant conglomeratic unit that forms a bluff along the crown of the landslide complex in this section.

Although the bulk of the hillside is the Góchar Formation conglomerate, there is a distinctive yellow mudstone unit that can be traced through this section of the landslide. This unit is affected by a number of dissolution soil pipes and other associated dissolution features. Some of the pipe structures are up to a 1.5m in diameter. This unit has been identified as the yellow "Marine Band" marker horizon described by Mather (1991). This observation is of particular significance to the landslide as any pipe structure within the slopes can either concentrate any water passing through them or directly destabilise parts of the slope as a result of collapsing. As discussed in Section 4.3, the presence of pipe structures is indicative of a dispersive, highly erodible material.

The eastern section of the landslide complex is part of a ridge-like structure that is affected by landslide activity on both sides. This northern slope forms the northern section of the overall landslide complex. The northern section is a relatively small dip-slope, translational/high angle rotational landslide. It is possible that the landslide

is being controlled by both the dip of the geology and the erosive nature of the carbonate mudstone that was described above.

The crown area of the landslide (and the top of the canyon wall) is at approximately the same height as the B river terrace level. A number of D or E terrace levels have been identified on the opposite side of the river (Harvey *et al.*, 1995; Mather *et al.*, 1995; Harvey, 2001). These areas are currently being used for agriculture. This spatial distribution of the river terraces would suggest that the incision of the river has occurred post river terrace B and prior to the formation of the D river terraces, which fits in with the incision history of the Rio Aguas as previously described. It would also imply that the landslide was initiated during this time interval, and is a relatively old feature within the landscape.

However, this time interval covers a considerable amount of the recent history of the study area. Geomorphological mapping and analysis of the spatial distribution of the river terraces in the area suggests that the landslide is probably related to the wave of aggression and incision after the Rio Aguas/Rambla Feos River Capture (i.e., post terrace C formation and prior terrace D formation). In support of this, Mather (2000) has estimated that this section of the Rio Aguas may have experienced up to a five-fold increase in the rate of incision after the Rio Aguas/Rambla Feos River Capture. The western section of the landslide complex would have initiated as a result of the formation of the over steepened canyon walls on the outside of this meander. The eastern section, being on the inside of the meander, would have been affected by fluvial erosion of the lower slopes, but not to the same extent.

Therefore, based on the field mapping observations, the factors that seem to be controlling the activity of this landslide are:

- The location of the landslide on the outside of a meander;

- The relative rapid incision of the drainage and, therefore, the relatively rapid formation of the valley side slopes;

- The geological dip and dip direction of the Góchar Formation; and

- The dissolution features (i.e., the pipe structures) and the dispersive nature of some of the units within the rock mass.

The landslide is not located near to any of the houses, roads or other infrastructure associated with the main town of Sorbas. There are some agricultural fields located just below the eastern section of the landslide.

5.2.5   The "Bird's Footprint" Rock Fall

Bird footprints have been found preserved within part of the white sandstone succession of the Sorbas Member (Doyle *et al.*, 2000). The landslide described here is a rock fall that has occurred immediately above one of the best locations for seeing these footprints. The author first visited the site in the spring of 1998, and has returned frequently to monitor the site, and has previously described the site in Hart *et al.* (2000).

The site is located a short distance to the west of the Los Beneficios Landslide at the western end of Sorbas (Landslide 1; Figure 5.2). The rock fall has occurred within the

canyon wall onto the upper section of the drainage channel. The active drainage channel is carved into bedrock and is split into two levels, with 2-3 m in height difference between them. They are located in a slightly wider channel.

The canyon wall predominantly consists of the thickly bedded, white sandstone interbedded with thin intercalations of calcareous mudstone of the Sorbas Member. Two joint sets are clearly visible in the cliff face. The upper most part of the cliff face is composed of semi-unconsolidated rock material and river terrace deposits. There is also a river terrace C capping the cliff face (Harvey *et al.*, 1995; Harvey, 2001).

The canyon wall is affected by rock fall activity (Dikau *et al.*, 1996) initiating from a partially wedged failure surface (Figure 5.19; Table 5.6). The landslide is thought to have occurred during a high magnitude flood event in 1973 (Mather & Griffiths, *pers. comm.*). However, it is unclear whether it was the flood event itself undercutting the slope or the associated rainfall that triggered the actual rock fall. The measured runout length for the landslide is possibly slightly shorter than might be expected for this type of landslide. This could be because the debris from the landslide has been removed by either flood or human activity in the drainage channel.

The landslide is not located near to any of the houses, roads or other infrastructure associated with the main town of Sorbas. There are also no agricultural areas close to the landslide. The landslide area is, however, of scientific importance (i.e., the presence of fossilised bird's footprints) and the local authorities, in conjunction with numerous universities, are trying to "open" up the site, possibly even to tourists. It is

suggested here that if this site was to be opened to the public, then this would require at least some form of stability assessment to be made of the cliff face.

Table 5.6 – Bird's Footprint landslide data

Landslide No.:	1
Grid Reference:	05769 41065
Height:	10m
Length:	4m *
Width:	5m
Angle of Reach:	24.0°
Volume:	300 m³

* = part of the debris has been removed by a combination of human and flood activity
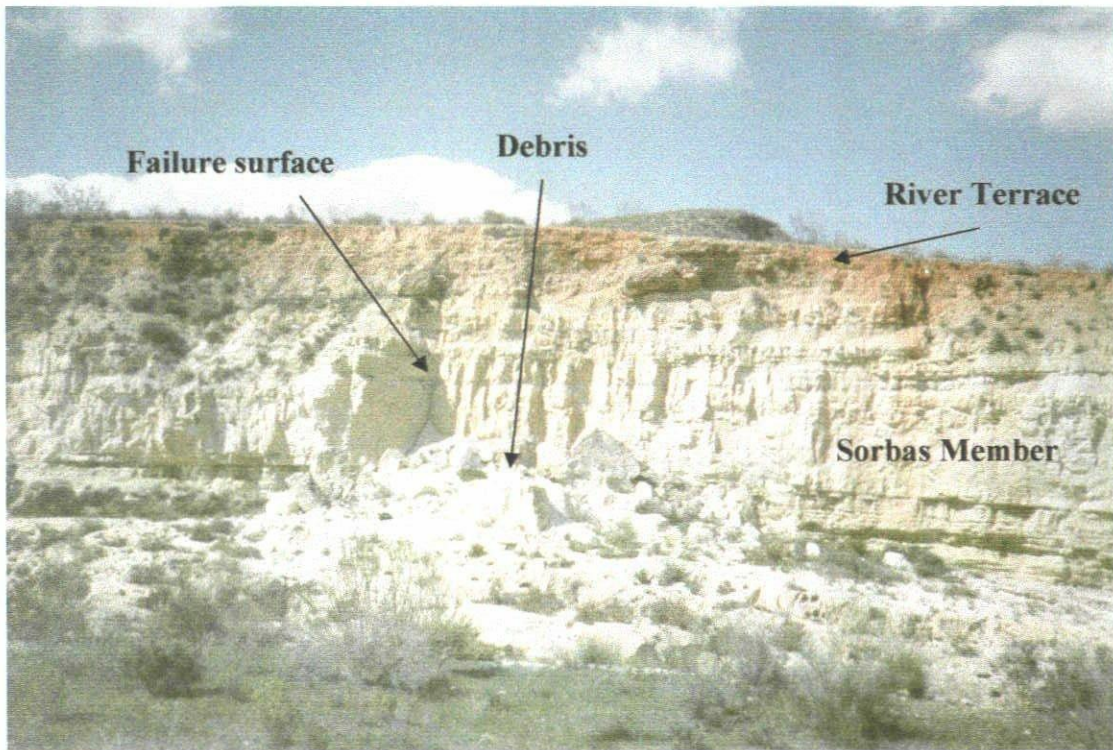
Figure 5.19 – Photograph of the "Bird's Footprint" rock fall (Grid Reference: 0576941065 / Facing north). The rock face is approximately 10-15m high at this point.

5.2.6 The Abandoned Meander Section

There are a number of relict and active landslides in the abandoned meander that is to the south and west of the Sorbas "knoll" (Figures 5.2 and 5.20). Hart & Griffiths (1999) and Hart *et al.* (2000) have described the majority of these landslides.

The abandoned channel has been incised to a depth of approximately 30-40 m below the surrounding countryside and the Góchar erosion surface. The canyon is a uniform width at approximately 100-150 m wide. The floor of the canyon is now used for agriculture and has been identified as a D2 or D3 river terrace (Harvey *et al.*, 1995; Harvey, 2001). The formation of this abandoned meander was described in the introduction to Section 5.2. The landslides all occur within the canyon walls.

The canyon walls under the town of Sorbas consist of the thickly bedded, fine to medium-grained, white sandstone interbedded with thin intercalations of fine-grained calcareous mudstone, of the Sorbas Member. The rock mass is affected by at least two clearly visible joint sets, which are approximately 60 degrees to each other. The canyon walls on the outside of the meander consist of both Sorbas Member bedrock and unconsolidated rock material.

Geomorphological mapping of the hillside above the areas of unconsolidated material identified two "hanging" valleys/gullies. On the aerial photographs these are picked out by the presence of drainage lines that have now been used for agricultural terraces. These hanging valleys/gullies relate to an older land surface that existed before the Río Aguas/Rambla Feos River Capture. These hanging valleys/gullies are

approximately 20 m above the canyon floor, suggesting that they were active before D3, but after B (the river terrace on which Sorbas is built and which caps slopes above the outside of the meander). They were then possibly filled in with loosely consolidated rock debris before being truncated by the incision of the canyon to its present level.

The in-fill is predominantly loosely consolidated white sandstone (Figure 5.21). The material ranges from coarse sand to angular/sub-angular boulders. The contact with the underlying white sandstone bedrock of the Sorbas Member can be seen in a number of places (Figure 5.21). The angular nature of the material would suggest that it has not travelled very far, and the lithology is very similar to the local bedrock. Mapping of the hillside above the deposit (above the meander on what would have been the palaeo-surface) has shown that the debris seems to be confined to the "palaeo-gullies". It is suggested that the debris represents a small landslide that initiated a relatively short distance to the south of the current abandoned meander. The mechanism may have been rock fall with some form of ravelling (possibly sporadic rock fall or stone fall) filling the gully with material. The debris, confined to the gullies, may have then travelled a short distance down slope. Subsequently, the gullies were truncated by the incision of the now abandoned meander.

When constructing the N-340 through the abandoned meander section, a number of road cuttings were created. These cut through the relict features, causing them to be reactivated. The failures from these relict features have been small rock falls and sporadic stone falls (Dikau *et al.*, 1996; Nicholson *et al.*, 2000). These slopes may be affected by water seeping along the relict drainage lines within the hanging

valleys/gullies through the unconsolidated material, as well as water on the cut-slope surface. Mitigation of these failures has included trimming the road cuttings back, as well as a drainage/catch ditch at the base of the slope. The road is also relatively wide at this point.

Many people (both locals and visitors) have commented on the apparent stability of the knoll on which the old part of Sorbas is built. The evidence used for this is the presence of the houses that are built right along the very edge of the canyon wall. However, field mapping has identified a rock talus slope that runs all the way around the foot of the Sorbas knoll. In addition to this, over the last six years, at least four landslides have occurred around the town, affecting this canyon wall. The most recent landslide (Landslide No. 20) occurred during the spring of 2003 within the abandoned meander opposite the locations described above. It was a rock fall that has undercut the foundations of a house (Figure 5.22). This rock fall may have been initiated by a combination of building work being undertaken in the house and the ongoing construction work for a footpath around the Sorbas knoll. This work has involved digging a path into some parts of the rock talus slope.
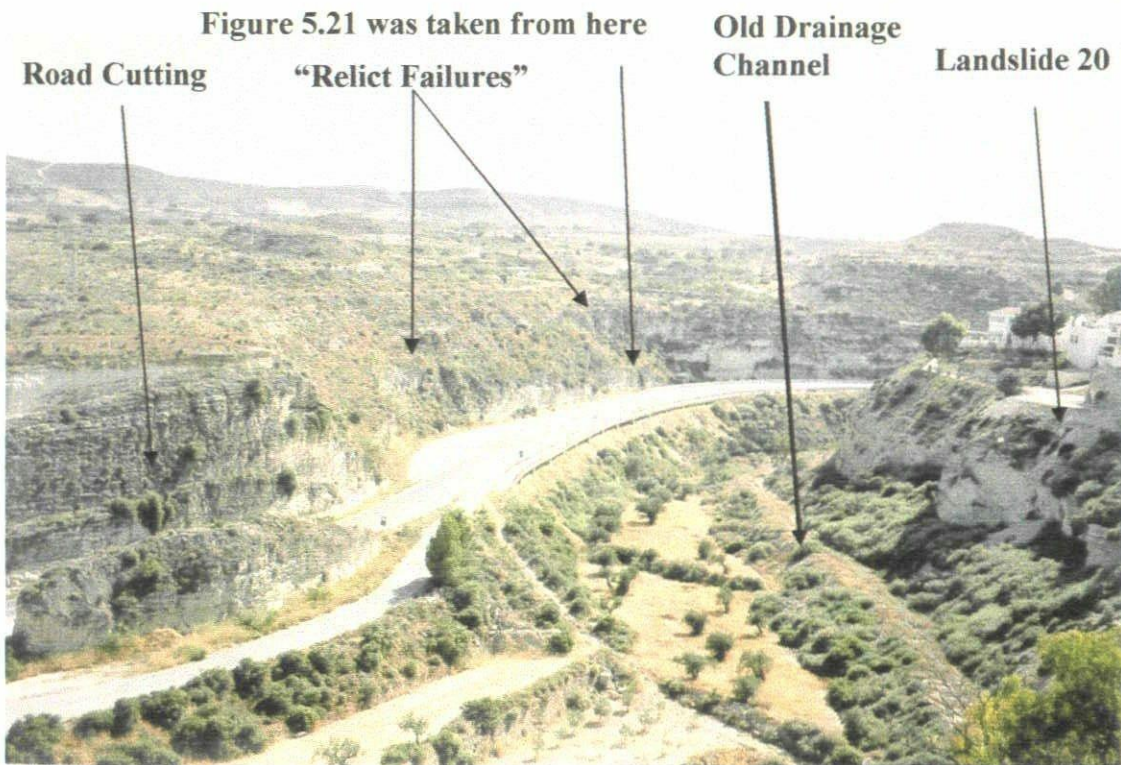
Figure 5.20 – Photograph of the abandoned meander and the N-340 (Grid Reference: 0578041063 / Facing southwest).
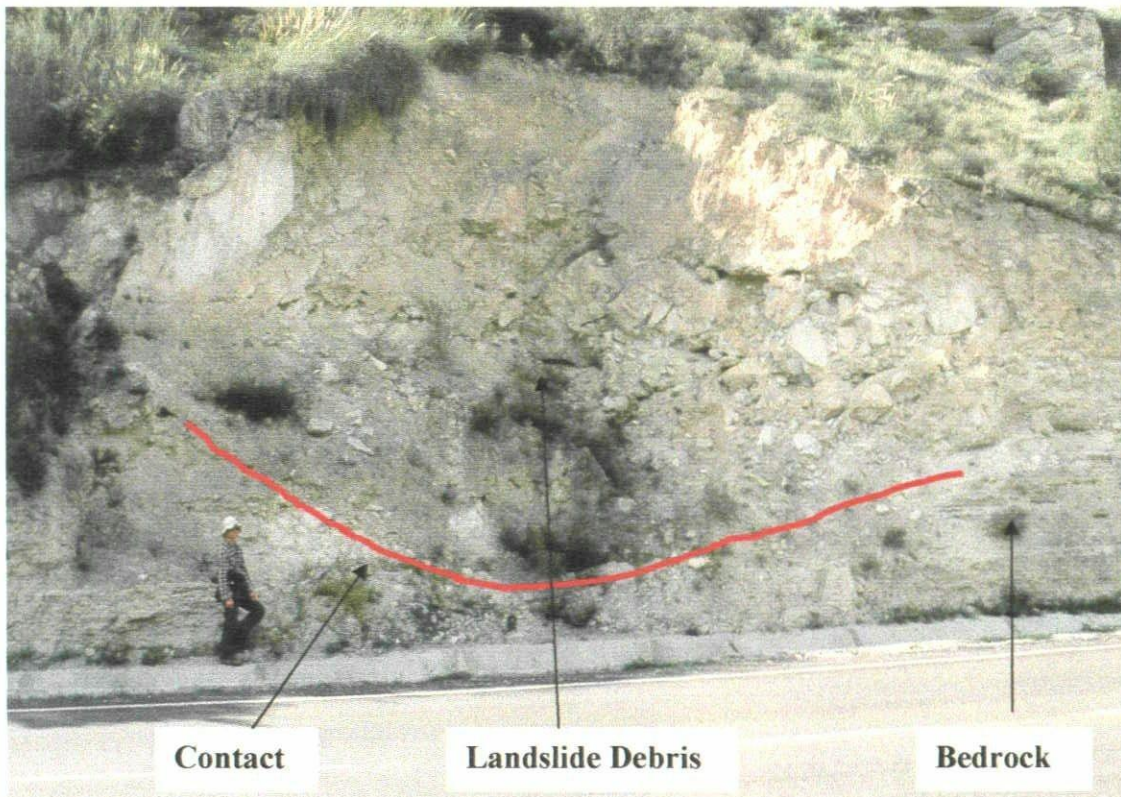
Figure 5.21 – Photograph of N-340 road cutting exposing unconsolidated landslide debris (Grid Reference: 057741062). Material is moving out of slope towards road. Author, for scale, is approximately 1.8m tall. The line shows the contact between the bedrock and displaced material.
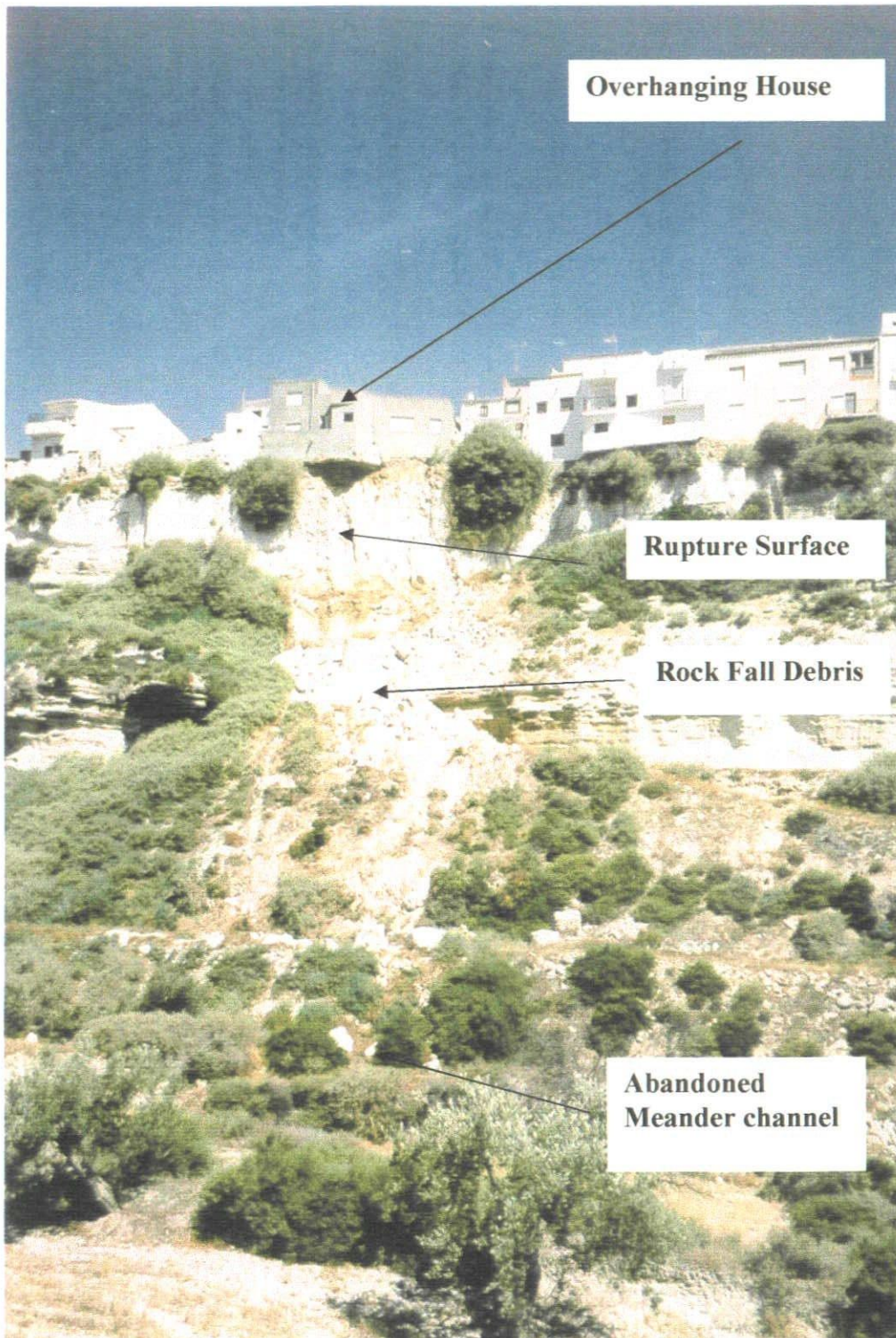
Figure 5.22 – Photograph of Landslide Number 20 that occurred during the Spring of 2003 (Grid Reference: 0577941062 / Facing northwest). The cliff face on which Sorbas is built is approximately 30-40m high at this point.

5.2.7 Cave-collapse Landslides

Several of the landslides mapped around Sorbas highlighted the important relationship between the geology and human activity (Hart & Griffiths, 1999; Hart *et al.*, 2000). The following examples will demonstrate how the geology (influenced by the human activity) has directly affected slope stability around the town of Sorbas. These examples will also underline the importance of repeat visits to a site and of talking to the local population about observed landslide activity and ongoing construction activity.

There are a number of caves found at various locations around the "knoll" on which the old part of Sorbas is built. These caves have been dug by the local inhabitants of Sorbas and seem to be used for storage. These locations are:

- The cliff face behind the new Sorbas museum (Landslide 16);

- The cliff above the eastern road into Alfarería (Landslide 21); and

- Beside the small street going from Alfarería up into the main part of Sorbas (Landslide 22).

The caves are all dug into the same part of the Sorbas Member. The Sorbas "knoll" predominantly comprises thickly bedded, moderately strong, white sandstone. The Sorbas Member is capped by a Quaternary river terrace deposit that can be found at a number of places around the Sorbas "knoll". Within the Sorbas Member, there is at least one unit of moderately weak, thinly laminated, calcareous mudstone that has a maximum thickness of approximately 2-3 m. It is within this mudstone unit that the

caves have been dug, with the floors and ceilings being left in the stronger sandstone units.

A number of these caves have collapsed, often giving rise to further failures in that part of the cliff face or increased signs of instability. These failures can be quite sizeable considering their location. For example, in 1998 a cave collapsed causing a landslide to occur behind what was a car mechanic's workshop (Table 5.7; Figures 5.2 and 5.23). The landslide had not destroyed the building but the cliff was still unstable (tension cracks were clearly visible), therefore still posing a risk to the building. The building was demolished and the landslide debris cleared away. The cliff face was then trimmed back and covered in shotcrete. As a further measure, a large retaining wall was built to cover the lower parts of the cliff face. Recently, a new museum for Sorbas has been built on the site to encourage tourists to visit Sorbas. It is unlikely that this part of the slope will fail again in the near future. However, other parts of this hillside are still vulnerable. These remedial measures will also have to be maintained. For example, the drainage pipes will have to be cleaned regularly or this could lead to a build up of water in the slope and subsequent failure.

Table 5.7 – New Museum landslide data

Landslide No.:	16
Grid Reference:	05778 41064
Height:	5m
Length:	3m
Width:	5m
Angle of Reach:	59.0°
Volume:	45 m^3
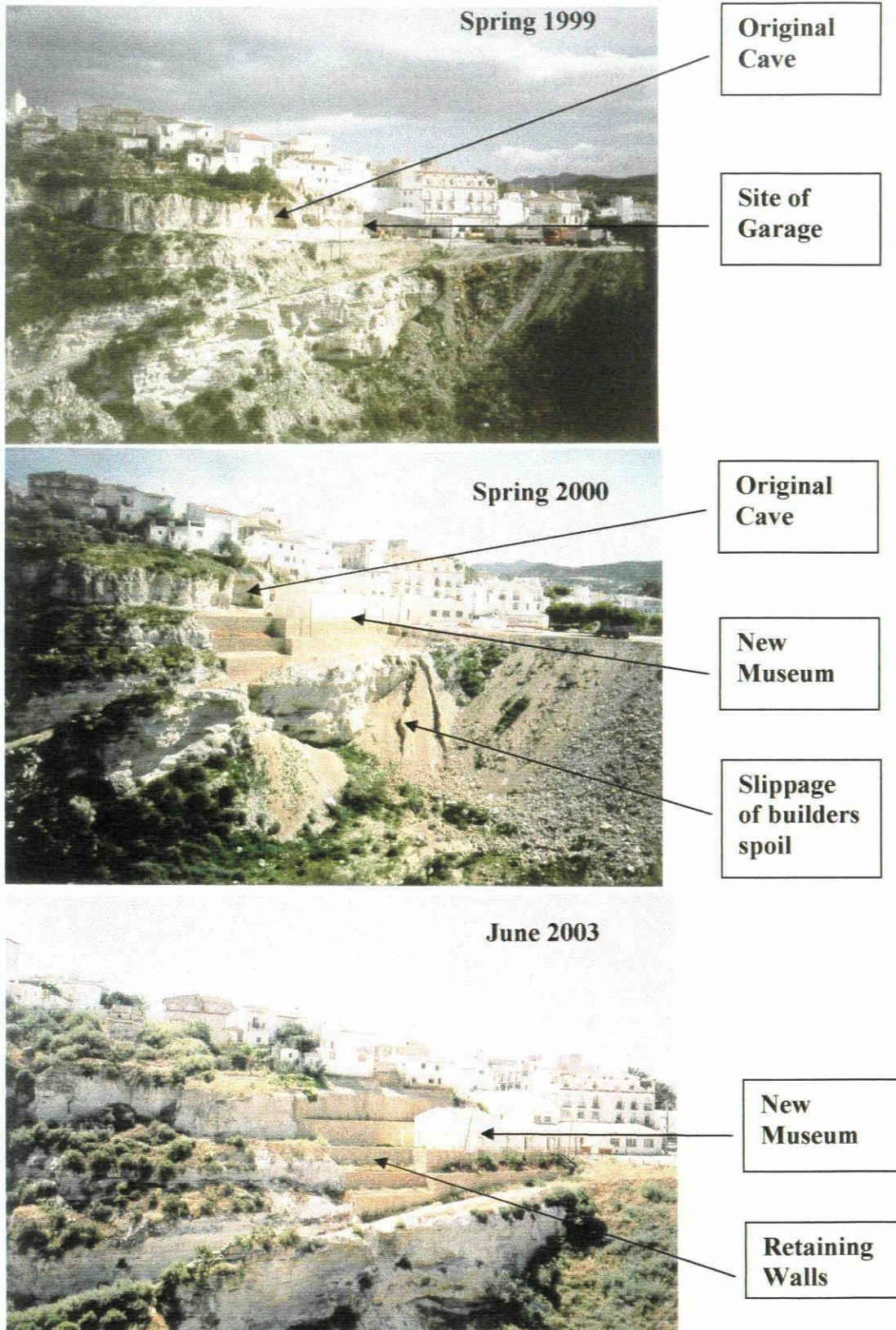
Figure 5.23 – Photographs of the new museum area taken during the mitigation works and construction of the museum (1999 and 2000) and after completion (2003). All photographs taken from Grid Reference 0577741065, facing southeast.

Another example is the cave collapse and rock fall that occurred on the small lane that links Alfarería Square to the main part of the old town. This rock fall was cleared up during 2000, with the backscar and debris being completely removed from the site (Figure 5.24). This photograph also shows where another cave exists but has been covered up by the construction of the building alongside the road. The newly cut rock face undercuts the properties located above this site. By 2003 this site had been abandoned and closed to the public. Structural supports have been built into the cliff, in an attempt to support the weight of the cliff face and the properties above. The author believes that further remedial work should be undertaken on this slope to stabilise it and prevent further failure. If nothing is done, the houses above and below the site are at risk. The houses above the slope are at risk from their foundations being undermined. The houses below the slope are at risk from the houses and other debris above them falling on to them. In addition to this, road users are also at risk from this slope failure.

From the point of view of carrying out a landslide investigation, these two examples (as well as a number of the other landslides around Sorbas) highlight an interesting problem. How many landslides have occurred around Sorbas and been cleaned up or the evidence "removed"? For example, the only indication of the original cave and subsequent landslide at the site of the new museum is the slight depression that has been left in the cliff face behind the small garden area behind the museum (Figure 5.23). The next question is then "how representative is the current data set of the level of landslide activity in the Sorbas area?" If, due to pressure on land use, landslides are cleared up relatively quickly after an event, then the landslide database for the Sorbas

area may be an under estimate. This problem, if not properly addressed, would also hinder any calculations of the frequency of landslide activity in the area.

These observations would imply that a number of different strategies would need to be adopted when working in such areas, including:

- Repeat visits to a site;

- An awareness of such practises;

- Consultation with local engineers and/or members of the local population; and

- The ability to identify where these events have occurred in the past (the "eye for landscape" of Hutchinson, 2001).

Field mapping has shown how the presence of these caves within the rock face (and therefore under parts of the town) can increase the inherent instability of the area. This could increase the risk to those who use, or work, in the caves, although the extent to which this occurs is difficult to assess. There is also the problem of settlement caused by the collapse of these caves. This would be difficult to assess and has not been investigated within this research project.
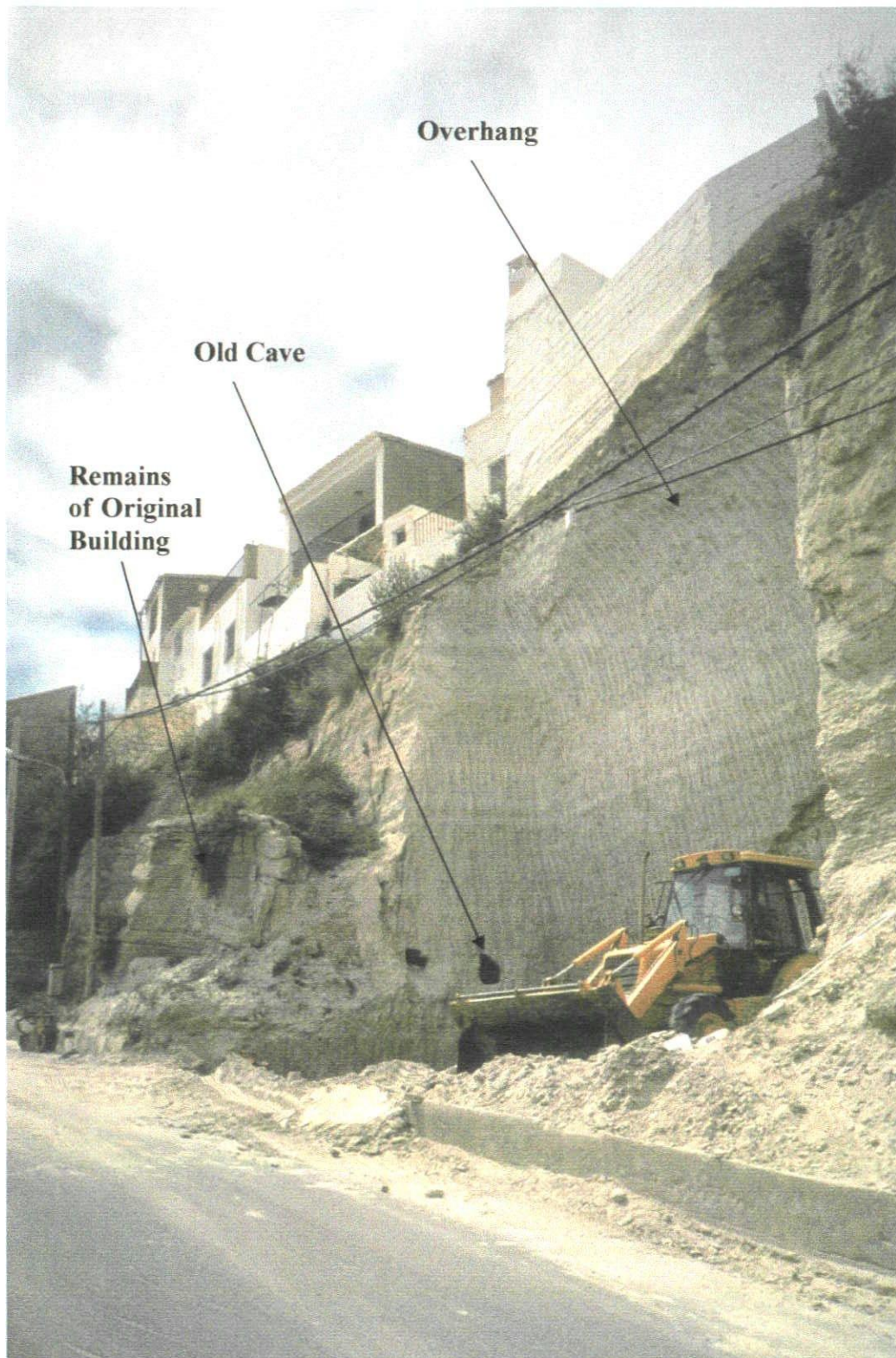
Figure 5.24 – Photograph of a site in the lane at the back of Sorbas that was affected by a landslide in 1998 which was cleared up in 1999 (Grid Reference: 0578241063). The site is now being redeveloped.

5.2.8   Synopsis of the Sorbas Case Study Area

The API and field mapping have identified a number of factors that control the landslide activity affecting this case study area. These are:

- The presence of the tension cracks and geologically controlled discontinuities within the Sorbas Member;

- The dispersive nature and therefore extreme weathering potential of the calcareous mudstones within Cariatiz Formation;

- The relative rapid incision of the drainage and, therefore, relatively rapid formation of the valley side slopes and canyon walls; and

- Human activity involving the construction of roads or buildings which involve either the loading or undercutting of slopes.

This case study area is within the part of the Rio Aguas study area that has been affected by the "wave of incision" relating to the Rio Aguas/Rambla Feos River Capture described in Section 2.4. By using the geomorphological mapping results it is possible to construct a tentative landscape history for the landslides.

1. Dissection of the Góchar erosion surface by the formation of the ancestral Lower Aguas.

2. The above dissection would have been driven by the differential uplift between the Sorbas and Vera Basins (Mather, 1991; Stokes, 1997; Mather *et al.*, 2001; Stokes *et al.*, 2002; Mather *et al.*, 2003).

3. The Río Aguas/Rambla Feos River Capture.

4. An increase in the gradient and stream power of the Río Aguas, leading to increased rates of drainage incision and slope erosion.

5. Incision of the Río Aguas and erosion of the Góchar erosion surface to almost present locations.

6. The modification of the slopes by human activity in the area.

5.3 The Gypsum Escarpment / River Capture Section

There are a number of places along the edge of the gypsum escarpment that are affected by landslide activity. Many of these landslides have been identified and described in Hart (1999) and Hart & Griffiths (2000). Eyers *et al.* (1998) and Davis *et al.* (2000) also identified some of the larger features as part of satellite image (Landsat or SPOT) or Airborne Thematic Mapper (ATM) image interpretation studies. This area was also identified as one of the parts of the study area with a high landslide density (Section 4.2.1; Figure 4.6), and therefore provides an excellent example of the problems being addressed by this research project (Hart, 1999; Hart & Griffiths, 1999; Griffiths *et al.*, 2002). The case study area covers approximately 10km^2 and is located approximately 10km east of Sorbas, some 55km north-east of Almería, the Provincial capital (Figures 1.2 and 2.1).

This case study area contains the site where the Río Aguas/Feos River Capture occurred (Figure 5.25). The API and subsequent field validation showed that over 25 landslides affect this case study area. It is, therefore, an ideal place to study how this geomorphological event has influenced the Río Aguas, the surrounding landscape and the observed landslide activity, both upstream and downstream of the river capture site. Field mapping showed that the majority of the landslides were associated with the Quaternary development of the drainage network, confirming the apparent close relationship between drainage/landscape evolution and the observed landslide activity (Hart & Griffiths, 1999; Griffiths *et al.*, 2002). The mapping also highlighted the presence of several relict landslide features, and confirmed the importance of

understanding the geomorphological history of an area before undertaking engineering works.

The case study area follows the course of the Río Aguas and the gypsum escarpment from just west of the village of El Río de Aguas del Los Molinos[#], downstream to the abandoned village of Marchalico Viñicas (Figure 5.25). The key locations within the study area are:

- El Río de Aguas del Los Molinos[#] (0582341054) – just upstream from the river capture site;

- The Río Aguas/Rambla Feos Capture Col (0584041045);

- Los Perales (0584541058) – just downstream from the river capture site; and

- Marchalico Viñicas (0585241073) – approximately 4 to 5 km downstream from the river capture site.

The geology of the case study area is a mixture of Neogene sedimentary basin fill, capped, in places, by Quaternary river terrace deposits (Figure 5.25). The succession generally dips to the north or north-west (i.e., towards the basin centre). The amount of dip varies, but is generally between 15° and 20°. Apart from the gypsum of the Yesares Member, each of these lithological units rests unconformably on the unit underneath it.

[#] The village of El Río de Aguas del Los Molinos is also known as Los Molinos
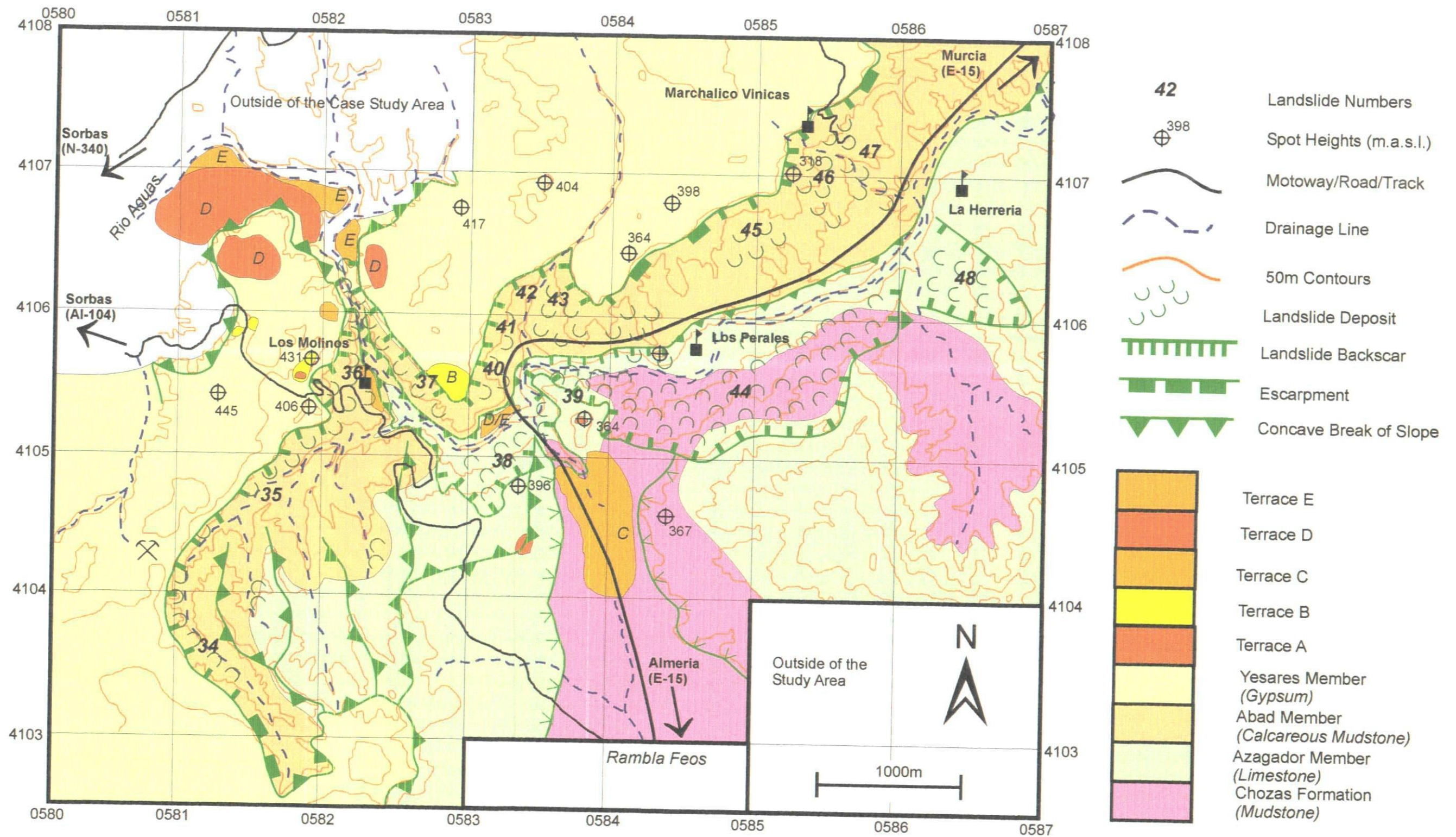
Figure 5.25 - Map of the Los Molinos - Gypsum Escarpment Case Study Area. River terrace levels are after Harvey *et al.* (1995).

Structurally, this part of the study area has experienced some of the highest uplift rates of the region, with approximately 160 m Ma^{-1} of uplift over the Plio-Pleistocene interval (Mather, 1991). This is associated with continued regional deformation during the Quaternary, which has been dominantly north-south compression, and east-west extension (Mather & Westhead, 1993). Field evidence for this comes from the Quaternary river terrace sediments in the area, some of which have been tilted up to 70° (Mather *et al.*, 1991; Mather & Stokes, 1996).

The river terrace deposits in this area record the incision of the drainage system, particularly after the Río Aguas/Rambla Feos river capture (Harvey & Wells, 1987; Mather, 1991; Harvey *et al.*, 1995). The distribution and nature of the river terrace deposits provide an insight into the formation of the present day Río Aguas valley and, therefore, are helpful in "dating" some of the observed landslide activity that is seen in the case study area.

The following sections are selected examples of the landslide activity that affects this case study area. The examples include four of the largest landslide complexes in the Río Aguas study area (Table 5.1). They are presented here in their downstream order from the village of Los Molinos to the abandoned village of Marchalico Viñicas (Figure 5.25).

5.3.1   Los Molinos

The village of Los Molinos is situated between 20 and 40 m above the present level of the Río Aguas. This section of the river is within a deeply incised valley/canyon beneath the level of the gypsum plateau (Yesares Member). Calcareous mudstone (Abad Member) forms both valley-side slopes within the canyon and erodes to form a typical badland-type landscape. The limestone of the Azagador Member outcrops along parts of the valley floor and makes up part of the southern valley-side slopes. It also forms an escarpment feature on the northern side of the Río Aguas near to the abandoned farmhouses at Carrasco (Grid reference: 0583241054). The Azagador Member is underlain by the calcareous mudstones of the Chozas Formation. This means that the slopes on the southwestern side of the Río Aguas valley are dip-slopes and those on the northeastern side of the valley are scarp-slopes.

5.3.1.1   Gypsum Escarpment Landslides

The whole length of the Gypsum Escarpment on the northern side of the Río Aguas is affected by landslide activity. There are combinations of failure mechanisms at work – rock falls, rock topples, high-angle rotational and non-rotational landslides, and sagging-type failures. These nearly all involve both the gypsum and underlying calcareous mudstones. The landslide activity is all related to the incision of the Río Aguas over steepening the valley side slopes.

This same situation can also be seen in the area along the length of gypsum escarpment that runs southwest from Los Molinos to the gypsum quarry and then

southeast to the Cerrón de Huelí (Grid reference: 0581341023) at the southern margin of the study area.

5.3.1.2   *The Los Molinos Relict Landslide*

The aerial photographic interpretation and field-based geomorphological mapping has enabled a number of relict features to be identified in the study area. However, subsequent erosion and/or human activity has meant that some of these features are more difficult to identify than others. One example is the landslide referred to here as "The Los Molinos Relict Landslide".

The landslide is located in the same area as the village of Los Molinos (Landslide No. 36; Figure 5.25). This village was abandoned (possibly during the Spanish Civil War) but has now been re-inhabited by an "alternative lifestyle" community (possibly since the 1970s). They have sought to rebuild some of the houses and irrigation ditches and use the agricultural terraces that are located beneath the village, but above the active channel for the Río Aguas.

The upper part of the Los Molinos village is built on moderately weak calcareous mudstones that are intercalated with shale and occasional beds of moderately strong, thin beds of sandstone (Abad Member). The lower part of the village and the agricultural terraces are built on a moderately strong, light coloured limestone (Azagador Member). The crown area of the landslide is in the gypsum of the Yesares Member.

Los Molinos is located on a lower valley slope 30-40m above the level of the Río Aguas active channel. The section of river below the village has standing water, with the water coming from natural springs in the gypsum a short distance upstream from Los Molinos.

The morphology of the landslide has been altered and heavily masked by the presence of the road AL-104, the agricultural terraces above the village and the village itself. The landslide was identified by an anomalous occurrence of randomly orientated, broken up blocks of gypsum that are held within a silty clay matrix outcropping underneath a part of Los Molinos (Figure 5.26). This material now infills what was probably a slight topographic low at the time of the landslide occurring.

A combination of geomorphological field mapping and aerial photographic interpretation were used to identify the possible location and size of the backscar and the debris accumulation. The backscar has been identified as the arcuate feature in the gypsum escarpment directly above the Los Molinos. Interestingly, the hollow formed by the landslide has been used for the switchbacks in the AL-104 as it passes out of the very steep sided Los Molinos valley (Figures 5.27 and 5.28).

The southern part of the backscar may have been removed by erosion of the gypsum escarpment and underlying calcareous mudstone. The debris accumulation has been either removed or extensively altered by the construction of the agricultural terraces and the road. However, particularly with the use of aerial photographs, a track of debris can be traced from the backscar down to the toe of the landslide. This has

meant that the geometry of the landslide can be measured in some places and inferred in others (Table 5.8).

Table 5.8 – Los Molinos relict landslide data

Landslide No.:	36
Grid Reference:	05820 41054
Height:	60m
Length:	350m
Width:	60m
Angle of Reach:	15.9°
Volume:	$1.10 \times 10^6 \, m^3$

The removal and/or masking of this landslide has made identifying the controlling factors difficult. However, it is assumed that those factors that have been observed or inferred as controlling other landslides in this immediate area would have also influenced this landslide. These factors are:

- The NE-SW and NW-SE tectonic related discontinuity pattern of the area;

- The presence of the pipe structures, tension cracks and geologically controlled discontinuities along the edge of the gypsum plateau;

- The presence of the minor drainage features and gullies in the area;

- The dispersive nature and therefore extreme weathering potential of the calcareous mudstones within the Abad Member; and

- The undercutting of the gypsum escarpment through erosion of the calcareous mudstones.

The crown area of this landslide is level with the Gypsum Plateau and the B or C river terrace levels (Harvey & Wells, 1987; Mather, 1991; Mather *et al.*, 1995; Harvey *et al.*, 1995; Harvey, 2001). The toe of the landslide is approximately the same height as river terrace level D3. This landslide has, therefore, occurred since the formation of this slope, which is after the Río Aguas/Rambla Feos River Capture and subsequent incision of the drainage system. It is possible that this landslide occurred at approximately the same time as the formation of the D3 terrace, and has been stable since then because it does not appear to have affected the E river terrace below the village.

The fact that both a village and a main road through the area have been built on this landslide makes this an interesting case study. Their presence has led to the re-activation of the landslide, albeit on a relatively small-scale. Some of the houses in the village that are built on the landslide show signs of structural damage that is slightly different in nature to the damage seen on other houses in the village (most of which are in some state of dis-repair). The local residents have also commented that the houses "appear to move" during rainstorms.

The AL-104 road also shows signs of subsidence and cracking. This may not be helped by the almost constant heavy lorry traffic travelling between the Hueli gypsum quarry and the gypsum processing plant on the coast at Carboneras.
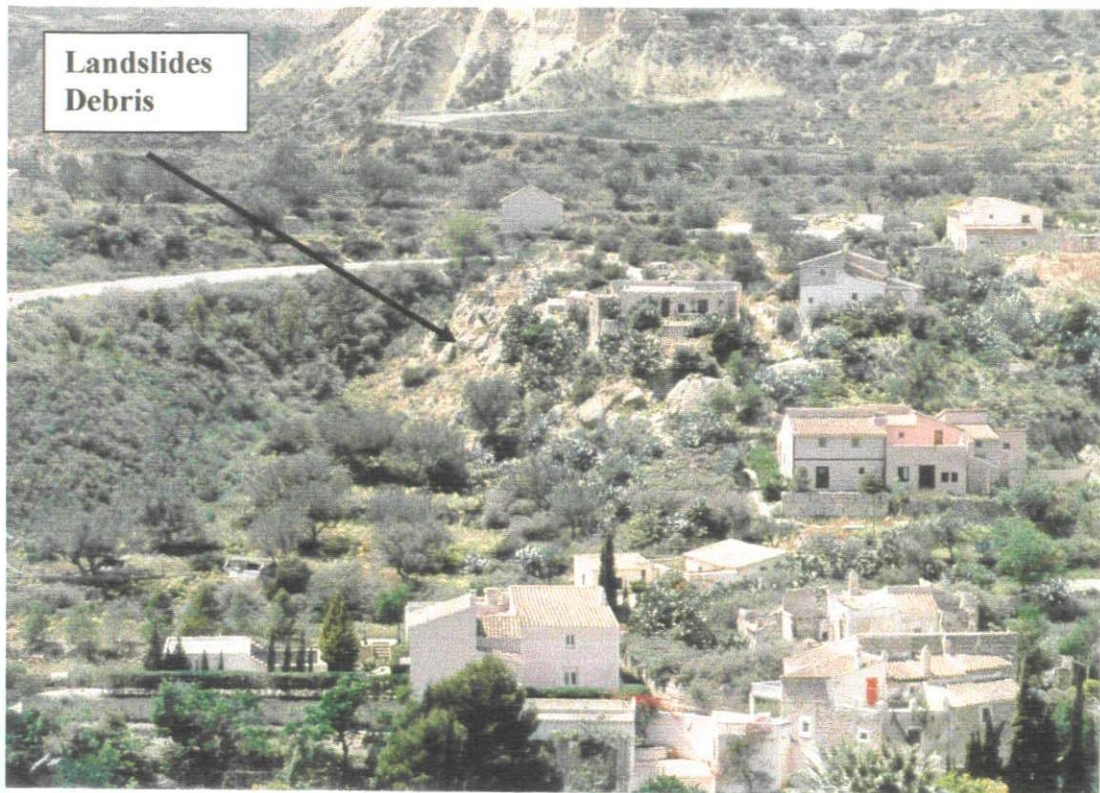
Figure 5.26 – Photograph of the debris of the relict feature under the houses of Los Molinos (Grid Reference: 0582641056 / Facing southwest).
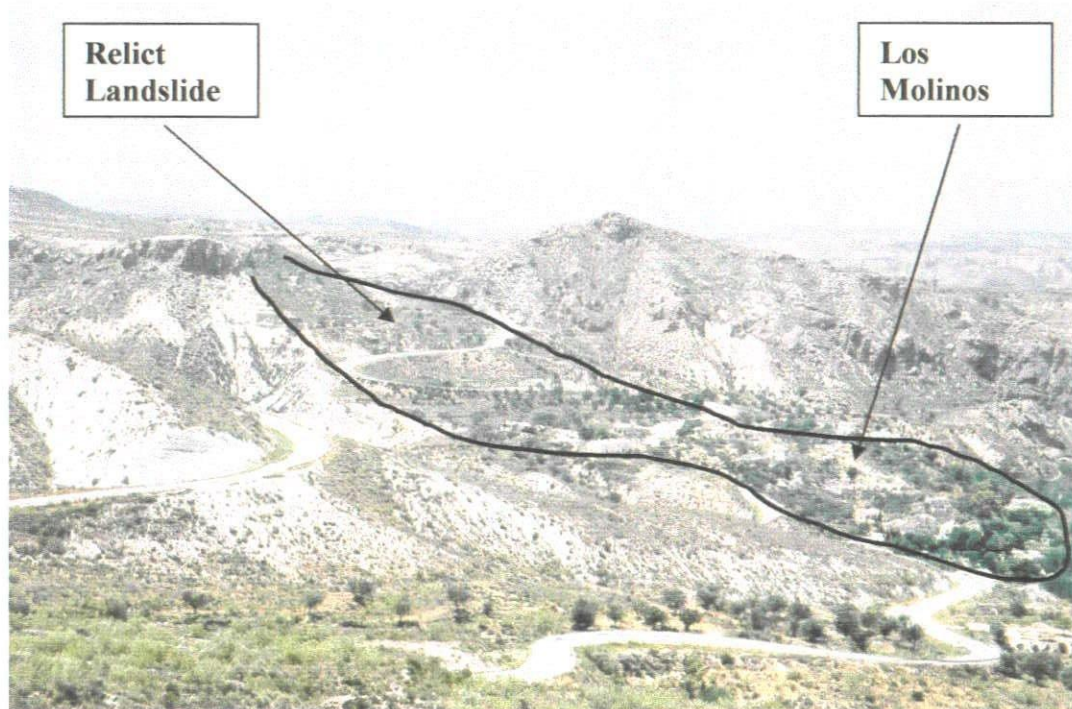
Figure 5.27 – Photograph of Los Molinos Relict Landslide and the main road (Grid Reference: 0583141047 / Facing northwest).
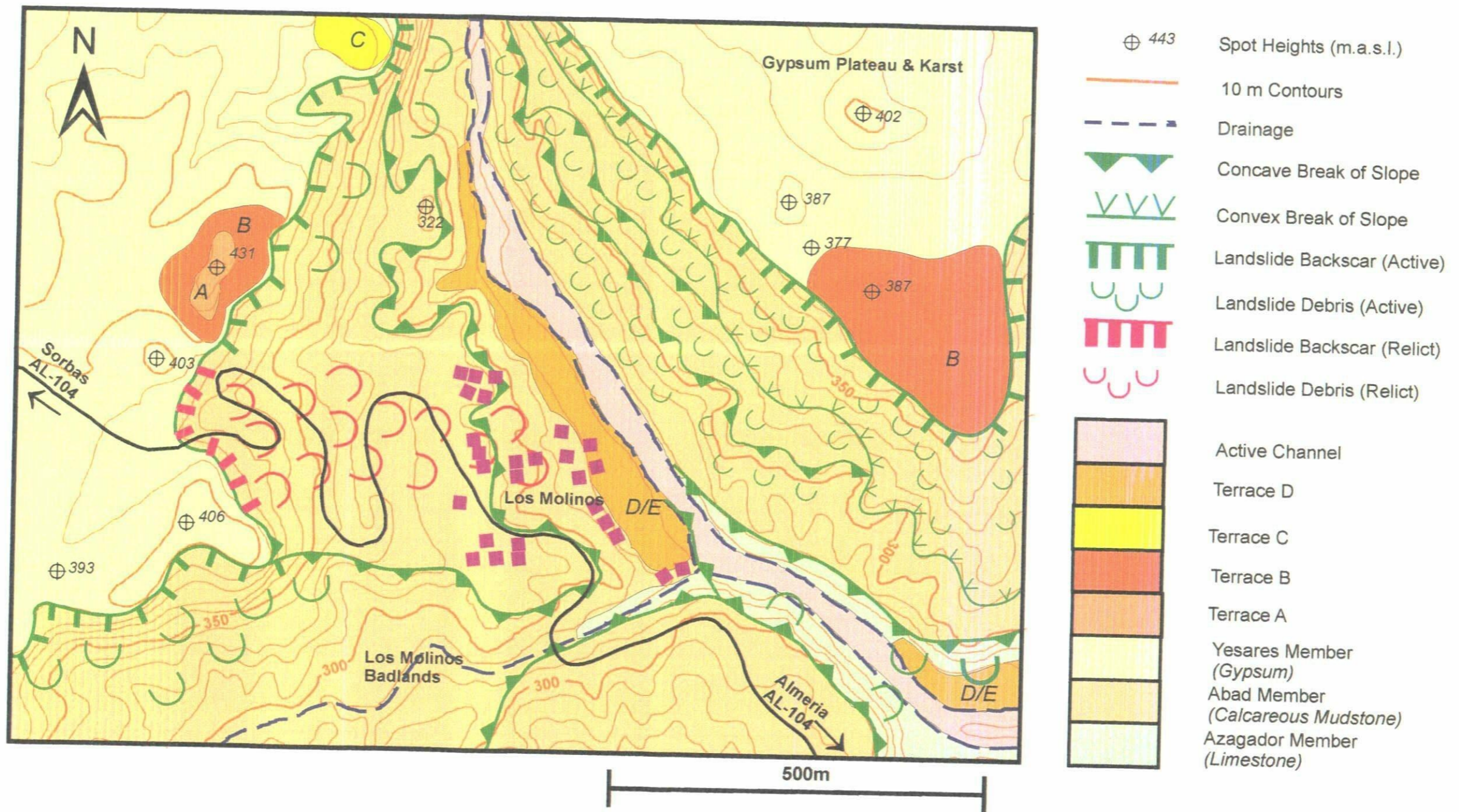
Figure 5.28 - Map of the Los Molinos Relict Landslide

5.3.1.3   The "Cerro Molatas / Carrasco Landslide" Complex

This landslide was identified and briefly described by Eyers *et al.* (1998) and Davis *et al.* (2000) as part of a satellite image interpretation study in the region. It has been described in more detail by Hart (1999) and Hart *et al.* (2000). The "Cerro Molatas / Carrasco Landslide" is located immediately to the west of the "Wind Gap" or "Capture Col" (Figures 5.25, 5.29 and 5.30; Landslide No. 38; Grid Reference: 05834105), at the southwestern end of the Los Molinos valley.

The landslide occurs within the light-coloured limestone of the Azagador Member and the underlying calcareous mudstones and shales of the Chozas Formation. The limestone rests unconformably on the Chozas Formation and dips towards the northwest at approximately 30-40 degrees. The limestone is affected by both jointing and dissolution features.

The landslide occurs on a dip-slope within the outside of a meander of the Río Aguas active channel (Figure 5.30). The toe of the landslide appears to be at the same level as the contemporary active channel of the Río Aguas. As stated above, the site is adjacent to the site of the Río Aguas/Rambla Feos River Capture and has experienced approximately 90-100 m of incision.
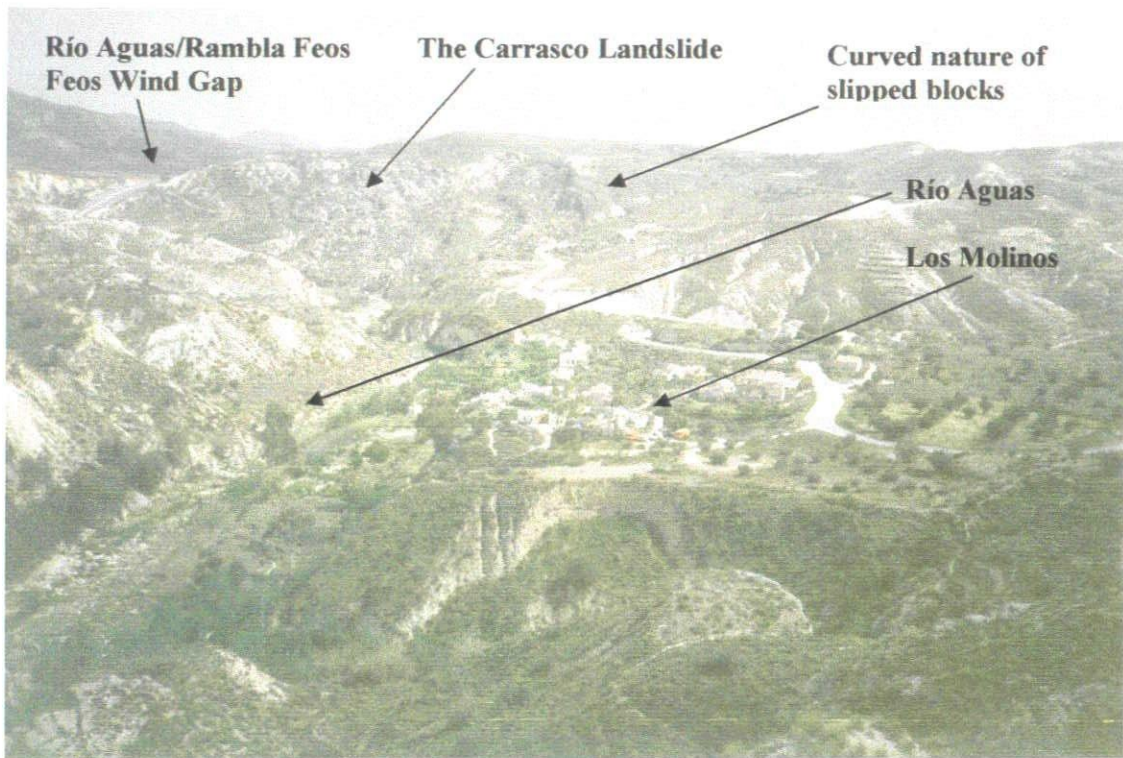
A.
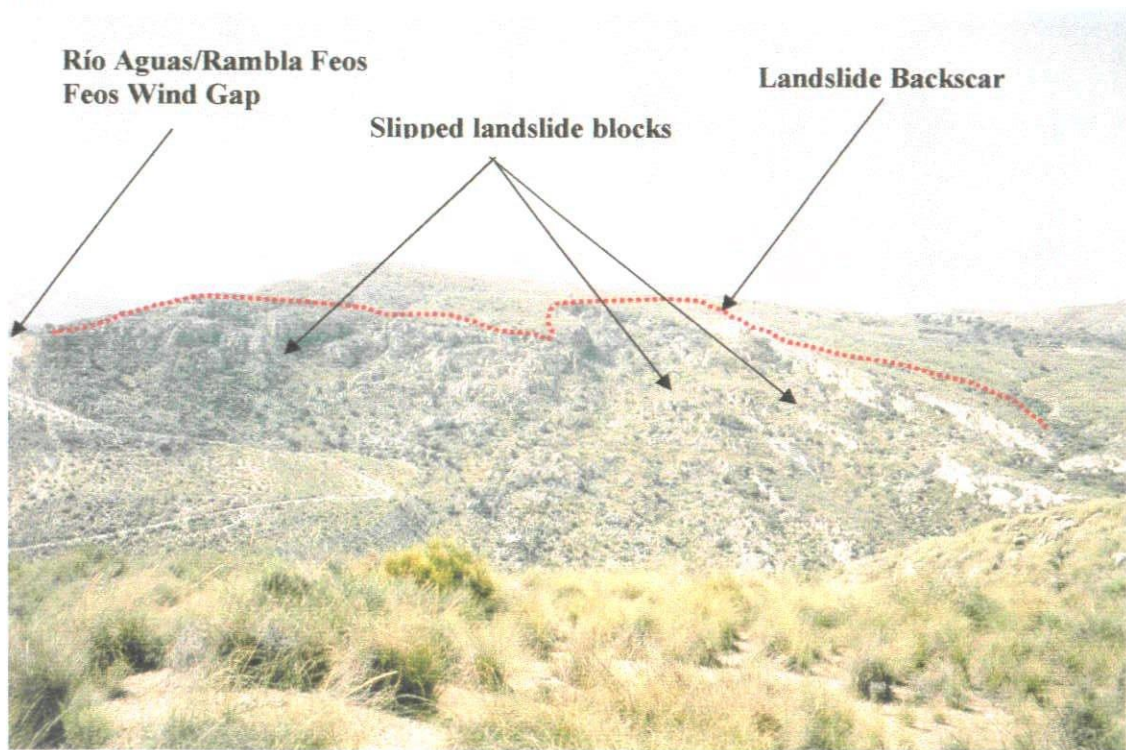
B.

Figure 5.29 – Photographs of the Cerro Molatas/Carrasco Landslide.

A. View from above Los Molinos Village (Grid Reference: 0581941055 / Facing east).

B. View from opposite side of the Río Aguas (Grid Reference: 0582941054 / Facing south).

The "Cerro Molatas / Carrasco Landslide" is a complex landslide exhibiting different types of failure mechanism. It is characterised by dip-slope translational movements with some smaller, high-angle non-rotational movements. There are also minor rock falls and topples along parts of the backscar. Although the slip-surface has not been found, the geomorphology of the landslide suggests that the slip-surface is along the contact between the limestone and underlying calcareous mudstone. Some of the details included in the landslide inventory are shown below (Table 5.9).

Table 5.9 – Cerro Molatas / Carrasco landslide data

Landslide No.:	38
Grid Reference:	0583 4105
Height:	150m
Length:	250m
Width:	250m
Angle of Reach:	31.0°
Volume:	$4.91 \times 10^6 \, m^3$

Geomorphological mapping within the landslide complex has shown that the limestone blocks have moved in a general downslope direction but with a degree of lateral migration across the slope (Figures 5.29 and 5.30). This would imply that the retrogression direction has changed from dip-slope to slightly oblique to it. This could be related to a combination of the shape or direction of the slip-surface, as well as the morphology of the hill slope.

Aerial photographic interpretation, supported by field mapping, has shown that the shape of the mass movement is closely controlled by the major discontinuity pattern for the area. For example, part of the landslide backscar has a very distinctive

rectangular shape trending NW-SE and NE-SW. There are also a series of lateral tension cracks running approximately parallel to each of the sides to the backscar. The majority of these occur along the western flank of the landslide backscar and would suggest that this is currently the most active part of the landslide complex. This could have implications for the AL-104 main road, which passes within 10 m of this part of the mass movement.

The landslide has occurred on a slope that was formed as a result of the incision of the drainage system after the Río Aguas/Rambla Feos River Capture. Due to the height of the crown area in relation to the height of the River Capture Wind Gap, and the dip-slope nature of the landslide, it is possible that there had been a considerably smaller landslide at this location before the river capture. However, the current landslide has formed as a result of the river capture and subsequent rapid incision of the Río Aguas and formation of the slopes in this area. The presence of tension cracks at various locations around the backscar of the landslide and the fact that it reaches the floor of the valley indicate that this landslide is still active.

The local AL-104 road is within 10m of the backscar to the landslide (Figure 5.30). Further failure of the backscar could start to undercut the road. There was also a dirt track that once went through part of the eastern section of the landslide. This was used to access El Tesoro and the piers to the motorway bridges.
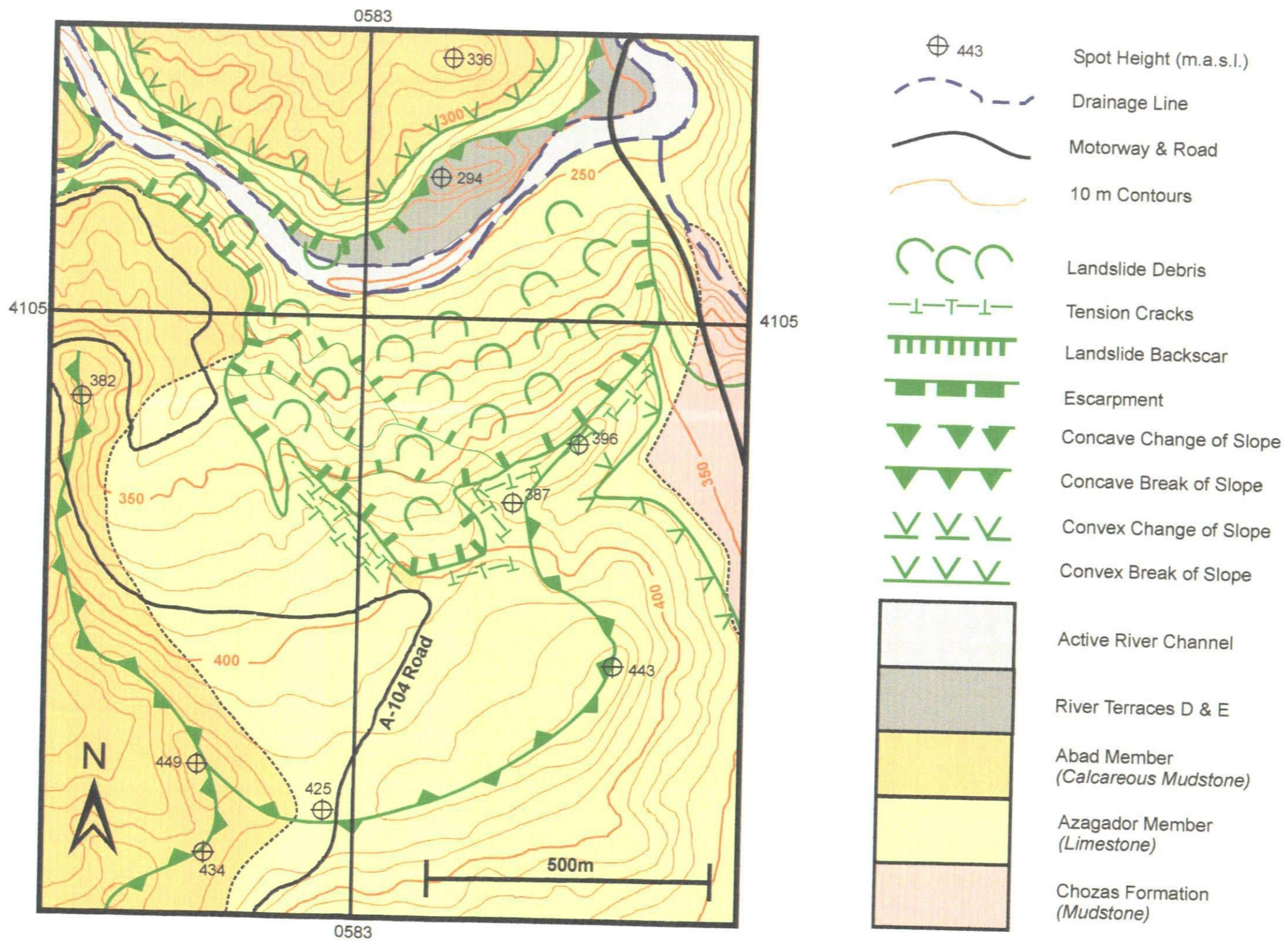
Figure 5.30 - Map of the Cerro Molatas/Carrasco Landslide

5.3.1.4   Landslide Related Geomorphological Feature

During the geological and geomorphological field mapping of the Los Molinos valley

an anomalous outcrop of sediment was identified. From a distance, the outcrop has a

similar weathering appearance to the surrounding area. However, closer inspection

revealed that the feature did not fit in with the surrounding geology or

geomorphology.

The anomalous outcrop is located approximately 10-20m above the present level of

the Río Aguas active channel, opposite the "Carrasco Landslide" (Figure 5.25). The

area is (despite appearances) relatively inaccessible and protected by the "Cuevas de

Sorbas, Parje Naturale" (Sorbas Caves Natural Park).

Behind the anomalous outcrop is a 20-30m high cliff face of moderately strong,

thickly bedded and lightly coloured, fossiliferous limestone (the Azagador Member).

This is overlain by approximately 50m of moderately weak, calcareous mudstone that

is intercalated with shale and the occasional thin bed of moderately strong sandstone

(the Abad Member). The Abad Member is capped by the moderately strong and

thickly bedded gypsum and interbedded calcareous mudstones of the Yesares

Member.

The geological units all dip towards the north, implying that the slopes above the

anomalous outcrop are scarp-slopes. A definite ledge in the valley slope marks the

contact between the limestone and the calcareous mudstone. This highlights the

differences in erosion rates of the two geological units.

The anomalous outcrop sits above, and behind, a relatively large area of river terrace. This is thought to be a either a level D3 (?) or E (more likely due to height above current channel) river terrace after Harvey & Wells (1987). The terrace is located on the inside of the Río Aguas active channel. Geomorphological mapping of the area showed that the anomalous outcrop seems to be in the downstream "shadow" of an outcrop of the Azagador Member limestone which is immediately to the west of the anomalous outcrop (Figures 5.30 and 5.31).

The anomalous outcrop is approximately 15m high, 150 m long and up to 50 m wide. Weathering of the northern side of the outcrop, along its contact with the limestone, means that it almost stands alone as an island defined by two steep gullies (along the northern and western sides).

A light grey weathering crust that makes the study of the sedimentology rather difficult covers the surface of the outcrop. However, there are three sections where it is possible to do so (Figure 5.31):

- A weathering hollow on the northern side of the outcrop (Figure 5.32a);

- A three-roomed man-made cave accessed through a hole in the front of the outcrop (this may have been used for cold storage by the owners of the abandoned farmhouse, but is now home to a swarm of African Bees – Figure 5.32b); and

- A weathering hollow at the eastern end of the outcrop.
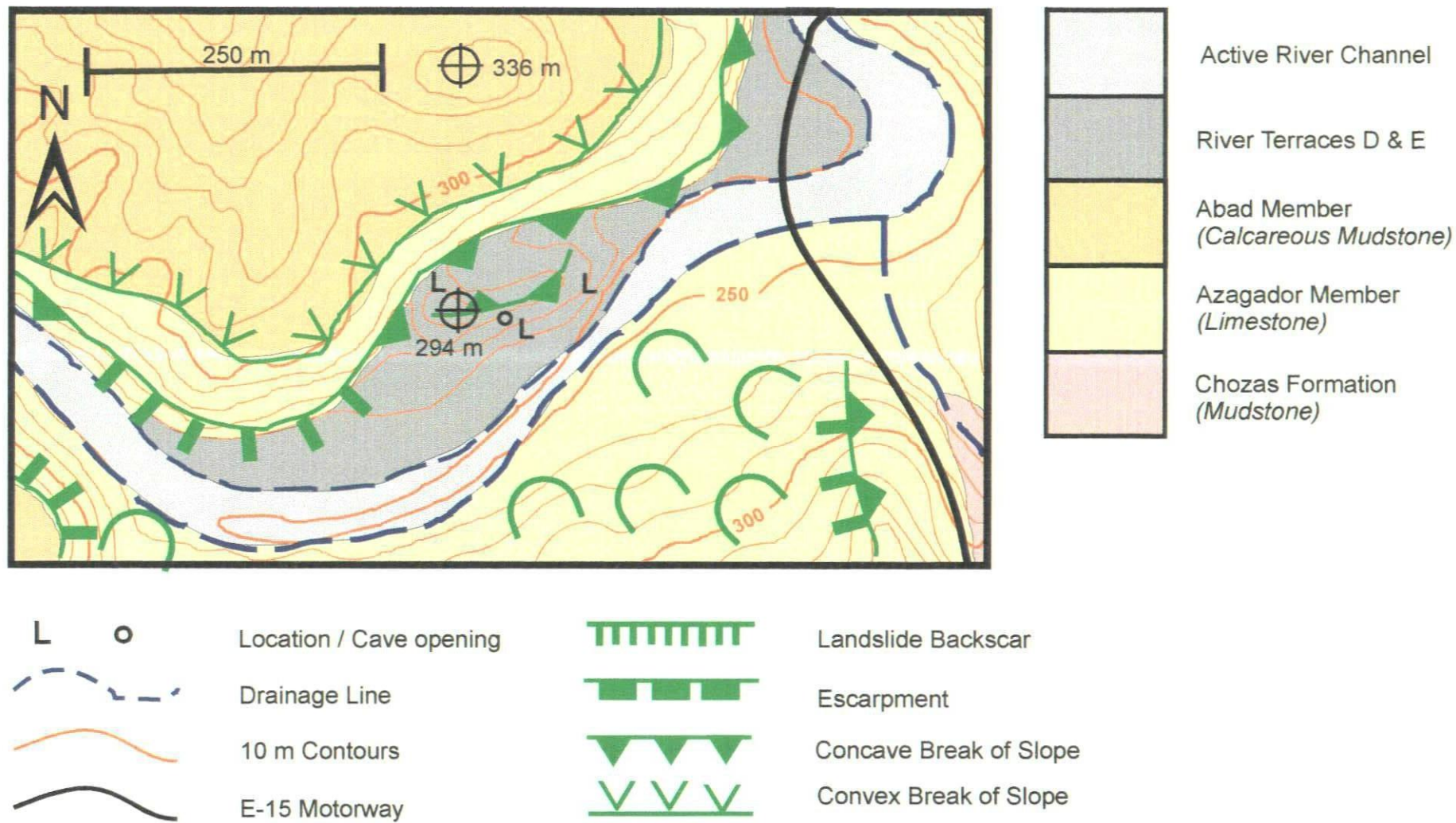
Figure 5.31 - Map of the "Unknown Geomorphological Feature" in the Los Molinos Valley
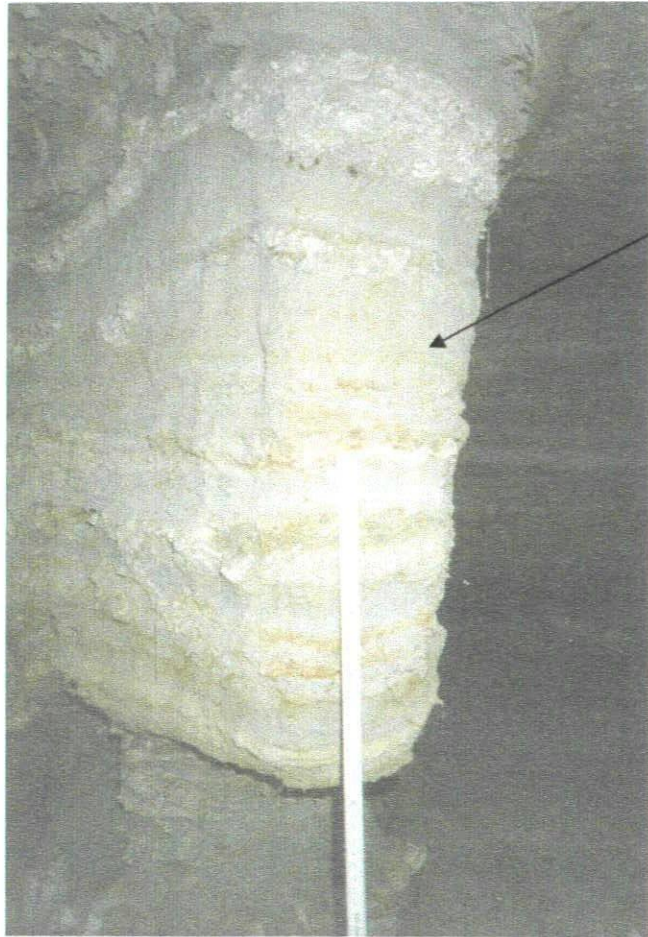
Fine grained, grey, white and red, unconsolidated sandstone and siltstone, with some interbedded pebble bands

Lobes of coarser material
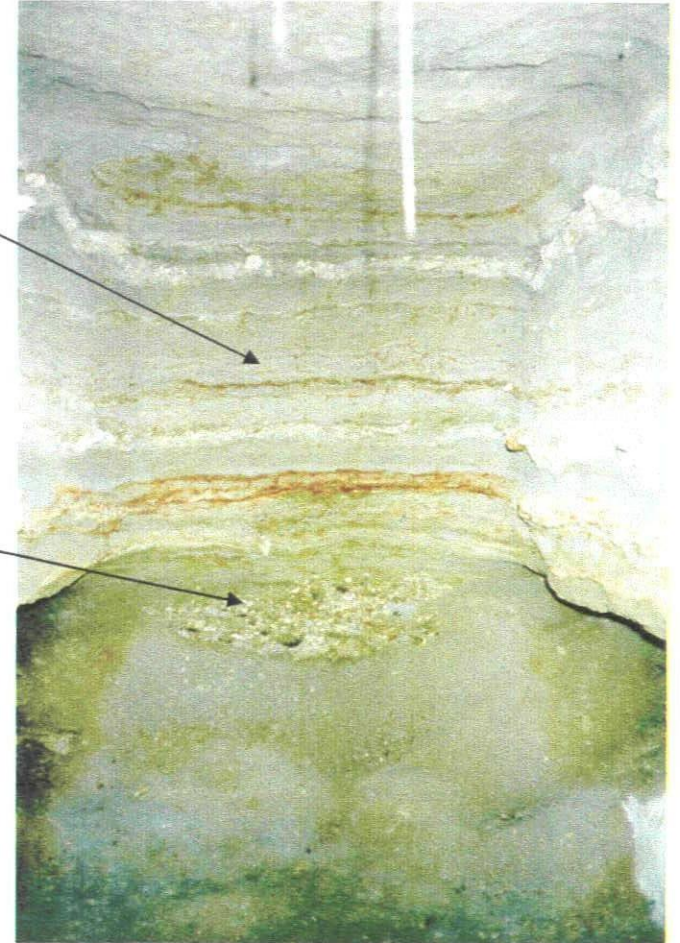
Figure 5.32a – Photographs from inside the cave section (Scale is 1 m ruler) showing the fine horizontal lamination of the sediments, with lobes of coarser material (Grid Reference: 0583241053).
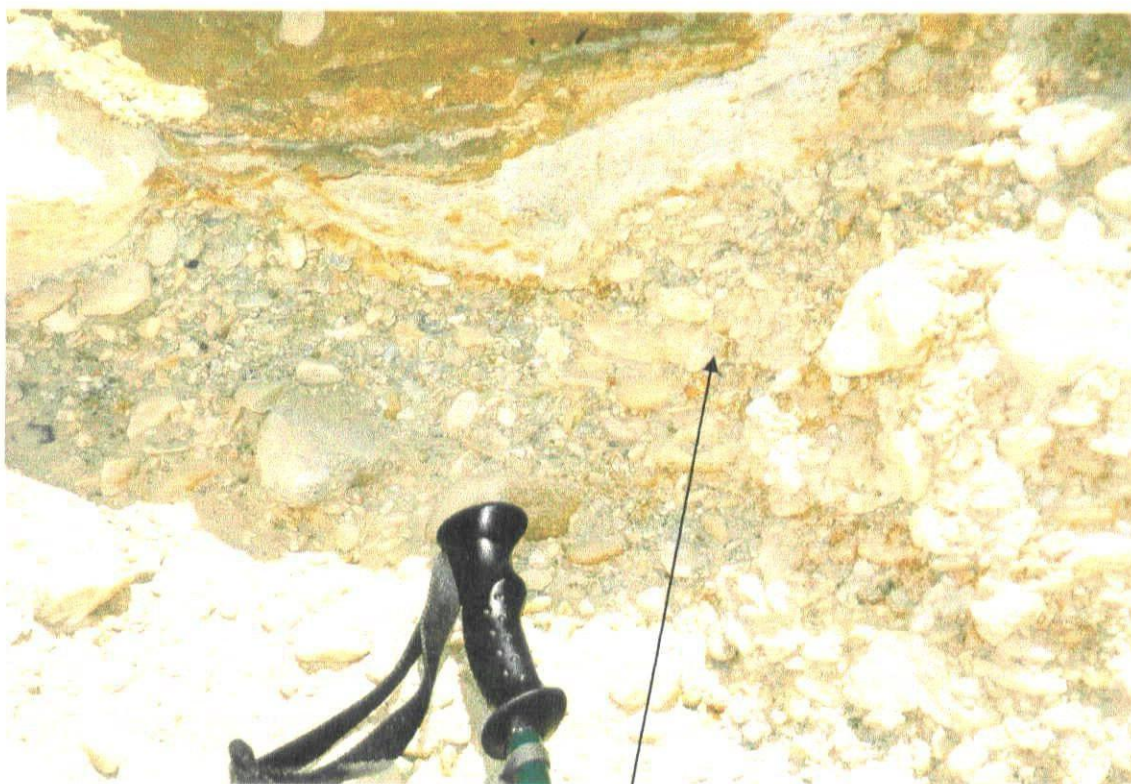
Chaotic distribution of gravels and pebbles & possible imbrication in places.

Figure 5.32b – Photographs of the second section (Scale is 1 m ruler) showing the chaotic nature and possible imbrication of the sediments (Grid Reference: 0583241053).

Sedimentological analysis at these sections showed:

- Thin horizontal laminations of rusty orange, brown, grey, and off-white/cream coloured, silts, clays and fine to medium grained, sub-angular sands;

- The mineralogy consisted predominantly of quartz and mica;

- The occasional layer (up to c.4cm thick) of coarser-grained quartz gravel;

- Towards the base of the outcrop there are layers of sub-angular to sub-rounded pebbles of white sandstone (Sorbas Member?), light coloured limestone (Azagador Member?) and moderately well rounded pebbles of mica schist and ironstones; and

- Internal structures within these pebble-rich layers show faint imbrication that possibly indicate a "flow" direction similar to the present river system. A small number of possible channel-like structures were also identified.

The sediment that makes up the outcrop is relatively unconsolidated and easily erodible. However, a number of very thin layers (up to c.2 cm thick) of black organic matter and thicker layers (up to c.6 cm thick) of cemented material have been identified. These cemented layers are rich in calcium carbonate and contain "pipe-like" structures that have been identified as rootlets. These have been interpreted as possible calcrete layers (M. Watkinson & G. Aillud, *pers. comm.*).

Samples from the three sections examined were brought back to the University of Plymouth for further analysis. The samples have been analysed using standard micropalaeontological techniques.

The sediment (including sediment taken from between the layers of calcrete and carbonate material) has yielded abundant, but poorly preserved foraminifera. The poor preservation, as well as etching and broken chambers, indicates that the foraminifera have been reworked by erosion of the parent rock (Figure 5.33; M. Oxford, C. Smart & M.B. Hart, *pers. comm.*). The foraminifera include both benthonic and planktonic taxa of Messinian age, indicating that they are derived from the calcareous mudstones of the Abad Member (Baggley, 2000; Section 2.3.4.2).

Fine-grained, laminated sediment tends to indicate deposition in a low energy environment with the material being derived locally. The coarser material could then be interpreted as occasional "storm" or "flood events" that could transport material in from slightly further afield from within the catchment area. The presence of rootlets and calcrete would suggest either a surface or sub-surface environment, with calcium-rich groundwater conditions.

The combination of predominantly locally derived sediment (containing relatively deep water planktonic and benthonic foraminifera), calcium-rich material (containing both rootlets and deep-water foraminifera) and carbonate-rich material possibly indicates a low energy, ephemeral environment for the deposition of the anomalous outcrop. This would tend to imply that the anomalous outcrop was either deposited under lacustrine conditions or as part of a river terrace.
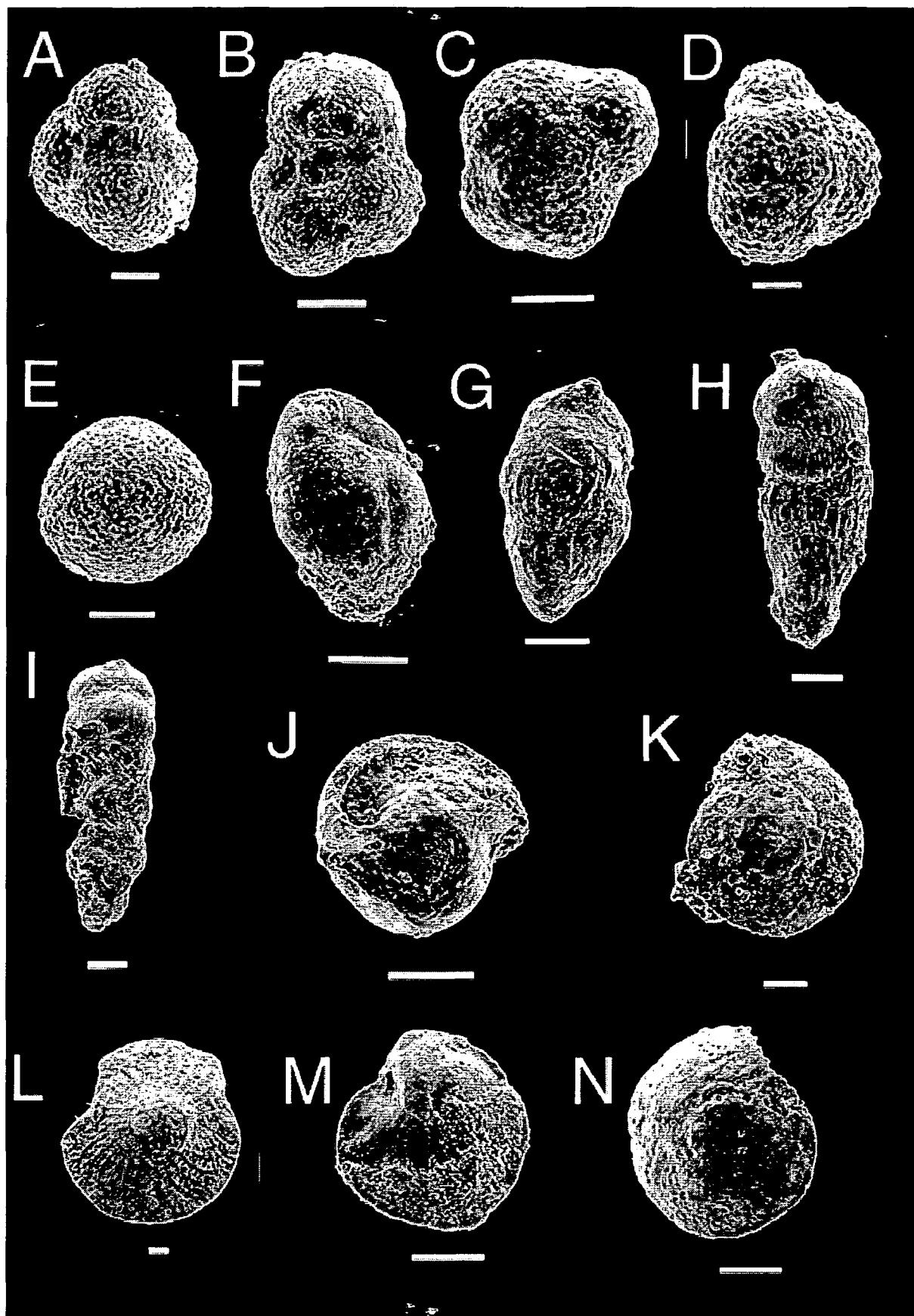
Figure 5.33 Foraminifera from the Geomorphological Feature in the Los Molinos Valley. **A.** *Globigerina* sp.; **B.** *Globigerinoides triloba* (Reuss, 1850); **C.** *Neogloboquadrina acostaensis* (Blow, 1959); **D.** *Neogloboquadrina acostaensis* (Blow, 1959); **E.** *Orbulina universa* d'Orbigny, 1839; **F.** *Bulimina* sp.cf. *Bulimina elongata* d'Orbigny, 1826; **G.** *Bulimina inflata* Seguenza, 1862; **H.** *Uvigerina* sp.cf. *Uvigerina peregrina* Cushman, 1923; **I.** *Bulimina fusiformis* Williamson, 1858; **J.** *Pullenia bulloides* (d'Orbigny, 1864); **K.** *Heterolepa dutempli* (d'Orbigny, 1846); **L.** *Elphidium crispum* (Linnaeus, 1758); **M.** *Epistominella exigua* (Brady, 1884); **N.** *Heterolepa dutempli* (d'Orbigny, 1846). Scale bars are all 100μm, except D which is 50μm. Compared to the specimens figured by Baggley (2000, pls 1-3) these specimens are broken, abraded and lacking clear ornament.

A similar dominantly fine-grained, sequence of laminated silt and clay with occasional intercalated organic soils and fluvatile debris has been described at Cortijo Urra (Grid reference: 0580441061) approximately 4 km upstream (Figure 5.34). Mather *et al.* (1991) and Harvey *et al.* (1995) described the Cortijo Urra deposit as the D2 part of the three-part D river terrace sequence. In the Cortijo Urra area, the deposit reaches a thickness of approximately 35m, and may extend below the modern river level (Mather *et al.*, 1991). The D2 terrace deposits at Cortijo Urra also contain numerous syn-sedimentary deformation structures, which are restricted only to this level (i.e. the significantly thinner, overlying D3 river terrace is not deformed). Mather *et al.* (1991) proposed that the deposition and deformation of this relatively thick river terrace deposit was the result of diapirism in the underlying gypsum, as well as possibly localised tectonic activity in the Cortijo Urra area. The diapirism activity in the gypsum was possibly initiated by the unroofing of the gypsum, as the overlying material was eroded away as a result of the incision of the Río Aguas and its tributaries, post river capture (Mather *et al.*, 1991). They argued that the diapirism and tectonic activity could have led to ponding of sediment and, therefore, the deposition of the D2 river terrace.

The question that is raised is whether or not the Cortijo Urra D2 river terrace deposit and the anomalous outcrop in the floor of the Los Molinos valley are related? The anomalous outcrop has not been affected by any deformation, but then it is 3 km downstream from Cortijo Urra. The anomalous outcrop is also a similar height above the current river level to both the D2 terraces at Urra and several of the D3 river terraces along this section of the Río Aguas (between Los Molinos and Urra).

Mather *et al.* (1991) describe the D2 terrace at Cortijo Urra as extending below the modern river bed. This would imply that the river had been cut to below the modern river level before the formation of the D2 terraces. The D2 terraces would therefore represent the infilling of the river channel. This level has then subsequently been incised by the Río Aguas before the deposition of the D3 river terraces. This brief history would imply that the base level of the Río Aguas has fluctuated during its incision history.

The D2 and D3 terraces (as mapped by Harvey *et al.*, 1995) in the area between the entrance to the gypsum canyon and the Cortijo Urra area, form reasonably large and level areas either side of the current active channel (Figure 5.34). The D3 terrace areas are also bounded by a series of closely spaced abandoned meander scars that suggest a very sinuous drainage pattern. This could indicate that the river, at that time, had a very low gradient and was, therefore, very close to – or at – the base level of the drainage network.

So how can these observations be explained? What would cause a "blip" in the incision of the Río Aguas and the formation of the relatively thick D2 terraces? One possibility is the occurrence of a landslide and the formation of a landslide dam downstream of Cortijo Urra, possibly within the Río Aguas canyon in the Los Molinos or Los Perales area. The river is very confined in these areas, and so a blockage of the river would have the greatest affect. The landslide mapping has identified a number of landslides that could have potentially blocked the river at this time. These are:

- The failures from the gypsum escarpment between the entrance to the gypsum canyon and Los Molinos (although these would possibly not explain the formation of the anomalous deposit);

- The "Tension Crack Ridge Landslide" (Section 5.3.4.1); or the

- The Cuesta del Honor landslide near to Los Perales (Section 5.3.4.2).

Any or all of these landslides could have blocked the Río Aguas during the formation of the D level river terraces. The sequence of events could possibly have been:

1. Occurrence of a landslide or landslides that blocks the Río Aguas to form a landslide dam;

2. Damming of water and sediment behind the dam;

3. Relative raising of the Río Aguas base level;

4. Relative decrease in the stream power of the Río Aguas;

5. Formation of tightly spaced meanders;

6. Deposition of fine grained material (?D2 terrace deposits);

7. Breach of the landslide dam; and

8. Continued incision of the Río Aguas.

Landslide dams are relatively short-lived phenomena that tend to leave very little evidence of their existence (Costa & Schuster, 1988). Often the evidence left behind consists of:

- Remains of meanders indicating that the stream power of the river was decreased, possibly as a result of base level being raised;

- Remains of landslide material at the sides of the river channel (the bulk of the material may be washed away when the dam is breached); and

- Flood deposits from when the landslide dam was breached. These can sometimes be catastrophic.

The tightly spaced D3 terrace meanders may be related to this event, a second, shorter-lived event (hence no apparent deposits) or some other factor that influenced the base level and/or the stream power of the Río Aguas.

Therefore the significance of the anomalous outcrop is that it may provide:

- Evidence for the formation of a landslide dam that blocked the Río Aguas for a period of time;

- The possibility of being able to link the deposit (and therefore any potential age or environmental conditions) to any of the river terraces or landslide activity in the immediate area;

- Evidence for the environmental conditions present at the time of deposition;

- Pollen or other micro/macrofossils that could provide a "dating" source for the deposit; and

- A "date" for the deposition of the carbonate layers within the anomalous deposit.

It is therefore potentially a significant source of information concerning the geology and geomorphology of the Los Molinos area and the development of the Río Aguas. It may even provide a link between the river terrace sequence and some of the landslide activity in the Los Molinos area.
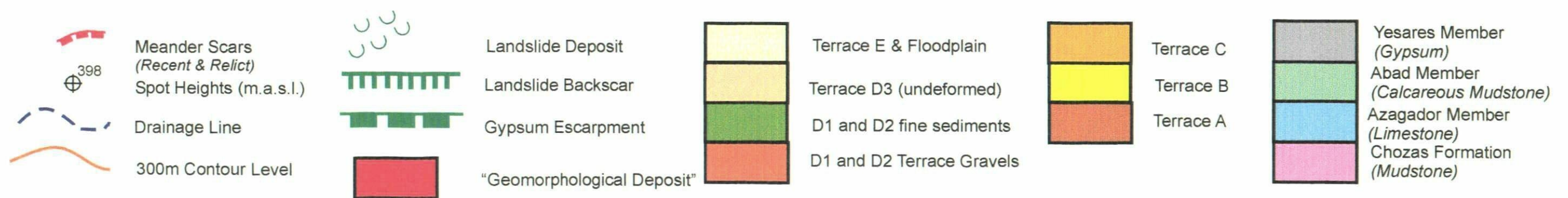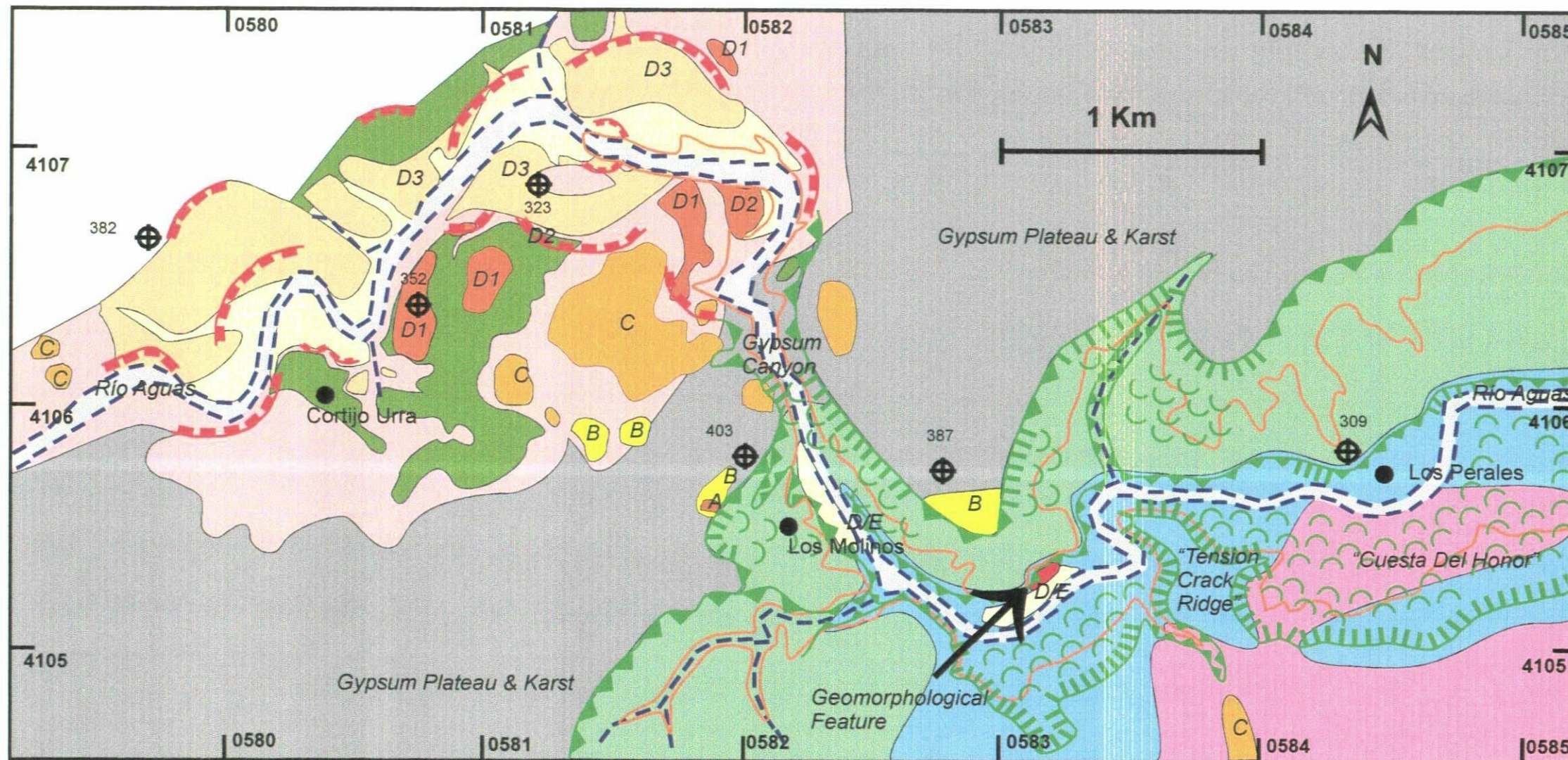
Figure 5.34 - Map of the terrace levels between CortijoUrra and Los Perales. The terrace levels are after Harvey *et al.* (1995) and Harvey (2001).

5.3.2   The Rambla Feos Wind Gap

The "Rambla Feos Wind Gap" marks the area where the ancestral drainage of the Sorbas Basin flowed southwards into the Carboneras Basin (Figure 2.1). It now marks the watershed between the Río Aguas and the Rambla Feos. The "Wind Gap" (or "Capture Col") is 80 m above the present level of the Río Aguas and forms a relatively level plateau between Cerro Molatas in the west and Cerro de la Matica and the Sierra Cabrera in the east (Figures 5.25 and 5.35).

Mapping of the river terraces by Harvey & Wells (1987) along the route of the Río Aguas and Rambla Feos identified a number of river terraces in this area. The floor of the Wind Gap has been "dated" as being a C river terrace (Harvey & Wells, 1987; Harvey *et al.*, 1995). This is underlain by the calcareous mudstones and sandstones of the Chozas Formation. The hills immediately to the west of the Wind Gap consist of the moderately strong limestones of the Azagador Member. Limestones of the Azagador Member also outcrop in the hills to the east of the Wind Gap, as well as the Chozas Formation and the mica schists (and other basement material) of the Sierra Cabrera.
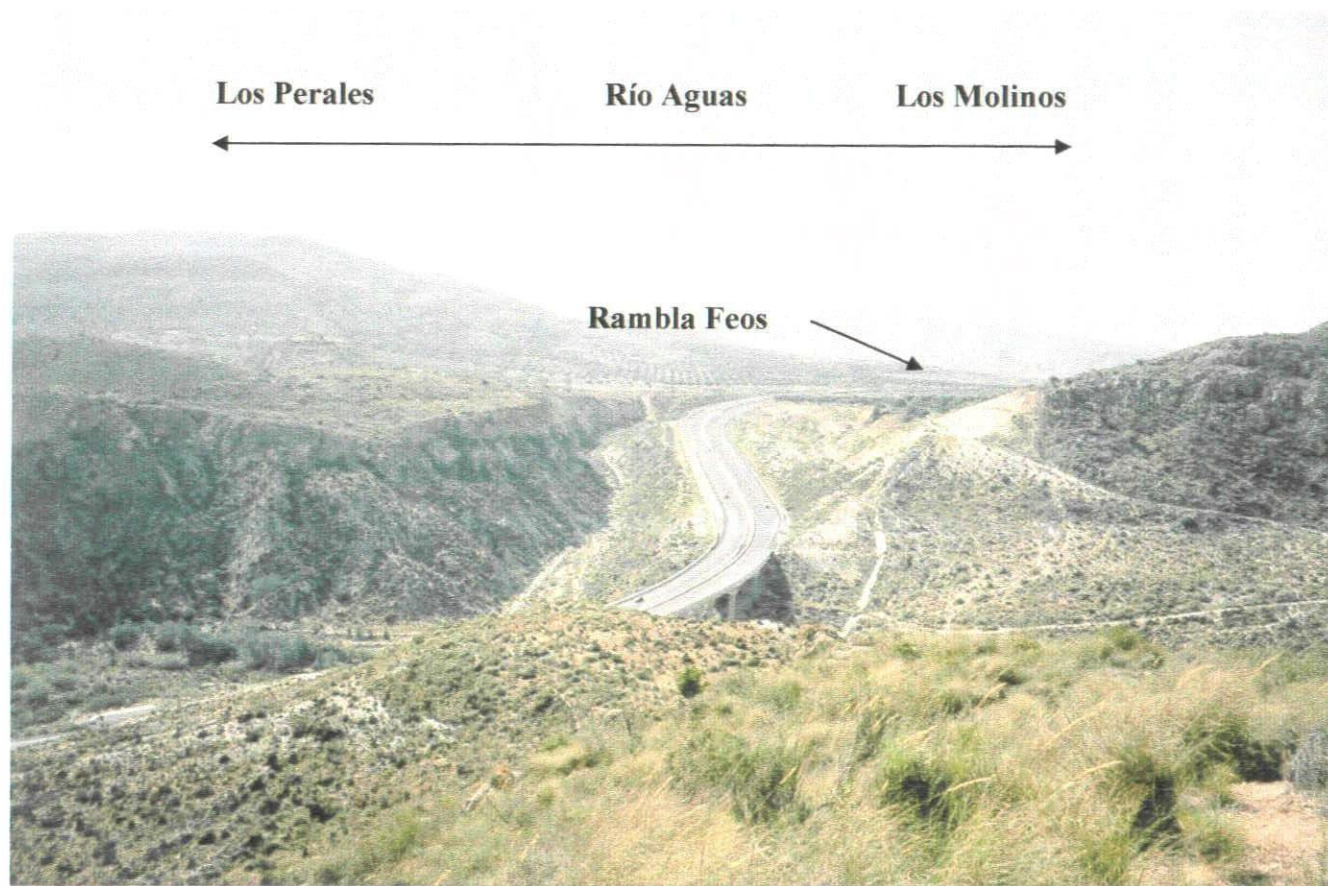
Figure 5.35 – Photograph of the Río Aguas/Rambla Feos Wind Gap (River Capture Site). The Río Aguas flows from right to left (Grid Reference: 0582941054 / Facing south southeast). The construction of the motorway has made use of the natural gap in the topography created by the Wind Gap.

5.3.3   The El Tesoro Landslides

El Tesoro is an abandoned village that is located in a relatively large, bowl shaped area immediately to the north of the Rambla Feos Wind Gap (Figure 5.25; Landslide Numbers 40-43; Grid Reference = 05834106). The village is immediately underneath the gypsum escarpment that is a continuation of the escarpment described in Section 5.3.1.1. Some of the landslides that occur in this area have been described by Hart (1999).

The village is built on the moderately weak, thinly bedded, laminated calcareous mudstones of the Abad Member. In this area, the Abad Member contains the occasional thin band of stronger, and more resistant, orange sandstone. The Abad Member is overlain by the moderately strong gypsum of the Yesares Member, which contains thin intercalations of moderately weak calcareous mudstone and siltstone. The Yesares Member thins out in the western part of this site (at the southern corner of the escarpment) and is replaced by deposits of Quaternary river terrace. These rest unconformably on the Abad Member. Below the Abad Member, the Río Aguas is cut into the limestone of the Azagador Member. All three geological units present in this area dip towards the north and northwest. The more resistant geological units in the area are affected by the NE-SW and NW-SE trending discontinuity pattern that is seen elsewhere in this case study area.

The village is built on scarp slopes in a relatively large bowl-shaped area that represents the outside of an older, higher level meander in the Río Aguas, that was formed after the Río Aguas/Rambla Feos River Capture. The valley side slopes are very steep and in

places vertical. The gypsum plateau above the area exhibits a number of different karst features that have been described by Calaforra & Pulido-Bosch (1997). One of the most significant karstic features observed above El Tesoro are pipe structures. In a number of places, these have developed into tension cracks that run parallel to the edge of the escarpment.

Numerous landslides affect this relatively small area (Table 5.10). One could argue that the whole escarpment shows evidence of instability and that the majority of the bowl area is either covered or affected by landslide debris (Figure 5.36). The majority of the landslide activity involves a combination of sagging/rock avalanche at the edge of the escarpment, rock fall, rock topple, followed by sliding (and sometimes possibly rolling). These movements are all due to erosion within the calcareous mudstones that is undercutting the gypsum. Examples of this type of failure can also be seen along the section of gypsum escarpment underneath Penon Diaz and the gypsum quarry and along the opposite side of the valley from Los Molinos (Figure 5.25).

It is interesting to note that landslides listed in Table 5.10 vary considerably in size, volume, runout length and angle of reach. In particular, the angle of reach of these landslides decreases with the volume of the displaced mass. This agrees with the results presented in Section 4.2.16. The size and runout length of these landslides may also reflect the topography, of both where the landslide initiated from and the ground over which it has moved.

On the eastern side of the El Tesoro area (Figure 5.25; Grid Reference = 05834106), a section of the escarpment has undergone a combination of rotational and non-rotational sliding. This has led to a stepped appearance in the hillside, which has subsequently

been modified by the construction of the village and agricultural terraces. Similar landslide activity can also be seen along parts of the canyon opposite the village of Los Molinos.

Field mapping has shown that dissolution features within the gypsum play an important role in the location of the landslides along the gypsum escarpment (Hart, 1999). An example of this is seen in the northern part of the El Tesoro area (Figure 5.25; Grid Reference = 05834106). Here a small number of drainage lines on top of the gypsum plateau drain into a natural pipe structure a short distance away from the edge of the escarpment. The gypsum in this section of the escarpment has broken up into a series of very large blocks. These blocks have then undergone a combination of either translational, forward rotational or toppling movements. Some of these blocks have then either toppled or fallen into the Barranco El Tesoro, following this initial sagging/rock flow-style movement.
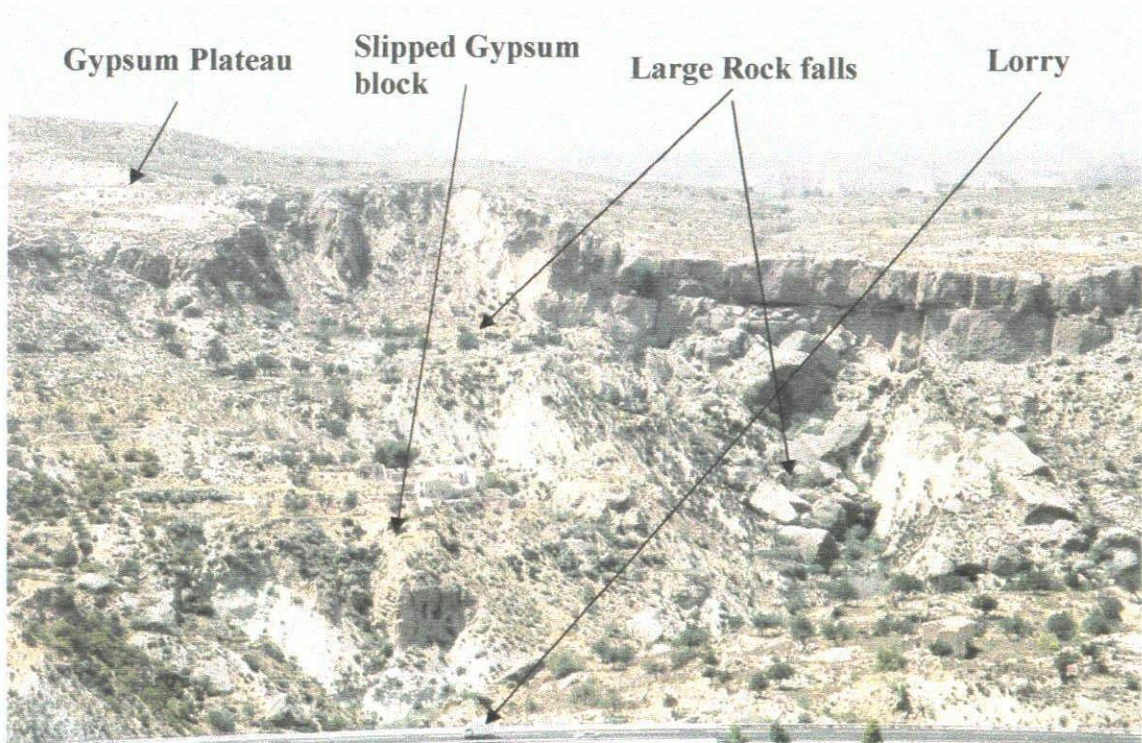
A.
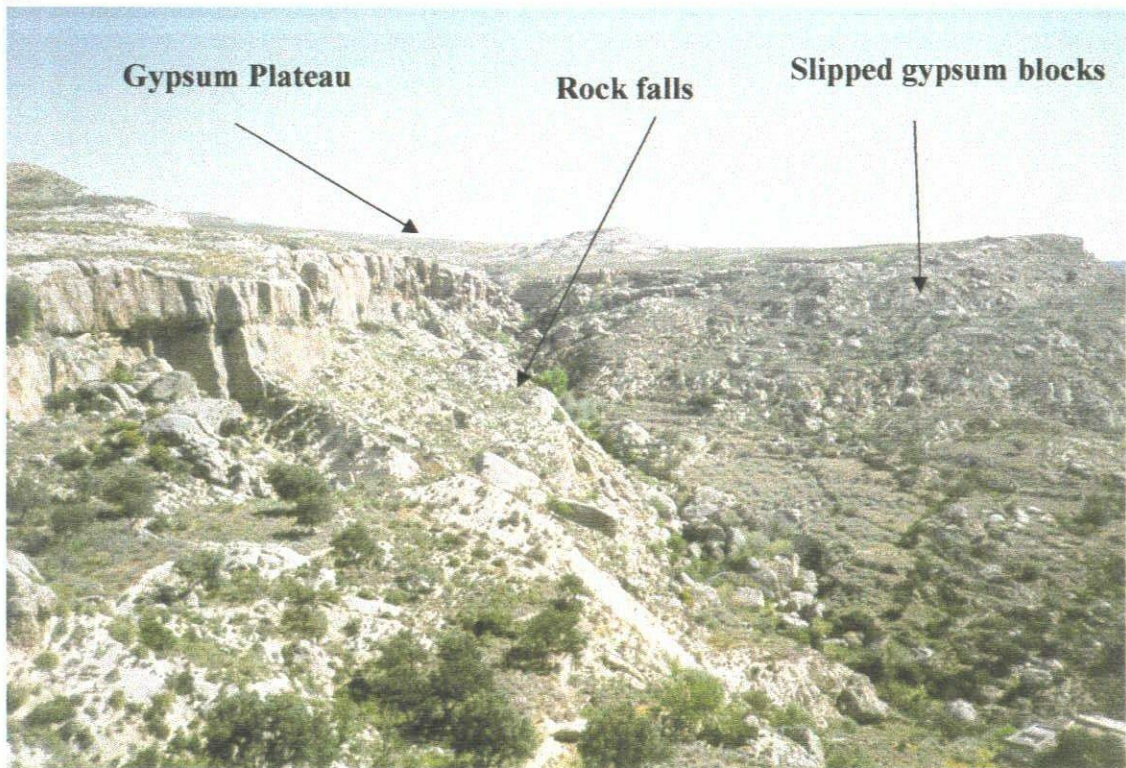
B.

Figure 5.36 – Photographs of the El Tesoro area. **A.** Large scale rock falls and topples within the El Tesoro area (Grid Reference: 0583841054 / Facing northwest). **B.** Looking north-eastwards along the edge of the El Tesoro Gypsum Escarpment and the large scale failures within the bowl-shaped landscape (Grid Reference: 0583041057).

Table 5.10 - Extract of data from the Landslide Inventory for four of the landslides mapped in the El Tesoro area.

	"West El Tesoro 02"	"West El Tesoro 03"
Landslide No.:	40	41
Grid Reference:	05831 41059	05831 41061
Height:	50m	110m
Length:	150m	250m
Width:	100m	100m
Angle of Reach:	18.0°	24.0°
Volume:	$0.015 \times 10^6 \, m^3$	$0.625 \times 10^6 \, m^3$

	"El Tesoro NW"	"EL Tesoro NE"
Landslide No.:	42	43
Grid Reference:	05834 41063	05837 41063
Height:	50m	100m
Length:	200m	500m
Width:	500m	400m
Angle of Reach:	14.0°	11.0°
Volume:	$2.0 \times 10^6 \, m^3$	$12.5 \times 10^6 \, m^3$

Numerous factors have been identified as influencing the landslide activity (and to a certain degree the bowl shape) of the area. These are:

- The NE-SW and NW-SE tectonic related discontinuity pattern of the area;

- The presence of the pipe structures, tension cracks and geologically controlled discontinuities along the edge of the gypsum plateau;

- The presence of the Barranco del Tesoro and other minor drainage features in the area;

- The dispersive nature and therefore extreme weathering potential of the calcareous mudstones within the Abad Member;

- The undercutting of the gypsum escarpment by erosion of the underlying mudstone; and

- The relative rapid incision of the drainage and therefore relatively rapid formation of the valley side slopes and canyon walls.

Apart from the abandoned village there is no other infrastructure located within the area. The motorway, which passes through the bowl area of El Tesoro, has been built on an elevated section over the Barranco del Tesoro. Movement of the large rotational failure on the eastern side of the area could possibly affect the piers of this elevated section.

5.3.4 Los Perales

The village of Los Perales is located approximately 1.5 km downstream from the site of the Río Aguas/Rambla Feos River Capture (Figure 5.25). It is situated approximately 20 m above the present level of the Río Aguas within a steep sided, asymmetrically shaped river valley. It is also located beneath the level of the gypsum plateau (Yesares Member). Immediately above the village (on the northern side of the Río Aguas), but below the gypsum plateau escarpment, is a lower escarpment cut into the limestone of the Azagador Member. Between the gypsum escarpment and the limestone escarpment are the calcareous mudstones of the Abad Member, which form a badland-style landscape. The valley floor and southern side of the valley are composed of the calcareous mudstones and conglomerate of the Chozas Formation, all of which dip to the north.

The orientation of the main Río Aguas valley at Los Perales suggests it is following the regional strike of the geological units of the area. Therefore, there are dip-slopes on the southern side of the Río Aguas valley and scarp-slopes on the northern side of the valley.

5.3.4.1 The "Tension Crack Ridge"

The name "Tension Crack Ridge" that is used here for the ridge that is located to the east of the "Wind Gap" and separates the Los Molinos valley from the Los Perales valley (Figures 5.25; Landslide No. 39; Grid Reference = 0583741054). The term refers to the very large tension cracks that can be clearly seen affecting this ridge Hart (1999) and Hart et al. (2000). Davis et al. (2000) also identified some of the features of this landslide as part of a satellite image interpretation study in the region.

The ridge is predominantly composed of light coloured limestone (the Azagador Member) that is dipping between 30° and 40° to the north and north-west. This unconformably overlies the calcareous mudstones and shales of the Chozas Formation. Geological mapping at the contact (wherever accessible) suggests that the contact between the two rock units has a dome-like shape with variable dip amount and dip direction. The limestone is affected by both jointing and dissolution features. The jointing follows the regional trend.

The ridge is located immediately to the east of the Rambla Feos Wind Gap, and to the south of where the Lower Aguas undercut and captured the drainage of the Sorbas Basin. The ridge is a dip-slope occurring on the inside of a deeply incised active meander channel. The slopes to the southeast of the ridge are also affected by landslide

activity (Section 4.4.2.6). The active channel of the Río Aguas has undergone

approximately 100 m of incision at this point and flows around three sides – the

southwestern, northwestern and northeastern sides - of the ridge (Figure 5.37).

Although the area to the north of the ridge is a large open area of badland erosion

undercutting the gypsum escarpment (El Tesoro), the current active channel has cut a

deep and very narrow channel through the limestone.

Aerial photographic interpretation, followed by geological and geomorphological field

mapping, has shown that the ridge is dissected by a series of large tension cracks within

the Azagador Member limestone (Figures 5.37, 5.38 and 5.39). These tension cracks

define a series of "blocks" which vary greatly in size and exhibit varying degrees of

movement, both in distance moved and angle of tilt. The tension cracks reach widths of

up to 10 m and lengths of over 100 m, and the blocks can be up to tens of metres across

and several tens to hundreds of metres in length. Field mapping also highlighted that

the tension cracks trend predominantly NW-SE and NE-SW (Figure 5.37). This trend

follows the discontinuity pattern for the case study area being discussed here, as well as

the overall tectonic regime for the region. Interestingly, the ridge itself follows this

trend, suggesting that its shape is controlled by the discontinuities in the limestone.
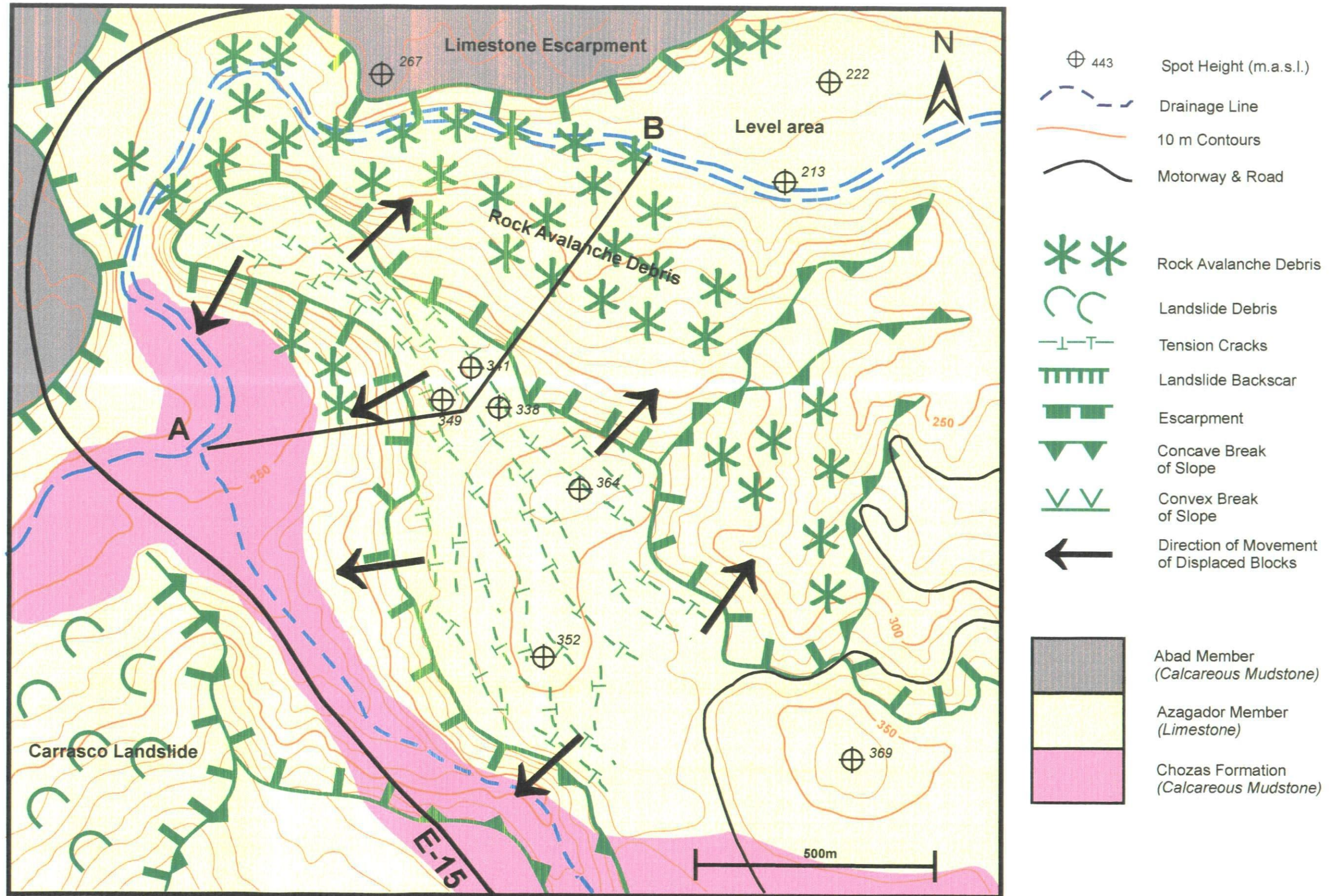
Figure 5.37 - Map of the "Tension Crack Ridge" Landslide at Los Perales
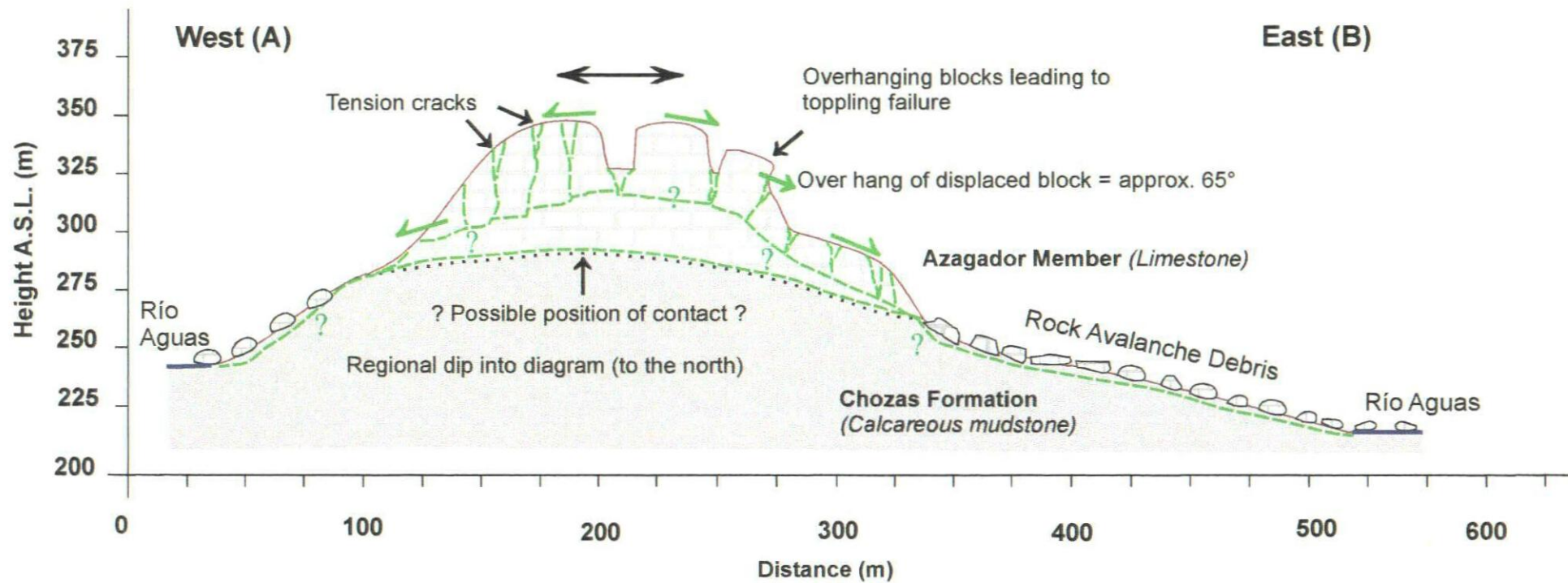
Figure 5.38 - Cross section through the "Tension Crack Ridge".
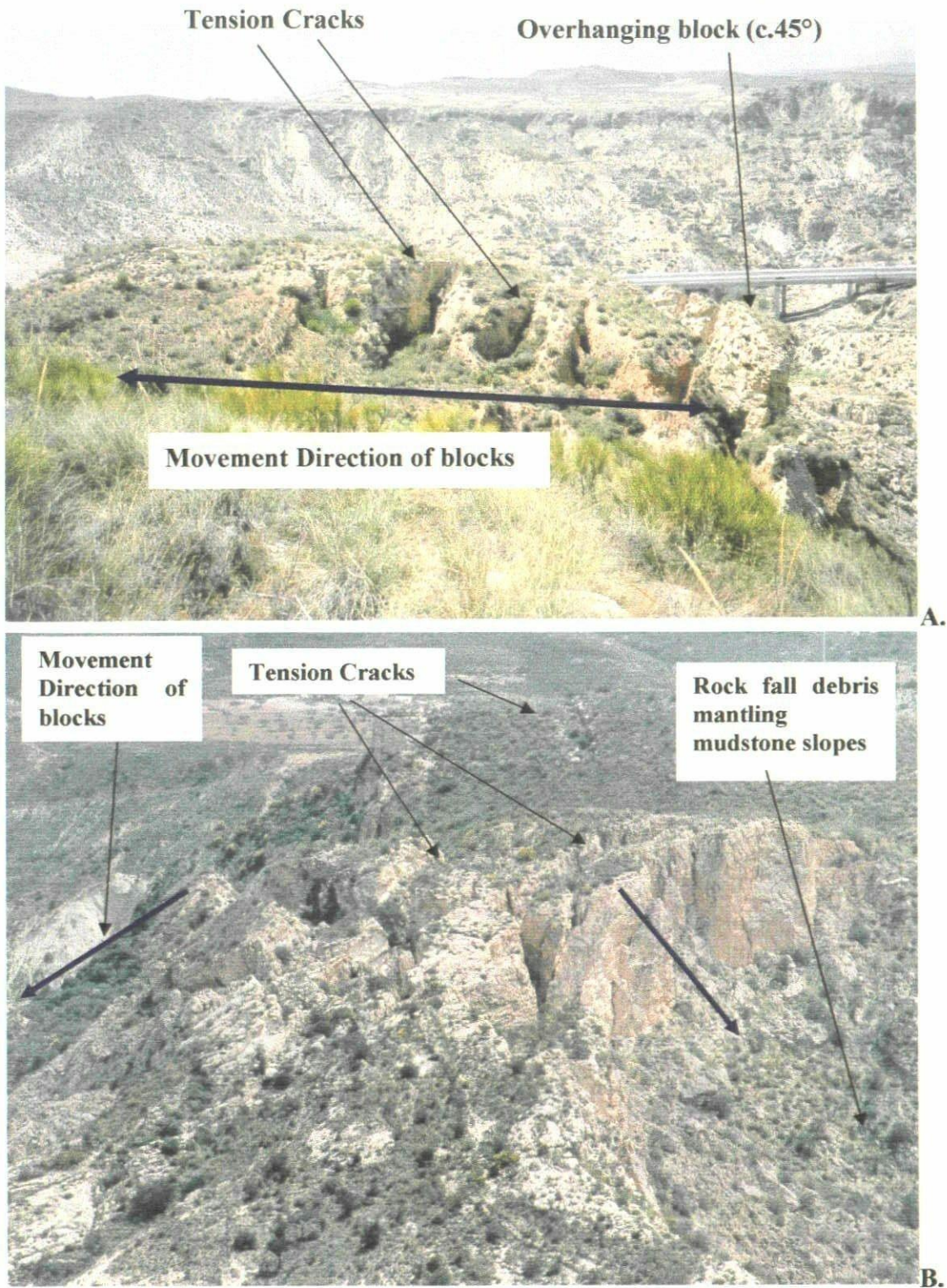
Figure 5.39 – Photographs of the "Tension Crack Ridge". The landslide involves blocks of Azagador Member limestone moving over mudstone (Chozas Formation). **A.** Looking along the ridge itself (Grid Reference: 0583841054 / Facing northwest). **B.** The ridge observed from the Gypsum Escarpment above El Tesoro (Grid Reference: 0583041055 / Facing east).

The western side of the ridge is a vertical rock face of the Azagador Member limestone (Figures 5.37 and 5.38). The base of the cliff face is covered by rock debris, which potentially covers an outcrop of the Chozas Formation. This rock debris is the result of rock falls from this cliff face.

The "snout" of the ridge is a relatively broad northwest facing dip-slope that is broken up by the numerous tension cracks described above (Figure 5.39). The Río Aguas at this point passes through a very narrow (<5 m wide) limestone canyon. There are also some very large boulders at the northern end of this canyon.

The northeastern side of the ridge forms a complex slope that is covered by a number of large blocks, boulders and rock debris (Figures 5.37, 5.38 and 5.40). It appears that the blocks (mentioned and described above) "move out" over the slope, and then either topple and slide or fall down the slope. The rock debris and boulders also fill the Río Aguas canyon below the slope.

Identification of the mechanisms involved in this complex landslide has not been straightforward. However, by studying the blocks, boulders, and the rock debris, as well as the distribution of the tension cracks it has been possible to gain an understanding of the movements and mechanisms affecting the ridge. The movements involve:

- The limestone sliding over the contact with the calcareous mudstones, with a slight outward component, as seen on the eastern side of the complex. These blocks then either fall or topple into the valley below. Examples of this are seen on the eastern side of the ridge;

- The larger blocks breaking up to form relatively small-scale rock avalanches as seen on the eastern side of the ridge; and

- High-angle, non-rotational shear failures within the calcareous mudstones, with the limestone carried short distances downslope as intact blocks. An example of this is seen on the western side of the ridge.

A cross section of the ridge (based on the geological and geomorphological mapping) highlights the role of the unconformity between the limestone and the underlying rock units, as well as the variation in the dip amount and direction of the unconformity (Figure 5.38).

Using the classification schemes of Varnes (1978) and Turner & Schuster (1996), this mass movement would be classified as being a combination of lateral spreading, with "smaller" translational and non-rotational movements. These continue until the rock mass becomes unstable, giving rise to rock falls, rock topples, and relatively small-scale rock avalanches. Parts of the landslide complex also exhibit some of the features associated with rock flow movements (Sackung) as defined by Dikau *et al.* (1997). Brunsden *et al.* (1996b) identified a similar combination of mechanisms affecting the Isle of Portland in southern England. This may suggest that this combination of controlling factors and geological and geomorphological setting is significant for landslide activity (i.e., a competent rock mass overlying a ductile rock mass, outcropping along a "ridge-like" structure, with active erosion on both sides).
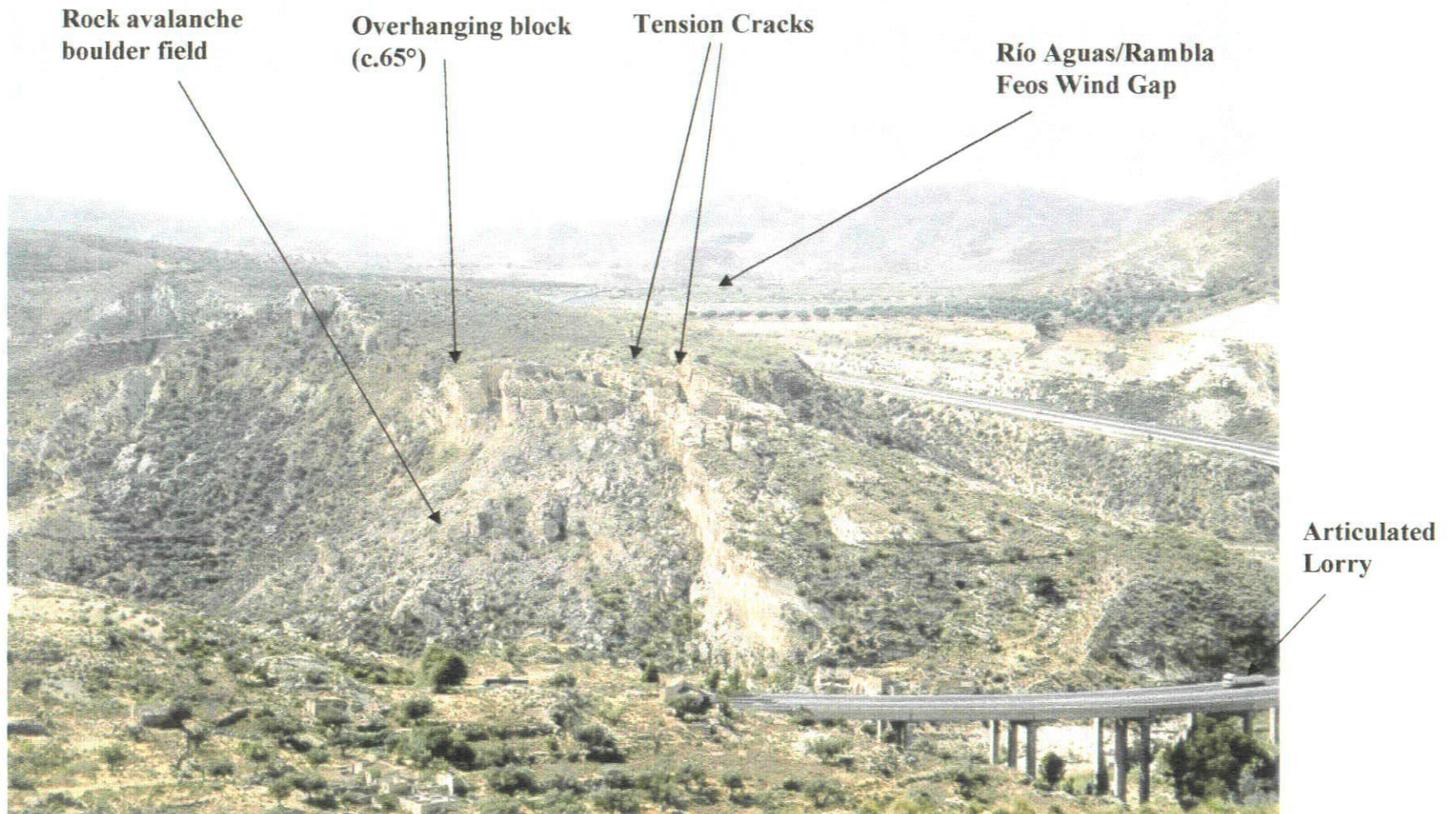
Figure 5.40 – Photograph of the boulder field on the eastern side of the "Tension Crack Ridge" (Grid Reference: 0583841063 / Facing south).

The details of the landslide, as contained within the landslide inventory for this study are shown in Table 5.11.

Table 5.11 – Tension Crack Ridge landslide data

Landslide No.:	39
Grid Reference:	05838 41053
Height:	140m
Length:	500m
Width:	400m
Angle of Reach:	Variable – depends on location
Volume:	14.7×10^6 m^3

The factors that appear to control the activity of this landslide are:

• The resistant but strongly jointed limestone overlying the weaker mudstones;

• The discontinuities within the limestone;

• The differences in permeability of the two rock units;

• The varying dip amount and direction of the geological units and the unconformable contact; and

• The relative rapid incision of the drainage and therefore relatively rapid formation of the valley side slopes and canyon walls.

An interesting question is how old is the landslide? The top of the ridge is roughly at the same height as the River Capture Wind Gap and, therefore, river terrace level C. It is possible that the ridge only became unstable once the Río Aguas had incised below the level of the limestone and mudstone contact. This would be post-river terrace C but before formation of the D river terrace levels.

If the ridge were to collapse towards the north and/or east, it would block the Río Aguas, particularly as the river is within a very narrow canyon in this area. This could result in the formation of a lake, although this would not take place very quickly considering the climate of the area and the amount of water in the river. The sizeable boulder field and rock talus slopes in this area suggests that this side of the ridge is very active. The extremely large size of some of the boulders in this area would also suggest that any failure in this area could have devastating effects on any infrastructure located in this area. However, the only infrastructure in the area, at this time, is the E-15 motorway. The motorway is on an elevated bridge section above the valley and the river (Figure 5.41).

Failure of the western side of the ridge could also affect the Río Aguas but possibly not to the same extent as described above. Although, there is a rock talus slope at the base of the ridge, it is dramatically smaller than the rock talus slope on the eastern side of the ridge. This would suggest that this side is more stable and, therefore, potentially poses a lower risk.

Río Aguas   "Cuesta Del Honor"   The Tension
                Landslide   Crack Ridge

Figure 5.41 – Photograph of the elevated section of the E-15 Motorway above the Río Aguas (Grid Reference: 0583041055 / Facing east).

5.3.4.2 *The "Cuesta del Honor" Landslide Complex*

The "Cuesta del Honor" landslide complex is situated directly to the south of Los Perales (Figure 5.25; Landslide No. 44; Grid Reference = 05844105). The landslide covers the whole of the valley side from the ridge crest down to the Río Aguas (Eyers *et al.*, 1998; Hart, 1999; Davis *et al.*, 2000; Hart *et al.*, 2000).

The valley slope (and therefore the landslide) is formed from the interbedded calcareous mudstones and sandstones of the Chozas Formation. Outcrops of Azagador Member limestone can be seen at the ridge crest of the hillside and in the floor of the valley. The dip of both of these units is towards the north. The limestone is thickly bedded and moderately strong, whereas the calcareous mudstones are thinly bedded, moderately weak and highly eroded. The interbedded sandstones form bands of more competent material that can be traced through the rock succession.

The geological dip of the area means that the landslide is located on a dip slope. The valley slope has a complex morphology, reflecting the complex history of landslide activity that affects the area. The Río Aguas forms a very narrow channel at the base of the valley slope. The north side of the channel is a wall of Azagador Member limestone. However, there is little evidence of this on the southern side of the river.

The landslide activity involves a combination of different mechanisms including rotational and non-rotational sliding. This is picked out by a series of blocks or "steps" within the hillside, some of which are slightly back-tilted (Figure 5.42). Both field mapping and API has shown that these vary in size and relative age. Many of the blocks are well degraded and vegetated. This suggests that this is an older feature

within the landscape and that the smaller movements are all part of a much larger landslide complex that affects almost the whole of the valley side slope (Table 5.12 and Figure 5.25). It is likely that the landslide initially started during the incision of the drainage system after the Río Aguas/Rambla Feos River Capture and has been developing since that time. However, there is a possibility that the upper parts of this valley slope were unstable before this time, as the Lower Aguas was at a lower level than the Rambla Feos prior to the river capture.

Table 5.12 – "Cuesta del Honor" landslide data

Landslide No.:	44
Grid Reference:	05850 41055
Height:	250m
Length:	750m
Width:	2000m
Angle of Reach:	18.0°
Volume:	$147.3 \times 10^6 \, m^3$

The location of the smaller movements within the overall landslide complex is possibly influenced by the presence of a small number of springs within the hillside, which can often be picked out by areas of more dense vegetation. The presence of these springs is probably controlled by the underlying geology (i.e., boundary contacts between the mudstone and sandstone layers in the Chozas Formation).

The geomorphological mapping of the lower valley side slopes has indicated that the landslide may have blocked the Río Aguas. The section of the valley slope opposite Cortijo de Lentiscar (Grid reference: 0585041061) is a large back-tilted block (on which an electricity pylon has been placed). The block is composed of disturbed and slightly unconsolidated material (blocks of mudstone, shale and conglomerate). The area was

difficult to map due to the very disturbed and wet nature of the ground (there was a spring in the area). A limestone cliff face on the northern side of the river restricts the width of the river at this point. The river also flows around the toe of this back tilted block, and is possibly out of "alignment" with the main trend of the river. This could be the result of the landslide blocking the river at this point, which has eroded around the back tilted block to cut the present river channel (Figures 5.25 and 5.42).

The field mapping and API identified a number of different factors that have, or are, potentially controlling this landslide. They are:

- The location of natural springs within the hillside;

- The dip of the geological units involved in the landslide activity;

- The variable properties of the material involved in the landslide activity; and

- The relative rapid incision of the drainage and, therefore, relatively rapid formation of the valley side slopes and canyon walls

The village of Los Perales is located on the opposite side of the valley from the landslide. It is also built above one of the river terrace levels in the area (possibly terrace level E). This is used for agriculture. The access road for Los Perales descends to the valley floor through the western part of the landslide. This part of the landslide does appear to be stable at present, although there are the remains of back-tilted blocks that indicate previous failures in this area (high-angle rotational slides).
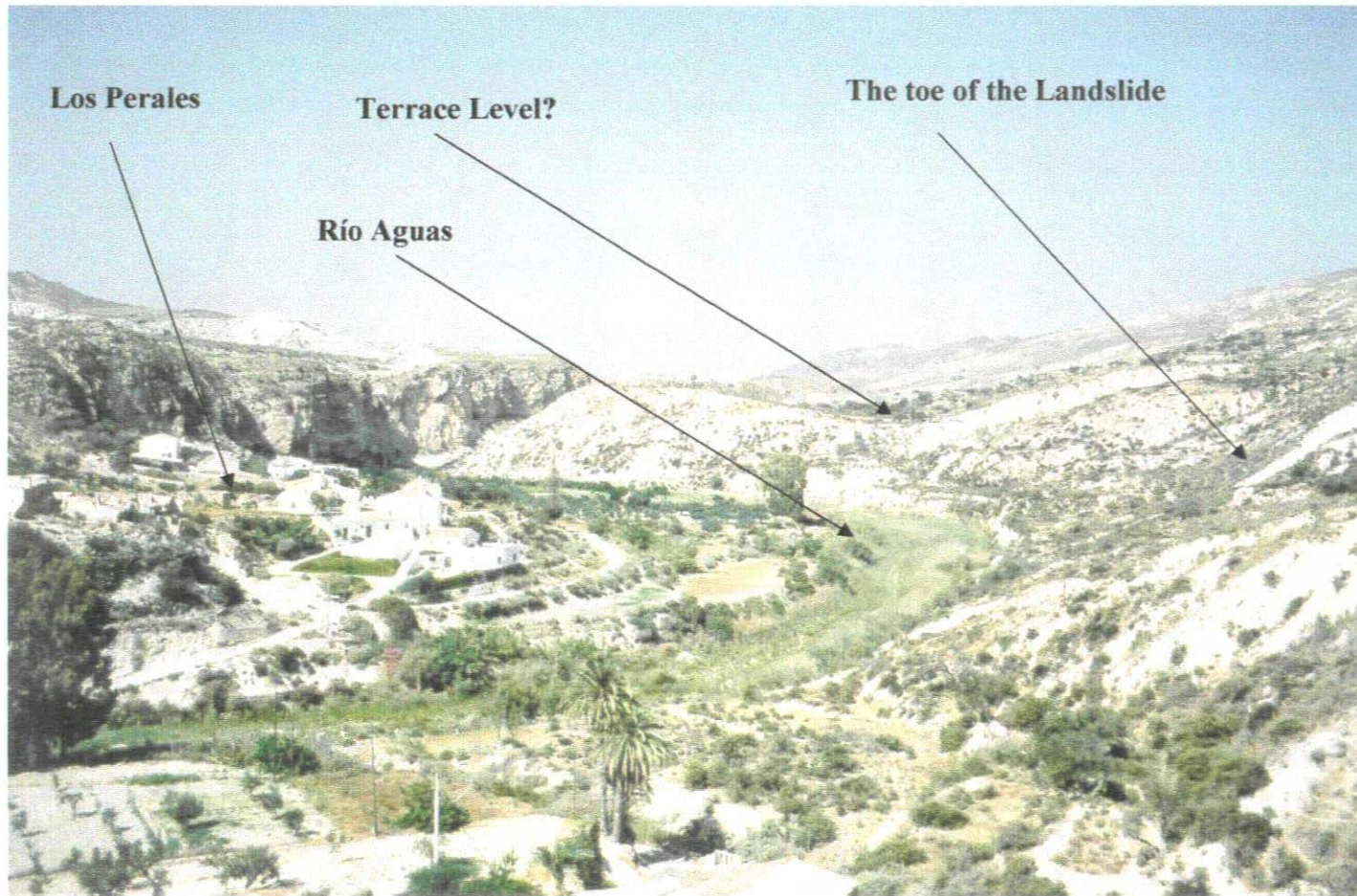
Figure 5.42 – Photograph of the toe area of the Cuesta del Honor Landslide and the village of Los Perales (Grid Reference: 0584341053 / Facing northeast).

5.3.5 Marchalico Viñicas

The abandoned village of Marchalico Viñicas is located just below the level of the eastern edge of the gypsum escarpment, above the Río Aguas. The village was possibly abandoned as a result of either the economic migration to the cities in the 1960s and 1970s or the Spanish Civil War. The village looks out over the eastern edge of the Sorbas Basin and the southern part of the Vera Basin (Figure 5.25). The village also provides an excellent view of a number of landslide features that affect this part of the study area (Eyers *et al.*, 1998; Hart, 1999; Hart *et al.*, 2000).

Between Los Perales and Marchalico Viñicas the Río Aguas valley opens up into a broader river valley. The valley side slopes below the gypsum plateau escarpment are composed of the calcareous mudstones of the Abad Member and weather to form a typical badland-style landscape. In the Los Perales valley area the limestone (Azagador Member) outcrops at river level. The dip-slopes on the southern slopes of the Río Aguas valley (which are outside of this case study area) comprise of the limestone and the mudstones and shales of the Chozas Formation. The landscape (particularly below Marchalico Viñicas) has been altered by the construction of the E-15 motorway, feeder roads and agricultural activity.

The village itself is built on the scarp-slopes of the Abad Member, immediately underneath the escarpment of the gypsum of the Yesares Member.

The village is approximately 150m above the current level of the Río Aguas active channel, at the site of a natural spring. The spring is found at the contact between the gypsum and the calcareous mudstones of the Abad Member, and is part of the extensive

378

karst system that is found within the gypsum (Section 2.3.5 and 2.5; Calaforra & Pulido-Bosch, 1997). The gypsum plateau above the village is one of the key example areas for some of the karst features described by Calaforra & Pulido-Bosch (1997) that have contributed to the area being designated the "Cuevas de Sorbas, Parje Naturale" (Sorbas Caves Natural Park). One of the most significant karstic features along the edge of the gypsum escarpment are pipe structures. In a number of places, these have developed into tension cracks that run parallel to the edge of the escarpment.

There are two distinct landslide features in this area, as well as several smaller features (Figure 5.43). The two larger landslides (Table 5.13) can be clearly distinguished from each other on the basis of their geomorphology. They are also clearly identifiable on both the colour and black and white aerial photographs of the study area. Field evidence suggests that these landslides are of different ages and are, therefore, referred to here as the "Relict" and "Recent" Landslides.
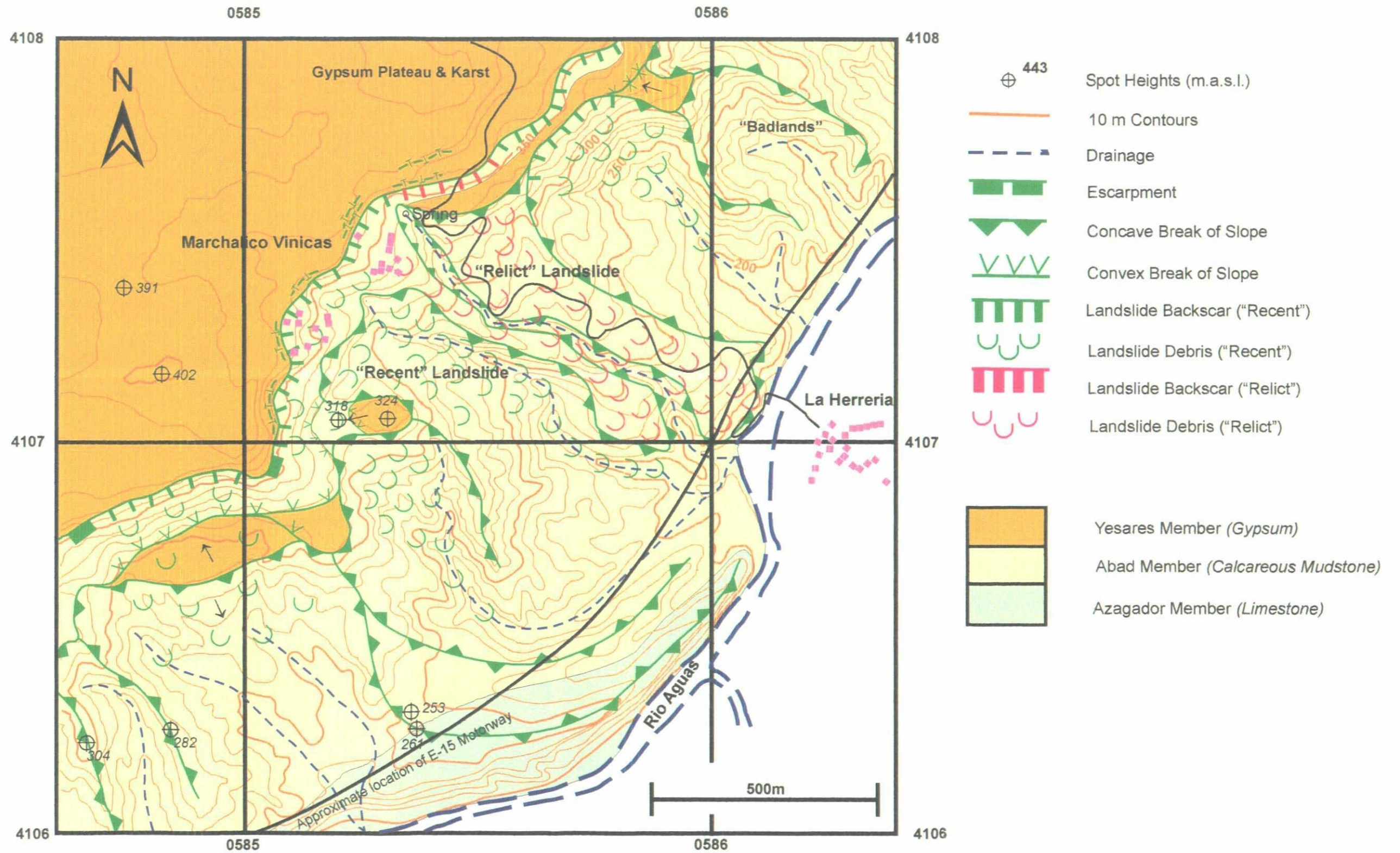
Figure 5.43 - Map of the Marchalico Viñicas area.

Table 5.13 – Extract of data from the Landslide Inventory for the "Relict" and "Recent" landslides at Marchalico Viñicas.

	"Recent" Feature	"Relict" Feature
Landslide No.:	46	47
Grid Reference:	05851 41071	05853 41074
Height:	180m	180m
Length:	800m	900m
Width:	200m	200m (min)
Angle of Reach:	13.0°	11.0°
Volume:	$15.1 \times 10^6 \ m^3$	$17.0 \times 10^6 \ m^3$

5.3.5.1 The "Recent" Feature

The "recent" landslide forms a very prominent feature on the ground and is clearly visible on aerial photographs and ATM images (Eyers *et al.*, 1998; Hart, 1999; Hart *et al.*, 2000). The reason for this is due to the extremely large gypsum boulders within the debris accumulation and the long runout of the debris. Geomorphological mapping of the area suggests that the landslide occurred as a combination of a large non-rotational movement within the Abad Member and collapse of the overlying gypsum. The debris then moved downslope as a large debris/rock avalanche.

The village is located directly under the backscar, in a small depression formed by the top of a slightly back tilted block (Figures 5.43 and 5.44). Parts of the village are also located within the runout of gypsum boulders that cover the upper slopes suggesting that the landslide occurred prior to the construction of the village. The spring (see above) is found at the back of one of the gullies mentioned above, and is covered by the edge of the runout (Figure 5.43).
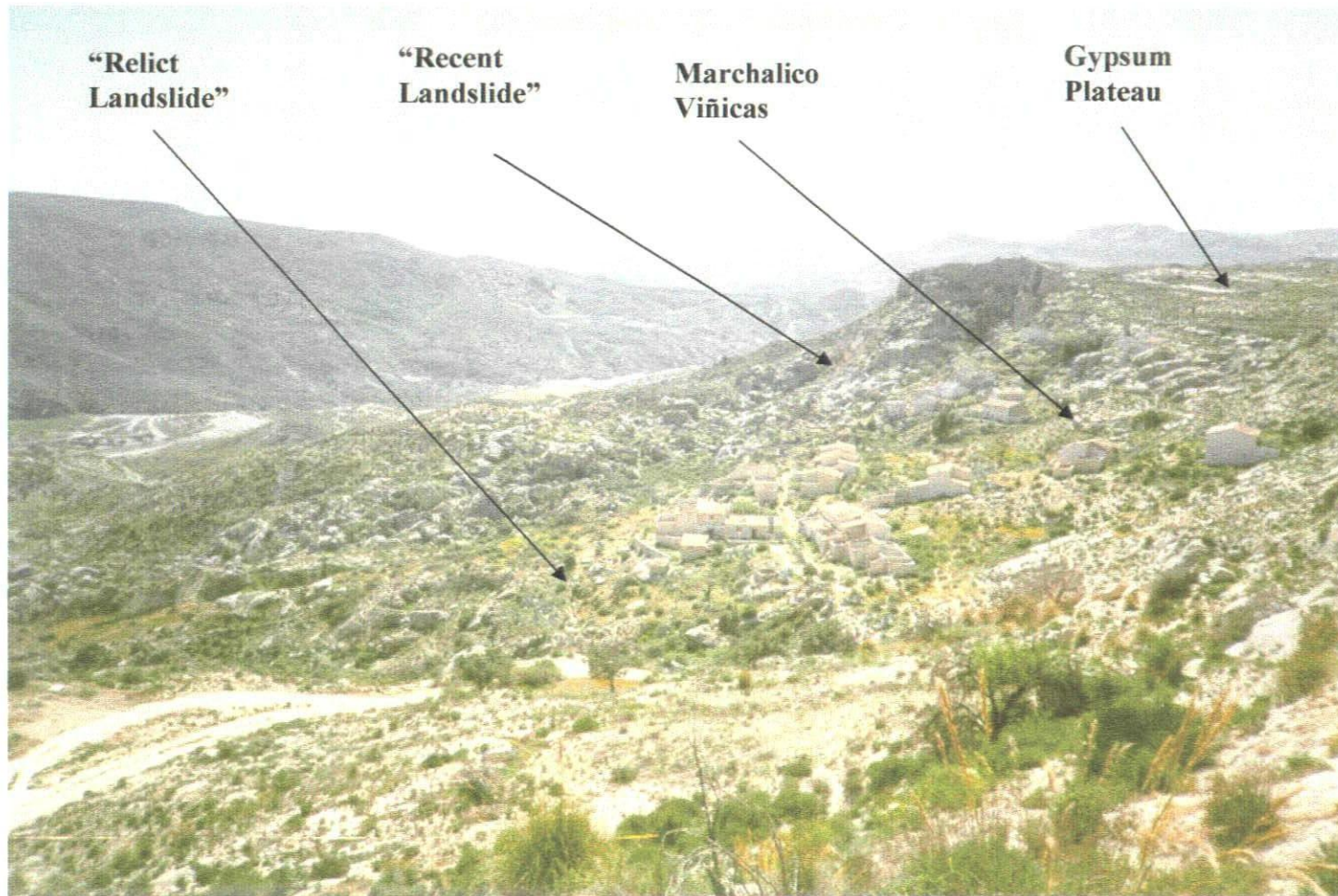
Figure 5.44 – Photograph of the Marchalico Viñicas abandoned village, the crown areas for both landslides described here and the edge of the Gypsum Escarpment (Grid Reference: 0585541077 / Facing southwest).

The debris accumulation in the crown area of the landslide (i.e., under the level of the gypsum escarpment) is not confined by the topography. In the middle section of the slope the debris accumulation is confined within two gullies. Further downslope the two gullies join together and the debris is completely confined within this topographic low. The landslide runout ends just above the motorway embankment. Although the toe area may have been modified by the construction of an embankment, there is no evidence that the debris would have travelled beyond the observed point.

This landslide is probably the result of a number of sagging and non-rotational movements (Dikau *et al.*, 1997) involving both the gypsum and underlying mudstone. Due toe the nature of the rock material involved the moving blocks would have broken up to form the observed rock debris. It would then have moved downslope as a rock flow. The presence of the spring near to the backscar area of the landslide may also be significant in explaining the mobility of the rock material. The initial movements along the edge of the Gypsum Escarpment may have been similar to the sagging movements seen at the Tension Crack Ridge and described by Brunsden *et al.* (1996b).

Further movement of the "recent" landslide may affect the houses of Marchalico Viñicas. However, as the buildings are abandoned and show signs of decay, any structural damage caused by landslide activity (past, present or future) would be difficult to ascertain. Recently, however, there was some speculation that a developer was looking to buy the site and use it for secluded holiday homes (Walsh, *pers. comm.*).

5.3.5.2 *The "Relict" Feature*

The "relict" landslide, which is located just to the north of the village and adjacent to the "recent" landslide, is a well-degraded and masked feature in the landscape. Although the landslide and surrounding slopes have been considerably modified by human activity, (i.e., the construction of the village, agricultural terraces and a track), it can be picked out on aerial photographs by its overall morphology. The landslide is approximately 800 m long, reaching from the gypsum escarpment down to just above the level of the Río Aguas active channel (Figure 5.43).

Geological and geomorphological field mapping of the landslide has indicated that the landslide has been modified by surface processes, erosion and more recent landslide activity. For example, the northern of the two gullies, down which the "recent" landslide has travelled, has dissected the "relict" landslide. The gully wall shows a section through the landslide, as well as the contact with the underlying geology (Figure 5.45). The landslide has also been dissected by the construction of the motorway and a feeder road (Figures 5.45 and 5.46). The toe of the landslide outcrops in the slope just above the active channel of the Río Aguas. However, this slope may have been affected by the construction of the motorway and feeder road.

The four sections mentioned above (the gully wall, two road cuttings and the toe area) have allowed the internal structure of the landslide to be studied. They show that the lower parts of the debris accumulation zone consist of a chaotic "jumble" of relatively large, well-rounded gypsum boulders, held within a calcareous mudstone/siltstone matrix (Figures 5.45 and 5.46). The contact between the debris accumulation and the original ground surface (i.e. the shear surface) shows evidence for scour and removal of

material, as well as for filling-in depressions on the original ground surface. The shear surface is at a much gentler angle than the current topography.

It is likely that the landslide involved a number of different failure mechanisms. The initial movement may have been similar to the sagging movements described for the Tension Crack Ridge and the "Recent Landslide" at this locality (see above). These movements may have then progressed into a number of non-rotational landslides (Dikau *et al.*, 1997). The cross sections through the landside (Figures 5.45 and 5.46) would indicate that the final movements of the landslide were very similar to a debris flow or rock avalanche. Again, the presence of the spring in the crown area of the landslide may have influenced the mobility and mechanism of the landslide.

The debris from the road construction has been tipped down some of the surrounding slopes into the river channel. However, it is possible to distinguish between the two types of material:

• The lack of matrix material in the tipped material;

• The conditions of the gypsum boulders - the tipped boulders are more broken and some are more angular; and

• The degree of weathering - the tipped material is slightly more weathered;

A.
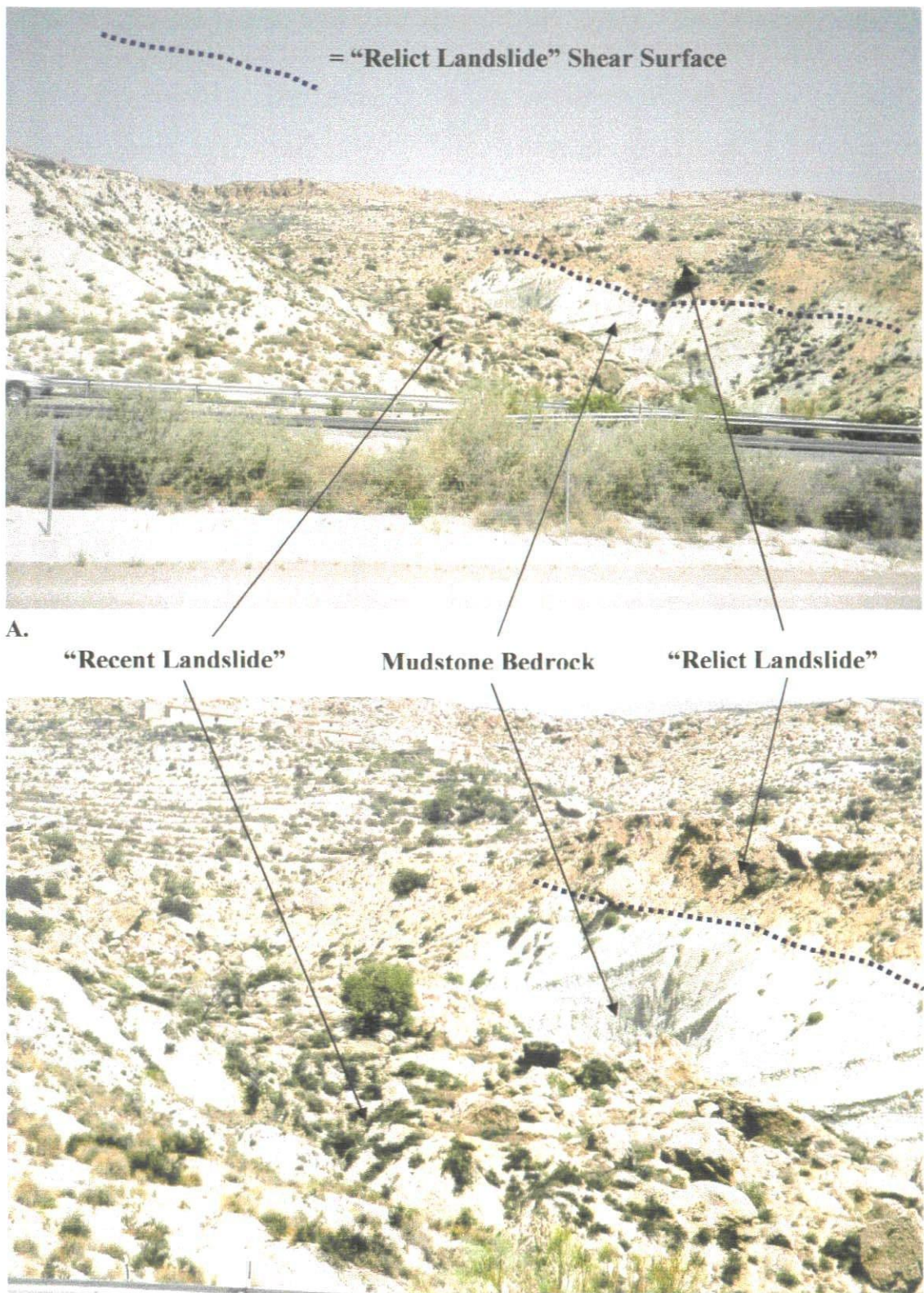
B.

Figure 5.45 – Photographs of a section through the Marchalico Viñicas "Relict" Landslide, exposed in a gully wall, adjacent to the E-15 Motorway (Grid Reference: 0586041067 / Facing northwest). Photograph B is a close-up of Photograph A.
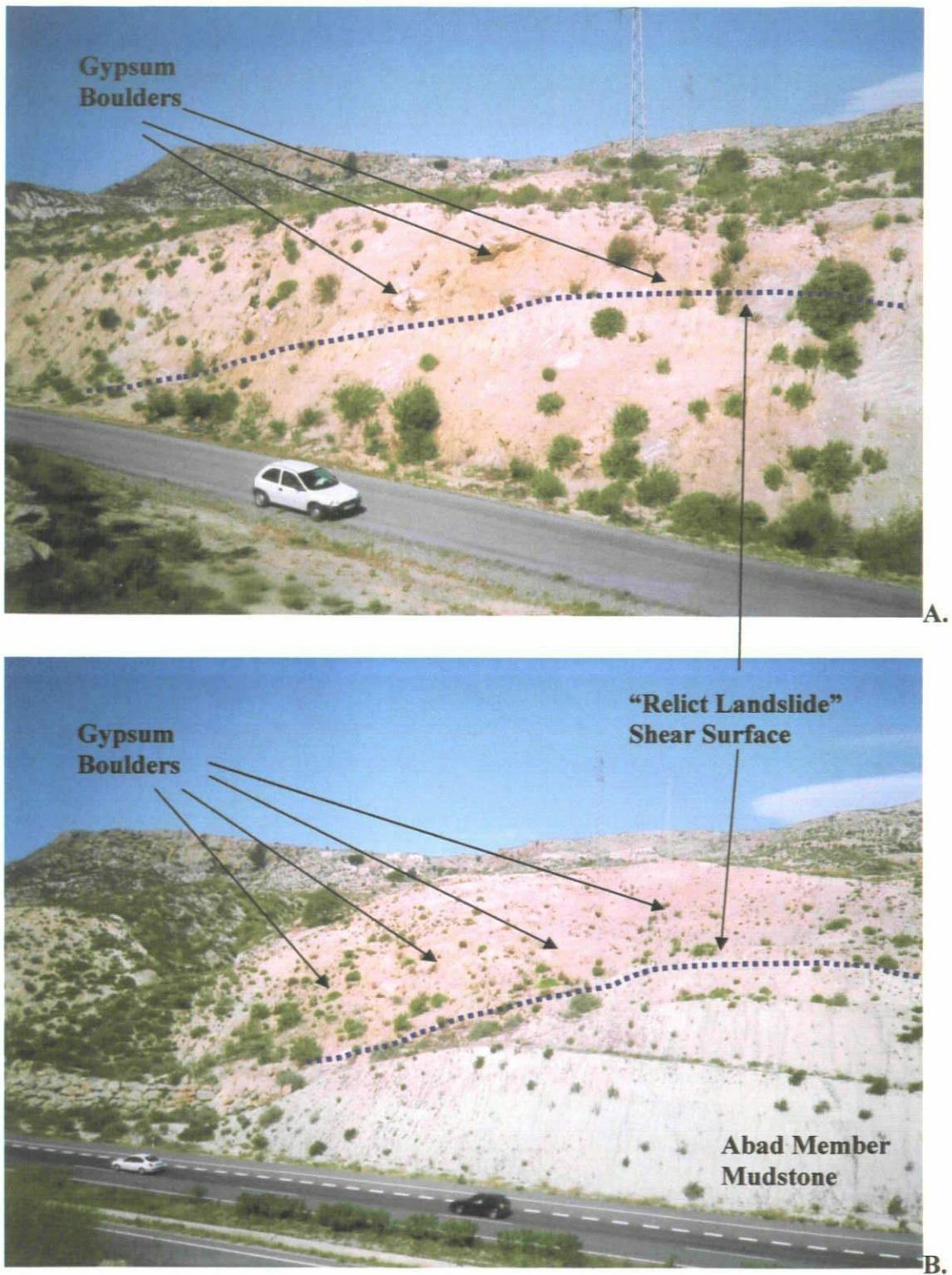
Figure 5.46 – Photographs of sections through the Marchalico Viñicas "Relict" landslide. **A.** Road cutting on the minor road to La Herrería. **B.** Motorway road cutting. Both photographs are taken from the tops of the road cuttings either side of the minor road to La Herrería, at the approximate Grid Reference 0586041070, facing almost northwest.

The field mapping revealed a number of tension cracks (several tens of metres long) that cut through the "relict" landslide feature within approximately 5m of the top of the motorway road cutting. They reach widths of approximately 10-20cm. These may indicate reactivation of this part of the "relict" landslide debris accumulation. The tension cracks also pass by the foundation block for a high voltage electricity pylon.

5.3.5.3 Other Landslide Features

Other sections of the gypsum escarpment adjacent to the two features described above have failed as either rock toppling failures or as a number of fairly large rock falls. The latter are the result of the gypsum being undercut by the erosion of the underlying calcareous mudstones. The topples may be the result of shear surfaces developing in the underlying calcareous mudstones, which then cause the gypsum blocks to rotate and topple forwards. The size and shape of the blocks are defined by the pipe structures and other discontinuities within the gypsum.

5.3.6   Synopsis of the Gypsum Escarpment Case Study Area

The API and field mapping have identified a number of factors that control the landslide activity affecting this case study area. These are:

- The presence of the active springs in the crown area for both the "relict" and "recent" failures at Marchalico Viñicas and in different parts of the Cuesta Del Honor landslide;

- The presence of the pipe structures, tension cracks and geologically controlled discontinuities along the edge of the gypsum plateau;

- The dispersive nature and therefore extreme weathering potential of the calcareous mudstones within the Abad Member;

- The undercutting of the gypsum escarpment; and

- The relative rapid incision of the drainage and, therefore, relatively rapid formation of the valley side slopes and canyon walls.

This last point is particularly interesting, as this site is downstream of the Río Aguas/Rambla Feos River Capture site. The idea of a "wave of incision" moving upstream from the river capture site has already been described (Section 2.4). Field mapping at this site, and upstream towards the river capture site, would indicate that a similar "wave of incision" was also felt downstream of the river capture site (Stokes, *et al.*, 2002; Mather *et al.*, 2002). This is not surprising, considering that the river capture would have meant that the catchment area for the ancestral Río Aguas (i.e., the "Lower Aguas") increased dramatically. This would have led to an increase in the stream power (and therefore erosion potential) of the river. However, unlike the area immediately upstream of the river capture site, where the "wave of incision" led to the formation of river canyons, the geology of the downstream section has led to the formation of a slightly more open river system.

By using the geomorphological mapping results it is possible to construct a tentative landscape history for the landslides:

1. Dissection of the Gypsum Plateau and Góchar erosion surface by the formation of the ancestral Lower Aguas, accompanied by landslide activity (e.g., the proto-Cuesta Del Honor and Carrasco landslides).

2. The above dissection would have been driven by the differential uplift between the Sorbas and Vera Basins (Mather, 1991; Stokes, 1997; Mather *et al.*, 2001; Stokes *et al.*, 2002; Mather *et al.*, 2003).

3. The Río Aguas/Rambla Feos River Capture.

4. An increase in the gradient and stream power of the Río Aguas, leading to increased rates of drainage incision and slope erosion.

5. Incision of the Río Aguas and erosion of the gypsum escarpment to almost present locations.

6. The failure of the "Relict" landslide.

7. The formation/incision of the present gully through spring activity, that cuts through the "Relict" landslide.

8. The failure of the "Recent" landslide, further modifying the landscape and the geomorphological fingerprint of the "Relict" landslide.

9. The modification of the slopes by human activity in the area.

5.4   Chapter Summary

A number of case studies have been chosen from within the study area to highlight some of the findings from the aerial photographic interpretation, the field investigations and some of the results and observations that were described and discussed in the previous chapter. The examples all came from two parts of the study area – the area around the town of Sorbas and the area immediately upstream and downstream of the Rio Aguas/Rambla Feos Wind Gap (Figure 5.1). Both of these areas are within the part of the study area most greatly affected by the Rio Aguas/Rambla Feos River Capture and are presented here as a series of "type localities" that have highlighted:

- The effects of the Rio Aguas/Rambla Feos River Capture;

- The link between the geology, geomorphology and observed landslide activity;

- The factors controlling the landslide activity and how these vary across the study area depending on the geological and geomorphological setting;

- The range of landslide activity that is seen within the study area (styles, failure mechanisms and geomorphological setting);

- The diversity of landslide failure mechanisms, including rock fall, rock topple, high-angle rotational sliding, non-rotational sliding, and Sackung failures (Dikau *et al.*, 1996); and

- The interaction between landslide activity and the infrastructure and population of the study area.

The factors affecting slope instability in these example areas has been shown to be:

- Unloading of the canyon walls and valley side slopes (due to the incision of the drainage network);

- Discontinuities within the rock mass and their orientation;

- Flood events (usually occurring during intense periods of rainfall);

- Sub-surface groundwater flow;

- Weathering of the materials involved; and

- Construction activity in the area.

The examples presented in this chapter have also highlighted the relative ages of the landslide activity within the study area. This is:

1. Contemporary landslide activity;

2. Those that occurred after the Río Aguas/Rambla Feos River Capture and during the incision; and

3. Those that initiated before the Río Aguas/Rambla Feos River Capture.

The case studies that have been described and discussed in this chapter have shown how the evolution of part of the drainage system of the study area has affected slope stability. These examples have highlighted how a river capture occurring approximately 100,000 years BP led to a wave of incision passing through part of the Río Aguas and some of its tributaries leading to a dramatic increase in base level lowering and incision. The incision led to the formation of river canyons and over steepened slopes. It is on these slopes that the majority of the landslides mapped by this study have occurred.

The information that has been presented in this chapter has been combined with the results from the previous chapter covering the analysis of the landslide distribution and the information described and discussed in Chapter 2 concerning the geology and geomorphology of the study area to develop a ground model for the Río Aguas study area. This is presented in the following chapter.

Chapter 6 – The Río Aguas Geological Model & Summary

"... if you do not know what you should be looking for in a site investigation,

you are not likely to find much of value" – Glossop (1968)

6 The Río Aguas Ground Model

6.1 <u>Introduction</u>

One of the main aims of this research project has been to develop a geological and geomorphological ground model for the Río Aguas catchment area. The previous two chapters have described the results from this landslide investigation. Chapter 4 describes the results from the statistical analyses, highlighting those geological, geomorphological and morphological factors that appear to be significant in explaining the mapped landslide activity. In particular, this makes use of the terrain classification that is described in Section 3.2.3. Chapter 5 uses a number of case studies to highlight the link between the mapped landslide activity and the geological and geomorphological setting of the study area (outlined in Chapter 2) and, in particular, the role of the Río Aguas/Rambla Feos River Capture. The details contained in the case studies are derived from the aerial photographic interpretation and field work, plus the results of the statistical analyses. This chapter provides a conclusion to this work and has the following aims:

- To demonstrate how these observations and results have been used to develop a geological and geomorphological ground model for the Río Aguas catchment area;

- To highlight topics of ongoing and/or further areas of research, relating to the topics covered by this study; and

- To summarise the findings of this study.

6.2 Rationale for the Development of the Ground Model

The ground conditions at any site are a product of the geological and geomorphological history. Hutchinson (2001), in the fourth Glossop Lecture, described the geomorphology of any site as "precious and fragile, the end result of an interplay of thousands to millions of years between solid and Quaternary geology, hydrogeology, climate, process and the nature of the ground as controlled by its physical properties". Brunsden (2002), in the fifth Glossop Lecture, quoting Skempton (1953), Terzaghi & Peck (1967), Peck (1969), Legget (1977), Henkel (1982), Fookes (1997) and Fookes *et al.* (2000) argued that to understand any particular site we must attempt to consider the total geological and geomorphological history of any site, including the event magnitude/frequency relationships.

In the first Glossop Lecture, Fookes (1997) referred to this as developing a geological model for a site based on the "Total Geological History" of the site, and stated that it included stratigraphy, structural geology, former and current geomorphological processes and the past and present climatic conditions.

Fookes (1997) suggested that geological models provide a way to conceptualise the ground conditions of a site and to make predictions. A geological model should provide a framework for the raw data being used, and allow for the identification of patterns both within the landscape and the data. To develop such a model, practitioners will draw on experience and published case histories (Fookes *et al.*, 2000). A site specific geological model is essential to make sense of the total geological history and predict

how this will influence the engineering performance of a site during, and after, engineering works (Total Geology Website, 2001).

Fookes (1997) argued that such ground models were conceptual and not prescriptive. There is no model "model" and, to a certain degree, it should be site specific. It was suggested by Fookes (1997) that the model should comprise geological cross-sections with, or without, surface geological plans. Larger areas might have complex block models.

The strength of the ground model is in enabling predictions to be made or situations anticipated for which explanations need to be sought in the geological materials, geological structure and in the ancient and active geological and geomorphological processes in the area. It provides a rational basis for interpretation of the geology from understanding and correlation of observed geological features and exposures. It can also provide an indication of the potential variation in the properties of the soil and/or rock mass (Fookes, 1997).

The Fookes *et al.* (2000) paper and the subsequent "Total Geology" website (Total Geology Website, 2001) have proposed a number of different idealised models for a number of different geological and geomorphological settings. Their closest geomorphological model to the Río Aguas study area is for a "hot dry climate" (Figure 6.1). This model was based on observations from North Africa, the Middle East and parts of Arizona (Fookes *et al.*, 2000). The closest geological models defined by Fookes *et al.* (2000) for the Río Aguas study area are:

- Hot arid and hot wet climates (Figure 6.1; based on Selley, 1985; Tucker, 1991; Emery & Myers, 1997); and

- open folds and joints (Figure 6.1; based on Price & Cosgrove, 1990).

Recently, Delgado *et al.* (2003) developed a geotechnical ground model for the Segura River flood plain of SE Spain, using subsurface data. The investigation focused on the bearing capacity and liquefaction potential of the subsurface material. It did not however, investigate the geomorphological history of the area or the presence of other geological hazards.

Therefore, although none of these models match what is seen in the Río Aguas study area, they do provide an insight into some of the landforms and processes that are found in the study area. They can, therefore, provide a starting point for developing a more site specific ground model for the Río Aguas.

several to hundreds of kilometres

Diagram A

Screes and alluvial fans may coalesce to form bajada (a flat or low angle apron of alluvial fans)

Valley/wadi/nulla/arroyo, sides may be duricrusted

Canyon/slot/gorge

Piedmont or mountain foot

Talus fans formed by rockfall

Talluvial and colluvial fans formed by rockfall and debris flow from the escarpment

Seif dune

Barchan dune

Plateau surface duricrust or loose coarse debris

Prevailing wind direction

Accumulated debris forms the piedmont, may be duricrusted

Coarse alluvium deposited during flood events

Outwash plain of fine alluvium

Ablated alluvial plain possibly with young duricrusts

Gilgai (cracking plastic clays subject to shrink/swell)

Ephemeral stream courses

Pediment - erosion surface in bedrock below mountain front, forms a pediplain when covered with alluvium

Playa lake with very high evaporation, cyclical muds and evaporites. Controlled by base level of basin centre or sea level

Eroded remnants of old land surfaces with thick duricrusts developed

A

Diagram B

Old duricrust on plateau, commonly true "laterite" or bauxite deposits

Resistant rock type

Dambo (channeless valley or catchment depression)

Deeply weathered ridges

Monolithic bornhardt

Mudflow and sheet wash deposits

Several kilometres

Deep weathering profiles, half orange relief

Landslide/ debris flow/earthflow

Quaternary terrace, possibly with duricrusts developed

Deep gullying in colluvial pediment/alluvial terraces

Deep weathering profile with corestones developed in massive rocks and deep saprolite in less massive rocks beneath old land surfaces. Depth of weathering profile controlled in part by distribution of discontinuities.

Terrace deposits

Floodplain

Gullying and erosion of colluvial and taluvial slopes

B

Diagram C

Longitudinal
Strike joints
Extension joints
(b-c) joints

Transverse joints
Cross joints
Dip Joints
Extension joints
(a-c) joints

Tectonic axes used to describe joint sets, orientation of axes varies around the fold

Zone of tension - open joints

Metres to kilometres

Dip angle

Dip direction

Zone of compression - tight joints

Thrusts develop in thick flexured unit

Shear joints
Diagonal joints
Forming a conjugate set

Bedding plane or intraformational shear (bed over bed slip) reduces shear strength below peak values and possibly as low as residual values

Strike direction

C

A = Hot arid climate
B = Hot wet climate
C = Open folds and joints

Figure 6.1 - Three of the models from Fookes *et al* (2000) that help to explain some of the features seen in the Río Aguas study area.

6.3 The Río Aguas Ground Model

The synoptic ground model of the overall ground conditions for the Río Aguas study

area presented here includes:

- The landslide inventory (Appendix B);

- Chapter 2 – the descriptions of the geology and geomorphology of the study

  area;

- Chapters 4 and 5 – descriptions of the results and many of the landslides mapped

  in the study area;

- A series of summary tables describing the various parts of the study area;

- A series of photographs highlighting different parts of the study area;

- An annotated map showing the distribution of the Land System and other

  features; and

- A three-dimensional model of the study area.

The geomorphological setting and geomorphology of the study area were described in

Chapter Two. This included a description of the main landforms and processes that are

found in the study area. This information, and the results from the aerial photographic

interpretation, were used to develop a terrain classification scheme based on the concept

of Land Systems, Facets and Elements for the study area. This classification was then

refined through the fieldwork and field validation of the API results, with the final

scheme being described in Chapter 3 (Table 3.2). This scheme has now been modified

to take into account the results from the statistical analysis of the landslide inventory

presented in Chapter 4, as well as the field and API observations of the landslide

activity affecting the study area, many of which were presented in Chapter 5 (Table 6.1 and Figures 6.2 to 6.9).

The ground model presented here highlights:

- The relationship between the underlying geology, the geomorphology (based on the project derived terrain classification) and the landslide distribution;

- The link between the landslide distribution, the Río Aguas/Rambla Feos River Capture and the extent of the resulting wave of incision picked out by the nick points within the drainage system;

- The relationship between the Río Aguas and other major tributaries such as the Rambla de Los Castaños and the Río Jauto;

- Those "anomalies" within the landscape that could provide further information about individual landslides or the evolution of a particular part of the study area; and

- A summary of the main findings of this study.
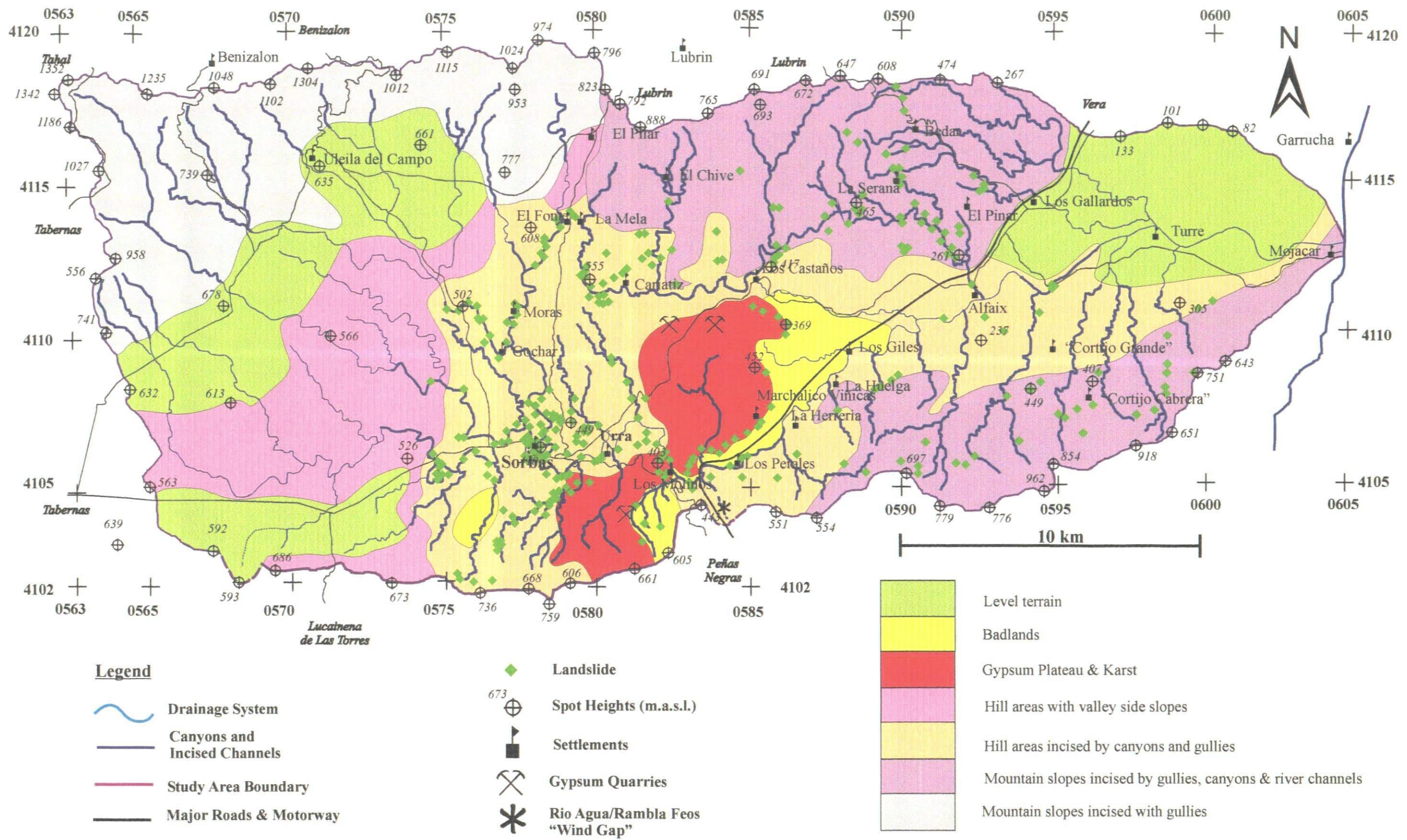
Figure 6.2 - The Ground Model map for the Río Aguas Catchment Study Area. This is based on the Land Systems map for the area and the landslide distribution.
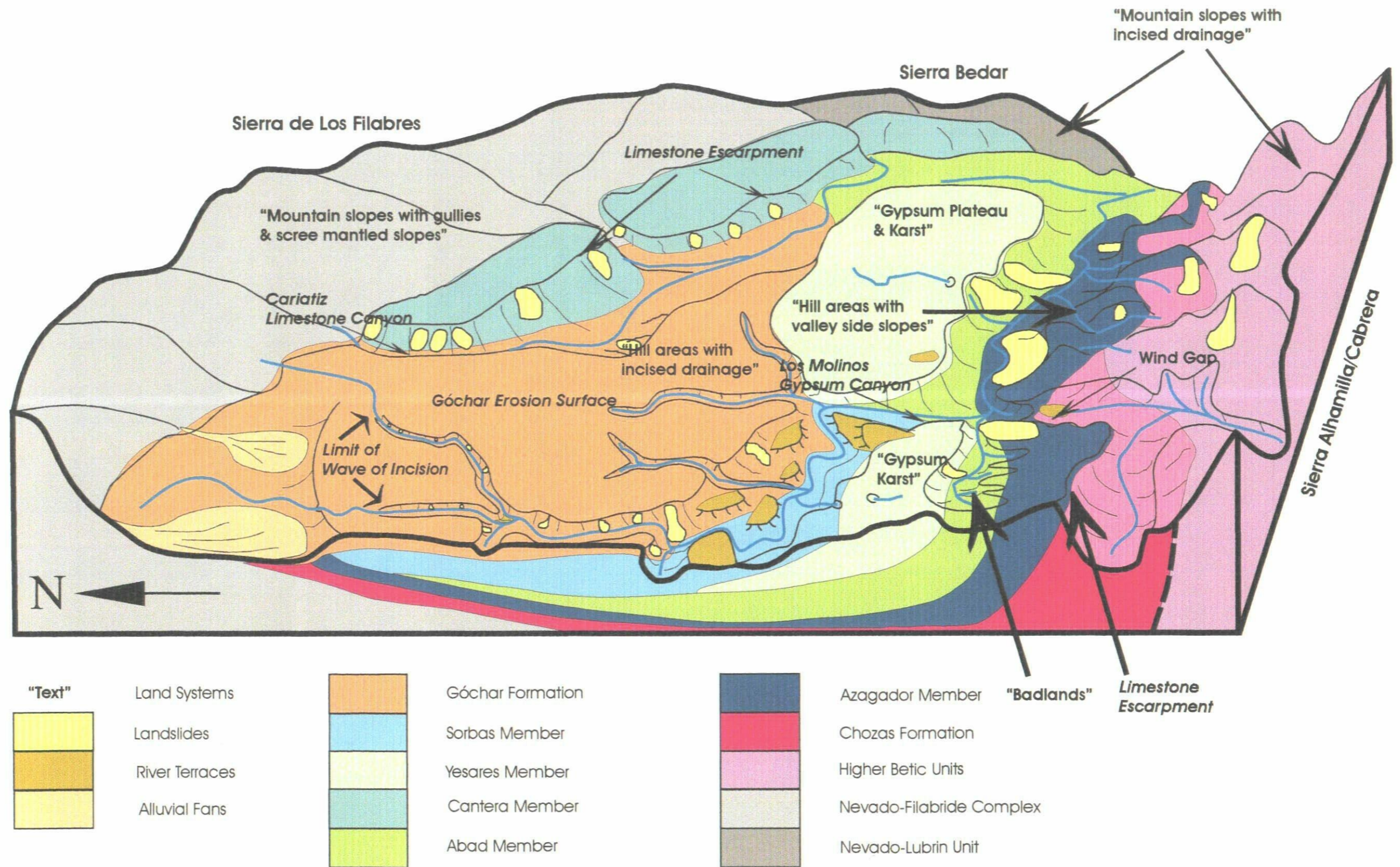
Figure 6.3 - Threee-dimensional Ground Model for the Río Aguas Catchment Area

Table 6.1 – Descriptions of the Ground Model units developed by this project for the Río Aguas Study Area, based on the terrain classification.

Land System	Location	Geology	Description	Landslide Activity	Fig. No.
Mountain slopes incised by gullies, canyons and river channels	Sierra Cabrera and Sierra Bédar	Basement Material (gneiss, mica schist, phyllite)	Steep mountain slopes, drainage channels are incised, narrow and steep, basin margin fault systems.	Rock falls and topples, as well as slope deterioration processes	6.4
Mountain slopes with gullies	Sierra Filabres	Basement Material (gneiss and mica schist)	Steep mountain slopes covered by scree material. Very little dissection of the drainage channels. Very steep slopes.	Rock falls and slope deterioration processes	6.5
Hill areas incised by canyons and gullies	The central western parts of the study area	Neogene sediments	Areas that have been incised by the drainage network. Characterised by steep sided gullies and canyons.	Rock falls and topples, with some high-angle rotational and non-rotational landslides	6.6
Hill areas with river valley side slopes	The central western parts of the study area away from the main drainage channels	Neogene Sediments	Areas with valley side slopes formed by the dissection of the drainage channel. Some gullies, but generally open side slopes	High-angle rotational and non-rotational landslides, translational landslides, as well as minor rock falls and topples	6.7

Table 6.1 (continued) – The Ground Model developed by this project for the Río Aguas Study Area.

Land System	Location	Geology	Description	Landslide Activity	Fig. No.
Gypsum Plateau and Karst	Central part of the study area	Yesares Member – gypsum interbedded with calcareous mudstone	Large area of level terrain. Very thin or no soil cover. Sparse vegetation cover. Characterised by dissolution features such as sinkholes, and cave systems, as well as other karstic features. The eastern edge of the plateau is marked by a distinctive escarpment.	Focused along the eastern escarpment. Characterised by high-angle rotational and non-rotational landslides, sagging and rock falls and topples.	6.8
Badlands	1. Between the Gypsum Plateau Land System and the Río Aguas 2. Barranco de Mocatán area	1. Abad Member 2. Zorreras and Góchar Formations	Typical "Badland" landscapes. Areas of high rates of erosion and dissection.	Predominantly affected by soil erosion and other "badland-type" processes. Landslide activity found in areas where badlands undercut stronger rock types.	6.9
Level Terrain	NE and SW parts of the study area, as well as areas below the Sierra Filabres	Neogene and Quaternary sediments	Relatively level terrain. Some parts of this area (i.e. central parts of Sorbas Basin) will relate to the Góchar erosion surface	No observed or mapped landslide activity	NA

Large rock fall and topple, in the area of one of the Vera Basin, basin margin faults.

A.
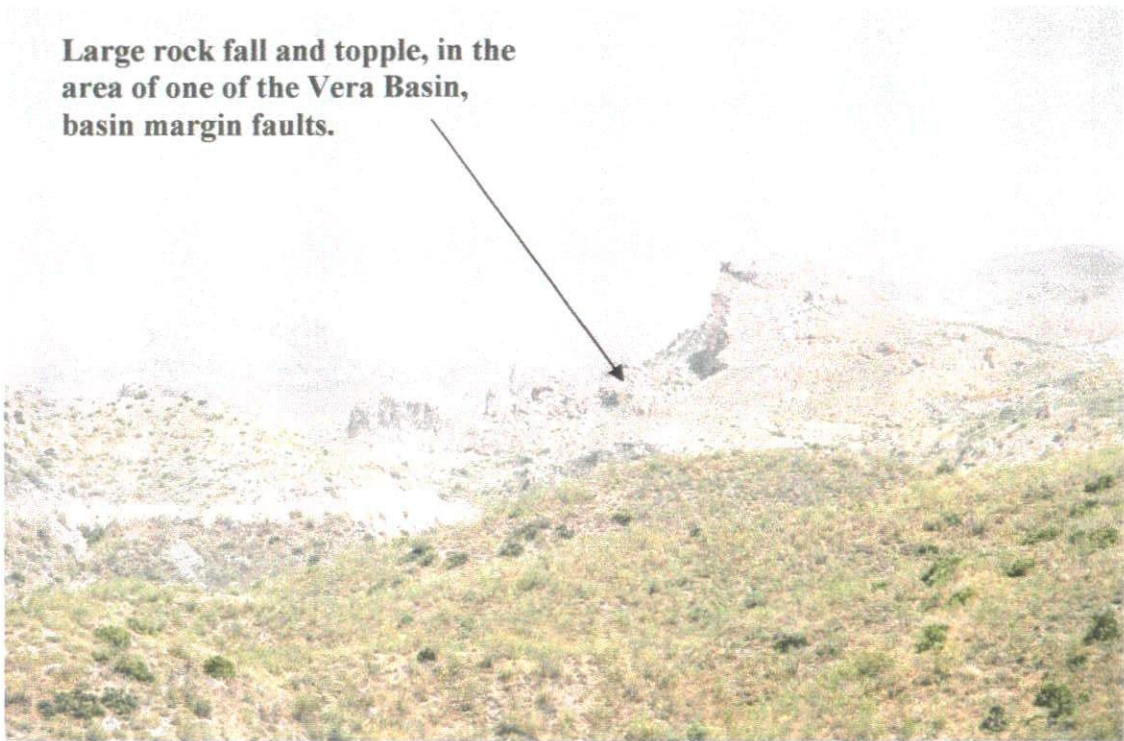
Large rock fall and topple, along the Río Jauto.
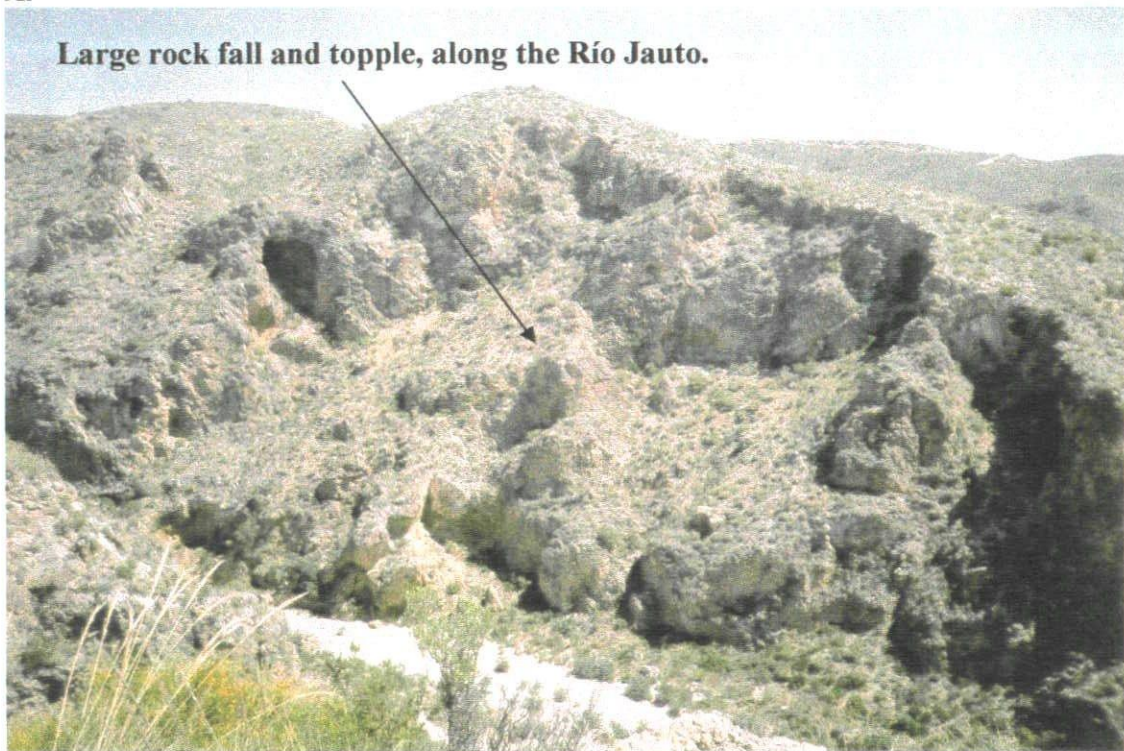
B.

Figure 6.4 – Landslides within the "mountain slopes with incised drainage" Land System. **A.** Landslides in mica schist (part of the Higher Betic Units) within the Sierra Cabrera (Grid Reference: 0594541077 / Facing east). **B.** Rock fall and topples in gneiss (part of the Higher Nevado-Filabrides Complex) within the Sierra Bédar (Grid Reference 0591541125 / Facing east).

"Mountain Slopes with gullies and scree-mantled slopes"

Sierra de Los Filabres

"Level Terrain (the "Góchar Erosion Surface")
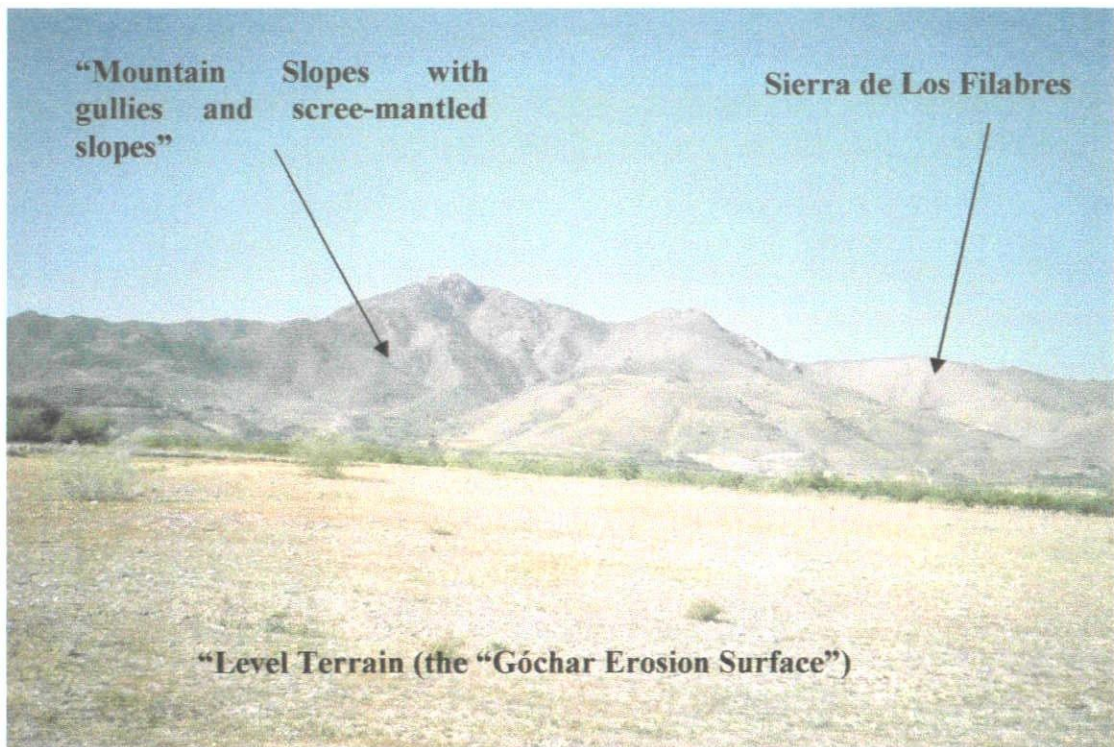
Figure 6.5 – The "Mountain slopes with gullies and scree-mantled slopes" Land System. The photograph is taken looking to the north from the roadside of the AL-813, approaching the village of Uleila del Campo. The highest peak in the picture is the "Ermita de la Virgen de la Cabeza" (1304 m above sea level). The slopes of this part of the Sierra de Los Filabres are formed from garnet mica schist of the Nevado-Lubrín Unit.
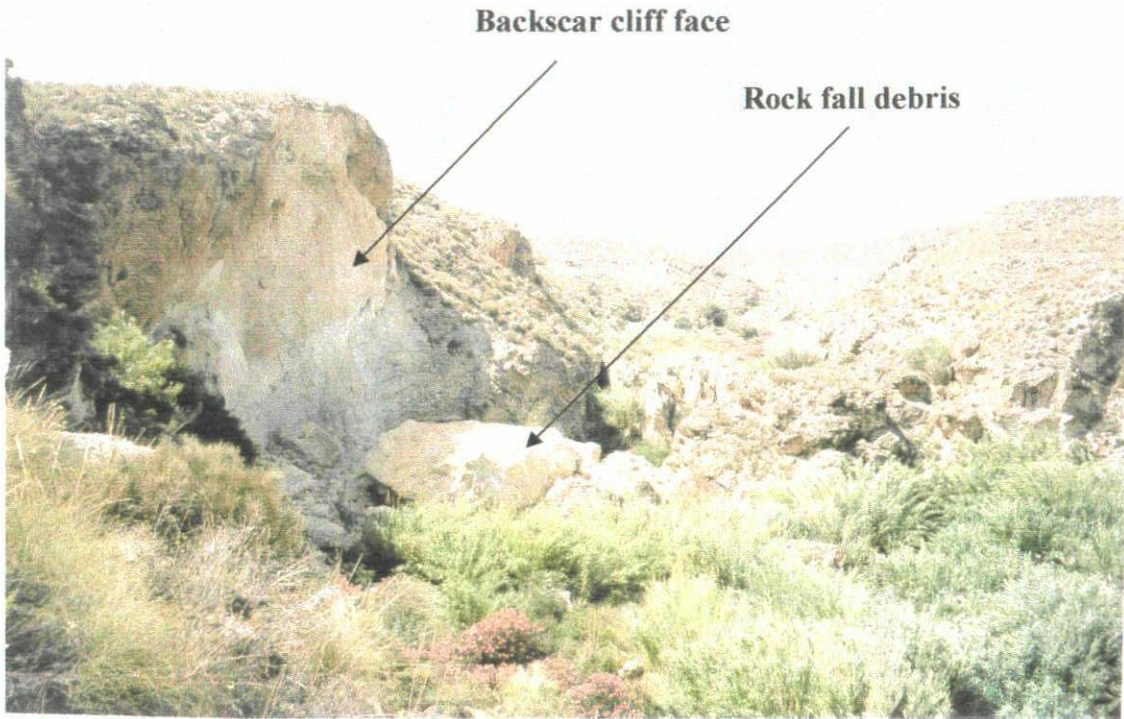
A.
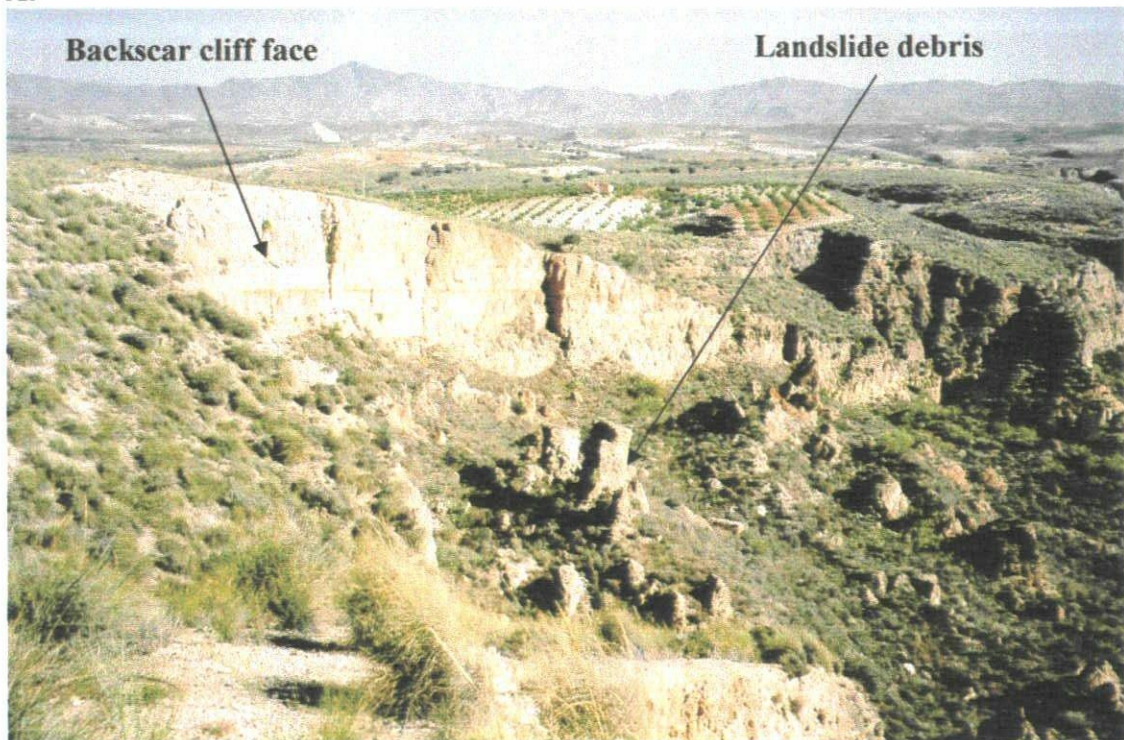
B.

Figure 6.6 – Landslides within the Land System "hill areas with incised drainage". **A.** Large rock fall just below a knick point in the Góchar Formation conglomerates and mudstone within the Rambla de Góchar (Grid Reference: 0576241106 / Facing north). The canyon is approximately 30m deep at this point. **B.** Non-rotational landslide within the Zorreras Member conglomerate and mudstone within the Barranco del Aguarón, near to Cortijo Urra (Grid Reference: 0579141074 / Facing north). The rambla has been incised approximately 30-40m below the surrounding countryside.

Translation landslide involving fine grained sediment sliding along the contact with underlying gypsum of the Yesares Member. Slope angle c. 30°.

Figure 6.7 – A translational landslide within the "Hill areas with valley side slopes" Land System. This landslide is located at "La Clauda" near to Cortijo Urra (Grid Reference: 0579541050 / Facing northeast from near to the farm "La Clauda").
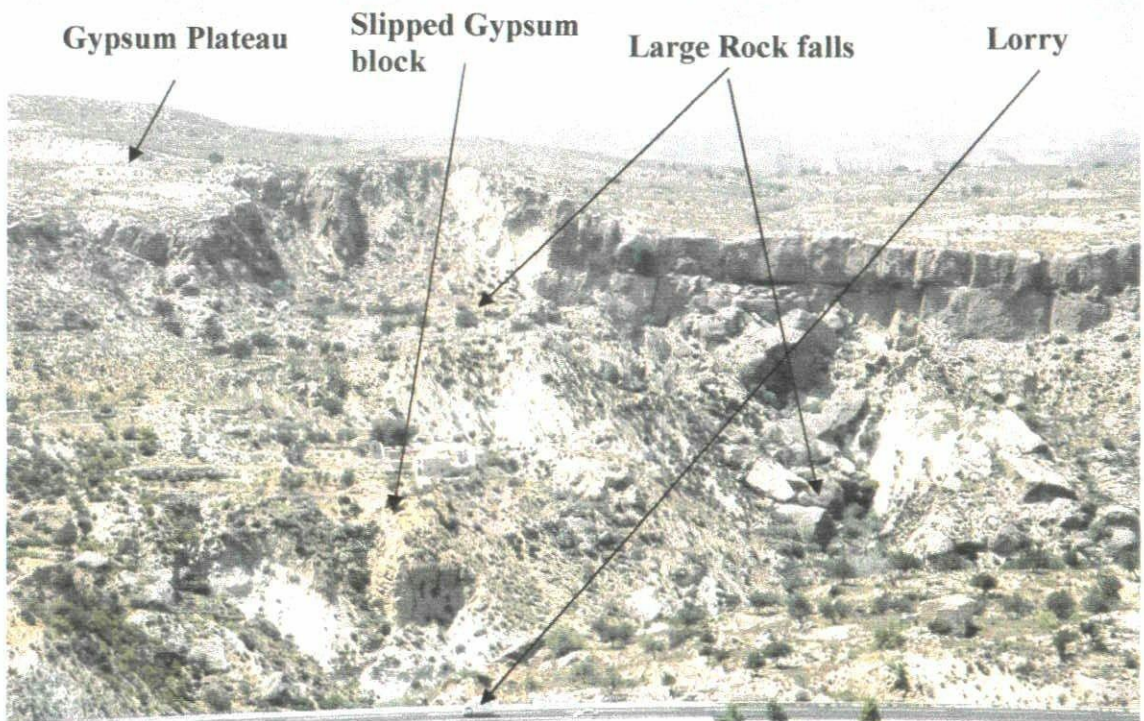
A.
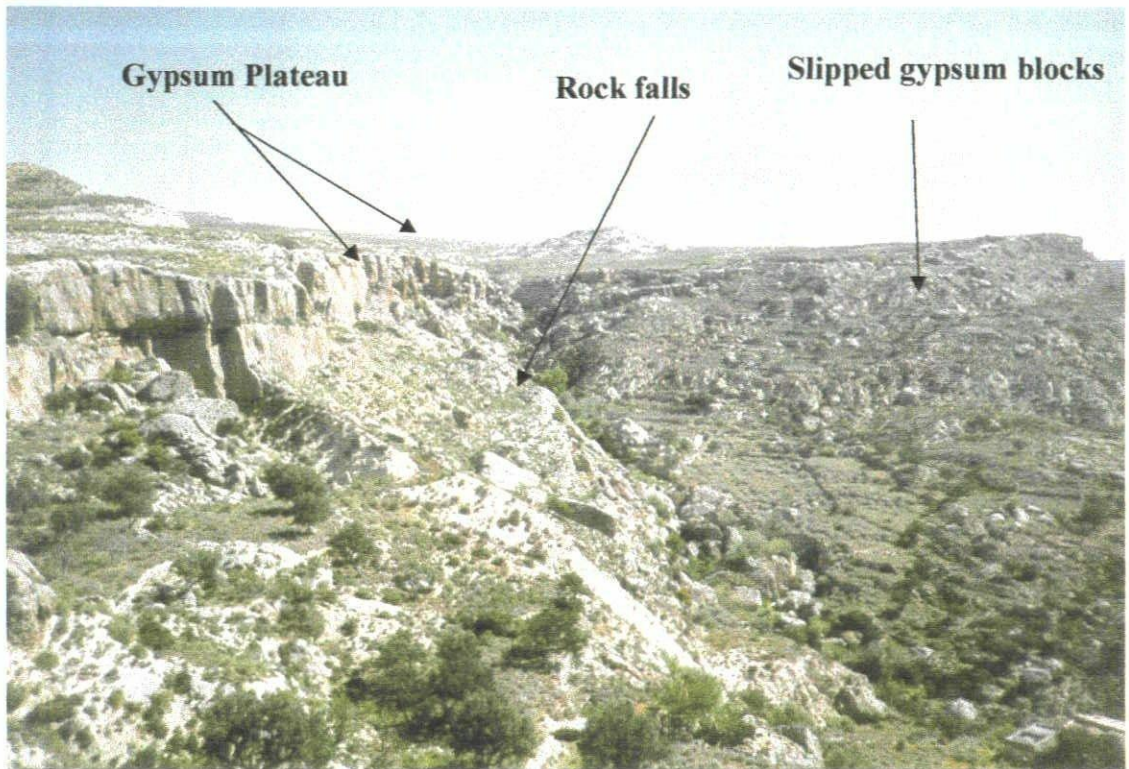
B.

Figure 6.8 – Landslides along the edge of the Land System "gypsum plateau and karst". **A.** Large scale rock falls and topples within the El Tesoro area (Grid Reference: 0583841054 / Facing northwest). **B.** Looking north-eastwards along the edge of the El Tesoro Gypsum Escarpment and the large scale failures within the bowl-shaped landscape (Grid Reference: 0583041057). .
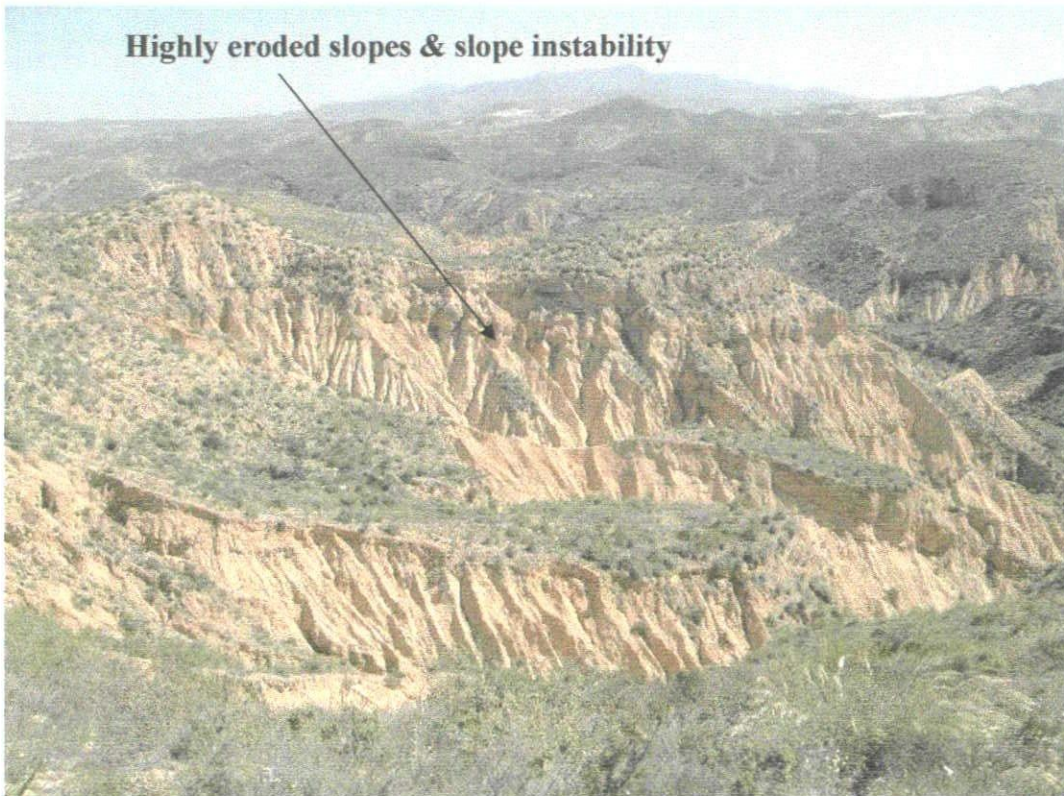
Figure 6.9 – Photograph of the Badlands at Mocatán near Sorbas. The area is heavily affected by soil erosion and dissolution features, often leading to small-scale slope instability (Grid Reference: 0576841036 / Facing east northeast along the Barranco de los Contreras).

6.4 <u>Summary</u>

As outlined in Section 1.5, the aims of this study have been to:

1.   Identify the types of landslide and landslide activity affecting the study area, including the main factors and controlling conditions that lead to the observed landslide activity.

2.   Investigate the link between the development of the drainage network, the Quaternary river terrace deposits, the landscape and the observed landslide activity.

3.   Develop a conceptual ground model for the Río Aguas catchment area, based on the desk study research, API, field observations and statistical analysis of the landslide inventory.

Most landslide investigations involve some form of landslide inventory database. Three such examples were discussed in Chapter 1. It was shown that these landslide inventories (often quoted as examples of "best practice") used either desk study sources or remotely sensed images (satellite data or aerial photographs) for the data collection and "High-tech" methods for the data analysis such as Geographical Information Systems (GIS). These studies have usually been undertaken without reference to a ground model for the area being considered (i.e., the landslides are almost studied in isolation from their geological and geomorphological setting) and were usually carried out in wet (monsoonal environments) with significant vegetation cover. These areas are often mountainous and/or heavily populated areas. The importance of developing and using a ground model for a given area was stressed in Section 6.2, when it was shown

that to understand any particular site, or landslide we must attempt to consider the total geological and geomorphological history of the site and the processes that have been active during that period. It was, therefore, noted that very few landslide inventory based projects have sought to use primary field mapping (in conjunction with remote sensing) and then to evaluate the data in its geological and geomorphological context, particularly in a relatively remote, arid environment.

This project has, therefore, sought to use the full range of land surface evaluation techniques to carry out a landslide investigation and develop both a landslide inventory and a geological and geomorphological ground model for the 425 km^2 catchment area for the Río Aguas. This is a relatively remote, rural and arid to semi-arid region of southeastern Spain. Although the geology and geomorphology of the area are well understood (as described in Chapter 2), the landslide activity of the area was less understood. Previous work had focused on the use of satellite image processing techniques for landslide mapping, rather than the landslides themselves.

The framework for the ground model was a project-derived terrain classification scheme based on the concept of Land Systems, Land Facets and Land Elements (Section 3.2). The ground model also broadly indicates areas of landslide susceptibility within the study area. The terrain classification and landslide inventory were both developed through a combination of aerial photographic interpretation and field mapping (Section 3.3). This methodology, in conjunction with the desk study, is regarded as the ideal way of developing any landslide inventory database or ground model.

The study area falls within the two Neogene sedimentary basins – the Sorbas and Vera Basins. The basin fill is a succession of marine calcareous mudstones, limestones, sandstones, conglomerates and gypsum. This is capped in a number of places by river terrace deposits. The northwestern and southeastern sections of the study area are bordered by Sierras composed of predominantly metamorphic rocks. The present drainage network was initiated during the Plio-Pleistocene and has incised through the sedimentary succession. This drainage network, which originally flowed southwards, has been modified by a number of river capture events.

One of these events (the Río Aguas/Rambla Feos River Capture approximately 100,000 years BP) has had a significant impact on the landscape in the south central part of the study area closest to the capture site. The river capture has led to:

- A relatively rapid drop in base level.

- An increase in the rate of incision, erosion and land surface lowering, especially in the areas closest to the river capture site.

- A wave of incision to pass through a section of the drainage network, leading to the over steepening of many of the valley sides slopes and formation of river canyons. The upstream extent of this wave of incision is picked out by a number of knick points. It is within the area affected by this wave of incision that the majority of the observed landslide activity is found.

It is this combination of events that has contributed to the majority of the landslide activity that is seen in the study area. Analysis of the landslide inventory database (described in Chapter 4 and summarised in Figure 6.10 and Tables 6.2 to 6.4) has shown that the landslide activity of the study area is closely controlled by the

underlying geology, geomorphological location and slope morphology of a particular site. The causes of individual landslides have been considered but due to the lack of exact dates and other historical information that has proven difficult. However, those factors that control the landslide activity of the study area have been considered and are summarised in Table 6.3.

Relative ages for the landslide activity can be estimated by comparing the spatial distribution of the landslides with the spatial distribution of a succession of Quaternary river terraces that have been mapped in the study area. These river terraces relate to the incision of the drainage network and described in detail in Sections 2.4 and 2.5. The link between the landslide distribution and the development of the landscape and drainage network has been described in Chapter 5. A number of "Landslide Type Localities" were also described. These were chosen to highlight the nature, variety and scale of the landslide activity that is seen within the parts of the Río Aguas catchment area most greatly affected by the Río Aguas/Rambla Foes River Capture described above and in previous chapters.

It is argued here, that to understand the landslide activity of the Río Aguas catchment area and be able to develop a working ground model for the area, one must understand the details of the underlying geology, the tectonic and structural setting of the region, the transition from marine to continental conditions and the formation and subsequent development of the drainage network. This approach is significant as:

- It has provided a working model for the assessment of landslide activity in the Río Aguas Catchment and will provide a valuable database for future infrastructure development; and

- The development of complex ground models is little understood, but the methodology is applicable world-wide (as suggested by Fookes, 1997 and Fookes *et al.*, 2000). The methodology developed here, for the Río Aguas Catchment Area, can therefore, be regarded as a pilot investigation (particularly, for an arid to semi-arid environment).

Of potential significance for the Río Aguas Catchment Area, the development of the ground model presented here has helped to identify;

- Clusters of landslides which are linked to changes or anomalies within the landscape or drainage network that may relate to geological or geomorphological processes such as faulting or river capture; and

- A lake deposit/river terrace (described in Section 5.3.1.4) that could provide further palaeontological, micropalaeontological, sedimentological and environmental information about that part of the study area and the development of the Río Aguas in the last 10,000 years.

0563 **0565** **0570** **0575** **0580** **0585** **0590** **0595** **0600** **0605**

4120

974
Benizalon
1024
1352 *1235* *1048* *1115* *796*
1342 *1304* *1012* Lubrin
1102 *953* *823* *691* *647* *608* *474*
1186 *792* *765* *672* *267*
888
1027 *661* El Pilar *693* Bedar *101* *82*
739 *777* *133* Garrucha
4115
635 El Chive La Seraña Los Gallardos
958 El Fonte La Mela *265* El Pinar Turre
556 *608* *555* *261* Mojacar
678 *417* Alfaix
502 Cariatiz Los Castaños *237* *305*
741 Moras *369* Los Giles "Cortijo Grande"
566 *452* La Huelga *407* *643*
4110 Gochar *449* "Cortijo Cabrera" *751*
632 *613* Marchalico Viñicas La Herreria *651*
526 Orra *854* *918*
Sorbas Los Perales *697* *962*
563 Los Molinos *779* *776*
4105 *605*
639 *551* *554* **0590** **0595**
592 *686* *668* *606* *661*
593 *673* *736* *759* *580* **4102**
4102
0563 **0565** **0570** **0575** **0580** **0585**

Legend

673 ⊕   **Spot Heights (m.a.s.l.)**

〰   **Drainage System**

───   **Major Roads & Motorway**

━━━   **Study Area Boundary**

▪   **Settlements**

⚒   **Gypsum Quarries**

✳   **Rio Agua/Rambla Feos "Wind Gap"**

◆   Landslides related to the incision of the drainage system after the Río Aguas/Rambla Feos River Capture

◆   Landslides originally associated with the initial incision prior to Río Aguas/Rambla Feos River Capture

◆   Landslides possibly relating to a river capture involving the Rambla de Los Castanos & Río Jauto - these landslides are still under investigation

Figure 6.10 - The Relationship between the landslide activity & the Drainage Network of the Study Area.

Table 6.2 – Summary of the results from this landslide investigation. The table shows those factors with the highest incidence of landslides, for each of the main factors considered by this study. All percentages are percentages of the total number of mapped landslides.

No. Landslides:	316
Size of Study Area:	425 km^2
Landslide Density:	Approximately 0.75 landslides/square km
Geological Unit:	Nevado-Filabride Complex = 16.8% / Sorbas Member = 15.5% Góchar Formation = 12.3% / Azagador Member = 9.5%
Rock Types:	Conglomerate = 14.6% / Limestone = 13.9% / Mica Schist = 10.4% / Sandstone = 10.1%
Landslide Mechanism:	Rock falls and topples = 66.8% Non-rotational Landslides = 21.2%
Landslide Activity	
State of Landslide Activity:	Dormant = c.80% ("a landslide that has not moved for more than one annual cycle of seasons, but where the causes of movement apparently remain" – WP/WLI, 1993)
Style of Landslide Activity:	Multiple = 80% (a landslide that exhibits "repeated development of the same type of movement along the same rupture surface and involving the same displaced material" – WP/WLI, 1993).
Distribution of Landslide Activity:	Retrogressing = 75% ("a landslide where the rupture surface is extending in the direction opposite to the movement of the displaced material" – WP/WLI, 1993).
Landslide Factor Analysis	
Slope Angle & Mechanism:	• Falls & Topples & Non-rotational Landslides = increasing landslide incidence with slope angle • Translational Landslides = highest landslide incidence on moderately steep slopes • "Other" Landslides = Highest landslide incidence on very steep slopes
Slope Angle & Rock Type:	• The highest incidence of landslides involving conglomerate, sandstone, limestone and schist occur on slopes > 60°. • For landslides involving gneiss the slope angle is >45° • For landslides involving gypsum overlying mudstone the highest incidence is on slopes >75°

Table 6.3 – Summary of the results from the analysis of landslides causative factors. All percentages are percentages of the total number of mapped landslides.

Landslide Causes	
Geological Factors:	These factors were identifiable in the field: • jointed or fissured material; • adversely orientated mass discontinuities (bedding, cleavage, faults or unconformities); • contrasts in permeability and its effects on groundwater; • alternating sequences of "hard rocks" over "soft rocks"; and • contrasts in stiffness (stiff, dense material over plastic material).
Morphological Factors:	These factors were inferred from field observations or eye-witness accounts: • tectonic uplift of the study area; • fluvial erosion of many of the slopes; • subterranean erosion through piping and dissolution features (Figure 4.45); and • vegetation removal (by erosion, forest fire or drought).
Physical Factors:	Insufficient detailed information and no dated landslides to allow for a full investigation of these factors. However, these factors were inferred from field observations or eye-witness accounts: • Intense, short period rainfall; and • Shrink and swell weathering of expansive soils and clays are important.
Human Factors:	These factors were inferred from field observations or eye-witness accounts: • excavation of slopes; • loading of the slope or at its crest; • defective maintenance or leaking of service pipes; • vegetation cover removal (deforestation); and • quarrying.

Table 6.4 – Summary of the results from the statistical analysis of the number of landslides occurring in the different combinations of geology, terrain classification and landslide failure mechanism considered by the project.

Geomorphology	Geomorphology & Mechanism	Geomorphology & Lithology	Geomorphology, Lithology & Mechanism
• Hill areas with incised drainage channels • Incised drainage channels with river terraces • Outside meanders of active drainage channels • 12.0% of the mapped landslides (38 landslides)	• Hill areas with incised drainage channels • Incised drainage channels with river terraces • Outside meanders of active drainage channels • Rock Falls and Topples • 7.6% of the mapped landslides (24 landslides)	• Mountain slopes incised by gullies, canyons and river channels • Hill and mountain area • Ridge crests • Basement material (Mica schist, gneiss, phyllite) • 4.7% of the mapped landslides (15 landslides)	• Mountain slopes incised by gullies, canyons and river channels • Hill and mountain area • Ridge crests • Basement Material (Mica schist, gneiss, phyllite) • Rock Falls and Topples • 4.7% of the mapped landslides (15 landslides)
• Hill areas with incised drainage channels • Incised drainage channels without river terraces • Outside meanders of active drainage channels • 7.0% of the mapped landslides (22 landslides)	• Mountain slopes incised by gullies, canyons and river channels • Hill and mountain area • Ridge crests • Rock Falls and Topples • 7.0% of the mapped landslides (22 landslides)	• Mountain slopes incised by gullies, canyons and river channels • Incised drainage channels with river terraces • Canyons side slopes • Mica schist • 4.7% of the mapped landslides (15 landslides)	• Mountain slopes incised by gullies, canyons and river channels • Incised drainage channels with river terraces • Canyons side slopes • Rock Falls and Topples • Mica Schist • 4.7% of the mapped landslides (15 landslides)
• Mountain slopes incised by gullies, canyons and river channels • Hill and mountain area • Ridge crests • 7.0% of the mapped landslides (22 landslides)	• Hill areas with incised drainage channels • Incised drainage channels with river terraces • Dip-slope escarpments • Rock Falls and Topples • 6.0% of the mapped landslides (19 landslides)	• Hill areas with incised drainage channels • Incised drainage channels with river terraces • Scarp-slope escarpments • Gypsum overlying calcareous mudstone • 3.8% of the mapped landslides (12 landslides)	• Hill areas with incised drainage channels • Incised drainage channels with river terraces • Scarp-slope escarpments • Gypsum overlying calcareous mudstone • "Other" – complex combination of mechanisms • 3.8% of the mapped landslides (12 landslides)

Geomorphology	Geomorphology & Mechanism	Geomorphology & Lithology	Geomorphology, Lithology & Mechanism
• Hill areas with incised drainage channels • Incised drainage channels with river terraces • Dip-slope escarpments • 6.6% of the mapped landslides (21 landslides)	• Mountain slopes incised by gullies, canyons and river channels • Incised drainage channels with river terraces • Canyons side slopes • Rock Falls and Topples • 5.4% of the mapped landslides (17 landslides)	• Hill areas with incised drainage channels • Incised drainage channels with river terraces • Outside meanders of active drainage channels • Conglomerate • 3.2% of the mapped landslides (10 landslides)	• Hill areas with incised drainage channels • Incised drainage channels with river terraces • Outside meanders of active drainage channels • Conglomerate • Rock Falls and Topples • 3.2% of the mapped landslides (10 landslides)
• Mountain slopes incised by gullies, canyons and river channels • Incised drainage channels with river terraces • Canyons side slopes • 5.4% of the mapped landslides (17 landslides)	• Hill areas with incised drainage channels • Incised drainage channels with river terraces • Scarp-slope escarpments • "Other" – complex combination of mechanisms • 4.1% of the mapped landslides (13 landslides)	• Gypsum plateau and karst • River valley formed by the dissection of the drainage system • Scarp-slope escarpment • Gypsum overlying calcareous mudstone • 2.5% of the mapped landslides (8 landslides)	• Gypsum plateau and karst • River valley formed by the dissection of the drainage system • Scarp-slope escarpment • Gypsum overlying calcareous mudstone • "Other" – complex combination of mechanisms • 2.5% of the mapped landslides (8 landslides)
• Hill areas with incised drainage channels • Incised drainage channels with river terraces • Scarp-slope escarpments • 5.4% of the mapped landslides (17 landslides)	• Hill areas with incised drainage channels • Incised drainage channels without river terraces • Outside meanders of active drainage channels • Non-rotational Landslides • 4.1% of the mapped landslides (13 landslides)	• Hill areas with incised drainage channels • Incised drainage channels with river terraces • Outside meanders of active drainage channels • Limestone and calcareous mudstone • 2.5% of the mapped landslides (8 landslides)	

6.5 Further Research

The purpose of the ground model developed by this project is to provide information about the geology and geomorphology of the study area, with specific reference to the landslide activity. The intention is that the ground model can continue to be refined as our understanding of the study area and the landslide activity increases. This would be through ongoing research into the different aspects of the geology and geomorphology of the study area, as well as through further field work, continued monitoring of the known landslides or unstable areas and additional remote sensing interpretation and interpretation.

One further development of the study that will be required is the use of a Geographical Information System (GIS). However, the GIS approach requires a large amount of accurate and detailed data to be effective and a substantial investment of time for data input. At the start of this project no digital data were available, which if a GIS approach had been adopted at the onset would have meant a considerable amount of time spent digitising all of the required data. There were also gaps in the published map data at scales larger than 1:50,000. However, digital contour data have now become available and as a continuation of this project the data could be used in conjunction with the results from this study to develop a GIS database. This would combine contour (and therefore slope data) with the geological, geomorphological and landslide information obtained during this research. It was, however, beyond the scope of this current project.

A few researchers have looked at using satellite imagery to investigate the landslide activity in the study area (i.e., Eyres *et al.*, 1998; Davies *et al.*, 2000). However, this

has mainly focused on using Landsat ETM data and ATM data, and in particular how it can be processed. With recent developments in high resolution satellite imagery (LRA Project, 2001, 2002, 2003; Petley *et al.*, 2003), this work could be developed much further within the Río Aguas study area.

This research project has, therefore, identified a number of areas where further research is needed. Within the study area, potential topics for further research are:

1. To continue to build and develop the landslide inventory for the study area (and thereby develop a longer-term view of the landslide activity in the study area).

2. To continue to assess those factors that are the most relevant in explaining the mapped landslide activity, including relict features such as the one described by Mather *et al.*, (2003).

3. To continue observing some of the landslide sites described in Section 5, to provide longer-term information on the development of these sites and their "life-time" in the landscape.

4. To obtain dates for as many of the river terrace levels as possible and establishing the Holocene phases of landslide history, as well as confirm the phases of incision and aggradation.

5. To continue to develop the ground model for the study area.

6. Development of the existing ground model to include other potential or existing hazards such as piping, soil erosion, soil liquefaction, rainfall activity and/or seismic activity.

7. Inclusion of subsurface data to develop a geotechnical aspect to the ground model (and therefore help in the inclusion of some of the potential hazards listed above);

8. Development of further ground models for neighbouring areas to gain a better understanding of the observed landslide activity and ground conditions in this region of SE Spain.

9. To undertake a detailed geotechnical investigation of some of the landslide sites described in Section 5.

10. To evaluate the role of the Quaternary climate changes on the development of the Río Aguas and the development on the present landscape and the observed landslide activity.

11. To investigate the development of the Rambla de Los Castaños and Río Jauto in the northern parts of the study area (this part of the drainage system developed separately from the bulk of the Río Aguas catchment area and was therefore unaffected by the Río Aguas/Rambla Feos river capture).

12. To investigate the development of the observed landslide activity in relation to the basin margin fault systems along the northern flanks of the Sierra Cabrera (this area has been extensively affected by landslide activity, faulting and thermal alteration of the underlying geology).

13. To further investigate the relict landslide features in the landscape and the information that they provide regarding the landscape and the processes acting on that landscape.

14. To further investigate the "anomalous outcrop" near Los Molinos including detailed micropalaeontological and palynological study of the outcrop's succession; possible carbon dating of the organic material that was found in the anomalous outcrop (landslide related geomorphological deposit in the Los Molinos Valley).

15. To refine the use and effectiveness of applying the angle of reach and the various geometric ratios for assessing the mobility and potential run-out length of potential landslides.

16. To develop a Geographical Information System (GIS) for the study area, containing data on the topography, geology, structural geology, engineering geology, geomorphology, terrain classification, landslide distribution, as well as any other available information and data (i.e., rainfall, seismic activity).

17. To use a GIS to investigate the spatial relationships between the landslide activity and the factors held within the database. Such investigations have been carried out in a number of different countries and geological/geomorphological settings, and the Río Aguas study area would make a good comparison.

18. To use the landslide inventory (and any GIS database that is developed) to carry out a complete landslide susceptibility, hazard and risk assessment of the study area.

19. To further investigate the relationships between landslide volume, runout and angle of reach for the Río Aguas landslides, comparing it with other similar studies. Such data could possibly be used to develop predictive runout models for any future landslides in the study area or other similar environments.

20. To apply and test the techniques described here in other parts of the region and other environments. These techniques should be directly applicable.

Chapter 7 – References

"...but there are just so many books...."

- A librarian at the University of Plymouth (2002).

Alcàntara-Ayala, I. & Thornes, J.B., 1996a. The environmental dimensions of mass failure in semi-arid Spain. In: Senneset, K. (Ed.), *Landslides, Glissements de Terrain, Proceedings of the 7ᵗʰ International Symposium on Landslides*, A.A. Balkema, Rotterdam, **3**, 1837-1842.

Alcàntara-Ayala, I. & Thornes, J.B., 1996b. Structure and hydrology in controlling mass failure in space and time: The case of the Guadalfeo failures. In: Chacón, J., Irigaray, C. & Fernández, T. (eds), *Landslides: Proceedings of the 8ᵗʰ International Conference and Field Trip on Landslides*, Granada, Spain 27ᵗʰ-28ᵗʰ September 1996, A.A. Balkema, Rotterdam, 89-96.

Aleotti, P. & Chowdhury, R., 1999. Landslide hazard assessment: summary review and new perspectives. *Bulletin of Engineering Geology and the Environment*, **58**, 21-44.

Alexander, E.D., 1989. Urban landslides. *Progress in Physical Geography*, **13**, 157-191.

Alexander, D., 1993. *Natural Disaster*. University College London Press, London, 632pp.

Alexander, R.W., Harvey, A.M., Calvo, A., James, P.A. & Cerda, A., 1994. Natural stabilisation mechanisms on badland slopes: Tabernas, Almería, Spain. In: Millington, A.C. & Pye, K. (eds), *Environmental Change in Drylands: Biogeographical and Geomorphological Perspectives*. Wiley, Chichester, 85-111.

Alexander, R.W., Spivey, D.B., Faulkner, H. & Willshaw, K., 1999. Badland morphology and geoecology: Mocatán system: Processes and patterns. In: Mather, A.E. & Stokes, M. (eds), *BSRG/BGRG SE Spain Field Meeting Guide Book*, University of Plymouth, England, 134-151.

Allum, J.A.E., 1982. *Photogeology and regional mapping.* Pergamon Press Ltd, Oxford, 111pp.

Alvado, J.C., 1986. *Sédimentation, déformation, et manifestations magmatiques néogènes associées au couloir de décrochement de Palomares: Bassin de Vera (Sud-Est de l'Espagne).* PhD. Thesis, Université Pierre et Marie Curie, Paris, 240pp.

Amor, J.M. & Florschutz, F., 1964. Results of the preliminary palynological investigation of samples from a 50-m boring in Southern Spain. *Boletin Real Sociedad Español de Historia Natural (Geologica)*, **62**, 251-255.

Anon, 1972. The preparation of maps and plans in terms of engineering geology: Geological Society Engineering Group Working Party. *Quarterly Journal of Engineering Geology*, **5**, 293-382.

Anon, 1982. Land surface evaluation for engineering practice. Report by a Working Party under the auspices of the Geological Society. *Quarterly Journal of Engineering Geology*, **15**, 265-316.

Bakker, H.E., De Jong, K., Helmers, H. & Biermann, C., 1989. The geodynamic evolution of the Internal Zone of the Betic Cordilleras (south-east Spain): a model based on structural analysis and geothermobarometry. *Journal of Metamorphic Geology*, **7**, 359-381.

Baggley, K.A., 2000. The late Tortonian-Early Messinian foraminiferal record of the Abad Member (Turre Formation), Sorbas Basin, Almería, South-east Spain. *Palaeontology*, **43**, 1069-1112.

Barnes, J.W., 1981. *Basic Geological Mapping.* Geological Society of London Handbook Series, **1**. Open University Press, London, 112pp.

Barragán, G., 1997. *Evolución geodinámica de la Depresión de Vera. Provincia de Almería. Cordilleras Béticas.* Unpublished PhD. Thesis, Universidad de Granada, Spain.

Begin, Z.B., 1988. Application of a diffusion-erosion model to alluvial channels which degrade due to base level lowering. *Earth Surface Processes and Landforms*, **13**, 487-500.

Begin, Z.B., Meyer, D.F. & Schumm, S.A., 1981. Development of longitudinal profiles of alluvial channels in response to base-level lowering. *Earth Surface Processes and Landforms*, **6**, 49-68.

Bell, F.G., 1993. *Engineering Geology*, Blackwell Science Ltd, Oxford. 359pp.

Berrisford, M.S. & Matthews, J.A., 1997. Phases of enhanced rapid mass movement and climatic variation during the Holocene: a synthesis. In: Matthews, J.A., Brunsden, D., Frenzel, B., Gläser, B & Weiß (eds), *Rapid mass movement as a source of climatic evidence for the Holocene*, European Science Foundation project "European palaeoclimate and man, **Special Issue No. 12**. Gustav Fischer Verlag, Stuttgart, 409-440

Bicker, R.J., 1966. *Geological investigations in the region west of Antas and Cuevas del Almanzora, south-eastern Spain*. Unpublished PhD Thesis, Municipal University, Amsterdam. 124pp.

Biermann, C., 1995. The Betic Cordilleras SE Spain. Anatomy of a dualistic collision-type orogenic belt. *Geologie en Mijnbouw*, **74**, 167-182.

Biju-Duval, B., Dercourt, J. & Le Pinchon, X., 1977. From the Tethys to the Mediterranean Seas: a plate tectonic model of the evolution of the western Alpine system. In: Biju-Duval, B. & Montadert, L. (eds), *Structural History of the Mediterranean Basin*. Technical Report, Paris, 143-164.

Braga, J.C. & Martín, J.M., 1996. Geometries of reef advance in response to relative sea-level changes in a Messinian (uppermost Miocene) fringing reef (Cariatiz reef, Sorbas Basin, SE Spain). *Sedimentary Geology*, **107**, 61-81.

Braga, J.C., Martín, J.M. & Wood, J.L., 2001. Submarine lobes and feeder channels of redeposited, temperate carbonate and mixed siliciclastic-carbonate platform deposits (Vera Basin, Almería, southern Spain). *Sedimentology*, **48**, 99-116.

Braga, J.C., Martín, J.M. & Quesada, C., 2003. Patterns and average rates of late Neogene-Recent uplift of the Betic Cordillera, SE Spain. *Geomorphology*, **50**, 3-26.

Brook, D., 1992. Department of the Environment research on geological hazards. *Geoscientist*, **2**, 44. [Abstract of papaer presented to the Engineering Group of the Geological Society meeting on Hazards to Development in Great Britain, March 1992.]

Brouwer, H.A., 1926a. Zur geologie der Sierra Nevada. *Geologische Rundschau*, 17, 118-137.

Brouwer, H.A., 1926b. Zur tektonik der betischen Kordilleren. *Geologische Rundschau*, 17, 332-336.

Brunsden, D., 1993. Mass movement; the research frontier and beyond: a geomorphological approach. *Geomorphology*, 7, 85-128.

Brunsden, D., 2001. A critical assessment of the sensitivity concept in geomorphology. *Catena*, 42, 99-123.

Brunsden, D., 2002. The Fifth Glossop Lecture: Geomorphological roulette for engineers and planners: some insights into an old game. *Quarterly Journal of Engineering Geology and Hydrogeology*, 35, 101-142.

Brunsden, D. & Thornes, J.B., 1979. Landscape sensitivity and change. *Institute of British Geographers, Transactions New Series*, 4, 463-484.

Brunsden, D. & Ibsen, M.-L., 1997. The temporal occurrence and forecasting of landslides in the European Community: summary of relevant results of the European Community EPOCH Programme. In: Matthews, J.A., Brunsden, D., Frenzel, B., Gläser, B. & Weiß, M.M. (eds), *Rapid mass movement as a source of climatic evidence for the Holocene*, Paläoklimaforschung 19 Gustav Fischer Verlag, Stuttgart, 401-407.

Brunsden, D., Doornkamp, J.C., Fookes, P.G., Jones, D.K.C. & Kelly, J.M.H., 1975. Large scale geomorphological mapping and highway engineering design. *Quarterly Journal of Engineering Geology*, 8, 227-253.

Brunsden, D., Ibsen, M.-L., Bromhead, E. & Collison, A., 1996a. Final national report, King's College London. In: Dikau, R., Schrott, L., Dehn, M., Hennrich, K. & Rasemann, S. (eds), *The temporal stability and activity of landslides in Europe with respect to climatic change (Project TESLEC)*. Final report, Part II, National reports. European Community. CEC. Environment Programme, Brussels. EV5V-CT94-0454. 309-408.

Brunsden, D., Coome, K., Goudie, S. & Parker, A.G., 1996b. The structural geomorphology of the Isle of Portland, southern England. *Proceedings of the Geologists' Association*, 107, 209-230.

BS5930, 1990. *Code of Practice for Site Investigations*. British Standards Institution, London.

Bull, W.B., 1988. *Marine-terrace survey near Mojacar, Spain*. Unpublished survey report BGRG, SE Spain Field Excursion.

Butzer, K.W., 1964. Climatic-geomorphologic interpretation of Pleistocene sediments in the Eurafrican sub tropics. In: Howell, F.C. & Bourliere, F. (eds), *African Ecology and Human Evolution*, Methuen, London, 1-25.

Calaforra, J.M., 1996. Some examples of gypsum karren. In: Fornós, J.J. & Ginés, A. (eds), *Karren Landforms*, University of Balearic Islands, Mallorca, 253-260.

Calaforra, J.M. & Pulido-Bosch, A., 1997. Peculiar landforms in the gypsum karst of Sorbas (Southeast Spain). *Carbonates and Evaporites*, 12, 110-116.

Calaforra, J.M. & Pulido-Bosch, A., 2003. Evolution of the gypsum karst of Sorbas (SE Spain). *Geomorphology*, 50, 173-180.

Calvo-Cases, A., Harvey, A.M. & Paya-Serrano, J., 1991. Process interactions and badland development in SE Spain. In: Sala, M., Rubio, J.L. & Garcia-Ruiz, J.M. (eds), *Soil Erosion Studies in Spain*, Geoforma Ediciones, Logroño, Spain, 75-90.

Candy, I., Black, S., Sellwood, B.W. & Rowan, J.S., 2003. Calcrete profile development in Quaternary alluvial sequences, southeast Spain: Implications for using calcretes as a basis for landform chronologies. *Earth Surface Processes & Landforms*, 28, 169-185.

Canton, Y., Domingo, F., Sole-Benet, A. & Puigdefabregas, J., 2001. Hydrological and erosion response of a badlands system in semiarid SE Spain. *Journal of Hydrology*, 252, 65-84.

Carrara, A., Cardinali, M., Detti, .R, Guzzetti, F., Pasqui, V. & Reichenbach, P., 1991. GIS techniques and statistical models in evaluating landslide hazard. *Earth Surface Processes and Landforms*, 16, 427-445.

Carrara, A., Guzzetti, F., Cardinali, M. & Reichenbach, P., 1999. Use of GIS technology in the prediction and monitoring of landslide hazard. *Natural Hazards*, 20, 117-135.

Carrión, J.S., 1992a. Late Quaternary pollen sequence from Carihuela Cave, Southeastern Spain. *Review of Palaeobotany and Palynology*, 71, 37-77.

Carrión, J.S., 1992b. A palaeoecological study in the western Mediterranean area. The Upper Pleistocene pollen record from Cova Beneito (Alicante, Spain). *Palaeogeography, Palaeoclimatology, Palaeoecology*, 92, 1-14.

Carrión, J.S. & Dupre, M., 1996. Late Quaternary vegetational history at Navarres, Eastern Spain. A two core approach. *New Phytology*, 134, 177-191.

Carrión, J.S. & Van Geel, B., 1999. Fine-resolution Upper Weichselian and Holocene palynological record from Navarres (Valencia, Spain) and discussion about factors of Mediterranean forest succession. *Review of Palaeobotany and Palynology*, 106, 209-236.

Carrión, J.S., Munuera, M. & Navarro, C., 1998. The palaeoenvironment of Carhuela Cave (Granada, Spain): a reconstruction on the basis of palynological investigations of cave sediments. *Review of Palaeobotany and Palynology*, 99, 317-340.

Carrión, J.S., Munuera, M., Navarro, C., Burjachs, F., Dupre, M. & Walker, M.J., 1999. The palaeoecological potential of pollen records in caves: the case of Mediterranean Spain. *Quaternary Science Reviews*, 18, 1061-1073.

Carrión, J.S., Navarro, C., Navarro, J. & Munuera, M., 2000. The distribution of cluster pine (*Pinus pinaster*) in Spain as derived from palaeoecological data: relationships with phytosociological classification. *The Holocene*, 10, 243-252.

Carrión, J.S., Andrade, A., Bennet, K.D., Navarro, C. & Munuera, M., 2001. Crossing forest thresholds: inertia and collapse in a Holocene sequence from south-central Spain. *The Holocene*, 11, 635-653.

Cendrero, A., Díaz de Terán, J.R., Farias, P., Fernández-Menéndez, S., González-Díez, A., Jiménez, M., Marquínez, J., Menéndez-Duarte, R. & Salas, L., 1994. Temporal distribution and contribution of landslides to landscape evolution from Late Pleistocene to Present ion the Cantabrian Cordillera, Spain. In: Casale, R., Fantechi, R. & Flageollet, J.C (eds), *Temporal occurrence and forecasting of landslides in the European Community*, European Commission, Brussels, EUR 15805 EN, 425-506.

Chacón, J., Irigaray, C. & Fernández, T., 1993. Methodology for large scale hazard mapping in a GIS. In: Novosad, S. & Wagner, P. (eds), *Landslides: Proceedings for the 7*[th] *International Conference and Field Workshop on Landslides*, Bratislavia, Czeck and Slovak Republics, A.A. Balkema, Rotterdam, 77-82.

Chacón, J., Irigaray, C. & Fernández, T., 1994. Large to middle scale landslides inventory, analysis and mapping with modelling and assessment of derived susceptibility, hazards and risks in a GIS. In: Oliveira, R., Coelho, A.G., Rodrigues, L.F. & Cunha, A.P. (eds), *Proceedings of the 7*[th] *International Congress International Association of Engineering Geology*, 5-9th Septmeber, Lisbon, Portugal, A.A. Balkema, Rotterdam, 4669-4678.

Chacón, J., Irigaray, C., Hamdouni, R.El. & Fernández, T., 1996. From the inventory to the risk analysis: Improvements to a large scale GIS method. In: Chacón, J., Irigaray, C. & Fernández, T. (eds), *Landslides: Proceedings of the 8*[th] *International Conference and Field Trip on Landslides*, Granada, Spain 27th-28th September 1996, A.A. Balkema, Rotterdam, 335-342.

Charman, J.H. & Griffiths, J.S., 1993. Terrain evaluation methods for predicting relative hazards from mass movements, fluvial erosion and soil erosion in the developing world. In: Merriman, P.A. & Browitt, C.W.A (eds), *Natural Disasters: Protecting vulnerable communities*, Thomas Telford, London, 167-183.

Christian, C.S. & Stewart, G.A., 1968. Methodology of Integrated Surveys. Proceedings of Conference on Aerial Surveys and Integrated Studies, Toulouse, UNESCO, 233-280.

Cloetingh, S., Van Der, Beek, P.A., Van Rees, D., Roep, Th.B., Biermann, C. & Stephenson, R.A., 1992. Flexural interaction and the dynamics of Neogene extensional basin formation in the Alboran-Betic region. In: Maldonado, A. (Ed.), Alboran Basin Special Issue. *Geo-Marine Letters*, 12, 66-75.

Cooke, R.U. & Doornkamp, J.C., 1990. *Geomorphology in environmental management*, Second Edition, Clarendon Press, Oxford, 410pp.

Coppier, G., Griveaud, P., De Larouzière, F.-D., Montenat, C. & Ott d'Estevou, P., 1989. Example of Neogene tectonic indentation in the eastern Betic Cordilleras: the Arc of Aguilas (Southeastern Spain). *Geodinamica Acta*, 3, 37-51.

Corominas, J., 1996. The angle of reach as a mobility index for small and large landslides. *Canadian Geotechnical Journal*, **33**, 260-271.

Costa, J.E & Schuster, R.L., 1988. The formation and failure of natural dams. *Geological Society of America Bulletin*, **100**, 1054-1068.

Crozier, M.J., 1973. Techniques for the morphometric analysis of landslips. *Zeitschrift für Geomorphologie*, **17**, 78-101.

Crozier, M.J., 1986. *Landslides: Causes, consequences and environments*. Croom Helm, London, 252pp.

Cruden, D.M., 1991. A simple definition of a landslide. *Bulletin of the International Association of Engineering Geology*, **43**, 27-29.

Cruden, D.M. & Varnes, D.J., 1996. Landslide types and processes. In: Turner, A.K. & Schuster, R.L. (eds), *Landslides: Analysis and Control*, Special Report **247**, Transportation Research Board, National Research Council, National Academy Press, Washington DC, 36-75.

Cruden, D.M. & Fell, R., (eds), 1997. *Landslide Risk Assessment*, Proceedings of the International Workshop on Landslide Risk Assessment, Honolulu, Hawaii, 19th-21st February 1997, A.A. Balkema, Rotterdam, 371pp.

Dai, F.C. & Lee, C.F., 2002. Landslide characteristics amd slope stability modelling using GIS, Lantau Island, Hong Kong. *Geomorphology*, **43**, 213-228.

Davies, A.M., Mason, P.J. & Moore, J.McM., 2000. Three dimensional visualisation of landslides in SE Spain using a Digital Elevation Model (DEM) and orthophotography. In: Bromhead, E., Dixon, N. & Ibsen, M.-L. (eds), *Landslides in research, theory and practice*, Thomas Telford, London, 403-408.

Davison, L., Fookes, P. & Baynes, F., 2003. Total geological history: a web-based modelling approach to the anticipation, observation and understanding of site conditions. In: Rosenbaum, M.S. & Turner, A.K. (eds), *New paradigms in subsurface prediction:Characterization of the shallow subsurface: Implications for urban infrastructurte and environmental assessment*, Springer-Verlag, Düsseldorf, 237-252.

Department of the Environment, 1990. *Planning policy guidance note 14: Development on Unstable Land*. HMSO, London.

Department of the Environment, 1996. *Planning policy guidance note 14 Annex: Development on Unstable Land: Landslide and Planning.* HMSO, London.

Dewey, J.F., Pitman, III, W.C., Ryan, W.B.F. & Bonnin, J., 1973. Plate tectonics and the evolution of the Alpine system. *Geological Society of America Bulletin*, **84**, 3137-3180.

Dikau, R., Brunsden, D., Schrott, L. & Ibsen, M.-L., 1996. *Landslide recognition: Identification, movement and causes.* John Wiley & Sons Ltd, Chichester, 251pp.

Doornkamp, J.C., Brunsden D., Jones, D.K.C., Cooke, R.U. & Bush, P.R., 1979. Rapid geomorphological assessments for engineering. *Quaterly Journal of Engineering Geology*, **12**, 189-204.

Doyle, P., Wood, J.L. & George, G.T., 2000. The shorebird ichnofacies: an example from the Miocene of southern Spain. *Geological Magazine*, **137**, 517-536.

Dronkert, H., 1976. Late Miocene evaporites in the Sorbas Basin and adjoining areas. *Memorie della Societa geologica italiana*, **16**, 341-361.

Dronkert, H., 1977. The evaporates of the Sorbas Basin. *Rev. Instit. Inv. Geol. Dip. Provincial Univ. Barcelona*, **32**, 55-76.

Dronkert, H., 1985. *Evaporite models and sedimentology of Messinian and recent evaporates.* Unpublished PhD Thesis, Municipal University of Amsterdam, GUA Paper, Geology, 24, 283pp.

Egeler, C.G., 1963. On the tectonics of the eastern Betic Cordilleras. *Geologische Rundschau*, **53**, 260-269.

Egeler, C.G. & Simon, O.J., 1969. Orogenic evolution of the Betic Zone (Betic Cordilleras, Spain), with emphasis on the nappe structures. *Geologie en Mijnbouw*, **48**, 296-305.

Emery, D. & Myers, K.J. (eds), 1997. *Sequence Stratigraphy*, Blackwell Science, Oxford, UK, 297pp.

EPOCH (European Community Programme) 1993. *Temporal Occurrence and Forecasting of Landslides in the European Community.* Flageollet, J.C. (Ed.), 3 volumes, Contract No. 90 0025.

Estaban-Parra, M.J., Rodrigo, F.S. & Castro-Diez, Y., 1998. Spatial and temporal patterns of precipitation in Spain for the period 1880-1992. *International Journal of Climatology*, **18**, 1557-1574.

Evens, N.C., 1996. *Natural Terrain Landsldie Study: Rainfall distribution and orographic effects in Hong Kong*. Discussion Note DN 3/96. Geotechnical Engineering Office, Hong Kong (unpublished).

Evens, N.C., 1997. *Natural Terrain Landslide Study: Preliminary assessment of the influence of rainfall on natural terrain landslide initiation*. Discussion Note DN 1/97. Geotechnical Engineering Office, Hong Kong (unpublished).

Evens, N.C., 1998. The natural terrain landslide study. In: Li, K.S., Kay, J.N. & Ho, K.K.S. (eds), Slope *Engineering in Hong Kong*, Proceedings of the Annual Seminar on Slope Engineering in Hong Kong, Hong Kong, 2nd May 1997. A.A. Balkema, Rotterdam, 137-144.

Eyres, R., Moore, J.McM., Hervás, J. & Liu, J.G., 1998. Integrated use of Landsat TM and SPOT panchromatic imagery for landscape mapping: case histories from southeast Spain. In: Maund, J.G. & Eddleston, M. (eds), *Geohazards in Engineering Geology*. Geological Society, London, Engineering Geology Special Publications, **15**, 133-140.

Fallot, P., 1948. Les Cordilleres Betiques. *Estud. Geol.*, **8**, 83-172.

Faulkner, H., Spivey, D. & Alexander, R., 2000. The role of some site geochemical processes in the development and stabilisation of three badland sites in Almeria, Southern Spain. *Geomorphology*, **35**, 87-99.

Fernández, T., Irigaray, C. & Chacón, J., 1994. Large scale analysis and mapping of determinant factors of landsliding affecting rock massifs in the eastern Costa del Sol (Granada, Spain) in a GIS. In: Oliveira, R., Coelho, A.G., Rodrigues, L.F. & Cunha, A.P. (eds), *Proceedings of the 7th International Congress International Association of Engineering Geology*, 5-9th Septmeber, Lisbon, Portugal, A.A.Balkema, Rotterdam, 4649-4658.

Fernández, T., Irigaray, C. & Chacón, J., 1996. GIS analysis and mapping of landslides determinant factors in the Contraviesa area (Granada, Spain). In: Chacón, J., Irigaray, C. & Fernández, T. (eds), *Landslides: Proceedings of the 8th*

International Conference and Field Trip on Landslides, Granada, Spain 27th-28th September 1996, A.A. Balkema, Rotterdam, 141-152.

Fookes, P.G., 1997. Geology for Engineers: the Geologcal Model, Prediciton and Performances. The First Glossop Lecture. *Quarterly Journal of Engineering Geology*, **30**, 293-424.

Fookes, P.G., Baynes, F.J. & Hutchinson, J.N., 2000. Total geological history: A model approach to the anticipation, observation and understanding of site conditions. In: *Proceedings of GeoEng2000*, Melbourne, **1**, 370-460.

Fortuin, A.R., Kelling, J.M.D. & Roep, T.B., 1995. The enigmatic Messinian-Pliocene section of Cuevas del Almanzora (Vera Basin, SE Spain) revisited: erosion features and strontium isotope age. *Sedimentary Geology*, **97**, 177-201.

Frizon de Lamotte, D., Andrieux, J. & Guezou, J.C., 1991. Cinématique des chevauchements néogènes dans l'arc betico-rifian: discussion sur les modèles géodynamiques. *Bulletin Société Géologique de France*, **162**, 611-626.

Frizon de Lamotte, D., Averbuch, O. & Guezou, J.C., 1995. Distinguishing lateral folds in thrust-systems. Examples from Corbières (SW France) and Betic Cordilleras (SE Spain). *Journal of Structural Geology*, **17**, 233-244.

Fry, N., 1984. *The Field Description of Metamorphic Rocks*. Geological Society of London Handbook Series, **3**. Open University Press, London, 110pp.

García-Hernández, A.C., López-Garido, A.C., Rivas, P., Sanz De Galdeano, C. & Vera, J.A., 1980. Mesozoic paleogeographic evolution of the External Zones of the Betic Cordillera. *Geologie en Mijnbouw*, **59**, 155-168.

García-Meléndez, E., Molina, I., Ferre-Julià & Aguirre, J., 1998. Multisensor data integration and GIS analysis for natural hazard mapping in a semiarid area (southeast Spain). *Advances in Space Research*, **21**, 493-499.

Gardiner, T.W., 1983. Experimental study of knickpoint and longitudinal profile evolution in cohesive, homogenous material. *Geological Society of America Bulletin*, **94**, 664-667.

Geotechnical Control Office, 1984. *Geotechnical Manual for Slopes*. Engineering Development Department, Hong Kong.

Gibbons, W. & Moreno, T. (eds), 2002. *The Geology of Spain*. The Geological Society, London, 632pp.

Gile, L.H., Peterson, F.F. & Grossman, R.B., 1966. Morphological and genetic sequences of carbonate accumulation in desert soils. *Soil Science*, **101**, 347-360.

Glade, T., 1998. Establishing the frequency and magnitude of landslide-triggering rainstorm events in New Zealand. *Environmental Geology*, **35**, 160-174.

Glossop, R., 1968. The rise of geotechnology and its influence on engineering practice. *Géotechnique*, **18**, 105-150.

Godt, J.W. & Savage, W.Z., 1999. El Niño 1997-98: direct costs of damaging landslides in the San Fransisco Bay Region. In: Griffiths, J.S., Stokes, M. & Thomas, R. (eds), *Proceedings of the 9th Interntional Conference and Field Trip on Landslides*, Balkema, Rotterdam, 162pp.

Gomez-Pugnaire, M., 2001. The basement geology of the Almeria Province. In: Mather, A.E., Martín, J.M., Harvey, A.M. & Braga, J.C. (eds), *A Field Guide to the Neogene Sedimentary Basins of the Almeria Province, SE Spain*. Blackwell Science Ltd, Oxford, 33-46.

González-Díez, A., Remondo, J., Díaz de Terán, J.R. & Cendrero, A., 1999. A methodological approach for the anlaysis of the temporal occurrence and triggering factors of landslides, *Geomorphology*, **30**, 95-113 [Special Issue: Temporal stability and activity of landslides in Europe with respect to climatic change (TESLEC), Schrott, L. & Pasuto, A. (eds)].

Goudie, A., 1981. *Geomorphological Techniques*. George Allen & Unwin, London. 395pp.

Goy, J.L, Zazo, C., Dabrio, C.J., Lario, J., Borja, F., Sierro, F.J., & Flores, J.A., 1996. Global and regional factors controlling changes in southern Iberia (Spain) during the Holocene. *Quaternary Science Reviews*, **15**, 773-780.

Goy, J.L. & Zazo, C., 1982. Niveles marinos cuaternarios y su relacion con la meotectonica en el litoral de Almería (Espana). *Bol. Real Espanola de Historia Natural*, **80**, 171-184.

Goy, J.L. & Zazo, C., 1986. Synthesis of the Quaternary in the Almería littoral, neotectonic activity and its morphologic features. *Tectonophysics*, **130**, 259-270.

Gregory, K.J. & Walling, D.E., 1973. *Drainage Basin Form and Process: A geomorphological approach*. Edward Arnold Ltd, London, 458pp.

Griffiths, J.S., 2001. Engineering geological mapping. In: Griffiths, J.S. (Ed.), *Land Surface Evaluation for Engineering Practice*. Geological Society, London, Engineering Geology Special Publications, **18**, 39-42.

Griffiths, J.S. & Edwards, J.G., 2001. The development of land surface evaluation for engineering practice. In: Griffiths, J.S. (Ed.), *Land Surface Evaluation for Engineering Practice*. Geological Society, London, Engineering Geology Special Publications, **18**, 3-9.

Griffiths, J.S., Mather, A.E. & Hart, A.B., 2002. Landslide susceptibility in the Rio Aguas catchment, SE Spain. *Quarterly Journal of Engineering Geology and Hydrogeology*, **35**, 9-17.

Griffiths, J.S., Mather, A.E., Stokes, M., Hart, A.B., 2003. Spatial and temporal issues for landslide hazard assessment in the Río Aguas Catchment, southeast Spain. *Proceedings of the Annual Conference of the International Association for Mathematical Geology*, University of Portsmouth, 7th-12th September 2003.

Guadagno, F.M. & Zampelli, S.P., 2000. Triggering mechanisms of the landslides that inundated Sarno, Quindici, Siano and Bracigliano (southern Italy) on May 5-6, 1998. In: Bromhead, E., Dixon, N., Ibsen, M.-L. (eds), *Landslides in research, theory and practice*, Thomas Telford, London, 671-676.

Guzzetti, F., Carrara, A., Cardinali, M. & Reichenbach, P., 1999. Landslide hazard evaluation: a review of current techniques and their application in a multi-scale study, Central Italy. *Geomorphology*, **31**, 181-216.

Hamdouni, R.El., Irigaray, C. & Chacón, J., 1996. Landslides inventory and determining factors in the Albuñuelas river basin (Granada, Spain). In: Chacón, J., Irigaray, C. & Fernández, T. (eds), *Landslides: Proceedings of the 8th International Conference and Field Trip on Landslides*, Granada, Spain 27th-28th September 1996, A.A. Balkema, Rotterdam, 21-30.

Hansen, A., 1984. Landslide Hazard Analysis. In: Brunsden, D. & Prior, D.B. (eds), *Slope Instability*. Wiley, Chichester, 523-602.

Hansen, M.J., 1984. Strategies for classification of landslides. In: Brunsden, D. & Prior, D.B. (eds), *Slope Instability*, Wiley, Chichester, 1-25.

Haq, B.U., Hardenbol, J. & Vail, P.R., 1988. Mesozoic and Cenozoic chronostratigraphy and cycles of sea-level change. In: Wilgus, C.K., Hastings, B.S., Kendall, C.G.St.C., Posamentier, H.W., Ross, C.A. & Van Wagoner, J.C. (eds), *Sea-Level Changes: an Integrated Approach*, Special Publication, Society of Economic Paleontologists and Mineralogists (SEPM), Tulsa, **42**, 71-108.

Harrison, S.P. & Digerfeldt, G., 1993. European lakes as palaeohydrological and palaeoclimatic indicators. *Quaternary Science Reviews*, **12**, 233-248.

Hart, A.B., 1999. An Introduction to the Landslides of the Sorbas Basin. In: Mather, A.E., Stokes, M. (eds), *BSRG/BGRG South-east Spain Field Meeting Guide Book*, University of Plymouth, England, 124-133.

Hart, A.B., & Griffiths, J.S., 1999. Mass movement features in the vicinity of the town of Sorbas, South-east Spain. In: Griffiths, J.S., Stokes, M.R., Thomas, R.G. (eds), *Landslides: Proceedings of the Ninth International Conference and Field Trip on Landslides*, Bristol, UK, 5th-16th September 1999, A.A. Balkema, Rotterdam, 57-63.

Hart, A.B., Griffiths, J.S. & Mather, A.E., 2000. The role of landsliding in landscape development in the Rio Aguas Catchment, South-east Spain. In: Bromhead, E., Dixon, N. & Ibsen, M.-L. (eds), *Landslides in research, theory and practice*, Thomas Telford, London, 701-706.

Hart, A.B., Hearn, G.J., Petley, D.N., Tiwari, S.C. Giri, N.K., 2003a. Using remote sensing and GIS for rapid landslide hazard assessment: Potential public sector uptake in Nepal and Bhutan. *Proceedings for the Permanent International Association for Road Congresses (PIARC) Conference, Sustainable Slope Risk Management for Roads*, Kathmandu, Nepal, March 2003.

Hart, A.B., Lamichhane, P., Jha, P., Subba, M. & GC, S., 2003b. A landslide database for Nepal. *Proceedings for the Permanent International Association for Road Congresses (PIARC) Conference, Sustainable Slope Risk Management for Roads*, Kathmandu, Nepal, March 2003.

Hart, A.B., Hearn, G.J. & Petley, D.N., *In Press*. (2004) Landslide susceptibility, hazard and risk mapping for infrastructure planning in mountainous areas. *Quarterly Journal of Engineering Geology and Hydrogeology*, **37**, xxx-yyy.

Harvey, A.M., 1982. The role of piping in the development of badlands and gully systems in southeast Spain. In: Bryan, R. & Yair, A. (eds), *Badland Geomorphology and Piping*, Geobooks, Norwich, 317-335.

Harvey, A.M., 1984a. Aggradation and dissection sequences on Spanish alluvial fans: influence on morphological development. *Catena*, 11, 289-304.

Harvey, A.M., 1984b. Geomorphological response to an extreme flood: a case from southeast Spain. *Earth Surface Procesess and Landforms*, 9, 267-279.

Harvey, A.M., 1987. Patterns of Quaternary aggradational and dissectional landform development in the Almeria Region, southeast Spain: a dry-region tectonically active landscape. *Die Erde*, 118, 193-215.

Harvey, A.M., 2001. Uplift, dissection and landform evolution: the Quaternary. In: Mather, A.E., Martin, J.M., Harvey, A.M. & Braga, J.C. (eds), *A Field Guide to the Neogene Sedimentary Basins of the Almeria Province, SE Spain*, Blackwell Science Ltd, Oxford, 225-322.

Harvey, A.M. & Wells, S.G., 1987. Response of Quaternary fluvial systems to differential epeirogenic uplift: Aguas and Feos river systems. *Geology*, 15, 689-693.

Harvey, A.M., Miller, S.Y. & Wells, S.G., 1995. Quaternary soil and river terrace sequences in the Aguas/Feos river systems: Sorbas Basin, Southeast Spain. In: Lewin, J., Macklin, M.G. & Woodward, J.C. (eds), *Mediterranean Quaternary River Environments*, A.A. Balkema, Rotterdam, 65-76.

Hearn, G.J. & Griffiths, J.S., 2001. Landslide hazard mapping and risk assessment. In: Griffiths, J.S. (Ed.), *Land Surface Evaluation for Engineering Practice*, Geological Society, London, Engineering Geology Special Publications, 18, 43.52.

Hearn, G.J., Hodgson, I. & Woddy, S., 2001. GIS-based landslide hazard mapping in the Scotland District, Barbados. In: Griffiths, J.S. (Ed.), *Land Surface Evaluation for Engineering Practice*. Geological Society, London, Engineering Geology Special Publications, 18, 151-157.

Hearn, G., Petley, D.N, Hart, A.B., Massey, C. & Chant, C., 2003. *Landslide Risk Assessment in the Rural Access Sector: Guidelines on best practice – remote sensing, landslide hazard and risk mapping, land use planning and management*

and route corridor selection. Report for the DFID funded project R7815 "Landslide Risk Assessment in the Rural Access Sector".

Hernandez, J., De Larouzière, F.D., Bolze, J. & Bordet, P., 1987. Le magmatisme néogène bético-rifain et le couloir de décrochement trans-Alborán. *Bulletin, Societé Géologique de France*, **8**, 257-267.

Heim, A., 1932. *Bergsturz und Menschenleben*. Zürich, Fretz und Wasmuth. (English translation by N.A.Skermer, 1989. *Landslides and human lives*. BiTech Publishers, Vancouver, British Columbia, Canada).

Henkel, D.J., 1982. Geology, geomorphology and geotechnics. *Géotechnique*, **32**, 175-194.

Hsü, K.J., 1975. Catastrophic debris streams (Sturzstroms) generated by rockfalls. *Geological Society of America Bulletin*, **86**, 129-140.

Hsü, K.J., 1978. Albert Heim: Observations on landslides and relevance to modern interpretations. In: Voight, B. (Ed.), *Rockslides and avalanches*, Elsevier, Amsterdam, **Vol. 1**, 71-93.

Hsü, K.J., Cita, N.B. & Ryan, W.B.F., 1972. The origin of the Mediterranean evaporites. *Initial Reports of the Deep Sea Drilling Project (DSDP)*, **XIII**, pt.2, 695-708.

Hsu, K.J. Montadert, L., Bernoulli, D., Cita, M.B., Erickson, A., Garrison, K.E., Kidd, K.B., Melieres, F., Muller, C. & Wright, R., 1977. History of the Messinian salinity crisis. *Nature*, **267**, 399-403.

Hsü, K.J., Montadert, L. Bernoulli, D. *et al* 1978. *Initial Reports of the Deep Sea Drilling Project 42A*. US Government Printing Office, Washington DC.

Huntley, B. & Birks, H.J.B., 1993. *An atlas of past and present pollen maps for Europe: 0-13K years ago*. Cambridge University Press, Cambridge,

Hutchinson, J.N., 1988. Morphological and geotechnical parameters of landslides in relation to geology and hydrology, General Report. In: Bonnard, C. (Ed.), *Landslides, Proceedings of the 5th International Symposium on Landslides*, **1**, A.A. Balkema, Rotterdam, 3-35.

Hutchinson, J.N., 1995. Keynote Paper: Landslide hazard assessment. *Proceedings of the 6th International Symposium on Landslides*, Christchurch, New Zealand, 3, 1805-1841.

Hutchinson, J.N., 2001. The Fourth Glosop Lecture: Reading the ground: Morphology and geology in site appraisal. *Quaterly Journal of Engineering Geology and Hydrogeology*, 34, 7-50.

Irigaray, C., Fernández, T. & Chacón, J., 1994. GIS landslide inventory and analysis of determinant factors in the sector of Rute (Cordoba, Spain). In: Oliveira, R., Coelho, A.G., Rodrigues, L.F. & Cunha, A.P. (eds), *Proceedings of the 7th International Congress International Association of Engineering Geology*, 5-9th September, Lisbon, Portugal, A.A.Balkema, Rotterdam,

Irigaray, C., Chacón, J. & Fernández, T., 1996a. Methodology for the analysis of landslide determinant factors by means of a GIS: Application to the Colmenar area (Malaga, Spain). In: Chacón, J., Irigaray, C. & Fernández, T. (eds) *Landslides: Proceedings of the 8th International Conference and Field Trip on Landslides*, Granada, Spain 27th - 28th September 1996, A.A. Balkema, Rotterdam, 163-172.

Irigaray. C., Chacón, J. & Fernández, T., 1996b. Comparative analysis of methods for landslide susceptibility mapping. In: Chacón, J., Irigaray, C. & Fernández, T. (eds) *Landslides: Proceedings of the 8th International Conference and Field Trip on Landslides*, Granada, Spain 27th - 28th September 1996, A.A. Balkema, Rotterdam, 373-384.

Irigaray, C., Fernández, T., Hamdouni, R.El, & Chacón, J., 1999. Verification of landslide susceptibility mapping: a case study. *Earth Surface Processes and Landforms*, 24, 537-544.

Irigaray, C., Lamas, F., Hamdouni, R.El, Fernández, T., & Chacón, J., 2000. The importance of the precipitation and the susceptibility of the slopes for the triggering of landslides along the roads. *Natural Hazards*, 21, 65-81.

Jalut, G., Amat, A.E., Bonnet, L., Gauquelin, T. & Fontugne, M., 2000. Holocene climatic changes in the Western Mediterranean, from south-east France to south-east Spain. *Palaeogeography, Palaeoclimatology, Palaeoecology*, 160, 255-290.

Jones, D.K.C. & Lee, E.M., 1994. *Landsliding in Great Britain*, Department for the Environment, HMSO, London, 361pp.

Keefer, D.K. 1984. Landslides caused by earthquakes. *Bulletin Geological Society of America*, **95**, 406-421.

Keefer, D.K., 1999. Earthquake-induced landslides and their effects on alluvial fans. *Journal of Sedimentary Research*, **69**, 84-104.

Keller, J.V.A., Hall, S.H., Dart, C.J. & McClay, K.R., 1995. The geometry and evolution of a transpressional strike-slip system – the Carboneras Fault, SE Spain. *Journal of the Geological Society*, **152**, 339-351.

Kelly, M., Black, S. & Rowan, J.S., 2000. A calcrete-based U/Th chronology for landform evolution in the Sorbas Basin, southeast Spain. *Quaternary Science Reviews*, **19**, 995-1010.

Kleverlan, K., 1989. Neogene history of the Tabernas Basin, (SE Spain) and its Tortonian submarine fan development. *Geologie en Mijnbouw*, **68**, 421-432.

Krijgsman, W., Hilgen, F.J., Raffi, I., Sierro, F.J., & Wilson, D.S., 1999. Chronology, causes and progression of the Messinian salinity crisis. *Nature*, **400**, 652–655.

Kuribayashi, E. & Tatsuoka, F., 1975. Brief review of liquetaction during earthquakes in Japan. *Soils and Foundations*, **15**, 81-92.

Kuribayashi, E. & Tatsuoka, F., 1977. History of earthquake-induced soil liquefaction in Japan. *Japan Ministry of Construction, Public Works Research Institute Bulletin*, **31**, 26pp.

Larouziére, F.D.De., Bolze, J., Bordet, P., Hernandez, J., Montenat, C. & Ott D'Estevou, P., 1988. The Betic segment of the lithospheric Trans-Alboran shear zone during the late Miocene. *Tectonophysics*, **152**, 41-52.

Lawrance, C., Byard, R. & Beaven, P., 1993. *Terrain Evaluation Manual*. Transportation Research Laboratory, State-of-the-Art Review 7, HMSO, London, 285pp.

Lazzari, M. & Salvaneschi, P., 1999. Embedding a Geographical Information System in a Decision Support System for landslide hazard monitoring. *Natural Hazards*, **20**, 185-195.

Lee, E.M., 2001. Geomorphological mapping. In: Griffiths, J.S. (Ed.), *Land Surface Evaluation for Engineering Practice*, Geological Society, London, Engineering Geology Special Publications, **18**, 53-56.

Lee, E.M., Jones, D.K.C. & Brunsden, D., 2000. The landslide environment of Great Britain. In: Bromhead, E., Dixon, N. & Ibsen, M.-L. (eds), *Landslides in research, theory and practice*, Thomas Telford, London, 911-916.

Leggett, R.F., 1977. *Cities and Geology*. McGraw-Hill Publishing, New York.

Leroi, E., Rouzeau, O., Scanvic, J.Y., Webber, C.C. & Vargas, G., 1992. Remote sensing and GIS technology in landslide hazard mapping in the Columbian Andes. *Episodes*, **15**, 32-33.

Linthout, K. & Vissers, R.L.M., 1979. On the classification of tectonic units in the Nevado-Filabride complex of the Northern Sierra de los Filabres, Betic Cordilleras, SE Spain. *Geologie en Mijnbouw*, **58**, 49-56.

Longergan, L. & White, N., 1997. Origin of the Betic-Rif Mountain Belt. *Tectonics*, **16**, 504-522.

López-Arroyo, A., Martin-Martin, A.J., Mezcua-Rodriguez, J., Muñoz, D. & Udias, A., 1980. *E; terremoto de Andalucia de 25 Diciembre de 1884*. Presidencia del Gobierno, Instituto Geográfico Nacional, Madrid.

Landslide Risk Assessment Project, 2001a. *Proceedings for the Mountain Hazards Research and Mitigation Seminar*, April 2001, Kathmandu, Nepal. Unpublished report for the DFID funded project R7815 "Landslide Risk Assessment in the Rural Access Sector".

Landslide Risk Assessment Project, 2001b. *Proceedings for the Landslide Susceptibility Mapping Technical Meeting: Preliminary Findings Seminar*, October 2001, Kathmandu, Nepal. Unpublished report for the DFID funded project R7815 "Landslide Risk Assessment in the Rural Access Sector".

Landslide Risk Assessment Project, 2002a. *Proceedings for the Bhutan studies: Final Seminar, September 2002, Thimphu, Bhutan*. Unpublished report for the DFID funded project R7815 "Landslide Risk Assessment in the Rural Access Sector".

Landslide Risk Assessment Project, 2002b. *Proceedings for the Mountain Hazards Research and Risk Minimisation Seminar*, November 2002, Kathmandu, Nepal.

Unpublished report for the DFID funded project R7815 "Landslide Risk Assessment in the Rural Access Sector".

Landslide Risk Assessment Project, 2003a. *Report on the project activities undertaken in Nepal.* Unpublished report for the DFID funded project R7815 "Landslide Risk Assessment in the Rural Access Sector".

Landslide Risk Assessment Project, 2003b. *Report on the project activities undertaken in Bhutan.* Unpublished report for the DFID funded project R7815 "Landslide Risk Assessment in the Rural Access Sector".

Landslide Risk Assessment Project, 2003c. *Best practice guidelines in the use of a Geographical Information System (GIS) for landslide susceptibility mapping ata regional scale.* Unpublished report for the DFID funded project R7815 "Landslide Risk Assessment in the Rural Access Sector".

Lucchitta, B.K., 1978. A large landslide on Mars. *Bulletin Geological Society of America*, **89**, 1601-1609.

Machette, M.N., 1985. Calcic soils of the southwestern United States. In: Weide, D.L. (Ed.), *Soils and Quaternary Geology of the South-western United States*, Geological Society of America Special Paper, **203**, 12-21.

Macklin, M.G., Lewin, J. & Woodward, J.C., 1995. Quaternary fluvial systems in the Mediterranean Basin. In: Lewin, J., Macklin, M.G. & Woodward, J.C. (eds), *Mediterranean Quaternary River Environments*, A.A. Balkema, Rotterdam, 1-25.

Mantovani, F., Soeters, R & Van Westen, C.J., 1996. Remote sensing techniques for landslide studies and hazard zonation in Europe. *Geomorphology*, **15**, 213-225.

Martin, J.M. & Braga, J.C., 1994. Messinian events in the Sorbas Basin in southeastern Spain and their implications in the recent history of the Mediterranean. *Sedimentary Geology*, **90**, 257-268.

Martin, J.M. & Braga, J.C., 1996. Tectonic signals in the Messinian stratigraphy of the Sorbas Basin (Almería, SE Spain). In: Friend, P.F. & Dabrio, C.J. (eds), *Tertiary Basns of Spain: the Stratigraphic record of crustal kinematics*, Cambridge Universtiy Press, Cambridge, 387-391.

Martin-Penela, A.J. & Barragán, G., 1995. Silification of carbonate clasts in a marine environment (Upper Miocene, Vera Basin, SE Spain). *Sedimentology Geology*, **97**, 21-32.

Martinez-Martinez, H.M. & Azanon, J.M., 1997. Mode of extensional tectonics in the SE Betics (SE Spain); implications for the tectonic evolution of the Peri-Alboran orogenic system. *Tectonics*, **16**, 205-225.

Mason, P.J., Rosenbaum, M.S. & Moore, J.McM., 1998. Digital image texture analysis for landslide mapping. In: Maund, J.G. & Eddleston, M. (eds), *Geohazards in Engineering Geology*, Geological Society, London, Engineering Geology Special Publications, **15**, 297-308.

Mather, A.E., 1991. *Late Caenozoic drainage evolution of the Sorbas Basin, Southeast Spain*. Unpublished PhD Thesis, University of Liverpool.

Mather, A.E., 1993a. Basin inversion: Some consequences for drainage evolution and alluvial architecture. *Sedimentology*, **40**, 1069-1089.

Mather, A.E., 1993b. Evolution of a Pliocene fan delta: links between the Sorbas and Carboneras Basins, SE Spain. In: Frostick, L. & Steel, R. (eds), *Tectonic Controls and Signatures in Sedimentary Successions*. International Association of Sedimentologists, Special Publication, **20**, 277-290.

Mather, A.E., 2000a. Impact of headwater river capture on alluvial system development: an example from SE Spain. *Journal of the Geological Society, London*, **157**, 957-966.

Mather, A.E., 2000b. Adjustment of a drainage network to capture induced base-level change: an example from the Sorbas Basin, SE Spain. *Geomorphology*, **34**, 271-289.

Mather, A.E. & Harvey, A.M., 1995. Controls on drainage evolution in the Sorbas Basin, Southeast Spain. In: Lewin, J., Macklin, M.G. & Woodward, J.C. (eds), *Mediterranean Quaternary River Environments*, A.A. Balkema, Rotterdam, 65-76.

Mather, A.E. & Stokes, M., 2000. Integrating research, teaching and the environment, a role for a specilised field meeting?: The 1999 BSRG/BGRG Southeast Spain Field Meeting Experience. *Geoscientist*, **10**, No.8, 4-6.

Mather, A.E. & Stokes, M., 2001. Marine to Continental Transition. In: Mather, A.E., Martin, J.M., Harvey, A.M. & Braga, J.C. (eds), *A Field Guide to the Neogene Sedimentary Basins of the Almeria Province, SE Spain*, Blackwell Science Ltd, 186-224.

Mather, A.E. & Stokes, M., 2003. Long-term landslide development in southern Spain. *Geomorphology Special Issue*, 50, 291pp.

Mather, A.E., Harvey, A.M. & Brenchley, P.J., 1991. Halokinetic deformation of Quaternary river terraces in the Sorbas Basin, South-east Spain. *Zeitschrift der Geomorphologie (Supplementband)*, 82, 87-97.

Mather, A.E., Martin, J.M., Harvey, A.M. & Braga, J.C., 2001a. Introduction to the Field Guide. In: Mather, A.E., Martin, J.M., Harvey, A.M. & Braga, J.C. (eds), *A Field Guide to the Neogene Sedimentary Basins of the Almeria Province, SE Spain*, Blackwell Science Ltd, 1-8.

Mather, A.E., Martin, J.M., Harvey, A.M. & Braga, J.C., 2001b. Introduction to the Neogene of the Sorbas Basin. In: Mather, A.E., Martin, J.M., Harvey, A.M. & Braga, J.C. (eds), *A Field Guide to the Neogene Sedimentary Basins of the Almeria Province, SE Spain*, Blackwell Science Ltd, 9-28.

Mather, A.E., Stokes, M. & Griffiths, J.S., 2002. Quaternary landscape evolution: a framework for understanding contemporary erosion, southeast Spain. *Land Degradation & Development*, 13, 89-109.

Mather, A.E., Griffiths, J.S. & Stokes, M., 2003. Anatomy of a "fossil" landslide from the Pleistocene of SE Spain. *Geomorphology*, 50, 135-149.

McClay, K.R., 1991. *The Mapping of Geological Structures*. Geological Society of London Handbook Series, John Wiley & Sons, Chichester, 161pp.

McEwen, A.S., 1989. Mobility of large rock avalanches: evidence from Valles Marineris, Mars. *Geology*, 17, 1111-1114.

Mitchel, C.W., 1991. *Terrain Evaluation: An introductory handbook to the history, principles and methods of practical terrain assessment*. Longman Scientific & Technical, Longman Group UK Ltd, Harlow, 441pp.

Miller, S.Y., 1991. *Soil chronosequences and fluvial landform development: studies in SE Spain and NW England*. Unpublished PhD Thesis, University of Liverpool.

Montenat, C. (Ed), 1990. *Les bassins Néogènes du domaine bétique oriental (Espagne).* *Doc. Trav. IGAL 12–13,* Paris (1990) 392 pp.

Montenat, C. & Ott d'Estevou, P., 1999. The diversity of Late Neogene sedimentary basins generated by wrench faulting in the eastern Betic Cordillera, Southeast Spain. *Journal of Petroleum Geology,* **22,** 61-80.

Montenat, C., Ott d'Estevou, P. & Masse, P., 1987. Tectonic sedimentary characters of the Betic Neogene basins evolving in a crustal transcurrent shear zone (SE Spain). *Bulletin Centres Recerches Exploration-Prodction Elf Aquitaine Pau,* **11,** 1-22.

Nathanial, P. & Symonds, A., 2001. Geographical Information Systems. In: Griffiths, J.S. (Ed.), *Land Surface Evaluation for Engineering Practice,* Geological Society, London, Engineering Geology Special Publications, **18,** 57-58.

Navarro, C., Carrrión, J.S., Navarro, J., Munuera, M. & Prieto, A.R., 2000. An experimental approach to the palynology of cave deposits. *Journal of Quaternary Science,* **15,** 603-619.

Nicholson, D.T., Lumsden, A.C. & Hencher, S.R., 2000. Excavation-induced deterioration of rockslopes. In: Bromhead, E., Dixon, N. & Ibsen, M.-L. (eds), *Landslides in research, theory and practice,* Thomas Telford, London, 1105-1110.

Olshansky, R., 1990. *Landslide hazard in the United States. Case studies in planning and policy development.* Garland Publishers, New York, 178pp.

Ott d'Estevou, P.,1980. *Evolution dynamique du basin Néogène de Sorbas (Cordillèras Bétiques Orientales, Espagne).* PhD Thesis, Université Paris VII, Denis-Diderot, 264pp.

Oveiero, G. & Zazo, C., 1971. Niveles marinos Pleistocenos en Almería (SE de Espana). *Quaternaria,* **15,** 145-159.

Pagnier, H., 1976. Depth of deposition of Messinian selenetic gypsum in the Basin of Sorbas (SE Spain). *Memorie della Societa geologica italiana,* **16,** 363-367.

Peck, R.B., 1969. Advantages and limitations of the observational method in applied soil mechanics. *Géotechnique,* **19,** 60-66.

Perez-Obiol, R. & Julia, R., 1994. Climatic change on the Iberian Peninsula recorded in a 30,000-year old pollen record from Lake Banyoles. *Quaternary Research*, **41**, 91-98.

Petley, D.N.,1998. Geomorphological mapping for assessment in a neotectonic terrain. *The Geographical Journal*, **164**, 183-201.

Petley, D.N., Crick, W.D.O. & Hart, A.B., 2002. The use of satellite imagery in landslide studies in high mountain areas. *The Proceedings of the 23rd Asian Conference on Remote Sensing (ARCS, 2002), Kathmandu, Nepal.* Available online at: www.gisdevelopment.net/aars/acrs/2002/hdm.48.pdf

Petley, D.N., Hearn, G.J. & Hart, A.B., *In Press.* (2004). Satellite remote sensing for planning and engineering purposes in Nepal and Bhutan. *Quarterly Journal of Engineering Geology and Hydrogeology*, **37**, xxx-yyy.

Phipps, P.J., 2001. Terrain systems mapping. In: Griffiths, J.S. (Ed.), *Land Surface Evaluation for Engineering Practice*, Geological Society, London, Engineering Geology Special Publications, **18**, 59-61.

Platt, J.P., 1982. Emplacement of a fold-nappe, Betic orogen, southern Spain. *Geology*, **10**, 97-102.

Platt, J.P. Van den Eeckhout, B., Janzen, E., Konert, G., Simon, O.J. & Weijermars, R., 1983. The structure and tectonic evolution of the Agilón fold-nappe, Sierra Alhamilla, Betic Cordilleras, SE Spain. *Journal of Structural Geology*, **5**, 519-538.

Platt, J.P. & Vissers, R.L.M., 1989. Extensional collapse of thickened continental lithosphere: a working hypothesis for the Alborán Sea and Gibraltar Arc. *Geology*, **17**, 540-543.

Pons, A. & Reille, M., 1988. The Holocene and Upper Pleistocene pollen record from Padul (Granada, Spain): A new study. *Palaeogeography, Palaeoclimatology, Palaeoecology*, **66**, 243-263.

Poisson, A.M., Morel, J.L., Andrieux, J., Coulon, M., Wernli, R. & Guernet, C., 1999. The origin and development of Neogene basins in the SE Betic Cordillera (SE Spain): a case study of the Tabernas-Sorbas and Huercal Overa Basins. *Journal of Petroleum Geology*, **22**, 97-114.

Postma, G. & Roep, T.B., 1985. Resedimented conglomerates in the bottomsets of Gilbert-type gravel deltas. *Journal of Sedimentary Petrology*, **55**, 874-885.

Price, N.J. & Cosgrove, J.W., 1990. *Analysis of Geological Structures*, Cambridge University Press, Cambridge, UK, 502pp.

Priem, H.N.A., Boelrijk, N.A.I.M., Hebeda, E.H. & Verschure, R.H., 1966. Isotopic age determinations on tourmaline granite-gneisses and a metagranite in the eastern Betic Cordillleras (southeastern Sierra de los Filabres), SE Spain. *Geologie en Mijnbouw*, **45**, 184-187.

Rengers, N., Soeters, R. & Van Westen, C.J., 1992. Remote sensing and GIS applied to mountain hazard mapping. *Episodes*, **15**, 36-45.

Rhodenburg, H. & Sabelberg, U., 1980. Northwest Sahara margin: terrestrial stratigraphy of the Upper Quaternary and some palaeoclimatic implications. In: Sarnthein, M., Seibold, E., Rognon, P., Van Zinderen Bakker, E.M. & Coetzee, J.A. (eds), *Sahara and surrouding seas: Sediments and climatic changes*, (Proceedings of an International Symposium, Mainz, 1st - 4th April 1979), *Palaeoecology of Africa*, **12**, 267-276.

Riding, R., Martín, J.M. & Braga, J.C., 1991. Coral-stromatolite reef framework, Upper Miocene, Almería, Spain. *Sedimentology*, **38**, 799-818.

Riding, R., Braga, J.C. & Martín, J.M., 1999. Late Miocene Mediterranean desiccation: topography and significance of the "Salinity Crisis" erosion surface on-land in southeast Spain. *Sedimentary Geology*, **123**, 1-7.

Rodriguez-Puebla, C., Encinas, A.H., Nieto, S., & Garmendia, J., 1998. Spatial and temporal patterns of annual precipitation variability over the Iberian Peninsula. *International Journal of Climatology*, **18**, 299-316.

Roep, ThB. & Beets, D.J., 1977. An excursion to coastal and fluvial sediments of Messinian-Pliocene age (Sorbas and Zorreras Members) in the Sorbas Basin, SE Spain. In: *Messinian Seminar, 3, Field Trip Guide, Field Trip 2, Málaga*, 22-36.

Roep, ThB & Van Harten, 1979. Sedimentological and ostracodological observations on Messinian post-evaporite deposits of some southwestern Spanish basins. In: Stournaras, G., Marcopoulou-Diacantoni, A. & Georgiades-Dikeoulia, E. (eds), Proceedings of the 7th International Congress on Mediterranean Neogene,

Athens, 27th October 1979, Annales Géologiques des Pays Héllniques, **3**, 1037-1044.

Roep, ThB., Beets, D.J., Dronkert, H & Pagnier, H., 1979. A prograding coastal sequence of wave-built structures of Messinian age, Sorbas, Almería, Spain. *Sedimentary Geology*, **116**, 27-56.

Rondeel, H.E., 1965. *Geological investigations in the western Sierra Cabrera and adjoining area, south-eastern Spain.* Unpublished PhD. Thesis, Municipal University, Amsterdam, 161pp.

Rose, J., Meng, X. & Watson, C., 1999. Palaeoclimate and palaeoenvironmental responses in the western Mediterranean over the last 140ka: evidence from Mallorca, Spain. *Journal of the Geological Society, London*, **156**, 435-448.

Ruegg, G.J.H., 1964. *Geologische Onderzoekingen in Het Bekken Van Sorbas, S Spanje.* Unpublished M.Sc. Thesis, Municipal University of Amsterdam, 67pp.

Sabelberg, U., 1977. The stratigraphic record of late Quaternary accumulation series in southwest Morocco and its consequences concerning the pluvial hypothesis. *Catena*, **4**, 204-214.

Sanz de Galdeano, C., 1990. Geologic evolution of the Betic Cordilleras in the western Mediterranean, Miocene to the present. *Tectonophysics*, **172**, 107-119.

Sanz de Galdeano, C., & Vera, J.A., 1992. Stratigraphic record and palaeogeographical context of the Neogene basins in the Betic Cordillera, Spain. *Basin Research*, **4**, 21-36.

Scheidegger, A., 1973. On the prediction of the reach and velocity of catastrophic landslides. *Rock Mechanics*, **5**, 231-236.

Schulte, L., 2002. Climatic and human influence on river systems and glacier fluctuations in southeast Spain since the Last Glacial Maximum. *Quaternary International*, **93-94**, 85-100.

Schulte, L. & Julià, R., 2001. A Quaternary soil chronosequence of Southeastern Spain. *Zeitschrift fur Geomorphologie*, **45**, 145-158.

Schumm, S.A., 1979. Geomorphic thresholds: the concept and its applications. *Institute of British Geographers, Transactions New Series*, **4**, 485-515.

Schuster, R.L., 1996. Socio-economic significance of landslides. In: Turner, A.K. & Schuster, R.L. (eds), *Landslides: Analysis and Control*, Special Report 247, Transportation Research Board, National Research Council, National Academy Press, Washington DC, 12-35.

Schuster, R.L. & Fleming, R.W., 1986. Economic losses and fatalities due to landslides. *Bulletin of American Association of Engineering Geologists*, 23, 11-28.

Seed, H.B., 1968. Landslides during earthquakes due to soil liquefaction. *American Society of Civil Engineers, Journal of the Soil Mechanics and Foundation Division*, 94, SM5, 1053-1122. [Reprinted in American Society of Civil Engineers, 1974, Terzhagi Lectures, 1963-1972: New York, *American Society of Civil Engineers*, p191-261.]

Selley, R.C., 1985. *Ancient Sedimentary Environments*, Third Edition, Cambridge University Press, Cambridge, UK, 317pp. [Orignially published by Chapman & Hall, London]

Shah, B.V., 1983. Is the environment becoming more hazardous? A global survey 1947 to 1980. *Disasters*, 7, 202-209.

Shreve, R.L., 1968. The Blackhawk landslide. *Geological Society of America, Special Paper*, 108, 47pp.

Skempton, A.W., 1953. Soil Mechanics in relation to geology. *Proceedings of the Yorkshire Geological Society*, 29, 33-62.

Skermer, N.A., 1985. Discussion of paper: "Nature and mechanics of the Mount st. Helens rockslide-avalanche of 18 May 1980". *Géotechnique*, 35, 357-362.

Soeters, R. & Van Westen, C.J., 1996. Slope instability recognition, analysis and zonation. In: Turner, A.K. & Schuster, R.L. (eds), *Landslides: Analysis and Control*, Special Report 247, Transportation Research Board, National Research Council, National Academy Press, Washington DC, 129-177.

Spivey, D., 1997. *Scale, process and badland development in Almeria Province*. Unpublished PhD Thesis, University of Liverpool.

Stapel, G., Moeys, R. & Biermann, C., 1996. Neogene evolution of the Sorbas Basin (Southeast Spain) determined by palaeostress analysis. *Tectonophysics*, 225, 291-305.

Starkel, L., 1966. Post-glacial climate and the moulding of European relief. *Proceedings of the International Symposium on World Climate 8,000 to 0 BC*, Royal Meterological Society, London, 15-32.

Starkel, L., 1985. The reflection of Holocene climatic variations in the slope and fluvial deposits and forms in the European mountains. *Ecologia Mediterranea*, **11 (1)**, 91-97.

Stokes, M., 1997. *Plio-Pleistocene drainage evolution of the Vera Basin, SE Spain*. Unpublished PhD Thesis, University of Plymouth, 390pp.

Stokes, M. & Sendra, J., 1996. Stratigraphical, sedimentological and palaeontological consequences of Pliocene fan-delta evolution, Vera Basin, SE Spain. In: Mather, A.E., Stokes, M. (eds), *BSRG/BGRG South-east Spain Field Meeting Guide Book*, University of Plymouth, England, 49-57.

Stokes, M. & Griffiths, J.S., 1999. Small-scale mass movement failures in Early to Mid Pleistocene fluvial deposits in the Vera Basin, South-east Spain. In: Griffiths, J.S., Stokes, M. & Thomas, R. (eds), *Proceedings of the 9th Interntional Conference and Field Trip on Landslides*, Balkema, Rotterdam, 135-147.

Stokes, M. & Mather, A.E., 2000. Response of Plio-Pleistocene alluvial systems to tectonically induced base-level changes, Vera Basin, SE Spain. *Journal of the Geological Society, London*, **157**, 303-316.

Stokes, M & Mather, A.E., 2003. Tectonic origin and evolution of a transverse drainage: the Río Almanzora, Betic Cordillera, Southeast Spain. *Geomorphology*, **50**, 59-81.

Stokes, M., Mather, A.E., & Harvey, A.M., 2002. Quantification of river-capture-induced base-level changes and landscape development, Sorbas Basin, SE Spain. In: Jones, S.J. & Frostick, L.E. (eds), *Sediment Flux to Basins: Causes, Controls and Consequences*, Geological Society, London, Special Publications, **191**, 23-35.

Swanston, D.N. & Schuster, R.L., 1989. Long-term landslide hazard mitigation programs: structure and experience from other countries. *Bulletin American Association of Engineering Geologists*, **26**, 109-113.

Terral, J.F. & Mengual, X., 1999. Reconstruction of Holocene climate in southern France and eastern Spain using qua anatomy of olive wood and archaeological charcoal. *Palaeogeography, Palaeoclimatology, Palaeoecology*, **153**, 71-92.

Terzaghi, K., 1950. Mechanism of Landslides. In: Paige, S. (Ed.), *Application of Geology to Engineering Practice*, Geological Society of America, New York, 83-123.

Terzaghi, K. & Peck, R.B., 1967. *Soil Mechanics in Engineering Practice*. Second Edition. John Wiley & Sons Inc., New York, 566pp.

Thompson, R. & Oldfield, F., 1986. *Environmental Magnetism*. Allen & Unwin, London.

Thornes, J.B., 1974. The rain in Spain. *Geographical Magazine*, **46**, 339-343.

Thornes, J.B. & Alcàantara-Ayala, I., 1998. Modelling mass failure in a Mediterranean mountain environment: climatic, geological, topographical and erosional controls. *Geomorphology*, **24**, 87-100.

Thorpe, R.S. & Brown, G.C., 1985. *The Field Description of Igneous Rocks*. Geological Society of London Handbook Series, **4**. Open University Press, 162pp.

Thurston, N. & Degg, M., 2000. Transferability and terrain reconstruction within a GIS landslide hazard mapping model: Derbyshire Peak District. In: Bromhead, E., Dixon, N. & Ibsen, M.-L. (eds), *Landslides in research, theory and practice*, Thomas Telford, London, 1467-1472.

Tianchi, Li., 1983. A mathematical model for predicting the extent of a major rockfall. *Zeitschrift für Geomorphologie Neue Folge*, **27**, 473-482.

Torres-Giron, M.L. & Recio-Espejo, J.M., 1997. Periglacial features of the Subbetic mountains of southern Spain (Córdoba Province). *Journal of Quaternary Science*, **12**, 275-282.

Total Geology Website, 2001. http://fbe.uwe.ac.uk/public/geocal/totalgeology/ - A website based on Fookes *et al.* (2001).

TRL, 1997. *Principles of Low Cost Road Engineering in Mountainous Regions*. TRL Overseas Road Note 16. Transportation Research Laboratory, Crowthorne, 149pp.

Troelstra, S.R., Van de Poel, H.M., Huisman, C.H.A, Geerlings, L.P.A. & Dronkert, H., 1980. Palaeoecological changes in the latest Miocene of the Sorbas Basin, SE Spain. *Géologie Méditerranéenne*, 7, 115-126.

Tucker, M.E., 1982. *The Field Description of Sedimentary Rocks*. Geological Society of London Handbook Series, 2. Open University Press, 124pp.

Tucker, M.E., 1991. *Sedimentary Petrology, An Introduction to the Origin of Sedimentary Rocks*. Second Edition. Blackwell Science, Oxford, UK.

Turner, A.K. & Schuster, R.L., 1996. *Landslides: Analysis and Control*, Special Report 247 of the Transportation Research Board, National Research Council, National Academy Press, Washington DC, 675pp.

Turner, K. & McGuffey, V.C., 1996. Organisation of investigation process. In: Turner, A.K. & Schuster, R.L. (eds), *Landslides: Analysis and Control*, Special Report 247, Transportation Research Board, National Research Council, National Academy Press, Washington DC, 121-128.

Van de Poel, H.M, Roep, ThB. & Pepping, N., 1984. A remarkable limestone breccia and other features of the Mio-Pliocene transition in the Agua Amarga Basin (SE Spain). *Géologie Méditerranéenne*, 11, 265-276.

Van Westen, C.J., Rengers, N., Terlien, M.T.J. & Soeters, R., 1997. Prediction of the occurrence of slope instability phenomena through GIS-based hazard zonation. *Geologische Rundschau*, 86, 404-414.

Varnes, D.J., 1958. Landslide types and processes. In: Eckel, E.B. (Ed.), *Landslides and engineering practice*, Special Report 29, Highways Research Board, National Research Council, Washington DC, 20-47.

Varnes, D.J., 1978. Slope movement types and process. In: Schuster, R.L. & Krizek, R.J. (eds), *Landslides: Analysis and control*, Special Report 176, Transportation Research Board, National Research Council, Washington DC, 11-33.

Varnes, D.J., 1984. *Landslide Hazard Zonation: A review of principles and practice*. UNESCO, Paris, 63pp.

Vissers, R.L., Platt, J.P. & Van Der Vaal, D., 1995. Late orogenic extension of the Betic Cordilleras and the Alboran Domain: a lithospheric view. *Tectonics*, 14, 786-803.

Voight, B., 1978 *Rockslides and avalanches, Natural Phenomena,* Elsevier, Amsterdam, **Vol. 1**, , 833pp.

Voight, B., Janda, R.J., Glicken, H., & Douglas, P.M., 1983. Nature and mechanics of the Mount st. Helens rockslide-avalanche of May 18, 1980. *Géotechnique,* **33**, 243-273.

Völk, H.R., 1967a. Relation between Neogene sedimentation and late orogenic movements in the Eastern Betic Cordilleras (SE Spain). *Geologie en Mijnbouw,* **46**, 471-474.

Völk, H.R., 1967b. *Zur Geologie und Startigraphie des Neogenbeckens von Vera, Südost-Spanien.* Unpublished PhD. Thesis, Municipal University of Amsterdam, 160pp.

Völk, H.R., 1979. *Quatare Reliefentwicklung in Südost-Spanien.* Heidelberger Geographische Arbieten, **58**, 146pp.

Völk, H.R. & Rondeel, H.E., 1964. Zur glied erung des jungtertiars im becken von Vera, Sudostspanien. *Geologie en Mijnbouw,* **43**, 310-315.

Wadge, G., 1988. The potential of GIS modelling of gravity flows and slope instabilities. *International Journal of Geographical Information Systems,* **2**, 143-152.

Weijermars, R., 1991. Geology and tectonics of the Betic Zone, SE Spain. *Earth Science Reviews,* **31**, 153-236.

Weijermars, R., Roep, T.H.B., Van Den Eeckhout, B., Postma, G. & Kleverlaan, K., 1985. Uplift history of a Betic fold nappe inferred from the Neogene-Quaternary sedimentation and tectonics (in the Sierra Alhamilla and Almeria, Sorbas and Tabernas Basins of the Betic Cordillera, SE Spain). *Geologie en Mijnbouw,* **64**, 379-411.

Wieczoek, G.F., 1984. Preparing a detailed landslide inventory map for hazard evaluation and reduction. *Bulletin of the Association of Engineering Geologists,* **21**, 337-342.

WP/WLI (Working Party on the World Landslide Inventory), 1990. A suggested method for reporting a landslide. *Bulletin of the International Association of Engineering Geology,* **41**, 5-12.

WP/WLI (Working Party on the World Landslide Inventory), 1991. A suggested method for a landslide summary. *Bulletin of the International Association of Engineering Geology*, **43**, 101-110.

WP/WLI (Working Party on the World Landslide Inventory), 1993. A suggested method for describing the activity of a landslide reporting a landslide. *Bulletin of the International Association of Engineering Geology*, **47**, 53-57.

WP/WLI (Working Party on the World Landslide Inventory), 1994. A suggested method for reporting landslide causes. *Bulletin of the International Association of Engineering Geology*, **50**, 71-74.

WP/WLI (Working Party on the World Landslide Inventory), 1995. A suggested method for describing the rate of movement of a landslide. *Bulletin of the International Association of Engineering Geology*, **52**, 75-78.

Wright, R.H. & Nilsen, T.H., 1974. *Isopleth map of landslide deposits southern San Fransisco Bay Region, California*, US Geological Survey Miscellaneous Field Studies Map MF550, scale 1:25,000.

Youd, T.L. & Perkins, D.M., 1978. Mapping liquefaction-induced ground failure potential. *American Society of Civil Engineers proceedings, Journal of the Geotechnical Engineering Division*, **104**, 433-446.

Zazo, C., Goy, J.L, Hoyes, M., *et al.*, 1981. Ensayo de sintesis sobre el Tirreniense Peninsular Español. *Estud. Geol.*, **37**, 257-262.

Appendix A – Publications

The following is a list of publications that have been written by while this study has been completed. A copy of all of the papers are also included.

Refereed Publications:

Griffiths, J.S., Mather, A.E. & Hart, A.B. (2002) Landslide susceptibility in the Rio Aguas Catchment, SE Spain. *Quarterly Journal of Engineering Geology and Hydrogeology*, 35, 9-17.

Hart, M.B. & Hart, A.B. (2000) Global Climate Change: A geological perspective. Geoscience in South West England, 10, 14-17.

Hart, A.B. & Hearn, G.J. (In preparation) Landslide susceptibility, hazard and risk mapping for low cost road planning in remote mountain areas. To be submitted to *Quarterly Journal of Engineering Geology and Hydrogeology* for publication in 2004.

Conference Proceedings & Non-Refereed Publications:

Hart, A.B., Hearn, G.J. Petley, D.N., Tiwari, S.C. & Giri, N.K. 2003. Using remote sensing and GIS for rapid landslide hazard assessment: Potential public sector uptake in Nepal and Bhutan. *Proceedings for the Permanent International Association for Road Congresses (PIARC) Conference "Sustainable Slope Risk Management for Roads"*, Kathmandu, Nepal, March 2003.

Hart, A.B., Lamichhane, P., Jha, P., Subba, M. & GC, S. 2003. A Landslide Database for Nepal. *Proceedings for the Permanent International Association for Road Congresses (PIARC) Conference "Sustainable Slope Risk Management for Roads"*, Kathmandu, Nepal, March 2003.

Petley, D.N, Crick, W.D.O. and Hart, A.B. 2002. The use of satellite imagery in landslide studies in high mountain areas. *The Proceedings of the 23rd Asian Conference on Remote Sensing (ACRS 2002), Kathmandu.* Available online at: http://www.gisdevelopment.net/aars/acrs/2002/hdm/48.pdf

Hart, A.B., Griffiths, J.S. & Mather, A.E. (2000) The role of landsliding in landscape development in the Rio Aguas Catchment, South East Spain. In: Bromhead, E., Dixon, N. & Ibsen, M.-L. (eds.) *Landslides in research, theory and practice*, Thomas Telford, London, 701-706.

Hart, A.B. & Griffiths, J.S. (1999) Mass movement features in the vicinity of the town of Sorbas, South-east Spain. In: Griffiths, J.S., Stokes, M.R. & Thomas, R.G. (eds.)

1

Landslides: Proceedings of the Ninth International Conference and Field Trip on Landslides, Bristol, UK, 5th-16th September 1999, A.A. Balkema, Rotterdam, 57-63.

Hart, A.B. (1999) An Introduction to the Landslides of the Sorbas Basin. In: Mather, A.E. & Stokes, M. (eds.) *BSRG/BGRG South East Spain Field Meeting Guide Book*, University of Plymouth, England, 124-133.

Conference Abstracts & Posters:

Hart, A.B., Griffiths, J.S. & Mather, A.E. (abstract) Differentiating between susceptibility, hazard and risk: a case study of landsliding in South East Spain. Abstract for a paper that was presented by Griffiths, J.S. at the RGS/IBG Conference, held at the University of Plymouth, January 2001.

Mather, A.E., Hart, A.B. & Griffiths, J.S. (abstract) Impact of Quaternary base-level change on hillslope erosion in the Rio de Aguas catchment, South-East Spain. Abstract submitted to the COST Conference, Almeria, September 2000.

Hart, A.B. (2000) Landslide activity, drainage development and risk assessment: The Sorbas Case Study, SE Spain. Poster presented at the European Union Concerted Action on Forecasting, Prevention and Reduction of Landslide and Avalanche Risks (CALAR) Conference "Living with Natural Hazards", Vienna, Austria 17th-19th January 2000.

Hart, A.B. (2000) Landslide activity, drainage development and risk assessment: The Sorbas Case Study, SE Spain. Poster presented at the 8th International Symposium on Landslides, Cardiff, Wales, 26th - 30th June 2000.

Scott Wilson Project Reports:

"Report on Project Activities undertaken in Nepal." Unpublished Report for the DFID funded project R7815 – "Landslide Risk Assessment in the Rural Access" Project.

"Report on Project Activities undertaken in Bhutan". Unpublished Report for the DFID funded project R7815 – "Landslide Risk Assessment in the Rural Access Sector" Project.

"Proceedings for the Regional Workshop held in Ilam, Nepal, 16th to 17th March 2003" (written in conjunction with other members of the LRA Project Team). Unpublished Report for the DFID funded project R7815 – "Landslide Risk Assessment in the Rural Access Sector" Project.

"Proceedings for the Regional Workshop held in Pokhara, Nepal, 16th to 18th February 2003" (written in conjunction with other members of the LRA Project Team). Unpublished Report for the DFID funded project R7815 – "Landslide Risk Assessment in the Rural Access Sector" Project.

"Best Practice Guidelines in the Use of a Geographical Information System for Landslide Susceptibility Mapping at a Regional Scale" Unpublished Report for the DFID funded project R7815 – "Landslide Risk Assessment in the Rural Access Sector" Project.

"Proceedings for the Mountain Hazard Research and Mitigation Seminar held in Kathmandu, Nepal, 18th to 23rd November 2002" (written in conjunction with other members of the LRA Team). Unpublished Report for the DFID funded project R7815 – "Landslide Risk Assessment in the Rural Access Sector" Project.

"Proceedings for Bhutan Studies: Final Seminar held in Thimphu, Bhutan, 27th September 2002" (in conjunction with other members of the LRA Team). Unpublished Report for the DFID funded project R7815 – "Landslide Risk Assessment in the Rural Access Sector" Project.

"Report on the GIS Workshop 7th to 9th October 2002, Thimphu, Bhutan". Unpublished Report for the DFID funded project R7815 – "Landslide Risk Assessment in the Rural Access Sector" Project.

"Landslide Factor and Susceptibility Analyses: Baglung and Arghakhanchi Project Development Areas and Ilam Project Test Area". Unpublished Report for the DFID funded project R7815 – "Landslide Risk Assessment in the Rural Access Sector" Project.

"Rainfall Analysis for the Baglung, Arghakhanchi and Ilam Project Study Areas". Unpublished Report for the DFID funded project R7815 – "Landslide Risk Assessment in the Rural Access Sector" Project.

Landslide susceptibility in the Río Aguas catchment, SE Spain

J.S. Griffiths[1], A.E. Mather[2] & A.B. Hart[1]

[1]Department of Geological Sciences University of Plymouth, Drake Circus, Plymouth, Devon PL4 8AA, United Kingdom (e-mail: j1griffiths@plymouth.ac.uk)
[2]Department of Geographical Sciences, University of Plymouth, Drake Circus, Plymouth, Devon PL4 8AA, United Kingdom

Abstract

The definitions of hazard and risk in natural hazard studies are well established in the scientific literature. However, many examples of landslide hazard assessment only identify the susceptibility of slopes to failure and make no statement on the frequency of occurrence that would be necessary for a complete hazard evaluation. In a research programme undertaken in SE Spain the issue of landslide susceptibility in a semi-arid neotectonic environment was examined, with some attempt to evaluate the hazard. This work involved establishing the occurrence of landsliding within the 550 km² Río Aguas catchment through remote sensing interpretation and field mapping. These data were compiled in an inventory containing the records of nearly 250 landslides that was analysed to establish the nature and extent of landslide susceptible situations. Within the catchment anticipated combinations of geological materials proved to be susceptible to failure, and relationships between landslide volume and travel angle were examined in relation to standard models. The highest incidence of contemporary landsliding appeared to be related to the proximity of a major river capture site, a geomorphological event that had been dated at 100 000 BP. This produced localized rapid incision, a ten fold increase in sediment removal and the creation of oversteepened slopes that were only recently degrading to their long-term angle of stability. In addition to contemporary landslides, field mapping identified anomalous geological structures that proved to be degraded erosional remnants of ancient landslides. Relating these remnants to the river terrace sequence in the region provided some control on the relative ages of these ancient or fossil landslides. It was concluded that any assessment of landslide risk in the study area would need to take into account not only geological materials and the contemporary geomorphological environment but also the geomorphological history of the region.

Keywords: landslides, susceptibility, hazard, SE Spain

When subject to careful investigation the causes and mechanisms of an individual landslide occurrence can generally be described in detail. Based on such studies it has been possible to develop general theories about landslide behaviour, and the state-of-the-art has recently been summarized in Turner & Schuster (1996). However, for most planning and feasibility studies in engineering the main requirement is for the potential of landslides occurring to be established and the scale of the hazard to be defined. This subject was examined in detail in the 1997 Honolulu Workshop on Landslide Risk Assessment (Cruden & Fell 1997). From this work it became apparent that, whilst the definitions of susceptibility, hazard and risk in landslide studies are well established in the scientific literature (Hearn & Griffiths 2001; Royal Society 1992) many studies failed to incorporate the necessary landslide frequency data to provide actual estimates of hazard. The Workshop also demonstrated that the methods for carrying out susceptibility, hazard and risk assessments were available but that more studies were needed both to provide the necessary base data on landslide occurrence and to refine and develop the techniques. Against this background this paper describes a research programme undertaken in SE Spain to examine the occurrence of landsliding within the 550 km² Río Aguas catchment (Fig. 1). Data were compiled in a landslide inventory from remote sensing interpretation and field mapping and this was analysed to establish the nature and extent of landslide susceptible situations. In this study it was recognized that there was a lack of information on landslide frequency, therefore, a genuine assessment of landslide hazard was not possible. The only control on landslide frequency that became apparent concerned some of the degraded ancient or 'fossil' landslides that had been identified. In places these could be related to the Quaternary terrace sequence of the area that had been dated approximately by Harvey et al. (1995). However, the recognition and occurrence of ancient landslides did not assist in the definition of the contemporary landslide hazard.

In addition to geological and geomorphological details, the landslide inventory contained data on the various elements at risk within the landscape. However, the vulnerability of the various elements and probability of occurrence of the identified risks was not been defined and this will require further research. The authors are presently undertaking further research on the triggering causes of the landslides in the region, notably seismic activity and rainfall conditions. This paper, therefore, concentrates on the underlying processes that need to be
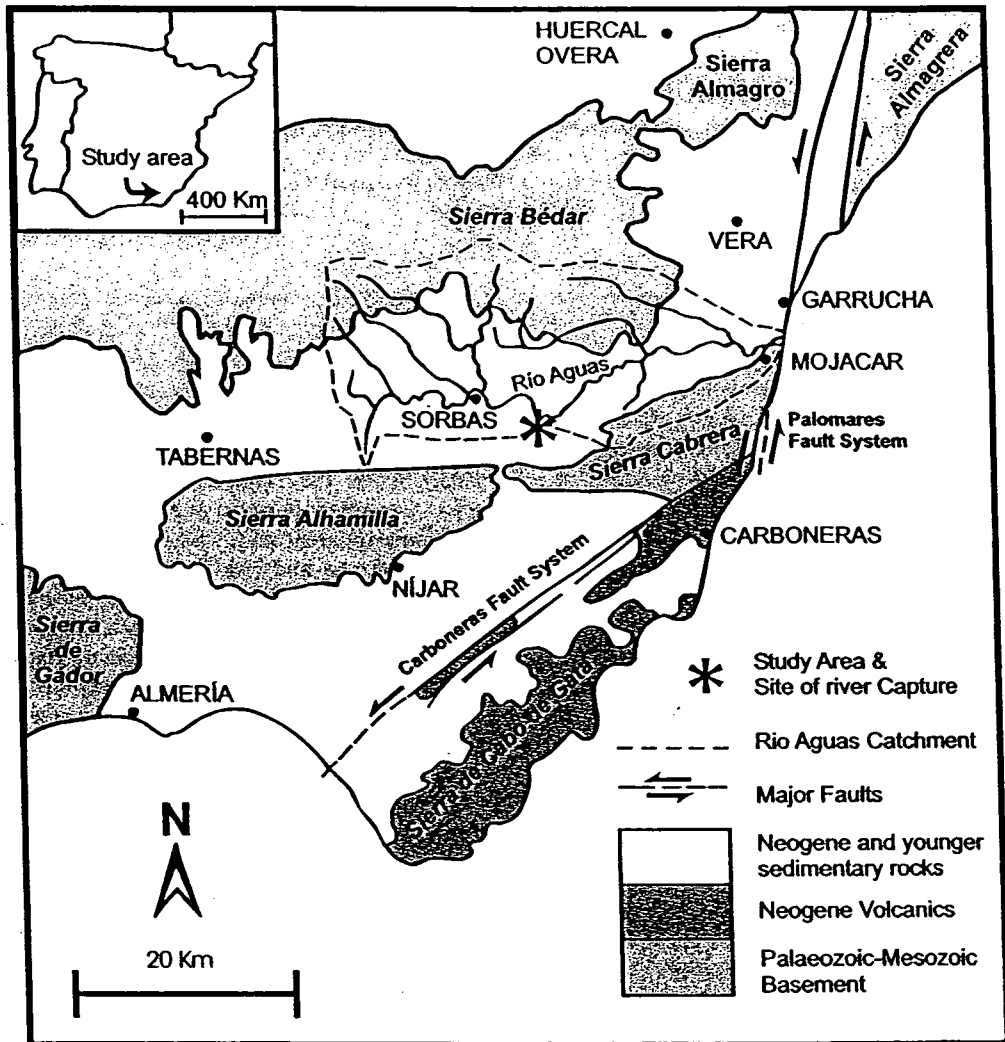
Fig. 1. Location map of the Almeria region showing the major tectonic units, fault systems and the Río Aguas catchment (after Mather & Harvey 1995).

taken in to account before the hazard and risk from landsliding can be evaluated.

The study area

The study area is located in the Almería Province of SE Spain. It has an arid climate with annual precipitation recently established as less than 210 mm (Esteban-Parra 1998). The area is seismically active with regular small magnitude events of less than 4, and major earthquakes with intensities of X on the Modified Mercalli Scale identified in the historic record (WWW 2001).

The modern Río Aguas catchment covers an area of approximately 550 km^2 and drains the Neogene sedimentary basins of Sorbas, and a small part of Vera. The study area is bounded by the Sierra de los Filabres to the

north, the Sierra Alhamilla/Cabrera to the south and a low drainage divide with Tabernas Basin to the west. To the east the Río Aguas drains in to the Mediterranean Sea near the town of Mojacar.

The general geology of the study area is presented in Figure 1 and the detailed stratigraphy in Figure 2. The Sorbas and Vera basins are part of the Trans-Alboran shear zone of Larouziére *et al.* (1988), a zone dominated by sinistral movement within the internal zone of the Betics. The mountains (sierras) surrounding the basins are composed of Mesozoic and older basement rocks which can be broadly divided into the Nevado Filabride and Alpujarride nappes (Egeler & Simon 1969; García-Hernández *et al.* 1980; Sanz de Galdeano 1990), whilst the faulting helps define the Neogene Basins. Localized variations in compression and extension directions were generated over the period of sedimentary
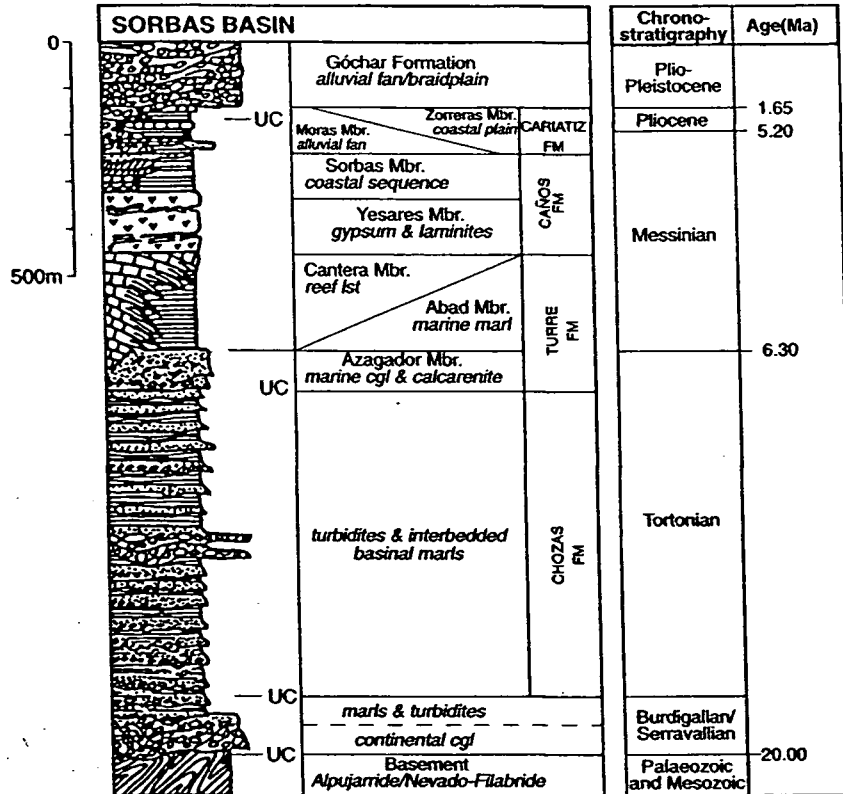
Fig. 2. Stratigraphy in the study area (after Mather 1991).

basin evolution (Keller et al. 1995). Within the Sorbas Basin, during the Quaternary, compression has been dominantly north–south, with associated east–west extension (Mather & Westhead 1993). Uplift rates for this part of the basin have been calculated at 160 m/Ma over the Plio/Pleistocene (Mather 1991). Rates were calculated using the current elevation of the last (lower Pliocene) marine incursion into the region, and corrected for sea level fluctuation (Mather 1991).

Differential uplift has increased regional gradients which, when combined with the variable lithologies of the basin fill, lead to ideal conditions for incision and river capture. The Río Aguas catchment has been affected by two significant river captures. The first occurred in the early Pleistocene and removed the headwaters of the original consequent drainage (Mather 1991, 1993, 2000b; Mather & Harvey 1995). The second river capture event is estimated to have occurred at about 100 ka (Harvey et al. 1995). This 100 ka date is substantiated by U/Th isochron methods used by Kelly et al. (2000) to date carbonate soils from the terrace landforms at c.88 ka (68–104 ka). This second river capture lowered base-levels at the point of capture (Figs 1 & 3) by c. 90 m (Harvey et al. 1995) and re-routed 73% of the original Sorbas Basin

drainage from the Níjar/Carboneras Basin in the south to the Vera Basin in the east (Fig. 1; Mather 2000b). This created a local base-level change both upstream and downstream on the Río Aguas and it has been estimated that there was a five fold increase in incision rates over most of the river network, whilst close to the point of capture incision rates may have increased ten fold (Mather 2000a). The sediment flux calculated for the post capture period in the main river showed an increase by a factor of between 2 to 9 (Stokes et al. 2002).

The change in the local base-level resulting from the second river capture had a profound effect on the geomorphology of the whole Sorbas Basin. Incized canyons have developed in the stronger geological strata, whereas large 'V' shaped valleys are predominantly found in the weaker lithologies. During the formation of this terrain, sediment has been eroded from the slopes to provide both suspended and bedload material to the fluvial system through a variety of hillslope processes. Given the rapid rates of incision over the past c.100 ka, the landscape has had little time to adjust and many hillside slopes may be regarded as over-steepened, and, hence, in a state of marginal stability.

Table 1. *Parameters compiled in the landslide inventory*

No	Parameter	Definition
1	Location	The geographical location of the landslide and the longitude and latitude co-ordinates of the centre of the landslide.
2	Land use	The use of the land either above, below or adjacent to the landslide and any remedial measures that have been undertaken.
3	Elevation	The elevation of the crown and the toe of the landslide.
4	Geometry	The height, width and length of the backscar and debris accumulation, as well as the area covered by and the volume of the debris accumulation.
5	Landslide mechanisms	The landslide failure mechanisms involved.
6	Angle of reach	The angle of reach of the landslide (measured as an indicator of landslide mobility).
7	Landslide activity	The state, style, distribution and rate of the landslide.
8	Causative factors	The factors that have been attributed as either decreasing the stability of the slope or actually triggering the landslide.
9	Morphology	The aspect, profile and angle of the slope.
10	Geomorphology	The Land System, Land Facet and Land Element in which the landslide is located.
11	Geology	The geology of the landslide. Additional information concerning the geotechnical properties of both the rock material and rock masses involved in the landslide are contained within a second database.
12	Vegetation	The type and extent of vegetation cover associated with the landslide.
13	Drainage	The nature of the drainage within and around the landslide.
14	References	Any published or unpublished material referring to the landslide.
15	Other information	Any other relevant information.

The landslide investigation

It is apparent that there is a high level of understanding about the recent geological history of the Sorbas and Vera basins and the role of fluvial activity in the development of the contemporary landscape (see above). A preliminary site reconnaissance in 1997, however, established that landsliding is a significant mechanism for sediment transfer from hillslopes to the fluvial network. Therefore, in March 1998 a research programme was initiated to investigate the scale and extent of landsliding in the region with the aims: to evaluate landslide causes and mechanisms, identify the controls on susceptibility and hazard, and establish the role of landslide processes in landscape development. This work was based on field mapping, remote sensing interpretation, data collation and analysis. In order to provide a direct link with the on-going investigations in sediment flux, it was decided to base the study on a single major drainage basin, namely the Río Aguas.

Landslide inventory

The first stage in any regional landslide study is the creation of a landslide inventory. In order to identify the situations where landslides were most likely to occur, the inventory compiled data on the range of parameters listed in Table 1. All data were encoded in a database to allow ease of analysis and this database was linked to other environmental information in a Geographical Information System. For the creation of the inventory the classification and reporting systems recommended by the UNESCO Working Party on World Landslide Inventory (WP/WLI (UNESCO Working Party for World Landslide Inventory), 1990, 1991, 1993; Cruden 1991) were adopted. The checklist for the causes of landsliding was based on the work of Brunsden (1993), and Dikau *et al.* (1996), although the interpretation of field situations was strongly influenced by the work of Professor Hutchinson summarized in his Glossop Lecture (Hutchinson 2001).

For the aerial photograph interpretation stereo images were used and landslides were identified by reference to the morphological and tonal indicators contained in Soeters & Van Westen (1996); TRL (1997); Rib & Liang (1978); Dikau *et al.* (1996). Two types of aerial photographs were used for the investigation:

(1) 1:30 000 black and white prints from the Spanish Catalunya Cartographic Institute, acquired on flights in September 1984, April 1985 and October 1985.

(2) 1:13 333 colour prints from the National Environment Research Council (NERC), acquired from a flight flown in the spring of 1996.

Fieldwork comprised geological and geomorphological mapping using standard systems and nomenclature (Barnes 1997; Cooke & Doornkamp 1990; Brunsden *et al.* 1975; Gardner & Dackombe 1983). The field mapping was used to both ground-truth the aerial photograph interpretation and identify landslides not easily identifiable on the aerial photographs, because their size was less than approximately 10 m x 10 m (i.e. 0.75 mm x 0.75 mm on 1:13 333 scale photographs).

To date, nearly 250 landslides have been mapped in the catchment (Fig. 3), an increase in 50 since the work

Sierra de los Filabres
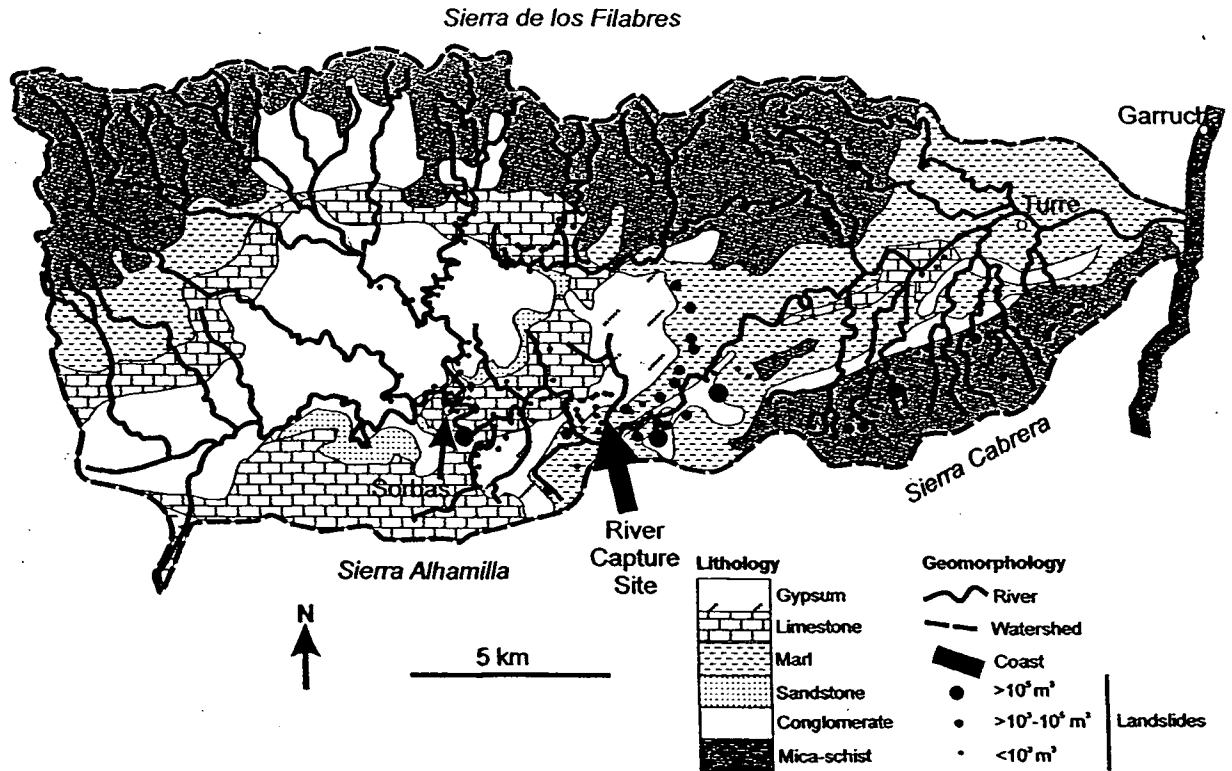
Fig. 3. Landslide distribution and bedrock lithology in the Río Aguas catchment.

was last reported (Hart *et al.* 2000). This gives a landslide density of approximately 0.45 landslides per km². Nearly 70% of the landslides identified were found to be rockfalls and a further 23% were non-rotational compound failures. The landslides varied in volume from tens of cubic metres up to several million cubic metres.

During initial site reconnaissance of the catchment it was apparent that the landslides occurred in certain geomorphological settings. Therefore, it was decided that some form of systematic representation of the landscape was needed that identified different geomorphological situations. After considerable debate on a range of landscape models, of the type proposed by Fookes (1997); Fookes *et al.* (2000), a terrain systems subdivision of the landscape was adopted. This terrain system classification is presented in Table 2. Each major terrain system was subdivided first into land facets and then into smaller land elements, as described by Phipps (2001). The terrain system was included in the database as an ordinal dataset as the requirement was simply to look at the cross-correlation between geomorphological settings and the occurrence of landslides of different types. The main terrain systems were primarily a function of the different bedrock lithologies, whereas the land facets more closely reflected the way the local geological structure and geotechnical properties of soils and rocks influenced geomorphological processes.

Whilst this particular land system classification is only appropriate for use in the study area, Waller & Phipps (1996) suggested the land systems approach can be used in a wide range of engineering studies at different scales.

For the classification of the geological materials two types of data were collected, the stratigraphic unit based on the stratigraphy presented in Figure 2, and a lithological description. The lithological description was carried out in the field using the standard engineering system presented in BS 5930 (BSI 1999).

Landslide susceptibility

Whilst the triggers of individual landslide events could rarely be identified a number of clear relationships between the location of a landslide and particular geological and geomorphological situations were established.

The Góchar Formation with 20% of recorded landslides, the Sorbas Member of the Caños Formation with 21% and the Turre Formation with 22% were the most susceptible stratigraphic units. Overall, because of its widespread occurrence within the Río Aguas catchment, 33% of recorded landslides were found to occur in the Caños Formation. Of the lithologies involved in landslides, conglomerates accounted for 30%, limestone 24%

Table 2. *Terrain systems classification used in the landslide inventory*

Terrain Systems	
1	Gentle slopes incized by canyons and gullies
2	Gentle slopes with terraced river valleys
3	Mountain slopes incized by river channels
4	Plateau area

Land Facets	
1	Hill / Mountain area
2	Incized river channel / canyon bounded by river terraces
3	Incized river channel / canyon without any river terraces
4	Open River valley bounded by river terraces
5	Open River valley bounded by slopes formed by the dissection of the drainage system
6	Terraces
7	Level terrain (Interfluve area)
8	Badlands
9	Gully System
10	Plateau area

Land Elements			
1	plateau area	17	river terrace surface
2	crest or ridge area	18	river terrace slope
3	scarp-slope escarpment / cliff face / canyon wall	19	artificial terrace
4	dip-slope escarpment/cliff face/canyon wall	20	man-made slope/road cutting
5	scarp-slope transportational mid-slope	21	scarp slope – inside of an active meander
6	dip-slope transportational mid-slope	22	inside of an active meander
7	slope perpendicular to dip direction	23	scarp slope – outside of an active meander
8	valley side slope	24	outside of an active meander
9	colluvial footslope / talus	25	dip-slope – inside of an active meander
10	gully side wall	26	dip-slope – outside of an active meander
11	scarp-slope gully side/wall	27	scarp slope – inside of an abandoned meander
12	dip-slope gully side / wall	28	inside of an abandoned meander
13	gully floor	29	scarp slope – outside of an abandoned meander
14	abandoned river channel or canyon	30	outside of an abandoned meander
15	floodplain	31	dip-slope – inside of an abandoned meander
16	active river channel or canyon	32	dip-slope – outside of an abandoned meander

and sandstone 22%. Where more than one lithology was involved in a failure the most widespread combination was gypsum over marl (22%) and limestone over marl (17%). When individual failures were examined, it was apparent that the scale and mode of failure (ie topple, wedge, planar) of many were controlled by the local discontinuity patterns. This is exemplified by the large-scale failure at Maleguica (Fig. 4), approximately 1/2 km south of Sorbas Town. This landslide has formed in marls and gypsum from the Yesares Member overlain by limestones and sandstones of the Sorbas Member. The bedding is dipping northwards out of the cliff face in Figure 4, and the shape of the eastern lateral scar (left side of Figure 4) and backscar are controlled by two joint sets perpendicular to the bedding and at 60° to each other. The overall failure, therefore, is a translational block slide along a bedding plane, with secondary toppling and rockfalls controlled by the joint pattern, that

has developed on the outside of a meander loop of the Rio Aguas.

The land systems approach to classifying the landscape highlighted some very interesting concentrations of landsliding. Not surprisingly the vast majority of the landslides occurred within the general category of 'Mountain Slopes Incized by River Channels', and within the land facets 70% of failures were associated with these incized rivers. At the land element level, however, the outside of active river meanders only accounted for 32% of failures (e.g. at Malaguica, Figure 4) and 21% were found to be on cliff-faces or canyon walls developed at the edge of dip-slope escarpments. Other notable geomorpho logical situations susceptible to landsliding were cliff faces or canyon walls developed at the edge of scarp slopes (9%) and on the inside of abandoned meander (8%). However, one general observation that coul

Fig. 4. Maleguica landslide, south of the town of Sorbas.

be made from the overall landslide distribution map was that the density of landslides was highest in the vicinity of the Late-Pleistocene river capture site (Fig. 3).

Landslide hazard

The majority of the landslides were identified as either active or recent but insufficient data were available to provide a genuine estimate of frequency that could be used as a basis for a hazard analysis. However, studies by Corominas (1986) demonstrated that the travel angle (i.e. the angle between the horizontal and a line drawn from the crest to the toe of a landslide) could be used as a mobility index for landslides. This would provide an indication of at least one facet of the hazard from landslides in a region, namely the extent of the area likely to be covered by a landslide event. For this study one of the relationships investigated was between landslide volume and travel angle (Fig. 5). In this analysis a minimum cut-off travel angle of 10 degrees could be identified, and the coefficient of determination (r^2) for the relationship between the angle of reach and the natural logarithm of the volume was 0.396. Given the subset of 153 landslides for which these parameters were available this was a very significant relationship and produced the regression equation:

$$Y = -3.171 \log_e (X) + 73.74$$

Where: Y = Angle of Reach (in degrees)
        X = Landslide Volume (in m^3)

The strength of this relationship for landslides within the Río Aguas catchment is a function of the relatively limited number of landslide types. However, with on-going investigations to determine the triggering causes of landslides and the attempts to define the frequency of occurrence of failures, this regression relationship will provide the basis for defining the scale of the runout hazard from landslide events of all magnitudes.

A further area of investigation stems from the results of the detailed geological mapping of the Sorbas Basin reported in Mather (1991). During this work sites were identified where the dip and dip direction of faults did not fit the overall pattern of faulting in the region and could not be ascribed to local tectonic structures or particular stratigraphic units. An investigation of one of these anomalous fault systems in a sub-catchment of the Río Aguas, the Mocatán catchment to the south of the town of Sorbas, has been carried out by Mather et al. (in press). This work has shown that an alternative interpretation is that some of these fault anomalies represent the degraded remnants of ancient landslides, labeled as 'fossil landslides' by Mather et al. (in press). On the basis of its relationship with the Sorbas Basin river terrace sequence established by Harvey et al. (1995), the Mocatán ancient landslide has been shown to have occurred soon after the second Río Aguas river capture event in the Late Pleistocene. Other possible ancient landslides have been identified and are subject to further investigation. If a Late Pleistocene history of landsliding can be established by reference to the river
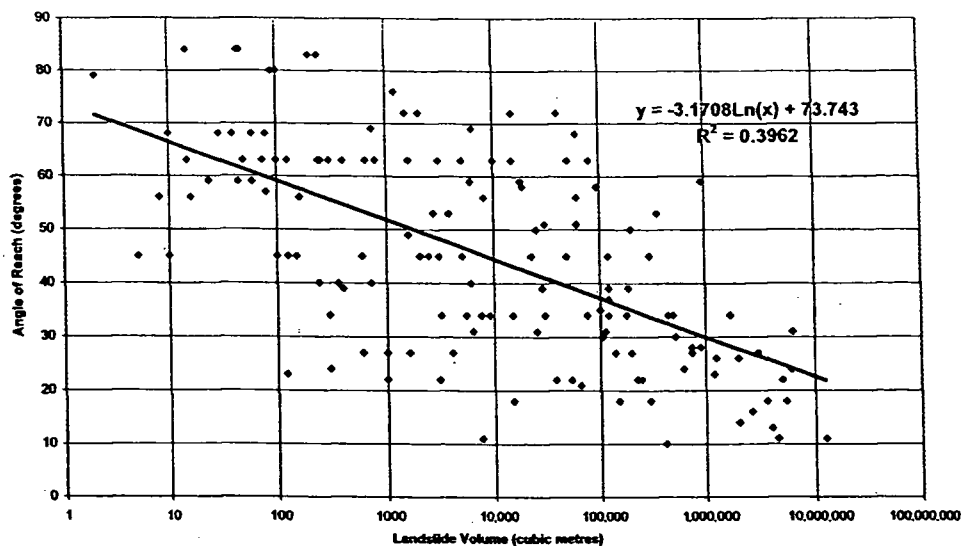
Fig. 5. Relationship between landslide travel distance and landslide volume, Río Aguas catchment.

terrace sequence then it might be possible to evaluate the landslide hazard over this period of time. However, it will not provide a realistic estimate of the contemporary landslide hazard.

Conclusions

The density of landsliding in the Río Aguas catchment exceeds that on any single lithology in Great Britain (Jones & Lee 1994), suggesting that the potential risk from landsliding in the area is high. One of the original aims of the research programme was to investigate the controls and causes of landsliding within a single catchment. Whilst certain lithologies and geomorphological situations were identified as particularly landslide susceptible, it became apparent during the investigation that the contemporary distribution of landsliding was best understood by reference to the geomorphological history of the area. The identified concentration of landslide activity around the site of a Late-Pleistocene river capture (Fig. 3) suggests that this resulted in a local change in base level. The erosion resulting from the river capture created a 'wave of incision' (Garcia *et al.* 1999) similar to the 'wave of aggression' identified by Bjerrum & Jørstad (1968) in relation to changes in sea level. This resulted in oversteepening of valleyside slopes, which in turn has led to the concentration of landslide activity. It is also likely that the contemporary landslide 'hazard' is accentuated by seismic activity in the area, although this has yet to be demonstrated.

This investigation illustrates the need for investigations of landslides to fully take into account the geological and geomorphological history of a region if the controls on current instability are to be understood.

References

BARNES, J.W. 1997. *Basic Geological Mapping* 3rd Edn. 133, John Wiley & Sons, Chichester.

BJERRUM, L. & JØRSTAD, F. 1968. Stability of rock slopes in Norway. *Norwegian Geotechnical Institute Publication No.*, 79, 1–11.

BRUNSDEN, D. 1993. Mass movement: the research frontier and beyond: a geomorphological approach. *Geomorphology*, 7, 85–128.

BRUNSDEN, D., DOORNKAMP, J.C., FOOKES, P.G., JONES, D.K.C. & KELLY, J.M.H. 1975. Large-scale geomorphological mapping for highway engineering. *Quarterly Journal of Engineering Geology*, 8, 227–253.

BSI (BRITISH STANDARDS INSTITUTE) 1999. *BS 5930: Code of Practice for Site Investigations.* London.

COOKE, R.U. & DOORNKAMP, J.C. 1990. *Geomorphology in Environmental Management.* 2nd Edn. Clarendon Press, Oxford.

COROMINAS, J. 1986. The angle of reach as a mobility index for small and large landslides. *Canadian Geotechnical Journal*, 33, 260–271.

CRUDEN, D.M. 1991. A simple definition of a landslide. *Bulletin of the International Association of Engineering Geology*, 43, 27–29.

CRUDEN, D. & FELL, R. (eds) 1997. *Landslide Risk Assessment* Balkema, Rotterdam.

DIKAU, R., BRUNSDEN, D., SCHROTT, L. & IBSEN, M-L. 1996. *Landslide Recognition* John Wiley & Sons, Chichester.

ESTEBAN-PARRA, M.J., RODIGO, F.S. & CASRO-DIEZ, Y. 1992. Spatial and temporal patterns of precipitation in Spain for the perod 1880–1992. *International Journal of Climatology*, 18, 1557–1574.

EGELER, C.G. & SIMON, O.J. 1969. Orogenic evolution of the Betic zone (Betic Cordilleras Spain) with emphasis on nappe structure. *Geologie en Mijnbouw*, 48, 296–305.

FOOKES, P.G. 1997. Geology for engineers: the geological model, prediction and performance. *Quarterly Journal of Engineering Geology*, 30, 293–424.

FOOKES, P.G., BAYNES, F. & HUTCHINSON, J.N. 2000. Total geological history: a model approach to understanding

site conditions. *Proceedings of GeoEng2000, Melbourne*, 1, 370–460.

GARCÍA, A.F., KU, T.L., CHADWICK, R., EL HAMDOUNI, R., IRIGARAY FERNANDEZ, C., CHACON MONTERO, J. & KELLER, E. A. 1999. Quaternary geology, geomorphology and calcic soils of the eastern Alpujarran corridor, Almeria, Southern Spain. *In:* MATHER, A. E. & STOKES, M. (eds) *BSRG/BGRG SE Spain Field Meeting Guide Book* University of Plymouth 97–123.

GARCÍA-HERNÁNDEZ, M., LÓPEZ-GARRIDO, A.C., RIVAS, P. SANZ DE GALDEANO, C. & VERA, J.A. 1980. Mesozoic palaeogeographic evolution of the External zones of the Betic Cordillera. *Geologie en Mijnbouw*, 59, 155–168.

GARDNER, V. & DACKOMBE, R. 1983. *Geomorphological Field Manual.* Allen & Unwin, London.

HART, A.B., GRIFFITHS, J.S. & MATHER, A.E. 2000. The role of landsliding in landscape development in the Rio Aguas Catchment. *Southeast Spain. ISSMGE and BGS 8th International Symposium on Landslides, Cardill, South Wales*, 26–30 June, 2000, 701–706.

HARVEY, A.M., MILLER, S.Y. & WELLS, S.G. 1995. Quaternary soil and river terrace sequences in the Aguas/Feos river systems: Sorbas basin, southeast Spain. *In:* LEWIN, J., MACKLIN, M.G. & WOODWARD, J.C. (eds) *Mediterranean Quaternary River Environments* Balkema, Rotterdam, 263–281.

HEARN, G.J. & GRIFFITHS, J.S. 2001. Landslide hazard assessment. *In:* GRIFFITHS, J. S. (ed.) *Land Surface Evaluation in Engineering Practice.* Engineering Geology Special Publication, 18, 43–52.

HUTCHINSON, J.N. 2001. Reading the ground: morphology and geology in site appraisal. *Quarterly Journal of Engineering Geology and Hydrogeology*, 34, 5–50.

JONES, D.K.C. & LEE, E.M. 1994. *Landsliding in Great Britain* HMSO, London.

KELLER, J.V.A., HALL, S.H., DART, C.J. & McCLAY, K.R. 1995. The geometry and evolution of a transpressional strike-slip system: the Carboneras fault. *SE Spain. Journal of the Geological Society, London*, 152, 339–351.

KELLY, M., BLACK, S. & ROWAN, J.S. 2000. A calcrete-based U/Th chronology for landform evolution in the Sorbas basin, southeast Spain. *Pleistocene Science Reviews*, 19, 995–1010.

LAROUZIÈRE, F.D., DE BOLZE, J., BORDET, P., HERNANDEZ, J., MONTENAT, C. & OTT D'ESTEVOU PH. 1988. The Betic segment of the lithospheric Trans-Alboran shear zone during the late Miocene. *Tectonophysics*, 152, 41–52.

MATHER, A.E. 1991. *Cenozoic drainage evolution of the Sorbas Basin SE Spain.* PhD Thesis, University of Liverpool.

MATHER, A.E. 1993. Basin inversion: Some consequences for drainage evolution and alluvial architecture. *Sedimentology*, 40, 1069–1089.

MATHER, A.E. 2000a. Adjustment of a drainage network to capture induced base-level change. *Geomorphology*, 34, 271–289.

MATHER, A.E. 2000b. Impact of headwater river capture on alluvial system development. *Journal of the Geological Society of London*, 157, 957–966.

MATHER, A.E. & HARVEY, A.M. 1995. Controls on drainage evolution in the Sorbas basin, southeast Spain. *In:* LEWIN, J., MACKLIN, M.G. & WOODWARD, J. (eds) *Mediterranean Quaternary River Environments* Balkema, Rotterdam, 65–76.

MATHER, A.E. & WESTHEAD, R.K. 1993. Plio/Quaternary strain of the Sorbas Basin, SE Spain: Evidence from sediment deformation structures. *Quaternary Proceedings*, 3, 57–65.

MATHER, A.E., GRIFFITHS, J.S. & STOKES, M. in press. Anatomy of a fossil landslide from the Pleistocene of SE Spain. *Geomorphology*.

PHIPPS, P.J. 2001. Terrain systems mapping. *In:* GRIFFITHS, J. S. (ed.) *Land Surface Evaluation in Engineering Practice.* Engineering Geology Special Publication, 18, 59–61.

RIB, H.T. & LIANG, T. 1978. Recognition and identification. *In:* SCHUSTER, R. L. & KRIZEK, R. J. (eds) *Landslides – Analysis and Control* 3, 33–79 National Academy of Sciences, Washington DC.

ROYAL SOCIETY 1992. *Risk: analysis, perception and management.* Report of the Royal Society Study Group, The Royal Society, London.

SANZ DE GALDEANO, C. 1990. Geologic evolution of the Betic Cordilleras in the Western Mediterranean, Miocene to the present. *Tectonophysics*, 172, 107–119.

SOETERS, R. & VAN WESTEN, C. J. 1996. Slope instability recognition. *In:* TURNER, A. K. & SCHUSTER, R. L. (eds) *Landslides Investigation and Mitigation.* Special report 247 of the Transportation Research Board, National Research Council, National Academy Press, Washington DC, 129–177.

STOKES, M., MATHER, A.E. & HARVEY, A.M. 2002. Quantification of river capture induced base-level changes and landscape development, Sorbas, SE Spain. *In:* JONES, S. & FOSTICK, L. (eds) *Sediment Flux to basin: causes, controls, consequences.* Special Publications, 192, Geological Society, London in press.

TURNER, A.K. & SCHUSTER, R. L. (eds) 1996. *Landslides Investigation and Mitigation.* Special report 247 of the Transportation Research Board, National Research Council, National Academy Press, Washington DC.

TRL (TRANSPORTATION RESEARCH LABORATORY) 1997. *Principles of low cost road engineering in mountainous regions, with special reference to the Nepal Himilaya.* Overseas Road Note 16, TRL/ODA.

WALLER, A.M. & PHIPPS, P. 1996. Terrain systems mapping and geomorphological studies for the Channel Tunnel link. *In:* Craig, C. (ed.) *Advances in Site Investigation Practice.* Thomas Telford, London, 25–38.

WP/WLI (UNESCO WORKING PARTY FOR WORLD LANDSLIDE INVENTORY) 1990. A suggested method for reporting a landslide. *Bulletin of the International Association of Engineering Geology*, 41, 5–12.

WP/WLI (UNESCO WORKING PARTY FOR WORLD LANDSLIDE INVENTORY) 1991. A suggested method for a landslide summary. *Bulletin of the International Association of Engineering Geology*, 43, 101–110.

WP/WLI (UNESCO WORKING PARTY FOR WORLD LANDSLIDE INVENTORY) 1993. A suggested method for describing the activity of a landslide. *Bulletin of the International Association of Engineering Geology*, 47, 53–57.

WWW 2001 Andalusian Institute of Geophysics, University of Granda website http://www.ugr.es/iag/eq_iageng.html

GLOBAL CLIMATE CHANGE; A GEOLOGICAL PERSPECTIVE.

M. B. Hart & A. B. Hart

Climate is changing globally! The world is about 0.6°C warmer than 100 years ago and, in the UK, seven of the warmest years ever recorded have been in the present decade. The 1990's have, so far, been about 0.5°C warmer than the 1961-1990 average and the five warmest years in the 340-year Central England Temperature Series have occurred since 1988.

Coupled with these temperature changes there is evidence of major change in the world's atmosphere. The levels of ozone in the atmosphere, particularly over Antarctica, are known to be decreasing. Concentrations of atmospheric carbon dioxide are known to be rising and this rise can be traced back to the industrial revolution; it is reportedly anthropogenic and not (apparently) part of a natural cycle.

The debates over the cause of these changes, and their impact, will continue well into the future. While many find it difficult to come to terms with the idea of climate change, geologists have a wealth of experience to bring to the discussions. Ten thousand years ago the last ice age maximum was coming to an end, with temperatures changing and sea level rising rapidly as a direct result of the melting icefields. Since that time there have been less severe, but nonetheless significant reversals of the warming trend. Historians have vividly described the effects of the "little ice age" when the River Thames regularly froze in winter over an extended period of years.

Geologists appreciate these global changes and have documented the climatic changes that have shaped the planet over periods of hundreds of millions of years. Using radiometric and palaeomagnetic time-scales we now have an appreciation of the natural rates of change that have left a record in the geological succession.

The current climatological data suggest a modern rate of change that is beyond our geological experience and, as a direct consequence of this, there have been established a number of key bodies; e.g., the UK Climate Impacts Programme and the Inter-Governmental Panel on Climate Change. Models of climate change, and the associated rise in global sea levels, are now available and it is the responsibility of the science community to present these in a way in which the general public can appreciate both the problem and the likely consequences. This must, however, be done in a measured way and we all have a responsibility in this regard. A classic example of this being hi-jacked by the media was the cliff-fall at Beachy Head in 1999. The chalk cliffs of Sussex have developed, by such falls over recent millennia and to attribute the last such event to "global warming" is to totally miss the point. Coastal stability may well be an issue for future investigation. Many major landslides (e.g., the Lyme Regis area) have a history back into the Pleistocene and will, almost certainly, be affected by changes in sea level and increased winter rainfall. Quick soundbites are, however, not the appropriate way by which to communicate the problems that may confront many coastal areas.

Geologically speaking, we are in an inter-glacial period in Earth History. The evidence suggests that extensive glacial conditions will return to N.W. Europe in the not too (geologically) distant future. The dilemma for humanity is which gets us first – ice-house or green-house?

*M.B.Hart, A.B.Hart, Department of Geological Sciences and Plymouth Environmental Research Centre,
University of Plymouth, Drake Circus, Plymouth PL4 8AA*

INTRODUCTION

The climate of the early Earth was probably very warm (Figure 1). This was the direct result of the build-up of gravitational energy, loss of kinetic energy and the heat liberated by short-lived radio-isotopes as the planet was forming 4,600 million years ago. Despite the calculated increase in solar luminosity during geological time, the surface temperature of the Earth has, in general, reduced since the Archean, apart from occasional warm intervals, especially in the Cretaceous. The main controls on the global climate, through the Phanerozoic appear to be:-

- the bio-regulatory effect of photosynthetic marine/terrestrial algae and plants;
- the movements of the crustal plates and the rate(s) of sea floor spreading;
- the increasing solar luminosity(?); and
- the variations in the proportion of "greenhouse" gases in the atmosphere.

Throughout this time the Earth has migrated between "green-house" and "icehouse" conditions, when large terrestrial and marine ice sheets expanded over significant areas of the globe. Between these major glacial expansions (shown in Figure 1) there may have been intervals with little (see Keller & Stinnesbeck, 1996; Miller et al., 1999) or no polar ice.

GLOBAL CLIMATE CHANGE

Throughout geological time the climate has been changing and it should come as no surprise that these natural processes are ongoing. The latest figures suggest that the average temperature of the planet is about 0.6°C warmer than one hundred years ago (Hulme & Jenkins, 1998). The warmest year since records began in the UK (the 340-year Central England Temperature Series) was 1999, with 1997, 1995 and 1990 also recording some of the highest values on record. The 1990's have been about 0.5°C warmer than the 1961-1990 average and 1999 is the warmest year since about 1204 (using tree-ring data as a proxy for temperature).

Over the next 100 years the rate of global warming (Hulme & Jenkins, 1998) is predicted to rise between 0.16°C per decade to 0.35°C per decade. In the same time period global sea level is predicted to rise from between 2.4 cm per decade to 10.0 cm per decade (see Table 1). These rates of change are quite dramatic and most geologists regard them as extra-ordinary. There have been times, however, when comparable rates of change have been recorded (e.g., the Younger Dryas period) although, for much of the geological record, such accurate measurements would be impossible.
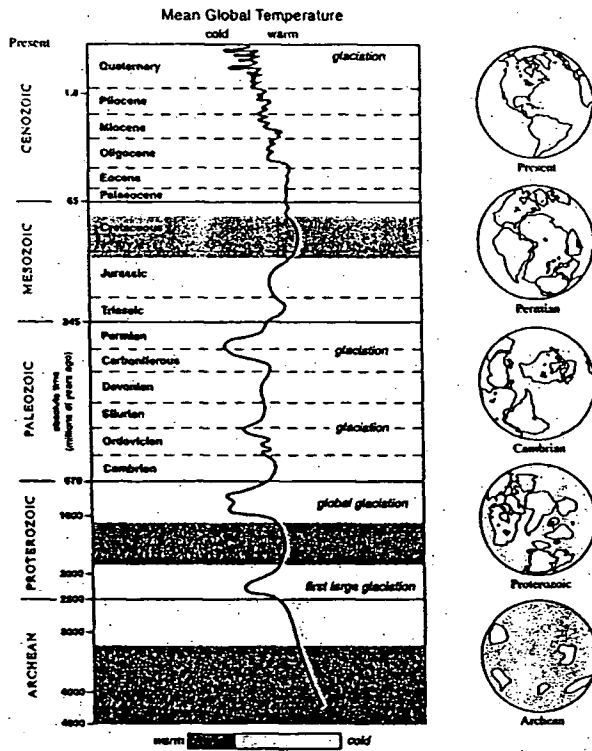
Figure 1. *Generalised temperature history of the Earth (adapted from Merritts et al., 1998).*

Figure 2. *Cooling of the Earth after the latest Cretaceous as recorded by oxygen isotopes in benthonic marine Foraminifera (adapted from Miller et al., 1987).*

THE CENOZOIC CLIMATIC DECLINE

After the mid-Cretaceous temperature maximum (Figure 1) global temperatures fell, although the details of the changes are relatively little known. In the mid-Late Turonian there was a dramatic drop in global sea level (Hancock & Kauffman, 1979; Hart, 1990 and references therein) the cause of which is not fully understood. Few authors have suggested that an Antarctic ice cap was present in the Cenomanian or Turonian (see Price, 1999, for a recent review) although it has been suggested (Keller & Stinnesbeck, 1996; Miller et al., 1999) that ice may have been present in the Maastrichtian. As indicated in Figure 2 there was little change between the latest Cretaceous and the earliest Cenozoic (aside from the short-term perturbations at the K/T boundary – however caused). The Cenozoic temperature maximum was in the Early Eocene and is marked, in the UK, by the presence of *Nummulites* spp. (a large, benthonic, foraminiferid) in the Hampshire Basin (Murray et al., 1989); the northernmost occurrence of this normally Tethyan genus. With the progressive build-up of glaciers on the Antarctic landmass, global temperatures declined through the remainder of the Palaeogene, with an associated drop in global sea levels. With the major ice advance in the Antarctic during the mid-Miocene the pattern of cooling accelerated and about 3.5 million years ago the Arctic Ocean began to be closed over by an ice sheet. During the Pleistocene the major advances of this ice sheet covered substantial parts of Northern Europe, Asia and North America. Since the last glacial maximum temperatures have improved rapidly (in geological terms), despite a major reversal in the Younger Dryas, attained modern levels about 11,600 years ago (Alley et al., 1993). Fluctuations in oxygen isotope ratios in ice cores provide a major source of information on which such interpretations are based.

Over the last 3,500 years dendrochronology not only provides a valuable time-scale but the relative size of the growth rings of trees such as the Bristlecone Pines of the Western USA provide a good proxy of temperature (Figure 3). From a maximum
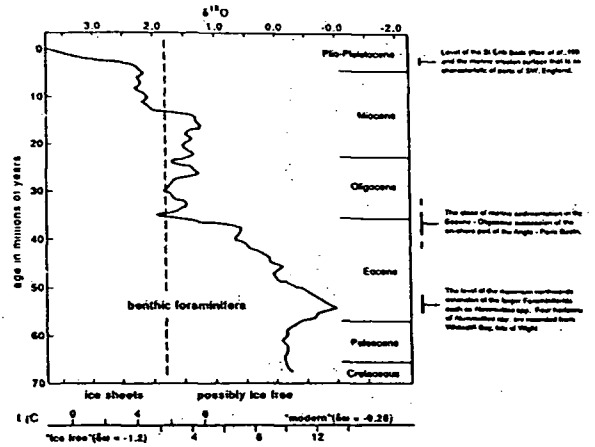
temperature in 1204, temperatures have fallen and, by the time the Central England Temperature Series began in 1659, temperatures were at a low level. Even at the beginning of the 19th Century the Little Ice Age was still having an effect, with warming only taking place after about 1820.

THE 19TH AND 20TH CENTURY WARMING

Since the industrial revolution in N.W.Europe there has been an increasing discharge of pollutants into the atmosphere. The years between 1750 and 1830 are generally regarded as the crucial years of the industrial revolution in the UK and elsewhere in Europe (Burke, 1974). With the near-exponential rise in the human population and the increasing use of fossil fuels, the emissions are carbon dioxide, chlorofluorocarbons, methane and nitrous oxide (Merritts et al., 1998). Unfortunately, for scientists trying to understand the present rise in temperature, this increasing anthropogenic impact on the atmosphere began
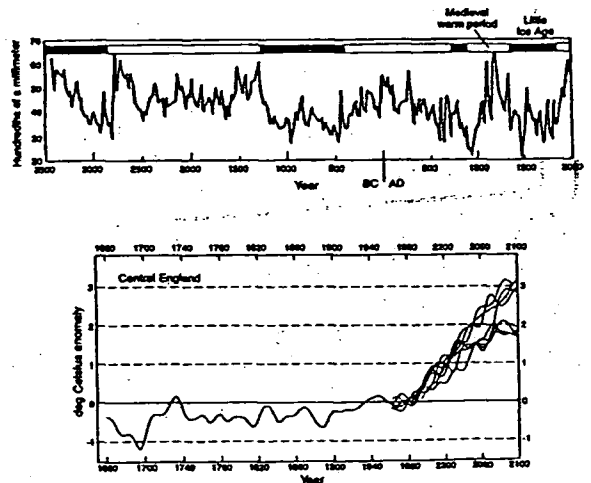
Figure 3. *Predicted temperature curve for the last 3500 years based on the proxy data from growth-ring thicknesses in the Bristlecone Pine trees in the western USA (based on Lamb, 1995, using data supplied by Professor V.C.La Marche). The lower graph shows the post-Little Ice Age data of the Central England Temperature Series to which have been added some of the present temperature predictions of the Climate Research Unit (Hulme & Jenkins, 1998).*

AUTHORS	BEST ESTIMATE (cm)	RANGE (cm)	TO (YEAR)
Hoffman et al. (1983)		56 - 345	2100
PRB (1985)		10 - 160	2100
Hoffman et al. (1986)		58 - 367	2100
Robin (1986)	80[1]	25 – 165[1]	2080
Thomas (1986)	100	60 - 230	2100
Jaeger (1988)	30	-2 - 51	2025
Raper et al. (1990)	21[2]	5 - 44[2]	2030
Van der Veen (1988)[3]		28 - 66	2085
Oerlemans (1989)	20	0 - 40	2025
Clayton (1990)	164	26 - 365	2030
Pugh (1990)[4]	110	90 - 170	2100
Warrick & Oerlemans (1990) [Based on IPCC 1990]	66	30 - 110	2100
IPCC "BAU" Scenario (1990)	47	18 - 109	2100
Church et al. (1991)[5]	35	15 - 70	2050
Wigley & Raper (1992) [Based on IPCC 1992]	-	15 – 90[6] (22 – 115)[7]	2100 / 2100
Wigley & Raper (1993)	46[8]	3 - 124[9]	2100
Woodworth (1993)	61		2087
Titus & Narayanan (1995)[10]	34	5 - 77[11]	2100
IPCC (1996)[12]	49	20 - 86	2100

Table 2. Estimations of change in global sea-level (after Hart, A.B., 1997).

[1] Estimated from global sea level and temperature change from 1880-1980 and global warming of 3.5+/-2.0°C for 1980-2080.
[2] Internally consistent synthesis of components.
[3] For a global warming of 2-4°C
[4] Surface air temperatures are assumed to increase linearly until 2050, to an average value of 3° higher than at present, and then to remain constant.
[5] Assumes rapid warming of 3°C by 2050 for best guess scenarios.
[6] Best guess with a temperature change of 1.7-3.8°C.
[7] Base case forcing with a temperature change of 2.1-5.0°C.
[8] For IPCC (1992) Policy Scenario B, best estimate model parameters.
[9] For IPCC (1992) forcing scenarios A & C with high and low model parameters, respectively.
[10] Incorporates subjective probability distributions for model parameter values based on expert opinion.
[11] Represents 90% confidence level.
[12] For the IPCC IS92a forcing scenario, using a climate sensitivity of 2.5°C for the mid projection and 1.5° & 4.5° for the low and high projections respectively. (See also Raper et al. 1996)

Table 1. Estimations of change in global sea level (after Hart, A.B., 1997).

at about the time of the end of the Little Ice Age. Are the two events related? If one looks at the temperature proxy provided by the tree-ring thicknesses (Figure 3) comparable changes in Medieval Times were – clearly - not caused by anthropogenic impacts.

One view is that the temperature rise we are experiencing is the natural cycle of the Earth's climate with glacial maxima at approximately 100,000 year intervals and the inter-glacials following the same pattern. If that is the case, curbing greenhouse gas emissions is both futile and economically suicidal. The alternative view is that there is a significant chance that the current warming is driven by anthropogenic activity and that to ignore it at the present time is both foolhardy and – in the long term – just as economically damaging.

The decisions about the global economic strategy are not to be considered in this report. If temperatures are rising and the climate is changing, whatever the cause, there will be an impact and some of the implications for the south-west of England are considered here.

IMPACTS IN SOUTH-WEST ENGLAND

South-west England is predicted to suffer changing climatic conditions over the next century and models are now available as part of the UK Climate Impacts Programme. As indicated in Table 2 the West Country may experience:-
* winters that are slightly warmer and significantly wetter;
* summers that are markedly warmer and slightly drier.
There are a number of consequences that follow from these predictions.

	2020's	2050's	2080's
average T°C	+0.5/1.3	+0.8/2.2	+1.2/3.0
summer T°C	+0.7/1.4	+0.9/2.4	+1.4/2.9
winter T°C	+0.5/1.4	+0.9/2.3	+1.2/3.0
total rainfall % change	+1.0/4.0	+3.0	+2.0/6.0
summer rainfall % change	-1.0/3.0	-1.0/10.0	-5.0/7.0
winter rainfall % change	+5.0/8.0	+7.0/13.0	+7.0/23.0
winter wind speeds	+1%	-1%	+1%
spring wind speeds	-3%	-2%	-1%
summer wind speeds	-1%	0%	+1%
autumn wind speeds	+2%	+2%	+2%

Table 2. Predicted changes in temperature, rainfall and wind speeds in South-west England (ranges of values given) based on the UK Climate Impacts Programme (Hulme & Jenkins, 1998). The general conclusions are that winters will be slightly warmer and significantly wetter while summers will be markedly warmer and slightly drier.

* the drier, warmer summers may allow for changes in some of the crops that can be grown in the region;
* there may be an impact on water supply, much of which is reservoir-based;
* there may be a significant risk of flooding during the winter months and flood protection works and/or drainage schemes should be considered a priority (e.g., problems in Devon during December 1999 and the significant flooding of the Somerset Levels;
* instability of hedge banks and soil run-off in the sunken lanes that are so typical of this region; and
* increased instability of pre-existing landslides that are already known to be triggered by excessive rainfall levels (Brunsden & Chandler, 1996).

The increased sea levels (see Table 1) would almost certainly affect the landslide stability on the Devon/Dorset coastline as the toes of the slips become attacked by the sea. That removal of material, coupled with more rainfall-induced activity, could significantly change the disposition of slides on Black Ven, Stonebarrow Hill, etc., and make occupancy of Higher Sea Lane in Charmouth (Conway, 1976; Denness et al., 1975) a problem.

The increase in winter rainfall is primarily due to the increased temperature of sea water in the North Atlantic Ocean and the generation of more active depressions. There is, below each depression, a significant "bulge" of sea water caused by the low pressure. This bulge, coupled with strong winds and high tides (or both) can cause significant coastal erosion or flooding. As illustrated by Hart (2000) it was a situation such as that outlined above that caused the disastrous flooding of East Anglia in 1953 and which, directly, led to the building of higher marine defences and the Thames Barrier. During December 1999 strong winds, an high tide and a depression-induced bulge threatened the Sussex coastline with flooding and severe damage. This was only averted by a last minute change in wind direction.

CONCLUSIONS

While the majority of environmental scientists believe that the present rise in global temperatures is anthropogenic in origin, there are those that would claim that it is the direct result of the Earth's natural evolution. Whatever the cause, the outcome is the same. The Earth is experiencing a rapid rise in global temperature

and this, coupled with the associated rise in global sea levels, will directly impact on the climate of south-west England. These changes will affect agriculture, coastal stability, land use, flood protection and water supplies.

ACKNOWLEDGEMENTS

REFERENCES

ALLEY, R.B.; MEESE, D.A., SHUMAN, C.A., GOW, A.J., TAYLOR, K.C., GROOTES, P.M., WHITE, J.W.C., RAM, M., WADDINGTON, E.D., MAYEWSKI, P.A. & ZIELINSKI, G.A. 1993. Abrupt increase in Greenland snow accumulation at the end of the Younger Dryas event. *Nature*, 362, 527-529.

BRUNSDEN, D. & CHANDLER, J.H. 1996. Development of an episodic landform change model based upon the Black Ven mudslide, 1946-1995. *In*: ANDERSON, M.J. & BROOKES, S.M. (Eds), *Advances in Hillslope Processes*, 2, 869-896, J. Wiley & Sons, Chichester.

BURKE, J. 1974. *An Illustrated History of England*. Book Club Associates, Norwich, 349pp.

CHURCH, J.A., GODFREY, J.S., JACKETT, D.R. & McDOUGALL, T.J. 1991. A model of sea level rise caused by ocean thermal expansion. *Journal of Climate*, 4, 438-456.

CLAYTON, K.M. 1990. Sea-level Rise and Coastal Defences in the UK. *Quarterly Journal of Engineering Geology*, 23, 283-287.

CONWAY, B.W. 1976. Coastal terrain evaluation and slope stability of the Charmouth–Lyme Regis area of Dorset. *British Geological Survey, Geophysical Division, Engineering* Geology Report No. EG76/10

DENNESS, B., CONWAY, B.W., McCANN, D.M. & GRAINGER, P. 1975. Investigation of a coastal landslip at Charmouth, Dorset. *Quarterly Journal of Engineering Geology*, 8, 119-140.

HANCOCK, J.M. & KAUFFMAN, E.G. 1979. The great transgressions of the late Cretaceous. *Journal of the Geological Society, London*, 136, 175-186.

HART, A.B. 1997. *A risk assessment of the inland area around Charmouth, West Dorset*. Unpublished M.Sc. Thesis, University of Portsmouth.

HART, M.B. 1990. Cretaceous sea level changes and global eustatic curves. *Proceedings of the Ussher Society*, 7, 268-272.

HART, M.B. 2000. Construction of the Thames Barrier: an application of micropaleontology to the solution of an environmental problem. *In*: MARTIN, R.E. (Ed.), *Environmental Micropaleontology, Volume 15, Topics in Geobiology*, Kluwer Academic/Plenum Publishers, New York, 429-459.

HEAPS, N.S. 1977. Development of storm surge models at Bidston. *Internal Report*, No. 51, Institute of Oceanography.

HOFFMAN, J.S., KEYES, D. & TITUS, J.G. 1983. *Projecting Future Sea Level Rise: Methodology, Estimates to the Year 2000, and Research Needs*. United States Government Printing Office # 055-000-0236-3, Washington, D.C.

HOFFMAN, J.S., WELLS, J.B. & TITUS, J.G. 1986. Future global warming and sea Level rise. In: SIGBJARNASON, G. (Ed.), *Iceland Coastal and River Symposium*, National Energy Authority, Reykjavik, 245-266.

HULME, M. & JENKINS, G.J. 1998. *Climate Change Scenarios for the U.K.: Scientific Report*. UKCIP Technical Report No. 1, Climate Research Unit, Norwich, 80pp.

IPCC 1992. *Climate Change 1992: The Supplementary Report to the IPCC Scientific Assessment*. HOUGHTON, J.T., CALLANDER, B.A. & VARNEY, S.K. (Eds), Cambridge University Press, Cambridge, 200pp.

IPCC 1996a. *Climate Change 1995: The Science of Climate Change*. Contribution of Working Group 1 to the Second Assessment Report of the IPCC. HOUGHTON, J.T., MEIRA FILHO, L.G., CALLANDER, B.A., HARRIS, N., KATTENBERG, A., MASKELL, K. & LAKEMAN, J.A. (Eds)..

IPCC 1996b. *Climate Change 1995: Impacts, Adaptions & Mitigation of Climate Change*. Contribution of Working Group II to the Second Assessment Report of the IPCC. WATSON, R.T., ZINYOWERA, M.C. & MOSS, R.H. (Eds).

IPCC 1996c. *Climate Change 1995: Economic & Social Dimensions of Climate Change*. Contribution of Working Group III to the Second Assessment Report of the IPCC. BRUCE, J.P., LEE, H. & HAITES, E.F. (Eds).

JAEGER, J. 1988. *Developing Policies for Responding to Climate Change: a Summary* of the Discussions and Recommendations of the Workshop held in Villach (1987) and Bellagio (1987). WMO/TD-No.225.

KELLER, G. & STINNESBECK, W. 1996. Sea-level changes, clastic deposits and megatsunamis across the Cretaceous-Tertiary boundary. *In*: MacLEOD, N., & KELLER, G. (Eds), *Cretaceous-Tertiary Mass Extinctions: Biotic and Environmental Change*. Norton, London, 415-449.

LAMB, H.H. 1995. *Climate History and the Modern World*, Routledge, London, 433pp.

MERRITTS, D., DE WET, A. & MENKING, K. 1998. *Environmental Geology: an earth system science approach*. W.H.Freeman & Company, New York, i–xxvi, 452pp.

MILLER, K.G., BARRERA, E., OLSSON, R.K., SUGARMAN, P.J. & SAVIN, S.M. 1999. Does ice drive early Maastrichtian eustacy. *Geology*, 27, 783-786.

MILLER, K.G., FAIRBANKS, R.G. & MOUNTAIN, G.S. 1987. Tertiary oxygen isotope Synthesis, sea level history and continental margin erosion. *Paleoceanography*, 2, 1-19.

MURRAY, J.W., CURRY, D., HAYNES, J.R. & KING, C. 1989. Palaeogene. *In*: MURRAY, J.W. & JENKINS, D.G. (Eds), *Stratigraphical Index of Fossil Foraminifera*, (2nd Edition), Ellis Horwood Ltd., Chichester, 490-536.

OERLEMANS, J. 1989. A projection of future sea level. *Climate Change*, 15, 151-174.

POLAR RESEARCH BOARD (PRB). 1985. *Glaciers, Ice Sheets and Sea Level: Effect of a CO₂-induced Climate Change*. Report of a Workshop held in Seattle, Washington, September 13-15, 1984, United States DOE/ER/60235-1.

PRICE, G.D. 1999. The evidence and implications of polar ice during the Mesozoic. *Earth Science Reviews*, 48, 183-210.

PUGH, D.T. 1990. Is there a sea level problem? *Proceedings of the Institute of Civil Engineers*, 88, 347-366.

RAPER, S.C.B., WARRICK, R.A. & WIGLEY, T.M.L. 1990. Global sea level rise: past and future. *In*: MILLMAN, J.D. (Ed.), *Proceedings of the SCOPE Workshop in Rising Sea Level and Subsiding Coastal Areas, Bancock 1988*, John Wiley & Sons, Chichester.

ROBIN, G. de Q. 1986. Changing sea level. *In*: BOLIN, B., DOOS, B.R., JAEGER, J. & WARRICK (Eds), *The Greenhouse Effect, Climatic Change and Ecosystems*, John Wiley & Sons, Chichester, 323-359.

TITUS, J.G. & NARRAYANAN, V. 1995. *The Probability of Sea Level Rise*. U.S. Environmental Protection Agency, Office of Policy, Planning and Evaluation, Climate Change Division, EPA230-R-95-008, EPA, Washington, DC, 186pp.

THOMAS, R.H. 1986. Future sea level rise and its early detection by satellite remote sensing. *In*: TITUS, J.G. (Ed.), *Effects of Changing Stratospheric Ozone and Global Climate, Volume 4, Sea Level Rise*.

VAN DER VEEN, C.J. 1988. Projecting future sea level. *Surveys in Geophysics*, 9, 389-418.

WIGLEY, T.M.L. & RAPER, S.C.B. 1992. Implications for climate and sea level of revised IPCC emissions scenarios. *Nature*, 357, 293-300.

WIGLEY, T.M.L. & RAPER, S.C.B. 1993. Future changes in global mean temperature and sea level. *In*: WARRICK, R.A., BARROW, E.M. & WIGLEY, T.M.L. (Eds), *Climate and Sea Level Change: Observations, Projections and Implications*, Cambridge University press, Cambridge.

WOODWORTH, P.L. 1993. Sea level changes. *In*: WARRICK, R.A., BARROW, E.M. & WIGLEY, T.M.L. (Eds), *Climate and Sea Level Change: Observations, Projections and Implications*, Cambridge University press, Cambridge.

Using remote sensing and GIS for rapid landslide hazard assessment: potential public sector uptake in Nepal and Bhutan

Hart, A.B., Hearn, G.J.
Scott Wilson Kirkpatrick & Co Ltd, Scott House, Basing View, Basingstoke, RG21 4JG, United Kingdom
Email: andrew.hart@scottwilson.com, gareth.hearn@scottwilson.com
Petley, D.N.
Department of Geography, University of Durham, Science Laboratories, Durham, DH1 3LE,
United Kingdom, Email: d.n.petley@durham.ac.uk
Tiwari, S.C.
Department of Local Infrastructure and Agricultural Roads, Kathmandu, Nepal
Giri, N.K.
Department of Roads, Thimphu, Bhutan

Abstract:
This paper presents the outputs from the Landslide Risk Assessment in the Rural Access Sector (LRA) project. This is a three-year research project investigating ways by which landslide hazard and risk can be assessed in the context of low cost roads in rural areas, developed in response to the clear need from government agencies for rapid and reliable methods for the assessment of landslide hazard for preliminary decision-making prior to committing large resources to expensive field investigations. The research has concentrated upon six field sites in Nepal and Bhutan, and has incorporated a range of techniques including remote sensing, aerial photography, field mapping, and GIS analysis, but the primary focus has been on the application of techniques that use desk study data sources to provide a preliminary assessment of landslide potential for planning and engineering purposes.

The Landslide Risk Assessment project has examined the contribution that a range of remote sensing platforms can make to landslide mapping, focussing on both the effectiveness of the techniques themselves and their economic worth. It is concluded that Landsat 7 ETM+ provides a very cost-effective data source for route corridor planning and the mapping of medium sized and large landslides. IKONOS is considerably more expensive but provides far greater ground resolution, offering similar feature detection to aerial photography. It is clear that in the near future the advantages offered by conventional aerial photograph interpretation will be eclipsed by advances in satellite imagery, but at present aerial photographs often remain the most practical sources of multi-environmental data for planning and engineering purposes.

With regard to landslide mapping, the LRA Project has demonstrated that a reasonable degree of confidence can be placed in the mapping of landslide susceptibility using simple lithological and topographical factors derived from published geological maps, topographic maps and aerial photographs. GIS enables the various data capture and analytical stages to be undertaken relatively easily and it is concluded that the technology should be taken up readily by government agencies with appropriate training and field checks.

Introduction

In recent years there has been increasing recognition of the importance of the provision of transport infrastructure for sustainable development in remote mountain areas (Jacoby 2000; Sarkar and Ghosh 2000 for example). A road network provides access to markets, the importation of commodities from beyond the surrounding area, and enables the population to access medical, educational and other social facilities. Thus, rural communities rely on the provision of reliable transport facilities for improved livelihood and economic growth.

However, most mountainous areas are also prone to the effects of a range of natural hazards, including seismic activity, landslides, floods, glacial lake outburst floods and avalanches. Of these, landslides possibly pose the greatest challenge to the infrastructural planner and road engineer, as well as a frequent threat to rural communities and infrastructure. Landslides regularly lead to fatalities, injuries, the loss of livelihood and economic disruption, road closures, blockage or destruction of drainage structures, undermining of foundations, and frequently cause damage to road carriageways, ranging from cracking and settlement to complete failure. Whilst roads are normally designed to provide access to rural communities, the construction and operation of a road will usually attract speculative development in this corridor. These roadside communities are also frequently at risk from landslide hazards (Hearn *et al.*, this volume). This may, for example, be a major factor in the large and increasing numbers of fatalities associated with landslides in Nepal. During 2002, for example, there were a total of 346 reported human fatalities and 73 reported injuries as the result of 110 reported landslides (Hart *et al.*, this volume). In addition to the human costs, at least 650 houses were damaged or destroyed and 500 cattle were lost. Of course these events led to

the closure of many of the country's roads for days or weeks, imposing a substantial impact on the national economy.

Therefore, the assessment of landslide susceptibility, hazard and risk is an essential requirement in the planning of any new transportation project. In recent years a range of techniques have been developed to facilitate this. However, most techniques are limited in the geographical area in which they can be applied; are complex to understand and apply; require a range of data that is frequently not available; and have an unknown level of reliability and accuracy. Therefore, in many rural road projects in developing countries, the level of landslide susceptibility, hazard or risk assessment that is undertaken is minimal, and decisions continue to be made under conditions of uncertainty and unreliability.

The situation is also exacerbated by rural population growth and, consequently, increasing demands on marginal land and for rural infrastructure and roads. Therefore, the government agencies involved with rural access and development require a rapid and reliable method for assessing landslide susceptibility and hazard. This is particularly important during the preliminary decision-making stages of any infrastructure development project, before limited resources and money are committed to expensive field investigations or construction activity.

The Landslide Risk Assessment Project

In order to address these problems, the "Landslide Risk Assessment in the Rural Access Sector" Project (LRA) was established in 2000. This three-year project, which has been funded by the UK Government through the Department for International Development (DFID), has been undertaken in collaboration with the Department of Local Infrastructure Development and Agricultural Roads (DoLIDAR) in Nepal and the Department of Roads (DoR) in Bhutan. Activities have included:

- Comprehensive worldwide reviews of remote sensing and landslide susceptibility and hazard mapping techniques

- Analyses of satellite imagery to evaluate its applicability to terrain evaluation and landslide susceptibility assessments for rural infrastructure planning purposes

- Interpretation of aerial photographs to map landslides and assess landslide frequency through sequential photography

- Field mapping and the compilation of landslide inventories to develop databases for landslide susceptibility mapping

- Surveys of land use and social impact parameters in landslide areas to assist in the development of rural risk assessment and risk management guidelines

- The development of techniques for landslide susceptibility, hazard and risk mapping for rural access planning

- The development of a database of reported landslide occurrence in Nepal using various data sources (including the national press)

- The production of Best Practice Guidelines based on the above studies.

The aim of the LRA Project is to develop a set of rapid, reliable and cost-effective techniques that can be used to provide a preliminary assessment of landslide potential. This information can then be used in the planning stages of a project, as well as during the design and engineering stages.

A systematic programme of remote sensing, field mapping, land use and social survey, landslide susceptibility analysis, and landslide hazard and risk assessment, has been completed in all six of the project study areas (three in each of Nepal and Bhutan). The results have been combined to yield outputs relevant to both countries, thus providing the basis for application outside the study areas. The focus has been to use data sources that would be available at the desk study stages of any project. This has included the examination of the ways in which remote sensing data, published map data and GIS-based methods can be used, as well as looking at how to overcome the problems of limited, out of date or inaccurate data.

Remote Sensing

Satellite, remote sensing technology is rarely used for infrastructure development projects, and particularly for route corridor selection for a variety of reasons, including cost, resolution and technological limitations (see Petley & Hearn, this volume). An assessment has been undertaken of the ways in which different

remotely sensed data sources, including Landsat 7 ETM+, SPOT, IRS, IKONOS, and conventional aerial photographs, can be used for landslide susceptibility and hazard mapping. The results of the research are encouraging. Overall, Landsat 7 ETM+ proved to be the most cost-effective satellite tool for delineating and mapping large landslides (greater than 50m in dimension). It also proved to be effective for the mapping of land use, vegetation cover and even soil type through the analysis of the multi-spectral data. It was also found to be effective for mapping areas of colluvium that might be susceptible to sliding, although field verification is required to validate interpretations, given some of the uncertainties of interpreting terrain at the relatively small scales offered by Landsat imagery. The high resolution IKONOS product proved to be the most effective satellite tool for mapping smaller landslides (10 m or less), especially where multi-spectral data were available (Petley *et al.*, 2002). However, at present the relatively high cost precludes its use in most rural infrastructure projects.

Aerial photographic interpretation (API) provides an effective tool for landslide mapping and terrain evaluation. The advantages of API over satellite image interpretation (SII) include the availability of stereo images and the visual-familiarity with the terrain shown in the photographs. The "low technology" method used for the interpretation of aerial photographs (i.e. a stereoscope) also means that the work can be carried out on site without the need for a computer to carry out multi-spectral analysis. However, the disadvantages include distortion and relief exaggeration in mountainous areas and the relatively high cost and practical difficulties of updating the images on a regular basis (Petley & Hearn, this volume). Potential applications of Landsat 7 ETM+, IKONOS and aerial photography are briefly discussed below.

Landsat 7 ETM+

The effectiveness of approaches using True Colour Composite (TCC) images, False Colour Composite (FCC) images, Principal Components Analysis (PCA), clay ratio analyses, iron oxide ratio analyses and Abram ratio analyses have all been tested. Of these, the TCC approach proved to be the most effective for mapping landslides. In particular a RGB457 FCC, pan-sharpened image using the panchromatic data, yielded excellent results. A RGB 542 FCC also proved relatively successful. In both cases morphological evidence obtained from a TCC was used in conjunction with the FCC images to support the identification of landslide areas (i.e. concave or convex slopes, drainage pattern, shadows, etc). The FCC's were also used to map land use patterns, wet areas, soil type and vegetation cover. For example, in some of the study areas, colluvium was clearly identifiable, as were areas of barren land, bare soil or seepage.

Petley *et al.* (2002) concluded that a multi-spectral analysis of a Landsat image could assist landslide factor mapping. The presence of disturbed ground, wet areas (or seepage lines), bare soil or colluvium is often indicative of either creep or incipient failure. However, wet areas have the same spectral signature as tin roofs, paddy fields and river alluvium. Therefore, the need for field verification is vital. The analysis should also not be done in isolation from the rest of the project, but as an integral part of the project, with both the computer specialist and the field specialist working together.

IKONOS

Although IKONOS data are considerably more expensive than the other satellite images such as Landsat 7 ETM+ or SPOT iv, they provide far greater ground resolution and allows similar feature identification to API. Because of the limited spectral capability of the IKONOS instrument (only four bands plus the panchromatic band are available), most interpretation has been undertaken using panchromatic and TCC images. In both cases, ridges, valleys and rivers were clearly evident; whilst land-cover information such as vegetation type, soil type and rock outcrops were also visible. Areas of bare soil were bright and lighter in comparison with the surrounding darker vegetation. This meant that recent and active landslides whose width and length exceeded 10 m were visible. Relict (inactive) landslides proved to be difficult to identify however due to the lack of stereo capability. The availability of stereo images would have further increased the effectiveness of the imagery, making it similar to 1:5,000 scale stereo aerial photographs in terms of ground surface interpretation. However, until this stereoscopic capability is widely available, and the cost is reduced, the widespread adoption of IKONOS imagery appears to be limited in developing countries.

Aerial Photographs

Aerial photography still remains the most practical and readily-available image data source. Its application for multi-environmental data collection, planning and engineering purposes has been well demonstrated, by many infrastructure development projects, as well as the LRA Project (Dhakal *et al.* 1999 for example). In Nepal, there is relatively recent aerial photographic coverage for the whole country. However, some parts of the country have several epochs of aerial photographs, providing a useful insight into how the landscape and land use has changed in these areas. In Bhutan, the situation is not as good as Nepal. There is limited photographic coverage of the country, with the majority of the photographs being taken during the early

1990's. Aerial photographs in Bhutan also suffer from the distortion affects caused by the very steep terrain. However, in both countries API mapping techniques proved useful in the mapping the landslide distribution and for classifying the terrain during the LRA Project.

Geographical Information Systems

A Geographical Information System (GIS) is a powerful computer-based tool for the storage, management and analysis of spatial data. Until recently GIS was a very specialised tool that was only really usable by specialists due to the complexity and cost of the required software and hardware. However, in recent years the availability of powerful, low cost computers and the development of user-friendly software systems have meant that GIS is now a tool that is applicable to a wide range of projects. Numerous government and non-government agencies in both Nepal and Bhutan are currently using GIS.

The LRA Project has generated very large amounts of complex data, for which a GIS has proven to be the ideal tool for storage, manipulation and analysis. GIS has proven to be effective in enabling the various data capture, data entry and data analysis activities to be undertaken relatively quickly and easily. It has also been demonstrated that a GIS can be effectively used for carrying out rapid assessments of landslide susceptibility over large areas. Thus, it is clear that GIS is a very powerful tool for the assessment of vulnerability of the infrastructure and population of a given area to landslides, and it is thus an excellent tool for planning purposes.

For each of the project study areas a GIS database has been developed to manage a wide variety of datasets, which include information pertaining to the topography, geology, geomorphology, land use, regional seismicity and infrastructure. These data have been obtained from a number of sources, including published and unpublished maps and reports; API, SII and field mapping. GIS was utilised to identify those factors that were significantly correlated with the distribution of mapped landslides in each study area. The results obtained from these analyses were used to create a set of landslide susceptibility maps for each of the six study areas.

One advantage of a GIS is the ability to produce maps that are of a very high graphical quality. Unfortunately this can lead to a feeling that the information that they are portraying is accurate, which of course, may not be the case. Output data can only be as good as the data that has been used as an input. If the input data quality is poor then the output will also be poor. In addition, it is critically important that the user understands what the computer is actually doing when it undertakes an analysis. It may therefore be necessary to have a GIS specialist working in conjunction with a field specialist so as to utilise the experience, skills and knowledge of both.

Landslide Susceptibility and Hazard Mapping

The LRA Project has carried out detailed landslide susceptibility mapping in three study areas in Nepal and three study areas in Bhutan (Table 1) using a combination of SII, API and field mapping. In each case the SII and API was completed first, with the field mapping being used for field verification, as well as for the collection of primary data (geology, structural geology, soil cover and social survey mapping). The data have been stored and analysed using a GIS.

The use of a GIS allowed spatial relationships between the landslide distribution and the contributory factors to be analysed (Table 2). The investigation involved the analysis of either single factors (i.e. rock type) or several factors combined together (i.e. bi-variate or multi-variate analysis – rock type and slope angle; or slope angle, slope aspect and structural geology). Standard statistical techniques were used to compare and test the significance of the results. This analysis was undertaken for each of the six study areas individually and then with the data from all study areas combined as a single data set. The combined database contains over 1300 landslides mapped by the LRA Project.

Table 1: Different data types and sources used during the research

Field Derived Data	Published Data	GIS Derived Data	Remote Sensing Derived Data
Landslide distribution	Contours	Elevation	Landslide distribution
Rock type	Rainfall	Slope angle	Terrain classification
Structural geology	Seismicity	Slope aspect	Land use
Terrain classification	Land use	Drainage line distances	
Land use	Social data	Lineament distances	
Infrastructure	Infrastructure		

Table 2: Statistics for each of the LRA Project Study Areas

Country	Study Area	Area (km square)	No. Landslides Mapped
Nepal	Baglung	528.45	232
	Arghakhanchi	327.05	389
	Ilam	363.86	226
Bhutan	Mongar – Trashigang	346.19	229
	Chhukha	201.91	41
	Sunkosh – Daga	251.18	219
Total		2,018.64	1,336

The landslide susceptibility analyses undertaken by the LRA Project have shown that, when working at the regional scale, the most significant factors determining landslide activity are slope angle and rock type. However, at the regional scale, mappable geological units are usually a combination of different rock types. For example, phyllite is often found in conjunction with limestone, and schist is often found in conjunction with gneiss. The predominant rock type has been identified in each case through field mapping and consultation with Nepalese and Bhutanese experts. However, in many cases it proved necessary to combine two or more rock types into a single "lithotype" (see below) if each of the rock types present was judged to be important in governing slope stability.

The simple landslide susceptibility scheme developed is therefore based upon a list of rock types, each of which has been divided into four slope angle classes. For each rock type–slope angle combination the density of landsliding across the six study areas has been determined to provide an indication of the susceptibility of the unit to the occurrence of landslides. This list, referred to as the "Regional Landslide Susceptibility Rating List" is provided in Table 3. In many cases the formations on the geological map will not exactly coincide with those in Table 3, and therefore, some interpretation of the geological data will be required. This can be supplemented by field mapping or verification.

To undertake an assessment using this scheme, it is necessary to obtain a map showing the distribution of rock types of the study area. This can usually be achieved from published geological maps, ideally at a scale of 1:25 000 or 1:50 000. In most cases these maps will be in paper not digital form, and will thus require tablet digitising. Field mapping can also provide an input and should where possible be used to validate the information being used. The slope angle information is generally available in the form of contour maps compiled by national mapping agencies. Increasingly, this is available in digital form. Standard functions within the GIS can then be used to convert the contour data into the necessary slope angle data with the specified classes.

Standard GIS functions are again used to create a single factor layer combining the rock type data with the slope angle data. The landslide susceptibility factor ratings given in Table 3 are used to create the landslide susceptibility map for the area being studied. An example of such a map for the Chhukha study area in Bhutan is shown in Figure 1.

Table 3: The regional landslide susceptibility rating list

Susceptibility Class	Rock Type	Slope Angle	Indicative landslide density (landslides/Sq km)
Low Landslide Susceptibility (Rating of 1)	Granite	0° - 20°	0.00
	Granite	20° - 30°	0.00
	Granite	30° - 40°	0.00
	Granite	> 40°	0.00
	Limestone/Dolomite with Quartzite, Phyllite &/or shale	0° - 20°	0.00
	Slate/shale with Limestone &/or Quartzite	0° - 20°	0.00
	Quartzite & Phyllite	0° - 20°	0.16
	Mica Schist & Gneiss	0° - 20°	0.20
	Limestone/Dolomite with Quartzite, Phyllite &/or shale	20° - 30°	0.20
	Mica Schist and other minor rock types	0° - 20°	0.22
	Gneiss & Mica Schist	0° - 20°	0.25
	Mica Schist & Phyllite	20° - 30°	0.26
	Mica Schist & Quartzite	0° - 20°	0.27
	Gneiss	0° - 20°	0.30
	Phyllite (with Quartzite &/or Limestone)	0° - 20°	0.30
	Limestone/Dolomite with Quartzite, Phyllite &/or shale	30° - 40°	0.36
	Quartzite & Phyllite	20° - 30°	0.36
Moderate Landslide Susceptibility (Rating of 2)	Limestone/Dolomite with Quartzite, Phyllite &/or shale	> 40°	0.40
	Mica Schist & Phyllite	0° - 20°	0.43
	Phyllite (with Quartzite &/or Limestone)	20° - 30°	0.46
	Mica Schist and other minor rock types	20° - 30°	0.48
	Mica Schist & Gneiss	20° - 30°	0.53
	Quartzite & Phyllite	30° - 40°	0.54
	Gneiss	20° - 30°	0.55
	Mica Schist	0° - 20°	0.56
	Slate/shale with Limestone &/or Quartzite	30° - 40°	0.59
	Mica Schist & Quartzite	20° - 30°	0.60
	Slate/shale with Limestone &/or Quartzite	20° - 30°	0.60
	Quartzite & shale &/or Sandstone	20° - 30°	0.62
	Quartzite & shale &/or Sandstone	0° - 20°	0.65
	Gneiss & Mica Schist	20° - 30°	0.66
	Slate/shale with Limestone &/or Quartzite	> 40°	0.67
High Landslide Susceptibility (Rating of 3)	Quartzite & Phyllite	> 40°	0.72
	Mica Schist	30° - 40°	0.75
	Mica Schist	20° - 30°	0.77
	Fine grained Sandstone (siltstone/mudstone)	0° - 20°	0.78
	Mica Schist	> 40°	0.80
	Mica Schist & Gneiss	> 40°	0.81
	Gneiss	30° - 40°	0.82
	Mica Schist & Phyllite	30° - 40°	0.83
	Phyllite (with Quartzite &/or Limestone)	30° - 40°	0.88
	Mica Schist and other minor rock types	30° - 40°	1.00
	Gneiss & Mica Schist	30° - 40°	1.00
	Mica Schist & Gneiss	30° - 40°	1.02
	Gneiss	> 40°	1.02
	Medium to coarse grained Sandstone	0° - 20°	1.03
	Quartzite & shale &/or Sandstone	30° - 40°	1.15
	Mica Schist & Quartzite	30° - 40°	1.19
	Quartzite & shale &/or Sandstone	> 40°	1.45
	Phyllite (with Quartzite &/or Limestone)	> 40°	1.55
	Mica Schist & Quartzite	> 40°	1.58
	Mica Schist and other minor rock types	> 40°	1.58
	Medium to coarse grained Sandstone	20° - 30°	1.64
	Gneiss & Mica Schist	> 40°	1.89
	Medium to coarse grained Sandstone	> 40°	2.15
	Medium to coarse grained Sandstone	30° - 40°	2.48
	Mica Schist & Phyllite	> 40°	2.62
	Fine grained Sandstone (siltstone/mudstone)	20° - 30°	2.91
	Fine grained Sandstone (siltstone/mudstone)	30° - 40°	3.33
	Fine grained Sandstone (siltstone/mudstone)	> 40°	6.85
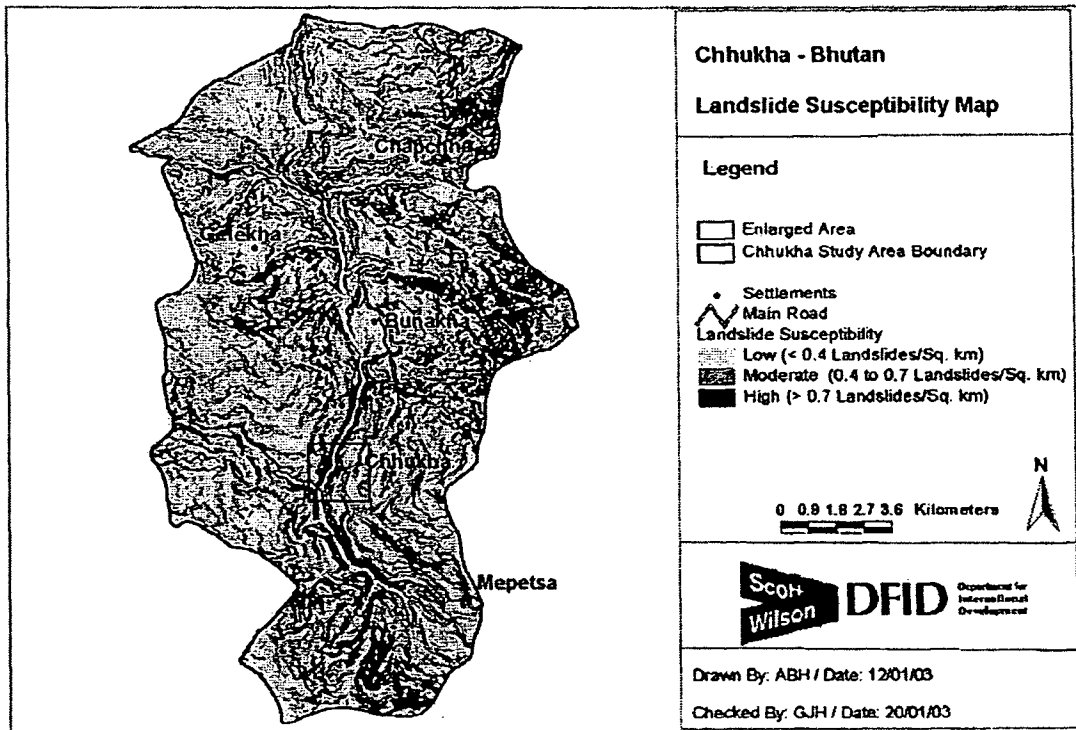
Figure 1: The Chhukha landslide susceptibility map as generated using the LRA methodology

To test this susceptibility model, the scheme was applied to each of the six study areas, as well as to two further test areas in Nepal. In each case the map was compared with the mapped landslide distribution and a number of standard statistical techniques were used to test the results. For each of the areas where the susceptibility model has been tested, it has performed well when compared to the existing landslide distribution, indicating that the model is potentially applicable to other areas within Nepal and Bhutan.

Of course it is essential to ensure that the outputs of the LRA Project are made available to potential users in the most cost-effective way. Because the LRA Project has been implemented in full co-operation with government agencies, namely DoLIDAR in Nepal and DoR in Bhutan, maximisation of output sustainability has been possible. It has been concluded that the use of landslide susceptibility maps in conjunction maps showing topography and infrastructure (Figure 2) is most useful to planners and engineers.

These maps can be developed to provide an indication of landslide hazard and risk. In the case of landslide hazard, this involved the incorporation of information regarding the frequency of landslide occurrence and the mapping of areas that will be affected by runout, lateral extension and retrogression. At present both of these parameters are difficult to define. Landslide frequency is best determined through the analysis of historical landslide records combined with precipitation and seismic records, but unfortunately data quality is rarely sufficient to establish clear relationships. Because of this, the best estimate that can be made is usually to assume a frequency based on the susceptibility class – i.e. that the highest susceptibility class = 100% probability in a given period, i.e. 20 years for the nominal design life of a low cost road. Runout is best determined in a general way based on the analysis of runout distances for existing landslides in similar materials. Risk can then be established by examining the potential cost of each landslide in terms of lives threatened and land use/infrastructure at risk.

Unlike many other schemes, the LRA landslide susceptibility model follows a relatively simple logic tree type approach. The simplicity of the LRA scheme means that potentially it could readily be applied to other areas outside of Nepal and Bhutan, as rock type and slope angle are likely to be significant factors in many other environments (see Petley and Hearn, this volume). However, it should be noted that the scheme described above is intended for use in, for example, the corridor selection of rural roads and should be used at a regional or district scale (i.e. c.1:200,000) and not for detailed planning and design. It will always require field verification as part of the analysis.

7
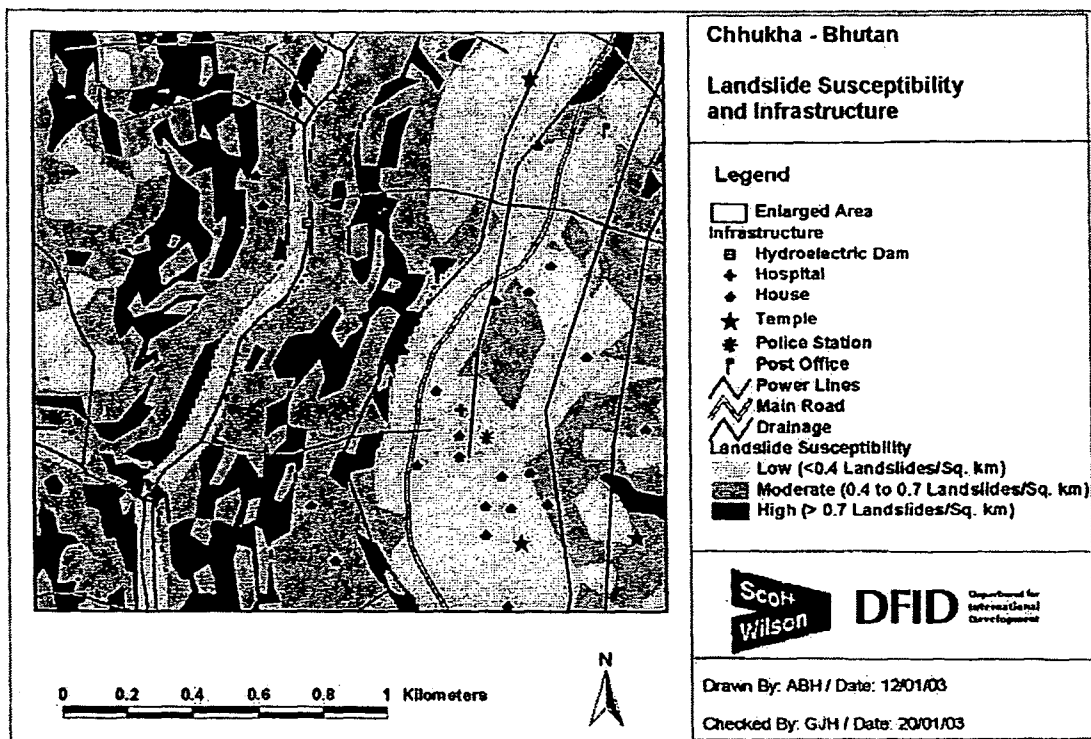
Figure 2: The Chhukha landslide susceptibility map overlain with information on topography and infrastructure vulnerability. This type of map has proven particularly useful for planning purposes.

LRA Sustainability in the Public Sectors of Nepal and Bhutan

As stated earlier, the aim of the project was to develop a set of rapid, reliable and cost-effective techniques that can be used to provide a preliminary assessment of landslide potential in any given area. This information can then be used during the planning and feasibility study stages of any rural development project. Therefore, the critical issue relates to whether or not the techniques developed by the LRA Project can be effectively used by the government agencies of Nepal and Bhutan who are involved with rural development (and more specifically rural access). Furthermore, do these government agencies have the technology and expertise to implement them?

As described by Petley and Hearn (this volume), at present satellite image remote sensing technology is rarely used in route corridor selection. There are a number of reasons for this. In the context of Nepal and Bhutan, there is a perception that the technology is expensive in comparison with conventional mapping techniques and requires specialised expertise and equipment. There are also concerns over the spatial resolution of the available images. Similar arguments are also used with respect to the use of GIS-based methods for route corridor selection – the technology is expensive, its use requires specialised training and the data is very expensive, not available or not sufficiently accurate for the purpose.

The LRA Project has demonstrated that the outputs are both manageable and practicable. Although currently, there are problems with the availability, accuracy or age of some of the available data, these are slowly being addressed by those agencies within Nepal and Bhutan that are working in the fields of geological and topographical survey. In both countries, the problem is sometimes not data availability, but knowing that the data are available, where to find it or how frequently it has been updated. There are many examples where data have been generated by some agencies from first principles despite the fact that the same data already existed within other government domains. Very often those agencies producing, creating or digitising the data are not publicising their data, or are unwilling or unable to pass it on to those who need it. Those agencies that require the data may not (or do not) have the resources to produce it themselves. This is an issue that is frequently discussed at LRA meetings, seminars and workshops by numerous government and non-government agencies, as well as private companies. Part of the problem is sometimes related to the cost of the data. Should there be a charge, and if so, how much? Should government agencies be sharing their data freely with each other? What is the role of private consultants?

8

The use of a GIS does require specialised training. However, the expertise is present in many government agencies and non-government organisations and companies within Nepal and Bhutan. There are also frequent workshops and training courses being organised in both countries, either by government agencies, private organisations and private companies (e.g. ESRI), or INGO's (e.g. ICIMOD).

Summary and Conclusions

While the LRA scheme is not intended to provide detailed slope assessment for design, it can allow broad assessments of landslide susceptibility (relative tendency of slopes to failure), landslide hazard (susceptibility combined with landslide probability and runout) and risk (damage potential) to be assessed in order to allow route corridor identification and assessment to proceed. The importance of developing a terrain evaluation-based ground model early in the planning stages of an infrastructure development project has been demonstrated. It is believed that the techniques developed by this project enable the mapping of landside susceptibility through the use of geological and topographical factors derived from published maps and API with a reasonable degree of confidence.

Training has formed an important component of the LRA Project. Seconded staff have been trained throughout the project duration and 15 training workshops have been held in Nepal and Bhutan covering the subjects of remote sensing, GIS, geology, geomorphology, field mapping and landslide management. A series of Best Practice Guidelines have been developed with the intention that they could be used by government and non-government agencies working in the field of rural access at every stage of the planning and implementation of a project.

In the context of developing countries such as Nepal and Bhutan, where resources are limited, there is a need for greater coordination and sharing of resources, experience and manpower. However, these problems are not insurmountable and it is therefore believed that the technology and techniques developed and applied by the LRA Project for the mapping of landside susceptibility and the planning of other rural infrastructure can be taken up readily by government agencies with appropriate training.

Acknowledgements

References

Dhakal, A.S., Amada, T. & Aniya, M. 1999. Landslide hazard mapping and the application of GIS in the Kulekhani watershed, Nepal. *Mountain Research and Development* 19 (1), 3-16.

Jacoby H.G. 2000. Access to markets and the benefits of rural roads. *Economic Journal* 110, (465), 713-737.

Hart, A.B., Lamichhane, P., Jha, P., Subba, M. & G.C., S. 2003. A Landslide Database for Nepal. *This volume.*

Petley, D.N, Crick, W.D.O. and Hart, A.B. 2002. The use of satellite imagery in landslide studies in high mountain areas. *The Proceedings of the 23rd Asian Conference on Remote Sensing (ACRS 2002), Kathmandu.* Available online at: http://www.gisdevelopment.net/aars/acrs/2002/hdm/48.pdf

Petley, D.N. & Hearn, G.J., 2003. Wide-scale applications of landslide susceptibility and hazard assessment. *This volume.*

Sarkar A.K. & Ghosh D. 2000, Development debate and practice. Identification and prioritisation of access problems in rural areas. *Development Southern Africa* 17, (1), 149-156.

A Landslide Database for Nepal

Hart, A.B.
Scott Wilson Kirkpatrick & Co Ltd, Scott House, Basing View, Basingstoke, RG21 4JG, United Kingdom
Email: andrew.hart@scottwilson.com
Lamichhane, P., Jha, P., Subba, M., GC, S.
Scott Wilson Kirkpatrick & Co. Ltd., PO Box No. 4201, Kathmandu, Nepal

Abstract:
Landslides are a fact of geology in Nepal. It is only in the geologically Recent time that they have become a fact of life: impacting on communities and infrastructure, and most notably roads. In order to be able to plan for landslides it is important to first ascertain where they are likely to occur. This is an inexact science but knowledge of where landslides have occurred in the past is a good starting point. The Landslide Risk Assessment Project has discussed landslide problems with several relevant agencies in Nepal and concluded that there is no single database that provides an overall picture of only landslide occurrence. Consequently, a detailed search has been undertaken to record landslides reported in the national press going back as far as 1968, using six different newspapers, covering both the Nepali and English language press. A database has been established that contains reference to over 730 reported landslides. Information on location, date and consequence of each reported landslide has been recorded wherever this data has been published. Additional data has been obtained from a number of Government or university departments within Nepal, including geological, seismic and rainfall data, as well as the location of major settlements and infrastructure. The database is unique in Nepal and probably unique in most countries. While the database is not statistically significant, given that only the bigger landslides with the greatest economic and social consequences will have been reported, it does provide the basis for analysing some of the relationships between the reported landslide activity and such factors as the geology or rainfall distribution of Nepal. The database also highlights the increasing economic risk and social impact associated with the landslide activity affecting Nepal.

Introduction

The combination of geological, topographical and climatic conditions found in Nepal promotes high levels of landslide activity. With an ever-growing population, landslide activity is increasingly impacting on communities and infrastructure, and in the remote rural areas of the country this impact is becoming increasingly difficult to manage. To be able to make any disaster preparedness plans it must first be ascertained where landslides are likely to occur. This is an inexact science but a working knowledge of where landslides have previously occurred, or the conditions that initiate landslide activity is a good starting point. It is also in these rural areas that the majority of the infrastructure development projects are currently being planned or executed. Hart *et al.*, (this volume) argue that an essential element of any proposed infrastructure project in these areas should be the assessment of landslide susceptibility, hazard and risk.

Carrying out such assessments requires a range of data that is frequently not available. The result is that in many developing countries, the level of landslide susceptibility, hazard or risk assessment that is undertaken for a rural road project is small or non-existent, and decisions continue to be made under conditions of uncertainty and unreliability (Hart *et al.*, this volume). One of the fundamental data sets required is a database of existing landslide activity. This may be in the form of a landslide distribution map or a database (digital or hard copy) of their occurrence. However, there are very few cases of such data sets being available for a whole country.

After consultation with a number of relevant agencies in Nepal it became apparent that there was no single database for landslide occurrence in the country, although there is a database for landslide and flood events maintained by the Ministry of Home Affairs (MoHA). Therefore, the Landslide Risk Assessment in the Rural Access Sector (LRA) Project established a database dealing solely with landslide activity affecting the country. As there is limited published data available on landslide occurrence in Nepal it was decided to use information reported in the national press. Five different newspapers were used, dating back to 1968 and covering both the Nepali and English language press. Additional data was obtained from a number of government or university departments within Nepal.

This paper briefly describes the database, the data it contains and some of the analysis that has been completed. A brief description of the results is also provided. The aim of the paper is to provide an indication of the level of landslide activity affecting Nepal and some of the impact it has on the country. The data presented in this paper provides a useful setting for the subject nature of this PIARC seminar.

The Landslide Database

The aim of the database is to provide an insight into the distribution, frequency and social-economic impact of the reported landslide activity across Nepal. It is not intended to be a definitive database covering all landslide activity within the country. The database contains information on over 730 reported landslides, covering the period from 1968 to 2002. For each landslide the following information has been recorded in the database:

- The location (name of village, town, Village Development Committee (VDC) and/or District Development Committee (DDC)
- The date of landslide occurrence (both English and Nepali calendar)
- The number of human casualties and fatalities
- The number of animals lost or killed
- The infrastructure damaged or lost
- Estimated cost of damage
- Any additional information, such as the causes (or inferred causes)
- The source of the information (i.e. the name of the newspaper)

The newspapers used during the study were the Gorkhapatra, Rising Nepal, Kantipur, the Kathmandu Post, and the Space Times Daily.

A number of data sets were obtained from the Department of Mines and Geology, the Department of Hydrology and Metrology, the Department for Disaster Management (Ministry of Home Affairs), the Department of Roads and the Central Departments of Geology and Geography (Tribhuvan University). This data included the geology and earthquake distribution of Nepal, the rainfall distribution, and the road network of Nepal.

The data is held within a Microsoft Access Database, as well as the ArcView Geographical Information System (GIS) software (Figure 1). Both of the software allows quick data entry and querying, with ArcView allowing the production of output maps. The GIS also allows the spatial distribution of the reported landslide activity to be investigated and compared against the other datasets such as the geology, rainfall and earthquake distribution of Nepal. A number of standard statistical techniques were used during this analysis, similar to those described by Hart *et al.*, (this volume) for carrying out the landslide susceptibility mapping for each of the LRA study areas.
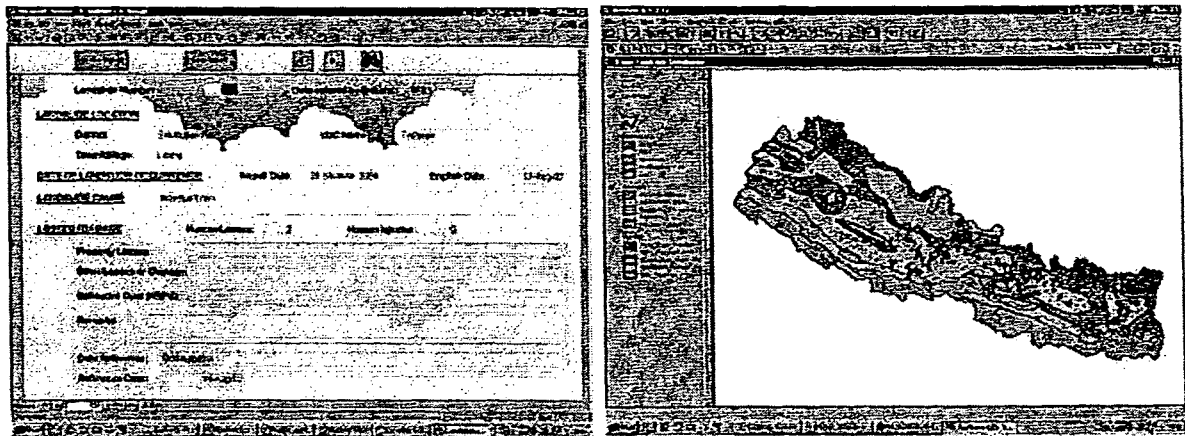
Figure 1: The landslide database is stored and analysed using MS Access and ArcView GIS.

Landslide Occurrence, Fatalities, Casualties and Damage

The landslide database for Nepal developed by the LRA Project contains information on over 730 landslides that have been reported in the national newspapers covering the period from 1968 to 2002. The database shows that during this period, landslide activity in Nepal has claimed the lives of over 2400 people, left over 500 people injured and caused over NRs 344.5 million (US$ 4.4 million) of damage (Table 1).

Table 1: Summary of landslide, fatality and casualty data contained within the LRA database.

	Landslides	Human Fatalities	Human Injuries	Houses Destroyed or Damaged	Estimated Cost (NRs.)
Minimum reported in a year	5	4	0	0	0
Maximum reported in a year	111 (2002)	342 (2002)	73 (1972/2002)	642 (2002)	242.5 million (1998)
Average reported per year (1968 to 2002)	20	70	15	96	9.8 million
Total reported for the period 1968 to 2002	734	2,441	516	3,366	344.5 million
Peaks in reported figures	1970, 1985, 1988, 1991, 1999, 2001, 2002	1970, 1972, 1976, 1982, 1983, 1985, 1988, 2001, 2002	1970, 1972, 1988, 2001, 2002	1971, 1983, 1985, 1987, 1998,1999, 2000, 2001, 2002	1982, 1986, 1988, 1998, 2001

A number of "peaks" can be seen in the data (Table 1; Figures 2, 3, 4 and 5). These dates have been compared with the available rainfall data for the period 1989 to 2000 (Figure 6) to see if they correspond to years with either "wet" or "dry" years (Table 2). A "wet" year has been defined as a year with high (or higher than average) rainfall recorded at a number of rainfall stations across the country and a "dry year" as a year with low (or lower than average) rainfall recorded at a number of rainfall stations. There seems to be a limited correlation between the number of reported landslides, human fatalities, injuries and houses destroyed and the relative amount of rainfall. This could be because the rainfall data only covers 12 years while the LRA landslide database covers 34 years.

Table 2: Reported Statistics for "Wet" and "Dry" Years

"Wet" Years	No. Reported Landslides	No. Reported Fatalities	No. Reported Injuries	No. Reported Houses Lost
1990	7	18	11	1
1993	8	29	2	27
1995	6	12	15	7
1998	29	79	9	151
2000	35	53	23	22
2002	111	342	72	321
"Dry" Years	**No. Reported Landslides**	**No. Reported Fatalities**	**No. Reported Injuries**	**No. Reported Houses Lost**
1992	5	24	3	0
1994	15	26	18	11
1997	13	22	2	49
1999	44	82	22	78

There does appear to be a lack of correlation between the "peaks" for some of the data listed in Table 1 or shown in Figures 2 to 5. For example, there is a peak in the estimated cost of the damage attributed to landslide activity for 1986 but this year is not represented by peaks in any of the other attributes. There is also a peak in the number of fatalities reported to have occurred as the result of landslide activity during 1976 but again this is not seen for any of the other attributes.

From about 1996, there appears to be a steady increase in the number of landslides, fatalities, injuries, and houses damaged or destroyed being reported each year (Figures 2, 3, and 4). The reported estimated cost of the damage caused by the landslide activity also appears to be increasing (Figure 5). This is also highlighted by the three-year running average figures that have been calculated using the data from 1968 to 2002 (Figures 3, 4 and 5). The question is whether this is an increase in the efficiency of landslide reporting or a

3

real increase in the occurrence of landslides, or a combination of both. Without an independent database for landslide activity (derived from field mapping or remote sensing) this issue cannot be easily resolved. However, it should be remembered that the number of reported human fatalities and casualties, or the estimated cost of the damage caused by a landslide may not necessarily reflect the number of reported landslides. For example, one or two large landslides may be more devastating or costly than ten or fifteen smaller events (which may be reported for other reasons such as damage to infrastructure).

Comparison of the fatality figures contained within the LRA database with the undifferentiated landslide and flood data collected by the Ministry of Home Affairs for the last 20 years (1983 to 2002) seems to suggest that it might be an increase in the level of reporting. For much of this period there seems to be little agreement between the data sets, except for the last few years (Figure 7). Interestingly, although the numbers of fatalities and injuries recorded by both the LRA and MoHA databases for the last two years have been very similar, there is a big discrepancy in the numbers of houses destroyed, as are recorded in the two databases (Table 3). It should however, be remembered that the LRA database deals solely with landslide activity while the MoHA database deals with both landslide and flood activity combined. Therefore part of the discrepancy between the two data sets will be the influence of the flood data. For example, Figure 3 shows that the MoHA database records that over 1200 people were killed in 1993 as a result of landslide and flood activity. This figure will mostly be due to the devastating floods that affected many parts of Nepal during the monsoon of that year.

Table 3: Comparison of the fatality, injury and houses destroyed figures contained within the LRA and MoHA Databases for 2001 and 2002. The LRA data is for landslides only. The MoHA data covers both landslide and flood activity.

Year	Fatalities		Injuries		Houses Destroyed	
	LRA	MoHA	LRA	MoHA	LRA	MoHA
2001	185	196	45	88	187	3,934
2002	342	444	72	108	321	21,559
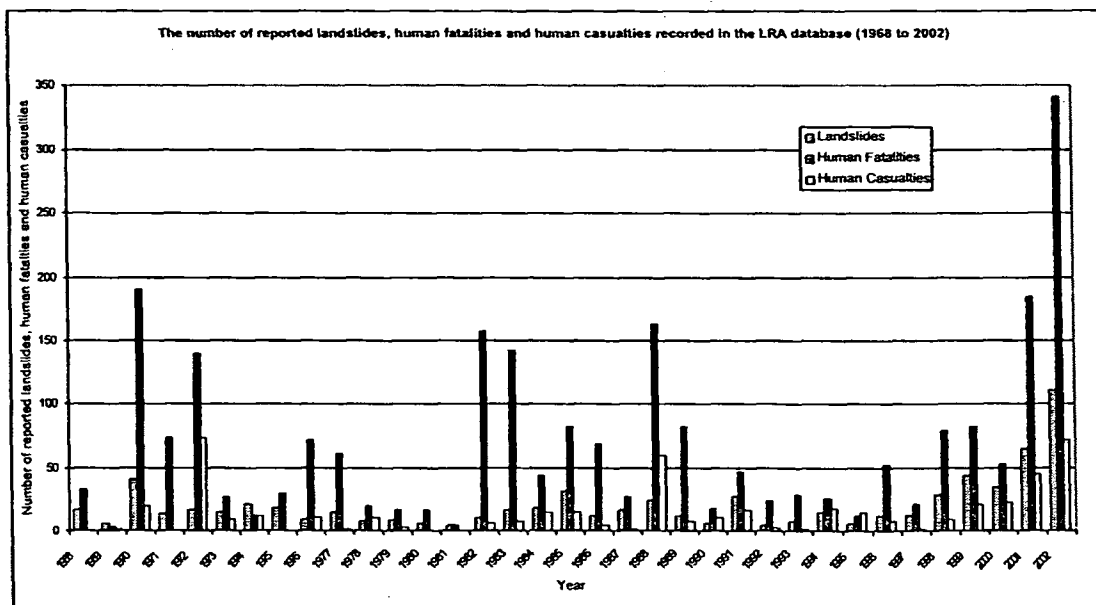
Figure 2: The number of reported landslides, human fatalities and human casualties per year from 1970 to 2002 recorded in the LRA Landslide Database.
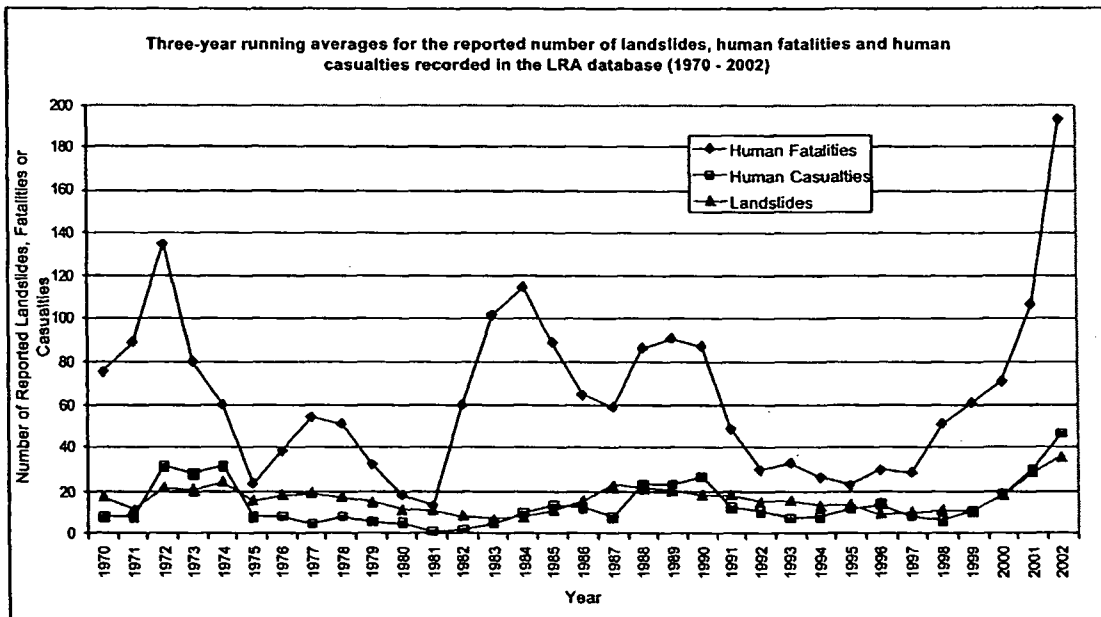
Figure 3: The running three-year average figures for the number of reported landslides, human fatalities and human casualties per year from 1970 to 2002 recorded in the LRA Landslide Database.
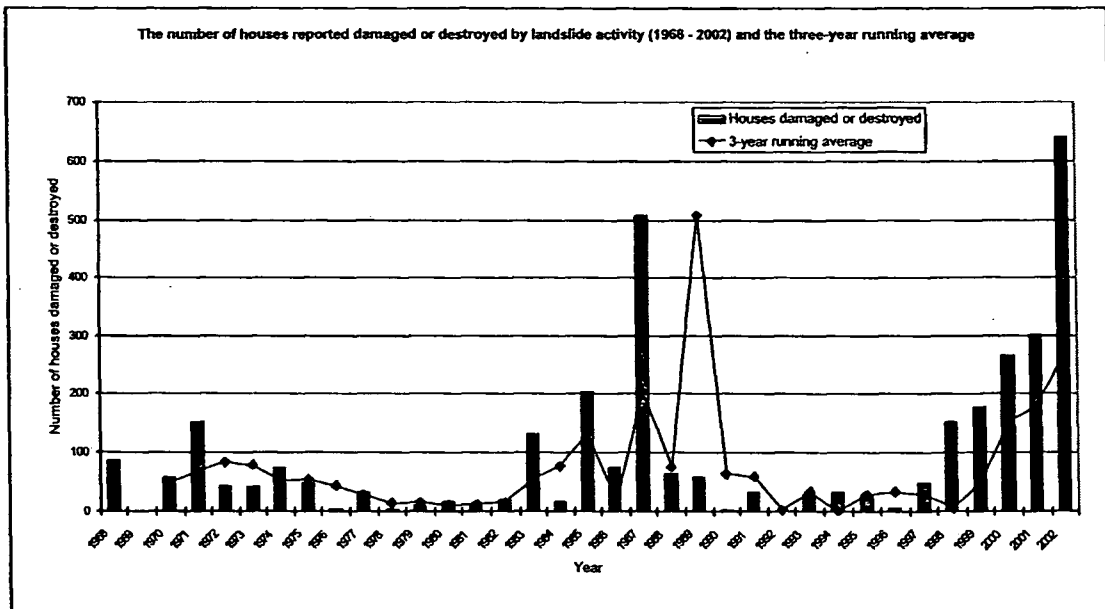
Figure 4: The number of reported houses damaged or destroyed by landslide activity per year from 1970 to 2002 recorded in the LRA Landslide Database.
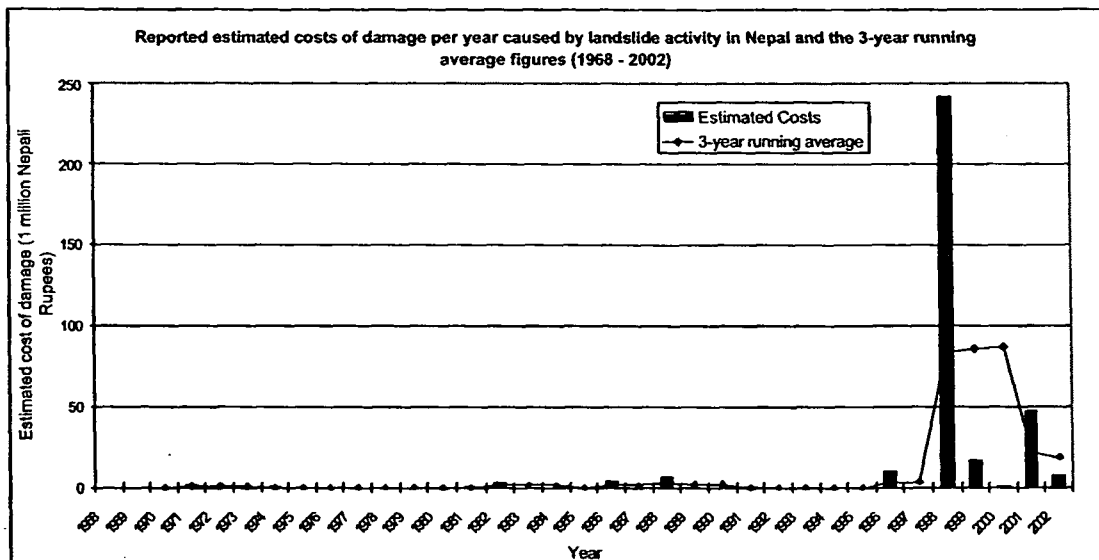
Figure 5: The estimated costs of the damage caused by landslide activity each year in Nepal that has been reported in the national press (1968 – 2002) and the three-year running average figures.
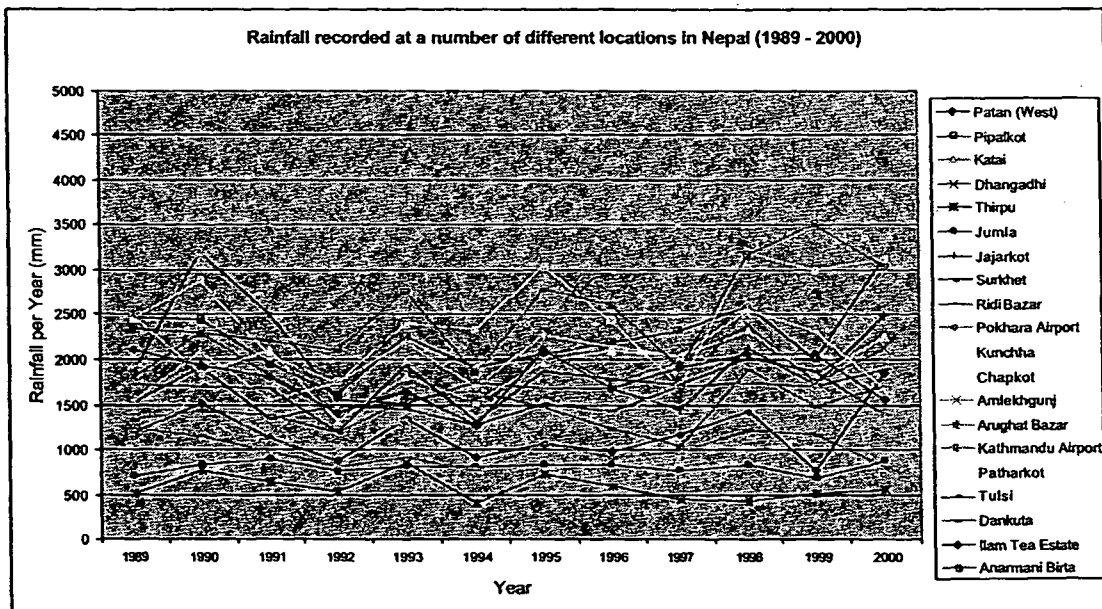
Figure 6: Comparison of the annual rainfall data from a number of rainfall stations located across Nepal for the period 1989 to 2000. (Data provided by the Department of Hydrology and Metrology, Nepal.)

This study has found that the estimated cost of the damage caused by landslide activity have only been recorded for approximately 10% of the reported landslides that are recorded in the LRA database. This means that the figure reported earlier in this paper of NRs. 334.5 million (over last 34 years) does not reflect the true picture for the country, and that it should be considerably higher. The problem might be that this information may not be reported as it may not be seen as important by the press unless it is a very high figure (and therefore "newsworthy"). Another problem associated with reporting the cost of a landslide is how to evaluate the cost of the damage. For examp le, in many cases the newspapers report that a landslide closed a section of road (i.e. the Prithvi Highway) for a number of days. The reported costs of road closures most likely relate to the capital costs of opening or reinstating the road only and not the added economic losses that result from a break in communications.

6
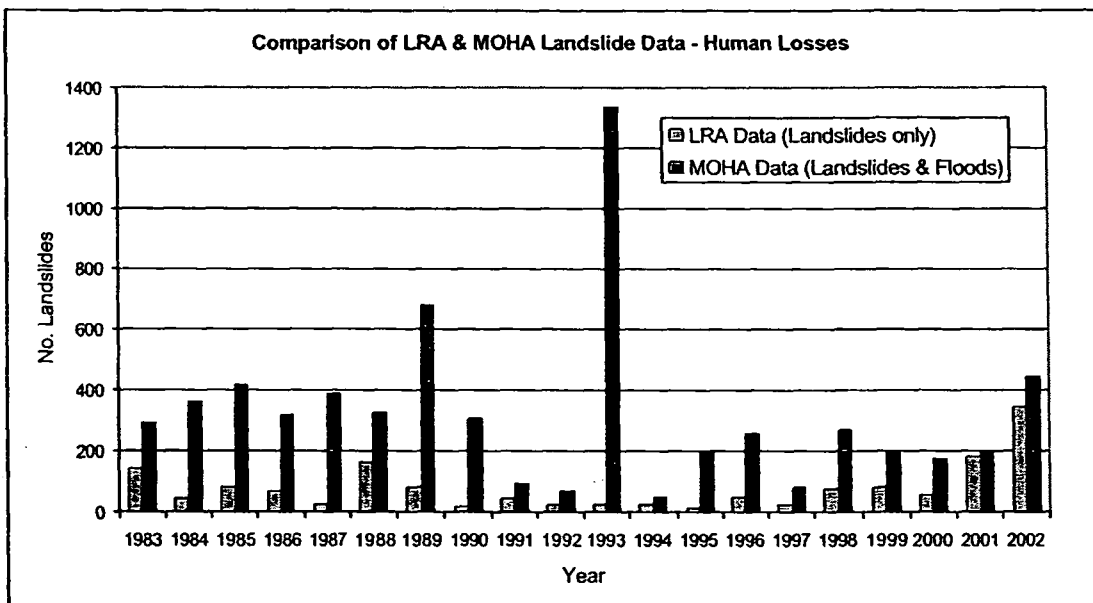
Figure 7: Comparison of the human fatality figures for the period 1983 to 2002 recorded in the LRA Landslide Database and the MoHA landslide and flood database.

If the cause of the landslide was reported in the newspaper article then this was also recorded in the LRA landslide database. This is most likely to be an inferred cause, as in many cases it is unlikely that a detailed investigation into the factors leading to the landslide's occurrence had been completed for purposes of newspaper reporting. As most of the landslides reported in the national press occurred during the monsoon, it is not surprising that rainfall is listed most frequently as the triggering mechanism (approximately 60%; Figure 8). Toe erosion or flood activity was also described in a number of cases as the cause of the reported landslide, although usually in conjunction with heavy rainfall or cloudburst events.
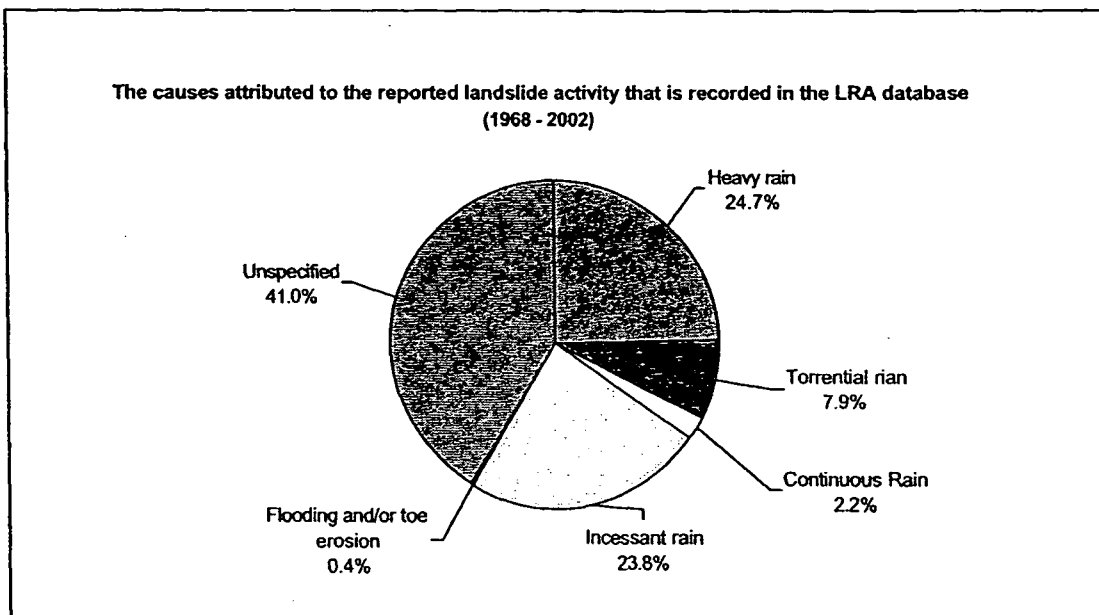
Figure 8: The causes attributed to the landslide activity reported in the national press (1968 – 2002).

Landslide Distribution

A source of bias in the LRA database is the fact that it will probably only contain those landslides that have impacted on the population and infrastructure of Nepal. It is therefore concluded that a large number of landslides that do not cause loss of life or damage to nationally-important infrastructure go unreported. This may mean that the distribution of reported landslides could be focused on the more populated parts of the country. To see how the reported landslide distribution reflects the population distribution of Nepal, the population density figures for each district were calculated using the 2001 population data. These were then compared with the number of reported landslides and the calculated reported landslide density figures for each district (Table 4). The comparison shows that those districts with the highest landslide densities are not necessarily those districts with the highest population densities. This may indicate that the reporting of the landslide activity affecting Nepal is not biased towards the major population centres of the country. This data also gives an indication of the relative level of risk posed to these districts by landslide activity.

By using a GIS it is possible to plot a map of the reported landslide distribution and compare it visually with the population centres and infrastructure such as the major road network for Nepal (Figure 9). This figure suggests that there is a very close connection between the reported landslide distribution and the major road network (and therefore some of the major population centres, such as Kathmandu and Pokhara). Is this a true representation of the situation or the result of reporting bias? How many of the reported landslides are natural failures and how many are the result of human (predominantly engineering) activity? It is often difficult to establish the cause of an individual landslide without a detailed ground investigation which has obviously been beyond the scope of this study. Another question that could be asked is whether this map supports the argument that road corridors attract ribbon development and therefore an increase in the level of risk posed by landslide activity associated within road corridors (Hearn et al, this volume).

Table 4: Comparison of the district population data for Nepal and the reported landslide density figures calculated using the figures held within the LRA database. The data shown is for the 20 districts with the highest reported landslide density figures.

Rank based on Slide Density*	District	Population	Area (Sq. km)	Population Density (pop/Sq. km)	Rank based on Population Density*	Reported Landslide Density (Landslides/ Sq. km)
1	Kathmandu	1,081,845	395	2,738.85	1	0.0380
2	Syangja	317,320	1,164	272.61	19	0.0369
3	Nuwakot	288,478	1,121	257.34	22	0.0294
4	Palpa	268,558	1,373	195.60	26	0.0218
5	Lalitpur	337,785	385	877.36	3	0.0208
6	Kavre	385,672	1,396	276.27	18	0.0208
7	Parbat	157,826	494	319.49	16	0.0202
8	Sindhupalchok	293,719	2,542	115.55	49	0.0189
9	Kaski (Pokhara)	380,527	2,017	188.66	29	0.0174
10	Dolakha	175,912	2,191	80.29	56	0.0132
11	Gulmi	296,654	1,149	258.18	21	0.0131
12	Baglung	268,937	1,784	105.75	41	0.0129
13	Dhading	338,658	1,926	175.83	31	0.0125
14	Khotang	231,385	1,591	145.43	44	0.0113
15	Okhaldhunga	156,702	1,074	145.91	43	0.0112
16	Terhathum	113,111	679	166.58	33	0.0103
17	Arghakhanchi	208,391	1,193	174.68	32	0.0101
18	Ilam	282,806	1,703	166.06	34	0.0100
19	Bhojpur	203,018	1,507	134.72	48	0.0093
20	Dhankuta	166,479	891	186.85	30	0.0090

* Nepal has 75 districts

8
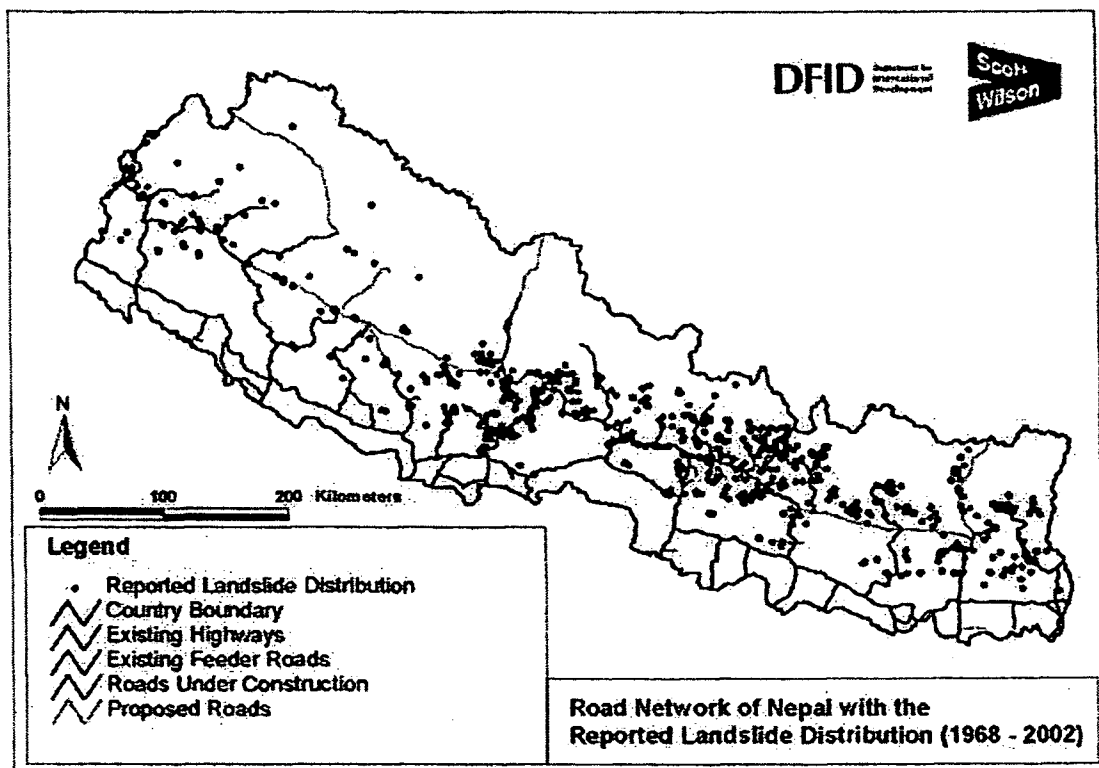
Figure 9: The reported landslide distribution with the major road network for NepaL The road network data was supplied by the Department of Roads, Nepal.

Data Analysis and Results

By importing the reported landslide database into ArcView GIS it is possible to examine the spatial relationships between the reported landslide distribution and several different factor layers of data held within the GIS. This analysis may help to identify those factors that, at the country scale, influence the landslide activity that affects the country. The factor layers used in this study are the geology, seismic activity and rainfall intensity of Nepal. Each factor layer was analysed using a number of standard statistical techniques, similar to those used for the landslide susceptibility mapping described by Hart *et al.*, (this volume). These were the Chi-Squared, O/E and landslide density statistics. Both the Chi squared and O/E statistics compare the distribution of the observed or reported landslides with the number of landslides that would be expected if the distribution of landslides was even or random across the whole area. The landslide density figures give an indication of the concentration of landslides found occurring within a given unit. The data used to calculate these figures is shown in Table 5.

The analysis of the importance of any factor has been undertaken using a standard Chi Sq test. This test is well established, providing an analysis of spatial distribution compared with a control dataset. Here, the control dataset has been generated by assuming an even distribution of landslides across the study area – i.e. that none of the factors involved in the analysis affect the landslide distribution. For each factor, $?^2$ has been calculated using the following formula:

$$?^2 = S\,((O\text{-}E)^2\,/\,E) \qquad \rightarrow \qquad \text{Equation 1}$$

Where: O = the observed number of landslides occurring in the area covered by that class or factor
         E = the expected number of landslides in that area if the distribution were even

9

Table 5: The data that was collected and the statistics calculated during the analysis of the reported landslide data held within the LRA database.

Area covered:	The area covered by the specified factor category (i.e. "Siwalik" within the geology factor layer).
% of total Area:	The % of the Nepal covered by the specified factor category.
Reported (Observed) No. Landslides (O):	The actual number of reported landslides that are found within the specified factor category.
Expected No. Landslides (E):	The number of landslides that would be expected to have occurred in the specified factor category if there was a uniform landslide distribution within the specified category.
O/E:	The ratio of the reported or observed number of landslides against the expected number of landslides.
Chi-squared (x^2) test:	The standard chi-squared statistic (described below).
Landslide Density:	The density of landslides occurring within the specified factor category.
% of total No. landslides	The % of the total number of landslides occurring in the specified factor category.

Therefore, a value of $x^2 = 0$ indicates a random distribution, whereas larger values of x^2 indicates a non-random distribution. However, x^2 values must be considered in terms of the degrees of freedom, which provides an indication of the probability that the distribution analysed occurred by chance. It is important to note that a high x^2 value does not necessarily mean that the technique is accurately determining the actual distribution, but rather one that is non-random. For this reason it is essential to consider the results in the context of the map to determine how well a non-random distribution coincides with the true distribution.

Another statistic that has been used is the O/E value. This basically divides the observed number of landslides by the expected number of landslides (if the distribution was even). Although not as powerful as the Chi-squared statistic this value can give a very quick indication as to the significance of a particular factor. For example:

For an O/E of less than one = the factor being considered may not be significant.
For an O/E of greater than one = the factor being considered may be significant.
An O/E value of one may indicate an even or random distribution.

Landslide density figures were also calculated for each of the classes within the different factor layers. This gives an indication of the concentration of landslides occurring within that class or category and helps to identify susceptible classes. For this investigation a combination of these statistics have been used, so as to reduce the risk of being misled by an individual statistic.

Rainfall Intensity

The rainfall intensity map (Figure 10) was produced by the Central Department of Geography at Tribhuvan University, using data provided by the HMG Department of Hydrology and Meteorology. The map divides Nepal into five different classes based on the average rainfall per 24 hours.

The results from the rainfall intensity factor analysis are shown in Table 6. The highest landslide density figures (and therefore the most susceptible landslide areas) occur where the rainfall intensity exceeds 300mm per 24 hours and the lowest landslide density figures (and therefore the least susceptible landslide areas) correspond with areas which have rainfall intensities less than 150mm per 24 hours. The Chi-Squared value of 385.3 with four degrees of freedom is highly significant.

10

Table 6: Summary of Rainfall Intensity Factor Analysis Results

Rainfall Intensity (mm / 24 Hours)	Area (Thousand Sq. km)	% of Nepal	Expected Landslides (E)	Reported Landslides (R)	R/E	Chi-Squared	Landslide Density (Slides/Sq. km)	% of Slides
Very High (Above 300)	0.9	0.6	4.5	23	5.17	77.4	0.0255	3.2
High (250 – 300)	4.1	2.8	20.2	79	3.91	171.1	0.0193	10.8
Moderately High (200 – 250)	49.9	33.7	246.3	352	1.43	45.4	0.0071	48.2
Moderate (150 – 200)	83.2	56.2	410.5	275	0.67	44.7	0.0033	37.7
Low (Below 150)	9.8	6.7	48.6	1	0.02	46.6	0.0001	0.1
Total	148.0	100.00	730.0	730	11.20	385.3	0.0049	100.0

Geology

The geology map (Figure 11) used in the analysis was provided by the Department of Mines and Geology. It shows the five main geological stratigraphic units found in Nepal. The landslide factor analysis has shown that the most susceptible stratigraphic unit to landslide activity in Nepal is the Lesser Himalayan Unit (Table 7). This unit appears to be considerably more susceptible than the other units. The Lesser Himalayan Unit comprises quartzite, meta-sandstone, phyllite, slate, schist, marble, dolomite and limestone (Table 8). The Chi-Squared value of 425.2 with four degrees of freedom is highly significant.

A large proportion of the population and infrastructure of Nepal is located within the Lesser Himalayan Unit. This implies that this population and infrastructure are at greatest risk from landslide activity. However, as the landslide occurrence data used in this investigation came from newspaper sources, this high correlation could also reflect a higher degree of reporting when compared to the more rural and remote areas of the country.

Table 7: Summary of Geology Factor Analysis Results

Geology	Area Covered (Thousand Sq. km)	% of Nepal	Expected Landslides (E)	Reported Landslides (R)	R/E	Chi-Squared	Landslide Density (Slides/Sq. km)	% of Slides
Lesser Himalayan	43.5	29.4	214.4	450	2.10	259.1	0.0104	61.6
Higher Himalayan	47.1	31.8	232.1	208	0.90	2.5	0.0044	28.5
Siwalik	14.8	10.0	73.1	36	0.49	18.8	0.0024	4.9
Tibetan Tethys	15.6	10.5	76.8	16	0.21	48.2	0.0010	2.2
Quaternary	27.1	18.3	133.6	20	0.15	96.6	0.0007	2.7
Total	148.0	100.0	730.0	730		425.2	0.0049	100.0

Table 8: Summary of the major rock types found in each of the major stratigraphic units of Nepal

Stratigraphic Unit	Major Rock Types
Quaternary	River terrace and lacustrine deposits (conglomerates and unconsolidated deposits)
Tibetan Tethys	Limestone, sandstone and shale
Siwalik	Sandstone, mudstone and conglomerate
Lesser Himalayas	Quartzite, meta-sandstone, phyllite, slate, schist, marble, dolomite and limestone
Higher Himalayas	Gneiss, schist and quartzite
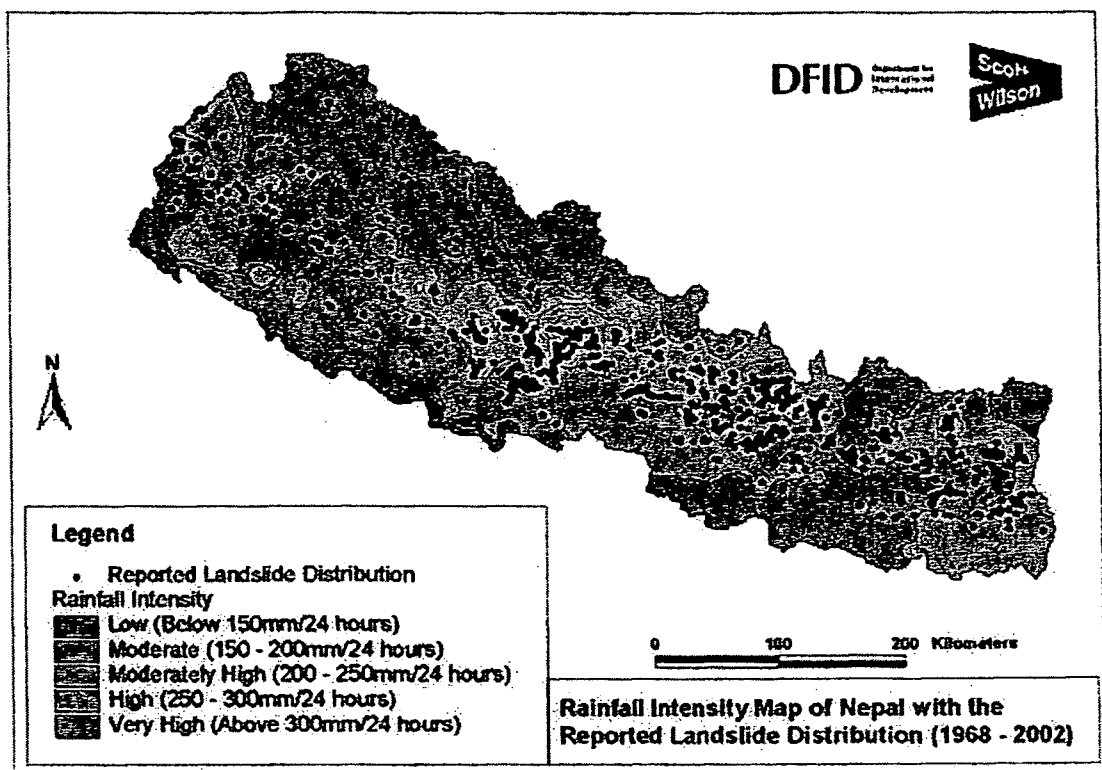
Figure 10: Rainfall intensity map for Nepal with the reported landslide distribution. The rainfall intensity data was supplied by the Department of Hydrology and Metrology and the Central Department of Geography, Tribhuvan University.
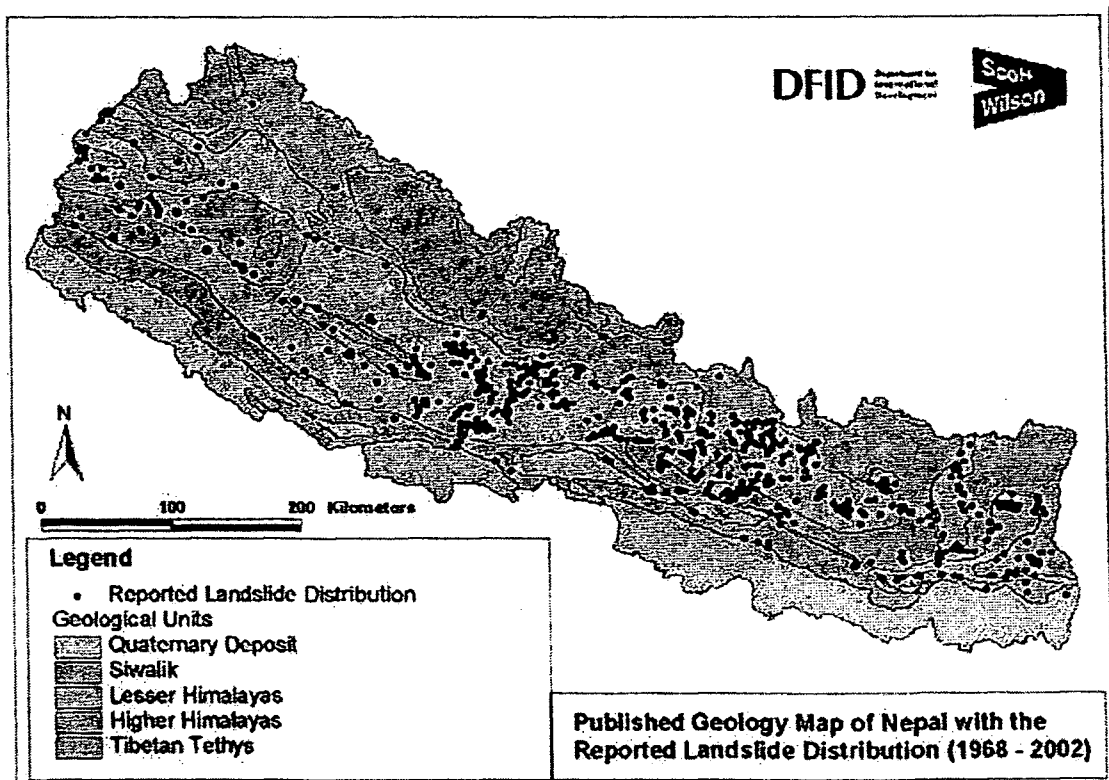
Figure 11: Published geology map for Nepal with the reported landslide distribution. The geology map was supplied by the Department for Mines and Geology.

Seismic Activity

Earthquake data for Nepal and the surrounding region was obtained from the United States Geological Survey (USGS) as well as from the Department for Mines and Geology in Nepal (Figure 12). The data displayed in Figure 12 shows the distribution of both the earthquake activity affecting Nepal and the reported landslide activity that is recorded in the LRA Database. The relationship between these data sets has been examined. However, the relationship between earthquake activity and associated landslide activity is a complex one (and is complicated even further if the earthquake occurs during the monsoon rains). The area affected by an earthquake and the number of landslides that might be triggered by an earthquake event, will vary according to the magnitude of the earthquake, the topography, geology and soil of the area. There is also the problem that unless the date and time of a landslide are known then it is very difficult to correlate it with a particular earthquake event.

During 1988, several large earthquakes affected Nepal and it is possible that these events led to some of the landslides that were reported to have occurred. There is a "peak" in the two data sets for 1988 (Figures 2 and 13). However, none of the reported landslides that have been recorded in the LRA database were attributed to earthquake activity (Figure 8).

Discussions held at the international mountain hazards seminar held in Kathmandu in November 2002 (organised by DoLIDAR and Scott Wilson and sponsored by the UK Department for International Development (DFID)) indicated that spatial relationships between seismic events and landslide occurrences are difficult to find because of the lack of detailed data available. Furthermore, it is common to find that many 'earthquake-generated landslides' do not occur instantaneously but as a result of heavy rain during following wet seasons. The lack of association is therefore considered to be due to the way in which seismic data is reported, the limited ground resolution of recorded data and the complex way in which many landslides are initiated.
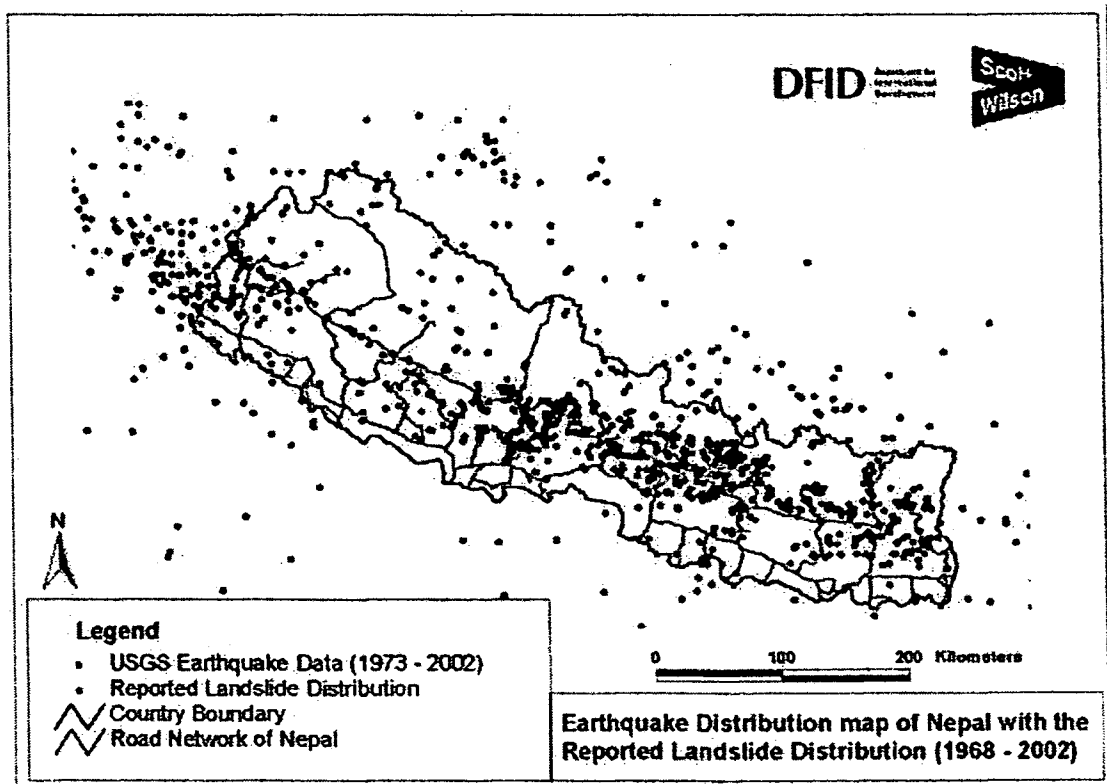
Figure 12: Earthquake epicentre distribution and reported landslide distribution map for Nepal. The earthquake epicentre distribution data was obtained from the United States Geological Survey (USGS) and the Department for Mines and Geology, Nepal

13
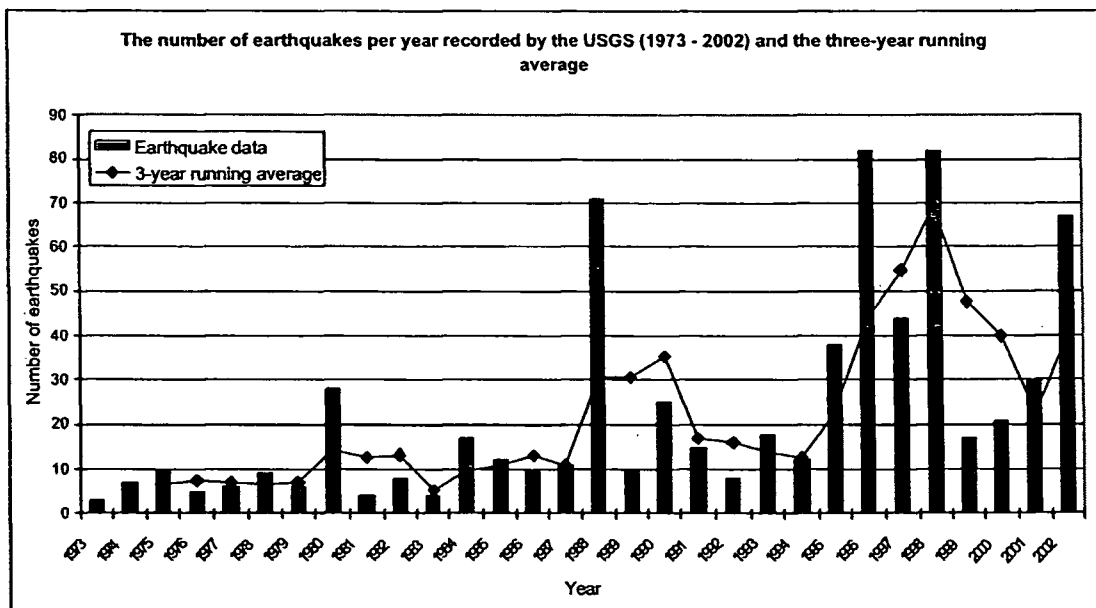
Figure 13: The number of earthquakes per year recorded by the USGS for the period 1973 to 2002 for Nepal. The earthquake data was obtained from the United States Geological Survey (USGS) and the Department for Mines and Geology, Nepal.

Summary

Landslide activity is an accepted fact of nature in Nepal, and therefore the creation of a database of reported landslide occurrence enables a better understanding of the geographical extent of this problem to be gained. This database, dealing solely with reported landslide activity, is unique to Nepal and probably most other developing countries. The database enables a quantification of the problem and identification of those parts of the country where either there is an elevated risk posed by the landslide activity or where more data needs to be collected so that a better understanding of the problem across the country as a whole can be gained. Such a database is therefore a valuable resource for policy makers, planners, engineers and researchers alike. Once established, such a database needs to be maintained and annually updated.

The data collected to establish the LRA database has been analysed both temporally and spatially. The spatial analysis of the landslide activity reported in the national press involved comparing the landslide distribution with a number of different factors. The analysis has shown that there is a close correlation between the reported landslide distribution and the geology and rainfall distribution of Nepal. Over 60% of the landslides occur in areas affected by rainfall intensities of greater than 200 mm of rain per 24 hours (Table 7) and within the Lesser Himalayan geological unit. This result confirms the widely accepted view that the landslide activity of Nepal is predominantly controlled by the geology and the climate of the country.

There is also a close association between the reported landslide distribution and the major population centres and road network of the country. In one sense, this is to be expected as it reflects the nature of the database – a database of reported landslide activity. The database developed by the LRA Project was not intended to reflect the natural landslide distribution of the country, but to provide an insight into how landslide activity affects the population and infrastructure of the country. This close correlation between the reported landslide activity and the country's infrastructure and population centres could also reflect the effects of human activity on the environment. For example, a large number of the landslides are reported to have occurred along the Prithvi Highway where steep and deep cut slopes have been formed in the Lesser Himalayan Unit.

The investigation has shown that over the last five years there has been an increase in the number of reported landslides and landslide related fatalities, injuries and damage to infrastructure, as well as other economic losses. Whether this is a true reflection of the situation (and therefore an increasing level of risk) or the result of an increase in public awareness (and therefore an increase in reporting) is still to be determined. It is interesting to note from Figure 2 that there are three main periods when landslide activity was reportedly

14

the highest. Excluding 2002, neither of these periods have a higher recorded incidence of landslide activity than the other. This might suggest that the efficiency of landslide reporting has not increased significantly over time; leading to the conclusion that time-series analysis is likely to be statistically significant. The lack of an independent, field or remote sensing based, landslide database for the country does not help to resolve this issue.

An enhancement of the database would be to differentiate between natural and human induced failures wherever possible. This would give a better understanding of how human activity across the country is contributing to the observed landslide problem.

If combined with field mapping, the assessment of aerial photographs and satellite imagery, as well as a more thorough document search (i.e. government records), the database of reported landslide activity developed by the LRA Project, as discussed in this paper, could become the starting point for a landslide database covering all aspects of landslide activity within Nepal. What is clear is that landslides pose a significant risk to population and infrastructure through the foothills and middle hills of Nepal. This distribution is linked to the weaker rock types and clusters along road corridors where slopes have been steepened for highway earthworks. However, landslides are by no means confined to these areas and appear to be triggered by threshold rainfall intensities of 250-300mm in 24 hours. In addition to the valuable data set collected by the LRA project, there is a wealth of information collected by MoHA, and it is clear that this latter database needs to be subdivided into human and economic losses caused by landslides and floods individually, as soon as possible.

The overall quality of the landslide database could be strengthened considerably by improved reporting at the level of local government with this information being fed through to the relevant authorities at central level. The creation and maintenance of such a database will eventually assist in the development of disaster preparedness plans and the allocation of resources for pre-emptive avoidance and mitigation.

References

Hart, A.B., Hearn, G.J., Petley, D.N., Tiwari, S.C. and Giri, N.K. 2003. Using remote sensing and GIS for rapid landslide hazard assessment: potential public sector uptake in Nepal and Bhutan. *This volume.*

Hearn, G J, Hart, J R and Tiwari, S C. 2003. Social and engineering management of landslides in road corridors. *This volume.*

Statistical Pocket Book, Nepal. 2002. HMG National Planning Commission Secretariat Central Bureau of Statistics.

Petley, D.N. and Hearn, G.J., 2003. Wide-scale applications of landslide susceptibility and hazard assessment. *This volume.*

THE USE OF SATELLITE IMAGERY IN LANDSLIDE STUDIES IN HIGH MOUNTAIN AREAS

David N. PETLEY*
William D.O. CRICK**
Andrew B. HART**

*Lecturer, Department of Geography, University of Durham
Stockton Road, Durham, DH1 3LE, United Kingdom
Tel: (44)-191-374-2099 Fax: (44)-191-374-2456
Email: d.n.petley@durham.ac.uk

**Engineering Geologists, Scott Wilson Kirkpatrick Ltd
Scott House, Basing View, Basingstoke, RG21 4JG, United Kingdom
Tel: (44)-1256-461161 Fax: (44) 1256 460582
Email: andrew.hart@scottwilson.com

KEY WORDS: Landslide, remote sensing, satellite, image interpretation, hazard

ABSTRACT

Landslides represent a serious threat to human life and activities in most high mountain chains. However, due to the difficult nature of such terrain, it is often difficult to assess directly the susceptibility of slopes to landsliding. Hence, remote sensing offers many attractions for the examination of landslide potential in such environments, especially in less developed nations in which resources are stretched and levels of environmental information are limited. However, there is a need to ensure that the techniques are effective, reliable, and offer value for money in terms of the amount and accuracy of data that can be extracted. Using a case-study, this paper compares the applicability of Landsat ETM+ and IKONOS imagery for the assessment of landslide susceptibility in natural terrain. This has been undertaken on the basis of six study areas located in upland areas of Nepal and Bhutan. In each case, the imagery has been used both to directly map landslides and to examine the occurrence of factors that might be important in landslide initiation, such as water seepage. The results from the imagery have been bench-marked using field surveys. The study has demonstrated that at present Landsat ETM+ remains the most cost-effective tool for mapping landslide susceptibility, due to its relatively low cost and high spectral resolution. However, its spatial resolution remains a significant limitation. This limitation is avoided by high resolution, multispectral IKONOS imagery, which finally allows even small landslides to be mapped in detail. However, the more limited spectral resolution is less useful for factor type mapping. Unfortunately, the high cost of this imagery will continue to preclude the development and use of this technique in developing countries.

1. INTRODUCTION

Recent research has demonstrated that in mountain chains undergoing high rates of uplift, landslides are an inevitable and essential environmental process (Petley and Read 1999 for example). Unfortunately this has important implications for humans, who are often adversely affected by landslides. As a result, the delineation of landslides is extremely important, but there is a general recognition that the process is difficult, especially where the slopes are covered in dense vegetation or are cultivated.

This is particularly the case in the Himalayas, where the on-going collision has allowed the generation of a high mountain chain characterised by steep, unstable slopes. The monsoonal climate allows the rapid growth of vegetation, although the environment is considerably altered by the activities of humans, in particular with respect to the drainage pattern and the landuse. Consequently landslides occur throughout the Himalayas. Unfortunately, landslide identification and delineation in this environment is problematic. The high, steep terrain means that the identification of mass movement features is difficult, especially where the features are not presently active. Many slopes are covered in forest or have been terraced for cultivation, meaning that surface forms are hard to identify. Finally, from a practical

perspective, access to the mountain areas is hindered by the absence of good quality roads – a Catch 22 situation given that the lack of roads is due in part to the problems associated with landslides.

Satellite remote sensing potentially offers a solution to at least some of these problems. Good quality, multispectral imagery can allow landslides to be identified using a combination of direct inspection and computer-based analyses. The availability of imagery with a sub-metre resolution means that even small landslides are potentially observable. However, research into the use of such techniques for landslide delineation has so far been limited. In this paper, the results of the application of various remote sensing methods for the delineation of landslides in the mountains of Nepal and Bhutan are described, demonstrating the very high potential that these techniques now offer.

2. SATELLITE REMOTE SENSING FOR LANDSLIDE MAPPING

Satellite imagery has been used in the analysis of landslide occurrence primarily through the analysis of colour composites. Several studies have experimented with the use of a true colour composite (TCC) (e.g. Sauchyn and Trench 1978; Greenbaum et al. 1996). In most cases the primary restriction has proven to be spatial resolution, with only landslides of approx. 50 m x 50 m or larger being easily resolved. Rather better results were achieved using the 5.8 m spatial resolution of the IRS-1 instrument however (Nagarajan et al. 1998).

False colour composite (FCC) images have proven useful in some cases, especially where a landslide scar provides a clear change in the surface properties, such as the removal of forest to expose bare soil. Greenbaum et al. (1995) successfully used this technique for the examination of landslides in Papua New Guinea for example. Similar results were also achieved by Rothery (1987) to identify rock avalanche deposits.

Mixed success has been achieved with the use of more complex analyses techniques. For example, Huang and Chen (1991) reported considerable success using a principal components analysis. Kusaka et al. (1996) on the other hand used the LANDSAT thermal bands to identify areas of perennially wet soil, which were linked with potential landslides. In all cases, spatial resolution has proven to be a key limitation, and shadows cause considerable problems.

3. THE STUDY SITE
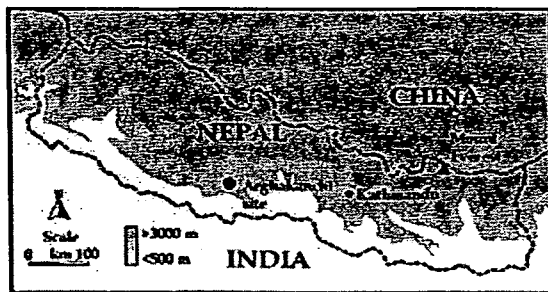
Figure 1: Field site location map

This study has examined the use of satellite imagery in six study areas within Nepal and Bhutan. However, this paper will concentrate upon one of the sites, located within the Arghakhanchi district of Nepal at approx. 83° 10'E, 27° 55'N (Figure 1). The study site has a surface area of 340 km², surrounding an existing agricultural road that has been severely affected by landslides. The road is orientated broadly north-south, running across terrain formed from young sedimemts including shales, sandstones, limestones, mudstones; and older metamorphosed rocks including quartzites, and schists. The area is forested, although there are extensive areas of cultivation and some and medium-sized settlements. The relief of the area extends from about 100 m above sea level on the Ganges plain to the south of the study area up to 2500 m in a ridgeline across which the road passes.

4. THE SATELLITE IMAGERY

This study has concentrated on the use of LANDSAT 7ETM+ and IKONOS imagery.

4.1 Landsat ETM+ imagery

A description of the Landsat 7ETM+ imagery can be found in table 1. In general the image is of very good quality, with no visible cloud, haze, distortions or noise. The image was referenced to the local Custom Transverse Mercator (Everest 1830) map projection system using quadratic polynomial rectification. High quality, scanned and mosaiced 1:25000 FinMap topographic maps were used for ground control points. The rectified image was checked against the base map. As the maximum error was 10 m the rectification was deemed to be acceptable. A sub-scene of the image to remove all but the study area was taken for ease of processing.

4.2 IKONOS imagery

IKONOS imagery has been acquired for 100 km² in the centre of the 340 km² study area. The imagery is formed from two north-south orientated, parallel strips (Table 2). Unfortunately, the two strips of data were noticeably difference in contrast and clarity, with strip 2 being considerably clearer than Strip 1. In addition, Strip 1 was affected by haze and had some thick cloud cover (7% of image). Overall however the terrain features were clearly visible, with individual houses, trees, terraces, water courses and roads being easy to identify. In many respects the image was similar to digital black and white aerial photography.

Date/Time of acquisition:	13th December 2000 c.09:30 local
Path/Row:	time
Sun azimuth:	142-41
Cloud cover (%):	SSE
	1

Bands		Resolution
B1	Visible blue	30 m
B2	Visible green	30 m
B3	Visible red	30 m
B4	Near infrared	30 m
B5	Mid Infrared	30 m
B6	Thermal Infrared	60 m
B62	Thermal Infrared	30 m (sub-sampled to 30m from B6)
B7	Mid Infrared	30 m
B8	Panchromatic	15 m

Table 1: Landsat ETM+ metadata

Both images were taken in the late afternoon so shadowing on northern and eastern slopes was a problem, but the shadow on northern, western, southern and south eastern slopes acted to highlight ground morphology. Both strips were georeferenced using quadratic polynomial rectification to the local coordinate system (as per the Landsat imagery) using scanned and mosaiced 1:25 000 topographic maps of the study area. The two images were then combined to form a single image and colour matched by contrast stretching.

Strip 1 (Western)		Strip 2 (Eastern)	
Date / Time:	24th January 2000, 17:12 (local)	Date / Time:	19th October 2000, 17:13 (Local time)
Sun Azimuth / Angle:	147°, 36°	Sun Azimuth / Angle:	152°, 48°
Cloud cover:	7%	Cloud cover:	0%
Bands	Resolution	Bands	
B1 (Panchromatic)	1m	B1 (Panchromatic)	1m

Table 2: IKONOS metadata

5. RESULTS

5.1 Landslide Mapping

5.1.1 Landsat 7 ETM+ Direct landslide mapping has been tested using both the Landsat and the IKONOS imagery. For the Landsat imagery this was undertaken using the false colour composite images. Comparison with the field landslide map suggested that the most effective technique utilises the RGB 457 FCC, pan sharpened using the panchromatic Band 8 and contrast stretched with a 99.9% transform in all bands. A 3x3-edge enhancement filter kernel was applied to increase the contrast. Bare soil in the resulting image varied from light to dark blue depending on light incidence and moisture content, meaning that landslides and areas of erosion were clearly highlighted. These were easy to differentiate from areas of forest (deep red) and cultivation (bright pink/orange). Little difference in colour was noted between landslides and other areas of bare soil. However, morphological evidence could be used to support the classification, including morphology (landslides typically have an arcuate back (upslope) scarp and a convex form) and slope (shadowing assisted in the elimination of areas of flat ground).

Some success was also achieved trough he use of the RGB 542 FCC, created using Pan sharpening from the panchromatic band, and enhanced with a 3x3 edge filter kernel and contrast stretching in each band. This composite highlighted wet, bare soil as blue tones, with increases in moisture content leading to a darkening of the blue colour. Vegetation appeared as a bright green and dry bare soil as brown tones. Thin vegetation representing areas of well-managed paddy cultivation (Khetland) were highlighted as purple colours. Other vegetation was represented by dark green colours and bare ground by deep brown colours. Areas of gravel alluvium were represented by a light pink colour. Water appeared dark blue. The ability to ascertain the soil moisture level of bare soil greatly assisted the interpretation. Best results were achieved where the RGB 542 and RGB 457 FCCs were examined together using a GIS.

The usefulness of a Principal Components Analysis (PCA) approach using an RGB 123 FCC was also tested. Again, this image was pan sharpened to increase clarity. The resulting image exhibited a very diverse range of colours (see fig 2). Areas of bare soils and landslides were particularly distinct and appeared almost white. In contrast to this all other colours were relatively dark. This was particularly useful for resolving relatively small finding small landslides.

Finally, testing was undertaken of the useful ness of the clay ratio, the iron oxide ratio and the Abrams ratio. In the Himalayan region the clay ratio was found to be of limited use as it did not distinguish adequately between vegetation and areas of clay rich soils. The iron oxide performed rather better, clearly differentiating between areas of vegetation and areas of bare soil. However, there was little advantage over the FCC approach. Finally, the Abrams Ratio, which projects the clay ratio, the iron oxide ratio and the NDVI (vegetation) ratio into the red green and blue colour guns respectively, was found to be rather more useful. The resulting image had an extremely diverse range of colours and was very good at distinguishing bare soil types from vegetation. Clay rich soils appear as red colours, whilst iron oxide-rich soils were seen as green colours and vegetation appears as blue. A mixture of iron soils and thin vegetation show as a cyan tone and granite soils with thin vegetation as magenta. Thus, this ratio appeared to give rather promising results and is worthy of further development.

After ground truthing, and through the use of the RGB 457 and RGB 457 FCCs, the RGB 123 PCA and the Abrams ratio a total of 67 landslides were identified from the imagery. The ground mapping detected a total of 388 landslides. Thus, although the imagery allowed the detection of a significant proportion of the total landslide population, more than 75% of the total were not detected. The reasons for this anomaly are:

- Landslides on the shadowed slopes in the imagery were consistently under represented. In areas affected by shadows the unvegetated slopes had a similar appearance to those that had vegetation due to their low reflectance in many of the bands.
- The spatial resolution of the Landsat 7 ETM+ instrument is still too low to allow the detection of many of the smaller landslides. Based upon the results from this study, 50 m remains the smallest landslide width and length that can be resolved confidently using this instrument. Unfortunately, although many landslides have a length in excess of 50 m, their width is very often less than this, such that the slide cannot be delineated.
- The spectral resolution is still not really good enough to be able to produce finely-tuned, high quality FCC images.

However, the results did show that for very large, relict landslides the use of Landsat 7 ETM+ produced better results than did ground mapping. Such very large slides are difficult to detect from the surface, but proved to be very obvious in FCC images.

Based upon the ground mapping and the satellite image interpretation, an analysis has been conducted of the typical spectral range of landslides in the Arghakanchi study area (Table 3). Using an algorithm based upon these parameters, and excluding areas with a slope angle of less 15°, it would be possible to delineate 21 of the 30 active landslides within the study area.

Band number	DN value
1	60-100
2	60-100
3	50-120
4	70-130
5	80-140
6	140-190
7	60-110

Table 3: Active landslide band ranges

The increase in accuracy of this classification was tremendous and 21 of the 30 active landslides were classified. 2 small debris flows were also identified. It also helped in the mapping of areas of erosion, discussed later.

In total 32 landslides were mapped by a combination of the techniques listed below before any ground truthing was completed. After some ground truthing this number was increased to 67 (details of the ground truthing exercise can be found in this section).

5.1.2 IKONOS Due to the high cost, for this study only the 1 m panchromatic imagery was acquired. Of course, this has restricted this part of the study to direct examination of the imagery (Figure 2). The black and white images were plotted onto high resolution paper at a scale of 1:5000 and 1:10 000 and interpreted much the same as regular aerial photography in conjunction with the digital imagery on screen.

Use of the IKONOS imagery proved to be very straightforward. Ridges, valleys and rivers were clearly evident, whilst land cover information such as vegetation type, soil type and rock outcrops were also visible. Areas of bare soil were bright and lighter in comparison with the surrounding darker vegetation, so recent and active landslides were visible. The smallest landslides that could be mapped were in the order of 10m in width and length. Relict (inactive) landslides were much more difficult to spot, and in particular the very large, relict features identified with Landsat 7 ETM+ and in the field were not visible.

Overall because of the crispness of the imagery medium sized recent landslides were mapped very easily. Improvements could be achieved with the availability of stereo images, which would have meant that the imagery is the equivalent of 1:5000 scale aerial photography, which is known to have great potential for landslide mapping.

In total 74 landslides were mapped using the IKONOS imagery, although the imagery covered only 50% of the study area. Thus, the effectiveness of the higher resolution of this imagery is clearly evident, demonstrating that the imagery offers great potential. Indeed, if stereo coverage were freely available the imagery would offer better potential than the standard 1:25 000 or 1:50 000 scale aerial photography.

For the Arghakanchi area multispectral IKONOS imagery were not available. For other study areas this imagery has been acquired. The construction of a FCC improved the visual appearance of the imagery but offered little in terms of improving the ability to resolve landslides, especially in view of the lower spatial resolution. The construction of other FCCs, using the VNIR band, proved to provide little advantage. Unfortunately, the limited spectral resolution remains a problem with the IKONOS instrument. The availability of mid IR and thermal IR bands would potentially improve the instrument very considerably.

5.2 Factor Mapping
Satellite imagery has the potential to allow the identification of factors that are important in the initiation of landslides, such as areas of increased soil moisture content and of disturbed ground. If this is possible,

then the imagery can potentially be used to delineate areas of high landslide susceptibility rather than just those that have already suffered slope failure.

5.2.1 Landsat 7 ETM+ A multispectral analysis of the Landsat imagery can allow landslide factor mapping to be completed. The presence of disturbed ground is frequently taken to be an indication of the presence of slow landslide processes such as creep (Dearman and Fookes 1974). In many cases this is an indication of incipient or ongoing failure. The use of the RGB 457 and RGB 542 FCC images allowed the identification of the morphological characteristics of creep, such as slopes with mottled texture and disrupted vegetation. In addition, colluvium was clearly identifiable on the RGB 457 image as it appeared as bright blue tones. In the PCA 123 image bare colluvium and alluvial fans appeared as green colours when in shadow, and as orange colours where there was bright sunlight, although some variation across the image was noted, presumably reflecting lithological differences.

Considerable success was also achieved in the identification of areas of high moisture content or water seepage. Based on a training area identified during a field visit, a wet are algorithm was constructed based upon the band parameters given in Table 4. This was completed by identifying potential areas with high moisture content. The spectral responses of these areas were then deduced to produce minimum and maximum ranges of DN values, from which classification algorithm was created using minimum and maximum values.

Band number	DN value
1	53-120
2	35-67
3	32-90
4	40-70
5	35-95
6	130-149
7	21-90

Table 4: Wet Area Secondary Classification Parameters

This classification highlighted irrigated paddy fields, shadowed hollows, areas of ponding, and river alluvium. Whilst in a number of cases this was successful in the identification of areas that are prone to landslides, this tended to be swamped by the occurrence of high moisture content for other (i.e. non landslide-related) reasons. For this reason, such an analysis has proven to be of limited use.

5.2.2 IKONOS For the Arghakanchi area multispectral imagery was not available, so similar factor analyses approaches were not possible. However, mapping of disturbed ground from the panchromatic imagery was possible based upon texture and ground cover type. This could have been enhanced through the analysis of .the multispectral imagery, but the improvement would have been limited given the low spectral resolution. The high spatial resolution of the IKONOS imagery could also be used to map elements that are vulnerable to the effects of landslides, which could greatly assist in the compilation of a landslide risk map.

6. CONCLUSIONS

LANDSAT 7 ETM+ offers many advantages in the mapping of landslides in high mountain chains, especially with respect to large features that are difficult to detect on the ground. The use of FCCs, and in particular the combination of the RGB 457 and the RGB 542 FCCs, PCA RGB 123 highlighted landslides well. However, the combination of the all of he techniques still allowed the delineation of only about 25% of the total number of landslides in the study area, the major limitation being the spatial resolution.

The results achieved using the IKONOS panchromatic imagery are very promising. The 1m spaltial resolution allows even small landslides to be mapped, with failures as small as 8 m length and width being identified. At present the multispectral capability of the instrument appears to offer relatively small advantage due to the limitations in spectral resolution. However, the greatest restriction in the use of this technique is the high acquisition cost of the imagery, which will prevent its widespread use in less developed countries.

REFERENCES

Dearman, W.R. and Fookes, P. 1974. Engineering geological mapping for civil engineering practice in the United Kingdom. *Quarterly Journal of Engineering Geology*, 5, 297-367.

Greenbaum, D., McDonald, A. J. W. and Marsh, S. H. 1996. Rapid methods of landslide hazard mapping. Proceedings of the Thematic Conference on Geologic Remote Sensing, 11, I.287-I.296.

Huang, S.L. and Chen, B.K. 1991 Integration of Landsat and terrain information for landslide study. Proceedings of the Thematic Conference on Geologic Remote Sensing, 8, 743-754

Kusaka, T., Ootsuka, M., Shikada, M. and Kawata, Y. 1996 Estimation of landslide areas using satellite imagery and spatial features of watersheds. Proceedings of the Thematic Conference on Geologic Remote Sensing, 11 II.415-II.420.

Nagarajan R., Mukherjee A., Roy A. and Khire, M.V. 1998. Temporal remote sensing data and GIS application in landslide hazard zonation of part of Western Ghat, India. International Journal of Remote Sensing 19 (4), 573-585.

Petley, D.N. and Reid, S. 1999. Landscape sensitivity and change at Taroko, eastern Taiwan. In Landscape Sensitivity and Change, edited by Smith, B. J., Whalley, W.B. and Warke, P.A. Special Publication of the Geological Society of London, 162, 179-195.

Rothery D.A. 1987. Decorrelation stretching and related techniques as an aid to image interpretation in geology. In: Proceedings of the Remote Sensing Society 13th annual conference, Nottingham, p. 194-203.

Trench, N. R. and Sauchyn, D. J. 1978. Application of Landsat data to the identification and delimitation of landslides in Colorado. Abstracts with Programs - Geological Society of America, 10 (7) 506.

The Role of Landsliding in Landscape Development in the Rio Aguas Catchment, South-east Spain

A. B. HART, J. S. GRIFFITHS Department of Geological Sciences, Plymouth and A. E. MATHER, Department of Geographical Sciences, University of Plymouth, Plymouth, UK

ABSTRACT

The Rio Aguas catchment covers an area of approximately 550km^2 and drains the majority of the Sorbas Basin and the southern part of the Vera Basin, in the Almeria Province of South-East Spain. These sedimentary basins formed during the mid-Miocene as a result of the interaction between the African and Iberian Plates. They have a complex sedimentary fill of mainly Neogene sediments bordered by Palaeozoic and Permo-Triassic basement rocks. Uplift since the Late Pliocene of approximately 160 m Ma^{-1} and associated deformation has caused a change from net deposition to net erosion in the basins, resulting in the formation of deeply incised canyons. The area has a semi-arid climate (less than 270mm per annum) and is also subject to regular seismic shocks (commonly around Richter magnitude 3, but historically up to 7). In this situation mass-movement processes would be expected to form a very significant component in the geomorphological development of the region and this has been confirmed by remote sensing and field studies. Based on these studies, the nature and extent of landsliding in the region are examined with an evaluation of their role in developing the contemporary landscape of the catchment.

INTRODUCTION

The drainage evolution of the river systems of South-east Spain are controlled by differential tectonic uplift, the underlying geology, base level changes (either related to changes in sea level and/or geomorphological controls such as river capture) and the climate (Harvey & Wells, 1987; Mather, 1991; Mather & Harvey, 1995; Stokes, 1997). These same factors have also influenced the formation and evolution of the present-day landscape. One facet of the development of the landforms within the region is the extent to which landsliding has contributed to the formation of the contemporary landscape. This is now the subject of a research programme at the University of Plymouth (Hart, 1999; Hart & Griffiths, 1999; Mather et al., in press).

A landslide investigation is being carried out in the catchment area of the Rio Aguas, in Almeria Province, Andalucia (Figure 1). The Rio Aguas Catchment covers an area of approximately 550km^2 and is centred on 37°08'N and 2°04'W (near to the village of Cariatiz, 6km Northeast of the town of Sorbas). The area has a semi-arid climate (receiving less than 270mm of rain per annum) and is also subject to regular seismic shocks (commonly around Richter magnitude 3, but historically up to 7). Previous work on the landslides in the region has looked at the effectiveness of using digital imagery (i.e. SPOT, Landsat Thematic Mapper and Airborne Thematic Mapper) in the mapping of landslides (Eyers et al., 1998). This work

particularly focused on the problems and limitations imposed by the spatial and spectral resolution of the images and how they can be overcome with the use of stretching, filtering and enhancement techniques.

The investigation currently being undertaken involves an assessment of the hazard and risk posed by landsliding in the area, as well as an assessment of the role played by landsliding in the development of the contemporary landscape and drainage network. The investigation has involved a detailed desk study which included an Aerial Photographic Interpretation (API) followed by field visits. The field visits enabled the collection of more detailed data and the "ground-truthing" of the API. The data are stored as a landslide inventory, compiled using the guidelines suggested by the *UNESCO Working Party on the World Landslide Inventory* which are summarised in the work of Turner & Schuster (1996, and references therein). The database includes information concerning the location of the landslides, their size, geometry, geology and geomorphology, the failure mechanisms involved, their state, style, distribution and rate of movement, and the elements at risk from the landsliding.

THE STUDY AREA

The Rio Aguas drains the majority of the Sorbas Basin and the southern part of the Vera Basin (Figure 1). These basins are part of the Internal Zone of the Betic Cordillera and were formed during the mid-Miocene Alpine Orogeny at the southern margin of the Iberian Craton (Weijermars, 1991). The basins are bounded to the north and south by mountain ranges composed of Palaeozoic and Permo-Triassic basement. The basin fills are a series of Neogene marls, limestones, sandstones and gypsum, which are capped by terrestrial conglomerates. The conglomerates represent the initiation of a fluvial drainage system across the basins during the Pliocene (Mather, 1991; Stokes, 1997).

Continued, differential, regional uplift during the Quaternary led to a switch from net deposition to net erosion within the sedimentary basins. In the Sorbas Basin, where uplift since the Late Pliocene has reached 160 m Ma^{-1}, this drainage was a weakly convergent network that drained the basin to the south through a low between the Sierra Alhamilla and Sierra Cabrera (i.e., the Rambla de Los Feos) (Mather, 1991, 1993a, 1993b). In the Vera Basin a drainage system was developed that drained the northern flanks of the Sierra Cabrera (the Lower Aguas). As the Sorbas Basin was uplifted in relation to the Vera Basin, the Lower Aguas continued an aggressive, westwards, headward retreat exploiting the regional strike of the basin fill and the similarly orientated basin margin fault systems (Harvey & Wells, 1987). The result was the capture of southwards flowing streams across the Sierra Alhamilla such as the Rambla de Los Feos approximately 100,000 years BP (Harvey *et al.*, 1995). The river capture caused rejuvenation through much of the drainage system and a rapid increase in the rate of incision (Harvey *et al.*, 1995) leading to the formation of relatively steep, if not over-steepened, valley sides and canyon walls.

The development of the contemporary drainage system in the Sorbas Basin has been through a combination of alternating periods of incision and aggradation, recorded as a series of river terraces levels (Harvey, 1984; Harvey *et al.*, 1995). The episodic nature of the incision and aggradation has been related to the variability of the Quaternary climate - incision during the Quaternary interglacials, and aggradation and major sediment production during the Quaternary glacials (Amor & Florschütz, 1964; Harvey, 1990).
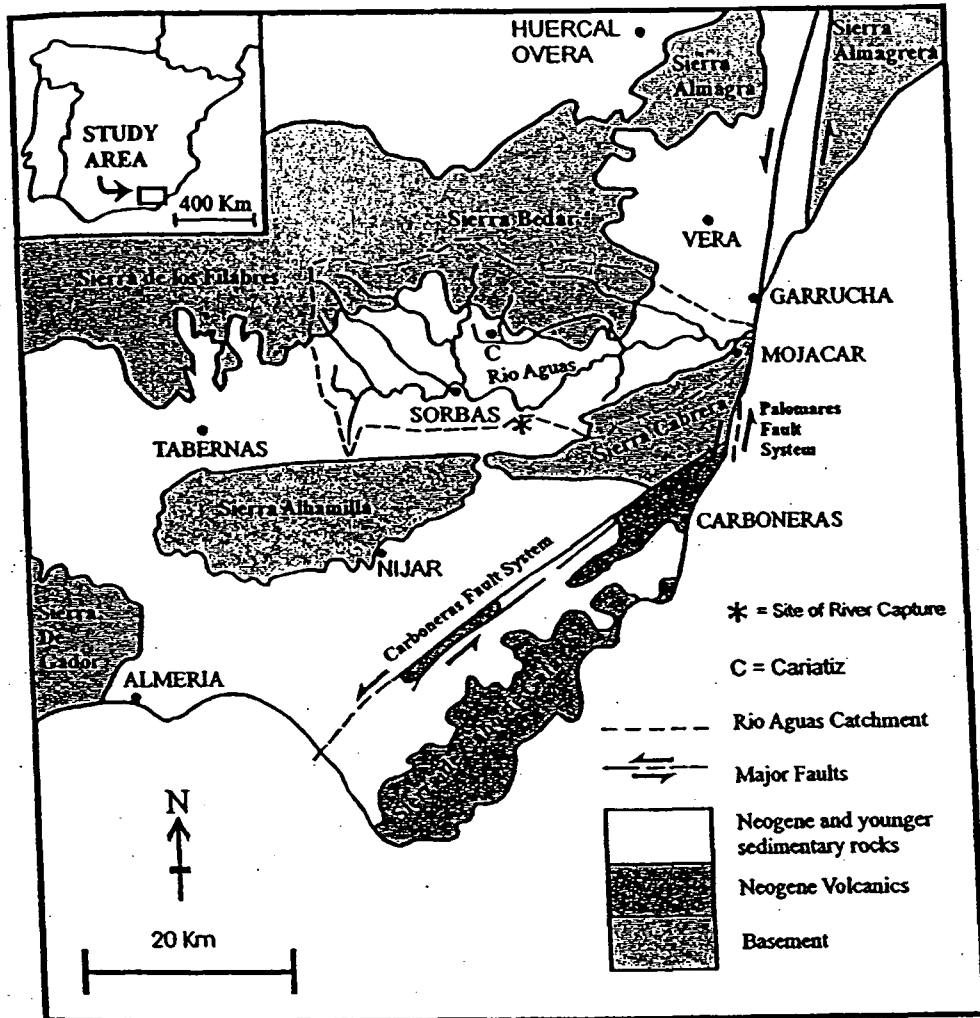
Figure 1. Simplified sketchmap of the Almeria region, showing major tectonic units, major fault systems and the Rio Aguas catchment area. Modified from Mather & Harvey (1995).

INITIAL RESULTS & DISCUSSION

To date, over 205 landslides have been mapped, giving the study area, a landslide density of approximately 0.37 landslides per km^2. The landslides vary considerably in their size from tens of m^3 to several million m^3. The majority of the landslides are rock falls. However, the larger landslides usually involve a combination of failure mechanisms, including rotational and non-rotational slides, debris flows and Sackung failures (Dikau *et al.*, 1996). An extract from the landslide database is given in Table 1.

The landslides observed within the study area appear to demonstrate at least three different stages of mass movement activity (Hart & Griffiths, 1999). There are the landslides that are presently active, those that occurred during the Quaternary development of the landscape and drainage network and those that appear to be pre-Quaternary in age. Some of these relict

features are now being reactivated by road construction (Landslide Numbers 1 and (
study of the landslides around the town of Sorbas (located approximately 7-8 km upst
from the river capture area) has shown that the majority of Quaternary landslides
Landslide Numbers 8 and 9) are related to the rejuvenation and incision of the drai
network (Hart & Griffiths, 1999, fig 1.). The canyon system around Sorbas reaches a dep
approximately 40-45 m and the canyon walls are generally near vertical. The sandston
which Sorbas is built is characterised by jointing and fractures related to the unloading o
canyon walls (Hart & Griffiths, 1999).

Table 1. Extract from the landslide database highlighting the different types of landsli
found in the study area, the size of the landslides and their relative ages.

No.	Location & Grid Ref.	Type of Failure	Geology	Volume (10^6 m^3
1	Marchalico Viñicas 0585341074	Relict (Quaternary) debris flow	Gypsum overlying marls	> 6.0
2	Marchalico Viñicas 0585141071	Non-rotational turned debris flow	Gypsum overlying marls	> 2.0
3	Los Perales 0584941052	Compound (listric) rock flow affecting at least 2 sides of a mountain ridge.	Steeply dipping limestone overlying marine marls	> 16.0
4	Gypsum Escarpment 0584741069	Non-Rotational slide on a single, non-circular, listric, failure surface	Gypsum overlying marls	> 10.0
5	El Tesoro 0583741063	Non-Rotational slide on a multistoried, non-circular, listric, failure surface with some rock falls & topples	Gypsum overlying marls	approx.
6	Sorbas road cutting 0577741061	Relict (Pre-Holocene / Post-Messinian) debris flow	Sandstone	**
7	Sorbas 0576941065	Rock fall	Sandstone	< 0.0003
8	NW of Sorbas (Los Beneficos) 0576941069	Non-Rotational compound slide on a single, non-circular, listric, failure surface.	Conglomerate, marls and sandstone.	approx.
9	SE of Sorbas (Maleguica) 0578041055	Non-Rotational compound slide on a multistoried, non-circular, listric, failure surface, with some rock falls	Gently dipping thickly bedded sandstone interbedded with thin beds of laminated marls	> 5.0
10	E of Sorbas (La Clauda) 0579641053	Translational movement sliding on planar failure surface (gently dipping lithological contact).	Thinly bedded, weak, sandstone overlying gypsum.	> 0.02

** It is not possible to calculate the volume of material involved as no backscar can be seen, ai
full extent of the displaced material cannot be measured.

One of the main contributions landsliding makes to the development of the landscape w
the study area is as a source of sediment for the drainage network. It is considered

landsliding accounts for a large (but not yet quantified) amount of the sediment that is transported into the fluvial system. It is also envisaged that this has been the case throughout the evolution of the drainage network, particularly during the periods of major sediment production during the Quaternary glacial intervals. A fluctuating Quaternary climate could have also influenced the type, state and style of landsliding within the area, which in turn would affect the amount of sediment being produced.

Quaternary glacial intervals in the western Mediterranean region were characterised by a pronounced seasonality, with extremely cold and wet winters, and summer drought (Macklin *et al.*, 1995). This may account for the greater runoff and relatively high lake levels seen at this time (Harrison & Digerfeldt, 1993), as well as the widespread occurrence of *Artemisia* steppe indicating increased aridity and a growing season soil moisture deficit (Huntley & Birks, 1993). The summer aridity would also account for the presence of well-developed calcrete profiles in the Vera and Sorbas Basins (Mather, 1991; Mather & Harvey, 1995; Stokes, 1997). This pronounced seasonality would increase the mechanical weathering experienced in the region, and hence explain the increased sediment production. The winter precipitation would also lead to higher pore water pressures, which would explain some of the landsliding that is seen within the study area (some of the extremely large rotational and non-rotational slides or debris flows).

CONCLUSIONS

Drainage evolution and the development of the contemporary landscape is controlled by the underlying geology, differential tectonic uplift, base level changes (caused by changes in sea level and/or geomorphological controls such as river capture), and the climate. As landsliding is also caused by these same factors it is apparent that landsliding plays as an important role in the development of the contemporary landscape. In the Rio Aguas catchment, the landslides contribute large amounts of sediment to the river system, and further research will enable these amounts to be quantified.

ACKNOWLEDGEMENTS

REFERENCES

Amor, J.M. & Florschutz, F. (1964) Results of the preliminary palynological investigation of samples from a 50 m boring in Southern Spain. *Bolétin de la Real Sociedad Español de Historia Natural (Geología)*, 62, 251-255.

Dikau, R., Brunsden, D., Schrott, L. & Ibsen, M-L. (eds) (1996) *Landslide Recognition: Identification, movement & causes*. Report No. 1 of the European Commission Environment Programme Contract No. EV5V-CT94-0454. John Wiley & Sons, Chichester.

Eyers, R., Moore, J.McM., Hervás, J. & Liu, J.G. (1998) Intergrated use of Landsat TM and SPOT panchromatic imagery for landslide mapping: case histories from Southeast Spain. In: Maund, J.G. & Eddleston, M. (eds) *Geohazards in Engineering Geology*, Engineering Geology Special Publication, Geological Society, London, 15, 133-140.

Harrison, S.P. & Digerfeldt, G. (1993) European lakes as palaeohydrological and palaeoclimatic indicators. *Quaternary Science Reviews*, 12, 233-248.

Hart, A.B. (1999) An introduction to the landslides of the Sorbas Basin. In: Mather, A.E. & Stokes, M. (eds) *BSRG/BGRG S.E. Spain Field Meeting Guide*, University of Plymouth, 124-133.

Hart, A.B.& Griffiths, J.S. (1999) Mass movement features in the vicinity of the town of Sorbas, South-east Spain. In: Griffiths, J.S., Stokes, M.R. & Thomas, R.G. (eds), *Landslides: Proceedings of the 9th International Conference and Field Trip on Landslides, Bristol, Uk, 5th-16th September 1999*, A. A. Balkema, Rotterdam, p57-63.

Harvey, A.M. (1984) Aggradational & dissection sequences on Spanish alluvial fans: influence on morphological development. *Catena*, 11, 289-304.

Harvey, A.M. (1990) Factors influencing Quaternary alluvial fan development in Southeast Spain. In: Rachocki, A.H. & Church, M. (eds) *Alluvial Fans: A Field Approach*. 247-269.

Harvey A.M. & Wells, S.G. (1987) Response of Quaternary fluvial systems to differential epeirogenic uplift : Aguas and Feos river systems, Southeast Spain, *Geology*, 15, 689-693.

Harvey, A.M., Miller, S.Y. & Wells, S.G. (1995) Quaternary soil and river terrace sequences in the Aguas/Feos river systems: Sorbas Basin, Southeast Spain. In: Lewin, J., Macklin, M.G. & Woodward, J.C. (eds) *Mediterranean Quaternary River Environments*, A.A. Balkema, Rotterdam, 263-281.

Huntley, B. & Birks, H.J.B. (1983) *An Atlas of Past and Present Pollen Maps for Europe 0-13,000 years ago*. Cambridge University Press, Cambridge.

Macklin, M.G., Lewin, J. & Woodward, J.C. (1995) Quaternary fluvial systems in the Mediterranean basin. In: Lewin, J., Macklin, M.G. & Woodward, J.C. (eds) *Mediterranean Quaternary River Environments*, A.A. Balkema, Rotterdam, 263-281.

Mather, A.E. (1991) *Late Caenozoic drainage evolution of the Sorbas Basin, Southeast Spain*, Unpublished Ph.D. Thesis, University of Liverpool.

Mather, A.E. (1993a) Basin inversion: some consequences for drainage evolution and alluvial architecture, *Sedimentology*, 40, 1069-1089.

Mather, A.E. (1993b) Evolution of a Pliocene fan delta: links between the Sorbas and Carboneras Basins, Southeast Spain. In: Frostick, L. & Steel, R. (eds) *Tectonic controls and signatures in sedimentary successions*. IAS Special Publication 20, 277-290.

Mather, A.E. & Harvey, A.M. (1995) Controls on drainage evolution in the Sorbas basin, Southeast Spain. In: Lewin, J., Macklin, M.G. & Woodward, J.C. (eds) *Mediterranean Quaternary River Environments*, A.A. Balkema, Rotterdam, 65-76.

Mather, A.E., Griffiths, J.S. & Stokes, M. (in press). Anatomy of a "fossil" landslide from the Pleistocene of Southeast Spain. *Geomorphology*.

Stokes, M. (1997) *Plio-Pleistocene drainage evolution of the Vera Basin, Southeast Spain*, Unpublished Ph.D. Thesis, University of Plymouth.

Turner, A.K. & Schuster, R.L. (eds) (1996) *Landslides: Investigation & Mitigation*. Transportation Research Board Special Report 276, National Academy of Sciences, Washington D.C.

Weijermars, R. (1991) Geology and tectonics of the Betic Zone, SE Spain. *Earth-Science Reviews*, 31, 153-236.

Mass movement features in the vicinity of the town of Sorbas, South-east Spain

A.B.Hart & J.S.Griffiths
Department of Geological Sciences, University of Plymouth, UK

ABSTRACT: A landslide investigation has been undertaken in the vicinity of Sorbas, Almeria Province, South-east Spain. Using the guidelines suggested by the UNESCO Working Party on the World Landslide Inventory, an inventory of the mass movements within the study area has been generated. The area has suffered a wide variety of mass movements, with a landslide density of approximately 4.6 landslides per Km^2. These mass movements range in size from a few tens of m^3 to a few million m^3. There is evidence that the major features may relate to Pleistocene climatic conditions very different to the semi-arid climate of the present day. Movements occurring at the present time appear to be on a smaller scale to those initiated earlier in the Pleistocene. The majority of the mass movements are rock falls, although there are also rock topples, rotational slides and lateral spreads.

1 INTRODUCTION

A landslide investigation has been carried out around the market town of Sorbas, in Almeria Province, Andalucia (Fig. 1). The study area is centred on latitude 37°06'N and longitude 2°07'W and covers approximately 5 km^2. The investigation has involved the interpretation of aerial photographs followed by a field visit to the study area to ground truth the data. The information collected has been compiled into an inventory following the guidelines suggested by the UNESCO Working Party on the World Landslide Inventory (IAEG 1990, UNESCO WP/WLI 1990, 1993, 1994, 1995).

Sorbas, with a population of under 3,000, is the main town in a rural area. The local economy is heavily dependant on agriculture (predominantly olives, almonds and citrus fruit), quarrying and, increasingly, rural tourism. The town is split into two parts, with the old town being built on an island within an incised drainage system (Fig. 1). The newer part of Sorbas is built on a level area to the west of the old town, on either side of the main Almeria to Murcia road (the N-340).

2 GEOLOGY AND GEOMORPHOLOGY

Sorbas is situated towards the centre of the Sorbas Basin, which is located within the Internal Zone of the Betic Cordillera (Weijermars 1991). The basin is bounded to the north and south by mountain ranges composed of Palaeozoic and Permo-Triassic basement material. This includes mica schists, phyllites, quartzites and low-grade metamorphic carbonate rocks. The basin fill consists of a series of Neogene marls, limestones and sandstones, as well as a large thickness of Messinian gypsum. This is capped by a conglomerate formed under terrestrial conditions at the end of the late Pliocene. The conglomerate represents the initiation of the fluvial drainage system across the basin.
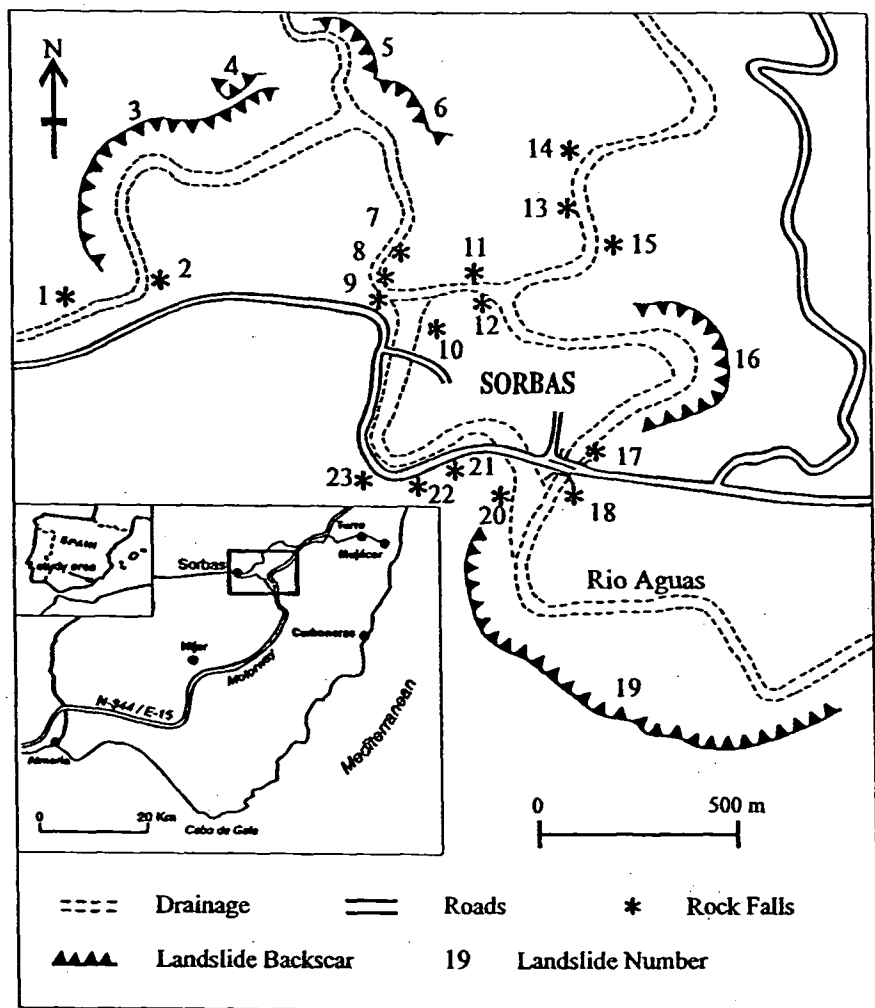
Figure 1. Map showing the location and distribution of the mass movement features around the town of Sorbas.

During the Quaternary, continued differential epeirogenic uplift of the region, led to a switch from net deposition to net erosion within the sedimentary basin. The result was the episodic incision of the drainage system, with the downcutting being punctuated by periodic aggradation, resulting in a fluvial landscape dominated by a sequence of river terraces, reflecting both climatic and tectonic controls (Harvey 1987, Mather & Harvey 1995). In the area around the town of Sorbas, the incision has reached a depth of about 90 m. This is within the canyon that contains the active drainage system (the Rio Aguas), that passes around the northern and eastern sides of the old town. The canyon that passes around the western and southern sides of the old town has been abandoned since the formation of the D3 terrace between 20,00 and 10,000 years BP (Harvey & Wells, 1987, Harvey et al. 1995). The river terrace sequence preserved around Sorbas nearly represents a complete incision history for the area. A detailed description of each of these levels is found in Harvey et al. (1995).

The geology of the study area comprises three Messinian units, with the regional dip of the bedding being to the north-north-west. These are :

58

- the Zorreras Member [youngest unit] - a rusty orange red, fine to medium grained sandstone capped by a conglomerate. Between the sandstone and conglomerate is a thin band of white sandstone. The sandstone is moderately weak, while the conglomerate is moderately strong. The conglomerate consists of polymict gravels with some pebbles, which are predominantly sub-rounded and clast supported.

- the Sorbas Member - a white medium grained sandstone that is interbedded with a thinly laminated marl. The sandstone is thickly bedded and moderately strong. The marl is moderately weak. The rock contains two joint sets that are oblique to each other and perpendicular to the bedding plane.

- the Yesares Member [oldest unit]- thickly bedded gypsum interbedded with thin laminations of marls. The size of the individual crystals can vary from approximately 1 to 12 cm. The strength of the rock is dependant on the size of the crystals as well as their state of weathering, which can also vary considerably.

3 RESULTS

Figure 1 shows the location and distribution of the landslides around Sorbas and Table 1. provides a summary of the information contained within the landslide inventory for the study area. This information shows that the area has a high landslide density of 4.6 landslides per Km^2 (roughly equal to the landslide density for the San Francisco Bay area and the average figure for the whole of the USA (Brabb 1989)). Rock fall is the most common failure mechanism being encountered. However, the largest mass movement features seen in the area exhibit a combination of failure mechanisms, usually rotational sliding, non-rotational sliding, rock fall and rock topple. The size of the landslides varies greatly from a few tens of cubic metres to a few million cubic metres.

The largest mass movement in the study area is found in the outside of the Rio Aguas meander, to the south-east of Sorbas (Mass Movement Number 19). This extensive mass movement can be clearly seen on aerial photographs and with ATM data (Eyers et al. 1998). The landslide is predominantly affected by rotational sliding giving rise to a series of back tilted blocks (Hart, in press). Most of these blocks are only a few tens of metres across. However, in the western section of the landslide, the rotating blocks have collapsed giving rise to a number of major rock falls and topples. The shape and size of the displaced blocks are controlled by the discontinuity pattern of the rock mass. The sandstone contains two joint sets that are both perpendicular to the bedding planes and almost at 90° to each other. There is also evidence to suggest that some parts of the mass movement are affected by faulting.

The construction of the main road along the southern edge of the canyon has possibly reactivated two relict features (Mass Movement Numbers 21 and 22). As a result, the road cuttings in these areas have been cut back and large ditches put in along the edge of the road to trap debris. These two mass movements (and also Mass Movement Number 20) are thought to represent fossil debris flows. They consist of randomly orientated blocks of the white Sorbas Member sandstone, contained within a sandy gravel of the same material. The debris flow is found within relict channels cut down into the Sorbas Member.

Another factor that seems to influence the stability of the canyon walls around parts of Sorbas is unloading as a result of the incision of the canyons. The instability seen at Mass Movement Numbers 7, 8, 9, 11, 12 and 23 are all characterised by large vertical fractures that run parallel to certain parts of the cliff face. All of these rock falls are within the white sandstone of the Sorbas Member and are therefore also affected by the jointing and dip direction of the bedding. In the case of Mass Movement Number 23, the unloading has also been influenced by the construction of the main road. The result is that part of the cliff face may be toppling out over the road.

Table 1. Part of the landslide inventory for the area around Sorbas.

Mass Movement Number	Grid Ref.	Mechanism	Approximate Volume (m³)	Angle of Reach	Lithological unit involved in landslide
1	0576941065	Rock fall	< 500	24	Sorbas Member
2	0577041065	Rock fall	< 500	30	Sorbas Member
3	0576941065	Rotational slide & rock fall	< 500,000	18	Zorreras Member
4	0577341071	Lateral Spread	> 10,000	22	Zorreras Member
5	0577641072	Rotational slide & rock fall	< 500,000	27	Zorreras Member
6	0577741071	Rotational slide & rock fall	< 500,000	39	Zorreras Member
7	0577841067	Rock fall	< 100	40	Sorbas Member
8	0577641066	Rock fall	< 5,000	30	Sorbas Member
9	0577741065	Rock fall	< 5,000	39	Sorbas Member
10	0577741064	Rock fall	< 5,000	22	Sorbas Member
11	0577941067	Rock fall	< 5,000	30	Sorbas Member
12	0577941065	Rock fall	< 5,000	32	Sorbas Member
13	0578341067	Rock fall	< 1,000	59	Zorreras Member
14	0578241068	Rock fall	< 100	59	Zorreras Member
15	0578241069	Rock fall	< 500	56	Zorreras Member
16	0578541063	Rock fall	< 1,000,000	68	Zorreras Member
17	0578241061	Rock fall	< 100	45	Sorbas Member
18	0578241060	Rock fall	< 10,000	34	Sorbas Member
19	0578041055	Rotational Slide & rock fall	> 1,000,000	18	Sorbas Member
20	0577941060	Relict feature	**	**	Sorbas Member
21	0577741061	Reactivation of relict feature	**	**	Sorbas Member
22	0577741061	Reactivation of relict feature	**	**	Sorbas Member
23	0577641062	Rock Topple	**	**	Sorbas Member

** It is not possible to work out the volume of material involved as no backscar can be seen, and the full extent of the displaced material cannot be calculated.

4 DISCUSSION

There are two different aspects to this study. First, there is the question of how the observed mass movements fit into the history of the landscape and drainage evolution of the area, and secondly, what sort of risk are these mass movements posing to the local population.

The mass movement features observed in the study area can be seen to represent (in a very broad sense) at least three different stages of mass movement activity. These are the mass movements that occurred at some point in the geological past, the mass movements that have occurred during the Quaternary as the river canyons were being formed, and the present day mass movement activity. The present day mass movements are probably the result of a combination of factors including the climate, seismic activity, unloading of the canyon walls due to the incision and construction activity. Examples of these mass movements have already been given.

The larger, and more complex mass movements, although still active today, are thought to have initiated under different climatic conditions. Due to their location on the outside of the meanders in the incised drainage system, it is possible to link their formation to the incision of the drainage and therefore, possibly, to the formation of the river terraces. Analysis of the river terrace deposits in the area have suggested that the climate during the Pleistocene, in this part of Spain, was drier and colder (Amor & Florschutz 1964, Harvey et al. 1995) especially in the glacial phases (Rohdenburg & Sabelberg 1973, Sabelberg 1977, Harvey & Wells 1987). During the Pleistocene the climatic and associated glacio-eustatic fluctuations (Sierro et al. 1999) have controlled the hydrography of the Sorbas Basin and other areas of South-east Spain. During the last glacial maximum (18,000 years BP) South-east Spain possibly had a near-tundra environment (McIntyre et al. 1976, fig.18) and may well have been arid (Brigg 1995). However, during the major Pleistocene inter-glacial intervals the climate may have been more temperate and, possibly, wetter. The major rotational landslides may well have initiated during these climatic fluctuations (Harvey & Wells 1987) when groundwater levels were higher. More recent modifications of these landslides are on a smaller scale (rock falls and topples) and more appropriate to an area with a semi-arid climate that receives only 260 mm of rain a year.

The risk posed by these landslides to those who live and/or work within the area varies considerably. All of the larger features occur in areas where, at present, they will have minimum effect on the population, whereas the smaller features are often in the populated parts of the study area. For example, there are the relict features above the main road (Mass Movement Numbers 21 and 22) or the rock falls below residential and business areas (Mass Movement Numbers 9, 10, and 12). There are also features like Mass Movement Number 17 which is located immediately above and adjacent to a private property, but also underneath part of the foundation of the old road bridge into Sorbas. Therefore, although one of the smallest mass movement features in the area, its very location makes the feature one of the most dangerous.

This risk is likely to increase. In the last ten years, the area has been opened up considerably. This has been the result of the upgrading of the road network and the construction of new roads such as the E-15 motorway. At the same time, the population of the area (and particularly around Sorbas) has been expanding. As development of the area proceeds, and new roads and buildings are constructed, it is probable that the current mass movements will start to have a greater affect on the local community, as well as the possible initiation of further mass movements.

5 SUMMARY

The area in the vicinity of Sorbas, South-east Spain, has been shown to have a landslide density of approximately 4.6 landslides per km². This figure is high and cannot be ignored, particularly as Sorbas, a strategic location within the region, is undergoing development and expansion. The landslide inventory will therefore prove to be a necessary reference for those involved in such developments.

This study is part of a wider project investigating the mass movement activity throughout the Rio Aguas catchment area. The data contained within the landslide inventory will be used to carry out a risk assessment of the landslide hazard affecting the area. The investigation will also involve an assessment of the role played by mass movement activity in the development of the present day drainage system and landscape (Hart et al, in prep.).

ACKNOWLEDGEMENTS

REFERENCES

Amor, J.M. & Florschutz, F. 1964. Results of the preliminary palynological investigation of samples from a 50 m boring in southern Spain. Boletin Real Sociedad Espanola de Historia Natural (Geologica). 62:251-255.

Bigg, G.R. 1995. Aridity of the Mediterranean Sea at the last glacial maximum : a reinterpretation of the $\delta^{18}O$ record. *Paleoceanography*, 10: 283-290.

Brabb, 1989. Landslides : extent and economic significance in the United States. In B.E. Brabb & B.L. Harrod (eds) Landslides : Extent and economic significance, A.A. Balkema, Rotterdam.

Eyers, R., Moore, J.McM., Hervás, J. & Liu, J.G. 1998. Integrated use of Landsat TM and SPOT panchromatic imagery for landslide mapping : case histories from Southeast Spain. In J.G. Maund & M. Eddleston (eds), Geohazards in Engineering Geology, Engineering Geology Special Publication, 15: 133-140. Geological Society, London.

Hart, A.B. In Press. An introduction to the landslides of the Sorbas Basin. In A.E. Mather & M. Stokes (eds) *Field guide for the BSRG/BGRG Joint Field Meeting, Almeria Province, S.E. Spain, September 1999*.

Hart, A.B., Griffiths, J.S. & Mather, A.E. In preparation. The role of landsliding in landscape developement in the Rio Aguas catchment, South-east Spain. *Proceedings of the 8th International Symposium on Landslides, Cardiff, 2000*.

Harvey, A.M. 1987. Patterns of Quaternary aggradtional and dissectional landform development in the Almeria region Southeast Spain : a dry region, tectonically active landscape. Die Erde. 118:193-215

Harvey, A.M. & Wells, S.G. 1987. Response of Quaternary fluvial systems to differential epeirogenic uplift : Aguas and Feos river systems, Southeast Spain. Geology 15: 689-693.

Harvey, A.M., Miller, S.Y. & Wells, S.G. 1995. Quaternary soil and river terrace sequences in the Aguas/Feos river systems : Sorbas Basin, Southeast Spain. In J. Lewin, M.G. Macklin & J.C. Woodward (eds), Mediterranean Quaternary River Environments: 263-281. A.A.Balkema, Rotterdam.

IAEG Commission on Landslides. 1990. Suggested nomenclature for landslides. Bulletin of the International Association of Engineering Geology, 41: 13-16.

Mather, A.E. & Harvey, A.M. 1995. Controls on drainage evolution in the Sorbas Basin, Southeast Spain. In J. Lewin, M.G. Macklin & J.C. Woodward (eds), Mediterranean Quaternary River Environments : 65-76. A.A. Balkema, Rotterdam.

McIntrye, A., Kipp, N.G., Be, A.W.H., Crowley, T., Kellogg, T., Gardner, J.V., Prell, W. & Ruddiman, W.F. 1976. Glacial North Atlantic 18,000 years ago : a CLIMAP Reconstruction. Geological Society of America Memior, 145: 43-76.

Rohdenburg, H. & Sabelberg, U. 1973. Northwestern Sahara margins : terrestrial stratigraphy of the Upper Quaternary and some palaeoclimatic implications. In E.M. Van Zinderen Bakker Sr. & J.A. Coetzee (eds), Palaeoecology of Africa and the Surrounding Islands 12: 267-276.

Sabelberg, U. 1977. The stratigraphic record of late accumulation series in southwest Morroco and its consequences concerning the pluvial hypothesis. Catena 4: 209-214.

Sierro, F.J., Flores, J.A., Zamarreño, I., Vázquez, A., Utrilla, R., Francés, G., Hilgen, F.J. & Krijgsman, W. 1999. Messinian pre-evaporite sapropels and precession induced oscillations in western Mediterranean climate. *Marine Geology*, 153: 137-146.

Weijermars, R. 1991. Geology and tectonics of the Betic Zone, SE Spain. Earth-Science Reviews, 31: 153-236.

UNESCO WP/WLI (Working Party on the World Landslide Inventory). 1990. A suggested method for reporting a landslide. Bulletin of the International Association of Engineering Geology, 41: 5-12.

UNESCO WP/WLI (Working Party on the World Landslide Inventory). 1991. A suggested method for a landslide summary. Bulletin of the International Association of Engineering Geology, 43: 101-110.

UNESCO WP/WLI (Working Party on the World Landslide Inventory). 1993. A suggested method for describing the activity of a landslide reporting a landslide. Bulletin of the International Association of Engineering Geology, 47: 53-57.

UNESCO WP/WLI (Working Party on the World Landslide Inventory). 1994. A suggested method for reporting landslide causes. Bulletin of the International Association of Engineering Geology, 50: 71-74.

UNESCO WP/WLI (Working Party on the World Landslide Inventory). 1995. A suggested method for describing the rate of movement of a landslide. Bulletin of the International Association of Engineering Geology, 52: 75-78.

(9) An Introduction to the Landslides of the Sorbas Basin.

ANDREW HART

Department of Geological Sciences & Plymouth Environmental Research Centre, University of Plymouth, Drake Circus, Plymouth, Devon, PL4 8AA, UK.

INTRODUCTION

The landscape and drainage pattern of the present day Sorbas Basin is the result of its tectonic history, the continued differential tectonic uplift, the underlying geology and the climate (Harvey & Wells, 1987; Mather, 1991; Mather & Harvey, 1995). These same factors have also influenced the formation and development of the numerous landslides that are seen within the region. One facet of the development of the landforms within the Sorbas Basin is the extent to which landsliding has contributed to the formation of the contemporary landscape.

This issue is being considered as part of a research project that has involved the compilation of a landslide inventory of all of the landslides affecting the Sorbas Basin. These data are being used to investigate the extent of landsliding, the causes and mechanisms involved, and the risk posed by landsliding to those who live and/or work within the area. The investigation has combined an aerial photographic interpretation and extensive desk study with data collected from the field (i.e. geomorphological mapping and discontinuity surveys). Some of the landslides visited on this field trip have also been studied by Eyers *et al.* (1998) using ATM data. Their work focused on how the spectral differences within ATM data can be used to identify areas affected by landslide activity.

The aim of this half day field trip is to study some of these landslides and the factors that led to their formation and development, the mechanisms involved, the risk that these features pose, as well as their role in the development of the present day landscape. The locations for this trip, as well as some of the landslide features that will be seen, are shown in Figure 1. All of these locations can be reached by car or minibus, and some of them can be reached on foot. A number of the sites are in environmentally sensitive areas that form part of the Sorbas Gypsum Karst Natural Park, therefore care must be taken when visiting these sites.

Directions to Stop 1.
From the top of the driveway to Urra head towards Sorbas along the AL-104 and then the N-340. The first stop is a pull-in just past the cemetery and shop (Venta La Viuda), opposite the road junction with the Lubrín road. From here it is a short walk to the top of the hill. The landslide at Maleguica is situated on the opposite side of the Rio Aguas.

Stop 1: Maleguica Landslide (GR 05784 41055)
[view point from hilltop opposite landslide = GR 05785 41058]
From the top of this hill, the Rio Aguas valley can be seen in the east and the town of Sorbas in the west (Figure 2). To the south the Rio Aguas has cut a wide canyon that reaches a depth of about 50-60 m below the main plateau surface. The landslide is located along the southern wall of the river canyon. Part of the canyon floor immediately below the hill, is being used to grow citrus fruit.

This fairly extensive landslide can be clearly seen on aerial photographs and with ATM data (Eyers *et al.*, 1998). The landslide can be divided into three parts (Figure 2.). There is an area of disturbed but vegetated ground to the left, a fairly rocky (and probably more active) section to the right, and a central section which forms a slightly disturbed, vegetated slope down into the canyon. The more active section is picked out by the presence of two cliff faces, which are almost perpendicular to each other (i.e. trending NW-SE and NE-SW) and the substantial accumulation of debris at the foot of these cliffs.

All three of these areas can be distinguished on the aerial photographs.
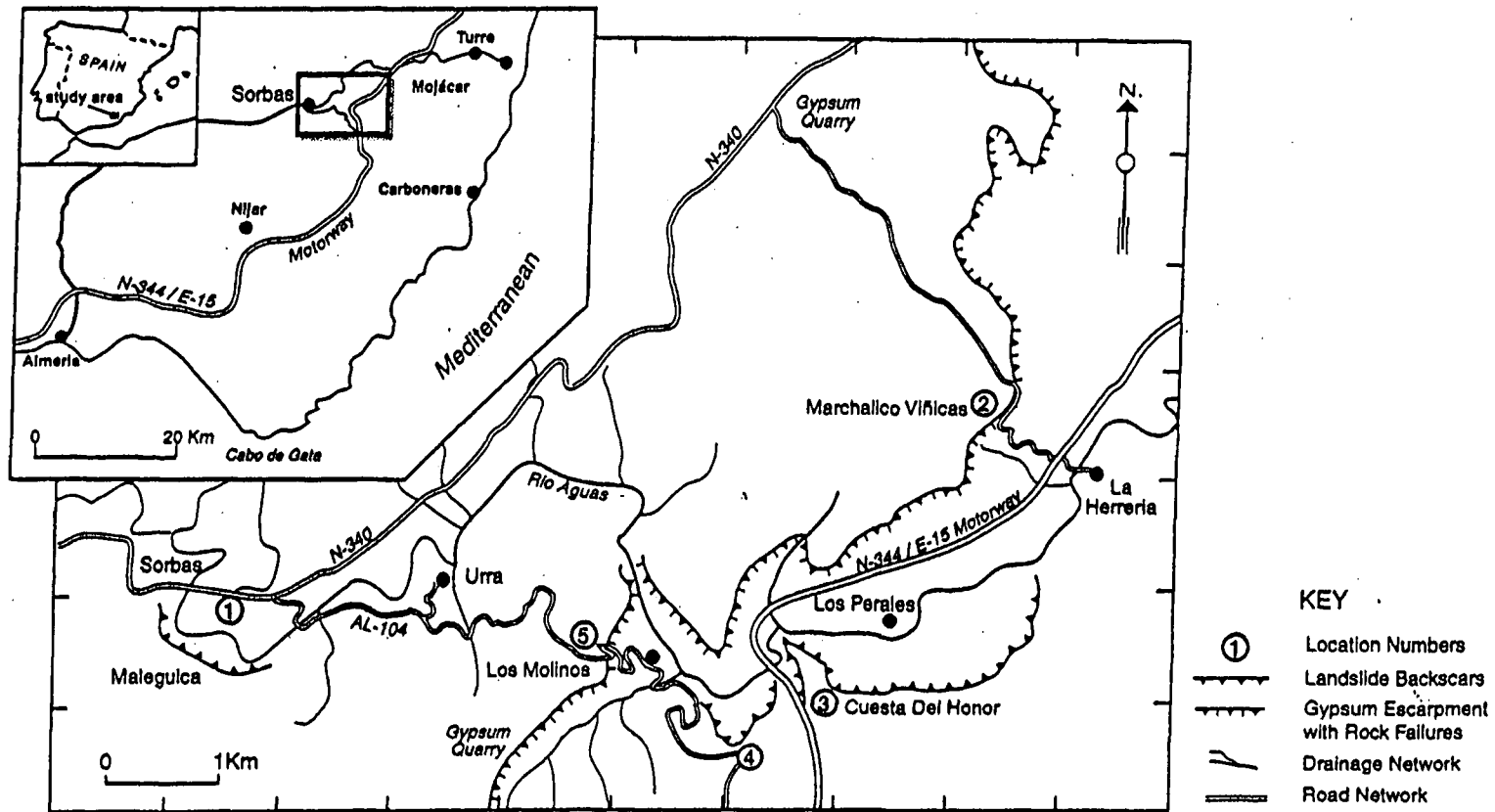
Figure 1. Simplified map showing the area around the town of Sorbas, some of the landslide features of the area and the field trip locations.

At the eastern end of the canyon there is a cliff face of laminated and massively bedded Messinian gypsum, which is interbedded with finely laminated marls (the Yesares Member). This is overlain by a light coloured limestone and sandstone, both from the Sorbas Member. The rock is well jointed in two directions, which are roughly at 60° to each other. This is clearly seen in the rock face. The jointing is almost perpendicular to the bedding surface, which in this area dips to the north and therefore out of the cliff face into the canyon. It is this combination of the discontinuity pattern and the bedding surface daylighting in the cliff face, that has given rise to the landsliding in this area.

The landslide is affected by a number of different failure mechanisms, with the predominant failure mechanism changing as the landslide has evolved. Geomorphological mapping has indicated that the eastern section of the landslide is predominantly affected by rotational sliding, shown up by the presence of 3 to 4 benches of back tilted blocks, which are progressively more degraded further down slope. Some of these benches are now being utilised for agriculture.

The central section of the landslide complex has also been affected by rotational sliding. However, this has then been complicated by a component of overriding by the "younger" blocks (i.e. those immediately below the backscar) over the blocks that make up the middle part of this section of the landslide complex. The result is that the top surfaces of the blocks in the area immediately beneath the backscar are either back-tilted, forward tilted or near horizontal. This can be picked out by the orientation of the joints in the heavily jointed, NE-SW trending cliff face.

Back tilted blocks can also be found in the apparently more active, western section of the landslide. This would indicate that this section of the landslide has also been affected by rotational sliding. However, since the formation of these back tilted blocks there has been a change in the failure mechanism to rock fall and topple. This is controlled by the discontinuity pattern within the rock mass, with the bedding plane dipping northwards out of the hillside in conjunction with two joint sets oblique to each other and perpendicular to the bedding. This discontinuity pattern is also responsible for the shapes of the slipped blocks in the other two sections of the landslide. Despite the switch in failure mechanism, large blocks are still being formed behind the present backscar of this section of the landslide, the backscars of which are parallel to the main backscar. The largest of these blocks is approximately 200 m long, reaches a maximum width of about 40-50 m and has possibly moved up to about 2 m both vertically and horizontally. This block is also broken up into several smaller blocks by a network of much smaller fractures, again all of which follow the discontinuity pattern of the rock mass. It is the break up of the larger blocks into these smaller units, that is giving rise to the rock falls and topples.

Transfer to Stop 2.
This locality is reached by driving along the N-340 towards Murcia, and then turning right into the gypsum quarry entrance at the cross-roads with the road to Cariatiz and the road to the gypsum quarry, the Gypsum Karst Natural Park and La Herreria (Kilometre Post 505). The road into the quarry bears off to the left, while the track to La Herreria is on the right, just before the quarry entrance. This is an unmetalled, gypsum topped track that follows the southern edge of the gypsum quarry. Once past the quarry, the track bears off to the right and goes across the gypsum plateau to the edge of the gypsum escarpment and the abandoned village of Marchalico Viñicas.

Stop 2: Marchalico Viñicas (GR 05854 41074)
From the top of the gypsum escarpment there is a clear view of the Rio Aguas valley which opens out into the southern part of the Vera Basin. The Mediterranean coast at Mojácar and the badland type topography that make up this area are usually visible on a clear day. The skyline is dominated by the Sierra Cabrera which runs from the coast inland and acts as the southern border to the Vera Basin. A number of landslides affect some of these slopes, particularly in the area near to the villages of La Huelga and La Herreria. Immediately below the gypsum escarpment is the abandoned village of Marchalico Viñicas (Figure 3). This village was probably abandoned during the 1950's and 1960's, when there was a migration from the rural parts of Spain to the larger towns and cities.

126

KEY

⊤⊤⊤⊤	Cliffs / Escarpments
▼▼▼	Convex Break of Slope
⋎ ⋎ ⋎	Concave Break of Slope
⋏A⋏	Rounded Ridge Crest
┴┴┴┴	Trough
↗	Slope Direction
⚏⚏⚏	Tension Cracks
◌◌	Debris Accumulation
⟍	Drainage Network
▭▭	Roads
▦	Neogene sandstone hills & valley side slopes
▤	Neogene gypsum valley side slope
▦	River valley floor
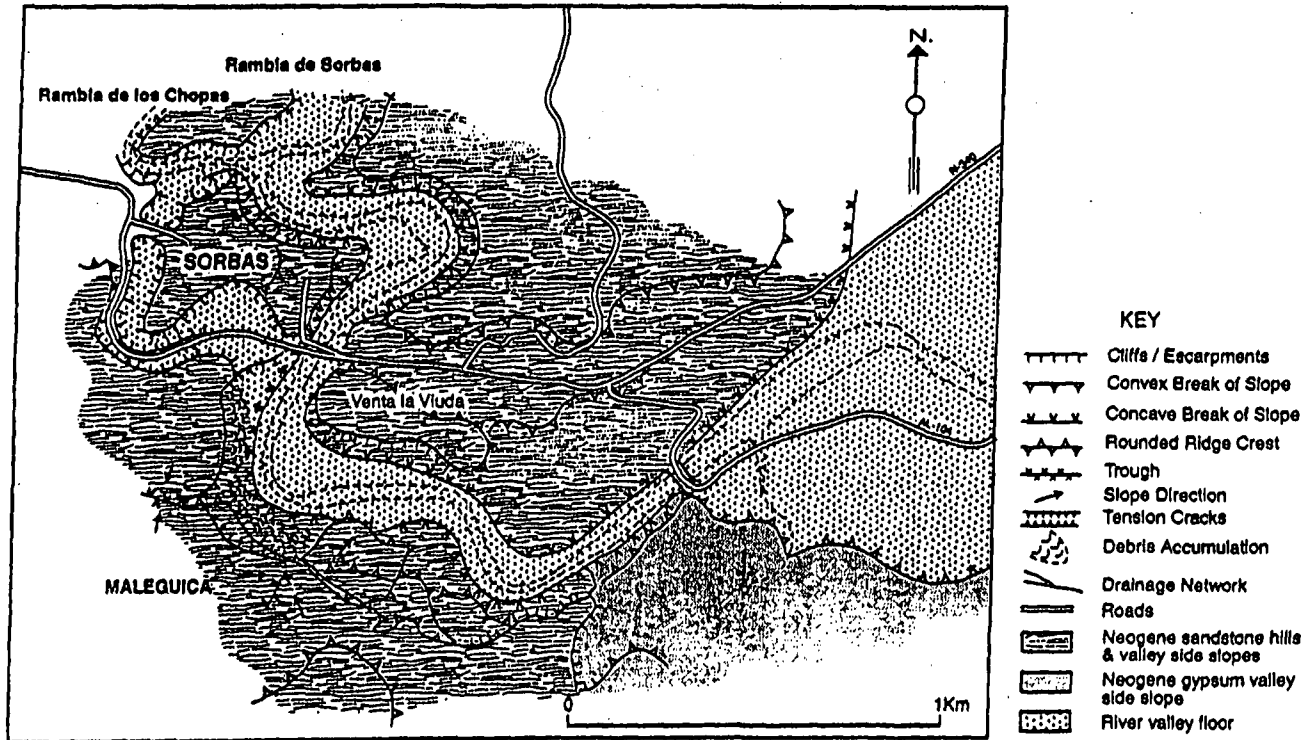
Figure 2. Simplified geomorphological map of the area around the Landslide at Maleguica, 1 Km south of the town of Sorbas. (Location 1)

The geology of the landslide area comprises laminated and massively bedded Messinian gypsum interbedded with finely laminated marls (the Yesares Member) underlain by the marls of the Abad Member.

The most recent landslide forms a fairly prominent feature on the landscape that can easily be identified in aerial photographs and ATM images (Eyers et al., 1998), as well as on the ground. The volume of debris and the size of some of the boulders that are involved is substantial. The failure seems to have initiated in the area around the village, possibly due to the presence of a spring located within the village at the base of the gypsum. In the head area the landslide is confined by the pre-existing topography, but further down slope it becomes confined to topographic lows. The lower part of the landslide forms a debris flow that extends almost down to the motorway (a distance of about 2-2.5 km.). However, the analysis of ATM data and geomorphological mapping has revealed the presence of a relict debris flow, consisting mainly of marls with very large gypsum boulders incorporated within it. This debris flow is parallel to the more recent debris flow and extends almost down to the Rio Aguas (a distance of approximately three kilometres). The runout for this relict flow has been modified by erosion and agricultural terracing, and has recently been cut by the construction of the motorway and the road down to La Herreria. The road cut on the La Herreria road allows a good opportunity to study the internal structure of the debris flow.

There appears to be a combination of failure mechanisms at work within this area. The gypsum contains numerous dissolution features which has created blocks within the gypsum near to the edge of the escarpment. These fail by either toppling or falling. There is also evidence for some degree of rotational sliding within the top part of the marls, with parts of the gypsum escarpment forming slightly back tilted blocks, but at a lower level to the rest of the gypsum plateau (Figure 3). This is possibly an "in-between phase" before complete failure within the marls leading to the formation of a sliding and then flowing debris mass.

Transfer to Stop 3.
From the abandoned village drive down the unmetalled, gypsum topped track and join the motorway, heading towards Almeria*. As you travel along the motorway there is the gypsum escarpment on the right, the edge of the Sierra Cabrera (consisting of the Azagador Member in this area) to the left and numerous landslide features on both sides of the road. At the point where the road takes a fairly sharp turn to the left the road crosses the Rio Aguas on an elevated section and then climbs up out of the canyon through the Aguas/Feos wind gap. This was formed during the late Pleistocene when the Rio Aguas/Feos drainage system was captured by the headward retreat of the lower Aguas (Harvey and Wells, 1987).

Turn off the motorway at the next junction (sign-posted Sorbas & Peñas Negras), turn right and go underneath the motorway. Just after the motorway junction on the other side of the bridge, there is a junction on the left with a metalled track sign-posted as going to Los Perales. This track runs alongside the motorway back towards the wind gap. At the point where the track starts to drop down into the Los Perales valley, there is a level area on the right which can be used as a pull-in.

* After heavy rains this track may become gullyed. If this is the case retrace the main road toward Sorbas, and take the turn off for Los Molinos, on the left before Sorbas town. Follow this road to the motorway intersection, pass under the motorway and take the tarmac minor road to Los Perales on the left. Follow this to stop 3 (see Figure 4), pull in on the left just before the road begins to drop significantly into the Aguas valley*

KEY

⊤⊤⊤⊤	Cliffs / Escarpments
▼▼▼	Convex Break of Slope
⊻ ⊻ ⊻	Concave Break of Slope
⋏⋏⋏	Rounded Ridge Crest
⋆⋆⋆	Trough
↗	Slope Direction
⊞⊞⊞	Tension Cracks
🝝	Debris Accumulation
⤳	Drainage Network
═══	Roads
▦	Neogene gypsum plateau
▨	Disected Neogene Marl plateau (badlands)
▦	River valley floor
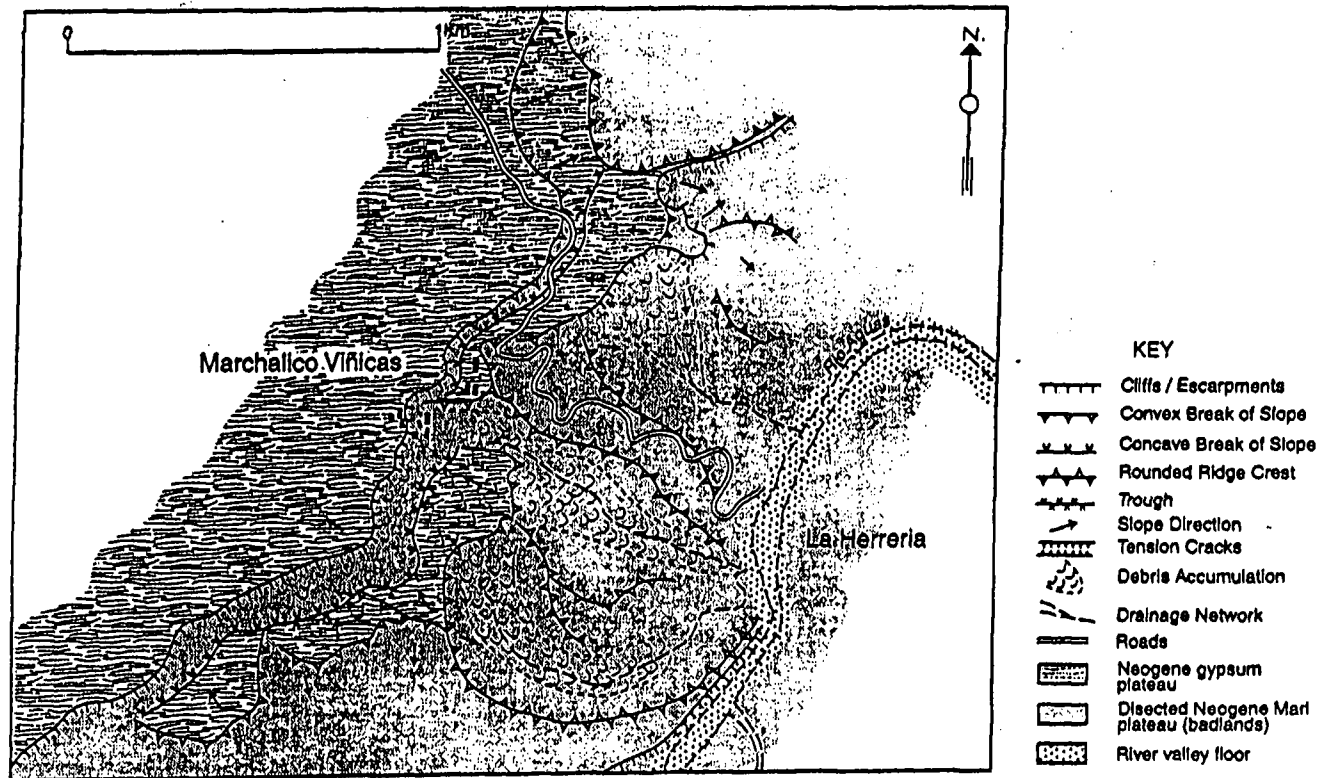
Figure 3. Simplified geomorphological map of the area around the abandoned village of Marchalico Viñicas, on the edge of the Gypsum Escarpment. (Location 2)

Stop 3: Los Perales Area (GR 05839 41051)

The geology of the Los Perales area consists of Messinian gypsum to the north, forming the gypsum escarpment, underlain by marls of the Abad Member. This is underlain by the Azagador Member and the marine marls of the Chozas Formation. The regional dip of the units within this area is to the north/north-west. The Rio Aguas has cut a subsequent drainage channel roughly along the contact between the marls of the Chozas Formation and the limestone of the Azagador Member. This was formed as the lower Aguas cut back towards the Rio Aguas/Feos drainage system.

The combination of rock type and regional dip has led to the formation of numerous landslide features along both sides of this part of the valley (Figure 4). To the north is the gypsum escarpment. In a number of places this has been affected by rock falls and topples caused by the gypsum being undercut by the marls. There has also been a non-rotational slide along one 200 m section of the escarpment, north of Cortijo de Lentiscar (GR 05845 41065), with the height difference between the top of the escarpment and the top surface of the slid block being approximately 50 m.

One particular area of instability within the valley itself, is the steep, south facing scarp slope located above the entrance to the village, just as the track crosses the river bed (GR 05843 41057). The base of the slope is the Chozas Formation marls, while the limestone forms a cliff at the top of the slope. This combination has meant that in some places, the limestone has been undercut, often resulting in rock falls and topples. In other parts of the scarp slope, blocks of the limestone have slipped downslope, possibly on shear surfaces within the marls. The section of scarp slope just upstream of where the track crosses the river bed, last failed in December 1998. Some of the people living within the valley reported seeing several blocks of the limestone start to slide, then topple as they broke up, and then fall down into the river bed below. No seismic shocks had been felt prior to the landslide, but there had been several sharp frosts during the week before.

The southern slopes of the valley are affected by a combination of rotational and non-rotational movement, forming a sizeable landslide complex. Again, this is due to the combination of the limestone overlying the marls, dipping northwards into the valley. Most of the landslide morphology is masked by a reasonably dense vegetation cover, although it is possible to pick out the larger slipped blocks.

Between the western end of this landslide complex and the Aguas/Feos wind gap there is a ridge that has been formed by the incision of the Rio Aguas, as it passes through a series of very tight meanders. These meanders are now incised into a very narrow limestone (Azagador Member) canyon. The ridge (Grid Reference 05837 41053) is composed of both the limestone and the underling marine marls of the Chozas Formation. There have been very large rock falls and topples on both sides of the ridge, with the largest failures being found on the northern side. The ridge is also dissected by a series of very large tension cracks. It is thought that these tension cracks indicate the lateral spreading (double-sided compound sagging, (Hutchinson, 1988)) of the ridge, as the limestone moves down-dip over the top of the marls.

Transfer to Stop 4.
Drive back towards the motorway junction, and follow the AL-104 towards Sorbas. The next stop is a lay-by on the right hand side of the road just as the road goes sharply around to the left and down into the Los Molinos (El Rio de Aguas) valley.

Stop 4: Eastern end of the Los Molinos Area (GR 05831 41046)

From the lay-by there is a good view through the Los Molinos valley area to the west and Rio Aguas/Foes Wind Gap and the Sierra Cabrera to the east. To the north there is the gypsum plateau with the Sierra Filabres in the distance. The second of the large gypsum quarries of the area is also quite clearly visible. Below the lay-by, the Rio Aguas flows through a very tight series of meanders over which the motorway passes on an elevated section.

KEY

⊤⊤⊤⊤	Cliffs / Escarpments
▽▽▽▽	Convex Break of Slope
⋁⋁⋁⋁	Concave Break of Slope
△△△△	Rounded Ridge Crest
⋏⋏⋏⋏	Trough
⟶	Slope Direction
⟋⟋⟋⟋	Tension Cracks
	Debris Accumulation
	Drainage Network
	Roads
	Neogene gypsum plateau
	Disected Neogene marl plateau (badlands)
	Neogene limestone hills & valley sides
	Neogene marl plateau
	River valley floor
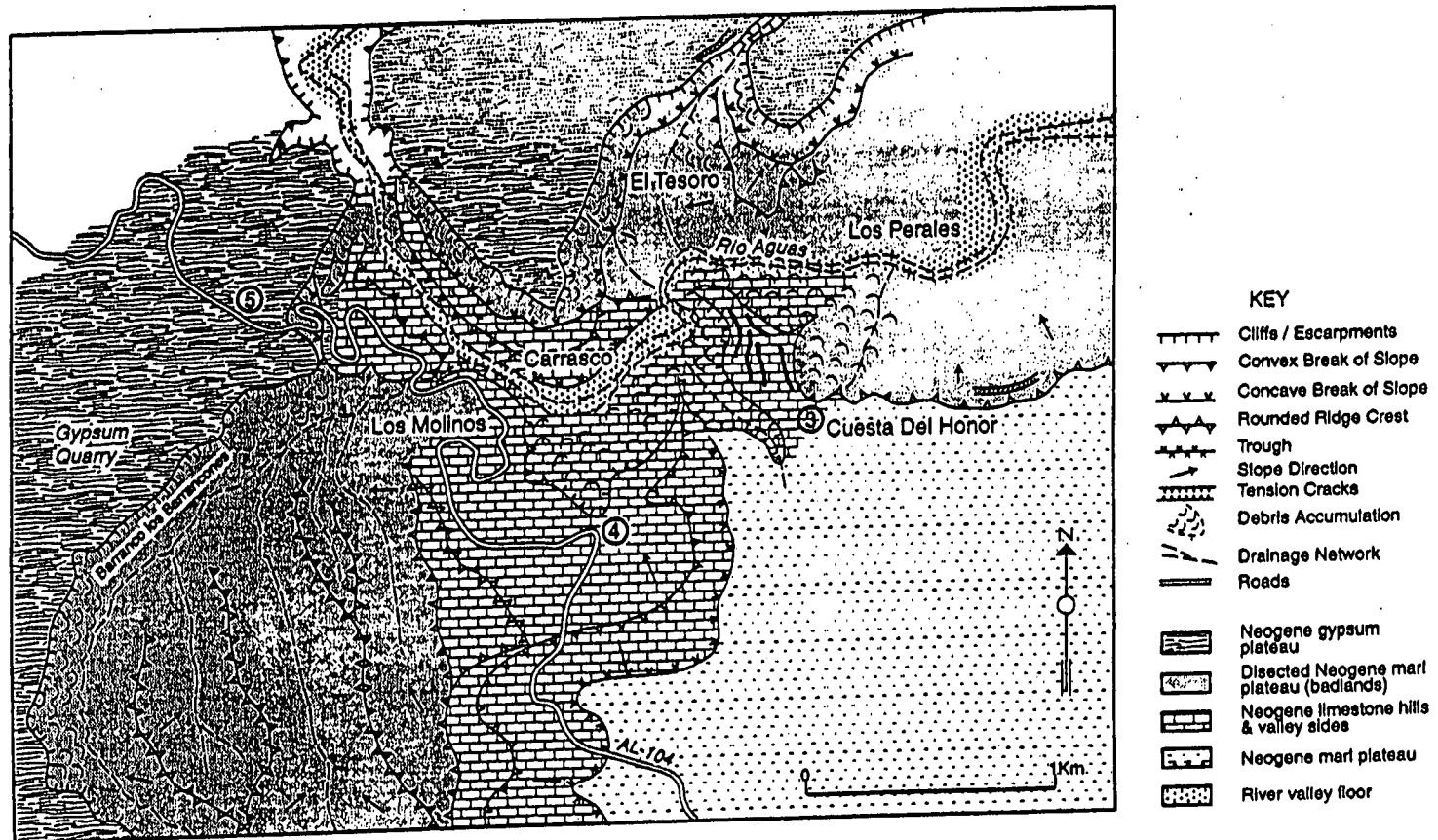
Figure 4. Simplified geomorphological map of the area between Los Molinos and Los Perales as well as parts of the Gypsum Escarpment (Locations 3, 4 & 5)

131

In this area the Rio Aguas has cut a gorge through the Messinian gypsum (Yesares Member), the marls of the Abad Member, the sandstones and limestone of the Azagador Member and the marine marls of the Chozas Formation. The dip of the units within this area is to the north/north-west. The gorge was cut by the combination of continued uplift and rapid antecedent incision after the capture of the Rio Aguas/Feos by the lower Rio Aguas.

Numerous landslide features can be seen affecting this area (Figure 4). There are rock failures along most of the gypsum escarpment in a similar fashion to the landsliding seen at Marchalico Viñicas. In the area between this lay-by and the motorway to the east is a dip slope rotational landslide (often referred to as the Carrasco Landslide) that occurs on the outside of a sharp meander in the Rio Aguas. This is found within the limestone of the Azagador Member and the marls of the Chozas Formation. The slip surface occurs either within the marls or along the unconformable contact between the two units.

The most active part of the landslide, is probably the area immediately below the lay-by. This section of the landslide has retreated further upslope than the rest of the landslide and is bounded by a more defined backscar. This backscar has a fairly distinctive, square shape. The aerial photographs for the area, show quite clearly how the shape of this landslide has been controlled by the major discontinuities of the area, which trend roughly NW-SE and NE-SW. There are also some fairly sizeable tension cracks running parallel with each of the sides of this square area, although these are mainly concentrated along the western flank of the landslide. The relative activity of this western flank of the landslide could be because of the agricultural terraces that are located to the west of the landslide. These terraces could allow water to collect within the hillside and then migrate towards the landslide area.

Transfer to Stop 5.
Continue driving towards Sorbas along the AL-104 through the village of Los Molinos (El Rio de Aguas). On the northern side of the valley various landslides can be seen affecting the gypsum escarpment. The road leaves the valley at the western end by crossing over the gypsum escarpment (Figure 4). Shortly after reaching the top of the gypsum escarpment there is a cross-roads. The road on the left goes to one of the gypsum quarries in the area and the abandoned village of Hueli. Turning off to the right, there is an unmetalled track and a lay-by cut into the gypsum. It is then a short climb up to the prominent conglomerate hill on the edge of the escarpment, following the footpath.

Stop 5: Western end of the Los Molinos Area (GR 05818 41055)
This hilltop is a popular viewpoint. It provides a good view down on to Los Molinos and along this stretch of the Rio Aguas. Further to the east there is the Sierra Cabrera, while slightly to the Northeast, there is the southern edge of the gypsum plateau across to the Marchalico Viñicas area. To the south, there is a view along the gypsum escarpment towards the gypsum quarry and the E-W trending limestone ridge, while to the west there is a good view towards Sorbas and the more central parts of the Sorbas Basin, with the Sierra de Los Filabres to the north and Northwest.

The gypsum escarpment in this area has been affected by various landslides. To the south, in the area adjacent to the gypsum quarry, there has been a very large rock fall, which could be related to the quarry activity. There has also been gypsum rock falls in the area just south of where the road comes up from Los Molinos. Opposite Los Molinos, there have been a number of landslides along the gypsum escarpment. The largest failures seem to have involved the gypsum and underlying marls undergoing a small degree of rotational sliding. In some places the gypsum seems to have been undercut by the marls resulting in topple failures and falls. Recently, some blocks of gypsum that had previously toppled over, have slid down the marl slopes into the Rio Aguas. The fresh backscars can be seen opposite the lower end of the village.

This viewpoint also allows a good oblique view into the Carrasco Landslide. Even with the vegetation cover, the tension cracks on the western flank of the landslide are clearly visible. The shape of these tension cracks give a good indication of how the western flank is retreating across towards the terraces, as well as back towards the road.

132

REFERENCES

EYERS, R., MOORE, J. McM., HERVÁS, J. & LIU, J.G. (1998) Integrated use of Landsat TM and SPOT panchromatic imagery for landslide mapping : case histories from Southeast Spain. In: Maund, J.G. & Eddleston, M. (Eds) *Geohazards in Engineering Geology*, Geological Society, London, Engineering Geology Special Publications, 15, 133-140.

HARVEY, A.M. & WELLS, S.G. (1987) Response of Quaternary fluvial systems to differential epeirogenic uplift : Aguas and Feos river systems. *Geology*, 15, 689-693.

HUTCHINSON, J.N. (1988) General Report : Morphological and geotechnical parameters of landslides in relation to geology and hydrogeology. In : C.Bonnard (Ed.) *Landslides, Proceedings of the 5th International Symposium on Landslides*, Balkema, Rotterdam, 1, 3-35.

MATHER, A.E. (1991) *Late Caenozoic drainage evolution of the Sorbas Basin, Southeast Spain.* PhD thesis, University of Liverpool.

MATHER, A.E. & HARVEY, A.M. (1995) Controls on drainage evolution in the Sorbas Basin, Southeast Spain. In : Lewin, J., Macklin, M.G. & Woodward, J.C. (eds) *Mediterranean Quaternary River Environments*, 65-76.

Notes

Appendix B – The Landslide Inventory

This is a copy of the landslide inventory that forms the basis of this research project. The

data is held in a *Microsoft Access* Database, but has been printed out using *Microsoft Excel*.

Slide No.	Ident Cert	Data Source	Grid Ref	Latitude (N)	Longitude (W)	Location	Land use 1	Position 1	Land use 2	Position 2	Land use 3	Position 3	Crown Elev (m)	Toe Elev (m)	Elev Diff (m)	RS Length (m)
201	1	5	591941132	37,09,35	1,57,55	Rambla Serena Tributary 1 (North side)	0	0					250	200	50	
202	1	5	591941132	37,09,35	1,57,55	Rambla Serena Tributary 2 (South side)							250	200	50	
203	1	6	591741124	37,09,12	1,58,05	Rio Jauto canyon East-side 1	0	0					200	140	60	
204	1	6	591641125	37,09,25	1,58,05	Rio Jauto Canyon East-side 2	0	0					230	150	80	
205	1	6	591441132	37,09,35	1,58,15	Rio Jauto Canyon East-side 3	0	0					250	150	100	
206	1	6	591241134	37,09,45	1,58,25	Rio Jauto Canyon East-side 4	0	0					300	160	140	
207	1	6	590741136	37,09,50	1,58,45	Rio Jauto Canyon East-side 5	0	0					350	180	170	
208	1	6	591941125	37,09,15	1,58,10	Rio Jauto Canyon West-side 1	0	0					200	140	60	
209	1	6	591441130	37,09,33	1,58,15	Rio Jauto Canyon West-side 2	0	0					250	150	100	
210	1	6	591041134	37,09,40	1,58,30	Rio Jauto Canyon West-side 3	0	0					270	170	100	
211	1	3	590541135	37,09,45	1,58,55	Rio Jauto Canyon West-side 4	0	0					350	190	160	
212	4	2	589541145	37,10,10	1,59,30	Cortijo Barranco Baeza	8	1	9	2	13	1	350	220	130	
213	1	3	590341144	37,10,00	1,59,00	Cortijo Molino del Seco	13	1					350	200	150	
214	2	3	589941135	37,09,48	1,59,05	Cortijo La Carabinera 1	0	0					350	210	140	
215	2	3	589541135	37,09,50	1,59,25	Cortijo La Carabinera 2	0	0					250	210	40	
216	4	10	588441144	37,10,12	2,00,15	Cerro Cabrero 1 (west facing)	0	0					450	250	200	
217	3	10	588441144	37,10,15	2,00,10	Cerro Cabrero 2 (northeast facing)	0	0					450	350	100	
218	3	10	588441144	37,10,10	2,00,10	Cerro Cabrero 3 (southeast facing)	0	0					450	350	100	
219	2	3	588541155	37,10,20	2,00,10	Barranco de la Parda/Loma del Cerro Cab	0	0					400	370	30	
220	1	1	588441136	37,09,43	2,00,23	Pago de Los Trances 1	0	0					300	230	70	
221	2	6	587641130	37,09,35	2,00,50	Pago de Los Trances 2	9	1	9	2			300	380	20	
222	4	6	588541137	37,09,55	2,00,50	Pago de Los Trances 3	9	4	13	4			400	250	150	
223	4	2	587741144	37,10,15	2,00,50	Barranco de Albarico	0	0					400	300	100	
224	1	2	590741127	37,09,20	1,59,45	Loma del Tallo 1	0	0					300	250	50	
225	1	2	590641127	37,09,20	1,59,47	Loma del Tallo 2	0	0					300	260	40	
226	1	2	590541127	37,09,20	1,59,50	Lome del Tallo 3	0	0					300	270	30	
227	1	1	589441159	37,11,08	1,59,35	Los Pinos 1	1	2	2	2	5	2	550	450	100	
228	2	6	589741153	37,10,45	1,59,25	Los Pinos 2	13	5					450	400	50	
229	2	6	589941153	37,10,45	1,59,18	Los Pinos 3 (Cerro de la Cruz)	0	0					450	400	50	
230	2	5	590041152	37,10,40	1,59,10	La Serena 1	13	2					450	380	70	
231	2	5	590041148	37,10,35	1,59,10	La Serena 2	0	0					400	360	40	
232	1	10	588041165	37,11,25	2,00,30	Fuente El Albarieo 2 (west facing)	0	0					750	650	100	
233	2	1	588541164	37,11,20	2,00,15	Fuente El Albarieo 1 (south facing)	0	0					750	680	70	
234	1	4	590041161	37,11,12	1,59,10	Cortijo del Hambre (Near Bedar)	12	2					550	450	100	
235	2	4	589841174	37,11,50	1,59,20	Cerro de las Angustias (Slopes above Bec	12	2					600			
236	2	10	590041182	37,12,20	1,59,10	Cerro del Silencio (N of Bedar)	0	0					550	510	40	
237	1	4	589941174	37,11,50	1,59,15	Pago de la Carrasquica (near Bedar)	12	2					600	500	100	

Slide No.	Ident Cert	Data Source	Grid Ref	Latitude (N)	Longitude (W)	Location	Land use 1	Position 1	Land use 2	Position 2	Land use 3	Position 3	Crown Elev (m)	Toe Elev (m)	Elev Diff (m)	RS Length (m)
238	2	4	592341153	37,10,45	1,57,40	La Gamberra (Rambla de las Norias 2)	0	0					290	220	70	
239	2	4	592641147	37,10,25	1,57,25	Rambla Trinchera 1 (south facing)	12	2					250	220	30	
240	2	4	592541145	37,10,20	1,57,25	Rambla Trinchera 2 (north facing)	12	2					270	210	60	
241	2	4	592641148	37,10,30	1,57,25	Rambla de las Norias 1	0	0					250	220	30	
301	1	5	591341105	37,08,10	1,58,20	Cortijada Las Flores	13	1	25	1			160	110	50	
302	1	12	592241115	37,08,40	1,57,42	Alfaix / Under the N-340 road bridge	12	1	12	2			120	110	10	
303	2	11	594941114	37,08,35	1,55,52	Rio Aguas canyon (Los Caparroses) 1	0	0					80	60	20	
304	2	11	594841115	37,08,35	1,55,52	Rio Aguas canyon (Los Caparroses) 2	0	0					80	60	20	
305	2	11	594941115	37,08,35	1,55,52	Rio Aguas canyon (Los Caparroses) 3	12	1					80	60	20	
401	1	12	574541085	37,07,10	2,09,40	Las Rellanas Pintas	13	1					470	460	10	
402	1	12	575641083	37,07,02	2,09,00	Cortijada de Cinta Blanca	13	1					470	450	20	
403	1	12	575541066	37,06,08	2,09,03	Cortijo Alto meander 1	9	1	13	2			460	420	40	
404	1	12	575541066	37,06,08	2,08,55	Cortijo Alto meander 2	9	1	13	2			460	420	40	
405	1	9	576441067	37,06,12	2,08,23	Rbla Chopas & Rbla Cinta Blanca	0	0					430	400	30	
406	1	9	574641058	37,05,48	2,09,35	Rbla del Chopas Switchback 1 (N of old rd	0	0					450	440	10	
407	1	9	574941052	37,05,25	2,09,35	Rbla del Chopas Switchback 2 (large failu							480	440	40	
408	1	12	574641053	37,05,30	2,09,32	Rbla del Chopas Switchback 3	0	0					450	445	5	
409	1	12	574741054	37,05,32	2,09,30	Rbla del Chopas Switchback 4	0	0					450	445	5	
410	1	12	574841055	37,05,35	2,09,34	Rbla del Chopas Switchback 5	0	0					450	445	5	
411	1	12	574741055	37,05,35	2,09,35	Rbla del Chopas Switchback 6	0	0					450	445	5	
412	1	9	574741058	37,05,40	2,09,34	Rbla del Chopas Switchback 7 (opposite c	0	0					460	430	30	
413	1	12	575341055	37,05,32	2,09,12	El Pilarico	0	0					430	425	5	
414	1	12	575641059	37,05,48	2,08,58	Los Pilaricos	0	0					440	430	10	
415	1	12	575941063	37,05,56	2,08,45	La Boquera	0	0					420	417	3	
416	1	12	576441058	37,05,40	2,08,26	Pozanco	0	0					470	410	60	
417	1	12	575041047	37,05,8	2,09,22	Barranco Chacho	0	0					450	445	5	
418	1	11	576441055	37,05,30	2,08,28	Canada de Miguel Campo	0	0					490	430	60	
419	1	12	576641053	37,05,23	2,08,14	Barranco del Mocatan/Mocatal	0	0					450	430	20	
501	1	12	576941065	37,06,05	2,08,01	Bird's foot locality 1	26	2					420	400	20	
502	1	12	577141065	37,06,05	2,07,58	Bird's Foot Locality 2	26	2					400	390	10	
503	1	9	576941069	37,06,20	2,08,00	Los Beneficos	9	1					440	400	50	
504	1	9	577341071	37,06,25	2,07,50	NE of Los Beneficos	9	2					430	410	20	
505	1	9	577641072	37,06,28	2,07,36	Sorbas Quarry	13	2					410	385	25	
506	1	9	577741071	37,06,22	2,07,32	Sorbas Playing Field (opposite)	0	0					430	380	40	
507	1	9	577841067	37,06,8	2,07,32	Sorbas Canyon (N of dodgy terrace)	0	0					380	370	10	
508	1	12	577741066	37,06,05	2,07,35	Dodgy Terrace (Jose's house)	1	1					400	360	40	
509	1	9	577741065	37,06,04	2,07,35	Sorbas 1st Aid 1	2	1	12	1			400	360	40	

Slide No.	Ident Cert	Data Source	Grid Ref.	Latitude (N)	Longitude (W)	Location	Land use 1	Position 1	Land use 2	Position 2	Land use 3	Position 3	Crown Elev (m)	Toe Elev (m)	Elev Diff (m)	RS Length (m)
510	1	9	577641066	37,06,05	2,07,34	Sorbas 1st Aid 2 (opposite)	0	0					380	360	20	
511	1	12	577841064	37,06,00	2,07,28	Behind the new pottery Museum	2	2					400	395	5	3
512	1	1	577741064	37,06,02	2,07,23	Sorbas Theatre	1	1	2	1	9	2	400	380	20	
513	1	9	577941065	37,06,04	2,07,22	N corner of Sorbas	1	1					400	360	40	
514	1	9	577941067	37,06,07	2,07,22	N of Sorbas N corner	0	0					400	360	40	
515	1	9	578541063	37,06,00	2,06,55	Alfereria	0	0					400	350	50	
516	1	9	578141062	37,05,55	2,07,12	Sorbas (Old Square)	1	1	1	2			400	380	20	
517	1	12	578241060	37,06,47	2,07,14	Sorbas (Chachos)	13	4					380	340	40	
518	1	12	578241061	37,05,51	2,07,10	E end of Sorbas Old Bridge	1	2	12	3	15	4	350	345	3	
519	1	12	578141061	37,05,52	2,07,16	W end of Sorbas Old Bridge	1	1	12	2			390	370	20	
520	1	11	577841063	37,05,55	2,07,25	Sorbas (Behind Fatima's Bar)	1	1	2	1	9	2	400	370	30	2
521	1	12	577741061	37,05,52	2,07,25	Sorbas road cutting 1 (Relict Feature)	12	2								
522	1	12	577741061	37,05,52,	2,07,25	Sorbas road cutting 1 (Reactivated)	12	2					390	380	10	
523	1	12	577741061	37,05,52	2,07,25	Sorbas road cutting 2 (Relict Feature)	12	2								
524	1	12	577741061	37,05,25	2,07,25	Sorbas road cutting 2 (Reactivated)	12	2					390	380	10	
525	1	12	577641062	37,05,55	2,07,35	Sorbas road cutting 3	12	2					400	390	10	
526	1	12	577941060	37,05,50	2,07,23	Opposite Fatima's (Relict Feature)	13	4	9	2			400	385	15	
527	1	9	578041055	37,05,31	2,07,08	Maleguica	9	2					400	350	50	
528	1	12	578741054	37,05,35	2,06,44	Gypsum outcrop rockfall 1	26	2					370	340	30	
529	1	12	578841054	37,05,35	2,06,45	Gypsum outcrop rockfall 2	26	2					370	340	30	
530	1	12	578941054	37,05,35	2,06,46	Gypsum outcrop rockfall 3	26	2					370	340	30	
531	1	9	578941054	37,05,28	2,06,41	Cortijo de Paco el Americano	5	2					400	350	50	
532	1	12	579041062	37,06,52	2,06,40	Gully system opposite Sorbas Cemetry 1	12	1					480	470	10	
533	1	12	579041062	37,06,52	2,06,40	Gully system opposite Sorbas Cemetry 2	12	1					490	480	10	
601	1	12	578341067	37,06,08	2,07,08	Cortijo de Porras / Sorbas construction ya	0	0					400	370	30	
602	1	12	578241068	37,06,13	2,07,11	Cortijo de Porras (SE Facing 1)	1	1					390	370	20	
603	1	12	578241069	37,06,18	2,07,11	Cortijo de Porras (SE Facing 2)	13	2					390	370	20	
604	1	12	578541069	37,06,18	2,06,58	Cortijo de Porras (N Facing 1)	0	0					395	370	25	
605	1	12	578641069	37,06,18	2,06,59	Cortijo de Porras (N Facing 2)	0	0					400	370	30	
606	1	9	578741072	37,06,25	2,06,52	Entrance to "Zoca Gully" (S - under the ro	12	1					420	370	50	
607	1	12	578541073	37,06,30	2,07,00	Entrance to "Zoca Gully" (N)	1	3	9	4			400	380	20	
608	1	12	578741073	37,06,30	2,06,52	"Zoca Gully" 1 (NW Facing)	9	1					420	400	20	
609	1	12	578641074	37,06,32	2,06,55	"Zoca Gully" 2 (W Facing)	9	1					420	390	30	
610	1	12	578541074	37,06,32	2,06,57	"Zoca Gully" 3 (E Facing)	9	1					410	380	30	
611	1	9	578141071	37,06,22	2,07,16	Zoca	1	2	13	4	9	2	430	400	30	
612	1	9	578041075	37,06,35	2,07,25	Rambla Sorbas (W-Side)	9	4	13	4			440	400	40	
613	1	9	578541073	37,06,30	2,07,05	Rambla Sorbas (E-Side)	1	4	9	4	13	2	400	380	20	

Slide No.	Ident Cert	Data Source	GridRef	Latitude (N)	Longitude (W)	Location	Land use 1	Position 1	Land use 2	Position 2	Land use 3	Position 3	Crown Elev (m)	Toe Elev (m)	Elev Diff (m)	RS Length (m)
614	1	12	577841078	37,06,45	2,07,24	Cortijo El Jahari (Rock Topple)	1	3	9	2			400	390	10	
615	1	12	577741077	37,06,45	2,07,30	Opposite Cortijo El Jahari	13	2								
616	1	12	578241080	37,06,52	2,07,18	Cortijo Tejica	9	1					420	390	30	
617	1	9	578441084	37,07,04	2,07,05	El Tieso	9	1	13	1	13	2	440	400	40	
618	1	9	578441088	37,07,00	2,07,00	Mayordomo	13	2					450	410	40	
619	1	12	576741093	37,07,35	2,08,10	Gochar	9	1	13	2			430	420	10	
620	1	12	5764110	37,08,00	2,08,20	Rambla de Gochar canyon (W-Side)	9	2	13	2						
621	1	12	5764110	37,08,00	2,08,20	Rambla de Gochar canyon (E-Side)	9	22	13	2						
622	1	12	576241106	37,08,20	2,08,38	Rambla de Gochar canyon - Terrapin Poo	9	1	28	2			450	430	20	
623	1	12	576241106	37,08,20	2,08,38	Rambla de Gochar canyon - Terrapin Poo	9	1	28	2			450	430	20	
624	1	12	576241106	37,08,20	2,08,38	Rambla de Gochar canyon - Terrapin Poo	9	1	28	2			450	430	20	
625	1	11	576141110	37,08,31	2,08,37	Rambla de Gochar / M.tial de los Charcor	0	0					460	455	5	
626	1	11	575841111	37,08,32	2,08,48	Rambla de Gochar / M.tial de los Charcor	0	0					470	460	10	
627	1	12	575141108	37,08,25	2,09,17	"Pepe" section 1	0	0					485	480	5	1
628	1	11	575341108	37,08,25	2,09,02	"Pepe" section 2							470	440	30	
629	1	12	577141097	37,07,50	2,07,58	Cortijo Entrada de Mora	0	0					440	430	10	
630	1	12	577041101	37,08,05	2,07,58	Cortijo de Zamora (opposite)	1	2	9	2	9	1	470	430	40	
631	1	12	577341104	37,08,10	2,07,45	Cortijo de Cavila (E)	13	1					480	430	50	
632	1	12	577141107	37,08,12	2,07,55	Cortijo de Cavila (N facing)	5	1					450	430	20	
633	1	12	577241130	37,08,20	2,07,42	Moras (S) (Ctjo Los Quicios)	13	2					470	440	30	
634	1	12	577341110	37,08,35	2,07,50	Moras (N) 2	13	1	5	1			460	445	10	
635	1	12	577441110	37,08,30	2,07,40	Moras (N) 1	0	0					460	450	10	
636	1	12	578141124	37,09,15	2,07,15	Rbla de La Mora 1 (limestone canyon)	0	0					520	500	20	
637	1	12	578141124	37,09,15	2,07,15	Rbla de La Mora 2 (lst canyon)	0	0					520	500	20	
639	1	12	578341126	37,09,20	2,07,06	Rbla de La Mora 3	9	1					520	500	20	
640	1	12	578241128	37,09,28	2,07,09	Rbla de La Mora 4	0	0					540	510	30	
641	1	12	578241130	37,09,32	2,07,03	Rbla de La Mora 5	0	0					550	515	35	
642	1	12	578241131	37,09,36	2,07,05	Rbla de La Mora 6	0	0					550	520	30	
643	1	12	578341132	37,09,41	2,07,05	Rbla de La Mora 7	0	0					540	530	10	
644	1	12	578841136	37,09,52	2,06,45	El Fonte 1	1	1					350	525	5	
645	1	12	578741138	37,10,00	2,06,00	El Fonte 2	0	0					525	520	5	
646	1	12	579341140	37,10,04	2,06,26	La Mela 1	9	2	13	2			560	555	5	
647	1	12	579341140	37,10,04	2,06,26	La Mela 2	9	2	13	2			560	555	5	
648	1	12	579341140	37,10,04	2,06,26	La Mela 3	9	2	13	2			560	555	5	
701	4	2	580541125	37,09,20	2,05,35	Cerro Pelado	9	2					550	530	20	
702	1	10	579741123	37,09,08	2,06,08	Rbla de Los Castanos (N of canyon) 1	9	4					570	550	30	
703	1	10	579641124	37,09,12	2,06,11	Rbla de Los Castanos (N of canyon) 2	9	4					550	540	10	

Slide No.	Ident. Cert.	Data Source	Grid Ref	Latitude (N)	Longitude (W)	Location	Land use 1	Position 1	Land use 2	Position 2	Land use 3	Position 3	Crown Elev.(m)	Toe Elev.(m)	Elev Diff (m)	RS Length (m)
704	1	7	579641120	37,09,00	2,06,15	Rbla de Los Castanos canyon (W-Side, e	13	1					540	490	50	
705	1	7	579641120	37,09,00	2,06,10	Rbla de Los Castanos canyon (E-Side, we	0	0					540	500	40	
706	1	11	579841118	37,08,48	2,06,02	Rbla de Los Castanos (S of canyon) 1	0	0					530	500	30	
707	1	12	580341116	37,08,52	2,05,45	Rbla de Los Castanos (N of Hill 487) 2	9	2					500	450	50	
708	1	12	580141113	37,08,36	2,05,50	Knoll W of Cariatiz (Hill 487) 1	9	2					480	440	40	
709	1	12	580341113	37,08,39	2,05,45	Knoll W of Cariatiz (Hill 487) 2	9	2					470	440	30	
710	1	12	579841113	37,08,30	2,06,04	Cariatiz (Relict Feature 1)	9	2	13	1			500	450	50	
711	1	12	580041112	37,08,34	2,06,00	Cariatiz (Relict Feature 2)	9	2	13	1			500	450	50	
712	1	12	580141112	37,08,33	2,05,52	Cariatiz (Relict Feature 3)	9	4	13	4			500			
713	1	11	580341111	37,08,32	2,05,47	Cariatiz (Relict Feature 4)	9	4	13	4			500			
714	1	11	580541111	37,08,31	2,05,38	Cariatiz (Relict Feature 5)	9	1	13	1			500			
715	1	7	581041122	37,09,05`	2,05,15	Limestone Escarpment behind Cariatiz, L	1	2	9	2	16	1	520	450	70	
716	1	7	581541125	37,09,20	2,04,50	Limestone Escarpment - Barranco del Chi	9	2	9	4			530	450	80	
717	1	12	582041122	37,09,10	2,04,36	Barranco del Chive (W-Side) 1	9	1	13	2			420	400	20	
718	1	12	581941123	37,09,10	2,04,40	Barranco del Chive (W-Side) 2	9	1	9	2	13	2	440	410	30	
719	2	5	581741130	37,09,35	2,04,45	La Rambla del Chive 1	9	2					480	450	30	
720	2	5	581541130	37,09,38	2,04,50	La Ramble del Chive 2	9	2					500	470	30	
721	1	11	582241126	37,09,18	2,04,29	Los Perez (Just to the north of the settlem	7	3	8	3			450	410	40	
722	1	7	582541128	37,09,25	2,04,15	Limestone Escarpment - Barranco del Ch	9	2	9	4			550	500	50	
723	1	7	582541124	37,09,10	2,04,10	Limestone Escarpment above Los Martine	9	4	9	2			550	450	100	
724	4	5	582741116	37,08,50	2,04,00	Los Martinez - Los Ramirez	9	4	9	2			425	400	25	
725	4	5	583741124	37,09,12	2,03,30	Cortijo de La Piedra 1	9	2					450	380	70	
726	4	5	584041123	37,09,05	2,03,15	Cortijo de La Piedra 2	9	2					450	370	80	
727	1	6	583841132	37,09,38	2,03,25	Cerro de La Piera	0	0					560	380	180	
728	2	5	585541123	37,09,05	2,02,10	Cerro de Solano 1	0	0					400	350	50	
729	4	5	585741125	37,09,10	2,02,05	Cerro de Solano 2	0	0					400	350	50	
730	4	5	585741126	37,09,12	2,02,00	Cerro de Solano 3	0	0					400	350	50	
731	4	5	586141128	37,09,20	2,01,48	Lomas de los Castanos 1	0	0					360	300	50	
732	4	5	585941129	37,09,28	2,01,25	Lomas de los Castanos 2	0	0					350	310	40	
733	4	2	582541143	37,10,12	2,05,12	Piedra Amarilla (near El Chive)	13	4					550	470	80	
734	4	2	584941152	37,10,42	2,02,40	Barranco de Cerrada	0	0					600	450	150	
735	4	2	585941142	37,10,10	2,01,55	Loma del Jaral 1	0	0								
736	4	2	585941142	37,10,10	2,01,55	Loma del Jaral 2	0	0								
801	1	7	575441021	37,03,42	2,09,00	Fuente El Taray 1	27	2					670	580	90	
802	1	7	575541020	37,03,38	2,08,55	Fuente El Taray 2	27	2					680	560	120	
803	1	7	576041019	37,03,35	2,08,40	Fuente El Taray 3	27	2					680	600	100	
804	1	7	576641019	37,03,38	2,08,15	Risco de Sanchez	27	2					670	600	70	

RS Slide No.	Ident. Cert	Data Source	Grid Ref	Latitude (N)	Longitude (W)	Location	Land use 1	Position 1	Land use 2	Position 2	Land use 3	Position 3	Crown Elev.(m)	Toe Elev.(m)	Elev Diff (m)	RS Length (m)
805	1	12	576741030	37,04,12	2,08,10	(Cortijo) Los Contreras 1	27	2					520	500	20	
806	1	12	576741031	37,04,14	2,08,10	(Cortijo) Los Contreras 2	27	2					510	500	10	
807	1	12	576841031	37,04,14	2,08,05	(Cortijo) Los Contreras 3	27	2					510	500	10	
808	1	12	576841032	37,04,18	2,08,08	(Cortijo) Los Contreras 4	27	2					530	500	30	
809	1	12	576741032	37,04,16	2,08,12	(Cortijo) Los Contreras 5	27	2					510	500	10	
810	4	12	576941042	37,04,50	2,08,5	Mocatan Relict Landslide	13	4					520			
811	1	9	577341041	37,04,45	2,07,47	Cerro de Juan Contreras - Bco de Los Co	0	0					465	450	15	
812	1	9	577241039	37,04,40	2,07,50	Bco de Los Contreras 2	0	0					480	450	30	
813	1	9	577941042	37,04,50	2,07,20	Bco de Los Contreras 3	0	0					450	420	30	
814	1	9	578141045	37,04,57	2,07,12	Bco de Los Contreras 4	0	0					450	410	40	
815	1	9	578241041	37,04,46	2,07,07	Bco de Las Alpargateras 1	0	0					450	420	30	
816	1	9	578341043	37,04,55	2,07,02	Bco de Las Alpargateras 2	0	0					450	410	40	
817	1	9	578441045	37,05,00	2,07,02	Bco de Infierno 1	0	0					450	400	50	
818	1	9	578541046	37,05,02	2,07,00	Bco de Infierno 2	0	0					450	400	50	
819	1	9	578641047	37,05,04	2,06,54	Bco de Infierno 3	0	0					450	400	50	
820	1	9	578641049	37,05,10	2,06,55	Bco de Infierno 4	0	0					450	400	50	
821	1	9	578941050	37,05,15	2,06,40	Bco de Infierno 5	0	0					400	390	10	
822	1	9	578741048	37,05,08	2,06,44	Bco de Infierno 6	0	0					420	380	40	
823	3	11	579341049	37,05,10	2,06,00	Bco de Infierno 7	0	0					400			
901	1	9	579641053	37,05,22	2,06,05	La Clauda	5	2					420	360	60	
902	1	9	580141060	37,05,45	2,05,52	Casa Linda 1	1	1					330	320	10	
903	1	9	580141059	37,05,45	2,05,55	Casa Linda 2	1	3					350	320	30	
904	1	9	579941059	37,05,44	2,06,02	Casa Linda 3 / Loma Sola	9	1					340	320	20	
905	1	12	580641063	37,06,56	2,05,34	Lindy's Landslide 1	0	0					340	310	30	
906	1	12	580841057	37,05,35	2,05,32	Urra (under the road bridge)	12	1					340	330	10	
907	1	12	580841059	37,05,40	2,05,27	Urra Estate 1	0	0							2	
908	1	9	581341065	37,06,00	2,05,06	Urra / Cortijo Los Indalecios	9	2					360	310	50	
909	1	9	581541066	37,06,08	2,04,51	Cortijo Los Indalecios	9	2					370	320	50	
910	1	12	581641069	37,06,15	2,04,55	Rio Aguas / Cortijo Los Indalecios	0	0					310	300	10	
911	1	12	581341073	37,06,28	2,05,06	Rio Aguas / Venta de la Tencia	0	0					310	305	5	
912	1	12	581541081	37,06,54	2,05,00	Road Cutting on the old N-340	13	2					350	340	10	
913	1	12	581141081	37,06,55	2,05,15	Rambla del Marchalico 1 (near to road)	0	0					390	380	10	
914	1	12	580941086	37,07,10	2,05,20	Rambla del Marchalico 2 (Small rockfall)	0	0					400	390	10	
915	1	9	580841090	37,07,20	2,05,25	Rambla del Marchalico 3 (East Facing)	9	1	9	2			400	360	40	
916	1	9	580541091	37,07,25	2,05,35	Rambla del Marchalico 4 (North Facing)	9	1	13	4			400	380	20	
917	1	9	580541092	37,07,30	2,05,35	Rambla del Marchalico 5 (South Facing)	0	0					410	370	40	
918	1	12	579941071	37,06,22	2,06,01	Bco del Aguaron	0	0					340	330	10	

Slide No	Ident Cert	Data Source	Grid Ref	Latitude (N)	Longitude (W)	Location	Land use 1	Position 1	Land use 2	Position 2	Land use 3	Position 3	Crown Elev (m)	Toe Elev (m)	Elev Diff (m)	RS Length (m)
919	1	9	579041077	37,06,40	2,06,40	Casa del Aguarico (NE Facing)	7	5	27	2	9	1	440	360	80	150
920	1	9	579241080	37,06,55	2,06,30	Casa del Aguarico (W Facing)	27	4	9	1	7	3	420	380	40	
921	1	9	579541077	37,06,40	2,06,20	Bcco East of Casa del Aguaron	9	1					430	370	60	
922	1	12	579541068	37,06,14	2,06,20	Hill 419 (W Facing)	27	2					410	400	10	
923	1	12	579541069	37,06,18	2,06,20	Hill 419 (NW Facing)	0	0					400	390	10	
924	1	12	579641070	37,06,20	2,06,24	Hill 419 (NE Facing)	0	0					400	390	10	
925	1	12	579641069	37,06,14	2,06,14	Hill 419 (SE Facing)	0	0					410	390	20	
926	1	12	579541065	37,06,02	2,06,20	Cortijo Boqueras Gully 1 (SE Facing)	9	1					370	340	30	
927	1	12	579341065	37,06,03	2,06,26	Cortijo Boqueras Gully 2 (NW Facing)	9	1					370	350	20	
928	1	12	579341067	37,06,08	2,06,28	Cortijo Boqueras Gully 3 (SW Facing)	9	1					380	350	30	
929	1	12	579141073	37,06,25	2,06,32	Alto de Zorreras	6	1	9	2	8	3	430	390	40	
930	1	12	579441061	37,05,50	2,06,25	Old N340 / Junta del Andalucia Shed	0	0					360	330	30	
1001	1	12	581941068	37,06,05	2,04,45	El Nacimiento 1 (S Facing)	0	0					320	300	20	
1002	1	12	581941063	37,05,53	2,04,40	El Nacimiento 2 (NE Facing)	9	1					350	300	50	
1003	1	12	582241064	37,05,55	2,04,32	El Nacimiento 3 (W Facing)	0	0					350	300	50	
1004	1	9	582141060	37,05,40	2,04,35	Los Molinos Canyon (W-Side, East facing	0	0					350	300	50	
1005	1	9	582241061	37,05,50	2,04,30	Los Molinos Canyon (E-Side, west facing)	0	0					350	300	50	
1012	1	12	581941056	37,05,32	2,04,41	Inspiration Point (Eagles Nest)	12	2					420	350	70	
1013	1	9	582241056	37,05,32	2,04,30	Los Molinos Campground	7	1					310	290	20	
1014	4	9	582041054	37,05,28	2,04,30	Los Molinos Relict Landslide	1	4	12	4			400	340	60	
1015	1	12	581941052	37,04,15	2,04,45	Inspiration Point South (situated south of	0	0					400	340	60	
1016	1	9	581241045	37,05,04	2,05,00	Penon Diaz	8	1					450	350	100	
1017	1	6	581541034	37,04,15	2,05,00	Las Majadas Viejas / Barranco los Barran	8	1					550	400	150	
1018	4	10	5824104	37,05,10	2,04,25	Barranco Los Madroneros	27	2	27	2			400	380	20	
1020	4	5	582041038	37,04,33	2,04,38	Loma de Jacinto/B.de Tocino	27	2	27	2			400	380	20	
1021	1	12	582941055	37,05,28	2,04,00	Gypsum Escarpment (above Carrasco)	27	2	7	2			350	320	30	
1022	1	12	583041051	37,05,18	2,04,00	Carrasco (Limestone Escarpment) (South	27	2	7	2			300	270	30	
1023	1	12	582741052	37,05,15	2,04,08	Carrasco (Limestone Escarpment) (North	12	1					300	260	40	
1024	1	9	5834105	37,05,11	2,03,55	Cerro Molatas (South of Carrasco) (aka "N	12	1					350	200	150	
1026	1	9	583041053	37,05,35	2,04,00	El Tesoro (West-side 1)	7	2					360	260	100	
1027	1	9	583141059	37,05,42	2,03,55	El Tesoro (West-side 2)	7	2					350	300	50	
1028	1	9	583141061	37,05,50	2,03,50	El Tesoro (West-side 3)	7	2					360	250	110	
1029	1	9	583441063	37,05,55	2,03,40	El Tesoro (NW)	7	2					350	300	50	
1030	1	9	583741063	37,05,50	2,03,30	El Tesoro (NE)	7	2					350	250	100	
1031	1	9	584041062	37,05,52	2,03,18	Gypsum Escarpment (Above Los Perales)	11	2					370	280	90	
1032	1	9	584341065	37,06,04	2,03,08	Gypsum Escarpment (Above Los Perales)	11	2					370	270	100	
1033	1	9	584541066	37,06,06	2,02,55	Gypsum Escarpment Rotational Failure (A	11	2					380	270	110	

Slide No.	Ident Cert	Data Source	Grid Ref	Latitude (N)	Longitude (W)	Location	Land use 1	Position 1	Land use 2	Position 2	Land use 3	Position 3	Crown Elev (m)	Toe Elev (m)	Elev Diff (m)	RS Length (m)
1034	1	9	585041069	37,06,15	2,02,38	Gypsum Escarpment (S of Marchalico Vir	11	2					380	250	130	
1035	1	8	584341057	37,05,35	2,03,07	Los Perales 1 (Jackie's Rockfall)	13	2					300	220	80	
1036	1	8	584641060	37,05,45	2,02,52	Los Perales - Cortijo de Lentiscar canyon	0	0					250	210	40	
1037	1	8	584941061	37,05,48	2,02,42	Los Perales - Cortijo de Lentiscar canyon	0	0					250	210	40	
1038	1	9	583841053	37,05,22	2,03,27	Tension Crack Ridge Landslide Complex	5	2	11	2	10	2	360	220	140	500
1039	1	9	585041055	37,05,25	2,02,40	Cuesta Del Honor Landslide Complex	9	4	13	4	1	5	450	200	250	
1040	1	1	585741055	37,05,30	2,02,05	Corral de la Molata	0	0					450	250	100	
1041	1	12	585141071	37,06,20	2,02,35	Marchalico Vinicas 1 (Large obvious featu	7	3	9	4	11	2	380	200	180	
1042	1	12	585341074	37,06,30	2,02,25	Marchalico Vinicas 2 ("Relict" Feature)	11	4	7	3	13	4	370	190	180	
1043	4	7	585241088	37,07,15	2,02,20	Cerro Alto del Yesar	0	0					350	300	50	
1044	1	4	586341103	37,08,05	2,01,40	Cerro del Majon (South Facing)	0	0					350	250	100	
1045	1	6	586041105	37,08,10	2,01,55	Cerro del Majon (NE Facing)	9	2					350	270	80	
1046	1	6	585541107	37,08,15	2,02,15	Cerro del Majon (North Facing)	9	2					380	300	80	
1047	1	6	585141109	37,08,22	2,02,30	Los Castanos/Cerro del Majon	9	2					400	310	90	
1048	1	6	585841098	37,07,50	2,02,00	Cerro del Mojon South	0	0					410	350	60	
1101	1	7	586541064	37,05,50	2,01,35	La Parrica	9	2					450	200	250	
1102	1	12	586841073	37,06,25	2,01,20	La Herreria	0	0					200	180	20	
1103	1	12	587141076	37,06,35	2,01,10	La Herreria / La Huelga cemetry	0	0					200	180	20	
1104	1	7	587841076	37,06,38	2,00,40	Barranco La Huelga	0	0					300	250	50	
1106	4	1	589341084	37,07,02	1,59,48	Los Quemadillos 1 (Bcco de los Quemadi	0	0					300	250	50	
1107	4	1	589341084	37,07,05	1,59,42	Los Quemadillos 2 (Bcco de los Quemadi	0	0					300	250	50	
1108	4	1	589741089	37,07,10	1,59,25	Los Quemadillos 4 (unamed Bcco - east f	0	0					260	200	60	
1109	4	1	589741089	37,07,15	1,59,22	Los Quemadillos 4 (unamed Bcco - west f	0	0					250	200	50	
1110	4	4	591941100	37,07,55	1,57,55	El Aguila 1 (east facing)	9	3					190	150	40	
1111	4	4	592141100	37,07,50	1,57,50	El Aguila 2 (west facing)	9	3					190	140	50	
1112	4	4	592641105	37,08,10	1,57,35	Loma de la Senora 1 (northwest facing) -	9	4	5	4			200	150	50	
1113	4	4	59341102	37,08,00	1,57,00	Loma de la Senora 2 (southeast facing)	0	0					200	100	100	
1114	1	4	594441107	37,08,20	1,56,15	Cortijo Nuevo del Aire (Cortijo Grande air	13	1	29	1			140	90	50	
1115	1	11	596041112	37,08,30	1,55,10	Cortijo de la Iruena	13	1					120	90	30	
1116	3	4	590241055	37,05,25	1,59,00	Alto del Muerto 1 (N Facing)	0	0					690	550	140	
1117	1	11	590441054	37,05,20	1,58,55	Alto del Muerto 2 (S Facing)	0	0					650	550	100	
1118	1	11	590741064	37,05,55	1,58,47	Bcco del Muerto	0	0					420	390	30	
1119	3	4	591741055	37,05,35	1,58,06	Cerro de la Fuente del Puerto 1 (west faci	0	0					550	450	100	
1120	3	4	591941055	37,05,35	1,57,56	Cerro de la Fuente del Puerto 2 (east faci	0	0					550	400	150	
1121	3	4	592341062	37,05,50	1,57,45	Cerro de la Fuente del Puerto 3 (southwes	0	0					500	400	100	
1122	3	4	593841065	37,06,00	1,56,43	La Carrasca	0	0					550	3500	200	
1123	3	4	593341078	37,06,50	1,56,15·	Loma del Colorado 1	13	2					350	250	100	

Slide No	Ident Cert	Data Source	Grid Ref	Latitude (N)	Longitude (W)	Location	Land use 1	Position 1	Land use 2	Position 2	Land use 3	Position 3	Crown Elev (m)	Toe Elev (m)	Elev Diff (m)	RS Length (m)
1124	3	4	594541085	37,07,00	1,56,40	Loma del Colorado 2	13	2					400	350	150	
1125	3	4	595141073	37,06,22	1,55,40	Barranco del Tremecin 1 (west side of Bc	0	0					500	300	200	
1126	3	4	595141073	37,06,20	1,55,40	Barranco del Tremecin 2 (east side of Bc	12	4					500	400	100	
1127	3	4	595841066	37,06,00	1,55,25	Cerro de los Peralicos 1 (higher)	0	0					700	600	100	
1128	3	4	595841075	37,06,02	1,55,20	Cerro de los Peralicos 2 (lower)	1	2	13	2			500	300	200	
1129	3	4	596241076	37,06,30	1,55,05	Cortijo Cabrera 1 ("La Molata" on the map	1	1	1	3	13	4	450	350	100	
1130	3	4	596541086	37,07,05	1,54,55	Cortijo Cabrera 2 (Cerro de la Pilica)	1	2	3	2	13	2	400	250	150	
1131	3	4	597541073	37,06,20	1,54,15	Cerro de los Ericos 1	0	0					700	600	100	
1132	3	4	598241075	37,06,30	1,53,40	Barranco de Mofar 1 (northeast facing) (e	0	0					650	450	200	
1133	3	4	598541080	37,06,40	1,53,30	Barranco de Mofar 2 (southwest facing) (v	0	0					600	450	150	
1134	3	4	598541083	37,06,52	1,53,30	Barranco de Mofar 3 (north facing) (west o	0	0					600	400	200	
1135	3	4	599541085	37,07,05	1,52,50	Cerro de Cucar - Risco del Moro	13	2					700	500	200	
1136	3	4	598541088	37,07,10	1,53,25	Majada de las Palomas 1 (southwest facir	0	0					450	300	150	
1137	3	4	598541090	37,07,15	1,53,15	Majada de las Palomas 2 (north facing)	0	0					450	350	100	
1138	3	4	598841099	37,07,46	1,53,00	Cerro de Judio	0	0					350	250	100	
1139	3	11	599741108	37,08,18	1,52,40	Cerro de los Caballones	13	1					300	250	50	
1140	3	11	600141111	37,08,25	1,52,12	Cerro de Juancho	13	1					160	140	20	
1141	1	11	588241059	37,05,40	2,00,35	Collado de la Limera	0						550	400	150	
1142	1	11	588941056	37,05,30	2,00,00	Rambla de la Parrica	13	2					550	400	150	

RS Width (m)	Runout Distance (m)	AZ Width (m)	AZ Height (m)	Volume (m^3)	H/L	Angle of Reach (tan H/L)	Type 1	Type 2	Type 3	Type 4	Type 5	Type 6	State	Style	Distribution	Cause 1	Cause 2	Cause 3	Cause 4	Cause 5	Cause 6	Cause 7	Cause 8
50	50	50		65,462.94	1	45	102	104					4	3	1								
75	50	75		98,194.41	1	45	102	104					4	3	1								
350	50	350		549,888.67	1.2	50	102	1103	1002	1102			4	3	1	4	6	7	8	11	14	21	25
250	50	250		523,703.50	1.6	58	102	1103	1002	1102			4	3	1	4	6	7	8	11	14	21	25
400	60	400		1,256,888.39	1.66	59	102	1103	1002	1102			4	3	1	4	6	7	8	11	14	21	25
350	250	350		6,415,367.82	0.56	29	102	1103	1002	1102			4	3	1	4	6	7	8	11	14	21	25
250	200	250		4,451,479.71	0.85	40	102	1103	1002	1102			4	3	1	4	6	7	8	11	14	21	25
250	50	250		392,777.62	1.2	50	102	1103	1002	1102			4	3	1	4	6	7	8	11	14	21	25
700	50	700		1,832,962.23	2	63	102	1103	1002	1102			4	3	1	4	6	7	8	11	14	21	25
250	60	250		785,555.24	1.66	59	102	1103	1002	1102			4	3	1	4	6	7	8	11	14	21	25
500	250	500		10,474,069.91	0.64	33	102	1103	1002	1102			4	3	1	4	6	7	8	11	14	21	25
100	200	100		1,361,629.09	0.65	33	102	1103	1002	1102			4	3	1	4	6	7	8	11	14	21	25
750	170	750		10,015,829.35	0.88	41	102	1103	1002	1102			4	3	1	4	6	7	8	11	14	21	25
200	150	200		2,199,554.68	0.93	43	102	1103	1002	1102			4	3	1	4	6	7	8	11	14	21	25
150	40	150		125,688.84	1	45	102	1103	1002	1102			4	3	1	4	6	7	8	11	14	21	25
200	400	200		8,379,255.93	0.5	27	102	1103	1002	1102			4	3	1	4	6	7	8	11	14	21	25
200	200	200		2,094,813.98	0.5	27	102	1103	1002	1102			4	3	1	4	6	7	8	11	14	21	25
200	200	200		2,094,813.98	0.5	27	102	1103	1002	1102			4	3	1	4	6	7	8	11	14	21	25
150	20	150		47,133.31	1.5	56	102	1103	1002	1102			4	3	1	4	6	7	8	11	14	21	25
200	100	20		733,184.89	0.7	35	102	1103	1002	1102			3	3	1	6	7	8	11	14	21	29	
200	50	200		104,740.70	0.4	22	102	1102	1002	1102			4	3	1	6	7	8	11	14	21	29	
700	150	700		8,248,330.05	1	45	400	500					4	3	7								
200	100	200		1,047,406.99	1	45	400	500					4	3	1	4	6	7	8	11	14	21	25
25	10	25		6,546.29	5	79	102	1103	1002	1102			4	3	1	4	6	7	8	11	14	21	25
20	10	20		4,189.63	4	76	102	1103	1002	1102			4	3	1	4	6	7	8	11	14	21	25
20	10	20		3,142.22	3	72	102	1103	1002	1102			4	3	1	4	6	7	8	11	14	21	25
500	350	500		9,164,811.17	0.29	16	102	1103	1002	1102			4	3	1	6	7	8	11	21	25	29	
100	30	100		78,555.52	1.66	59	102	1102	1002	1102			4	3	1	4	6	7	8	11	14	21	25
20	30	20		15,711.10	1.66	59	102	1102	1002	1102			4	3	1	4	6	7	8	11	14	21	25
20	30	20		21,995.55	2.33	67	102	1102	1002	1102			4	3	1	4	6	7	8	11	14	21	25
50	30	50		31,422.21	1.33	53	102	1102	1002	1102			4	3	1	4	6	7	8	11	14	21	25
50	200	50		523,703.50	0.5	26	102	1102	1103	1002			4	3	1	4	6	7	8	11	14	21	25
							102	1102	1103	1002			4	3	1	4	6	7	8	11	14	21	25
100	100	100		523,703.50	1	45	102	203					4	3	1	4	6	7	8	11	14	21	25
							102	1102	1103	203			4	3	1	4	6	7	8	11	21	25	29
10							102						4	5	1	6	8	11	18	21	25	29	
450	200	450		4,713,331.46	0.5	27	102	402	1101	1102	1002		4	3	1	4	6	11	21	25	31	37	40

RS Width (m)	Runout Distance (m)	AZ Width (m)	AZ Height (m)	Volume (m^3)	H/L	Angle of Reach (tan H/L)	Type 1	Type 2	Type 3	Type 4	Type 5	Type 6	State	Style	Distribution	Cause 1	Cause 2	Cause 3	Cause 4	Cause 5	Cause 6	Cause 7	Cause 8
200		180					102	1103	1002	1102			4	3	1	4	6	7	8	11	14	21	25
100	50	100		78,555.52	0.6	31	102	1103	1002	1102			4	3	1	4	6	7	8	11	14	21	25
200	100	200		628,444.19	0.6	31	102	1103	1002	1102			4	3	1	4	6	7	8	11	14	21	25
150	50	140		117,833.29	0.6	31	102	1103	1002	1102			4	3	1	4	6	7	8	11	14	21	25
100	100	100		261,851.75	0.5	26	104						1	3	1								
10	4	10	2	209.48	2.5	57	102						4	3	1	6	7	8	11	14	21	25	29
10							102	104					4	3	1	6	7	8	11	14	21	25	
15							102	104					4	3	1	6	7	8	11	14	21	25	
10							102	104					4	3	1	6	7	8	11	14	21	25	40
5	5	5	2	130.93	2	63	102						4	3	1	2	7	8	14	21	30		
8	3	10	8	251.38	2	63	102						4	3	1	2	7	8	14	21	30		
125	50	125	30	130,925.87	0.8	39	401						4	3	7	2	4	6	7	8	9	10	14
100	40	100	30	83,792.56	1	45	401						4	3	7	2	4	6	7	8	9	10	14
200	10	200	20	31,422.21	3	72	403	102					4	3	1	2	4	6	7	8	9	10	14
5	5	20	8	130.93	2	63	104						4	3	5	6	7	8	10	11	14	18	21
400	30	400	30	251,377.68	1.33	53	402	104					4	3	5	6	7	8	9	10	11	14	18
5	5	5	1	65.46	1	45	104						4	5	1	6	7	10	11	14	18	21	25
5	5	5	1	65.46	1	45	104						4	5	1	6	7	10	11	14	18	21	25
5	5	5	1	65.46	1	45	104						4	5	1	6	7	10	11	14	18	21	25
5	2	5	1	26.19	2.5	68	104						4	5	1	6	7	10	11	14	18	21	25
150	20	150	20	47,133.31	1.5	56	401						4	3	5	6	7	8	9	11	14	18	21
5	5	5	5	65.46	1	45	104						4	3	1	6	7	8	11	14	21	25	29
5	5	5	5	130.93	2	63	101						4	3	1	6	7	8	11	14	21	25	29
3	2	4	2	9.43	1.5	56	102	202					4	3	1	6	7	8	11	14	21	25	29
100	50	100	40	157,111.05	1.2	50	403						4	3	5	6	7	8	11	14	21	25	29
5	12	5	2	157.11	0.4166	23	102	104					4	3	1	6	7	8	10	14	21	25	29
100	50	100	40	157,111.05	1.2	50	403						4	3	5	6	7	8	11	14	21	25	29
10	5	10	5	523.70	4	76	102						4	3	1	6	7	8	9	10	14	21	30
10	9	15	2	942.67	2.22	24	101	102	203				4	3	5	4	7	8	11	14	21	29	
10	5	10	5	261.85	2	63	102	203					4	3	5	4	7	8	11	14	21	29	
600	150	600	40	2,356,665.73	0.33	18	403	406	102	203	1000	1100	4	3	5	2	6	7	8	9	10	11	14
70	50	70	15	36,659.24	0.4	22	401						4	3	5	2	6	7	8	9	10	11	14
150	20	150	20	39,277.76	1.25	51	402	104	203				4	3	5	2	6	7	8	9	10	11	14
150	25	150	25	78,555.52	1.6	58	402	104	203				4	3	5	2	6	7	8	9	10	11	14
5	6	5	2	157.11	1.66	59	101	102					4	3	1	6	7	8	11	14	21	25	29
10	15	10	5	3,142.22	2.66	69	101	102					1	3	1	6	7	8	11	14	21	25	29
75	15	70	6	23,566.66	2.66	69	101	102					1	3	1	6	7	8	11	14	21	25	29

RS Width (m)	Runout Distance (m)	AZ Width (m)	AZ Height (m)	Volume (m^3)	H/L	Angle of Reach (tan H/L)	Type 1	Type 2	Type 3	Type 4	Type 5	Type 6	State	Style	Distribution	Cause 1	Cause 2	Cause 3	Cause 4	Cause 5	Cause 6	Cause 7	Cause 8
50	15	50	5	7,855.55	1.33	53	101	102					1	3	1	6	7	8	11	14	21	25	29
5	3	5	3	39.28	1.66	59	102						4	5	5	6	7	8	11	21	25	29	31
20	50	20	3	10,474.07	0.4	22	101	102	202				4	3	5	6	7	8	11	14	21	25	29
25	40	15	4	20,948.14	1	45	101	102	201	202			4	3	1	6	7	8	11	14	21	25	29
20	35	15	3	14,663.70	1.14	49	101	102	201	202			4	3	1	6	7	8	11	12	21	25	29
700	30	700	45	549,888.67	1.66	59	402	1102	1103	1105	1002	102	4	3	1	2	3	6	8	9	11	14	18
50	10	50		5,237.03	2	63	401	1102	1002				4	3	1	8	9	10	11	18	21	25	31
50	60	50	3	62,844.42	0.66	34	101	102	201	202			4	3	1	6	7	8	11	12	21	25	29
5	2	4	1	15.71	1.5	56	102						3	3	1	6	7	8	11	12	21	25	29
10	10	10	1	1,047.41	2	63	102	103					1	2	1	6	7	8	11	21	29	31	32
10	20	10		3,142.22	1.5	56	101	102	202				1	3	1	6	7	8	11	14	21	25	29
							400	702					7										
20							104	1102	1103				1	3	1	4	17	21	25	29	31	40	
							400	702					7										
30							104	1102	1103				1	3	1	4	17	21	25	29	31	40	
10		10					104	201	1102	1103			1	3	1	6	7	8	11	17	21	25	29
							903						7										
800	150	800	45	3,142,220.97	0.06	18	102	203	400	600	800		4	2	5	6	7	8	11	14	21	25	29
	5	10	3		6	80	101						4	3	1	4	6	8	9	14	21	25	29
	3	8	3		10	84	101						4	3	1	4	6	8	9	14	21	25	29
	3	5	3		10	84	101						4	3	1	4	6	8	9	14	21	25	29
50	75	50	20	98,194.41	0.66	34	401						4	3	1	6	7	8	9	10	11	17	21
10	20	10	8	1,047.41	0.5	27	102	104	1002	1102	1103		4	3	1	6	7	8	11	21	25	40	
6	5	6	8	157.11	2	63	102	104	1002	1102	1103		4	3	1	6	7	8	11	21	25	40	
75	10	75	20	11,783.33	3	72	104						4	3	1	6	7	8	10	11	18	21	25
5	10	10	4	523.70	2	63	104	1001	1002	1101	1102		3	3	1	6	7	8	9	10	11	14	18
50	10	50	10	5,237.03	2	63	104	401	1001	1002	1101	1102	3	3	1	6	7	8	9	10	14	14	18
30	30	20	10	11,783.33	0.833	40	104	401	1001	1002	1101	1102	3	3	5	6	7	8	9	10	14	14	18
60	30	50	15	28,279.99	1	45	104	401	1001	1002	1101	1102	3	3	5	6	7	8	9	10	14	14	18
30	30	30	20	23,566.66	1.666	59	401	101	1001	1002	1101	1102	3	3	5	6	7	8	9	10	14	18	31
70	50	75	10	36,659.24	0.4	22	402	1001	1002	1101	1102	600	3	3	5	6	7	8	9	10	14	18	21
80	30	100	10	25,137.77	0.666	34	402	1001	1002	1101	1102	600	3	3	5	6	7	8	9	10	14	18	21
80	80	80	10	100,551.07	0.375	21	401	600	1001	1002	1101	1102	3	3	5	6	7	8	9	10	14	18	21
160	30	160	10	75,413.30	1	45	402	1001	1002	1101	1102	600	3	3	1	6	7	8	9	10	14	18	21
100	50	100	10	78,555.52	2	63	104	402	1001	1002	1101	1102	3	3	1	6	7	8	9	10	14	18	21
600	75	600	20	942,666.29	0.533	28	104	402	1001	1002	1101	1102	3	3	1	6	7	8	9	10	14	18	21
500	50	500	10	261,851.75	0.4	22	104	402	1001	1002	1101	1102	3	3	1	6	7	8	9	10	14	18	21

RS Width (m)	Runout Distance (m)	AZ Width (m)	AZ Height (m)	Volume (m^3)	H/L	Angle of Reach (tan H/L)	Type 1	Type 2	Type 3	Type 4	Type 5	Type 6	State	Style	Distribution	Cause 1	Cause 2	Cause 3	Cause 4	Cause 5	Cause 6	Cause 7	Cause 8
15	10	15	4	785.56	1	45	203	204	1001	1002	1101	1102	3	3	1	6	7	8	9	10	18	21	25
5	4	6	2				104	1001	1002	1101	1102		3	3	1	6	7	8	9	10	14	14	18
20	15	20	10	4,713.33	2	63	104	401	1001	1002	1101	1102	3	3	1	11	14	18	21	25	29		
125	50	120	20	130,925.87	0.8	39	104	401	1001	1002	1101	1102	3	3	1	11	14	18	21	25	29	30	
200	20	200	20	83,792.56	2	63	104	401	1001	1002	1101	1102	3	3	1	11	14	18	21	25	29	30	
5	10	5	3	261.85	1	45	104	1002	1102				3	3	1	11	14	21	25	29	30		
							100	1001	1002	1101	1102		3	3	1	10	21	25	29	30			
							100	1001	1002	1101	1102		3	3	1	10	21	25	29	30			
100	25	100	5	26,185.17	0.8	39	100	1001	1002	1101	1102		3	3	1	10	21	25	29	30			
100	25	100	5	26,185.17	0.8	39	100	1001	1002	1101	1102		3	3	1	10	21	25	29	30			
10	6	10	15	628.44	3.3	73	102	104	203	204			1	5	1	10	21	25	29	30			
4	3	4	2	31.42	1.66	59	104						4	3	1	6	7	8	9	10	21		
5	4	5	2	104.74	2.5	68	104						4	3	1	6	7	8	9	10	21		
1	1	1	2	2.62	5	79	102						3	5	1	7	8	14	21	25	29		
							102	1002	1101	1102			1	5	1	6	7	8	9	10	14	18	21
5	5	5	3	130.93	2	63	102	104	1001	1002	1101	1102	4	3	1	6	7	8	9	10	14	18	21
125	20	125	20	52,370.35	2	63	402	104	1001	1002	1101	1102	4	3	5	6	7	8	9	11	14	21	25
100	20	100	30	52,370.35	2.5	68	402	102	1001	1002	1101	1102	4	5	1	6	7	8	9	14	21	25	29
50	10	50	20	5,237.03	2	63	402	1001	1002	1101	1102		4	3	5	6	7	8	9	10	14	21	25
15	10	15	10	2,356.67	3	72	402	1001	1002	1101	1102		4	5	5	6	7	8	9	10	14	21	25
100	20	100	2	10,474.07	0.5	27	501						4	1	1	6	7	8	11	14	17	21	25
25	5	25	5	654.63	2	63	104	1001	1002	1101	1102		4	3	1	6	7	8	11	21	25	29	30
100	10	100	15	10,474.07	2	63	102	104	203				4	3	1	6	7	8	14	21	25	29	
100	10	100	15	10,474.07	2	63	102	104	203				4	3	1	6	7	8	14	21	25	29	
40	10	40	4	4,189.63	2	63	102	104	203	204			4	3	1	6	7	8	14	21	25	29	
10	5	10	2	785.56	6	80	102	104	203	204			4	3	1	6	7	8	14	21	25	29	
5	3	5	1	274.94	10	84	102	104	203	204			4	3	1	6	7	8	14	21	25	29	
5	3	5	1	235.67	10	84	102	104					4	3	1	6	7	8	14	21	25	29	
10	5	10	1	261.85	2	63	501	102	103				4	3	1	6	7	8	14	21	25	29	
4	5	5	4	52.37	1	45	104	401	1001	1002	1101	1102	4	3	1	6	7	8	9	10	14	18	21
5	4	5	4	52.37	2.5	68	101	1001	1002	1101	1102		4	3	1	6	7	8	9	10	14	18	21
5	2	5	3	26.19	2.5	68	102	104	203				4	5	1	6	7	8	11	21	25	29	
5	2	5	3	26.19	2.5	68	102	104	203				4	5	1	6	7	8	11	21	25	29	
5	2	5	3	26.19	2.5	68	102	104	203				4	5	1	6	7	8	11	21	25	29	
	20				1	45	102	1101	1103	1002			4	3	1	6	7	8	10	11	14	21	25
50	30	50		23,566.66	1	45	102	104					4	3	1	6	7	8	18	21	25	29	
							102	104					4	3	1	6	7	8	18	21	25	29	

RS Width (m)	Runout Distance (m)	AZ Width (m)	AZ Height (m)	Volume (m^3)	H/L	Angle of Reach (tan H/L)	Type 1	Type 2	Type 3	Type 4	Type 5	Type 6	State	Style	Distribution	Cause 1	Cause 2	Cause 3	Cause 4	Cause 5	Cause 6	Cause 7	Cause 8
750	75	750	30	1,472,916.08	0.666	34	102	104	203				4	3	1	6	7	8	14	18	21	25	29
500	75	500	20	785,555.24	0.533	28	102	104	203				4	3	1	6	7	8	14	18	21	25	29
							102	104	203				4	3	1	6	7	8	18	21	25	29	
250	100	200	10	654,629.37	0.5	27	102	104	401				4	2	5	6	7	8	18	21	25	29	30
50	25	50	15	26,185.17	1.6	58	104	102	401				4	3	1	6	7	8	11	14	21	25	29
100	25	100	10	39,277.76	1.2	50	104	102	401				4	3	1	6	7	8	11	14	21	25	29
	150	100	40		0.33	18	400						7			6	7	8	9	10	11	14	18
	150	100	30		0.33	18	400						7			6	7	8	9	10	11	14	18
							400						7			6	7	8	9	10	11	14	18
							400						7			6	7	8	9	10	11	14	18
							400						7			6	7	8	9	10	11	14	18
1250	250	1000		11,456,013.96	0.28	16	102	104	203	204			4	3	1	6	7	8	9	10	11	18	21
700	250	700		7,331,848.93	0.32	18	102	104	203	204			4	3	1	6	7	8	9	10	11	18	21
60	30	50	10	18,853.33	0.666	34	401						4	3	5	6	7	8	9	10	11	14	18
150	150	10	5	353,499.86	0.2	11	401						4	3	5	6	7	8	9	10	11	14	18
80	50	80		62,844.42	0.6	31	401						4	3	1	6	7	8	9	10	11	14	18
100	60	100		94,266.63	0.5	26	401						4	3	1	6	7	8	9	10	11	14	18
100	70	100	15	146,636.98	0.571	30	401						4	3	5	6	7	8	9	10	11	14	18
750	100	750	10	1,963,888.11	0.5	27	102	104	203	204			4	2	1	6	7	8	9	10	11	18	21
500	350	500	15	9,164,811.17	0.286	16	402	102	104	203	204		4	3	1	6	7	8	9	10	11	18	21
40	75	40		39,277.76	0.33	18	500	400					4	3	7	7	8	11	21	25	29		
200	100	200		733,184.89	0.7	35	504						7			7	8	11	21	25	29		
100	200	100		837,925.59	0.4	22	504						7			7	8	11	21	25	29		
200	150	200		2,827,998.87	1.2	50	102	1103	1002	102			4	3	1	7	8	11	21	25	29		
75	50	75		98,194.41	1	45	504						4	3	7	7	8	11	21	25	29		
25	40	25		26,185.17	2	63	500						4	3	7	7	8	11	21	25	29		
25	40	25		26,185.17	2	63	500						4	3	7	7	8	11	21	25	29		
200	60	200		314,222.10	0.83	40	504						4	3	7	7	8	11	21	25	29		
100	20	100		41,896.28	2	63	504						4	3	7	7	8	11	21	25	29		
100	40	100		167,585.12	2	63	500	100					7										
200	100	150		1,571,110.49	1.5	56	102	1101	1102	1002	500		4	3	1								
							102	1101	1102	1002	500		4	3	1								
							102	1101	1102	1002	500		4	3	1								
100	200	50	2	942,666.29	0.45	24	102						4	3	1	7	8	9	10	11	18	21	25
120	350	40	2	2,639,465.62	0.34	19	102						4	3	1	7	8	9	10	11	18	21	25
500	250	500	1	6,546,293.69	0.4	22	102						4	3	1	7	8	9	10	11	18	21	25
200	180	200	1	1,319,732.81	0.39	21	102						4	3	1	7	8	9	10	11	18	21	25

RS Width (m)	Runout Distance (m)	AZ Width (m)	AZ Height (m)	Volume (m^3)	H / L	Angle of Reach (tan H/L)	Type 1	Type 2	Type 3	Type 4	Type 5	Type 6	State	Style	Distribution	Cause 1	Cause 2	Cause 3	Cause 4	Cause 5	Cause 6	Cause 7	Cause 8
10	5	10	5	523.70	4	76	102						4	3	1	6	7	8	9	10	14	21	
5	5	5	2	130.93	2	63	102						4	3	1	6	7	8	9	10	14	21	
10	5	10	2	261.85	2	63	102						4	3	1	6	7	8	9	10	14	21	
10	5	10	5	785.56	6	81	102						4	3	1	6	7	8	9	10	14	21	
20	5	20	2	523.70	2	63	102						4	3	1	6	7	8	9	10	14	21	
													7										
100	50	100		39,277.76	0.3	17	401						4	3	1	7	8	9	10	14	18	21	30
150	50	150		117,833.29	0.6	31	401						4	3	1	7	8	9	10	14	18	21	30
50	20	50		15,711.10	1.5	56	102						4	3	1	7	8	9	10	14	18	21	30
100	25	50		52,370.35	1.6	58	401	102	1001	1002	1101	1102	4	3	1	7	8	9	10	14	18	21	30
150	50	150		117,833.29	0.6	31	401	102	1001	1002	1101	1102	4	3	1	7	8	9	10	14	18	21	30
100	40	100		83,792.56	1	45	401	102	1001	1002	1101	1102	4	3	1	7	8	9	10	14	18	21	30
50	30	40		39,277.76	1.666	59	401	102	1001	1002	1101	1102	4	3	1	7	8	9	10	14	18	21	29
50	40	50		52,370.35	1.25	51	401	102	1001	1002	1101	1102	4	3	1	7	8	9	10	14	18	21	29
70	60	70		109,977.73	0.833	40	401	102	1001	1002	1101	1101	4	3	1	7	8	9	10	14	18	21	29
250	70	250		458,240.56	0.714	36	102	1001	1002	1101	1102		4	3	1	7	8	9	10	14	18	21	29
20	10	20		1,047.41	1	45	102	1001	1002	1101	1102		4	3	1	7	8	9	10	14	18	21	29
100	50	100		104,740.70	0.8	39	401	102	1001	1002	1101	1102	4	3	1	7	8	9	10	14	18	21	29
							102									7	8	9	10	14	18	21	29
150	150	150	10	706,999.72	0.4	22	501						4	2	5	7	9	10	11	18	21	25	
30	15	30	7	2,356.67	0.666	34	401	1002	1102				4	3	5	6	7	8	9	10	11	14	21
150	40	150	20	94,266.63	0.75	37	401	1002	1102				4	3	5	6	7	8	9	10	11	14	21
25	20	25	10	5,237.03	1	45	401	1002	1102				4	3	5	6	7	8	9	10	11	14	21
100	20	100	4	31,422.21	1.5	56	104	400	1002	1102			4	3	1	10	11	14	21				
20	5	10	6	523.70	2	63	104	400	1005				1	3	5	7	8	9	10	11	14	18	21
0	2	5	1	0.00	1	45	104						4	5	1	2	4	18	21	30			
100	75	100	10	196,388.81	0.666	34	402	504					4	2	1	7	8	9	10	11	21	25	
180	75	150	40	353,499.86	0.66	34	402	504					3	2	1	7	8	9	10	11	21	25	
8	5	10	1	209.48	2	63	102	104					4	3	1	6	7	8	10	11	14	21	
20	10	25	4	523.70	0.5	27	104	1001	1002	1101	1102		1	3	1	3	6	7	21	8	10	11	14
15	4	15	1	314.22	2.5	68	104	1001	1002	1101	1102		4	3	1	3	6	7	8	9	10	18	21
15	12	10	2	942.67	0.833	40	100	1002	1101	1102	1001		4	3	1	6	7	8	10	11	14	21	25
5	5	6		130.93	2	63	100	1002	1101	1102	1001		4	3	1	4	6	7	8	10	11	14	21
150	60	150	20	188,533.26	0.666	34	401	1001	1002	1101	1102		4	3	5	4	6	7	8	9	10	11	14
300	60	250	10	188,533.26	0.333	18	402	1001	1002	1101	1102		4	3	5	4	6	7	8	9	10	11	14
90	60	100	20	113,119.95	0.666	34	402	1001	1002	1101	1102		4	3	5	4	6	7	8	9	10	11	14
15	12	15	2	942.67	0.833	40	104	1001	1002	1101	1102		4	3	1	6	7	8	10	14	21	25	29

RS Width (m)	Runout Distance (m)	AZ Width (m)	AZ Height (m)	Volume (m^3)	H/L	Angle of Reach (tan H/L)	Type 1	Type 2	Type 3	Type 4	Type 5	Type 6	State	Style	Distribution	Cause 1	Cause 2	Cause 3	Cause 4	Cause 5	Cause 6	Cause 7	Cause 8
500	200	500	50	4,189,627.96	0.4	22	402	403	1001	1002	1101	1102	4	3	5	6	7	8	9	10	11	14	18
250	70	250	30	366,592.45	0.571	30	402	403	1001	1002	1101	1102	2	3	5	6	7	8	9	10	11	14	18
250	125	250	40	981,944.05	0.48	26	402	403	1001	1002	1101	1102	2	3	5	6	7	8	9	10	14	18	21
15	12	15	4	942.67	0.833	40	401						4	3	7	7	8	9	10	18	21	30	
15	20	15	2	1,571.11	0.5	27	401						4	3	7	7	8	9	10	18	21	30	
20	25	20	2	2,618.52	0.4	22	401						4	3	7	7	8	9	10	18	21	30	
15	30	10	1	4,713.33	0.666	34	101	1102	1103	1105			4	3	1	7	10	14	17	18	20	21	25
25	30	25	4	11,783.33	1	45	102	104	203	204	1000	1100	2	3	5	6	7	8	9	10	11	18	21
20	20	25	4	4,189.63	1	45	102	104	203	204	1000	1100	2	3	5	6	7	8	9	10	11	18	21
30	45	30	4	21,209.99	0.666	34	102	104	203	204	1000	1100	2	3	5	6	7	8	9	10	11	18	21
5	50	8	1	5,237.03	0.8	39	104						4	3	1	6	7	8	9	10	11	18	21
25	50	25	5	19,638.88	0.6	31	104	400	1001	1002	1101	1102	2	3	5	6	7	8	9	10	11	14	20
75	25	75	15	19,638.88	0.8	39	104						4	3	5	6	7	8	9	10	11	14	18
20	40	25	30	20,948.14	1.25	51	104	203					4	3	1	6	7	8	9	10	11	14	18
10	30	10	20	7,855.55	1.666	59	102	104	203				4	3	1	6	7	8	9	10	11	14	18
500	75	500	10	981,944.05	0.666	34	903	203	104	401			4	3	1	6	7	8	9	10	11	14	18
750	100	750	40	1,963,888.11	0.5	27	903	203	104	402	904		4	3	1	6	7	8	9	10	11	14	18
60	100	50	20	219,955.47	0.7	35	903	104	204				4	2	1	6	7	8	9	10	11	18	21
10	15	10	18	1,571.11	1.33	53	401						4	5	5	9	10	11	14	18	21	25	30
100	350	60	20	1,099,777.34	0.171	10	702						7										
75	100	50	5	235,666.57	0.6	31	903	104	203				4	2	1	6	7	8	9	10	11	18	21
600	100	600	5	3,142,220.97	1	45	903	104	203	402			4	2	1	6	7	8	9	10	11	18	21
1250	600	1250		58,916,643.23	0.25	14	903	104	203	402			4	3	1	6	7	8	9	10	11	18	21
20	30	20		6,284.44	0.66	34	102	104					4	3	1	6	7	8	10	11	14	18	21
30	30	30		9,426.66	0.66	34	102	104					4	3	1	6	7	8	10	11	14	18	21
10	20	8	1	3,142.22	1.5	56	104	102					4	3	1	7	8	9	10	11	18	21	25
15	10	10	20	2,356.67	3	72	102	104	203				4	5	1	6	7	8	10	14	21	25	29
150	15	150	10	47,133.31	2.66	69	102	104	203				4	5	1	6	7	8	10	14	21	25	29
250	250	250	100	4,909,720.27	0.6	31	102	203	403	504			3	2	5	6	7	8	9	10	11	14	18
100	200	70	10	1,047,406.99	0.5	27	903	104	203	102			4	3	1	7	8	9	10	11	18	21	25
100	150	70	10	392,777.62	0.333	18	903	104	203	102			4	3	1	7	8	9	10	11	18	21	25
100	250	50	50	1,440,184.61	0.44	24	903	402	203	104	102		4	3	5	6	7	8	9	10	11	18	21
500	200	500	20	2,618,517.48	0.25	14	903	402	203	104	102		4	2	5	6	7	8	9	10	11	18	21
400	500	500	50	10,474,069.91	0.2	11	903	402	203	104	102		4	2	5	6	7	8	9	10	11	14	18
200	150	75	10	1,413,999.44	0.6	31	903	204	104				4	2	1	6	7	8	9	10	11	18	21
300	300	100	10	4,713,331.46	0.333	18	903	204	104				4	2	1	6	7	8	9	10	11	18	21
300	250	300	80	4,320,553.84	0.44	24	903	401	104	203			4	2	5	6	7	8	9	10	11	18	21

RS Width (m)	Runout Distance (m)	AZ Width (m)	AZ Height (m)	Volume (m^3)	H/L	Angle of Reach (tan H/L)	Type 1	Type 2	Type 3	Type 4	Type 5	Type 6	State	Style	Distribution	Cause 1	Cause 2	Cause 3	Cause 4	Cause 5	Cause 6	Cause 7	Cause 8
300	300	200	20	6,127,330.90	0.433	23	903	402	203	104			4	2	5	6	7	8	9	10	11	18	21
25	20	30	2	20,948.14	4	76	104	1103	1105				4	2	1	6	7	8	9	10	11	14	18
10	5	10	4	1,047.41	8	83	104	203	102				4	3	1	6	7	8	11	14	21	25	29
12	5	12	4	1,256.89	8	83	104	203	102				4	3	1	6	7	8	11	14	25	29	
400	500	400	75	14,663,697.87			805	903	901	403	104	203	1	3	7	6	7	8	9	10	11	14	18
	750	2000	200		0.333	18	403	303	102				1	3	1	7	8	9	10	11	14	18	21
300	500	300	75	7,855,552.43	0.2	11	403	303	102				4	3	1	7	8	9	10	11	14	18	21
200	800	100	50	15,082,660.67	0.225	13	903	403	702	203	102		4	2	1	6	8	9	10	11	14	18	21
200	900	100	50	16,967,993.25	0.2	11	903	403	702	203	102		4	2	1	6	8	9	10	11	14	18	21
							903	402	203	104			4	2	1	6	8	9	10	11	14	18	21
150	450	75	10	3,534,998.59	0.22	12	903	402	203	104			4	2	1	6	8	9	10	11	14	18	21
500	125	500		2,618,517.48	0.64	33	903	402	203	104			4	2	1	6	8	9	10	11	14	18	21
200	250	150		2,094,813.98	0.32	18	903	402	203	104			4	2	1	6	8	9	10	11	14	18	21
125	300	120		1,767,499.30	0.3	17	903	402	203	104			4	2	1	6	8	9	10	11	14	18	21
350	500	350		5,498,886.70	0.12	7	903	402	203	104			4	3	1	6	8	9	10	11	14	18	21
400	500	400		26,185,174.77	0.5	26	402	203	102				4	2	5	6	7	8	9	10	14	18	21
20	10	20	5	2,094.81	2	63	102						4	3	1	6	7	8	10	14	21		
20	10	20	5	2,094.81	2	63	102						4	3	1	6	7	8	10	14	21		
300	20	350	15	157,111.05	2.5	68	102	203	401				4	2	5	4	5	6	7	8	11	14	18
100		90					102						4	3	1	6	7	8	9	10	11	14	21
100		90					102						4	3	1	6	7	8	9	10	11	14	21
150		140					102						4	3	1	6	7	8	9	10	11	14	21
60		50					102						4	3	1	6	7	8	9	10	11	14	21
							102						4	3	1	6	7	8	9	10	11	14	18
							102						4	3	1	6	7	8	9	10	11	14	18
250		250					402	540					4	3	1	6	7	8	9	10	11	14	18
2000		2000					102						4	3	1	6	7	8	9	10	11	14	18
1000		1000					102						4	3	1	6	7	8	9	10	11	14	18
50	15	50	2	11,783.33	2	63	401	1001	1002	1101	1102		4	3	1	6	7	8	9	10	11	14	21
	250				0.56	29	102	1101	1103	1002	1105		4	3	1	4	6	7	8	9	10	11	21
150	200	150		1,571,110.49	1	45	102	1101	1103	1002	1105		4	3	1	4	6	7	8	9	10	11	21
150	150	150		353,499.86	0.2	11	102	1101	1103	1002	1105		4	3	1	4	6	7	8	9	10	11	21
	200				0.5	27	102	1101	1103	1002	1105		4	3	1	4	6	7	8	9	10	11	21
	100				1.5	56	102	1101	1103	1002	1105		4	3	1	4	6	7	8	9	10	11	21
	200				0.5	27	102	1101	1103	1002	1105		4	3	1	4	6	7	8	9	10	11	21
200	600	200		12,568,883.89	0.33	18	102	1101	1103	1002	1105		4	3	1	4	6	7	8	9	10	11	21
	100				1	45	102	1101	1103	1002	1105		4	3	1	4	6	7	8	9	10	11	21

RS Width (m)	Runout Distance (m)	AZ Width (m)	AZ Height (m)	Volume (m^3)	H/L	Angle of Reach (tan H/L)	Type 1	Type 2	Type 3	Type 4	Type 5	Type 6	State	Style	Distribution	Cause 1	Cause 2	Cause 3	Cause 4	Cause 5	Cause 6	Cause 7	Cause 8
1200	300			28,279,988.75	0.5	27	102	1101	1103	1002	1105		4	3	1	4	6	7	8	9	10	11	21
300	150	300		4,713,331.46	1.33	53	102	1101	1103	1002	1105		4	3	1	4	6	7	8	9	10	11	21
400	200	400		4,189,627.96	2	63	102	1101	1103	1002	1105		4	3	1	4	6	7	8	9	10	11	21
	150				0.66	34	102	1101	1103	1002	1105		4	3	1	4	6	7	8	9	10	11	21
700	400	700		29,327,395.74	0.5	27	102	1101	1103	1002	1105		4	3	1	4	6	7	8	9	10	11	21
400	400	400		8,379,255.93	0.25	14	102	1101	1103	1002	1105		4	3	1	4	6	7	8	9	10	11	21
	200				0.75	37	102	1101	1103	1002	1105		4	3	1	4	6	7	8	9	10	11	21
330	300	300		5,184,664.60	0.33	18	102	1101	1103	1002	1105		4	3	1	4	6	7	8	9	10	11	21
750	350	750		27,494,433.51	0.57	30	102	1101	1103	1002	1105		4	3	1	4	6	7	8	9	10	11	21
750	400	750		23,566,657.29	0.375	21	102	1101	1103	1002	1105		4	3	1	4	6	7	8	9	10	11	21
400	400	400		16,758,511.85	0.5	27	102	1101	1103	1002	1105		4	3	1	4	6	7	8	9	10	11	21
1250	250	1250		32,731,468.46	0.8	39	102	1101	1103	1002	1105		4	3	1	4	6	7	8	9	10	11	21
90	400	100		2,827,998.87	0.375	21	102	1101	1103	1002	1105		4	3	1	4	6	7	8	9	10	11	21
200	200	200		2,094,813.98	0.5	27	102	1101	1103	1002	1105		4	3	1	4	6	7	8	9	10	11	21
150	100	150		785,555.24	1	45	102	1101	1103	1002	1105		4	3	1	4	6	7	8	9	10	11	21
500	100	500		1,309,258.74	0.5	27	102	1101	1103	1002	1105		4	3	1	4	6	7	8	9	10	11	21
400	50	400		209,481.40	0.4	22	102	1101	1103	1002	1105		4	3	1	4	6	7	8	9	10	11	21
100	150	100		1,178,332.86	1	45	102	1105	1103				4	3	1	4	6	7	8	9	10	11	21
200	150	150		2,356,665.73	1	45	102	1102	1105	1103			4	3	1	4	6	7	8	9	10	11	21

Cause 9	Cause 10	Cause 11	Cause 12	Mit. 1	Mit. 2	Aspect	Simple Profile	Angle	System	Facet	Element	Veg Cover	Veg Type	Drainage Conditions	Upper Unit Name (1)	Lower Unit Name (2)	Other Unit Name (3)	Upper Lithology (1)	Lower Lithology (2)	Other Lithology (3)
				0	0	5	6	6	2	4	9	3	4	3	10			11		
				0	0	2	6	6	2	4	9	3	4	3	10			11		
29				0	0	6	6	6	2	4	9	2	4	3	10			10		
29				0	0	6	6	6	2	4	9	2	4	3	10			10		
29				0	0	6	6	6	2	4	9	2	4	3	10			10		
29				0	0	5	6	6	2	4	9	2	4	3	10			10		
29				0	0	5	6	6	2	4	9	2	4	3	10			10		
29				0	0	2	6	6	2	4	9	2	4	3	10			10		
29				0	0	2	6	6	2	4	9	2	4	3	10			10		
29				0	0	1	6	6	2	4	9	2	4	3	10			10		
29				0	0	1	6	6	2	4	9	2	4	3	10			10		
29	40			0	0	4	1	5	2	4	35	2	4	3	10			11		
29				0	0	5	6	6	2	4	18	2	4	3	10			10		
29				0	0	1	6	6	2	4	9	2	4	3	10			10		
29				0	0	5	6	6	2	4	9	2	4	3	10			10		
29				0	0	7	2	5	2	2	2	2	4	3	10			10		
29				0	0	2	2	5	2	2	2	2	4	3	10			10		
29				0	0	4	2	5	2	4	2	2	4	3	10			10		
29				0	0	5	6	6	2	4	18	2	4	3	10			10		
				0	0	2	4	3	2	4	18	2	4	3	10			10		
				0	0	1	6	6	2	4	24	2	4	3	10			10		
				0	0	4	1	4	3	4	8	3	9	3	10			10		
29				0	0	2	4	3	2	4	8	2	4	3	10			11		
29				0	0	5	6	6	2	4	9	2	4	3	10			10		
29				0	0	1	6	6	2	4	9	2	4	3	10			10		
29				0	0	5	6	6	2	4	9	2	4	3	10			10		
				0	0	5	1	5	2	2	2	2	4	3	10			10		
29				0	0	5	4	4	2	4	18	2	4	3	10			11		
29				0	0	6	4	4	2	4	18	2	4	3	10			11		
29				0	0	6	4	4	2	4	18	1		3	10			11		
29				0	0	1	4	4	2	4	35	2	4	3	10			11		
29				0	0	7	1	3	2	2	35	2	4	3	10			10		
29				0	0	5	1	4	2	2	2	2	4	3	10			10		
29				0	0	2	1	4	2	2	2	2	4	3	10			10		
				0	0	3	1	5	2	2	35	3	4	3	10			10		
				0	0	4	1	4	2	2	2	2	4	3	10			10		
				0	0	3	7	5	2	2	2	2	4	5	10			10		

Cause 9	Cause 10	Cause 11	Cause 12	Mit. 1	Mit 2	Aspect	Simple Profile	Angle	System	Facet	Element	Veg Cover	Veg Type	Drainage Conditions	Upper Unit Name (1)	Lower Unit Name (2)	Other Unit Name (3)	Upper Lithology (1)	Lower Lithology (2)	Other Lithology (3)
29				0	0	3	6	5	2	4	18	2	4	3	10			10		
29				0	0	5	4	5	2	4	17	2	4	3	10			10		
29				0	0	2	2	5	2	4	9	1		3	10			10		
29				0	0	2	4	5	2	4	24	2	4	3	10			10		
				0	0	6	6	5	3	4	18	1	1	3				8		
32	40			0	0	2	6	6	3	4	4	1		3	6d			8		
				0	0	8	6	6	3	4	4	2	4	3	6d			8		
				0	0	1	6	6	3	4	4	2	4	3	6d			8		
				0	0	4	6	6	3	4	4	2	4	3	6d			8		
				0	0	5	3	5	4	6	18	2	4	3	2			1		
				0	0	6	6	6	4	6	18	2	4	3	2			1		
18	21			0	0	2	6	6	4	6	18	3	4	3	2			1		
18	21			0	0	2	6	6	4	6	18	3	9	3	2			1		
18	21	30		0	0	6	6	5	4	6	8	2	4	3	2			1		
25	29	30		0	0	7	6	5	3	3	18	2	4	3	2			1		
21	25	29	30	0	0	8	6	6	3	3	18	2	4	3	2			1		
				0	0	5	5	1	3	3	17	2	4	3	2			1		
				0	0	2	5	1	3	3	17	2	4	3	2			1		
				0	0	6	5	1	3	3	18	2	4	3	2			1		
				0	0	3	5	1	3	3	18	2	4		2			1		
25	29	30		0	0	4	1	4	3	3	18	2	4	3	2			1		
				0	0	1	5	1	3	3	18	2	4	3	2			1		
				0	0	7	1	3	3	5	18	3	4	3	2			1		
				0	0	6	6	5	3	5	18	2	4	3	2			1		
				0	0	1	6	5	4	5	18	3	4	3	2			1		
				0	0	7	6	6	3	10	35	2	4	3	5a	5a		7	5	
				0	0	4	6	3	4	10	10	2	4	3	2			1		
				0	0	4	1	5	3	10	19	1		3	2			1		
				0	0	5	6	6	3	3	3	1	4	3	5a			7		
				0	0	7	5	5	3	3	28	2	4	3	5a			7		
18	21	25	30	0	0	3	5	7	3	3	18	3	9	3	4	2		1	7	
18	21	25	30	0	0	2	4	5	3	10	6	3	4	3	2	4		1	7	
18	21	25	30	0	0	6	6	6	3	3	18	2	4	3	2	4		1	7	
18	21	25	30	0	0	6	6	6	3	3	18	2	4	3	2	4		1	7	
				0	0	6	6	6	3	3	4	1		3	5a			7		
32	40			0	0	3	6	6	3	3	4	1		5	1	5a		1	7	
32	40			0	0	2	6	6	3	3	18	1		3	5a			7		

Cause 9	Cause 10	Cause 11	Cause 12	Mit 1	Mit 2	Aspect	Simple Profile	Angle	System	Facet	Element	Veg Cover	Veg Type	Drainage Conditions	Upper Unit Name (1)	Lower Unit Name (2)	Other Unit Name (3)	Upper Lithology (1)	Lower Lithology (2)	Other Lithology (3)
32	40			0	0	6	6	6	3	3	21	2	4	3	5a			7		
32	35	38	40	7	0	7	6	6	3	3	4	1	1	5	5a	5a		7	6	
32	40			7	0	1	6	6	3	3	4	2	6	5	5a			7		
32	40			0	0	1	6	6	3	3	21	2	4	3	5a			7		
32	40			0	0	5	6	6	3	3	21	2	4	3	5a			7		
21	25	30		0	0	7	6	6	3	3	18	2	4	3	4a	2		1	7	
32	36	38	40	7		3	6	5	3	3	4	1		4	5a			7	5	
				7	0	7	6	6	3	3	4	1		3	5a			7		
32	40			7	0	7	6	6	3	3	4	1		4	5a			7		
38	40			7	0	3	5	6	3	3	4	1		5	5a			7		
32	40			7	0	4	12	6	3	3	4	1		3	5a			7		
				7	1	8			3	3	28	2	4	5	5a			7		
				7	1	8	7	5	3	3	33	2	4	5	5a			7		
				7	1	1			3	3	28	2	4	5	5a			7		
				7	1	1	7	5	3	3	33	2	4	5	5a			7		
31	40			7	1	2	9	6	3	3	33	2	4	5	5a			7		
				0	0	7			3	3	9	2	4	3	5a			7		
				0	0	2	1	7	3	3	22	3	9	3	5a	5b		7	2	
				0	0	7	6	6	3	3	4	1		3	5b			2	5	
				0	0	7	6	6	3	3	4	1		3	5b			2	5	
				0	0	7	6	6	3	3	4	1		3	5b			2	5	
25	29			0	0	2	6	6	4	5	2	2	4	3	5a	5b		7	2	
				0	0	3	6	5	3	10	10	3	4	3	5a			7		
				0	0	5	6	5	3	10	10	3	4	3	5a			7		
29				0	0	8	6	6	3	3	18	2	4	3	4	2		5	1	
21	25	29		0	0	3	6	5	3	3	18	2	9	3	4	2		5	1	
21	25	29	31	0	0	4	6	6	3	3	18	2	9	3	4	2		5	1	
25	30	37		0	0	1	4	5	3	3	18	2	9	3	4	4	2	5	7	1
25	30	37		0	0	1	4	5	3	3	18	2	9	3	4	4	2	5	7	1
25	29	30	40	0	0	1	4	6	3	10	10	3	9	3	4	4		5	7	
25	29	30	34	0	0	6	4	6	3	10	10	3	9	3	4	4		5	7	
25	29	30	34	0	0	8	1	4	3	10	10	2	4	3	4	4		5	7	
25	29	30	34	0	0	7	1	4	3	10	10	2	4	3	4	4		5	7	
25	29	30	34	0	0	3	1	4	3	10	10	2	4	3	4	4		5	7	
25	29	30	31	7	0	4	6	6	3	3	24	1		5	4	2		5	1	
25	29	30	34	0	0	2	6	6	3	3	9	2	9	3	4	2		5	1	
25	29	30	34	0	0	6	5	7	3	3	9	2	9	3	4	2		5	1	

Cause 9	Cause 10	Cause 11	Cause 12	Mlt. 1	Mlt. 2	Aspect	Simple Profile	Angle	System	Facet	Element	Veg Cover	Veg Type	Drainage Conditions	Upper Unit Name (1)	Lower Unit Name (2)	Other Unit Name (3)	Upper Lithology (1)	Lower Lithology (2)	Other Lithology (3)
29	30			0	0	6	6	6	3	3	9	2	9	3	2	4		1	5	
21	25	29	30	0	0	3	6	6	3	3	9	1		3	4	4		5	1	
				0	0	1	6	6	3	3	18	2	4	3	2			1		
				0	0	7	6	6	3	3	18	2	4	3	2			1		
				0	0	7	6	6	3	3	18	2	4	3	2			1		
				0	0	1	6	6	3	3	18	2	4	3	2			1		
				0	0	3	6	6	3	3	9	2	9	3	2			1		
				0	0	7	6	6	3	3	9	2	9	3	2			1		
				0	0	3	6	6	3	3	9	2	4	3	2			1		
				0	0	7	6	6	3	3	9	2	4	3	2			1		
				0	0	3	6	6	3	3	9	2	4	3	2			1		
				0	0	7	4	3	3	10	10	2	4	3	6d			8		
				0	0	7	4	3	3	10	10	2	4	3	6d			8		
				0	0	8	5	5	3	6	18	1		3	6d			8		
29	30			0	0	8	6	6	3	6	18	1		3	6d			1		
29	30			0	0	4	1	7	3	3	23	2	4	3	2			1		
29	30	34		0	0	3	6	6	3	4	18	2	9	3	2			1		
30	32	40		0	0	7	6	6	3	4	18	2	9	3	2			1		
29	30	34		0	0	1	5	3	3	4	18	4	9	3	1	2		1	1	
29	30	34		0	0	8	6	6	3	4	18	3	9	3	2			1		
29				0	0	4	5	3	3	4	6	1		3	2	2		1	7	
				0	0	8	5	5	3	3	17	1		3	2	2		1	7	
				0	0	4	6	6	3	4	4	1		3	6b			8		
				0	0	4	6	6	3	4	4	1		3	6b			8		
				0	0	7	6	5	3	4	7	2	4	3	6b			8		
				0	0	2	6	5	3	4	7	2	4	3	6b			8		
				0	0	7	6	6	3	4	19	2	4	3	6b			8		
				0	0	4	3	4	3	4	6	2	4	3	6b			8		
				0	0	4	3	3	3	4	6	2	4	3	6b			8		
25	29	30		0	0	7	6	6	4	6	8	3	4	3	6d			1		
25	29	30		0	0	4	3	5	4	6	18	3	4	3	6d			1		
				0	0	7	5	4	4	6	4	2	4	3	6d			8		
				0	0	7	5	4	4	6	4	2	4	3	6d			8		
				0	0	7	5	4	4	6	4	2	4	3	6d			8		
29				0	0	9	6	5	3	4	3	2	4	3	6d			8		
				0	0	8	5	7	3	4	8	3	9	3	6b			8		
				0	0	8	5	7	3	3	8	3	9	3	6b			8		

Cause 9	Cause 10	Cause 11	Cause 12	Mit 1	Mit 2	Aspect	Simple Profile	Angle	System	Facet	Element	Veg Cover	Veg Type	Drainage Conditions	Upper Unit Name (1)	Lower Unit Name (2)	Other Unit Name (3)	Upper Lithology (1)	Lower Lithology (2)	Other Lithology (3)
				0	0	3	6	7	3	3	4	2	4	3	6b			8		
				0	0	7	6	7	3	3	4	2	4	3	6b			8		
				0	0	5	5	7	3	3	8	3	4	3	6b			8		
				0	0	5	4	1	3	3	18	2	4	3	6b	6c		8	5	
30				0	0	1	6	5	3	3	18	2	4	3	6b	6c		8	5	
				0	0	1	6	5	3	3	18	2	4	3	6b	6c		8	5	
21	25	29	30	0	0	2			3	3	8	3	9	3	2	4		1	1	
21	25	29	30	0	0	1			3	3	8	3	9	3	2	4		1	1	
21	25	29	30	0	0	1			3	3	8	3	9	3	2	4		1	1	
21	25	29		0	0	2			3	3	8	3	9	3	2	4		1	1	
21	25	29		0	0	1			3	3	8	3	9	3	2	4		1	1	
25	29	30		0	0	9	1		3	3	4	3	9	3	6b	6c		8	5	
25	29	30		0	0	7	1		3	3	8	3	9	3	6b	6c		8	5	
21	25	29	30	0	0	1	1	4	3	3	18	2	4	3	6b	6c		8	5	
21	25	29	30	0	0	7	1	4	3	3	18	2	4	3	6b	6c		8	5	
21	25	29		0	0	2	4	3	3	3	24	2	4	3	6b	6c		8	5	
21	25	29		0	0	1	4	3	3	3	24	2	4	3	6b	6c		8	5	
21	25	29		0	0	7	1	4	3	3	18	3	9	3	6b	6c		8	5	
25	29	30		0	0	2	6	5	3	3	18	2	4	3	6b	6c		8	5	
25	29			0	0	6	5	4	3	3	6	3	4	3	6b	6c		8	5	
				0	0	4	4	3	4	6	8	3	6	5	6b			8	5	10
				0	0	2	4	4	3	2	8	3	4	3	10			11		
				0	0	2	4	4	3	2	8	3	4	3	10			11		
				0	0	3	6	5	2	2	35	2	4	3	10			11		
				0	0	7	6	5	4	4	8	2	4	3	10			11		
				0	0	1	3	5	4	4	8	2	4	3	10			11		
				0	0	1	3	5	4	4	8	2	4	3	10			11		
				0	0	8	3	5	4	4	8	2	4	3	10			11		
				0	0	6	3	5	4	4	8	2	4	3	10			11		
				0	0	5	4	4	2	2	18	2	4	3	10			11		
				0	0	5	1	4	2	4	18	2	4	3	10			11		
				0	0	5	4	4	2	4	8	2	4	3	10			11		
				0	0	5	4	4	2	4	8	2	4	3	10			11		
29				0	0	1	4	2	4	2	6	3	9	3	6b			8		
29				0	0	1	4	2	4	2	6	3	9	3	6b	0		8	0	
29				0	0	1	4	2	4	2	6	3	9	3	6b	0		8	0	
29				0	0	1	4	2	4	2	6	3	9	3	6b	0		8	0	

Cause 9	Cause 10	Cause 11	Cause 12	Mit 1	Mit 2	Aspect	Simple Profile	Angle	System	Facet	Element	Veg Cover	Veg Type	Drainage Conditions	Upper Unit Name (1)	Lower Unit Name (2)	Other Unit Name (3)	Upper Lithology (1)	Lower Lithology (2)	Other Lithology (3)
				0	0	8	1	5	3	10	19	2	4	3	5a			7		
				0	0	4	1	5	3	10	20	2	4	3	5a			7		
				0	0	8	1	5	3	10	19	2	4	3	5a			7		
				0	0	2	1	5	3	10	20	2	4	3	5a			7		
				0	0	6	1	5	3	10	19	2	4	3	5a			7		
				0	0	7			3	10	10	2	4	3	2			1		
				0	0	4	4	3	3	4	20	2	4	3	2	2		1	6	
				0	0	8	4	3	3	4	20	2	4	3	2	2		1	6	
				0	0	8	4	3	3	4	22	2	4	3	5a	5a		4	7	
				0	0	8	4	3	3	4	22	2	4	3	5a	5a		4	7	
				0	0	8	4	3	3	4	22	2	4	3	5a	5a		4	7	
				0	0	8	4	3	3	4	22	2	4	3	5a	5a		4	7	
30				0	0	8	6	5	3	4	22	2	4	3	5a	5a		4	7	
30				0	0	8	6	5	3	4	4	2	4	3	5a	5a		7	4	
30				0	0	8	6	5	3	4	4	2	4	3	5a	5a		7	4	
30				0	0	5	6	5	3	4	20	2	4	3	5a	5a		7	4	
30				0	0	1	6	5	3	4	22	2	4	3	5b			2		
30				0	0	5	6	5	3	4	20	2	4	3	5a			7	4	
				0	0	0	6	6	3	4	4	1		3	5b			2		
				0	0	8	5	3	4	5	6	3	4	3	5a	5b		7	2	
25	30	34		0	0	7	5	7	4	5	18	3	4	3	5a			7		
25	30			0	0	8	5	7	4	5	18	3	4	3	5a			7		
25	30			0	0	1	6	6	4	5	18	3	4	3	5a			7		
				0	0	7	6	6	4	5	18	2	4	3	1	5a		1	7	
25	32	40		0	0	7	6	6	3	3	10	2	4	3	5b			2		
				0	0	1	6	5	4	3	10	3	4	3	1			7		
				0	0	1	2	4	4	5	28	3	4	3	5a			7		
				0	0	8	6	6	4	5	28	3	4	3	5a			7		
				0	0	2	3	5	4	5	25	1		3	5a			4		
17	21	23		0	0	7	6	6	4	5	18	2	4	3	1	5a		1	4	
29	31	40		0	0	7	7	6	3	3	33	1		5	5a			7		
				0	0	2	6	6	3	5	18	1		3	5a			4		
25				0	0	4	6	5	3	10	18	1		3	5a			7	4	
18	21	30		0	0	3	1	5	3	3	18	3	4	3	2			1		
18	21	30		0	0	1	1	5	3	3	24	3	4	3	2			1		
18	21	30		0	0	5	1	5	3	3	18	2	4	3	4			5		
30				0	0	6	6	5	3	3	18	2	4	3	2			1		

Cause 9	Cause 10	Cause 11	Cause 12	Mit 1	Mit 2	Aspect	Simple Profile	Angle	System	Facet	Element	Veg Cover	Veg Type	Drainage Conditions	Upper Unit Name (1)	Lower Unit Name (2)	Other Unit Name (3)	Upper Lithology (1)	Lower Lithology (2)	Other Lithology (3)
21	25	30		0	0	2	1	6	3	3	18	3	4	3	2	4a		1	6	
21	25	30		0	0	6	1	6	3	3	18	3	9	3	2	4a		1	6	
25	29	30		0	0	4	6	6	3	3	18	3	4	3	4a	4a		5	6	
				0	0	7	4	4	4	5	8	3	9	3	4a	4a		6	7	
				0	0	8	3	4	4	5	8	3	9	3	1	4a		1	5	
				0	0	2	3	4	4	5	8	3	9	3	1	4a		1	5	
29	37			0	0	4	5	4	4	5	10	3	4	3	1	4a		1	5	
25	29			0	0	4	6	6	4	10	10	3	4	3	5a	5a		7	5	
25	29			0	0	8	6	6	4	10	10	3	4	3	5a	5a		7	5	
25	29			0	0	6	6	6	4	10	10	3	4	3	5a	5a		7	5	
25	29	30	37	0	0	6	6	6	4	3	10	1		3	1	4a	4a	1	6	7
21	25	37	39	0	0	4	7	5	4	4	8	1			1	2	5a	1	1	7
21	25			0	0	5	6	5	3	3	18	2	4	3	1			1		
21	25			0	0	2	6	5	3	3	4	2	4	3	5b	6c		2	5	
21	25			0	0	7	6	6	3	3	4	2	4	3	5b	6c		2	5	
21	25	30		0	0	3	6	6	3	3	4	2	4	3	5b	6c		2	5	
21	25	30		0	0	6	6	6	3	3	3	2	4	3	5b	6c		2	5	
25	30	31		0	0	3	6	6	3	3	3	2	4	3	1	5b	6c	1	2	5
34	36			0	0	8	6	6	3	3	10	2	4	3	1			5		
				0	0	3			3	3	9	2	9	3	5b	6c		2	5	
25	30	40		0	0	5	6	6	3	3	3	2	4	3	5b	6c		2	5	
25	30	40		0	0	3	6	6	3	3	3	2	4	3	5b	6c		2	5	
25	30	40		0	0	2	6	6	3	3	3	2	4	3	5b	6c		2	5	
40				0	0	1	5	6	3	4	10	2	4	3	6d	7		8	5	
40				0	0	1	5	6	3	3	10	2	4	3	6d	7		8	5	
29	30			0	0	5	1	5	3	3	3	2	4	3	1	6c		1	5	
				0	0	5	6	6	3	3	3	1		3	6d			8		
				0	0	2	5	6	3	3	4	1		3	6d			8		
21	25	29	34	0	0	8	1	2	3	3	22	3	4	3	6d	7		8	5	
29	30	34		0	0	3	1	5	3	3	3	2	4	3	5b	6c		2	5	
29	30	34		0	0	3	1	5	3	3	3	2	4	3	5b	6c		2	5	
25	29	30		0	0	4	1	6	3	3	3	2	4	3	5b	6c		2	5	
25	29	30		0	0	4	1	6	3	3	3	2	4	3	5b	6c		2	5	
21	25	29	30	0	0	6	1	7	3	3	3	2	4	3	5b	6c		2	5	
25	29	30		0	0	4	6	6	3	3	3	2	4	3	5b	6c		2	5	
25	29	30		0	0	4	6	6	3	3	3	2	4	3	5b	6c		2	5	
25	29	30		0	0	4	6	6	3	3	5	2	4	3	5b	6c		2	5	

Cause 9	Cause 10	Cause 11	Cause 12	Mit 1	Mit 2	Aspect	Simple Profile	Angle	System	Facet	Element	Veg Cover	Veg Type	Drainage Conditions	Upper Unit Name (1)	Lower Unit Name (2)	Other Unit Name (3)	Upper Lithology (1)	Lower Lithology (2)	Other Lithology (3)
25	29	30		0	0	5	1	7	3	3	3	2	4	3	5b	6c		2	5	
21	25	29	30	0	0	5	6	6	3	3	3	2	4	3	6d	7		8	5	
				0	0	4	6	6	3	3	4	2	4	3	6d			8		
				0	0	5	6	6	3	3	4	2	4	3	6d			8		
21	25	29	30	0	0	9	1	7	3	3	21	3	9	3	6d	7		8	5	
25	30	37		0	0	8	1	7	3	3	6	4	9	3	6d	7		8	5	
25	30	37		0	0	2	1	4	3	3	8	4	9	3	6d	7		8	5	
25	29	30		0	0	3	1	7	1	6	3	2	4	3	5b	6c		2	5	
25	29	30		0	0	3	1	7	1	6	3	2	4	6	5b	6c		2	5	
25	29	30		0	0	2	1	4	1	6	3	2	4	3	5b	6c		2	5	
25	29	30		0	0	5	12	4	1	6	3	2	4	3	5b	6c		2	5	
25	29	30		0	0	2	12	4	1	6	3	2	4	3	5b	6c		2	5	
25	29	30		0	0	1	12	4	1	6	3	2	4	3	5b	6c		2	5	
25	29	30		0	0	3	12	4	1	6	3	2	4	3	5b	6c		2	5	
25	29	30		0	0	3	6	6	1	6	3	2	4	3	5b	6c		2	5	
25	29			0	0	8	1	4	3	2	6	3	4	3	6d			8		
				0	0	2	6	5	3	3	22	2	4	3	6d			8		
				0	0	6	6	5	3	3	22	2	4	3	6d			8		
21	25	29		0	0	6	1	5	3	4	9	2	4	3	8			18		
25	29			0	0	3	4	4	2	4	18	2	4	3	9			18		
25	29			0	0	7	4	4	2	4	17	2	4	3	9			18		
25	29			0	0	3	4	4	2	4	18	2	4	3	9			18		
25	29			0	0	7	4	4	2	4	17	2	4	3	9			18		
21	25	29		0	0	3	6	6	3	4	9	3	4	3	6d			8		
21	25	29		0	0	7	6	6	3	4	9	3	4	3	6d			8		
21				0	0	8	1	2	3	6	22	3	9	5	6d			8		
21	25	29		0	0	4	6	5	3	4	3	3	4	3	6d			8		
21	25	29		0	0	6	6	5	3	4	9	3	4	3	6d			8		
25	29			0	0	6	6	5	3	4	20	2	4	3	6d			8		
25	29			0	0	1	2	3	2	2	2	2	4	3	9			18		
25	29			0	0	4	2	3	2	2	2	2	4	3	9			18		
25	29			0	0	3	2	3	2	4	2	2	4	3	9			18		
25	29			0	0	7	2	3	2	2	2	2	4	3	9			18		
25	29			0	0	3	2	3	2	2	2	2	4	3	9			18		
25	29			0	0	6	2	3	2	2	2	2	4	3	9			18		
25	29			0	0	1	2	3	2	2	35	2	4	3	9			18		
25	29			0	0	7	2	3	2	2	2	2	4	3	8			18		

Cause 9	Cause 10	Cause 11	Cause 12	Mit	Mit 2	Aspect	Simple Profile	Angle	System	Facet	Element	Veg Cover	Veg Type	Drainage Conditions	Upper Unit Name (1)	Lower Unit Name (2)	Other Unit Name (3)	Upper Lithology (1)	Lower Lithology (2)	Other Lithology (3)
25	29			0	0	1	2	3	2	2	2	2	4	3	8			18		
25	29			0	0	1	2	3	2	4	35	2	4	3	9			18		
25	29			0	0	7	2	3	2	4	35	2	4	3	9			18		
25	29			0	0	9	2	3	2	2	2	2	4	3	9			18		
25	29			0	0	1	2	3	2	2	35	2	4	3	9			18		
25	29			0	0	8	2	3	2	2	2	2	4	5	9			18		
25	29			0	0	9	2	3	2	2	2	2	4	5	9			18		
25	29			0	0	2	2	3	2	2	35	2	4	3	9			18		
25	29			0	0	2	2	3	2	4	35	2	4	3	9			18		
25	29			0	0	7	2	3	2	4	2	2	4	3	9			18		
25	29			0	0	1	2	3	2	4	2	2	4	3	9			18		
25	29			0	0	8	2	3	2	2	2	2	4	3	9			18		
25	29			0	0	6	2	3	2	2	2	2	4	3	9			18		
25	29			0	0	1	2	3	2	2	2	2	4	3	9			18		
25	29			0	0	7	2	3	2	2	2	2	4	3	9			18		
25	29			0	0	4	2	3	2	2	3	2	4	3	6d			8		
25	29			0	0	4	2	3	2	2	3	2	4	3	6d			8		
25	29			0	0	5	2	3	2	2	2	2	4	3	9			18		
25	29			0	0	7	1	3	2	2	35	2	4	3	9			18		

Appendix C – Landslide Inventory Ratings

The following tables contain the numerical codes that were used in the Landslide Inventory developed by this research project. They are discussed in Chapter 3.

Copy of Table 3.4: The different types of data contained in the landslide inventory database.

Category	Data that were collected
Location	The geographical location of the landslide including the grid reference and the longitude and latitude co-ordinates of the centre of the landslide.
Certainty of Identification	The data source used (i.e. field mapping and/or API) and the certainty of identification of the landslide.
Land use	The land use of the area in which the landslide has occurred and the relative position of the landslide to the land use. Any remedial measures that have been undertaken were also recorded.
Elevation	The elevation of the crown and toe area of the landslide.
Geometry	The height, width and length of the backscar and debris accumulation, as well as the area covered by the landslide and the volume of the debris accumulation.
Angle of Reach	The angle of reach of the landslide, measured from the crown to the toe.
Landslide Mechanisms	Up to six landslide mechanisms were recorded for each landslide, using the definitions described by Cruden (1991), Dikau *et al.* (1996) and Turner & Schuster (1996) and outlined in Section 3.4.2
Landslide Activity	The state, style, distribution and rate of the landslide, based on the definitions of the WP/WLI (1990, 1993, 1994, 1995).
Landslide Age	Relative age of the landslide based on a project-derived scheme.
Causative Factors	Up to ten factors attributed to either controlling or actually triggering the landslide, per landslide using the WP/WLI definitions (WP/WLI, 1990, 1993, 1994, 1995).
Slope Morphology	The aspect, profile and angle of the slope on which the landslide has occurred.
Geomorphology	The Land System, Land Facet and Land Element in which the landslide has occurred, as described in Section 3.2.3.
Geology	The geology of the slopes in which the landslide has occurred. Additional information concerning the geotechnical properties of both the rock material and rock masses involved in the landslide are contained within a second database.
Vegetation	The type and density of the vegetation covering the slopes on which the landslide has occurred.
Drainage	The type of drainage within and around the landslide.
References	Any published or unpublished material referring to the landslide.
Other Information	Any other relevant information.

Table C.1: Classification for the identification certainty and data source for each of

the mapped landslides and the landslide inventory codes.

Code	Identification Certainty
1	Backscar and deposit clearly identifiable
2	Back scar only (Deposit has been removed)
3	Deposit only (Backscar has been removed)
4	Presence of either backscar and/or the deposit are uncertain (i.e., an eroded (relict) feature that is covered with vegetation, shadowing effects on the aerial photographs or erosion)
5	Debatable identification

Code	Data Source	Code	Data Source
1	Black & White API only (no field validation)	7	B&W API with detailed field validation
2	Colour API only (no field validation)	8	Colour API with detailed field validation
3	Both sets of aerial photographs only (no field validation)	9	Both sets of API with detailed field validation
4	B&W API with limited field validation	10	Very limited field mapping (i.e., observed at distance)
5	Colour API with limited field validation	11	Limited field mapping only
6	Both sets of API with limited field validation	12	Detailed field mapping only

Table C.2: Land use classification and landslide inventory codes

	Land Use		Land Use		Land Use
1	Private/residential buildings	11	Motorway	21	Buried storage structures
2	Public buildings (schools, shops)	12	Major road	22	Above ground storage structures
3	Recreational buildings	13	Minor road / dirt track / access road	23	Buried water pipelines
4	Public access areas (sports fields)	14	Railway lines	24	Canals
5	Farm buildings	15	Bridges	25	Reservoirs
6	Industrial buildings	16	Electricity pylons	26	Sites of Scientific Interest
7	Disused/abandoned buildings	17	Buried electrical cables	27	Abandoned Fields / terraces
8	Mine workings / quarries	18	Telephone pylons	28	Municipal Sites
9	Fields for crops / terraces	19	Buried telephone cables	29	Airport Runway
10	Fields for cattle	20	Buried gas pipelines	30	

Table C.3: Landslide Failure Mechanisms

Mechanism	Code	Description
100 Rock Fall	101	Rock Fall with detachment from a planar failure surface.
	102	Rock Fall with detachment from a wedge-shaped failure surface.
	103	Rock Fall with detachment from a stepped failure surface.
	104	Rock Fall with detachment from a vertical failure surface.
200 Rock Topple	201	Rock Topple with detachment from a single pre-existing discontinuity.
	202	Rock Topple with detachment from a single tension failure surface.
	203	Rock Topple with detachment from multiple pre-existing discontinuities.
	204	Rock Topple with detachment from multiple tension failure surfaces.
300 Rotational (Sliding)	301	Rotational movement (sliding) on a single, circular failure surface.
	302	Rotational movement (sliding) on a successive, circular failure surface.
	303	Rotational movement (sliding) on a multiple, circular failure surface.
400 Non-rotational	401	Non-Rotational Compound movement (sliding) on a single, non-circular, listric, failure surface.
	402	Non-Rotational Compound movement (sliding) on a progressive, non-circular, listric, failure surface.
	403	Non-Rotational Compound movement (sliding) on a multi-storied, non-circular, listric, failure surface.
	404	Non-Rotational Compound movement (sliding) on a single, non-circular, bi-planar, failure surface.
	405	Non-Rotational Compound (sliding) on a progressive, non-circular, bi-planar, failure surface.
	406	Non-Rotational Compound (sliding) on a multi-storied, non-circular, bi-planar, failure surface.
500 Translational (Sliding)	501	Translational Movement (sliding) on a planar failure surface.
	502	Translational Movement (sliding) on a stepped failure surface.
	503	Translational Movement (sliding) on a wedge-shaped failure surface.
	504	Translational Movement (sliding) on a non-rotational failure surface.
600 Lateral Spreading	601	Lateral Spreading of ductile or soft material that deforms in a layer beneath hard rock.
	602	Lateral Spreading of ductile or soft material that deforms in a weak unstratified layer.
	603	Lateral Spreading of ductile or soft material that deforms in a collapsible structure.

Mechanism	Code	Description
700 Debris Movement	701	Debris Movement by flow on a natural unconfined slope.
	702	Debris Movement by flow on a natural channelised slope.
	703	Debris Movement by flow on a complex unconfined slope.
	704	Debris Movement by flow on a complex channelised slope.
800 Rock Flow (Sackung, Sagging)	801	Rotational ROCK FLOW (sagging, Sackung) affecting a single side of a mountain
	802	Compound (listric) ROCK FLOW (sagging, Sackung) affecting a single side of a mountain
	803	Compound (bi-planar) ROCK FLOW (sagging, Sackung) affecting a single side of a mountain
	804	Rotational ROCK FLOW (sagging, Sackung) affecting more than one side of a mountain
	805	Compound (listric) ROCK FLOW (sagging, Sackung) affecting more than one side of a mountain
	806	Compound (bi-planar) ROCK FLOW (sagging, Sackung) affecting more than one side of a mountain
	807	ROCK FLOW (sagging, Sackung) movement on a stepped discontinuity that may involve toppling.
900 Other Types of Movement	901	Rock Avalanche
	902	Creep
	903	Cambering
1000 Semi- Continuous Rock Slope Deterioration	1001	Grain Ravelling
	1002	Stone Ravelling
	1003	Block Ravelling
	1004	Flaking
	1005	Wash Erosion
	1006	Solution or Karstification
	1007	Flexural Toppling
1100 Sporadic Deterioration	1101	Grain Fall
	1102	Stone Fall
	1103	Block Fall
	1104	Contour Scaling
	1105	Slab Fall
	1106	Slab Topple

Table C.4: Landslide Activity definitions and codes used in the Landslide Inventory

State of Landslide Activity - WP/WLI (1993)			
Code		**Title**	**Definition**
1		Active	a landslide that is currently moving
2		Re-activated	a landslide that is active again after being inactive for a period of time
3		Suspended	a landslide that has moved within the last annual cycle of seasons, but is not moving at present
4	Inactive	Dormant	a landslide that has not moved for more than one annual cycle of seasons, but where the causes of movement apparently remain
5		Abandoned	a landslide that has not moved for more than one annual cycle of seasons because the causes of movement are no longer present
6		Stabilised	a landslide where remedial measures prevent further movements from occurring
7		Relict	a landslide which has clearly developed under geomorphological and climatic conditions different from those experienced at present

Inactive = a landslide that has not moved for more than one annual cycle of seasons.

Style of Landslide Activity - WP/WLI (1993)		
Code	**Title**	**Definition**
1	Complex	A landslide exhibiting at least 2 types of movements, in which the types are in sequence
2	Composite	A landslide exhibiting at least 2 different types of movement, all of occur in different areas of the displaced mass
3	Multiple	A landslide exhibiting repeated development of the same type of movement along the same rupture surface and involving the same displaced material
4	Successive	a landslide exhibiting movement which is identical to earlier movements, but in contrast to a multiple movement does not share displaced material or a rupture surface with it
5	Single	A landslide exhibiting a single movement of displaced material often as an unbroken block

Distribution of Landslide Activity - WP/WLI (1993)		
Code	**Title**	**Definition**
1	Retrogressing	The rupture surface is extending in the direction opposite to the movement of the displaced material
2	Advancing	The rupture surface is extending in the direction of movement of the displaced material
3	Widening	The rupture surface is extending at one or both lateral margins
4	Confined	Those landslides which have a scarp but no rupture surface visible in the foot of the displaced material
5	Enlarging	The rupture surface is enlarging in 2 or more directions
6	Diminishing	A landslide where the displaced material is decreasing in volume
7	Moving	A landslide where the displaced material continues to move but whose rupture surface shows no visible changes

Table C.5: Two schemes for the Estimated Ages of Landslide Activity based on geomorphological mapping.

Code	Description
1	Unknown
2	Ongoing since before the Río Aguas/Rambla Feos River Capture Therefore between the Gochar erosion surface and the Present (i.e., during the incision of the drainage network)
3	Before the Río Aguas/Rambla Feos River Capture. Therefore between the Gochar erosion surface/Terrace A and the Terrace C
4	Ongoing since the Río Aguas/Rambla Feos River Capture up to Present. Therefore between Terrace C and the Present river level
5	Since the Río Aguas/Rambla Feos River Capture but before terrace E
6	Since Terrace D
7	Modern landslide activity
A	Unknown
B	Before river capture
C	After river capture
D	Recent

Table C.6: Landslide Causes based on WP/WLI (1994).

Geological Factors	1	plastic weak material	**Morphological Factors**	11	tectonic uplift
	2	sensitive material		12	volcanic uplift
	3	collapsible material		13	glacial rebound
	4	weathered material		14	fluvial erosion of the slope toe
	5	sheared material		15	wave erosion of the slope toe
	6	jointed or fissured material		16	glacial erosion of the slope toe
	7	adversely orientated mass discontinuities (including bedding, schistosity, cleavage)		17	erosion of the lateral margins
	8	adversely orientated mass discontinuities (including faults, unconformities, flexural shears, sedimentary contacts)		18	subterranean erosion (solution, piping)
	9	contrast in permeability and its effects on ground water		19	deposition loading the slope crest
	10	contrasts in stiffness (stiff, dense material over plastic)		20	vegetation removal (by erosion, forest fire, drought)
Physical Factors	21	intense, short period, rainfall	**Human Factors**	31	excavation of the slope or at its toe
	22	rapid melt of deep snow		32	loading of the slope or at its crest
	23	prolonged high precipitation		33	drawdown (of reservoirs)
	24	rapid drawdown following floods, high tides or breaching of natural dams		34	irrigation
	25	earthquake		35	defective maintenance of drainage system
	26	volcanic eruption		36	water leakage from services (water supplies sewers, storm-water drains)
	27	breaching of crater lakes		37	vegetation cover removal (deforestation)
	28	thawing of permafrost		38	mining and quarrying (open pits or underground galleries)
	29	freeze and thaw weathering		39	creation of dumps of very loose waste
	30	shrink and swell weathering of expansive soils		40	artificial vibration (including traffic, pile driving, heavy machinery)

Table C.7: Slope Aspect

Code	Aspect	Code	Aspect	Code	Aspect	Code	Aspect
1	N	3	E	5	S	7	W
2	NE	4	SE	6	SW	8	NW

9 = more than one slope aspect direction

Table C.8: Slope Profile

Code	Slope Profile	Code	Slope Profile
1	Complex	6	Cliff (escarpment)
2	Convex	7	Cut slope
3	Straight	8	Simple embankment
4	Concave	9	Benched embankment
5	Benched	10	

Table C.9: Slope Angle

Code	Angle	Code	Angle	Code	Angle
1	0° - 15°	3	31° - 45°	5	61° - 75°
2	16° - 30°	4	46° - 60°	6	76° - 90°

Table C.10: The Land System, Land Facet and Land Element classification scheme

and the landslide inventory codes.

Code	Land System	Code	Land System
1	Gypsum Plateau & Karst area	2	Mountain slopes in basement material incised by canyons and river channels
3	Mountain slopes in basement material with gullies	4	Hill areas incised by canyons and gullies
5	Hill areas with river valley side slopes	6	Badlands
7	Level Terrain		
Code	**Land Facet**	**Code**	**Land Facet**
1	Plateau area	2	Hill / Mountain area
3	Incised river channel / canyon bounded by river terraces	4	Incised river channel / canyon without any river terraces
5	Open River valley bounded by river terraces	6	Open River valley bounded by slopes formed by the dissection of the drainage system
7	Terraces	8	Level terrain (Interfluve area)
9	Badlands	10	Gully System
11	Barranco (narrow, incised drainage channel)		
Code	**Land Element**	**Code**	**Land Element**
1	Plateau area	2	crest or ridge area
3	Scarp-slope escarpment / cliff face / canyon wall	4	dip-slope escarpment / cliff face / canyon wall
5	Scarp-slope transportational mid-slope	6	dip-slope transportational mid-slope
7	Slope perpendicular to dip direction	8	valley side slope
9	Canyon side wall	10	gully side wall
11	Scarp-slope gully side/wall	12	dip-slope gully side / wall
13	Gully floor	14	Colluvial footslope / talus
15	active river channel or canyon	16	abandoned river channel or canyon
17	inside of an active meander	18	outside of an active meander
19	Scarp slope on the inside of an active meander	20	Scarp slope on the outside of an active meander
21	Dip-slope on the inside of an active meander	22	Dip-slope on the outside of an active meander
23	inside of an abandoned meander	24	outside of an abandoned meander
25	Scarp slope on the inside of an abandoned meander	26	Scarp slope on the outside of an abandoned meander
27	Dip-slope on the inside of an abandoned meander	28	Dip-slope on the outside of an abandoned meander
29	Active river terrace surface	30	Active river terrace slope
31	Abandoned river terrace surface	32	Abandoned river terrace slope
33	man-made slope/road cutting	34	Artificial (agricultural) terrace
35	Mountain side slope		

12

Table C.11: The Formation name and lithology classification scheme and the landslide inventory codes. This is based on the geology of the study area as described in Chapter 2.

Code	Formation Name	Code	Formation Name
1	Quaternary Deposits	6	Turre Fm
2	Gochar Fm	6a	*Santiago Mb*
3	Cuevas Fm	6b	*Cantera Mb*
4	Cariatiz Fm	6c	*Abad Mb*
4a	*Zorreras Mb*	6d	*Azagador Mb*
4b	*Moras Mb*	7	Chozas Fm
5	Caños Fm	8	Umbria Fm / Mofar Fm
5a	*Sorbas Mb*	9	Higher Betic Units
5b	*Yesares Mb*	10	Nevado-Filabride Complex
		11	Nevado-Lubrin Unit
Code	**Lithology**	**Code**	**Lithology**
1	Conglomerate	10	schist
2	Gypsum	11	gneiss
3	Clay	12	granite/granodiorite
4	Shale	13	gabbro/dolerite
5	Calcareous mudstone	14	basalt and other basic lava
6	Siltstone/mudstone	15	ultra-basic rocks
7	Sandstone	16	volcanic tuff and pyroclastic deposit
8	Limestone	17	breccia
9	Slate	18	

Table C.12: The Vegetation cover and type, and drainage conditions of the slope in which the landslide has occurred and the landslide inventory codes.

Code	Vegetation Cover	Code	Vegetation Cover
1	No Vegetation	3	Moderately covered
2	Sparsely covered	4	Densely covered
Code	**Vegetation Type**	**Code**	**Vegetation Type**
1	Temporarily Barren (i.e., fire)	6	Olive grove
2	Permanently barren	7	Deciduous woodland or forest
3	Pasture	8	Coniferous woodland or forest
4	Scrub (Bushes)	9	Combination
5	Vineyard	10	Other (specify)
Code	**Drainage Conditions**	**Code**	**Drainage Conditions**
1	Spring Line	4	Artificial drainage
2	Standing water	5	Combination of artificial and natural drainage
3	Natural drainage	6	Close proximity to natural spring line

Mitigation and/or Remediation

None = 0

Surface drainage = 1   Underground drainage = 2

Gabions = 3   Rock bolts/anchors = 4

Loading at landslide toe = 5   Loading at landslide crown = 6

Removal of material = 7   Netting = 8